

PCT-8

The International Polymer Conference of Thailand

PROCEEDINGS BOOK

June 14th-15th, 2018

Amari Watergate Bangkok Hotel,
Bangkok, Thailand



PST

Organized by Polymer Society of Thailand

PROCEEDINGS



The International Polymer Conference of Thailand

Annual Polymer Conference

June 14th – 15th, 2018

Amari Watergate Bangkok Hotel,
Bangkok, Thailand

Organized by



The Polymer Society of Thailand (PST)

Message from the President

PCT-8: Time for joining together to create innovations on polymeric materials for our society

Assoc. Prof. Dr. Pranee Phinyocheep
President of the Polymer Society of Thailand
PCT-8 Chair



It has been since 1999 that the Polymer Society of Thailand (PST) was founded by a group of Thai academic and industrial polymer scientists. As the members of the Society are increasing with the world's growth of research studies in polymeric materials, the International Polymer Conference of Thailand (PCT), organized annually by PST, is one of the most successful events in Thailand, which can draw people from different universities, and industrial sectors across the country to share their knowledges and innovations for the benefit of our society. The conference is also a stage in encouraging young polymer scientists to express their ideas and innovations.

The worthiness of Polymer Conference of Thailand (PCT-8) this year aims not only at the dissemination of the most recent advances in polymer science and technology commonly practiced among technocrats, it also focuses on the augmentation of a closer collaboration between the universities and the industrial enterprises. Emphasis will be placed upon the principles and practices, which address the concerns of the present and future generations. It is envisaged further that a tie of collaboration between the university research and the industry's R&D will result in improving the capacity to acquire and use the science and technology developed elsewhere for a constructive response to the status of the government's Eastern Economic Corridor under Thailand 4.0 national strategy.

The charm of this year conference is our honor to have eminent speakers covering rubber, plastic, fiber, film and coating from Universities and Industries. Five scientific sessions are being organized, which are Recent Developments in Polymer Design, Bioplastics and Polymers for Sustainability, Biomedical Polymers, Rubbers/Elastomers and Polymer Blends and Composites, with a special session of Polymer Industry Trends. Four honorable Plenary speakers will lead the conference; Prof. Toshikazu Takata from Tokyo Institute of Technology, Japan; Prof. Chua Chee Kai from NTU, Singapore; Prof. Guy Louarn from University of Nantes, France; Prof. Changwoon Nah from Chonbuk National University, South Korea. The PCT-8 is also pleased to have 8 Keynote speakers from abroad; Prof. Hiroshi Tamura (Kansai University, Japan); Prof. Kazuaki Matsumura (JAIST, Japan); Prof. Masanobu Naito (National Institute of Materials Science, Japan); Prof. Seiichi Kawahara (Nagaoka University of Technology, Japan); Prof. Salit Mohd Sapuan (University Putra, Malaysia); Assoc.Prof. Kheng Lim Goh (Newcastle University, Singapore); Dr. Thai Hwee Tatz (Dow Singapore Development Center); and Mr. Pradip Kumar Dubey (Aditya Birla Chemicals, Thailand); and 4 Thai Keynote speakers; Assoc.Prof. Hathaikarn Manuspiya (Chulalongkorn University); Asst.Prof. Amorn Chaiyasat (RMUTT); Dr. Duangporn Polpanich (NANOTEC) and Dr. Jittiporn Krueenate (PTTGC). Additionally, an Invited speaker; Dr. Teh Chin Hoe from Bruker Biospin AG, 46 oral presentations and 54 poster presentations will make the conference fulfilled with scientific ambience.

The PCT-8 organizing committee wishes to take this event to congratulate the efforts and accomplishments of young polymer scientists by recognizing them as "PCT-8 Rising Star"; Asst.Prof. Anoma Thitithammawong from Prince of Songkla University, Pattani Campus; Assoc.Prof. Thammasit Vongsetskul from Mahidol University and Ms. Thipa Naiyawat from Aditya Birla Chemicals (Thailand).

On behalf of the Polymer Society of Thailand, I would like to express my sincere thanks for the success of high quality conference to all of the committee who have put tremendous efforts to organize this PCT-8 conference. In addition, I would like to state special thanks to valuable supports for the Platinum sponsors from the PTT Global Chemical Public Company Limited, the Aditya Birla Chemicals (Thailand), and the Bara Scientific Co., Ltd.; Gold sponsor from the SCG Chemicals Co., Ltd., the Silver sponsor from Bruker BioSpin AG, the Bronze sponsors from the IRPC Public Company Limited and the Thailand Research Fund; the financial assistance for students' registration fee from the M.B.J. Enterprise Co., Ltd., and support from eight booth exhibitors *i.e.* Synchrotron Light Research Institute; HORIBA (Thailand) Limited, Vana Science Co., Ltd, LMS Instruments Co., Ltd; Richteck Paint Co., Ltd.; S.M. Chemicals Supplies Co., Ltd.; Becthai Bangkok Equipment & Chemical Co., Ltd. and Technovation International Co., Ltd including support from Siam Synthetic Latex Co., Ltd. My deepest gratitude goes to all speakers, poster presenters and audiences who participate in this conference.

Finally, I wish the PCT-8 conference a fruitful success, and hope that you have a happy stay, enjoy the sharing and exchanging of your expertise as well as bright mind to create innovations on polymeric materials for our society.

Pranee Phinyocheep

Board of Polymer Society of Thailand

Advisory board



Asst. Prof. Dr. Krisda Suchiva
Rubber Technology Research Centre,
Mahidol University

Prof. Dr. Pattarapan Prasassarakich
Department of Chemical Technology,
Chulalongkorn University



Prof. Dr. Supawan Tantayanon
Department of Chemistry,
Chulalongkorn University

Prof. Dr. Suda Kiatkamjornwong
Department of Imaging and Printing Technology,
Chulalongkorn University



Prof. Dr. Suwabun Chirachanchai
The Petroleum and Petrochemical College,
Chulalongkorn University

Dr. Banja Junhasavasdikul
Innovation Group



President
Assoc. Prof. Dr. Pranee Phinyocheep
Department of Chemistry, Mahidol University



Vice President
Dr. Chaya Chandavas
PTT Global Chemical Public Company Limited

Secretariat
Assoc. Prof. Dr. Panya Sunintaboon
Department of Chemistry, Mahidol University



Treasurer
Assoc. Prof. Dr. Thanyalak Chaisuwan
The Petroleum and Petrochemical College,
Chulalongkorn University

Reception Secretary
Assoc. Prof. Dr. Pakorn Opaprakasit
Sirindhorn International Institute of Technology,
Thammasat University



Board of Polymer Society of Thailand

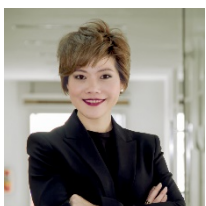
(continued)



Reception Secretary
Dr. Wonchalerm Rungswang
 SCG Chemicals Company Limited



Registrar
Assoc. Prof. Dr. Apirat Laobuthee
 Department of Materials Engineering, Kasetsart University



Public Relations
Asst. Prof. Dr. Wanvimol Pasanphan
 Department of Materials Science, Kasetsart University



Academic Committee
Asst. Prof. Dr. Winita Punyodom
 Department of Chemistry, Chiang Mai University



Academic Committee
Asst. Prof. Dr. Kannika Sahakaro
 Department of Rubber Technology and Polymer,
 Prince of Songkla University, Pattani Campus



Committee
Assoc. Prof. Dr. Taweechai Amornsakchai
 Department of Chemistry, Mahidol University



Committee
Asst. Prof. Dr. Varawut Tangpasuthadol
 Department of Chemistry, Chulalongkorn University



Committee
Dr. Pasaree Laokijcharoen
 National Metal and Materials Technology Center (MTEC)



Committee
Mr. Somsak Borrisuttanakul
 TPBI Public Company Limited



Committee
Mr. Bamrung Jadsadaphongphaibool
 M.B.J Enterprise Company Limited



Committee
Ms. Rattanapatum Piladang
 Plastics Institute of Thailand

Conference Committee

Chair

Assoc. Prof. Pranee Phinyocheep

Mahidol University

(President of the Polymer Society of Thailand)

International Advisory Committee

- | | |
|-----------------------------------|--|
| 1. Prof. Garry L. Rempel | University of Waterloo, Canada |
| 2. Prof. Laurent Fontaine | Le Mans Universite, France |
| 3. Prof. Philippe Daniel | Le Mans Universite, France |
| 4. Prof. Jean Francois Pilard | Le Mans Universite, France |
| 5. Prof. Bruno Vergnes | Ecole des Mines de Paris – CEMEF, France |
| 6. Prof. Guy Louarn | University of Nantes, France |
| 7. Prof. Anke Blume | University of Twente, Netherlands |
| 8. Prof. Jacques W.M. Noordermeer | University of Twente, Netherlands |
| 9. Prof. Masayoshi Okubo | Nanjing Tech University, China |
| 10. Prof. Yuko Ikeda | Kyoto Institute of Technology, Japan |
| 11. Prof. Seiichi Kawahara | Nagaoka University of Technology, Japan |
| 12. Prof. Tashikazu Takata | Tokyo Institute of Technology, Japan |
| 13. Prof. Kazuaki Matsumura | Japan Advanced Institute of Science and Technology |
| 14. Assoc. Prof. Masanobu Naito | National Institute for Materials Science, Japan |
| 15. Prof. Hiroshi Tamura | Kansai University, Osaka |
| 16. Prof. Hyoung Jin Choi | Inha University, Korea |
| 17. Prof. Changwoon Nah | Chonbuk National University, Korea |
| 18. Prof. Hazizan Md Akil | Universiti Sains Malaysia, Malaysia |
| 19. Assoc. Prof. Nadras Othman | Universiti Sains Malaysia, Malaysia |
| 20. Prof. Salit Mohd Sapuan | Universiti Putra Malaysia, Malaysia |
| 21. Prof. Bhuvanesh Gupta | Indian Institute of Technology, India |
| 22. Assoc. Prof. Chi-How Peng | National Tsing Hua University, Taiwan |
| 23. Prof. Katrina Cornish | Ohio State University |
| 24. Assoc. Prof. Kheng Lim Goh | Newcastle University in Singapore, Singapore |

Scientific Committee

- | | |
|---|--|
| 1. Prof. Garry L. Rempel | University of Waterloo, Canada |
| 2. Prof. Guy Louarn | University of Nantes, France |
| 3. Prof. Seiichi Kawahara | Nagaoka University of Technology, Japan |
| 4. Prof. Tashikazu Takata | Tokyo Institute of Technology, Japan |
| 5. Prof. Kazuaki Matsumura | Japan Advanced Institute of Science and Technology |
| 6. Prof. Masanobu Naito | National Institute for Materials Science, Japan |
| 7. Prof. Hiroshi Tamura | Kansai University, Osaka |
| 8. Prof. Changwoon Nah | Chonbuk National University, Korea |
| 9. Assoc. Prof. Nadras Othman | Universiti Sains Malaysia, Malaysia |
| 10. Prof. Salit Mohd Sapuan | Universiti Putra Malaysia, Malaysia |
| 11. Assoc. Prof. Kheng Lim Goh | Newcastle University in Singapore, Singapore |
| 12. Prof. Katrina Cornish | Ohio State University |
| 13. Assoc. Prof. Pranee Phinyocheep | Mahidol University |
| 14. Assoc. Prof. Panya Sunintaboon | Mahidol University |
| 15. Assoc. Prof. Sombat Thanawan | Mahidol University |
| 16. Assoc. Prof. Taweechai Amornsakchai | Mahidol University |
| 17. Assoc. Prof. Thammasit Vongsetskul | Mahidol University |
| 18. Asst. Prof. Anyarat Watthanaphanit | Mahidol University |
| 19. Prof. Suda Kiatkamjornwong | Chulalongkorn University |
| 20. Prof. Pattarapan Prasassarakich | Chulalongkorn University |
| 21. Assoc. Prof. Napida Hinchiranan | Chulalongkorn University |
| 22. Assoc. Prof. Sirilux Poompradub | Chulalongkorn University |
| 23. Asst. Prof. Kanoktip Boonkerd | Chulalongkorn University |

24. Asst. Prof. Varawut Tangpasuthadol	Chulalongkorn University
25. Asst. Prof. Wanpen Tachaboonyakiat	Chulalongkorn University
26. Assoc. Prof. Apirat Laobuthee	Kasetsart University
27. Assoc. Prof. Rangrong Yoksan	Kasetsart University
28. Asst. Prof. Amornrat Lertworasirikul	Kasetsart University
29. Asst. Prof. Wanvimol Pasanphan	Kasetsart University
30. Asst. Prof. Chantiga Choochottiros	Kasetsart University
31. Dr. Piyawanee Jariyasakoolroj	Kasetsart University
32. Assoc. Prof. Pakorn Opaprakasit	Thammasat University
33. Asst. Prof. Paiboon Sreearunothai	Thammasat University
34. Dr. Chariya Kaewsaneha	Thammasat University
35. Asst. Prof. Chonlada Ritvirulh	King Mongkut's Institute of Technology Ladkrabang
36. Asst. Prof. Suparat Rukchonlatee	King Mongkut's Institute of Technology Ladkrabang
37. Dr. Nonsee Nimitsiriwat	King Mongkut's University of Technology Thonburi
38. Asst. Prof. Suttinun Phongtamrug	King Mongkut's University of Technology North Bangkok
39. Asst. Prof. Amorn Chaiyasat	Rajamangala University of Technology Thanyaburi
40. Dr. Chatchai Veranitisagul	Rajamangala University of Technology Thanyaburi
41. Dr. Robert Molloy	Chiang Mai University
42. Asst. Prof. Winita Punyodom	Chiang Mai University
43. Assoc. Prof. Sunan Saikrasun	Maharakham University
44. Assoc. Prof. Metha Rutnakornpituk	Naresuan University
45. Dr. Gareth Michael Ross	Naresuan University
46. Asst. Prof. Anoma Thitithammawong	Prince of Songkla University, Pattani Campus
47. Asst. Prof. Kannika Sahakaro	Prince of Songkla University, Pattani Campus
48. Dr. Sunisa Suchat	Prince of Songkla University, Surat Thani Campus
49. Asst. Prof. Polpat Ruamcharoen	Songkhla Rajabhat University
50. Assoc. Prof. Sayan Saengsuwan	Ubon Ratchathani University
51. Dr. Pasaree Laokijcharoen	National Metal and Materials Technology Center

Organizing Committee

1. Assoc. Prof. Pranee Phinyocheep	Mahidol University
2. Asst. Prof. Krisda Suchiva	Mahidol University
3. Prof. Supawan Tantayanon	Chulalongkorn University
4. Prof. Suwabun Chirachanchai	Chulalongkorn University
5. Prof. Suda Kiatkamjornwong	Chulalongkorn University
6. Prof. Pattarapan Prasassarakich	Chulalongkorn University
7. Dr. Banja Junhasavasdikul	Innovation Group
8. Dr. Chaya Chandavasut	PTT Global Chemical Public Company Limited
9. Assoc. Prof. Panya Sunintaboon	Mahidol University
10. Assoc. Prof. Taweechai Amornsakchai	Mahidol University
11. Assoc. Prof. Thanyalak Chaisuwan	Chulalongkorn University
12. Asst. Prof. Varawut Tangpasuthadol	Chulalongkorn University
13. Assoc. Prof. Apirat Laobuthee	Kasetsart University
14. Asst. Prof. Wanvimol Pasanphan	Kasetsart University
15. Assoc. Prof. Pakorn Opaprakasit	Thammasat University
16. Asst. Prof. Kannika Sahakaro	Prince of Songkla University, Pattani Campus
17. Asst. Prof. Winita Punyodom	Chiang Mai University
18. Dr. Pasaree Laokijcharoen	National Metal and Materials Technology Center (MTEC)
19. Dr. Wonchalerm Rungswang	SCG Chemicals Company Limited
20. Mr. Somsak Borrisuttanakul	TPBI Public Company Limited
21. Mr. Bamrung Jadsadaphongphaibool	M.B.J Enterprise Company Limited
22. Ms. Rattanapatum Piladang	Plastics Institute of Thailand
23. Mr. Therdsak Leokprasirtkul	PTT Global Chemical Public Company Limited

Regional Organizing Committee

1. Dr. Robert Molloy
Chiang Mai University
2. Assoc. Prof. Metha Rutnakornpituk
Naresuan University
3. Assoc. Prof. Jatuphorn Wootthikanokkhan
King Mongkut's University of Technology Thonburi
4. Assoc. Prof. Yodthong Baimark
Mahasarakham University
5. Asst. Prof. Chiraphon Chaibundit
Prince of Songkla University, Hat Yai Campus
6. Asst. Prof. Polphat Ruamcharoen
Songkhla Rajabhat University
7. Asst. Prof. Rukkiat Jitchati
Ubon Ratchathani University
8. Asst. Prof. Suttinun Phongtamrug
King Mongkut's University of Technology North Bangkok
9. Asst. Prof. Preeyaporn Chaiyasat
Rajamangala University of Technology Thanyaburi
10. Asst. Prof. Chanchai Thongpin
Silpakorn University
11. Asst. Prof. Rapee Utke
Suranaree University of Technology
12. Dr. Patchara Punydamoonwongsa
Mae Fah Luang University
13. Dr. Piyaporn Na Nongkhai
Burapha University
14. Dr. Sunisa Suchat
Prince of Songkla University, Surat Thani Campus
15. Dr. Uthen Thubsuang
Walailak University
16. Dr. Achara Kleawkla
Maejo University
17. Ms. Boontharika Thapsukhon
University of Phayao

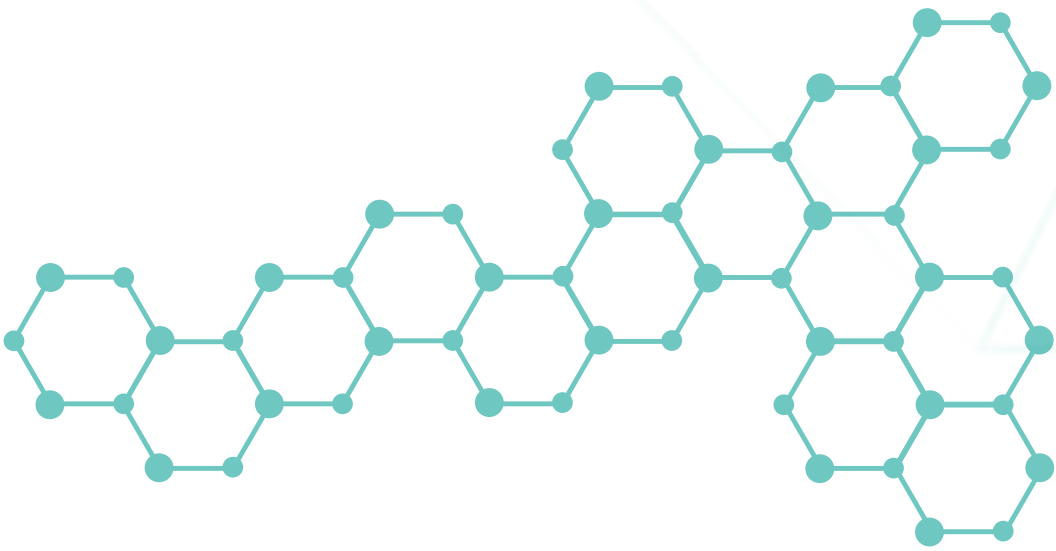
Contents

Session/Code	Title / Speaker	page
Plenary Lectures		
PLENARY-1	Effect of Mobile Polymer Chains at Cross-Link Points on Toughness Prof. Toshikazu Takata	1
PLENARY-2	Polymer-Based Additive Manufacturing: Emerging Trends Prof. Chua Chee Kai	2
PLENARY-3	Molecular Structures and Long-Term Mechanical Properties of Virgin and Recycled Polyolefins: A Case Study Applied to the Water Pipe Systems Prof. Guy Louarn	3
PLENARY-4	Recent Advances in Rubber Reinforcing and Functional Applications of Rubber Elasticity Prof. Changwoon Nah	4
Keynote lectures		
PDES-KN1	Degradation Control of Polysaccharides and the Biomedical Applications Assoc. Prof. Kazuaki Matsumura	5
PDES-KN2	Iodine Transfer Polymerization: Some Applications in Polymer Colloids Asst. Prof. Amorn Chaivasat	6
BPLA-KN1	Facile and Rational Modulation of Ubiquitous Plant Polyphenols: Novel Multifunctional Coating Precursors from Nature Assoc. Prof. Masanobu Naito	7
BPLA-KN2	Cellulose; Fascinating Biopolymer for Biomedical toward Energy Applications Assoc. prof. Hathaikarn Manuspiya	8
BMED-KN1	Biomedical Application of Chitin and Chitosan Prof. Hiroshi Tamura	9
BMED-KN2	Stimuli-responsive Polymeric Materials for Medical Diagnostics and Cell Labelling Dr. Duangporn Polpanich	10
RUBB-KN1	Characterization of Vulcanized Natural Rubber through Rubber State NMR Spectroscopy Prof. Seiichi Kawahara	11
COMP-KN1	Natural Fibre Composites: Malaysian Perspective Prof. Salit Mohd Sapuan	12
COMP-KN2	Natural Fiber Composite Materials: A Holistic Approach to Value Creation Dr. Jittiporn Kruenate	13
COMP-KN3	Polymer Composites Reinforced by Carbon Nanotubes and Carbon Fibres Assoc. Prof. Kheng Lim Goh	14
PIDT-KN1	Global Trends in Polymer Industry Mr. Pradip Kumar Dubey	15
PIDT-KN2	Mega Trends in Packaging and Properties and Applications of Innovative Packaging Resins-Ionomers Dr. Thai Hwee Tatz	16
INVT-1	NMR Application for Polymers Dr. Teh Chin Hoe	17
PST Rising Star Award Lecture		
RISESTAR-1	Overview of Thermoplastic Elastomers Research and Product Development Asst. Prof. Anoma Thitithammawong	18
RISESTAR-2	Electrospun Ultrafine Fibers: Versatile and Tunable Materials for Storing Electricity and Improving Enzyme Performance Assoc. Prof. Thammasit Vongsetskul	19
RISESTAR-3	Chemical Modifications and Value added Epoxy Resins: an Industrial Perspective Thipa Naiyawat	20
I. Session: Recent Development in Polymer Design		
PDES-O5	Development of Infrared-reducing Coating from Poly(3,4 Ethylenedioxythiophene) Polystyrene Sulfonate Krittana Lam, Jedsada Manyam, Chookiat Tansarawiput, Pakorn Opaprakasit and Paiboon Sreearunothai	21-25
PDES-P4	Preparation of Poly[(acrylic acid)-co-(potassium acrylate)] Superabsorbent Polymer Nonpan Dispat, Sirilux Poompradub and Suda Kiatkamjornwong	26-31
PDES-P6	Polyisocyanurate Foams Preparation Catalyzed by Mixtures of Copper-Amine Complexes and Potassium 2-Ethylhexanoate Teeraporn Suwannawet, Duangruthai Sridaeng and Nuanphun Chantarasiri	32-37
PDES-P8	Electron Beam-cured Overprint Varnish as a Green Printing Arnunthorn Ruengpattaradet, Thananchai Piroonpan, Anan Kempanichkul, Pichayada Katemake and Wanvimol Pasanphan	38-43

Session/Code	Title / Speaker	page
II. Session: Bioplastics and Polymers for Sustainability		
BPLA-O1	Effect of Modified Coconut Residue Fiber on Biodegradable Composite Foam Properties <i>Worraphol Nansu, Sukunya Ross, Gareth Ross and Sararat Mahasaranon</i>	44-52
BPLA-O2	Preparation of Nanocrystalline Cellulose by Using Eco-friendly Green Solvent as Pre-treatment <i>Gan Pei Gie, Sam Sung Ting and Muhammad Faiq bin Abdullah</i>	53-57
BPLA-O3	Effect of Different Crosslinkers on the Mechanical Properties of Nanocrystalline Cellulose/Chitosan Film Composite <i>Sam Sung Ting, Gan Pei Gie and Muhammad Faiq bin Abdullah</i>	58-62
BPLA-O4	Development of Low-cost Hydrophobic Sachet for Storage of Ethylene Scavenger for Use in Extending Fruit Shelf Life <i>Nisanart Naksin, Korakot Sombatmankhong, Pakorn Opaprakasit, Wanida Chooaksorn, Nichakorn Pathumrangsarn and Paiboon Sreearunothai</i>	63-68
BPLA-P11	Effects of Hydrophobic Starch/Nanosilica Hybrid Filler on Properties of Poly(lactic acid) Composites <i>Jindamas Supphasupsiri and Kawee Srikulkit</i>	69-75
BPLA-P12	Preparation of Cellulose Hydrogel-coated Fertilizers for Agricultural Applications <i>Nuntaporn Sutayo, Somrudee Nilthong, Nattakan Soykeabkaew and Orawan Suwanton</i>	76-81
BPLA-P13	Rheological and Viscoelastic Properties of Poly(Butylene Succinate)/Poly(Ethylene Terephthalate) Blends <i>Nattakarn Hongsrirphan, Kiattisak Chutivasanaskun, Paphada Kantipongpipat, Jirawat Thanokiang and Pajaera Patanathabutr</i>	82-88
BPLA-P14	Preparation and Properties of Biodegradable Citric Acid Modified Thermoplastic Rice Starch Films <i>Kittichai Sornsumdaeng, Panpailin Seeharaj and Jutarat Prachayawarakorn</i>	89-93
BPLA-P15	Influence of Waste Paper Fiber on the Physical Properties of Natural Rubber Graft Cassava Starch <i>Rangsima Jarusuwanwong, Lalisa Bunmechimma and Sa-Ad Riyajan</i>	94-99
BPLA-P16	Effect of Glycerol Contents on Properties of Hydrogel Sponge from Basil Seed Mucilage <i>Siriporn Tantiwatcharothai and Jutarat Prachayawarakorn</i>	100-104
BPLA-P17	Preparation and Properties of Thermoplastic Dialdehyde Cassava Starch Film by Sodium Metaperiodate <i>Sasikorn Poomkaew and Jutarat Prachayawarakorn</i>	105-109
BPLA-P18	Encapsulation of Agrochemical via Chitosan-functionalized W ₁ /O/W ₂ Double Emulsions <i>Chomphunut Thammaphichai, Nuttaporn Pimpha and Panya Sunintaboon</i>	110-115
BPLA-P19	Starch Foams Based on Rice Starch/Rice Straw Fiber <i>Nisa Promsen, Suparada Tagan and Linda Thiraphattaraphun</i>	116-120
BPLA-P20	PVA/CaHPO ₄ Film from Cockle Shell for Biodegradable Film <i>Nattapong Pinpru and Somsak Woramongkolchai</i>	121-127
BPLA-P21	Preparation and Property Improvement of Stereocomplexed PLL/PDL-PEG-PDL Blends <i>Aphinan Saengsrirchan, Puttinan Meepowpan, Patnarin Worajittiphon, Robert Molloy and Winita Punyodom</i>	128-132
III. Session: Biomedical Polymers		
BMED-O1	Synthetic Strategies for Molecularly Imprinted Polymer of Very-Low-Density Lipoprotein <i>Suticha Chunta and Peter A. Lieberzeit</i>	133-137
BMED-O3	<i>Cordyceps Militaris</i> Extract-Loaded Chitosan Nanoparticles and Their Release Characteristics <i>Jittap Pranjan and Orawan Suwanton</i>	138-143
BMED-O11	Preparation of Poly(Lactic Acid)/Alumina Composites for Dentistry Application <i>Nathawat Kanchanawaleekun, Nattakarn Hongsrirphan and Pajaera Patanathabutr</i>	144-148
BMED-P1	The Applicability of PMAMPC-functionalized Fe ₃ O ₄ NPs for Biosensor Application <i>Supannika Boonjamnian, Thanida Trakulsujaritchock and Piyaporn Na Nongkhai</i>	149-153
BMED-P2	Improvement in Mechanical Property of Hydroxyapatite Reinforced Chitosan/Collagen Scaffolds for Bone Tissue Engineering <i>Nareerat Thongtham, Suwimon Boonrungsiman and Orawan Suwanton</i>	154-159

Session/Code	Title / Speaker	page
BMED-P6	Synthesis and Characterization of Hydrogels Composed of Crosslinked poly(vinyl alcohol) and <i>Mesona Chinensis</i> Extract for Biomedical Use as Wound Dressings Chadaporn Srimai and Runglawan Somsunan	160-164
BMED-P8	Fabrication of High Magnification Microscope Lens using Confined Sessile Drop Technique Wisansaya Jaikandee, Sanong Ekgasit, Supeera Nootchanat, Parintorn Jangtawee, Porapak Suriya, Chutiparn Lertvachirapaiboon, Kazunari Shinbo, Keizo Kato and Akira Baba	165-169
IV. Session: Rubbers and Elastomers		
RUBB-O2	Development of Styrene Butadiene Rubber (SBR) Nanocomposites Reinforced with Polyethylene Glycol (PEG) Treated Nano Titanium Dioxide (TiO ₂) Kumarjyoti Roy and Pranut Potiyaraj	170-175
RUBB-O6	Influence of Free Fatty Acid in Eco-Friendly Oil on Physical Properties of Carbon Black-Filled Styrene Butadiene Rubber and Natural Rubber Blend Siwarote Boonrasri, Naruemon Thongkong and Pongdhorn Sae-Oui	176-181
RUBB-O8	Study the Effects of NCO Index on Mechanical Properties of Natural Rubber based Cationic Waterborne Polyurethane – New Approach to Water-Based Adhesive Applications Nathapong Sukhawipat, Nitinart Saetung, Anuwat Saetung, Jean-Francois Pilard and Sophie Bistac	182-187
RUBB-P1	Microphase Separation on Thermal/Dynamic Mechanical Properties of Olefin Block Copolymer-Thermoplastic Elastomers Orraithai Chamnan, Nanwarinparch Pucknansawhet and Chantima Deeprasertkul	188-191
RUBB-P2	Study of Porous Pipes made from GRT/NR/Reclaimed Rubber Reinforced with Waste Tire Fibers for Agricultural Applications Pattawee Pinitkul, Boonharn Ou-udomying and Ittipol Jangchud	192-196
RUBB-P3	Influence of Sulphur Crosslink Type on the Strain-induced Crystallization of Sulphur-Vulcanized Natural Rubbers by In-situ Synchrotron WAXD Watcharin Sainumsai, Shigeyuki Toki and Krisda Suchiva	197-204
RUBB-P4	Effect of Maturation and Compounding Latex on Properties of Nitrile Latex Gloves Siri Kirkmanee, Ittipol Jangchud, Suchet Khaenyook and Suparat Rukchonlatee	205-210
V. Session: Polymer Blends and Composites		
COMP-O1	Effects of Fiber Surface Modifications on Mechanical Properties of Pineapple Leaf Fiber – Acrylonitrile Butadiene Styrene (PALF-ABS) Composites Nanthaya Kengkhetkit, Tawechai Amornsakchai, Pornsawan Amornsakchai and Thanita Boonmee	211-217
COMP-O11	Effects of Type and Amount of Additives in Polypyrrole Composites on Metal Adsorption and Chemical Oxygen Demand Reduction Aopeau Invittaya, Neungrutai Saesaengseerung and Amornpon Changsuphan	218-222
COMP-P3	The Adsorption of Copper Ions onto Semi-interpenetrating Polymer Network Hydrogel Composed of HEMA and HEC Amlika Rungrod and Runglawan Somsunan	223-229
COMP-P4	Effect of Ethylene Ethyl Acrylate Copolymer on Mechanical Properties of Polymer Composite from Polypropylene Mixed with Barium Sulfate Nattharanet Treeraritchalerm and Suparat Rukchonlatee	230-235
COMP-P6	Modification of Natural filler filled-PLA with Ethylene Ethyl Acrylate Copolymer Nisakorn Watchara, Chonlada Ritvirulh and Suparat Rukchonlatee	236-242
COMP-P7	Effect of Foaming Agent on Natural Rubber Foam for Oil Spill Cleanup Siripak Songsaeng, Patchanita Thamyongkit and Sirilux Poompradub	243-248
COMP-P10	Process and Property Relationship of Pineapple Leaf Fiber/PHBV Composites Pongsathorn Chaleerat, Rapeephun Dangtungee, Suchart Siengchin	249-253
COMP-P12	Ag/PDMS Nanocomposite for Flexible Conductive Stripes Porapak Suriya, Supeera Nootchanat, Parintorn Jangtawee, Wisansaya Jaikandee, Chutiparn Lertvachirapaiboon, Akira Baba and Sanong Ekgasit	254-259

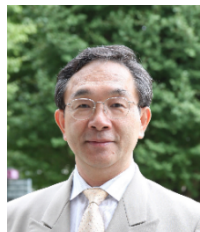
PLENARY AND KEYNOTE SPEAKERS



Effect of Mobile Polymer Chains at Cross-Link Points on Toughness

Jun Sawada and Toshikazu Takata

Department of Chemical Science and Engineering, Tokyo Institute of Technology
Ookayama, Meguro, Tokyo 152-8552, Japan
Phone +81 3 5734 2898, Fax +81 3 5734-2888, E-Mail: ttakata@polymer.titech.ac.jp



Present Professor, Department of Chemical Science and Engineering,
Tokyo Institute of Technology, Japan

Research Interests:

To develop novel molecules and materials with unique property and function in supramolecular chemistry based on organic and polymer chemistry.

Abstract

Elastomers having rotaxane structures at the cross-link points known as rotaxane cross-linked polymer (RCP) are characterized by the movable polymer chains at the cross-link points and show unique properties and functions that have never been achieved with any covalently cross-linked polymer (CCP).^[1-4] The movable polymer chain at the cross-link points makes possible an equalization of tension for external stimuli or stress to produce high swelling ability for solvents, high elasticity, and high stress-releasing ability. We have hitherto prepared various RCPs showing recyclable and stimuli-responsive nature.^[1-4] Herein, we would like to focus on the preparation of elastomers toughened by rotaxane cross-links using a few rotaxane cross-linkers having vinylic and nitrile *N*-oxide functions placed on both the wheel and axle components of their rotaxane structures.

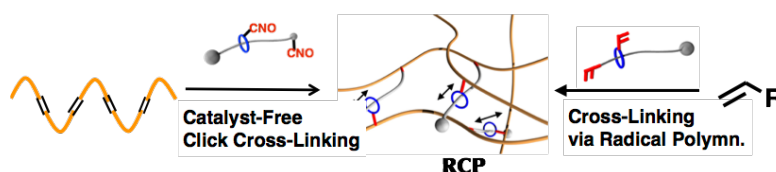


Figure 1. Synthesis of rotaxane-cross-linked polymers (left) by direct cross-linking of unsaturated bond-containing polymers with nitrile *N*-oxide-functionalized rotaxane cross-linker and (right) by cross-linking via radical copolymerization of vinyl monomers and vinyl group-functionalized rotaxane cross-linkers.

Direct cross-linking of unsaturated bond-containing polymers using a rotaxane cross-linker having two nitrile *N*-oxide groups on its wheel and axle components^[5-10] was carried out under catalyst-free and/or solvent-free conditions to afford the corresponding RCPs. Meanwhile, a similar rotaxane cross-linker possessing two vinyl groups in its axle and wheel components was added as a cross-linker into the radical polymerization systems of vinyl monomers such as butyl acrylate to obtain solvent-insoluble polymer as RCP_{BA} ^[11-13]. Mechanical property of RCP_{BA} was compared with covalently cross-linked polymers (CCP_{BA}) prepared from a mixture of BA and a typical covalent cross-linker. The observed big difference (Figure) suggests the excellent function of the rotaxane cross-linkers capable of endowing the cross-linked polymers with toughness. Effect of the mobility and/or mobile length of the rotaxane components on the toughening of cross-linked polymers will be mainly discussed.

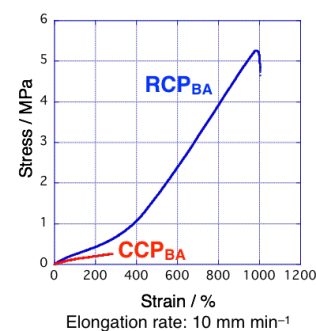


Figure 2. S-S Curve of RCP_{BA} and CCP_{BA}

Keywords: Toughened Elastomer, Rotaxane Cross-Link, Polymerization, Polymer Reaction

References:

- T. Takata *et al.* [1] *Angew. Chem. Int. Ed.*, **43**, 966 (2004). [2] *Macromolecules*, **41**, 8496 (2008). [3] *Angew. Chem. Int. Ed.*, **50**, 4872 (2011). [4] *Chem. Eur. J.*, **19**, 5917 (2013). [5] *ACS Macro Lett.*, **3**, 324 (2014). [6] *Angew. Chem. Int. Ed.*, **55**, 2778 (2016). [7] *ACS Macro Lett.*, **3**, 286 (2014). [8] *Polymer*, **54**, 4501 (2013). [9] *Chem. Commun.* **49**, 7723 (2013). [10] *Polym. Chem.*, **8**, 1445 (2017). [11] *ACS Macro Lett.*, **4**, 598 (2015). [12] *Polym. Chem.*, **8**, 1878 (2017). [13] *Macromol. Symp.*, **372**, 115 (2017).

Polymer-Based Additive Manufacturing: Emerging Trends

Chee Kai Chua

Singapore Centre for 3D Printing, School of Mechanical and Aerospace Engineering, Nanyang Technological University, Singapore 639798

Phone +65 6790 4897, Fax +65 6791 1859, E-Mail: mckchua@ntu.edu.sg



Present Professor, School of Mechanical and Aerospace Engineering, Nanyang Technological University, Singapore

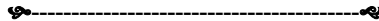
Research Interests:

Geometric Modelling, Rapid Prototyping, Additive Manufacturing, 3D Printing, Reverse Engineering, Biomedical Engineering Design, Tissue Engineering

Abstract

The evolution of polymer-based additive manufacturing (AM) is shaped by two driving forces: printability requirements from AM process and multi-dimensional requirements from application environment. An ideal polymer development is to fulfill both requirements concurrently with cost effectiveness. This requires a fundamental understanding of material-application relationship in AM as well as the role of polymer in AM. In general, polymer can be used in AM to make final parts or assemblies in all four engineering materials (polymer, composite, ceramic and metal). Recent developments have extended the dimensions of conventional prototypes such as number of materials and colour and have also propelled polymer-based AM from conventional prototyping into functional prototyping and small batch production across a variety of industries, including aerospace, medical, automotive, sportswear, consumer, etc. This plenary talk will present three groups of representative examples: industrial case studies, research literatures and projects conducted at Singapore Centre for 3D Printing (SC3DP). In particular, recent advances in multi-material printing, large format printing, high speed printing, composite printing, bioprinting and 4D printing, are highlighted as emerging trends in the future of polymer-based additive manufacturing.

Keywords: 3D printing, Additive manufacturing, Rapid prototyping, 4D printing, Composite



Molecular Structures and Long-Term Mechanical Properties of Virgin and Recycled Polyolefins : A Case Study Applied to the Water Pipe Systems

Guy Louarn¹ M. Alzerreca^{1,2}, D. Orditz² and O. Correc²

¹*Institut des Matériaux Jean Rouxel (IMN) ; CNRS-Université de Nantes, Nantes - France*

²*Centre Scientifique et Technique du Bâtiment (CSTB) Aquasim, Nantes -France*

Phone +33 240 683 112, E-Mail: guy.louarn@cnrs-imn.fr



Present Professor, University of Nantes, France

Research Interests:
Polymers and composites science

Abstract

According to a recent economic study, the European Union produces 49.9 million tons of plastics in 2017; polyethylene accounted for 29.8% (PE) and polypropylene (PP) for 19.3%^[1]. Polyolefins in particular constitute a significant percentage of household waste: 40 % of all polyolefin-derived products are considered to have a short service life; and 27% of plastics end up in landfills. Although polyolefin plastics can be mechanically recycled, regenerated, or incinerated, they do not decompose under natural conditions - a cause for considerable environmental concerns. Plastic manufacturers have begun to recycle their waste products in an attempt to address this problem. These waste products can be recycled internally or transferred to specialized plastic recyclers for further processing into reusable pellets. Similarly, the recycling of post-consumer plastics can offer an opportunity to reduce the amount of wasted plastic material and could save energy and raw materials for future generations.

For instance, water pipes and fittings are often polyolefins thermoplastics made, but nowadays, recycled materials, especially coming from post-consumer materials, are not used according to the standards^[2]. This recommendation is due to a lack of knowledge on these materials properties and their long-term mechanical behavior which does not guarantee a minimum service lifetime.

The present study compared virgin, reprocessed and recycled HDPE, provided by manufacturers of plastic. Mechanical testing (creep and fatigue) was used to assess the effects of degradation processes that can occur in the reprocessing of post-industrial (internally or externally reprocessed) and post-consumer (recycled) polymers. In addition, size-exclusion chromatography, ¹³C solid-state NMR, thermal analysis, oxidative induction time and melt flow index measurements were used to analyze the short-term and long-term evolution of the mechanical properties of these materials. Additionally, the presence of contaminants and/or catalytic residues in the recycled and regenerated HDPE was examined using X-ray fluorescence and energy dispersive X-ray spectroscopy. The gathered data were then used to explain the resistance and ability to withstand various types of imposed service conditions, and attempt to answer the question: are products made from post-consumer recycled polyolefins able to achieve the level of performance required by industry standards?

To illustrate the topic, a case study will be presented on virgin and recycled HDPE used in gravity sewer systems^[3].

Keywords: Polyethylene, Post-consumer, Lifetime, Creep, Fatigue

References:

- [1] Plastics : the Facts 2017. An analysis of European plastics production, demand and waste data, Plastics Europe (2017)
- [2] AFNOR, Plastics piping systems for non-pressure underground drainage and sewerage - Structured-wall piping systems NF EN 13476.
- [3] M. Alzerreca et al., Mechanical properties and molecular structures of virgin and recycled HDPE polymers used in gravity sewer systems, polymer testing 46 (2015) 1-8



Recent Advances in Rubber Reinforcing and Functional Applications of Rubber Elasticity

Changwoon Nah^{1*} and Wonseok Wang¹

¹BK21 Plus Haptic Polymer Composite Research Team, Department of Polymer-Nano Science and Technology, Chonbuk National University, Jeonju 54896, Republic of Korea
Phone +82 63 270 4281, Fax +82 63 270 2341, *E-Mail: cnah@jbnu.ac.kr



Present Professor, Department of Polymer-Nano Science and Technology, Chonbuk National University, Republic of Korea

Research Interests:

Functional rubbers including dielectric elastomer actuators or generators, stretchable electrode system and sensors and reinforcing mechanism of elastomeric polymers by various nanofillers

Abstract

The application of carbon blacks (CBs) is found to be very fascinating, since it can improve the mechanical properties of rubbers such as; modulus, strength (tensile, tear, and fatigue), and wear resistance. The mechanism of the reinforcement by CBs is largely explained by three factors: 1) hydrodynamic volume of CB, 2) rubber-CB interactions, and 3) interactions among CB particles. Recently, a generalized concept of CB reinforcement has been proposed by Fukahori considering a two-layer bound rubber model^[1], though the theory is still under discussion amongst rubber scientists.

To develop rubber composites with specific functionalities, various kinds of nano-sized fillers have been reinforced in rubber matrices in our laboratory and based on their properties, the mechanism of reinforcement of carbon nanotube (CNT) has been proposed^[2], which is significantly different than CBs reinforcement, though both carbon black and carbon nanotubes are basically made of same carbonaceous materials. The most striking feature that made CNT reinforcement different than CBs is a weak interaction (lower amount of bound rubber formation and even a slipping under compression) between rubbers and CNTs. The high modulus and strength of CNT reinforced composites is thus attributed to the large aspect ratio of CNTs that helped in overcoming the disadvantage of poor adhesion with rubber matrices. We have also been able to notice an unusual fracture morphology^[3] in prepared rubber compounds reinforced with organo-modified layered clays of platelet shape and surprisingly shown different morphology than the typical 'cross-hatched' morphology shown by CB-filled rubber compounds. Similarly, the reinforcing behavior of some other nanofillers will also be discussed in this presentation.

Since rubbers have been used for long time due to their unique elasticity suitable for various applications such as tires, belts, mounts, and seals, and where the extremely harsh conditions are required, hence no other polymers can accomplish the role of rubbers. Recently, elastic function of rubbers has attracted a great attention for various applications including stretchable displays, dielectric elastomer actuators, sensors, generator and seals for fuel cell vehicles; hence this presentation will cover various applications and issues in the light of recent developments in functional rubber composites. The applications of rubber elasticity in fabrication of bubble shaped actuator^[4], liquid lens^[5], disk-shape rubber generator^[6], and stretchable electrodes based on wrinkled rubbers (Figure 1)^[7] would also be covered to explain the importance of rubber composites.

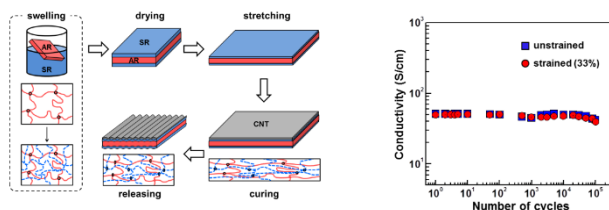


Figure 1. Stretchable electrode system based on wrinkles: (Left) Preparation procedure and (Right) Conductivity of the system under dynamic strain of 33%.^[7]

Keywords: Rubber, Reinforcing, Elasticity, Nano-sized fillers

References:

- [1] Y. Fukahori, Rubber Chem. Technol., 80 (4), 701 (2007).
- [2] C. Nah, J. Y. Lim, R. Sengupta, B. H. Cho, A. N. Gent, Polym. Int., 60, 42 (2011).
- [3] C. Nah, H. J. Ryu, S. H. Han, J. M. Rhee, M.-H. Lee, Polym. Int., 50, 1265 (2001).
- [4] L. Ren, R. H. Lee, H. R. Park, H. Ren, C. Nah, I. -S. Yoo, J. Microelectromech. Syst., 22, 1057 (2013).
- [5] B. Jin, J. -H. Lee, Z. Zhou, G. Zhang, G.-B. Lee, H. Ren, and C. Nah, Opt. Eng., 55, 017107 (2016).
- [6] R. H. Lee, U. Basuli, M.-Y. Lyu, E. S. Kim, C. Nah, J. Appl. Polym. Sci., 131, 40076 (2014).
- [7] G. -B. Lee, S. G. Sathi, D. -Y. Kim, K. -U. Jeong, and C. Nah, Polym. Test., 53, 329 (2016).

Degradation Control of Polysaccharides and the Biomedical Applications

Kazuaki Matsumura^{1*} and Wichchulada Chimpibul², Punnida Nonsuwan,^{1,2}

¹Japan Advanced Institute of Science and Technology, Nomi, 923-1292, Japan

²Chulalongkorn University, Bangkok 10330

Phone +81 761 51 1680, Fax +81 761 51 1149, *E-Mail: mkazuaki@jaist.ac.jp



Present Associate Professor, Japan Advanced Institute of Science and Technology, Japan

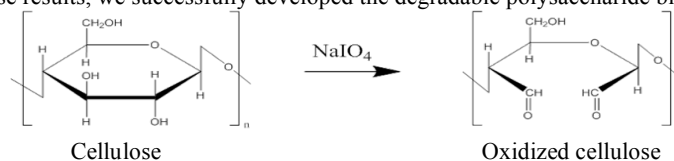
Award 2014 Young Scientist Award of the Japanese Society for Cryobiology and Cryotechnology

Research Interests:
Functional polymeric biomaterials

Abstract

The evolution of the field of tissue engineering goes in parallel with the coherent demand for new scaffolding materials with definite properties such as controlled porosity and pore size distribution, biocompatibility and biodegradation. Among these materials, natural polymers predispose especially interest because of their biocompatibility, biodegradation, and exuberance. Polysaccharides are natural polymers that include cellulose, chitin, dextran, starch and so on. We found that aldehyde introduced dextran via Malaprade oxidation can be degraded at the glycoside bonds through the reaction with amino groups. By using this phenomenon, a novel biodegradable adhesive hydrogel consisting of dextran and epsilon-poly(L-lysine) (dextran-PL) with multiple biomedical applications was developed [1,2]. Periodate oxidation in aqueous media almost stoichiometrically introduces aldehyde groups in dextran molecules, and aldehyde dextran can react with the primary amino groups in PL at neutral pH to form a hydrogel. The gelation time of the hydrogel can be easily controlled by the extent of oxidation in dextran. The degradation of dextran-PL hydrogel in PBS was easily controlled by the extent of oxidation in dextran. Here we propose novel main chain scission mechanism of oxidized dextran triggered by reaction with amine using GPC and ¹H- and ¹³C-NMR and elucidated the molecular mechanism of degradation during the reaction with amine (Fig.1) [3]. And we utilized this mechanism to invest cellulose with biodegradation for the development of degradable cell scaffolds for tissue engineering application.

Oxidizing cellulose scaffold to dialdehyde cellulose by sodium periodate (NaIO₄) was carried out (Scheme 1). The cellulose scaffold which was prepared by using 1-butyl-3-methylimidazolium chloride as a solvent, was oxidized using periodate oxidation, which oxidizes carbohydrate by glycol cleavage to provide dialdehyde. Aldehyde groups introduced into cellulose were quantified by simple iodometry. Oxidized cellulose scaffold was degraded in the amino acid solution triggered by the reaction between aldehyde groups and amino groups. During immersion of the cellulose scaffolds in the amino acid solution, the mass loss of the scaffolds was evaluated by measuring of weight of oxidized cellulose scaffold before and after degradation. From these results, we successfully developed the degradable polysaccharide biomedical devices.



Scheme 1. Aldehyde introduction by Malaprade oxidation of cellulose

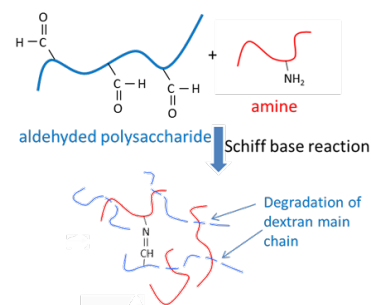
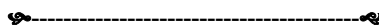


Fig.1 Schematic illustration of degradation of oxidized polysaccharide via Schiff base reaction

Keywords: Biodegradation, Polysaccharides, Tissue engineering, Scaffolds

References:

- [1] Matsumura K, Nakajima N, Sugai H, Hyon SH, Self-degradation of tissue adhesive based on oxidized dextran and poly-L-lysine, Carbohydr Polym, 113, 32-38, (2014)
- [2] Hyon SH, Nakajima N, Sugai H, Matsumura K, Low cytotoxic tissue adhesive based on oxidized dextran and epsilonpoly-L-lysine, J Biomed Mater Res A, 102A, 2511-2520, (2014)
- [3] Chimpibul W, Nagashima T, Hayashi F, Nakajima N, Hyon SH, Matsumura K. Dextran Oxidized by a Malaprade Reaction Shows Main Chain Scission Through a Maillard Reaction Triggered by Schiff Base Formation Between Aldehydes and Amines. J Polym Sci Part A. Polym Chem, 54, 2254-2260, (2016)



Iodine Transfer Polymerization: Some Applications in Polymer Colloids

Amorn Chaiyasat^{1,2}

¹*Department of Chemistry, Faculty of Science and Technology, Rajamangala University of Technology Thanyaburi, Thanyaburi, Pathumthani, 12110, Thailand*

²*Advanced Materials Design and Development (AMDD) Research Unit, Faculty of Science and Technology, Rajamangala University of Technology Thanyaburi, Thanyaburi, Pathumthani, 12110, Thailand*



Present Assistant Professor, Department of Chemistry, Faculty of Science and Technology, Rajamangala University of Technology Thanyaburi, Thailand

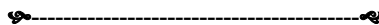
Research Interests:

Conventional and controlled/living radical polymerization in aqueous dispersed systems, Micro- and Nanoencapsulations, Functional Polymers

Abstract

Several techniques of controlled/living radical polymerization (CLRP) have been studied in order to synthesize the polymer having narrow molecular weight distribution and design of macromolecular architecture such as block and graft copolymers. Many techniques of CLRPs have successfully applied to aqueous dispersed systems such as nitroxide-mediated polymerization, atom transfer radical polymerization, reversible addition fragmentation chain transfer and organotellurium-mediated living radical polymerization. The iodine transfer polymerization (ITP) is one of the most popular CLRP techniques because it contains many advantages such as low-cost, environmental friendly reagent and without the utilization of heavy metal compounds. To the best of my knowledge, there are a few researches using ITP in aqueous dispersed systems. Some examples of ITP applied in aqueous dispersed systems will be presented as a follow. The stable polymer particle with submicrometer-sized was successfully prepared by ITP in an emulsifier-free emulsion polymerization (emulsion ITP) based on the self-assembly nucleation. High performance synthesis of microcapsules encapsulating various core materials such as heat storage materials, fragrance and metal oxides was also carried out by ITP in microsuspension polymerization (*ms* ITP). In addition, ITP was also used to synthesize polyacrylic acid (PAA) containing hydroxyl group prior to ring-opening polymerization of poly (L-lactide) (PLLA) to prepare a novel PAA-*b*-PLLA pH-responsive polymeric micelles for use in drug delivery systems.

Keywords: Iodine transfer polymerization, Emulsion ITP, *ms* ITP, Polymeric micelles



Facile and Rational Modulation of Ubiquitous Plant Polyphenols: Novel Multifunctional Coating Precursors from Nature

Masanobu Naito

Research and Services Division of Materials Data and Integrated System (MaDIS), National Institute for Materials Science (NIMS), 1-2-1 Sengen, Tsukuba, Ibaraki, Japan 305-0047
Phone +81 29-860-4783, E-Mail: NAITO.Masanobu@nims.go.jp



Present Group Leader, Data-driven Polymer Design Group, Research and Services Division of Materials Data and Integrated System, Japan Assoc. Professor, The university of Tokyo and Tsukuba university, Japan

Research Interests:

Surface chemistry, adhesive, coating materials, and the development of environmentally benign antifouling polymer materials.

Abstract

Naturally abundant building blocks such as DNA, protein, polysaccharide, chitin, and others have been extensively studied from both fundamental perspective and wide range practical applications for decades. Many advantages including inexpensive, wide availability, multiple functional groups along with their unique intrinsic properties make these precursors useful for various chemical/physical manipulations. For instance, hydrosoluble biopolymers have been wisely modified by simple incorporation of hydrophobic moieties, which exhibit exotic phenomena, such as formation of micelle, hydrogel and liquid crystal, with pertinent biocompatible medical, biological, and optical applications. On the other hand, hydrosoluble plant polyphenols like catechin, tannic acid (TA) are another class of important natural raw materials found in variety of plant parts and well-known for antioxidant, antimicrobial, and other activities. Despite such ready availability and diverse scope of manipulation, chemical modifications like hydrophobization of plant polyphenols have rarely been carried out and major studies have been pursued only in aqueous media.

Recently, we developed a facile chemical modification approach to modify water-soluble tannic acid (TA) to partially *n*-alkyl (C_6 , C_{10} , or C_{16}) substituted TA (PATA). Interestingly, our simple strategy enables wide range solubility of TA in organic media with broad polarity range such as *n*-hexane, chloroform, diethyl ether, ethyl acetate and others. Consequently, (ultra)thin film of PATAs was effortlessly fabricated on various metal/alloy and glass substrates. Several studies have revealed that thin-film of PATAs are highly efficient as anticorrosion, contact based antibacterial and adhesive coatings on various substrates.

Keywords: Polyphenol, Antibacterial, Tannic acid

References:

- [1] H. Ejima, J. J. Richardson, K. Liang, J. P. Best, M. P. Koevenden, G. K. Such, J. Cui and F. Caruso, *Science*, 2013, **341**, 154.
- [2] T. S. Sileika, D. G. Barrett, R. Zhang, K. H. A. Lau and P. B. Messersmith, *Angew. Chem. Int. Ed.*, 2013, **52**, 10766.
- [3] D. Payra, M. Naito, Y. Fujii and Y. Nagao, *Chem. Commun.* 2015, DOI: 10.1039/c5cc07090b.

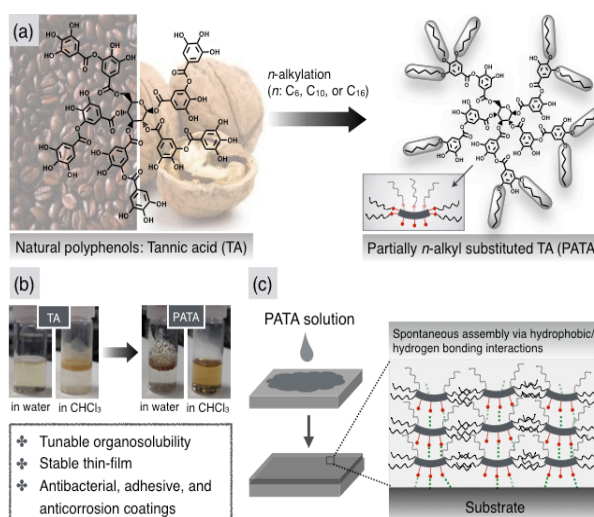
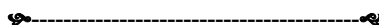


Figure (a) Chemical structure of tannic acid (TA) and some natural sources in the background. Facile chemical modification via *n*-alkylation of TA to a novel organosoluble PATA. (b) Comparison of solubility between TA & PATA in water/organic media. (c) Self-assembly of PATA on solid surfaces to a stable and multifunctional thin-film.



Cellulose; Fascinating Biopolymer for Biomedical toward Energy Applications

Hathaikarn Manuspiya^{1,2}

¹*Petroleum and Petrochemical College, Chulalongkorn University, Bangkok, TH 10330*

²*Center of Excellence on Petrochemical and Materials Technology, Bangkok, TH 10330*



Present Deputy Director, Center of Excellence on Petrochemical and Materials Technology
Associate Professor of the Petroleum and Petrochemical College, Chulalongkorn University, Thailand

Research Interests:

Electronic and optoelectronic materials and devices, Ferroelectric oxides, Low loss and tunable microwave materials, Nanostructure science and technology, Polymer Blends and Polymer nanocomposites.

Abstract

The current widespread interest in nanotechnology and nanomaterials promoted the growth of research in cellulosic nanomaterials. Cellulose is one of the most plentiful biopolymers on Earth, representing about 1.5 trillion tons of the total annual biomass production. Cellulose can be abundantly obtained from plant-based materials such as cotton, wood, and hemp. Cellulose can also be synthesized from algae, tunicates and some bacteria. Bacterial cellulose (BC) is a purified form of cellulose that is free of lignin and hemicellulose. The BC can be produced by several types of bacterial species that mainly belong to the genus *Acetobacter*. The BC has microfibrils that are arranged in a 3D web-shaped structure, providing a porous geometry and high mechanical strength. Compared to plant cellulose, the BC has considerably higher crystallinity (80–90%), water absorption capacity, and degree of polymerization (up to 8000). The preparation of BC offers an opportunity to provide control of the products' properties in-situ, via specific BC production methods and culture conditions. There is a growing body of work on the production of BCs and bacterial cellulose nanocrystals (BCNCs) from BC fibers. This review describes developments in BC and BCNCs production methods and factors affecting their yield and physical characteristics. The BC, alone or in combination with different components (e.g., biopolymers and nanoparticles), can be used for a wide range of applications, such as medical products, electrical devices, sensor packaging and food ingredients.

The latest use of BC in the electronic, food, and biomedical fields is discussed with its applications in composite will be reviewed. Oxidation/sulfonation reaction and plasma surface treatment of BC extracted from sugar cane bagasse can be modified to sulfonated cellulose with high hydrophilicity, biocompatibility, and surface area which improved thermal properties, wettability, and air permeability. The modified BC is then combined with biodegradable polymers, i.e. Poly(lactic)/Poly(butylene succinate) (PLA/PBS) blends, to produce green separator membranes in *Li-ion batteries*. On the other hand, acid hydrolysis of BC under controlled conditions would produce BCNCs with specific characteristics, i.e. morphology, particle size, surface charge, crystallinity, crystallite size, and thermal stability; hence, the resulting BCNCs will have different characteristics which are useful in various applications. For *sensory applications*, BCNCs can be modified with metallic nanoparticles, i.e. silver nanoparticles (AgNPs) and alginate-molybdenum trioxide nanoparticles (MoO₃NPs). The BCNCs hybrid metallic nanocomposites were developed for hydrogen sulfide (H₂S) gas optical sensor in food packaging applications where the MoO₃NPs were used as the metal oxide source that are readily reduced to a colored sub-oxide by atomic hydrogen produced H₂S gas, and AgNPs were used as the H₂S reactive metal. For *biomedical applications*, BCNCs with suitable properties can be selected for further cationic surface modification by the physical adsorption with amines and amine-containing polymers such as methacrylamide to form complexation with siRNA. The resulting complexation would potentially be used in gene delivery nanocarriers.



Biomedical Application of Chitin and Chitosan

Hiroshi Tamura* and Tetsuya Furuike

*Faculty of Chemistry, Materials and Bioengineering, Kansai University, Osaka 564-8680
Phone +81 6 63680871, Fax +81 6 6330 3770, *Email: Tamura@kansai-u.ac.jp*



Present Professor, Department of Chemistry and Materials Engineering,
Faculty of Chemistry, Materials and Bioengineering, Kansai
University, Japan

Research Interests:

Natural occurring polymer, Polysaccharide chemistry especially chitin/chitosan, Gelatin

Abstract

Chitin, the second abundant natural polysaccharide on earth, has been studied to clarify its biological functions including biodegradability and low toxicity in animal body. Chitin is also known to have a couple of crystalline structure dependent on the function in animal body. The outer skeletal chitin consisted of α -chitin and squid pen is consisted of β -chitin. α -Chitin has been proposed to form much tighter crystalline structure than that of β -chitin. According to finding of mild solvent for chitin, calcium chloride saturated methanol, α - and β -chitin molecule has been suggested to become loose coil structure in solution due to the destruction of rigid hydrogen bonds^[1]. The hydration of α -chitin molecule was achieved by the addition of large excess of water to chitin solution. The smooth chitin hydrogel was prepared by the removal of calcium ion and methanol through extensive dialysis against water. β -Chitin has been found to become hydrogel following the vigorous mechanical agitation of chitin powder in water without any chemicals, whereas α -chitin was hardly prepared the hydrogel by similar process. On the other hand, chitosan, a deacetylated product of chitin, dissolves into water by the formation of salt with organic acids such as formic acid, acetic acid, ascorbic acid and etc., because CS is cationic polymer, which has amino group ($-\text{NH}_2$) consisting of glucosamine units and has a pKa value of about 6.5. In addition, CS is used as a prominent biomaterial, because it has a lot of properties such as antibacterial activity, biocompatibility, biodegradability and wound healing ability^[2,3]. However, it is hard to maintain its molecular weight constant for long standing at room temperature. Chitosan hydro-gel was also prepared from the organic acid solution. Neutralization of the solution gave the chitosan hydro-gel, which is stable in wet state for long period. Resulted chitosan hydro-gel dissolves quickly by the addition of minimum amount of acids such as hydrochloric acid, acetic acid and so on^[4]. Chitin and chitosan are little digestible in human intestine system due to β -1,4 glycoside linkage of chitin and chitosan. Chitin is also known to accelerate the recovery of epidermal cells on wound healing^[5]. Chitosan accelerates the formation of Fibroblast in animal body^[6]. Based on these findings, chitin and chitosan were used as main component for several scaffolds, coating component of fiber and membrane for biomedical purpose. The examples are reported.

Keywords: Chitin, Chitosan, Hydrogel, Polysaccharide

References

- [1] H. Tamura, H. Nagahama, S. Tokura, *Cellulose*, 13 (4), 357-364 (2006).
- [2] A. Anitha, V.V. D. Rani, R. Krishna, V. Sreeja, N. Selvamurugan, S. V. Nair, H. Tamura, R. Jayakumar, *Carbohydrate Polymers*, 78 (4), 672-677 (2009).
- [3] R. Jayakumar, M. Prabakaran, P. T. S. Kumar S. V. Nair, H. Tamura, *Biotechnology advances*, 29 (3), 322-337 (2011).
- [4] H. Tamura, K. Wada, R. Rujiravanit, S. Tokura, *J. Metals, Materials and Minerals*, 15, 19-21 (2005).
- [5] J. F. Prudden, G. Nishihara, *Gynecology & Obstetrics*, 115, 283 (1957).
- [6] S. Minami, Y. Okamoto, A. Matsuhashi, Y. Shigemasa, T. Tanigawa, Y. Tanaka and S. Tokura, "Chitin derivative in life science" Eds. by S. Tokura and I. Azuma, Japan Soc. Chitin/Chitosan Press. 1992, pp68.



Stimuli-responsive Polymeric Materials for Medical Diagnostics and Cell Labelling

Jaruwan Joothamongkon, Raweewan Thiramanas, Udom Asawapirom, Kulachart Jangpatarapongsa, Pramuan Tangboriboonrat and **Duangporn Polpanich***

NANOTEC, National Science and Technology Development Agency, PathumThani 12120

*Phone +66 2117 6700, Fax +66 2564 6985, *E-mail: duangporn@nanotec.or.th*



Present Senior Researcher at FNI Laboratory, NANOTEC, NSTDA Thailand

Research Interests:

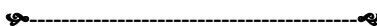
Polymer colloids and capsules for biomedical applications, Surface functionalization, Biomaterials, Biosensors

Abstract

Stimuli-responsive substances, which are able to alter their properties in response to environmental change, represent one of the most exciting prospects in current nanotechnology. Their combination with polymeric materials presents a wide range of possibilities in design of a novel materials for using in biomedical applications. In this present work, encapsulation of magnetic (Fe_3O_4) and light (near infrared dye) responsive substances into polymer matrix for applying in medical diagnostics and cell labelling has been focused. For medical diagnostics application, the idea involved in the use of dual behaviors of Fe_3O_4 encapsulated in polysaccharide including magnetic separator and catalytic activity to develop a novel technique named magneto-polymerase chain reaction-colorimetry (magneto-PCR-colorimetry) for detection of *Vibrio cholera*. This bacterium is responsible for the world pandemics of cholera, a life-threatening diarrhea disease. In which, PCR product was directly amplified on the surface of forward primer modified MPNP and then easily concentrated by a magnet. By employing the catalytic activity of MPNP under optimized conditions, the analysis of PCR product bound MPNP yielded a high sensitivity (10^3 cfu/mL) and specificity in buffer system within 4 h. The proposed technique was more simple and rapid compared to the PCR-ELISA and safer compared to the PCR-gel electrophoresis. It would be potentially adapted to identify other pathogenic bacteria.

In addition, we synthesized poly(ϵ -caprolactone) (PCL) nanoparticles encapsulated with near infrared (NIR) conjugated polymer dye *via* emulsion-diffusion method. Among various surfactants, the synthesized nanoparticles using Kolliphor® P188 showed the highest fluorescent intensity. Effect of the quantity of dye loading on size and optical properties of nanoparticles was studied. Using NIR spectroscopy, the nanoparticles exhibited the fluorescence emission at 921 nm with a large Stokes shift of 276 nm in aqueous solution. The synthesized NIR polymeric nanoparticles have great potential as fluorescent label for future biomedical applications.

Keywords: Magnetic nanoparticles, Near infrared dye, Polymer, Encapsulation



Characterization of Vulcanized Natural Rubber through Rubber State NMR Spectroscopy

Seiichi Kawahara

*Department of Materials Science and Technology, Faculty of Engineering,
Nagaoka University of Technology, Nagaoka, Niigata 940-2188, Japan*



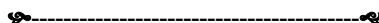
Present Professor, Department of Materials Science and Technology, Faculty of Engineering, Nagaoka University of Technology, Nagaoka, Niigata 940-2188, Japan

Awards:
2014 Sparks-Thomas Award, Rubber Division, American Chemical Society

Research Interests:
Polymer/Textile materials, Polymer chemistry

Abstract

Rubber state NMR spectroscopy was applied to investigate structure of crosslinking junctions of crosslinked natural rubber and crosslinked chloroprene rubber. The crosslinked rubbers were prepared with sulfur and various accelerators in the presence of ZnO and stearic acid. The NMR measurements were performed by field gradient magic angle spinning solid state NMR spectroscopy. Intensities of small signals in ^1H -NMR spectra and ^{13}C -NMR spectra were related to crosslink density of the crosslinked rubbers. Outstanding mechanical properties were investigated in terms of not only crosslink density but also intensities of the signals.



Natural Fibre Composites: Malaysian Perspective

Salit Mohd Sapuan

Department of Mechanical and Manufacturing Engineering, Universiti Putra Malaysia, 43400 UPM Serdang, Selangor, Malaysia

Phone +60193863191, Fax +603 86567122, E-Mail: sapuan@upm.edu.my



Present Professor of composite materials, Department of Mechanical and Manufacturing Engineering, Universiti Putra Malaysia (UPM), Malaysia

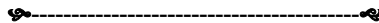
Research Interests:

Natural fibre composites, Materials selection for composites, Design for manufacture and design for sustainability.

Abstract

The objectives of this presentation are to review recent work and highlight some research findings related to development and characterization of natural reinforced polymer composites performed in Malaysia. Important results of the development and characterization are discussed, taking into account of different types of natural fibres as reinforcements in polymer composites with different types of polymer matrices either from synthetic polymers or plant based sources. Design for manufacture and design for sustainability in product development from natural fibre composites are introduced and discussed. Total design approach of natural fibre composite product development was performed emphasizing on the conceptual design and materials selection of such materials. In Malaysia, natural fibres typically used as reinforcements in polymer composites include kenaf, oil palm, pineapple leaf, sugar palm and rice husk fibres, used either in the woven, unidirectional, random chopped, particulate form or even in the form of nanocellulose. For the biopolymers, plant based starches were used to produce biopolymer matrices from sugar palm, cassava, sago and corn after adding suitable plasticizers such as glycerol and sorbitol. The natural fibre composites were used to develop different types engineering products such as safety helmets, furnitures, food packaging and rescue boats. In conclusions, natural fibre composites are potential candidate materials for engineering products due to some advantages that they offer such as light weight, low cost, environmentally friendly, comparable specific strength and stiffness properties to glass fibre composites, corrosion resistance, abundantly available and renewable.

Keywords: Natural fibres, Biocomposites, Mechanical properties



Natural Fiber Composite Materials: A Holistic Approach to Value Creation

Jittiporn Kruenate

PPT Global Chemical Public Company Limited, 59 Ratniyom Rd., Noenphra, Mueng Rayong 21150 Thailand
Phone +66(0)3899-4670, E-Mail: jittiporn.k@pttgcgroup.com



Present Vice President, Science and Innovation Center; Corporate Innovation;
PTTGC; Thailand

Research interest:

NFC materials, Creating values of renewable resources toward NFC materials

Abstract

Since last decade, the interest in NFC materials has been rapidly growing due to the advantages of these NFC materials with regard to their sustainability and value creation. In order to be perceived as emerging sustainable composite materials, the mechanical performance and economic efficiency of the NFC materials need to be accomplished. PTTGC, one of the leading chemical companies in Asia, has a very strong direction to focus on the sustainability outlook. Creating values of renewable resources toward NFC materials is a very challenging task. The objective of this presentation is to provide an overview perspective of value creation of NFC products.



Polymer Composites Reinforced by Carbon Nanotubes and Carbon Fibres

Kheng Lim Goh

*School of Mechanical & Systems Engineering, Newcastle University in Singapore, Singapore. 567739
Phone +65 97578847, E-Mail: kheng-lim.goh@ncl.ac.uk*



Present Associate Professor, School of Mechanical & Systems Engineering,
Newcastle University in Singapore, Singapore

Research interest:

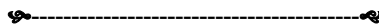
Investigation of the fundamentals of fibre and particle reinforced composites, Repair of connective tissues, Synthesis and characterisation of polymer- and biopolymer-based composites reinforced by nanoparticles

Abstract

This talk is intended to connect the current understandings of fundamental findings of polymer composites reinforced by carbon nanotubes and carbon fibres to industry applications. The fundamental understandings will address the interaction of carbon nanotubes/fibres with polymer matrix (that implicate the structure-function relationship). The industry applications will highlight current findings of the structural monitoring of the performance of these polymer composites and mechanical damage, as used in aviation, a mission critical area.

Recently, interest in reinforcing polymer composites by carbon nanotubes (CNTs) for mission critical engineering applications, such as aviation, has increased. This comes on the back of increased deployment of composite laminates made from polymer composites reinforced by long carbon fibres in many parts of the aircraft, mainly the fuselage, and new findings of how CNT can be dispersed uniformly and aligned along the fibre-matrix interface to enhance the interfacial toughness. CNTs can be physically bond with polymeric matrix. However, at the lengthscale of CNT, modeling the elasticity and failure behavior of CNTs and the local environment of the CNT, and how the underlying mechanics affect the overall composite material becomes a complex task. Current approach addresses multi-scale modeling strategies involving multiple spatial and temporal scales in hierarchical or concurrent manner. Here I shall offer an insight into various multiscale modeling techniques in studying the mechanical response of CNTs, such as continuum approach, quasi-continuum approach and molecular dynamics simulation, and how these approaches are integrated with analytical and numerical micromechanics models to predict the average macroscopic properties of the polymer composite. For the purpose of this talk, the focus is on composites made up of carbon fiber-reinforced polymers (CFRPs), which are now well-known in industries such as aviation and marine, and more recently in automotive (e.g. Mercedes-Benz SLR McLaren, BMW i8). Although the CFRPs can be made to high specific strength and stiffness, they are also susceptible to damage by projectiles. Damage occurs when the project impacts at a direction perpendicular to the plane of the laminate. While most damaged structures may be repaired using methods such as scarf/bonding and resin-injection, the demand in mission critical areas, such as aviation, then requires robust structural health monitoring (SHM) of the the composite structures, especially after repair. Traditionally, the SHM involves non-destructive testing methods which are performed off-line. Recently, there are studies to integrate structural health monitoring (SHM) systems within composite structures. One such method is the introduction of CNTs in CFRP. While CNT is known for its capability for reinforcing a material, it is less known for its damage sensing capability. Here I shall review some of our understandings on the use of CNTs in FRPs for SHM as well as discuss the gaps in the results obtained in the laboratory and industrial applications.

Keywords: Polymer composites, Carbon nanotubes, Carbon fibres



Global Trends in Polymer Industry

Pradip Kumar Dubey, Amit Dixit and Sirirat Changmongkol

Aditya Birla Chemicals (Thailand) Limited (Epoxy Division), Rayong-Thailand 21150
Phone: +66 38 683 981 / 685 233, Website: www.epotec.info



Present SBU Head of the Global Epoxy Business for Aditya Birla Chemicals, Thailand

Research Interests:

Development of polymer composite products

Abstract

The global polymer industry is projected to grow at CAGR of 3.9% over the next 5 years. The polymer industry segmented based on the type of polymers; thermoplastics, thermosets and elastomers, and further by applications has been experiencing increase in demand driven by growth in end use markets, such as packaging, automotive, infrastructure, transportation and telecommunication mainly from emerging economies of developing nations. Polymer is continuously substituting metals, glass, paper, and other traditional materials in various applications due to lightweight, high strength-weight ratio, design flexibility and cost economics. In addition polymeric materials are increasingly being considered as alternatives to support the global drive towards sustainability. While many established markets in the world are relatively mature, the industry continues to show strong growth. It is notable that there are significant opportunities in a number of developing world regions where the pace of growth is accelerating on the back of economic expansion and rising incomes. Further the growth is also being driven by the ongoing process of innovation and performance advances for a wide variety of polymers and compounds combined with the growing sophistication in the manufacturing technology for plastic products. In this paper, the global macroeconomic and industry trends covering the external forces shaping the industry are discussed which is followed by detailed analysis of the emerging trends and growth opportunities in the polymer industry.

Keywords: Polymers, Thermoplastics, Thermosets, Elastomers, Trends



Mega Trends in Packaging and Properties and Applications of Innovative Packaging

Resins – Ionomers

Thai Hwee Tatz

Dow Singapore Development Center



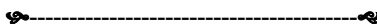
Present Senior Research Scientist for Packaging and Specialty Plastics at Dow
Singapore Development Centre

Research Interests:

Innovative packaging structure design and 100% recyclable packaging film structures to support the sustainable initiatives of the food industry

Abstract

The presentation will cover the global trends in food packaging, basic chemistry of a family of innovative packaging resins - Surlyn ionomers. Surlyn ionomers have many unique properties such as high hot tack, abrasion resistance, stiffness, easy tear, thermoformability, retard microbial growth, burst peel behaviour and easy peel from glass and ceramic. Based on these unique properties, applications such as vacuum skin packaging for meat and seafood, burst peel for cereal packaging, self-venting for microwave re-heating and cooking of food, lock and peel frangible pouch, easy tear condom packaging, high speed packaging of snack and thermoforming easy tear and peel medical pouch were developed.



NMR Application for Polymers

Teh Chin Hoe

Product Specialist (NMR) Bruker (Malaysia)
Phone: 019 7960988, E-Mail: Chin_Hoe.Teh@bruker.com



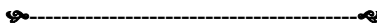
Present Product Specialist (NMR) Bruker (Malaysia)

Research Interests:

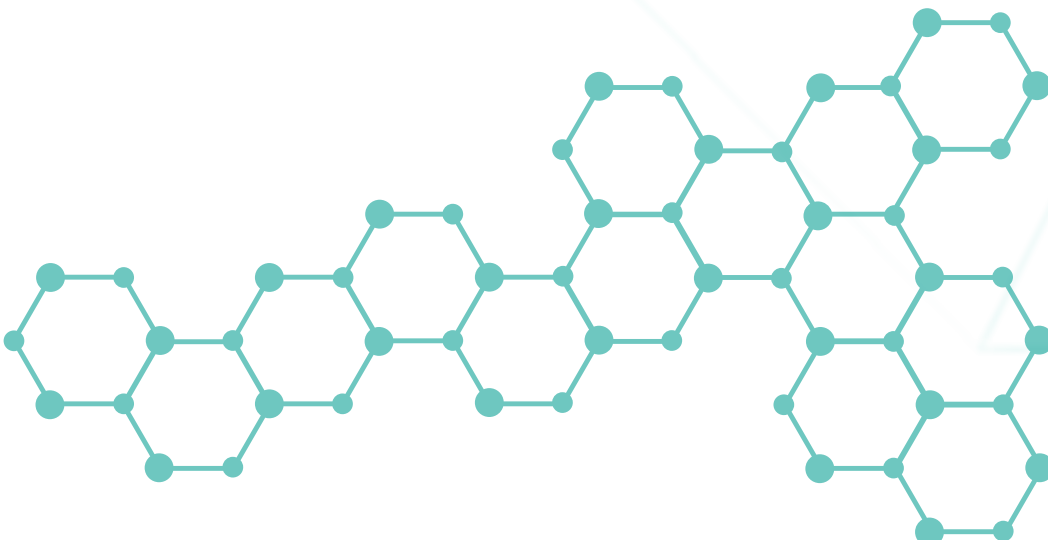
High resolution NMR spectroscopy

Abstract

High resolution NMR spectroscopy has proved to be the most powerful method available for characterizing the structures of polymers. The chemical shift, not only can reveal the structural information of the polymers but also its electronic structures. Therefore, polymers with cis- or trans- isomers and polymers which demonstrate different tacticities (isotactic, syndiotactic, and atactic) can be easily detected in the spectra. In addition, area of NMR signal, commonly referred as integral, provide the quantitative insight to the polymers which can be subsequently used in determining the polymer compositions.



RISING STAR



Overview of Thermoplastic Elastomers Research and Product Development

Anoma Thitithammawong

Department of Rubber Technology and Polymer Science, Faculty of Science and Technology, Prince of Songkla University, Pattani Thailand 94000

**E-Mail: anoma.t@psu.ac.th*



Present Assistant professor, Department of Rubber Technology and Polymer Science, Faculty of Science and Technology, Prince of Songkla University

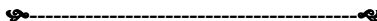
Research Interests:

Polymer blend and thermoplastic elastomer, Modification of natural rubber and Its application, Photosensitive and luminescent polymers, Polymer composites

Abstract

The presentation covers the overview of academic research on thermoplastic elastomer in particular a group of elastomer/thermoplastic blends. The blend system was deeply investigated to understand effect of various factors on blend behaviors in both micro- and macroscopic scales. Cure behaviors, crystallinity, phase morphology, and mechanical, elastomeric and surface properties were discussed. Additionally, the research works related to industrial product development were also presented in which natural rubber was applied for the study.

Keywords: Thermoplastic Elastomer, Natural Rubber, Product Development



Electrospun Ultrafine Fibers: Versatile and Tunable Materials for Storing Electricity and Improving Enzyme Performance

Thammasit Vongsetskul

*Department of Chemistry, Faculty of Science, Mahidol University, Rama 6 Road, Ratchathewi, Bangkok 10400
Phone: 02-201-5110, Fax: 02-354-7151, E-mail: thammasit.von@mahidol.ac.th*



Present Associate Professor, Department of Chemistry, Faculty of Science, Mahidol University

Research Interests:

Fabrication and applications of nanostructured materials (electrospun ultrafine fibers in particular), Polymer-surfactant complexes and their applications

Abstract

Ultrafine fibers with high surface area are normally produced by electrospinning. This technique is simple, convenient, repeatable, scalable, and providing an ability to tune their dimension. Due to their high-surface-area character, these fibers are used in various applications such as filtration. In this talk, my research works on these fibers for storing electricity and improving enzyme performance will be presented. Nowadays, electricity from environmentally-friendly sources such as sunlight and wind is gained a great attention because of global warming caused by fossil fuel-based power plants. Unfortunately, it normally fluctuates in a day, but we need to use electricity for 24 hours. Therefore, powerful and trustable energy storage devices for electric grids are required to be developed. Here, it will be demonstrated that our fabricated fibers can improve battery safety and performance successfully. The other research area is improving enzyme performance. Enzymes are known as efficient, environmentally-friendly, and highly specific biocatalysts. However, the uses of enzymes are limited by sensitivity to pH and temperature changes and reusability due to regular protein properties. To solve the mentioned problems, enzymes are normally immobilized onto the inert and insoluble materials. However, the activity of the immobilized enzymes is normally reduced. Therefore, a solid support with high surface area, ultrafine fibers, is applied to increase the amount of the bound enzymes. It is found that these fibers can solve the problems efficiently.



Chemical Modifications and Value added Epoxy Resins: an Industrial Perspective

Thipa Naiyawat

¹Aditya Birla Chemical (Thailand) Ltd., Research Centre: Epoxy Division; Rayong, Thailand

²Aditya Birla Chemicals, Performance Material Research Centre, Mumbai, India

Phone: 081-9409483, E-Mail: thipa.naiyawat@adityabirla.com



Present Deputy General Manager (DGM)- Research & Development (R&D)
Aditya Birla Chemical (Thailand) Ltd., and Aditya Birla Chemicals,
Performance Material Research Centre, Mumbai, India

Research Interests:

Low crystallization Bisphenol F epoxy resin, Controlled conversion resins for powder coatings, Multifunctional epoxy resins for aviation and oil drilling, Bio based epoxy resins and Bisphenol free epoxy

Abstract

In Industrial environment understanding of polymers at molecular level, impact of functional groups, knowledge of chemical modifications, impact of such modifications on performance properties, can leads to quick turnaround of technical success to commercial success. Another key challenge is maintaining a pipeline full of new products.

In my professional journey, I learned a disciplined stage gate approach for new product development key to quick churning of ideas to successful commercial launch of new molecules. Applications of Epoxy polymers are diverse and range from civil, coating, composites and electrical sector. It involves whole range of Reactive diluents to liquid, semi-solid, solid epoxy resins.

In my research carrier, I got opportunity to work Reactive diluents (2002); Standard Liquid epoxy bisphenol based (2004); Solid epoxy resins by Taffy process and Advancement process; With changes in mega trends in epoxy chemistry, our focus shifted to Bisphenol free epoxy resins, Bio-sourced epoxy resins, specialty Multifunctional, high heat resistant epoxy resins to super specialty recyclable epoxy resins.

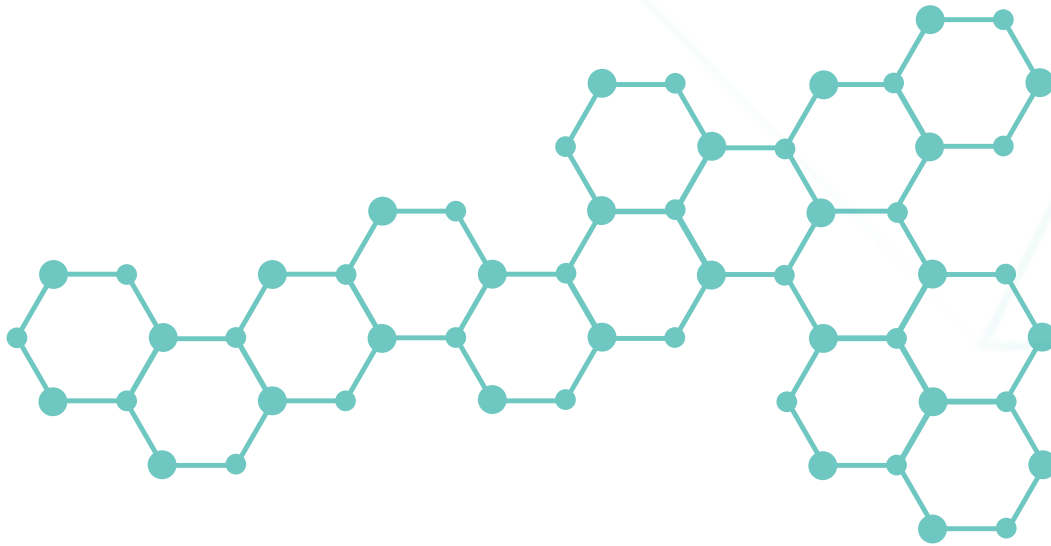
We as a team could achieve these accomplishments due to collaborative research environment and excellent ecosystem created for innovation by leaders at Aditya Birla Research Centre. Here Synthetic chemistry teams work hand in hand in hand with formulation experts, regulatory experts and IP cell, to extract maximum value out of new products and provide solutions to our global customers in much better way.

The environment friendly epoxy resins like waterborne, recyclable epoxies, bio-sourced epoxies and bisphenol free epoxy seems to be promising in near future and we in universities research teams should focus on such projects.



PDES

RECENT DEVELOPMENT IN POLYMER DESIGN



Development of Infrared-Reducing Coating from Poly(3,4-Ethylenedioxythiophene) Polystyrene Sulfonate

Krittana Lam¹, Jedsada Manyam², Chookiat Tansarawiput², Pakorn Opaprakasit¹ and Paiboon Sreearunothai^{1*}

¹School of Bio-Chemical Engineering and Technology, Sirindhorn International Institute of Technology (SIIT), Thammasat University, Phatum Thani 12121, Thailand

²National Nanotechnology Center (NANOTEC), National Science and Technology Development Agency (NSTDA), Thailand Science Park, Klong Luang, Pathum Thani 12120, Thailand

*E-mail: paiboon_sree@siit.tu.ac.th

Abstract

Infrared-reducing coating is useful for reducing heat transfer from sunlight through windows. Transparent conductive oxides (TCO) such as indium tin oxide (ITO) have high optical transparency and near infrared reflective properties which make it suitable for window coating. However, TCO is expensive and requires complicated process to make thin film coating. In this work, infrared (IR)-reducing glass coating employing poly(3,4 ethylenedioxythiophene) polystyrene sulfonate (PEDOT:PSS) was developed and tested for heat reducing performance. Heat-insulating PEDOT:PSS thin film was prepared using tetraethyl orthosilicate (TEOS) as a binder and applied using a wired bar coater. The optical and infrared shielding performance of the coatings were evaluated using an ultraviolet-visible-near-infrared (UV-Vis-NIR) spectrometer. The obtained film showed infrared shielding property with about 25% reduction in the NIR region (750-2500 nm) while maintaining high transparency in the visible region of over 85%. The film also showed good scratch resistance upon TEOS addition with the pencil hardness level of 3H increased from 6B level in that of the pristine film. Illumination test showed that window coated with the developed film can attain the temperature reduction by about 1.3-3.4 °C compared to that of the uncoated glass. The wettability of the film was also examined and the water contact angle results indicated that the coated film displayed more hydrophilicity than that of the uncoated glass which may promote the water wetting of the coated glass leading to facile cleaning.

Keywords: poly(3,4-ethylenedioxythiophene) polystyrene sulfonate, PEDOT:PSS, infrared reducing coating

1. Introduction

Windows are one of the most important building components where sunlight and heat can enter. The conventional technology that commonly used such as curtain shades and blinds is good at cutting down the heat entered through window but also blocks the useful visible light as well. The near-infrared range (700-2500nm) accounts for about 52% of energy in the solar spectrum sent to the earth (1). Coating technologies that can reduce this part of the energy has been made commercially available, such as the low emissivity (low-E) coatings that can reduce both the ultraviolet (UV) and/or infrared (IR) radiation, but this coating is normally applied from

factory (2). Heat-reducing coatings for application on windows require the retaining of optical transparency in addition to effectiveness in blocking of the near-infrared spectra (3).

Transparent conductive oxides (TCOs) such as indium tin oxide (ITO), antimony-doped tin oxide (Sb: SnO₂, ATO) and aluminum doped zinc oxide (AZO) have high optical transparency in the visible spectral range and NIR reflective properties which make them suitable for heat-insulating coating(4). However, for ITO, despite having the best properties out of the three

TCOs, is expensive and requires complicated process to make thin films (5,6).

Poly(3,4-ethylenedioxythiophene) polystyrene sulfonate or PEDOT:PSS is an inherently conducting polymers (ICP) which features high conductivity, optical transparency, and low-cost alternatives to the vacuum sputtered conductive oxides (TCO) that have been extensively used in these applications. It also has a good physical and chemical stability and can also be water processable (7,8) rendering it to be easily applied by various coating and printing techniques. This compound thus has a high potential to be used in heat-cut coating applications. This work aims to study the infrared-shielding properties of a PEDOT:PSS thin film as well as its adhesion, physical, and chemical stability on the glass surface.

2. Experimental methods

2.1 Materials

PEDOT:PSS (1.3 wt% dispersion in H₂O) and TEOS were obtained from Sigma-Aldrich and Merck, respectively. The wired bar coater was purchased from H.J.UNKEL which produces a 6.86-micron wet film thickness. Commercial borosilicate glass of 4 x 6 inch and 2mm-thickness was used as a substrate.

2.2 Sample preparation

Coating solution was prepared by mixing TEOS with the PEDOT:PSS solution in the ratio of 0wt% and 5wt% TEOS in PEDOT:PSS. The solution was mixed using a mechanical stirrer for 6 hours at room temperature until the mixture became homogeneous. The glass substrate was cleaned by rinsing with acetone, ethanol, and IPA to remove oil and dirt contaminants before coating. Then, the solution was coated onto a glass substrate using the wire-bar coater with an active area of 4x6 inches. The film with TEOS was also baked at various temperatures for 30 min to improve its hardness using a hot plate.

2.3 Characterizations of the coated film

The spectral transmittance measurement was conducted using an Agilent Cary 7000 Universal Measurement Spectrometer in the wavelength range of 250-2500 nm. The transmittance was measured in a straight-line configuration without any polarization filter.

The mechanical properties of the coating were determined according to the ASTM standard D 3363, using QHQ-A pencil hardness tester. The pencil hardness test is a simple method to measure the hardness of the film. The pencil (Mitsubishi) with varying in hardness from 6B to 6H was placed on the film at a 45° angle under the load of 500 g. The hardness grades of the film were evaluated by using Dino-Lite Digital Microscope for inspection of the damage on the surface of the film.

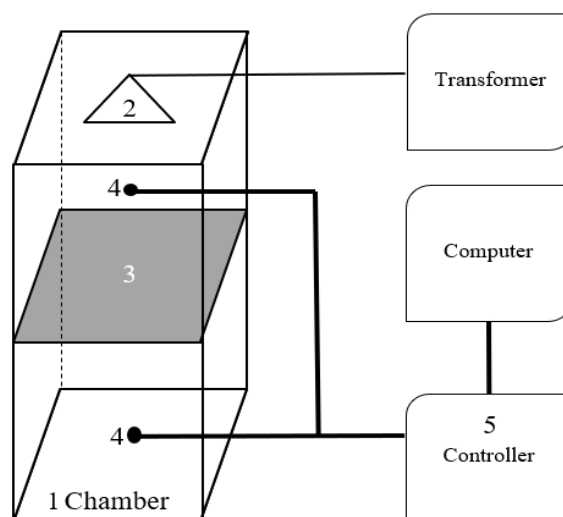


Fig. 1 Schematic diagram of the illumination set-up for measurement of the temperature reduction using the developed coating compared to that of the un-coated glass. 1-sealed acrylic chamber, 2-halogen lamp, 3-sample placement holder, 4-temperature sensors, 5- Arduino Mega 2560 controller board

The temperature reduction performance of the coating was also evaluated using a home-built illumination test chamber. The set-up is shown in Fig. 1. The device consists of an acrylic chamber with the size of 4 x 6 x 15 inch with a sample holder in the middle, a 150W-halogen lamp as a stimulated light/heat source, temperature sensors connected to an Arduino Mega 2560 microcontroller. The difference in the bottom chamber

temperatures when coated and un-coated glass windows were placed in the sample holder were used to demonstrate the effect of heat shielding performance of the coating in term of the temperature reduction after the coating was employed.

The water contact angle measurement was measured using a Dino-Lite Digital Microscope (AM4815) with the amount of water in each drop of 5 microliters.

3. Results and Discussion

3.1 Optical properties and a digital photograph

To study optical properties of the coating, the transmittance spectra of the PEDOT:PSS/TEOS film is shown in Fig. 2. For the PEDOT:PSS/TEOS film, a good NIR reducing performance in the range of 800 to 2500 nm was observed with more than 80% transmittance in the visible region (400-700nm). In the near-infrared region, PEDOT:PSS film demonstrates reduced infrared transmittance between 60-70 % compared to the value of over 90% for the un-coated glass substrate. The PEDOT:PSS coating film appeared to be smooth and transparent as shown in Fig. 3.

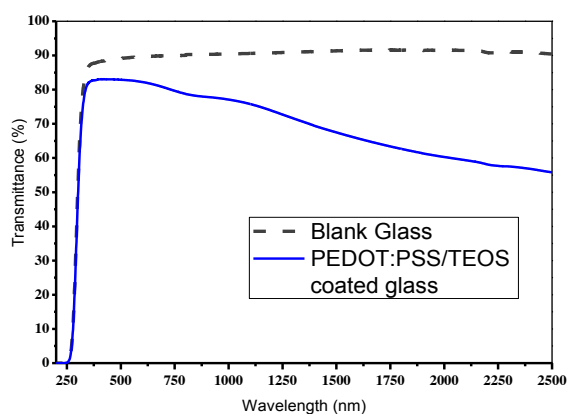


Fig. 2 UV-Vis-NIR spectra of PEDOT:PSS/TEOS coating and the glass substrate

3.2 Mechanical properties

The mechanical strength of the PEDOT:PSS film was determined using the pencil hardness test and results shown in Table 1. The pure PEDOT:PSS film (without TEOS) showed quite weak mechanical strength. The film

could be scratched by just a 6B pencil. The hardness of the film was enhanced when TEOS was added such that no scratch by a 1B pencil was observed.

The effect of annealing temperature on the mechanical strength of the PEDOT:PSS/TEOS film was also studied. In this case, the film coated without any annealing showed the hardness of HB. This is increased to 2H grade upon annealing the film at 60°C and to a 3H grade upon annealing at 100°C for 30 min. The mechanical strength of the film could be observed to improve over ten grades from 6B to 3H as a result of both TEOS additives in combination with a moderate 100°C annealing treatment.



Fig. 3 Digital photograph of PEDOT:PSS film coated onto the glass substrate showing its high visible transparency

3.3 Temperature reduction performance

A heat shielding performance and the temperature reduction has been carried out in a sealed acrylic chamber. Fig. 4 demonstrates the change of the inner air temperature in the chamber from initial to the final temperature. Increasing air temperature depends on the irradiation time when the chamber has been heated by the halogen lamp. From the testing results show that the air temperature in the chamber which was covered by the PEDOT:PSS film has the rate of increasing lower than that covered by blank glass. The final temperature of the chamber covered with the blank glass and the PEDOT:PSS coated glass was 36.2 and 34.9 °C, respectively. The difference in the temperature reduction

Table 1 Effect of the additive: TEOS as binder and annealing temperature (T_c) of the coated glass on its pencil hardness grade

Pencil Hardness Test / Standard ASTM D 3363				
Grades	Neat PEDOT:PSS film, no TEOS	5%wt TEOS annealed at RT	5%wt TEOS annealed at 60°C	5%wt TEOS annealed at 100°C
3H	Film was gouged	Film was gouged	Film was gouged	Film was gouged
2H	Film was gouged	Film was gouged	Film was gouged	Film was scratched
1H	Film was gouged	Film was gouged	Film was scratched	Film was scratched
F	Film was gouged	Film was gouged	Film was scratched	No scratches
HB	Film was gouged	Film was scratched	No scratches	No scratches
1B	Film was gouged	No scratches	No scratches	No scratches
2B	Film was gouged	No scratches	No scratches	No scratches
3B	Film was gouged	No scratches	No scratches	No scratches
4B	Film was gouged	No scratches	No scratches	No scratches
5B	Film was scratched	No scratches	No scratches	No scratches
6B	Film was scratched	No scratches	No scratches	No scratches

Coating Hardness Results

Gouge	4B	F	2H	3H
Scratch	> 6B	B	HB	F

between the PEDOT:PSS coated and the blank glass was 1.3 °C.

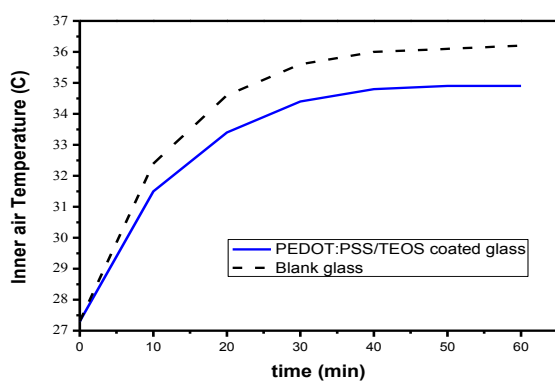


Fig. 4 The temperature of the air inside the chamber covered with either the blank glass or the PEDOT:PSS coated glass as a function of irradiation time.

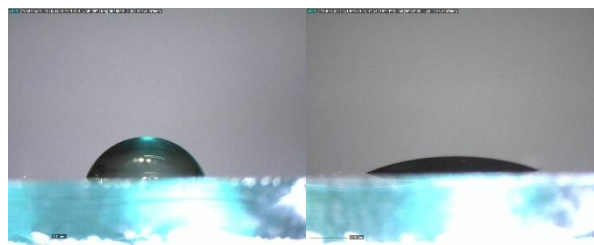


Fig. 5 Photographs shows the water contact angle of water droplet on a blank glass (left, 69°) and on a PEDOT:PSS/TEOS coated glass substrate (right, 18°). The PEDOT:PSS/TEOS coated glass shows smaller water contact angles than that of the pristine glass. 3.4 Wettability of the PEDOT:PSS film

Hydrophilicity of the PEDOT:PSS film was assessed by measuring the contact angle of water droplets on their surfaces blank glass, neat PEDOT:PSS and after adding TEOS. As observed in Fig. 5, the water contact angle of water droplet on blank glass was $69 \pm 3^\circ$ and The neat PEDOT:PSS samples obtained from wire bar coater

have a water contact angle value of $16\pm 3^\circ$, indicating their high hydrophilicity. After adding TEOS 5wt%, the film show slightly higher water contact angle values of $18\pm 3^\circ$. From this result, the films coated with PEDOT:PSS/TEOS are more hydrophilic than the blank glass, and potentially can be easily wet and cleaned by water washing providing facile cleaning coating.

4. Conclusion

Infrared reducing glass coating has been developed using the PEDOT:PSS polymer in combination with TEOS binder. The developed coating shows more than 85% optical transparency in the visible light range. In the near-infrared region, PEDOT:PSS film demonstrates reduced infrared transmittance between 60-70% compared to the value of over 90% for the un-coated glass substrate. Adding TEOS does not change the transmission spectrum much, but significantly increased the film scratch resistance from the 6B pencil to the 3H pencil level. Illumination test measurement shows that window coated with the developed film can attain the temperature reduction by about 1.3 °C compared to that of the uncoated glass. The PEDOT:PSS/TEOS films shows a water contact angle value of 16° lower than the 69° value of the blank glass indicating more hydrophilic surface which could help promote the water wetting and facile cleaning of the coated surface. The developed coating has potential to be applied in many fields, especially in infrared shielding applications.

Acknowledgment

Krittana gratefully acknowledges TAIST-Tokyo Tech and STEM scholarships from NSTDA. Financial supports from SCG Chemicals and the Centre of Excellence in Materials and Plasma Technology (M@P Tech), Thammasat University are also gratefully acknowledged.

References

1. ASTM G173 - Standard Tables for Reference Solar Spectral Irradiances: Direct Normal and Hemispherical on 37 Tilted Surface. Am Soc Test Mater. 2008;3(Reapproved 2008):1-21.
2. Wang L, Hang J, Shi L, Sun X, Xu F. Preparation and characterization of NIR cutoff antimony doped tin oxide/hybrid silica coatings. Mater Lett [Internet]. 2012;87:35-8. Available from: <http://dx.doi.org/10.1016/j.matlet.2012.07.065>
3. Lampert CM. Heat mirror coatings for energy conserving windows. Sol Energy Mater. 1981;6(1):1-41.
4. Afre RA, Sharma N, Sharon M, Sharon M. Transparent Conducting Oxide Films for Various Applications : a Review. 2018;53.
5. Guzman G. ATO coatings : liquid based deposition processes for Photovoltaic and other applications Background Properties of ATO Applications of ATO thin films Photovoltaic applications of ATO Wet chemical deposition processes of ATO Applications. Thin Film. 2010;1-29.
6. Faculty TA, Halim A, Fulfillment IP. THIN FILMS MADE FROM COLLOIDAL ANTIMONY TIN OXIDE NANOPARTICLES FOR TRANSPARENT CONDUCTIVE APPLICATIONS A Thesis Presented to by Abigail Halim of the Requirements for the Degree. 2013;(May).
7. Lubianez RP, Kirchmeyer S, Gaiser D, Starck HC, Place I. Advances in PEDOT : PSS Conductive Polymer Dispersions. 1(617).
8. Polymer IC. Principles and Applications of an Intrinsically Conductive Polymer.

Preparation of Poly[(acrylic acid)-*co*-(potassium acrylate)] Superabsorbent Polymer

Nonpan Dispat¹, Sirilux Poompradub^{1,2*}, Suda Kiatkamjornwong^{3,4}

¹Department of Chemical Technology, Faculty of Science, Chulalongkorn University, Bangkok 10330

²Center of Excellence on Petrochemical and Materials Technology, Bangkok 10300

Phone +66 2218 7518, Fax +66 2255 5831, *E-Mail: sirilux.p@chula.ac.th

³Faculty of Science, Chulalongkorn University, Bangkok 10330

⁴FRS(T), the Royal Society of Thailand, Sanam Suepa, Dusit, Bangkok 10300

Abstract

Superabsorbent polymer (SAP) is a material containing hydrophilic functional group such as carboxylic group through loosely crosslinked three-dimensional networks of flexible chains. It can absorb, retain a large amount of water or aqueous solution and release the retained moisture to the surrounding environment. In this research, SAPs were synthesized by acrylic acid (AA) and potassium acrylate (KAA) as the base monomers by free radical chain polymerization. Ammonium persulfate (APS), *N, N, N', N'*-tetramethylenediamine (TEMED) and *N, N'*-methylenebisacrylamide (MBA) were used as an initiator, a co-initiator and a cross-linker, respectively. SAPs were then characterized by Fourier-transform infrared spectroscopy and scanning electron microscopy. The effects of reaction temperature, initiator concentration and co-initiator concentration on the water absorbency were investigated. The highest water absorbency of the SAP ($450 \pm 29 \text{ g g}^{-1}$) was obtained using 0.013% mol APS (by mol AA), 0.27% mol TEMED and partially neutralized AA by potassium hydroxide at 65°C. The water absorbency of so-prepared SAP was 1.5 times higher than that of a commercial SAP (290 g g^{-1}). Reusability of the prepared SAP was much higher than the commercial SAP.

Keywords: acrylic acid, potassium acrylate, superabsorbent polymer, water absorbency

1. Introduction

In the past decades, drought due to climate changes, global warming and flood caused by typhoon and heavy rains directly destroy agricultural production and food chains and adversely affect human life. Superabsorbent polymer (SAP) is one interesting material that can be developed to increase water availability in soil. It helps soil to hold water after heavy rain and reduces the irrigation requirement.^[1] SAPs consisting of hydrophilic functional groups are loosely crosslinked to give three-dimensional networks of flexible polymer chain.^[2] SAPs are able to absorb large amounts of water and release the retained moisture to the surrounding environment by capillary, osmotic and hydration forces without dissolution or loss of structure.^[3] Because of their high

water-absorbing capacity, SAPs are widely used in many products^[4], such as disposable diapers, feminine napkins, soil amendment for agriculture and horticulture, gel actuators, water-blocking tapes, drug-delivery systems, absorbent pads, *etc.*

Acrylic acid and acrylamide are used commonly as substrates for synthesis of SAPs because they are widely used in the absorbent industries with a variety of water absorbency. Acrylic acid has more hydrophilic functional groups than does acrylamide. There are many factors affecting the water absorbency of SAPs, just to mention about the some important ones: type and amount of initiator^[5], polarity of polymer chains^[6] and crosslinking density^[7]. Potassium acrylate (KAA) resulting from neutralization of acrylic

acid by potassium hydroxide (KOH) can increase polarity of AA monomer before synthesis of SAPs, resulting in the enhancement of water absorbency^[8] and can be used as a potassium fertilizer containing SAP.

In this work, the influences of reaction temperature, initiator and co-initiator concentrations and KOH partially neutralized AA monomer on the water absorbency (WA) of poly[(acrylic acid)-*co*-(potassium acrylate)] SAP were investigated. Water absorbency of the prepared SAP was compared to that of commercial one. Finally, reusability of the prepared SAPs in comparison with the commercial one was investigated.

2. Experimental Methods

2.1 Materials

Acrylic acid (AA), commercial grade 99.97%, was supplied by Thai Mitsui Specialty Chemicals. Potassium hydroxide (KOH) and ammonium persulfate (APS analytical purity) were purchased from Ajax. *N, N'*-methylenebisacrylamide (MBA) and *N, N, N', N'*-tetramethylethylenediamine (TEMED, analytical grade), were obtained from Sigma-Aldrich. Acetone (commercial grade) and nitrogen gas (99.99%) were purchased from Zen point and Praxair, respectively. Commercial SAP was supplied by a local company, Thailand.

2.2 Synthesis of poly[(acrylic acid)-*co*-(potassium acrylate)] SAPs

Alkaline aqueous solution, 40 ml (30% w KOH) was added into 30 g commercial AA (dissolved in 120 ml deionized water) in an ice bath. Then, aqueous solution of the neutralized acrylate was mixed with 0.0165 g MBA in a four necked reactor flask equipped with a mechanical stirrer under nitrogen gas bubbling for removal of oxygen gas from the reactor. The reactor was placed in a thermostat oil bath to control the reaction temperature at 65°C. After the agitation at 220 rpm for 10 min, the APS initiator and TEMED co-initiator were added. At the completion of the polymerization time, the reaction was stopped. The viscous gelly-like product was soaked in

acetone for dewatering, cut into small pieces ($\approx 0.5 - 1$ cm) and dried in an oven at 65°C until a constant weight of SAP was obtained. Water absorbency (WA) is determined by Eq. (1).

$$\text{Water absorbency (g g}^{-1}\text{)} = \frac{\text{weight of the swollen SAP} - \text{weight of the dry SAP}}{\text{weight of the dry SAP}} \quad (1)$$

2.3 Characterization

Fourier transform infrared spectroscopy (FTIR) is used to identify the functional groups of SAPs. FTIR spectra of SAPs dispersed in a KBr pellet were analyzed using Spectrum One (Perkin Elmer, Germany). The IR peaks were scanned and recorded at the wave numbers from 500 to 4000 cm^{-1} with a resolution of 4 cm^{-1} for 64 scans.

The surface morphology and the elemental composition of SAPs were characterized by Scanning electron microscopy coupled with Energy Dispersive X-ray Spectroscopy (SEM/EDXS, JEOL, JSM-7610F and Oxford, X-Max N 20), operated at an acceleration voltage of 15 kV.

3. Results and Discussion

3.1 Influence of reaction temperature on water absorbency

The effect of reaction temperatures (55, 60 and 65°C) on the polymerization time to gelation or solidification of the synthesized SAPs is shown in Figure 1. The reaction time was recorded after the initiator (APS) was added until the polymer was formed to a complete gel. Increase in the reaction temperature resulted in decreases of the polymerization time. High temperature accelerates the reaction rate which leads to the earlier gelation of SAP. The highest water absorbency (387 ± 12 g g^{-1}) was obtained at the reaction temperature of 65°C, so this temperature was chosen for the next experiment.

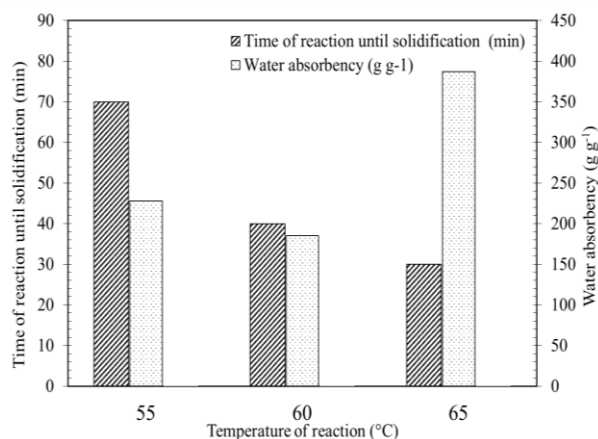


Figure 1 Effect of reaction temperature on water absorbency of SAPs (0.025% mol MBA crosslinking agent, 0.003% mol APS initiator and 0.27% mol of TEMED co-initiator)

3.2 Influence of APS initiator concentration and neutralization on water absorbency

The water absorbency of the prepared SAPs using APS initiator at different concentrations (0.0015 and 0.0140% mol of AA with a constant amount of MBA crosslinking agent of 0.025% mol and reaction temperature of 65°C is shown in Figure 2. Increase in the initiator concentration for the non-neutralized SAPs did not affect or changed the water absorbency. On the other hand, in case of the partially neutralized SAPs, increases in the initiator amount resulted in the increase of water absorbency as seen in Figure 2. Accordingly, the neutralization process can be concluded as one of the most important factors that affects the water absorbency. This process can be improved the polarity of SAPs.

3.3 Influence of *N,N,N',N'*-tetramethylethylenediamine (TEMED) co-initiator on water absorbency

The water absorbency of the so prepared SAPs using MBA crosslinking agent of 0.025% mol, APS initiator 0.0140% mol with a fixed TEMED co-initiator amount of 0.27% mol and reaction temperature of 65°C is shown in Figure 3. Water absorbency of both non-neutralized and neutralized SAPs increased with

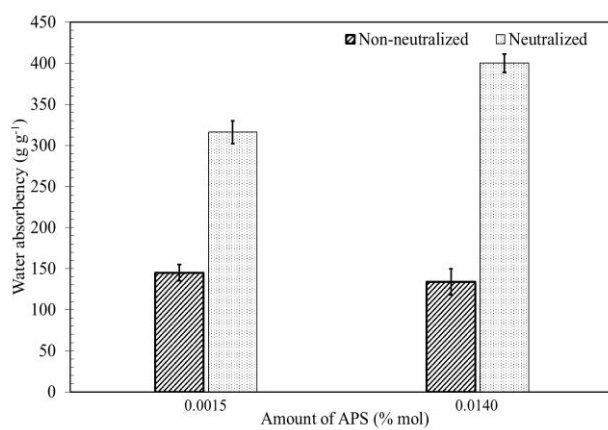


Figure 2 Effect of APS initiator amount on water absorbency of SAPs (0.025% mol MBA crosslinking agent with and without KOH neutralization, synthesized at 65°C)

the addition of TEMED within the concentration ranges of 11 and 12%. Furthermore, the neutralized SAPs with TEMED showed the highest water absorbency (450 ± 29 g g⁻¹). This result could be explained that the addition of TEMED affected the morphology of SAPs. As seen in the inserted Figure 3, it was found that the small porosity was clearly observed and distributed amongst the large porosity, while the morphology of the neutralized SAPs without TEMED showed merely large porosity. The highest water absorption SAP currently synthesized was used to compare with the commercial one in terms of morphology in relation with water absorbency.

3.4 Reusability test of the SAPs

Figure 4 shows the water absorbency of prepared SAP synthesized using MBA cross-linker 0.025% mol, APS initiator 0.0140% mol with a fixed TEMED co-initiator of 0.27% mol and reaction temperature of 65°C compared with the commercial SAP. The prepared SAP in this study shows the highest water absorbency at 450 ± 29 g g⁻¹ while the commercial one renders the low water absorbency of 290 g g⁻¹. The reusability test of both SAPs according to Eq. (2) showed that the efficiency of the prepared SAP decreased only by 7%, while the efficiency of the commercial SAP decreased by 26%.

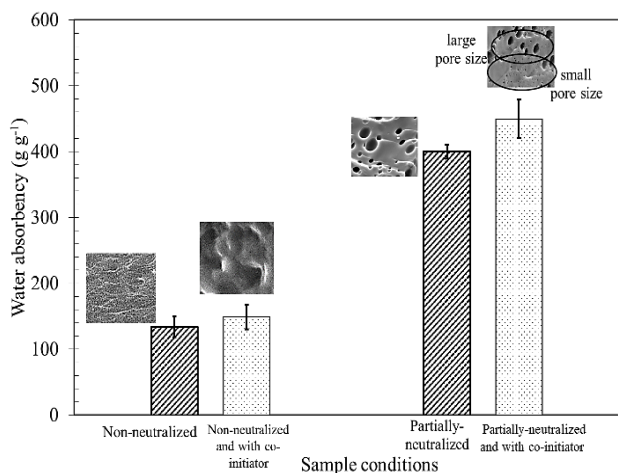


Figure 3 The effect of TEMED co-initiator on the water absorbency of SAPs (0.025% mol MBA crosslinking agent, 0.0140% mol APS initiator, 0.27% mol TEMED co-initiator synthesized at 65 °C)

Water absorbency (%)

$$= \frac{\text{Water absorbency}_{n+1}}{\text{Water absorbency}_n} \times 100 \quad (2)$$

where n is the number of repeating uses.

Consequently, the efficiency of water absorbency of prepared SAP in this study was higher than that of the commercial SAP. More explanation shall be investigated.

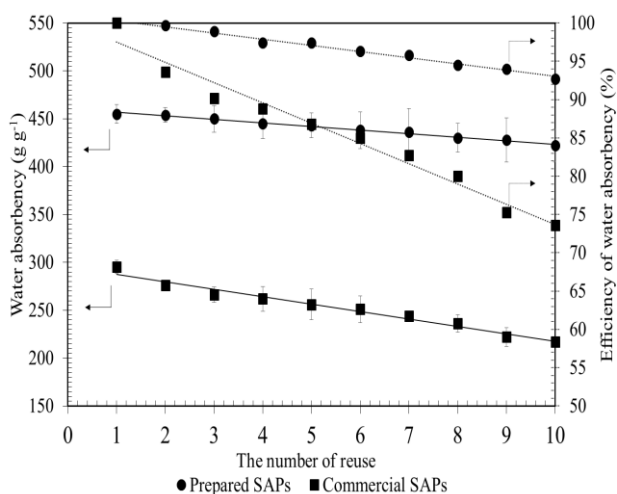


Figure 4 The reusability test of the prepared and commercial SAPs.

3.5 Characterization of SAPs

Figure 5 shows the FTIR spectra of commercial and prepared SAPs. Both spectra show the similar peaks. Absorption peaks at 3360 and 2900 cm⁻¹ are attributed to stretching vibration of the oxygen-hydrogen bonds (O-H) in the structure of carboxyl group (-COOH) and carbon-hydrogen bonds (C-H) in the structure of the methylene group (-CH₂), which are the acrylic monomer structure. In addition, the absorption peaks appeared at 1700, 1560 and 1450 cm⁻¹ indicate an asymmetric stretching and a symmetric stretching vibration of the carbonyl group (C=O) in the structure of acid functionality (-COOH). The stretching peak of carbon and oxygen bond (C-O) is observed at 1400 cm⁻¹.

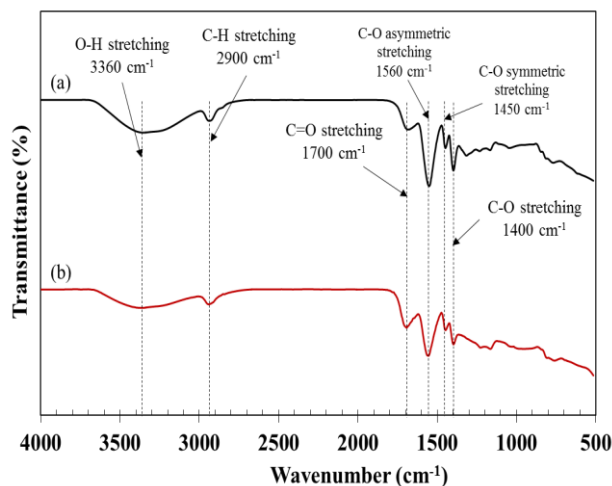


Figure 5 FTIR spectra of (a) commercial SAP, (b) SAP prepared with partially-neutralized AA, 0.025% mol MBA, 0.0140% mol APS and 0.27% mol TEMED.

3.6 Surface morphological studies

The surface appearance and structure of the commercial and prepared SAPs synthesized from the partially KOH-neutralized AA, 0.025% mol MBA, 0.0140% mol APS and 0.27% mol TEMED observed by SEM are depicted in Figure 6. It was found that the commercial SAP (Figure 6(a)) was less porous with low water absorbency (290 g g⁻¹). On the other hand, SEM images of the prepared SAP (Figure 6(b)) had more porosity with higher water absorbency (450 ± 29 g g⁻¹).

It could be that, besides the chain flexibility to hold more water, the larger the pore size, the higher water absorbency was obtained. Moreover, the prepared SAP gave the 1.5-fold higher water absorbency when compared with the commercial one.

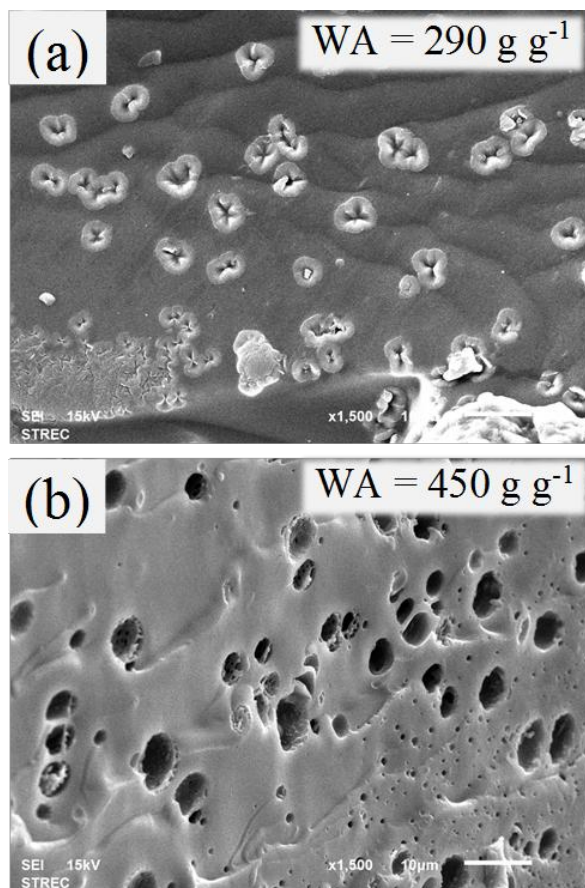


Figure 6 SEM images of (a) commercial SAP (b) prepared SAP with partially-neutralized AA, 0.025% mol MBA, 0.0140% mol APS and 0.27% mol TEMED.

4. Conclusion

Poly[(acrylic acid)-*co*-(potassium acrylate)] super absorbent polymer was prepared by the free radical chain polymerization in the presence of 0.025% mol MBA crosslinking agent, 0.0140% mol APS initiator, 0.27% mol TEMED co-initiator synthesized at 65°C. Under this condition, the highest water absorption of SAP was obtained at $450 \pm 29 \text{ g g}^{-1}$. Infrared spectroscopy technique confirmed the success of AA/KAA copolymeric SAPs.

Acknowledgment

The authors would like to thank the full support from Distinguished Professor Grant (DPG6080001), the Thailand Research Fund for the current research.

Partial support from the Center of Excellence on Petrochemical and Materials Technology, Chulalongkorn University for the first author's thesis expenditure for the academic year of class 2016.

References

- [1] Liu, X. and Chan, Z., "Application of potassium polyacrylate increases soil water status and improves growth of bermudagrass (*Cynodon dactylon*) under drought stress condition", *Sci. Hortic.*, 197, 705–711 (2015).
- [2] Kiatkamjornwong, S., "Superabsorbent Polymers and Superabsorbent Polymer Composites", *Science Asia*, 33:1, 39-43 (2007).
- [3] Buwalda S. J., Boere K. W.M., Dijkstra P. J., Feijenc J., Vermonden T. and Hennink W. E., "Hydrogels in a historical perspective: From simple networks to smart materials", *J. Control. Release*, 190, 254–273 (2014).
- [4] Laftah, W. A., Hashim, S., and Ibrahim, A. N., "Polymer Hydrogels: A Review" *Polym.-Plast. Technol. Eng.*, 50:14, 1475-1486 (2011).
- [5] Li, A., Wang, A. and Chen, J., "Studies on poly (acrylic acid)/attapulgit superabsorbent composite. I. Synthesis and characterization" *J. App. Polym. Sci.*, 92, 1596–1603 (2004).
- [6] Chen, X.P., Shan, G., Huang, J., Huang, Z. and Weng, Z. "Synthesis and properties of acrylic-based superabsorbent" *J. App. Polym. Sci.*, 92, 619–624 (2004).
- [7] Lira, L., Martins, K. and Torresi, S., "Structural parameters of polyacrylamide hydrogels obtained by the Equilibrium Swelling Theory" *Eur. Polym J.*, 45, 1232–1238 (2009).

-
- [8] Lu, S., Duan, M. and Lin, S., "Synthesis of Superabsorbent Starch-graft-Poly(potassium acrylate-co-acrylamide) and Its Properties" *J. App. Poly. Sci.*, 88, 1536–1542 (2003).
- [9] *Handbook of Bioengineering*, New York, McGraw-Hill : 21-27 (1989).

Polyisocyanurate Foams Preparation Catalyzed by Mixtures of Copper-Amine Complexes and Potassium 2-Ethylhexanoate

Teeraporn Suwannawet¹, Duangruthai Sridaeng² and Nuanphun Chantarasiri^{3*}

¹Program in Petrochemistry and Polymer Science, Faculty of Science, Chulalongkorn University, Bangkok 10330

²Department of Chemistry, Faculty of Science, Rangsit University, Pathum Thani 12000

³Department of Chemistry, Faculty of Science, Chulalongkorn University, Bangkok 10330

Phone +66 2218 7639, Fax +66 2218 7598, *E-mail: nuanphun.c@chula.ac.th

Abstract

A new catalyst system for the preparation of polyisocyanurate (PIR) foam was developed. The mixture of copper-amine complex and potassium 2-ethylhexanoate [copper-amine complex:potassium 2-ethylhexanoate (K-15)] was used as catalyst. Two copper-amine complexes, namely $\text{Cu}(\text{OAc})_2(\text{en})_2$ and $\text{Cu}(\text{OAc})_2(\text{trien})$; where OAc = acetate, en = ethylenediamine and trien = triethylenetetramine, were used as catalyst for blowing and gelling reactions. K-15 was used as a catalyst for trimerization reaction. PIR foams prepared from $\text{Cu}(\text{OAc})_2(\text{en})_2$:K-15 and $\text{Cu}(\text{OAc})_2(\text{trien})$:K-15 were compared with those prepared from a commercial catalyst system, *N,N'*-dimethylcyclohexylamine (DMCHA):K-15. The experimental results showed that both $\text{Cu}(\text{OAc})_2(\text{en})_2$:K-15 and $\text{Cu}(\text{OAc})_2(\text{trien})$:K-15 had better catalytic activity than DMCHA:K-15. Both $\text{Cu}(\text{OAc})_2(\text{en})_2$ and $\text{Cu}(\text{OAc})_2(\text{trien})$ has very weak odor as compared to DMCHA, which has strong odor.

Keywords: polyisocyanurate foam, catalyst, copper-amine complex

1. Introduction

Polyisocyanurate (PIR) foam is thermosetting polymer used as insulation materials. The important property of PIR foam is the better thermal stability than polyurethane foam due to isocyanurate group. PIR foam has lightweight, low density and good mechanical properties [1-4].

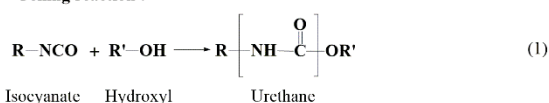
PIR foam synthesis is described in three main reactions, namely blowing reaction, gelling reactions and trimerization reaction. Blowing reaction is the reaction between isocyanate and water to produce unstable carbamic acid, which immediately decomposes into an amine and carbon dioxide (reaction 1). Gelling reaction is reaction between an isocyanate with polyols to generate polyurethane (reaction 2). Trimerization reaction is reaction between isocyanates that produces isocyanurate group

(reaction 3) [5]. However, these three reactions are slow and therefore the catalysts are required for preparation of PIR foams.

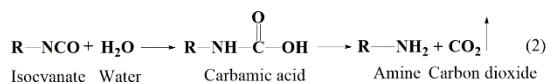
Two types of catalysts are needed in the preparation of PIR foam, namely blowing/gelling and trimerization catalysts. Tertiary amines, such as *N,N'*-dimethylcyclohexylamine (DMCHA), are used as commercial catalysts in gelling and blowing reactions. For trimerization reaction, the commercial catalyst used are potassium salts of carboxylic acids, such as potassium 2-ethylhexanoate (K-15). Mechanism of gelling and trimerization reactions are shown in Scheme 1 and 2, respectively. Tertiary amine catalyst has strong odor which is an important problem in the preparation PIR foam in large scale.

From our previous work [6], copper amine complexes, namely copper-ethylenediamine $[\text{Cu}(\text{OAc})_2(\text{en})_2]$ and copper-triethylenetetramine $[\text{Cu}(\text{OAc})_2(\text{trien})]$ were used as blowing and gelling catalyst for preparation of rigid polyurethane foams (Scheme 3). $\text{Cu}(\text{OAc})_2(\text{en})_2$ and $\text{Cu}(\text{OAc})_2(\text{trien})$ were prepared in the form of solution in water (aqueous solution) which can be used in the preparation of rigid polyurethane foams without purification. The aqueous solution of $\text{Cu}(\text{OAc})_2(\text{en})_2$ and $\text{Cu}(\text{OAc})_2(\text{trien})$ has very weak odor as compared to DMCHA.

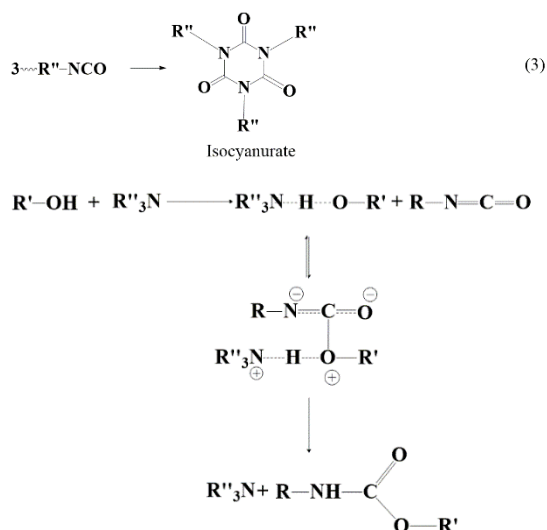
Gelling reaction :



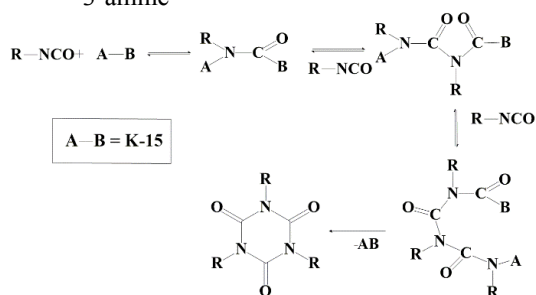
Blowing reaction :



Trimerization reaction :



Scheme 1 Mechanism of gelling reaction catalyzed by 3° amine



Scheme 2 Mechanism of trimerization reaction catalyzed by K-15

In this work, PIR foam will be prepared by using $\text{Cu}(\text{OAc})_2(\text{en})_2$:K-15 and $\text{Cu}(\text{OAc})_2(\text{trien})$:K-15. Aqueous solutions of two copper-amine complexes, namely $\text{Cu}(\text{OAc})_2(\text{en})_2$ and $\text{Cu}(\text{OAc})_2(\text{trien})$ will be used. Various mole ratios of copper-amine complex to K-15 and isocyanate indexes will be employed. The reaction times, rise profile and amount of isocyanurate group in PIR foam will be investigated. The results will be compared with PIR foam prepared from the commercial catalysts, DMCHA:K-15.

2. Experimental Methods

2.1 Materials

Copper (II) acetate monohydrate $[\text{Cu}(\text{OAc})_2 \cdot \text{H}_2\text{O}]$, ethylenediamine (en) and triethylenetetramine (trien) were obtained from Aldrich. Distilled water was used as a chemical blowing agent. Polyol (Polymaxx[®] 4221, sucrose-based polyether polyol, hydroxyl value = 440 mg of KOH/g, functionality = 4.3, viscosity at 25 °C = 5500 cP), polysiloxane surfactant (Tegostab[®] B8462), polymeric 4,4'-methylene diphenyl diisocyanate (PMDI, Raycore[®] B9001, % NCO = 31.0 wt%, average functionality = 2.7), *N,N'*-dimethyl cyclohexylamine (DMCHA, a commercial catalyst for gelling and blowing reaction) and potassium 2-ethylhexanoate (Dabco[®] K-15, a commercial catalyst for trimerization reaction) were supplied by IRPC Public Company Limited (Figure 1).

2.2 Synthesis of copper-amine complex aqueous solutions

The copper-amine complex aqueous solutions were synthesized from $\text{Cu}(\text{OAc})_2 \cdot \text{H}_2\text{O}$ and amines using water as a solvent according to the procedure reported in the literature [6]. The obtained aqueous solutions contained 25 wt% of copper-amine complexes in water which can be further used as a catalyst to prepare PIR foams without purification.

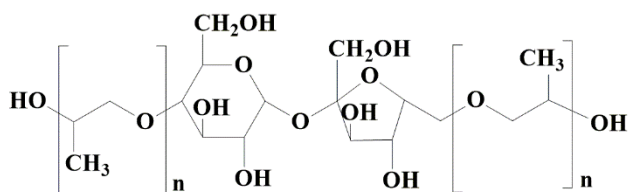
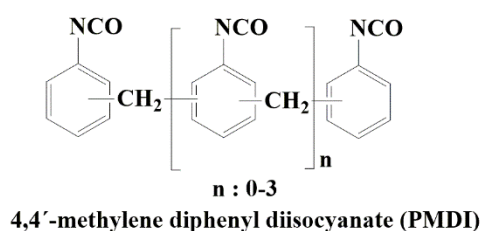
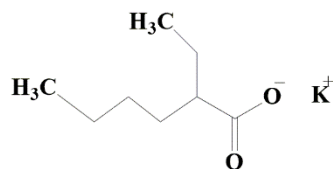
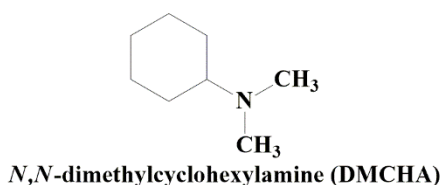


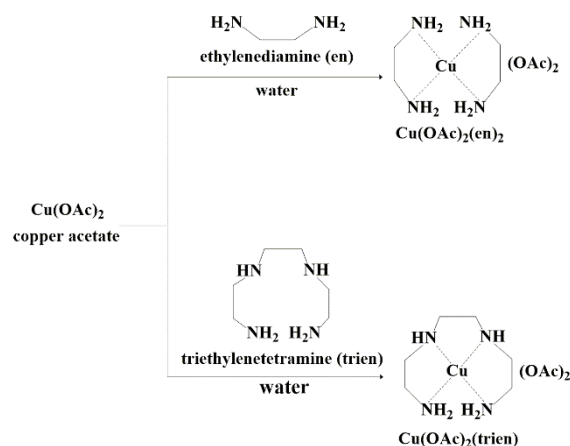
Figure 1. Structure of DMCHA, K-15, PMDI and polyol

2.2.1 Synthesis of copper-ethylenediamine complex aqueous solution [Cu(OAc)₂(en)₂]

A solution of ethylenediamine (0.42 ml, 6.28 mmol) in water (4 ml) was stirred at room temperature for 15 minutes. After that, Cu(OAc)₂.H₂O (0.624 g, 3.12 mmol) was added into the solution. The reaction mixture was stirred at room temperature for 24 hours. The aqueous solution of Cu(OAc)₂(en)₂ was obtained as an odorless dark purple solution. UV: λ_{max} (H₂O) = 229 nm, ε = 6,559.

2.2.2 Synthesis of copper-triethylenetetramine complex aqueous solution [Cu(OAc)₂(trien)]

The synthesis of Cu(OAc)₂(trien) aqueous solution was done by using the same procedure as Cu(OAc)₂(en)₂. Triethylenetetramine (0.43 ml, 2.89 mmol), Cu(OAc)₂.H₂O (0.577 g, 2.89 mmol) and water (4 ml) were used in the synthesis. The aqueous solution of Cu(OAc)₂(trien) was obtained as an odorless dark blue solution. UV: λ_{max} (H₂O) = 258 nm, ε = 4,365.



2.3 Preparation of PIR foams using cup test method

The preparation of PIR foams using cup test method was done by following ASTM D7487-13. PIR foam formulation is shown in Table 1. In the first step, polyol, surfactant, catalyst for gelling and blowing reaction (DMCHA or copper-amine complexes), catalyst for trimerization reaction (K-15) and blowing agent (distilled water) were mixed in a paper cup (700 ml) by hand mixing for 20 seconds to obtain homogeneous mixture. In the second step, PMDI was added into the mixture and mixed by mechanical stirrer at 2,000 rpm for 20 seconds. The reaction times (gel time, cream time, tack free time and rise time), rise profile and free rise density were investigated. The density of RPUR foam was measured according to ASTM D1621-04. The specimens were cut into a cubic shape with the dimensions of 3.0 x 3.0 x 3.0 cm³.

Table 1 PIR foam formulation (pbw)^a

Formulation	Catalyst	
	DMCHA	Copper-amine complexes
Polyol (Polymaxx [®] 4221)	100	100
Surfactant (Tegostab [®] B8460)	2.5	2.5
Blowing agent (H ₂ O)	3, 4	4
Gelling and blowing catalysts (DMCHA or copper-amine complexes)	0.5	0.5
Trimerization catalyst (K-15)	2, 2.5	2
PMDI (Raycore [®] B9001)	24.46 ^b , 24.52 ^c , 26.87 ^d , 26.93 ^e	26.87 ^d , 30.23 ^f

^a Parts by weight (pbw) is 1 g in 100 g of polyol

^b NCO index =160, H₂O = 3 pbw and K-15 = 2 pbw

^c NCO index =160, H₂O = 3 pbw and K-15 = 2.5 pbw

^d NCO index =160, H₂O = 4 pbw and K-15 = 2 pbw

^e NCO index =160, H₂O = 4 pbw and K-15 = 2.5 pbw

^f NCO index =180, H₂O = 4 pbw and K-15 = 2 pbw

3. Results and Discussion

3.1 Preparation of PIR foams by cup test method

The reaction time in the preparation of PIR foams were investigated, namely cream time (the time when polyol and isocyanate mixture begins to change from the liquid state to a creamy appearance and foam expansion subsequently starts), gel time (the time when polymerization occurs and the foam start to stiffen), rise time (the time when the foam reach its maximum height), tack free time (the time when the outer skin of the foam loses its stickiness or polymerization is completed). PIR foams catalyzed by copper-amine complex:K-15 were compared with those catalyzed by DMCHA:K-15, which is used commercially.

3.1.1 Preparation of PIR foams catalyzed by DMCHA:K-15

In the first step, the optimum foam formulation was investigated in DMCHA:K-15 catalyst system at the isocyanate index of 160. Two mole ratios of DMCHA:K-15, 0.5:2 and 0.5:2.5 were employed (Table 2). It was found that PIR foams prepared at these two mole ratios had similar cream time, gel time, rise time and tack free time. The amount of blowing agent (water) was varied at 3 and 4 pbw to investigate the change in PIR foam density. As the amount of water level increased, the reaction times also increased. The height of PIR foam increased and the foam density decreased. Therefore, the ratio of DMCHA:K-15 = 0.5:2 and the amount of water = 4 pbw were used in the next step.

3.1.2 Preparation of PIR foams catalyzed by copper-amine complex:K-15

Considering the PIR foams prepared from copper-amine complex:K-15 catalyst at the mole ratio of 0.5:2.0 and isocyanate index of 160 (Table 2). Both Cu(OAc)₂(en)₂:K-15 and Cu(OAc)₂(trien):K-15 gave shorter tack free time than DMCHA:K-15. These results indicate that copper-amine complex:K-15 has better gelling catalytic activity than DMCHA:K-15. Although copper-amine complex:K-15 gave shorter rise time than DMCHA:K-15, PIR foams catalyzed by copper-amine complex:K-15 had higher density than that catalyzed by DMCHA:K-15. The NCO index was increased from 160 to 180. The PIR foams prepared at NCO index = 180 had longer reaction times and density than those prepared at NCO index = 160.

3.2 Rise profile

From Figure 1, rise profile of PIR foams shows that the order of catalyst activity in blowing reaction is Cu(OAc)₂(en)₂:K-15 > Cu(OAc)₂(trien):K-15 > DMCHA:K-15. This result is in agreement with the rise time (Table 1). Cu(OAc)₂(trien):K-15 had lower reactivity than Cu(OAc)₂(en)₂:K-15 due to the steric hindrance of trien in Cu(OAc)₂(trien).

Table 2 Reaction times, density and height of PIR foams catalyzed by DMCHA or copper-amine complex:K-15

Catalysts	Mole ratio of catalysts	H ₂ O (pbw)	NCO index	Cream time (sec)	Gel time (sec)	Tack free time (sec)	Rise time (sec)	Density (kg/m ³)	Height (cm)
DMCHA:K-15	0.5:2.0	3	160	26±0.0	39±0.0	109±0.6	102±1.0	43.46±0.10	16.0±0.2
		4	160	25±0.0	39±0.0	130±0.0	115±0.6	38.47±0.51	18.9±0.1
	0.5:2.5	3	160	23±0.6	37±0.0	106±0.6	79±2.9	45.91±0.51	15.2±0.1
		4	160	23±0.0	38±0.6	114±0.6	82±0.6	37.61±0.63	18.8±0.1
Cu(OAc) ₂ (en) ₂ :K-15	0.5:2.0	4	160	28±1.0	41±1.0	87±1.5	66±0.6	44.78±0.97	17.4±0.1
			180	32±0.0	44±0.0	92±1.0	73±0.0	48.91±0.66	17.0±0.1
Cu(OAc) ₂ (trien):K-15	0.5:2.0	4	160	32±0.0	50±0.0	98±1.5	77±0.6	42.71±0.68	17.3±0.1
			180	40±0.0	68±0.6	130±0.6	104±1.2	45.64±0.75	17.7±0.1

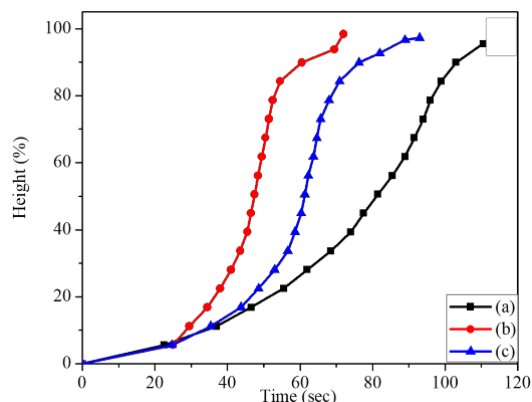


Figure 1 Rise profiles of PIR foams prepared at the NCO index = 160, H₂O = 4 pbw and catalyzed by (a) DMCHA:K-15 (100% height), (b) Cu(OAc)₂(en)₂:K-15 and (c) Cu(OAc)₂(trien):K-15 at the mole ratio of 0.5:2.0.

3.3 Isocyanate (NCO) conversion of PIR foams

Isocyanate conversion of RPUR foams was determined from the IR absorption band of the NCO group at 2277 cm⁻¹ (Figure 2) as shown in the following equation [7].

$$\text{NCO conversion (\%)} = [1 - \text{NCO}^t / \text{NCO}^i] \times 100$$

Where NCO^t is the area of isocyanate peak at time t, which is the time after the foam was kept at room temperature for 48 hours to complete the polymerization reaction and NCOⁱ is the area of the

isocyanate peak at initial time. The isocyanate peak area was normalized by the aromatic ring peak at 1595 cm⁻¹. Table 3 shows that all of PIR foams have high NCO conversion in the range 97.5-99.2%. PIR/PUR ratio was calculated from the peak area of isocyanurate and urethane at 1415 and 1220 cm⁻¹, respectively. PIR foams prepared at NCO index = 180 have higher PIR/PUR ratio than those prepared at NCO index = 160. This is because there are more NCO compounds (PMDI) to undergo trimerization to give isocyanurate groups.

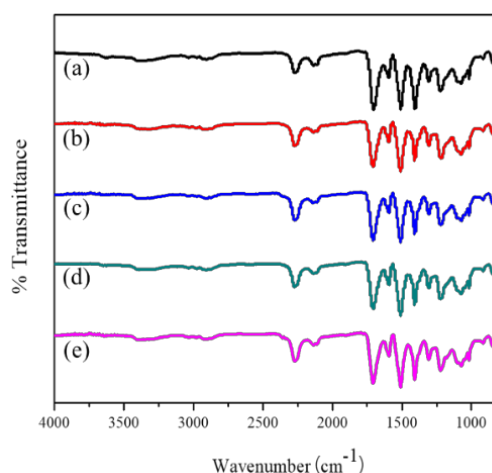


Figure 2 FTIR spectra of PIR foams: (a) DMCHA:K-15 (NCO index = 160), (b) Cu(OAc)₂(en)₂:K-15 (NCO index = 160), (c) Cu(OAc)₂(en)₂:K-15 (NCO index = 180), (d) Cu(OAc)₂(trien):K-15 (NCO index = 160), (e) Cu(OAc)₂(trien):K-15 (NCO index = 180)

Table 3 Isocyanate conversion of PIR foams catalyzed by DMCHA or copper-amine complex:K-15

Catalysts	NCO index	NCO conversion (%)	PIR/PUR ratio
DMCHA: K-15	160	99.2	0.81
Cu(OAc) ₂ (en) ₂ : K-15	160	98.5	0.80
	180	97.5	1.04
Cu(OAc) ₂ (trien) ₂ : K-15	160	98.5	0.92
	180	97.5	1.15

4. Conclusion

Good catalyst for PIR foam should give short tack free time, low density and high PIR/PUR ratio. PIR foams catalyzed by copper-amine complex:K-15 showed better gelling catalytic activity than DMCHA:K-15. When NCO index was increased, the PIR/PUR ratio also increased. The future work about modification of PIR foam formulation to obtain the required properties of PIR foam is under investigation.

Acknowledgement

The authors would like to thank IRPC Public Company Limited for supplying the chemicals used in the preparation of PIR foams.

References

- [1] Randal, D.; Lee, S. In *Huntsman polyurethanes-The polyurethanes book*; Wiley: *The United Kingdom* **2002**; Chapter 9, pp 141-145; Chapter 15, pp 229-233.
- [2] Eagels, H. W.; Pirkl, H. G.; Albers, R.; Albach, R. W.; Krause, J.; Hoffmann, A.; Casselmann, H.; Dormash, J. Polyurethanes: Versatile materials and sustainable problem solvers for today's challenges, *Angewandte Chemie International Edition* **2013**, *52*, 9422-9441.
- [3] Park, D. H.; Park, G. P.; Kim, S. H.; Kim, W. N. Effects of isocyanate index and environmentally-friendly blowing agents on the morphological, mechanical, and thermal insulating properties of

polyisocyanurate-polyurethane foams, *Macromolecular Research* **2013**, *21*, 852-859.

[4] Hu, Q.; Hong, T.; Zhou, Z.; Gao, J.; Xue, L. The effect of the trimerization catalyst on the thermal stability and the fire performance of the polyisocyanurate-polyurethane foam, *Fire and Materials* **2018**, *42*, 119-127.

[5] Silva, A. L.; Bordado, J. C. Recent developments in polyurethane catalysis: Catalytic mechanism review, *Catalysis Reviews-Science and Engineering* **2008**, *46*, 31-51.

[6] Noiasa, P. Preparation of rigid polyurethane foams catalyzed by copper-amine complexes prepared in water, Master's Thesis, Department of Chemistry, Faculty of Science, Chulalongkorn University, **2016**.

[7] Modesti, M.; Lorenzetti, A. An experimental method for evaluating isocyanate conversion and trimer formation in polyisocyanate-polyurethane foams, *European Polymer Journal* **2001**, *37*, 949-954.

Electron Beam-cured Overprint Varnish as a Green Printing

Arnunthorn Ruengpattaradet¹, Thananchai Piroonpan,¹ Anan Kempanichkul,^{1,3}
Pichayada Katemake^{1*} and Wanvimol Pasanphan^{2,3*}

¹Department of Imaging and Printing Technology, Faculty of Science, Chulalongkorn University, Bangkok10330

²Department of Materials Science, Faculty of Science, Kasetsart University, Bangkok 10900

³Center of Radiation Processing for Polymer Modification and Nanotechnology (CRPN), Department of Materials
Science, Faculty of Science, Kasetsart University, Bangkok 10900

Phone +66 2562 5555, Fax +66 2942 8290, *E-Mail: pichayada.k@chula.ac.th (P.K.) and wanvimol.p@ku.ac.th (W.P.)

Abstract

In this work, the electron beam-overprint varnish (EB-OPV) was developed as green and alternative technique for coating and curing in printing/finishing processes. Tri-propylene glycol diacrylate (TPGDA cross-linking agent) was added into epoxy acrylate main resin to obtain OPV (TPGDA: EA = 60:40). The OPV formulation was irradiated by EB with the doses of 0-50 kGy. Chemical structure of the EB-cured OPV samples were characterized by FT-IR. The gel fraction of the EB-cured OPV was determined using gravimetric measurement method. Color difference of OPV coating formula after EB curing was observed using colorimeter. In addition, the EB-OPV was coated onto three types of material substrates (i.e., polyethylene terephthalate (PET), polyvinyl chloride (PVC) and commercial photography paper) using k bar coater for controlling coating thicknesses of 4-6 micrometers and 50 micrometers. The effective dose of EB for curing were in the range of 5-30 kGy due to completed curing and no colour changing. Surface morphology of EB-OPV coated paper was observed by SEM. Cross-cut tape test (ASTM D3359) demonstrated that the EB-OPV show great surface adhesion on all material substrates. The EB-OPV showed complete curing and good surface quality as comparable with the conventional UV-OPV.

Keywords: Overprint varnish (OPV); epoxy acrylate; electron beam curing; coating

1. Introduction

Coating is a thin layer covering on the surface of an object substrate generally applied in finishing processes for decorative appearance, information, protective barrier and functionalization. The overprint varnish (OPV) is applied to an entire printed surface after printing that is a combination of oils, resins, waxes, solvents, monomer, oligomer and other materials used as to increase surface properties, for example increase of gloss for better appearance and increase of the protective barrier from abrasion and tear due to handling or contact with moisture, chemical or other potential sources of damage. Moreover, it is also referred to an overcoating applied to a printed product following printing as finished process. Overprint is applied for entire printing surface nevertheless for only partial parts of a printed surface, it

is called spot varnish. The importance property of OPV formulation is compatible with ink or other coating materials. It is important to ensure that the OPV coating process is not a cause of ink bleeding and other printing defects. The OPV coating process composes of two main steps, i.e., (i) applying liquid coatings on substrate and solidifying of coatings solution via several methods (e.g., oxidation, ultraviolet (UV) light curing, electron beam (EB) curing) depending on type of coating formulation. The coating formulation includes (i) solvent-based coatings, (ii) water-based (aqueous) coatings, (iii) oil-base coatings and (iv) radiation curable coatings. In this work, radiation curable coatings formulation is focused. In coating and printing technology, radiation is referred to UV light and high energy EB.

It is known that different application requires different type of coating processes, such as Gravure, Flexo, roller-coater, offset, and screen. For this work, EB curable coatings formulation was applied for roller-coater coating.

The OPV is mostly cured by ultraviolet (UV) light and it is called UV-OPV. The curing process is a process that transform monomer in liquid form to three-dimension network of polymer in solid form by polymerization and cross-linking reaction. UV is the one of the famous technologies for curing processes. The formulation of UV-OPV curing basically compose of resin or prepolymer, one or several reactive diluents or cross-linking agents, photo-initiators (PIs) as well as some additives. PIs is a free radical initiator generator to induce radical cross-linking polymerization reaction based on photochemistry reaction.

It is known that most of the PIs are toxic and it is able to migrate from the substrate to goods. In addition, IPs also influent to colour fading and produce fog on the printed products.

There are several issues in food safety report about PIs problem in coating and printing process, such as it has been reported that the most widely used PIs (i.e., isopropylthioxanthone, ITX) in ink, coating and adhesive applications [1]. ITX has been investigated its negative effect in vivo studies [2-4]. The Italian Competent Authorities alerted the European Commission about the detection of ITX in some baby milk and other dairy products at concentration levels in the range of about 100 - 400 ug/L. It caused the withdrawal of more than 30 million litres of milk for babies from European market. Besides, the European Food Safety Authority (EFSA) also observed the levels of ITX ranging from < 5 to 249 ug/L in fruit juices, fruit nectars, and drinks. German Research Institute also published positive finding of ITX of 405 µg/kg in TetraPack fruit juices. Without effective barrier, PIs can migrate through the package from non-food contact side to another food contact side packaging causing food contamination. Benzophenone (BP) is also one of the most common PIs, found in breakfast cereals with the concentrations up to 3728 mg/kg reported by

EFSA [5]. It has been reported that BP exhibited some evidence of carcinogenic activity in rats and mice [6] and hypospadias and allergic skin reaction [7].

Electron beam (EB) accelerator is a type of ion accelerator producing energetic electrons by electrostatic and electromagnetic fields. EB processing is an irradiation process using the accelerated electron for treating, synthesizing, modifying the materials for a variety purposes. Since the early 1980s, EB has be used for curing the OPV, called EB-OPV [8]. The EB transfer their energy to the coating compound mainly monomer or crosslinking agent. The distribution of the radicals in the matrix is a function of the electron beam energy. The high linear energy transfer (LET) of accelerated electron (150-200 keV) results in a high random concentration of free radicals in medium. Primary radiation induced chemical reaction which start a long sequence of spontaneously occurring reactions, or propagation resulting in polymerization and crosslinking. Accordingly, coating liquid is transfer solid form. The greater curing efficiency, the better conversion forming stable coating network on substrate.

Basically, EB-OPV and UV-OPV coating systems usually contain similar component, i.e., oligomer and monomer that is the binder system or reactive diluents (~60-80%), pigment (absent in clear coatings) (10 - 20%), PIs (5 - 15 %) and minor additives (5 -10%). However, EB-OPV is not necessary to have PIs in this system because of radiation-induced free radical and chemical reaction mechanism. For avoiding the toxicity problems of PIs in printing and packing industries, the EB-OPV is a technical challenge of green printing for the future. Since, cost of EB equipment has come down significantly over the last decade. Recently, the new and competitive manufacturing using EB machine and overall reliability of the curing units has significantly increased in the world. For the near future, "Green Economy" [9] that is an economy that results in improved human well-being and social equity, while significantly reducing environmental risks and ecological scarcities, is a trend to apply in many countries. Therefore, in printing and packing industry, EB curing is the touchable technology

for coating and curing in printing/finishing processes for printing and packing industries. In this work, EB-OPV formula was developed and characterized in terms of effect of EB irradiation dose on coating formulation and surface properties of commercial coated photography paper, polyethylene terephthalate (PET) and polyvinyl chloride (PVC) sheets.

2. Experimental Methods

2.1 Materials

Epoxy acrylate (EA) and tri-propylene glycol diacrylate (TPGDA) were supported by Anwill (Thailand) Co. Ltd. The chemical structures are shown in Fig. 1(A) and 1(B), respectively. The commercial graded photography paper, polyethylene terephthalate (PET) and polyvinyl chloride (PVC) sheets were supplied by Anwill (Thailand) Co. Ltd. Electron beam curing system (250 keV) in a nitrogen atmosphere is supported by National Metal and Materials Technology (MTEC), Thailand.

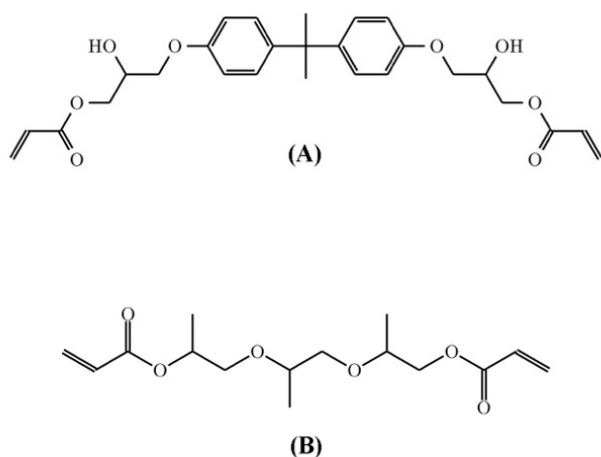


Fig. 1 Chemical structures of (A) EA and (B) TPGDA

2.2 Preparation of OPV coating

A universal popular and approved UV-OPV formula in printing industry was prepared for EB curing method. TPGDA (60% w/w) was added into EA (40%w/w) viscous solution. The TPGDA/EA was mixed and stirred to obtain homogeneous OPV coating solution. The viscosity of the OPV coating solution was measured using Brookfield Dial Viscometer. The liquid sample was irradiated using EB with the doses of 0-50 kGy. The un-

cured residue was removed in an acetone solution for 24 h. Gel fraction of the EB irradiated sample was calculated from $(W_{\text{cured}}/W_{\text{initial}}) \times 100$, W_{cured} and W_{initial} are weight of cured polymer and weight of an initial composition, respectively.

2.3 Preparation EB-OVP coated substrates

The OPV (TPGDA/EA) solution was coated onto commercial photography paper, PET and PVC sheets using k bar coater (No.1, 4-6 μm) and silk screen (No. 120, 50 μm). The coated samples were irradiated using accelerated EB with energy of 125 keV in EB curing system under nitrogen atmosphere. Similarly, pure EA and TPGDA were also coated onto the studied substrates for comparative study. Surface adhesion on all material substrates were characterized by cross-cut tape test (ASTM D3359) [10].

3. Results and Discussion

3.1 Physical appearance

The designed formula for EB curing, called EB-OPV including EA and TPGDA were irradiated with EB by varying irradiation doses of 0, 5, 10, 15, 20, 25, 30, 35, 40, 45, and 50 kGy. Fig. 2 shows gel fraction information of all EB irradiated samples after curing with different doses. It was found that gel fraction initially increased upto ~90% when the samples were irradiated only the dose of 5 kGy. The gel fractions were saturated around 90-100% after irradiation with the dose higher than 5 kGy. The result demonstrated that designed EB-OPV (TPGDA/EA), EA and TPGDA can be efficiently cured by transforming from liquid state to solidified state by EB curing process. It is known that EB curing is a process combining between free radical induced polymerization and crosslinking mechanism.

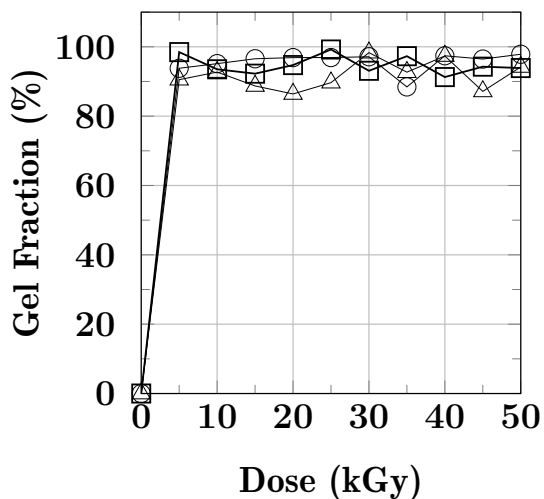


Fig 2. Gel fraction of EA (○), TPGDA (Δ) and TPGDA /EA (□)

To observe the optimum dose of EB-OPV without color change after EB curing, the colours of all irradiated EB-OPV samples were measured by numerically measured in L*a*b* colour space by Konica Minolta CR-400 colorimeter. In the colour space, L* indicates lightness (bright or dark colour), a* and b* are the chromaticity coordinates indicating colour directions; where +a* is the red direction, -a* is the green direction, +b* is the yellow direction and -b* is the blue direction. The colour difference (ΔE_{ab}) was calculated from $\Delta E_{ab} = \sqrt{(L_D^* - L_0^*)^2 + (a_D^* - a_0^*)^2 + (b_D^* - b_0^*)^2}$; where L_D^* , a_D^* , b_D^* and L_0^* , a_0^* , b_0^* are the numerical colors of the irradiated sample and without irradiation sample (liquid form).

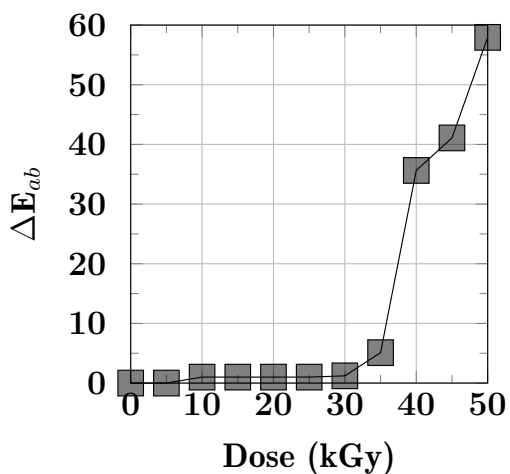


Fig. 3 Colour difference (ΔE_{ab}) of EB-OPV at different doses

Fig. 3 shows colour differences at different EB irradiation doses. The EB-OPV irradiation with the doses ranging between 5 to 35 kGy displayed transparency without colour change. On the other hand, the irradiated EB-OPV with dose over 35 kGy exhibited transparency with colour change to dark-brown depending on EB doses. Therefore, the dose of 30 kGy is an optimum EB irradiation dose for curing our EB-OPV with this EB curing system.

3.2 Morphologies

The morphologies in cross section of un-coated substrate and EB-cured OPV coated substrates, i.e, PVC, photograph paper and PET are revealed in Fig. 4. It is important to report that UV-OPV could not be strongly adhere on the surface of PVC and PET sheets. Although it could be cured into solidified coating layer, it was removed easily from the surface (data not shown). By using EB curing, EB-OPV exhibit good surface adhesion not only on paper (Fig. 4B) but also on PVC (Fig. 4A) and PET (Fig. 4C) plastic sheets.

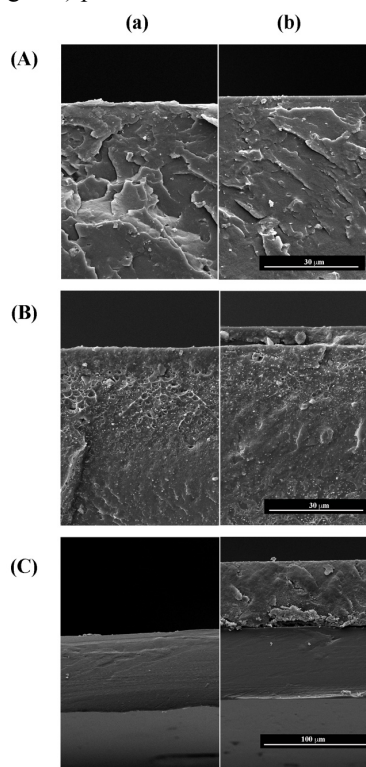


Fig. 4 SEM images of (a) uncoated and (b) coated EB-OPV on (A) PVC (k bar coater No.1) (B) photography paper (k bar coater No. 1) and (C) PET (silk screen No. 120)

The penetration range of 125 keV EB in plastics is about 250 μm and the effective depth is about 115 μm . In addition, the energy transferring of electron material behave like a “colour blind” interaction, therefore its penetration is not affected by pigments and opaque substrates.

From SEM image, the thickness of EB-OPV coating layer on PVC sheet, photograph paper and PET sheet were 4, 6 and 50 μm , respectively. EB penetrates to longer distance than all coating layers, thus it could interact not only the EB-OPV but also the surface-interface between EB-OPV and the substrates. Theoretically, free radicals are generated by energy transferring of the accelerated electrons along with their movement, thus chemical reaction are also generated via free radical along with their paths. In this case, radical-radical interaction between EB-OPV and substrate interface occurred leading to form the chemical bonding. This causes strong adhesion between EB-OPV layer and the substrate.

To confirm the performance of EB-OPV coated substrate, the adhesion property was also measured using cross-cut tape test (ASTM D3359). Classification number can be assessed from the surface of cross-cut area from which flaking has occurred. The results showed that EB-OPV coated on PVC, paper and PET is classified in No.5. It is interpreted that edges of the cuts are completely smooth; none of the squares of the lattice is detached. It can be summarized that EB-OPV effectively provide stable and strong coating on substrate.

3.3 Chemical interaction

The chemical structure or functional groups of the EB irradiated and non-irradiated samples were characterized by FT-IR (Fig. 5). For non-irradiated EA (Fig. 5A(a)), FT-IR spectra show C=C stretching at 1635 cm^{-1} of alkenes group, C-H in-plane bending at 1407 cm^{-1} , alkyl (=C-H) bending at 827 cm^{-1} , para disubstituted aromatic ring at 808 cm^{-1} , carbonyls group (C=O) at 1720 cm^{-1} , C-O and O-H stretching at 1180 and 3400 cm^{-1} , respectively. After 30 kGy EB irradiation, FTIR spectrum of cured EA (Fig. 5A(b)) shows decrease of the alkenes

group at the chain end of EA as found the disappearance of the peaks at 1635 cm^{-1} (C=C), 827 cm^{-1} (=C-H), and 1407 cm^{-1} (C-H) implying crosslinking-polymerization mechanism (curing). The FT-IR results confirm that EA was successfully cured using EB irradiation.

For non-irradiated TPDGA (Fig 5B(a)), FT-IR spectrum also shows signal of alkenes group at 1635 cm^{-1} (C=C stretching) and at 827 cm^{-1} (=C-H) as the functional end-group of TPDGA crosslinking agent. It was also observed C-H in-plane bending at 1407 cm^{-1} and ethers group at 1180 cm^{-1} from ether (C-O) stretching. The FT-IR spectrum of 30 kGy-irradiated TPDGA (Fig. 5B (b)) also shows the decrease of double bond structure as similar to the irradiated EA. The FTIR results indicated that of irradiated TPDGA confirm that TPDGA itself can be cured by EB. Both results demonstrated that EB processing can be applied for completely curing the epoxy acrylate and TPDGA.

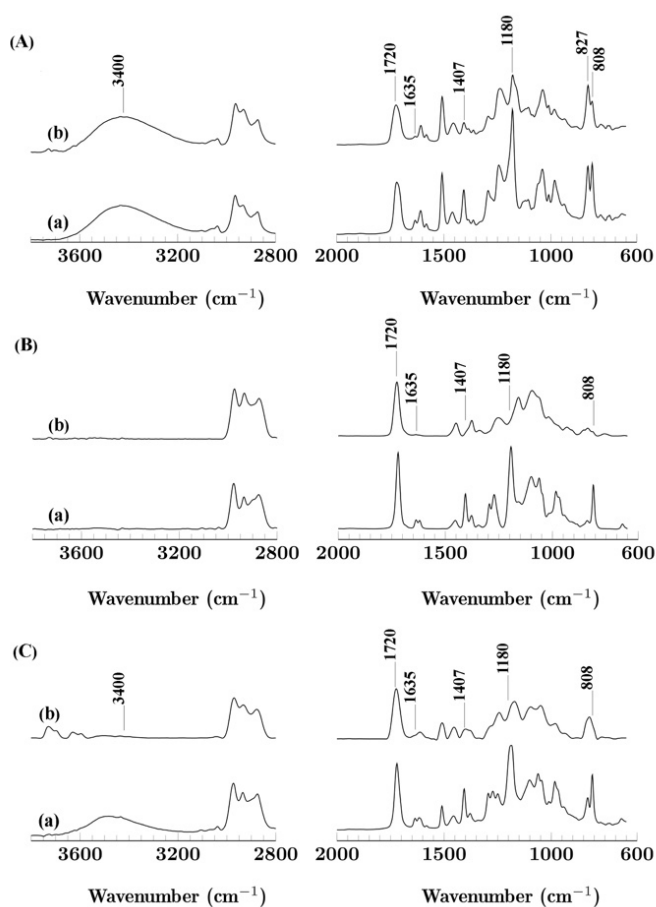


Fig. 5 FT-IR spectra of (A) EA, (B) TPDGA and (C) EA/TPDGA (a) before and (b) after EB irradiation

For TPDGA/EA formula (EB-OPV) (Fig. 5C(a)), the FTIR spectra show signals of EA and TPGDA as revealed previously. After EB irradiation (Fig. 5C(b)), the FT-IR peaks of EB-OPV around 1635 cm⁻¹ of alkenes group decreased. The peaks around 700-800 cm⁻¹ indicating the combination peak of (=C-H) in EA and TPDGA structures were changed to be a peak at 808 cm⁻¹. The result confirms the crosslinking polymerization occurred via free radical reaction.

4. Conclusion

The universal OPV formula of EA (40%) and TPGDA (60%) was proven to be used as EB-OPV. The selected EB-OPV is perfect curable by EB (125 keV) with the optimum dose of 30 kGy under nitrogen atmosphere. The color of the coating still remain transparency without yellowish formation. With EB curing process, the surface adhesion between EB-OPV and substrate can be improved because of the chemical bonding at the surface interface. The EB-OPV would be an alternative and sustainable green printing for the future printing and packaging industries.

Acknowledgement

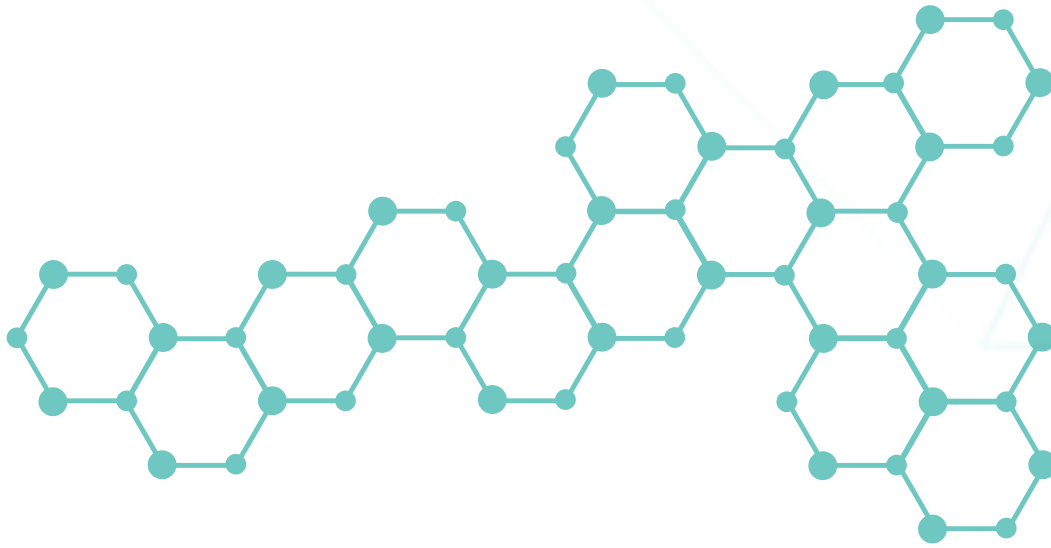
The authors gratefully acknowledge the Research and Researchers for Industries (RRI), The Thailand research fund, Thailand for grant supporting. This research is mainly supported by Technical Cooperation Project (THA1010 and THA1011), International Atomic Energy Agency (IAEA). The authors acknowledge the National Metal and Materials Technology Centre (MTEC), Ministry of Science and Technology, Thailand for supporting low energy electron beam facility.

References

- [1] C. Benetti, R. Angeletti, G. Binato, A. Biancardib, G. Biancotto, "A packaging contaminant: Isopropylthioxanthone (ITX) in dairy products", *Analytica Chimica Acta*: 32–138, 617 (2008).
- [2] G. Segratini, J. Manes, D. Giardina, Y. Picoal, "Determination of Isopropyl Thioxanthone (ITX) in Fruit Juices by Pressurized Liquid Extraction and Liquid Chromatography–Mass Spectrometry", *Journal of Agricultural and food chemistry* : 7949-7952, 54 (2006).
- [3] F. Momo, S. Fabris, R. Stevanato, "Interaction of isopropylthioxanthone with phospholipid liposomes", *Biophysical Chemistry*: 36–40, 127(2007).
- [4] A. Peijnenburg, J. Riethof-Poortman, H. Baykus, L. Portier, T. Bovee, R. Hoogenboom, "AhR-agonistic, anti-androgenic, and anti-estrogenic potencies of 2-isopropylthioxanthone (ITX) as determined by in vitro bioassays and gene expression profiling", *Toxicology in Vitro*: 1619–1628, 24 (2010).
- [5] M. Van Bossuyt, E. Van Hoeck, T. Vanhaecke, V. Rogiers, B. Mertens, "Printed paper and board food contact materials as a potential source of food contamination", *Regulatory Toxicology and Pharmacology*: 10-19, 81 (2016).
- [6] M.C. Rhodes, J.R. Bucher, J.C. Peckham, G.E. Kissling, M.R. Hejtmancik, R.S. Chhabra, "Carcinogenesis studies of benzophenone in rats and mice", *Food and Chemical Toxicology*: 843–851, 45 (2007).
- [7] Y. Zhang, Z. Du, X. Xia, Q. Guo, H. Wu, W. Yu, "Evaluation of the migration of UV-ink photoinitiators from polyethylene food packaging by supercritical fluid chromatography combined with photodiode array detector and tandem mass spectrometry", *Polymer Testing*: 276-282, 53 (2016).
- [8] M. Laksin, "Electron Beam Curing in Packaging", *RADTECH Report*: (2010).
- [9] Environment Management Group, "Working towards a Balanced and Inclusive Green Economy: A United Nations System-wide Perspective": (2011).
- [10] ASTM Designation: D 3359 – 97 Standard Test Methods for Measuring Adhesion by Tape Test.

BPLA

BIOPLASTICS AND POLYMERS FOR SUSTAINABILITY



Effect of Modified Coconut Residue Fiber on Biodegradable Composite Foam Properties

Worraphol Nansu, Sukunya Ross, Gareth Ross and Sararat Mahasaranon*

Biopolymer group, Department of Chemistry, Faculty of Science,
Naresuan University, Phitsanulok, 65000, Thailand

Research Center for Academic Excellence in petroleum, petrochemical and advanced material,
Faculty of Science, Naresuan University, Phone +66897089494; fax: +665596-3401., *E-mail: sararatm@nu.ac.th

Abstract

Environmental friendly materials are produced to solve one of the biggest waste problems from petroleum based plastic including film, food packaging foam trays, transportation packaging materials, etc. Natural resources are the main alternative materials for replacing petroleum based polymers. Cassava starch is one biodegradable material that has many advantages. In contrast, there are also some disadvantages including high moisture sensitivity, poor water resistance and brittle mechanical performance. Poor properties of starch can be improved by modifying the structure or adding a filler or other agents. Coconut residue fiber was mixed to modify the structure into the starch composite foam. Biodegradable composite foam was prepared by a compression molding technique. The following composite foam properties were measured; physical, mechanical, chemical, thermal properties and biodegradability. This research focused on the use of coconut residue fiber for improving the foam properties, the fiber was modified with monochloroacetic acid in 40%w/v NaOH solution. Biodegradable composite foam was prepared with cassava starch, modified coconut residue fiber (MCRF), coconut residue fiber (CRF), boric acid (crosslinking agent) and additives. MCRF was incorporated in 0 and 2wt% and CRF was added in 0, 2, 4, 6 and 8wt%. Results of the composite foam showed good physical and mechanical properties such as a decreased in density, high water absorption, moisture absorption, high hardness and high tensile strength with greater amounts of MCRF and CRF. Moreover, the cell size distribution of the biodegradable composite foam presented open cell, close cell structure and high thickness cell walls, with greater amounts of MCRF, CRF and crosslinking agent. This work produced biodegradable composite foam with natural resources that are low cost, environmental friendly, non toxicity and biodegradability.

Keywords: Cassava starch; Coconut residue fiber; Modified coconut residue fiber; Composite foam

1. Introduction

Commercial plastic from synthetic polymeric materials are used in a wide range of applications such as films, bottles, foam trays, transportation packaging, cushioning foams, and food packaging. These materials are one of the biggest causes of waste and are difficult to degrade under atmospheric conditions. Although, these products can be recycled, they have still great effect on the environment [1]–[4]. A lot of research has reported replacement materials in order to solve the plastic waste problem. Using renewable resources are an ideal candidate because they are environmentally friendly and non-toxic, for example, polysaccharides (starch) and natural fibers. Cassava starch is the main renewable

resource product of Thailand and can be used to produce renewable materials. However, starch has many limitations such as moisture and water sensitivity, poor mechanical properties (brittle) and retrogradation [5]–[7]. To improve the properties of starch many methods have been investigated, including filler addition, reinforcement agents, modifying starches structure, plasticizing agents and also crosslinking agents. Natural fibers are one group of raw materials used to reinforced composite materials. There are obtained from natural courses such as bamboo, kenaf, jute, ramie, sisal, cotton, flax, wood, hemp, sugarcane bagasse (SCB), cereal straws, rice straws, rice husk and coconut coir etc [2], [5], [6], [8]–[11]. The

chemical structure of fibers is similar to starch and therefore can be easily reacted with starch. Coconut residue fiber (CRF) is a waste product from coconuts after the coconut milk has been extracted. CRF has good physical properties such as being lightweight, white color, high porosity and good hydration properties [12]–[15]. This research focuses on coconut residue fiber mixed with composite foam. Coconut residue fiber modified with monochloroacetic acid and coconut residue fiber without structural modification were mixed within a cassava starch matrix. Biodegradable composite foams were produced by using a compression molding technique, with a temperature and time of 180 °C and 9 minutes, respectively. Boric acid was used as a crosslinking agent to further improve the properties of composite foam. Biodegradable composite foam can be applied in many applications as foam packaging, cushioning foam, and transportation material because of their low production cost, being environmentally friendly and also non-toxicity.

2. Experimental Methods

2.1 Materials

Commercial grade cassava starch (Biyok brand) was bought from the local supermarket. The solid waste coconut residue fiber after coconut milk extraction was obtained from a coconut shop in Phitsanulok, Thailand. Commercial grade polyvinyl alcohol from Ajax Finechem Pty Ltd., boric acid was used for a crosslinker from Fisher Scientific UK., analytical grade glycerol from Fisher Chemical Company, Mold releasing agent used was magnesium stearate from TTK Science Ltd., Sodium hydrogen carbonate in analytical grade from BP/USP, Micro pearls caustic soda 99% form AGC Chemicals Thailand, 10%w/v Sodium hypochlorite solution from TTK Science Ltd. Analytical grade monochloroacetic acid, commercial grade isopropanol, 95% Ethanol commercial grade, Analytical grade glacial acetic acid. Parallel mold plate was designed in a square shape in size of 15.0 cm x 15.0 cm with a thickness of 3.0 mm. Middle mold plate was notched for air bubble

release, during the foam baking process in the compression machine.

2.2 Coconut residue fiber preparation

Solid waste coconut residue fiber after extraction of the coconut milk was obtained from coconut milk shop, moisture was removed in a hot air oven at 60 °C for 24 hr. After that, dried coconut residue fiber was treated with 5%w/v alkali solution at 160 °C for 2 hr. Next the alkali solution was removed with distilled water until the fiber had neutral pH and bleached with 2.5%w/v sodium hypochlorite at 70 °C for 90 minutes. Afterwards it was washed with distilled water 3 times. Coconut residue fiber was then dried in a hot air oven at 60 °C for 24 hr and blended by blender machine (500w spec.) and sieved with 60 mesh sieve size.

Modified coconut residue fiber was prepared using the obtained coconut residue fiber, 10 g was put in solution mixture of isopropanol (400 mL) and 40%w/v NaOH solution (50 mL) with a stand stirrer for 30 min. Monochloroacetic acid was added into the mixture at a ratio 1:1 of fiber: monochloroacetic acid, after which it was mixed for 60 min. The solution mixture was kept in a hot oven at 60 °C for 30 min. The solid and solution phase of solution mixture was then separated. The solid phase was washed with 95% ethanol (300 mL) and the pH adjusted to neutral with glacial acetic acid. Finally, Modified coconut residue fiber was dried in a hot air oven at 60 °C overnight. [16]

2.3 Bio-composite foam preparation

Biodegradable composite foam formulations are presented in table 1. Cassava starch was mixed with coconut residue fiber (CRF) contents of 0, 2, 4, 6 and 8wt%, modified coconut residue fiber (MCRF) was varied between 0 and 2wt% by dry starch weight respectively. Also added were magnesium stearate, 5%w/v polyvinyl alcohol solution, distilled water and glycerol as a plasticizing agent. Afterwards, boric acid was added into starch mixture and finally sodium hydrogen carbonate as the blowing agent. The starch mixture was blended for 10 minutes with multi-function stand mixer (Model CK 4848 1000W CASIKO) and poured into a hot mold plate. A compression machine

which was used with a temperature at 180 °C and time of 9 minutes to obtain the final foam sheets. These biodegradable composite foam sheets were kept in a desiccator at 50% humidity for 7 days before foam characterization.

Table 1. Biodegradable composite foam formulation

Starch (g)	5% w/v PVA (g)	MCRF (g)	CRF (g)	Boric acid (g)
70.00	30.00	0	0	0.30
70.00	30.00	0	1.40	0.30
70.00	30.00	0	2.80	0.30
70.00	30.00	0	4.20	0.30
70.00	30.00	0	5.60	0.30
70.00	30.00	1.40	0	0.30
70.00	30.00	1.40	1.40	0.30
70.00	30.00	1.40	2.80	0.30
70.00	30.00	1.40	4.20	0.30
70.00	30.00	1.40	5.60	0.30

2.4 Bio-composite foam characterization

2.4.1 Coconut residue fiber and composite foam morphology

The morphology of composite foam was characterized by scanning electron microscope (SEM) model Leo1455VP, which coconut residue fiber and tensile tested composite foam specimens prepared on a sample holder with two-layer carbon tape. All of samples were heated in a hot air oven at 60 °C for removing the moisture in samples after that they were sputter coated with a thin layer of gold before testing.

2.4.2 Composite foam density

Biodegradable composite foam specimens were cut to size (2.0 x 2.0 cm) and 5 specimens of each sample tested. The samples thickness was measured by a digital vernier caliper, after which they were weighed with analytical balance. All of results were averaged to foam bulk density which was calculated using equation 1. When m is mass (g) and v is volume (cm³) of foam. [9]

$$\text{Foam density} = \frac{m}{v} \quad (1)$$

2.4.3 Moisture and water absorption

Moisture absorption testing of the biodegradable composite foams was examined using 5 samples which were cut to size (2.0 x 2.0 cm) and dried in a hot air oven at 105 °C for 2 hr to remove any moisture in composite foam. This was to obtain a constant initial weight (W_i). Composite foams were kept into a desiccator at 75% humidity during testing and the biodegradable composite foam specimens of final weights (W_f) were measured everyday for 1 month. The percentage of moisture absorption was calculated by the following equation 2. [17]

For water absorption testing of composite foam specimen preparation was similar to moisture absorption method. The biodegradable composite foam samples were dried in an oven at 105 °C, 2 hr for constant initial weight (W_i) and they were immersed in 20 mL distilled water per specimen in a covered cup. The water absorption weight was measured on 1, 2, 4, 8, 16, 24, 48 hr and 3, 5 and 7 days. The water on the surface samples were removed by blotting with tissue paper before weighing for final weight (W_f). Equation 2 was used to calculate the water absorption. [18]

$$\% \text{Moisture and water absorption} = \frac{W_f - W_i}{W_i} \times 100 \quad (2)$$

2.4.4 Tensile and Hardness testing

Biodegradable composite foam samples for tensile testing were cut to size (25 mm x 100 mm) again 5 specimens of each sample were used and followed ASTM D638M-91A for tensile testing according to ASTM 1992. The gauge length of samples were set at 50 mm and a 1kN load cell used at 0.1kN and cross ahead speed 5 mm/min. [19] Hardness testing used a shore A durometer machine. The each of sample was tested 5 times and the data was calculated for the average.

2.4.5 Biodegradation in soil

Biodegradability testing followed the previous research, biodegradable composite foam samples (5 specimens) were prepared to size (2.0 x 2.0 cm) placed in a hot air oven at 105 °C for 2 hr to remove moisture. Foam specimens were weighed with an analytical balance to obtain the first constant weight (W_0). The specimens were put into the control agricultural soil plastic box.

Time of testing was 30 days after that foam specimens were picked up from the plastic box and the soil on the surface was removed with tissue paper. The specimens were dried in an oven at 105 °C for 2 hr and weighed for final weight (W_f). The percentage of biodegradability in soil was calculated using equation 3. [20]

$$\% \text{Biodegradation} = \frac{W_o - W_f}{W_f} \times 100 \quad (3)$$

3. Results and Discussion

3.1 CRF and composite foam morphology

Coconut residue fiber morphology presented different structures, coconut residue fiber without surface treatment is depicted in Fig 1 (a) and shows hollow tube structure, which looks like a honey comb with a smooth surface. [13] Fig 1 (b) Treated coconut residue fiber (TCRF) showed different surface structure, which saw collapsed hollow tubes and rough surface and also gave a high surface area. Fig 1. (c) Modified coconut residue fiber obtained a rough structure due to the CRF being attracted by chemical reagent between carboxymethylation and modification process. Starch foam mixed with different amounts of MCRF presented different morphologies shown in Fig 2.

Starch foam was produced without MCRF in Fig 2. (a), (b) and shows small pore cell size and high wall thickness. Moreover, the starch granules were incompletely melted, while starch foam mixed with MCRF had increased cell size and decreased cell wall thickness, with greater amounts of MCRF. This is due to the increased compatibility of starch mixture as MCRF interacts with the chain ends of starch. High percentages of MCRF helped the starch granules to be able to melt completely. In Fig 2 (c), (d). Biodegradable composite foam was mixed with MCRF and CRF. CRF content was added at 0, 2, 4, 6 and 8 %wt and SEM images shown in Fig 3. Composite foam morphology presented different cell size and thickness cell wall when the composite foam was mixed with different CRF contents. Morphology of composite foam without CRF showed heterogeneous cell sizes. Mainly, it exhibited small cell size and thin cell walls. In contrast, large cell size was generated when

CRF was loaded in the starch foam matrix due to the hydration properties of CRF Fig 3 (c), (d). [13] Moreover, CRF showed a good distribution of starch in the matrix and adhesion between the fiber and starch. This is due to the chemical structure of the fiber being similar to starch (polysaccharide structure).

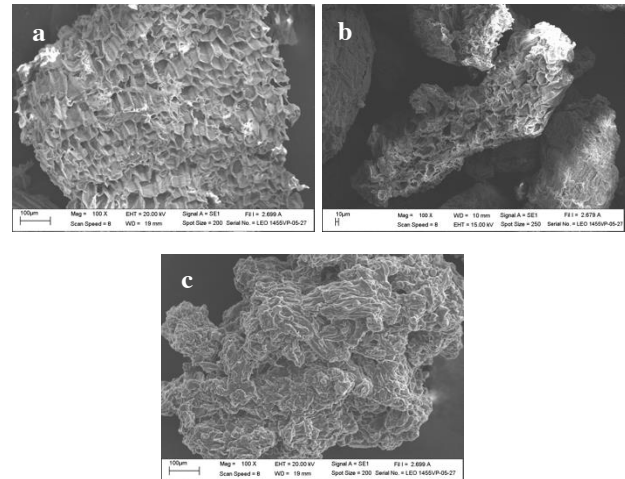


Fig 1. SEM images of coconut residue fiber at 100X magnification (a). Without treated CRF, (b). Treated CRF, (c). MCRF

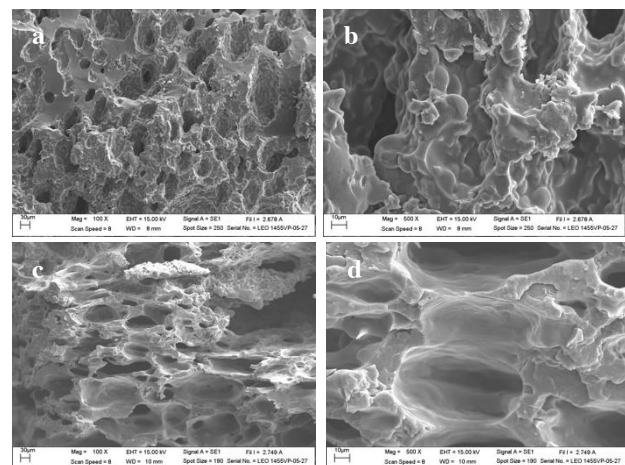


Fig 2. SEM images of composite foam (a). 0MCRF 100X, (b). 0MCRF 500X, (c). 2MCRF 100X, (d). 2MCRF 500X magnification.

3.2 Composite foam density

Composite foam density results are shown in Fig 4. The amount of MCRF affected the foam density of starch foam, as foam without MCRF showed the highest density of 0.62 g/cm³. Increasing MCRF concentration presented a decrease in density (0.49 g/cm³ at 2wt% of MCRF), due to MCRF reacting with the starch structure and decreased surface tension of starch that generated

large cell size. CRF was added in to the starch matrix influences the composite foam bulk density (Fig 4). The trend of composite foam density was to decrease slightly when the percentage of CRF increased due to high porosity of fiber and good distribution in starch matrix. when compared to the other CRF contents, 8wt% of CRF gave the lowest density of 0.39 g/cm³. However, composite foam density depended on the type of starch and filler. These have been reported in previous research including cassava starch and malt bagasse composite foam (0.415 to 0.450 g/cm³); cassava starch, cellulose and sunflower protein 0.45–0.58 g/cm³. [21]

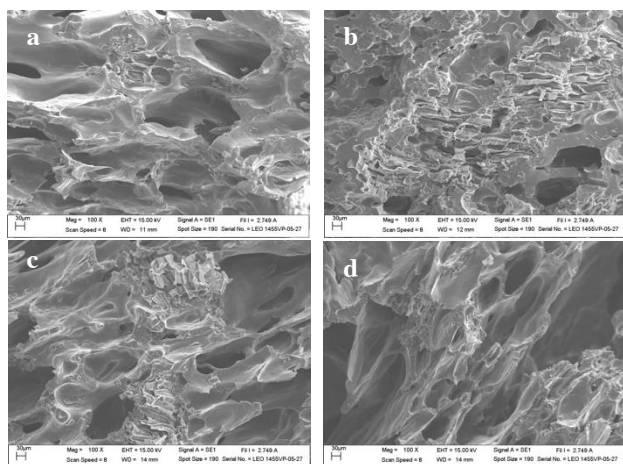


Fig 3. SEM images of composite foam mixed with 2MCRF at 100X magnification (a). 2CRF, (b). 4CRF, (c). 6CRF, (d). 8CRF.

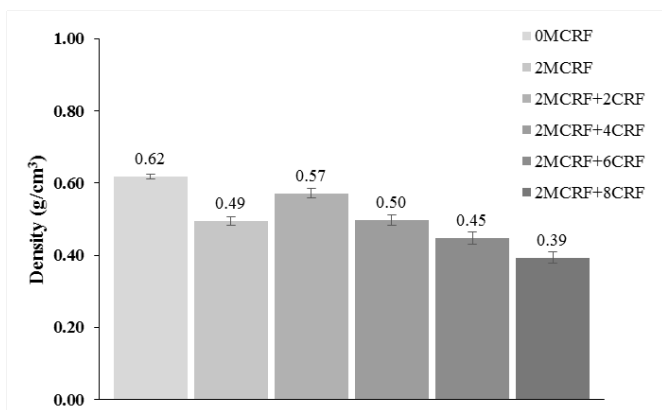


Fig 4. Composite foam density in different amount of MCRF and CRF

3.3 FTIR spectra composite foam

An infrared spectroscopic technique was used for chemical properties characterization of modified coconut residue fiber and composite foam. Fig 5 (a) shows the FTIR spectra of CRF without treatment,

treated CRF and modified CRF. The spectra show a wavelength band at 3400 cm⁻¹ which is –OH stretching group. The absorption band at 2900-2800 cm⁻¹ is methyl and methylene group. The band at 1740 cm⁻¹ is related to carbonyl group of CRF, which consisted of fatty acids in the composition of CRF. However, percentage transmittance of treated coconut residue fiber (TCRF) carbonyl peak is lower than CRF because of some removal of the coconut oil. MCRF absorption peak presented a band at 1600, 1400 and 1050 cm⁻¹ that consisted of COO–, –CH₂ and –O– group of commercial CMC which related to carboxymethylcellulose spectra. [22]–[24]

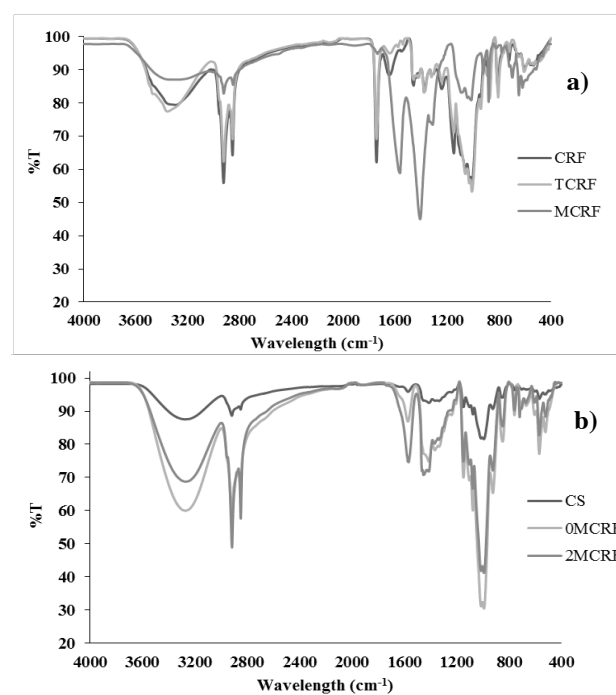


Fig 5. FTIR spectra of (a). CRF spectra and (b). Composite foam spectra

FTIR spectra of composite foam are depicted in Fig 5 (b) and shows wavelength band absorption at 3400 cm⁻¹ is –OH stretching group. The peak at 1600 cm⁻¹ is carbonyl group and 1062 cm⁻¹ (CH–O–CH₂ stretching). The carbonyl group peak disappeared in cassava starch (CS) but it was presented in composite foam and intensity of transmittance was related to MCRF content.

3.4 Moisture and water absorption

Moisture absorption was observed under control conditions with different amounts of MCRF that affected the moisture absorption of the composite foam. Fig 6 (a)

shows the moisture absorption of the composite foam and found the composite foam prepared with 2wt% of MCRF had high moisture absorption in the first week until to third week after that it rapidly increased in the final week. In contrast, composite foam prepared without MCRF showed low moisture absorption when compared with 2wt% MCRF composite foam. After the first week, the composite foam without MCRF rapidly absorbed moisture. These results are related to the hydrophilic character of starch and high surface area of starch, which was opposite to 2wt% MCRF foam that had strong interactions and low surface area. CRF was mixed into starch composite foam at different concentrations and showed the least different moisture absorption result due to CRF being embedded in the starch matrix with strong interactions, therefore, the moisture was hardly attracted to starch.

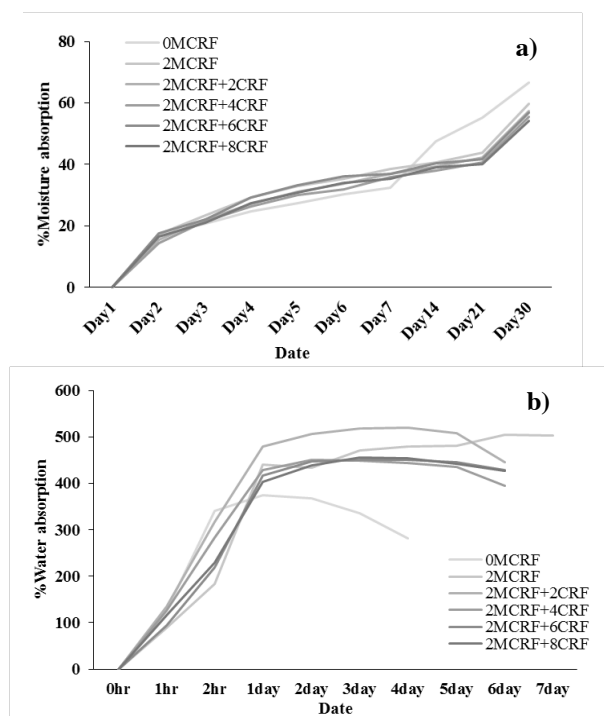


Fig 6. (a). Moisture absorption (b). Water absorption of composite foam

Water absorption of the composite foam was observed, and the results shown in Fig 6 (b). Composite foam without MCRF gave rapid water absorption in the initial time period and the highest water absorption was 375.4 6% at day 1, when the time passed to day 4, the composite foam had broken. This is due to weak interactions and starch granules being incompletely

melted, which means water can easily move into the starch structure. On the other hand, when composite foam was mixed with MCRF, the results showed that the water was slowly absorbed when compared to the composite foam without MCRF because MCRF can easily dissolve in the water and also there is good interactions between starch and MCRF. This means the composite foam with MCRF shows higher stability in water. However, composite foam still broke when it was tested for 7 days and showed the highest absorption of 504.63% at day 6.

CRF was added into the composite foam and affected the water absorption. The results showed high water absorption with increasing CRF concentration. After 1 day, the percentage of water absorption was consistent; the composite foam mixed with CRF broke after 6 days of testing. However, when the composite foam was mixed with CRF, it had a high percentage of water absorption but had less stability than composite foam without CRF.

3.5 Mechanical properties

Hardness of composite foam was characterized using a shore A durometer machine. The results are presented in Fig 7 and show the different hardness properties related to percentage of MCRF added. Composite foam without MCRF showed a hardness value lower than 2wt% MCRF, 26.83 and 37.64, respectively. MCRF is strongly bonded with starch and the starch granules are completely melted in foaming process that was shown in the SEM image in Fig 2 (d). Furthermore, added CRF influenced the hardness property of composite foam showed that the tendency of hardness increased with increased CRF concentration because CRF embedded and well distributed in the starch matrix. Moreover, the base chemical structure of CRF is similar to starch providing good adhesion between the two phases. However, the highest concentration of CRF produced a slightly decreased hardness value due to CRF generating large pore cell sizes in the foam and decreased the interactions between CRF and matrix phase.

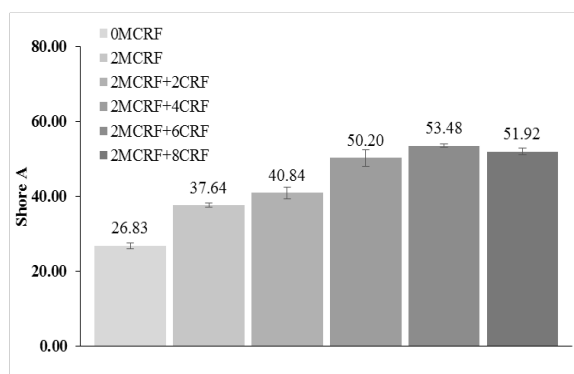


Fig 7. Hardness properties of composite foam

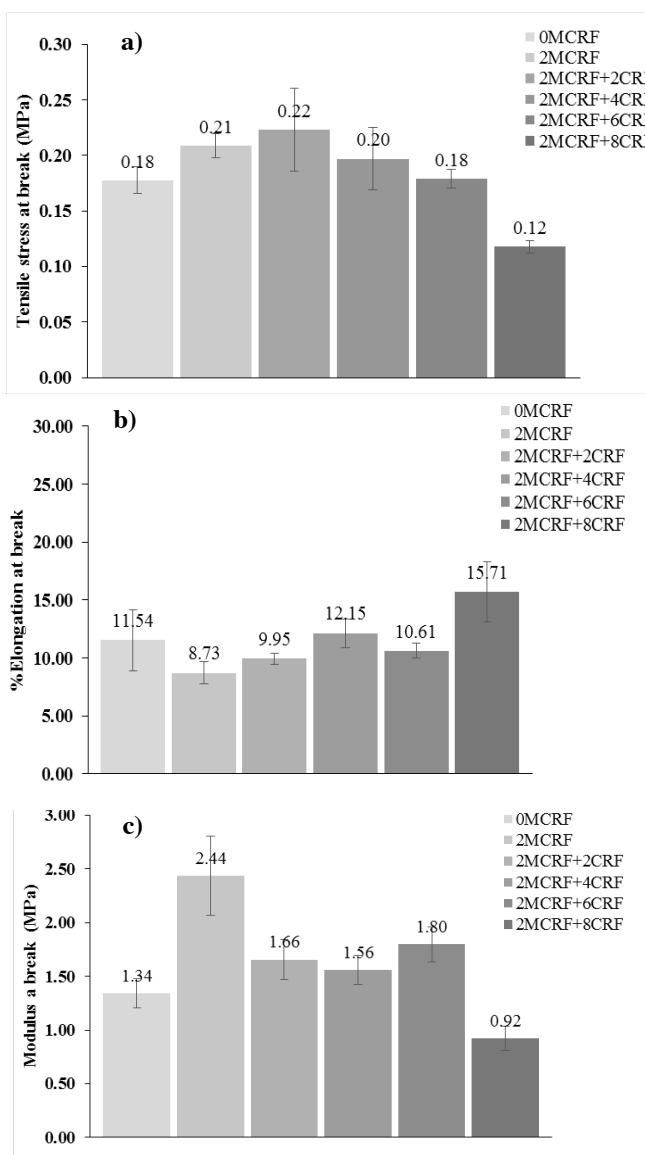


Fig 8. Tensile properties of composite foam (a). Tensile strength (b). %Elongation at break (c). Modulus at break

Tensile testing of the composite foam followed ASTM D638M-91A. Composite foam produced without MCRF and mixed with 2wt% MCRF presented different

tensile strength, Fig 8 (a) without MCRF composite had a 0.18MPa, which was lower than 2wt% MCRF composite (0.21MPa) due to MCRF reacting with the starch structure and having a homogenous phase. Moreover, greater CRF content increased the strength of composite foam but when CRF was mixed at high concentrations the strength decreased because of high porosity in the foam structure. Moreover, composite foam produced with MCRF and CRF showed decreased tensile modulus at break similar to tensile strength trends that was related to plasticizer affected of moisture in the foam matrix (Fig 8 (c)). On the other hand, in Fig 8 (b) the elongation at break tendency of composite foam slightly increased with increasing CRF contents because of the high adhesion force between the starch matrix and CRF, which was observed in the SEM data. Moreover, the moisture was rapidly absorbed by CRF, this moisture is attracted to starch structure and acts as a plasticizer.

3.6 Biodegradability

Biodegradability of the composite foam was tested via examining the biodegradation in soil. Fig 9 shows the degradation results obtained. Composite foam without MCRF had the lowest biodegradation (22.51%). When the CRF amount was increased, a corresponding increase in biodegradation of composite foam was also seen. CRF was added into the starch foam at 2, 4, 6 and 8wt%, and these contents gave degradation results of 24.74, 26.72, 28.20 and 35.30% respectively. Composite foam was produced with higher CRF content showed rapid degradation because the CRF can be easily degraded by bacterial and fungi in the present in the soil.

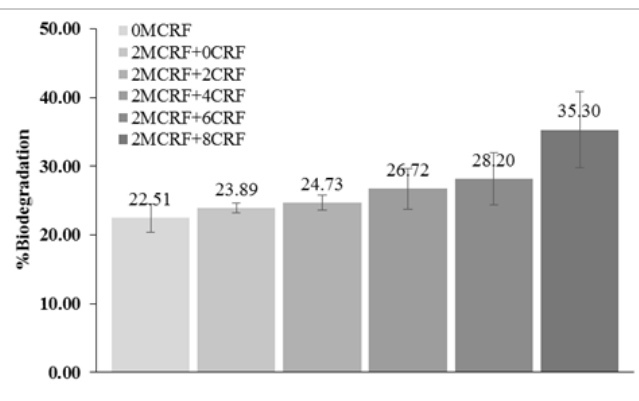


Fig 9. Biodegradation in soil of composite foam

4. Conclusion

Coconut residue fiber is the one of most plentiful natural fibers and can be easily obtained across Thailand from coconut milk shops. The chemical structure of CRF used in this research was modified before addition into cassava starch foam. This biodegradable composite foam was prepared via a baking process with hot mold hydraulic press. The results showed that addition of the fiber into the biodegradable composite foam improved the physical, mechanical, chemical properties and as well as the biodegradability. The morphology of CRF was characterized by SEM that showed the improved structure obtained. CRF had a structure similar to honey combs, with high porosity and a white color. Composite foam was mixed with MCRF and CRF and showed good morphology, strong interactions between starch, MCRF and CRF phases. Moreover, increased content MCRF fully melted in starch matrix, which was confirmed by FTIR spectra due to the starch and fiber had the similar chemical composition. Mechanical properties were improved when MCRF and CRF were added in starch matrix. Biodegradation in soil of composite foam has faster degradation with higher percentage of CRF. However, composite foam can displace synthetic petroleum materials because it had low cost and environmental friendly. Moreover, it can be widely used applications including foam tray for food packaging, transportation protection, insulating material and cushioning foam.

Acknowledgement

The authors wish to thank Naresuan University for the financial support. We thank science lab center for the instrument analysis, Science achievement scholarship of Thailand (SAST) and research center for academic excellence in petroleum, petrochemical and advanced material.

References

- [1] B. F. Bergel, L. M. da Luz, and R. M. C. Santana, "Comparative study of the influence of chitosan as coating of thermoplastic starch foam from potato, cassava and corn starch," *Prog. Org. Coatings*, vol. 106, pp. 27–32, 2017.
- [2] K. Pornsuksomboon, B. B. Holló, K. M. Szécsényi, and K. Kaewtatip, "Properties of baked foams from citric acid modified cassava starch and native cassava starch blends," *Carbohydr. Polym.*, vol. 136, pp. 107–112, 2016.
- [3] A. Boonchaisuriya and J. Chungsiriporn, "Biodegradable foams based on cassava starch by compression," *5th PSu-UNS Int. Conf. Eng. Technol.*, pp. 71–74, 2011.
- [4] N. Soykeabkaew, C. Thanomsilp, and O. Suwanton, "A review: Starch-based composite foams," *Compos. Part A Appl. Sci. Manuf.*, vol. 78, pp. 246–263, 2015.
- [5] A. Edhirej, S. M. Sapuan, M. Jawaid, and N. I. Zahari, "Cassava/sugar palm fiber reinforced cassava starch hybrid composites: Physical, thermal and structural properties," *Int. J. Biol. Macromol.*, vol. 101, pp. 75–83, 2017.
- [6] K. Kaewtatip, M. Pongroi, B. Holló, and K. Mészáros Szécsényi, "Effects of starch types on the properties of baked starch foams," *J. Therm. Anal. Calorim.*, vol. 115, no. 1, 2014.
- [7] F. Debiagi, R. K. T. Kobayashi, G. Nakazato, L. A. Panagio, and S. Mali, "Biodegradable active packaging based on cassava bagasse, polyvinyl alcohol and essential oils," *Ind. Crops Prod.*, vol. 52, 2014.
- [8] M. G. Lomelí Ramírez, K. G. Satyanarayana, S. Iwakiri, G. B. De Muniz, V. Tanobe, and T. S. Flores-Sahagun, "Study of the properties of biocomposites. Part I. Cassava starch-green coir fibers from Brazil," *Carbohydr. Polym.*, vol. 86, no. 4, pp. 1712–1722, 2011.
- [9] N. Soykeabkaew, P. Supaphol, and R. Rujiravanit, "Preparation and characterization of jute-and flax-reinforced starch-based composite foams," *Carbohydr. Polym.*, vol. 58, no. 1, pp. 53–63, 2004.
- [10] T. E. Motaung and R. D. Anandjiwala, "Effect of alkali and acid treatment on thermal degradation

- kinetics of sugar cane bagasse,” *Ind. Crops Prod.*, vol. 74, pp. 472–477, 2015.
- [11] L. R. P. F. Mello and S. Mali, “Use of malt bagasse to produce biodegradable baked foams made from cassava starch,” *Ind. Crops Prod.*, vol. 55, pp. 187–193, 2014.
- [12] S. Sulaiman, A. R. Abdul Aziz, and M. Kheireddine Aroua, “Optimization and modeling of extraction of solid coconut waste oil,” *J. Food Eng.*, vol. 114, no. 2, pp. 228–234, 2013.
- [13] S. N. Raghavendra, S. R. Ramachandra Swamy, N. K. Rastogi, K. S. M. S. Raghavarao, S. Kumar, and R. N. Tharanathan, “Grinding characteristics and hydration properties of coconut residue: A source of dietary fiber,” *J. Food Eng.*, vol. 72, no. 3, pp. 281–286, 2006.
- [14] T. P. Trinidad *et al.*, “Dietary fiber from coconut flour: A functional food,” *Innov. Food Sci. Emerg. Technol.*, vol. 7, no. 4, pp. 309–317, 2006.
- [15] S. N. Raghavendra, N. K. Rastogi, K. S. M. S. Raghavarao, and R. N. Tharanathan, “Dietary fiber from coconut residue: Effects of different treatments and particle size on the hydration properties,” *Eur. Food Res. Technol.*, vol. 218, no. 6, pp. 563–567, 2004.
- [16] P. Rachtanapun, S. Luangkamin, K. Tanprasert, and R. Suriyatem, “Carboxymethyl cellulose film from durian rind,” *LWT - Food Sci. Technol.*, vol. 48, no. 1, pp. 52–58, 2012.
- [17] W. Sanhawong, P. Banhalee, S. Boonsang, and S. Kaewpirom, “Effect of concentrated natural rubber latex on the properties and degradation behavior of cotton-fiber-reinforced cassava starch biofoam,” *Ind. Crops Prod.*, vol. 108, no. July, pp. 756–766, 2017.
- [18] R. L. Shogren, J. W. Lawton, and K. F. Tiefenbacher, “Baked starch foams: Starch modifications and additives improve process parameters, structure and properties,” *Ind. Crops Prod.*, vol. 16, no. 1, pp. 69–79, 2002.
- [19] M. K. Uslu and S. Polat, “Effects of glyoxal cross-linking on baked starch foam,” *Carbohydr. Polym.*, vol. 87, no. 3, pp. 1994–1999, 2012.
- [20] S. Mali, F. Debiagi, M. V. E. Grossmann, and F. Yamashita, “Starch, sugarcane bagasse fibre, and polyvinyl alcohol effects on extruded foam properties: A mixture design approach,” *Ind. Crops Prod.*, vol. 32, no. 3, pp. 353–359, 2010.
- [21] N. Soykeabkaew, C. Thanomsilp, and O. Suwantong, “A review: Starch-based composite foams,” *Compos. Part A Appl. Sci. Manuf.*, vol. 78, pp. 246–263, 2015.
- [22] V. Pushpamalar, S. J. Langford, M. Ahmad, and Y. Y. Lim, “Optimization of reaction conditions for preparing carboxymethyl cellulose from sago waste,” *Carbohydr. Polym.*, vol. 64, no. 2, pp. 312–318, 2006.
- [23] P. Rachtanapun and R. Suriyatem, “Value Added of Durian Husks: Synthesis of Carboxymethyl Cellulose from Durian Husk,” *Dep. Packag. Technol.*, p. 55, 2009.
- [24] A. H. Saputra, M. Hapsari, and A. B. Pitaloka, “Synthesis and Characterization of CMC from Water Hyacinth Cellulose Using Isobutyl-Isopropyl Alcohol Mixture as Reaction Medium,” *Contemp. Eng. Sci.*, vol. 8, no. 33, pp. 1571–1582, 2015.

Preparation of Nanocrystalline Cellulose by Using Eco-Friendly Green Solvent as Pre-Treatment

Gan Pei Gie^{1*}, Sam Sung Ting¹ and Muhammad Faiq bin Abdullah¹

¹ School of Bioprocess Engineering, Universiti Malaysia Perlis (UniMAP), Kompleks Pusat Pengajian Jejawi 3, 02600 Arau, Perlis, Malaysia.

*E-Mail: peigie023@gmail.com

Abstract

The objective of the present research was to isolate the NCC from EFB using DES pre-treatment. Nanocrystalline cellulose (NCC) was successfully isolated from oil palm empty fruit bunch (EFB), a major by-product biomass generated by oil palm industry, by sulphuric acid hydrolysis preceded by deep eutectic solvent treatment and bleaching. Field emission scanning electron microscopy (FESEM) of treated EFB cellulose showed individualized fibers indicating the removal of unwanted impurities such as lignin and hemicellulose from the raw EFB fibers. The average diameter of NCC is less than 20nm. The samples were also characterized by X-ray diffraction (XRD). The raw EFB, treated cellulose and NCC showed a crystallinity of 38.7%, 52.2% and 65.3%, respectively. FTIR results showed that the lignin and hemicellulose were successfully removed after chemical pre-treatment. Therefore, NCC obtained from EFB has great potential to be used as reinforcing agent in the manufacturing of nanocomposites.

Keywords: Nanocrystalline Cellulose, Green Solvent and Acid Hydrolysis

1. Introduction

Oil palm empty fruit bunch (EFB) is a natural fibre which has great relevance to Malaysia, as a great amount of biomass is produced by oil palm industry [1]. For every one ton of processed oil palm fresh fruit bunch, 0.23 ton of EFB will be produced [2]. In Malaysia, around 17 million tons of EFB is produced annually [3]. However, EFB (consists of 44.2% cellulose, 33.5% hemicellulose and 20.4% lignin) is still considered an under-utilized resource [4]. Therefore, there is a growing interest in utilizing EFB as a value-added product due to its high cellulose content, low cost and abundant source.

Nanocrystalline cellulose (NCC) has gained significant interest due to its unique and attractive characteristics such as high aspect ratio, low density, low thermal expansion and remarkable mechanical properties [5]. It has a relatively high aspect ratio with a diameter of 2–20 nanometers and lengths of 100

nanometers to several micrometers [6]. NCC can be isolated from various lignocellulosic materials by different isolation methods. Among these isolation techniques, sulphuric acid hydrolysis is the most common method for the preparation of NCC [7]. Under strong acid conditions, the amorphous domains of cellulose are hydrolysed as they are more susceptible to be attacked by acids in contrast to crystalline domains [8]. Furthermore, sulphuric acid hydrolysed NCC also exhibited a more stable dispersion compared to other acids. This is due to the grafting of sulphate group on the surface of NCC which provides a repulsive force stabilizing the NCC suspension [9]. Studies have been conducted on the isolation of NCC from the various natural fibers using acid hydrolysis. For instance, [10] successfully isolated the NCC from EFB using acid hydrolysis. The obtained NCC showed a diameter ranged from 4-15 nanometers.

The transformation of EFB fibres into NCC by acid hydrolysis preceded by deep eutectic solvent (DES) as pre-treatment was attempted. Sheltami et al. [11] isolated the treated cellulose by carrying out alkali and bleaching treatment. Same method was also employed by Ching and Ng [12] for extracting the treated cellulose. However, to the best of our knowledge, there is no attempt in using DES as pre-treatment in producing NCC yet. DES used in this research as the pre-treatment solvent is an attempt to produce biodegradable, recyclable and environmentally friendly solvent, to isolate the valuable components from EFB [13]. The morphological transformation of the samples was observed with field emission scanning electron microscopy (FESEM). The crystallinity index of cellulose samples was determined using X-ray diffraction (XRD).

2. Experimental Methods

2.1 Materials

EFB fibres were supplied by Taclico Company Sdn. Bhd. Sodium chlorite, sodium hydroxide and acetic acid were purchased from Sigma–Aldrich while glycerol and sulphuric acid were purchased from Merck. Potassium carbonate was purchased from HmbG.

2.2 Preparation of EFB Fibres

EFB was cleaned using tap water to wash off the impurities such as dust and sand from the fibres surface. The cleaned fibres were dried in the oven at 60°C for 24 hours. The dried fibres were ground and sieved through a 125µm sieve mesh.

2.3 Synthesis of Deep Eutectic Solvent (DES)

DES was prepared by mixing potassium carbonate and glycerol at a molar ratio of 1:7. DES mixture was heated at 80°C for 2 hours until a homogenous transparent liquid was formed. The DES was stored in the desiccator with silica gel for further use.

2.4 Preparation of Cellulose from EFB Fibres

Raw EFB fibre was added into DES mixture and heated at 80°C for 2 hours. The DES-treated

fibre was washed continuously with distilled water until a neutral pH was obtained. Bleaching of EFB fibres was also performed at 80 °C for 2 hours. Both DES treatment and bleaching were repeated thrice in order to remove the hemicellulose and lignin. The cellulose was then dried at 50°C for 24 hours and stored in the drying cabinet.

2.5 Preparation of NCC by acid hydrolysis

Acid hydrolysis was performed using 64 wt% sulphuric acids at 45 °C for 45 minutes with strong agitation. The ratio of obtained cellulose to sulphuric acid solution was set as 1:20. The hydrolysis was terminated by adding iced distilled water. The suspension was centrifuged at 8,000 rpm for 10 minutes at 20°C. The resulting suspension was sonicated for 10 minutes in water bath sonicator before refrigerated for further use.

3. Characterization

3.1 Field emission scanning electron microscopy (FESEM)

The morphological characteristics of EFB cellulose and NCC was investigated using NOVA NANOSEM 450. The sonicated NCC dispersion was dropped onto a sample holder and dried at room temperature. Prior to the examination, the samples were sputter coated with platinum. Images were acquired by using an accelerated voltage of 5 kV. The average cellulose diameter was measured using Image J (Version 1.37, National Institutes of Health, Bethesda, MD, USA, 2015).

3.2 X-ray diffraction (XRD)

A desktop D2 Phaser X-ray diffractometer (Bruker Corporation, USA) was employed to examine the crystallinity index of cellulose samples and NCC obtained from EFB at 40 kV and 30 mA. Data were collected in a 2θ angle between 5 and 40°. The crystallinity index was calculated using equation below [14]:

$$CI = \frac{I_{002} - I_{AM}}{I_{002}} \times 100\% \quad (1)$$

Where I_{002} is the maximum peak intensity for the crystalline region and I_{AM} is the minimum peak

intensity for the amorphous region.

3.3 Fourier transform infrared (FTIR) spectroscopy

FTIR Spectra were carried out for raw EFB fiber, treated cellulose and NCC using Perkin-Elmer Model Series 2. Samples were analyzed using KBr technique with a wavenumber of 4000 to 450 cm^{-1} at a resolution of 4 cm^{-1} .

4. Results and Discussion

4.1 Field emission scanning electron microscopy (FESEM)

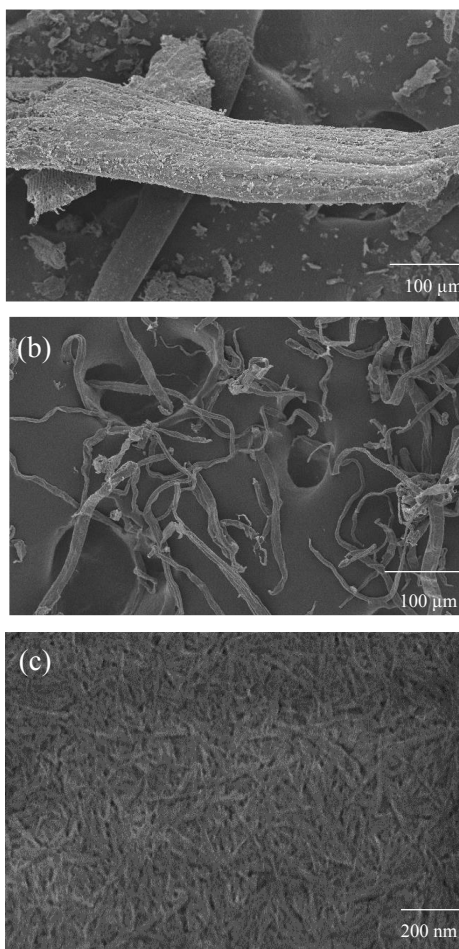


Figure 1: FESEM micrographs of EFB (a) raw fibre, (b) treated cellulose and (c) NCC

The FESEM micrographs of raw EFB fibre, treated cellulose and NCC was illustrated in Figure 1. Figure 1 (a) shows the surface of original ground EFB fibres which consisting packs of microfibrils with the deposition of non-cellulosic compounds such as lignin, wax, pectin and hemicellulose [15]. However, it could be noticed that after the pre-treatment the surface of cellulose became roughened

and unordered as shown in Figure 1 (b). The individualised fibres indicated that the lignin and hemicellulose were removed extensively by DES treatment and bleaching [16]. Figure 1 (c) exhibited the morphology of rod-like shape NCC with an average diameter of less than 20 nanometres. The aggregation of NCC could be observed in the micrograph. It could result by the water evaporation step during sample preparation, drying method and also the strong hydrogen bonding between NCC [17].

4.2 X-ray diffraction (XRD)

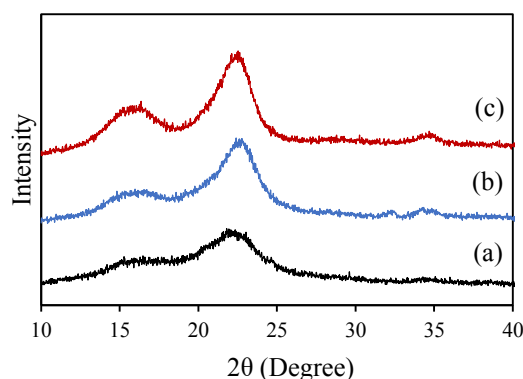


Figure 2: X-ray diffractogram of EFB (a) raw fibre, (b) treated cellulose and (c) NCC

XRD analysis was performed to evaluate the crystallinity of the EFB fibres after various chemical treatments. XRD patterns of raw EFB fibres, treated cellulose and NCC were shown in Figure 2. All diffractograms showed peaks around 16°, 22.5° and 34° 2θ angles attributed to the diffraction planes of (101), (002) and (040) respectively and indicated to be the crystal lattice of cellulose type I [8]. The peak intensity of (002) plane increased extensively after the chemical treatments. This showed that the cellulose became more crystalline due to the removal of amorphous structure such as hemicellulose and lignin [18].

Table 1: Percentage of Crystallinity of Cellulose Samples

Samples	Crystallinity Index (%)
Raw Fibre	38.7
Treated Cellulose	52.2
NCC	65.3

The crystallinity values of cellulose samples are tabulated in Table 1. From Table 1, it was clear that the crystallinity of NCC was significantly enhanced compared to raw EFB fibres. The sulphuric acid hydrolysis treatment applied to prepare NCC selectively hydrolysed the amorphous domains surrounding and embedding the cellulose but leaving the crystalline segments intact, hence, the crystallinity of NCC increased [15].

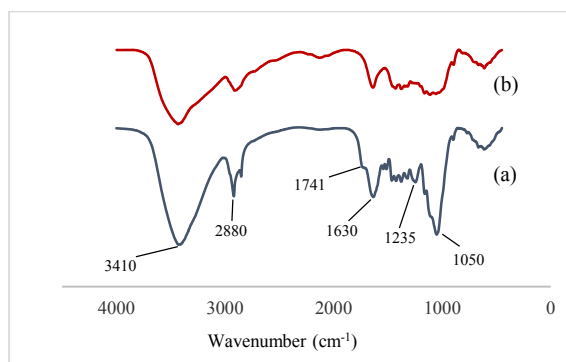


Figure 3: FTIR Spectra of EFB (a) raw fibre and (b) NCC

4.3 Fourier transform infrared (FTIR) spectroscopy

FTIR spectra of samples raw EFB fibres and NCC was displayed in Figure 3. FTIR spectra for raw fibres and NCC showed a peak at 3410 cm^{-1} was dominated to the stretching vibration of -OH groups whereas the peak at 2880 cm^{-1} was related to the C-H stretching vibration [19]. The band at 1741 cm^{-1} in the spectra was corresponding to the raw fibres was associated to the C=O stretching of acetyl group, which is a characteristic group of hemicellulose [20]. This group disappeared in NCC which proved the removal of hemicellulose after chemical pre-treatment. The band at 1630 cm^{-1} was attributed to the OH group of absorbed water by cellulose sample [20]. The peak at 1245 cm^{-1} could be assigned to the C-O-C of aryl-alkyl ether in lignin. The peak disappeared in NCC which suggested the removal of lignin [11]. Peak at 1050 cm^{-1} was assigned to the C-O stretching vibration.

5. Conclusion

NCC was successfully prepared by acid hydrolysis from the EFB fibres. DES treatment and

bleaching had effectively removed the non-cellulosic constituents of EFB. The average diameter of NCC produced was less than 20 nm. Crystallinity of raw EFB fibre, treated cellulose and NCC were 38.7%, 52.2% and 65.3% respectively. FTIR results revealed that the lignin and hemicellulose were successfully removed.

References

- [1] N. Razali *et al.*, "Influence of acid hydrolysis reaction time on the isolation of cellulose nanowhiskers from oil palm empty fruit bunch microcrystalline cellulose," *BioResources*, vol. 12, no. 3, pp. 6773–6788, 2017.
- [2] A. Abdulrazik, M. Elsholkami, A. Elkamel, and L. Simon, "Multi-products productions from Malaysian oil palm empty fruit bunch (EFB): Analyzing economic potentials from the optimal biomass supply chain," *J. Clean. Prod.*, vol. 168, pp. 131–148, 2017.
- [3] R. A. Bakar, S. Z. Darius, S. Kulaseharan, and N. Jamaluddin, "Effects of ten year application of empty fruit bunches in an oil palm plantation on soil chemical properties," *Nutr. Cycl. Agroecosystems*, vol. 89, no. 3, pp. 341–349, 2011.
- [4] W. T. Owi, H. Lin, S. T. Sam, H. Chia, and S. Zakaria, "Comparative Study of Microcelluloses Isolated From Two Different Biomasses with Commercial Cellulose," *BioResources*, vol. 11, no. 2, pp. 3453–3465, 2016.
- [5] X. Yang *et al.*, "Effects of preparation methods on the morphology and properties of nanocellulose (NC) extracted from corn husk," *Ind. Crops Prod.*, vol. 109, no. August, pp. 241–247, 2017.
- [6] H.-M. Ng *et al.*, "Extraction of cellulose nanocrystals from plant sources for application as reinforcing agent in polymers," *Compos. Part B Eng.*, vol. 75, pp. 176–200, 2015.
- [7] P. P. Zhang *et al.*, "Effects of acid treatments

- on bamboo cellulose nanocrystals,” *Asia-Pacific J. Chem. Eng.*, vol. 9, pp. 686–695, 2014.
- [8] F. Kallel, F. Bettaieb, R. Khiari, A. Garcia, J. Bras, and S. E. Chaabouni, “Isolation and structural characterization of cellulose nanocrystals extracted from garlic straw residues,” *Ind. Crops Prod.*, vol. 87, pp. 287–296, 2016.
- [9] C. D. Jayaweera, D. W. T. S. Karunaratne, S. T. S. Bandara, and S. Walpalage, “Investigation of the effectiveness of nanocellulose extracted from Sri Lankan Kapok, as a filler in Polypropylene polymer matrix,” *3rd Int. Moratuwa Eng. Res. Conf. MERCon 2017*, pp. 1–6, 2017.
- [10] N. S. Lani, N. Ngadi, A. Johari, and M. Jusoh, “Isolation, Characterization, and Application of Nanocellulose from Oil Palm Empty Fruit Bunch Fiber as Nanocomposites,” *J. Nanomater.*, vol. 2014, 2014.
- [11] R. M. Sheltami, I. Abdullah, I. Ahmad, A. Dufresne, and H. Kargarzadeh, “Extraction of cellulose nanocrystals from mengkuang leaves (*Pandanus tectorius*),” *Carbohydr. Polym.*, vol. 88, no. 2, pp. 772–779, 2012.
- [12] Y. C. Ching and T. S. Ng, “Effect of preparation conditions on cellulose from oil palm empty fruit bunch fiber,” *BioResources*, vol. 9, no. 4, pp. 6373–6385, 2014.
- [13] J. A. Sirviö, M. Visanko, and H. Liimatainen, “Deep eutectic solvent system based on choline chloride-urea as a pre-treatment for nanofibrillation of wood cellulose,” *Green Chem.*, vol. 17, no. 6, pp. 3401–3406, 2015.
- [14] M. Mariño, L. Lopes da Silva, N. Durán, and L. Tasic, “Enhanced materials from nature: nanocellulose from citrus waste,” *Molecules*, vol. 20, no. 4, pp. 5908–23, 2015.
- [15] M. Rahimi Kord Sofla, R. J. Brown, T. Tsuzuki, and T. J. Rainey, “A comparison of cellulose nanocrystals and cellulose nanofibres extracted from bagasse using acid and ball milling methods,” *Adv. Nat. Sci. Nanosci. Nanotechnol.*, vol. 7, no. 3, 2016.
- [16] C. W. Zhang, S. Q. Xia, and P. S. Ma, “Facile pretreatment of lignocellulosic biomass using deep eutectic solvents,” *Bioresour. Technol.*, vol. 219, pp. 1–5, 2016.
- [17] P. G. Gan, S. T. Sam, M. F. Abdullah, N. N. Zulkepli, and Y. F. Yeong, “Characterization of Nanocrystalline Cellulose Isolated from Empty Fruit Bunch Using Acid Hydrolysis,” *Solid State Phenom.*, vol. 264, pp. 9–12, 2017.
- [18] M. S. Mohaiyiddin *et al.*, “Characterization of nanocellulose recovery from *Elaeis guineensis* frond for sustainable development,” *Clean Technol. Environ. Policy*, vol. 18, no. 8, pp. 2503–2512, 2016.
- [19] J. Lamaming, R. Hashim, O. Sulaiman, C. P. Leh, T. Sugimoto, and N. A. Nordin, “Cellulose nanocrystals isolated from oil palm trunk,” *Carbohydr. Polym.*, vol. 127, pp. 202–208, 2015.
- [20] R. Li, J. Fei, Y. Cai, Y. Li, J. Feng, and J. Yao, “Cellulose whiskers extracted from mulberry: A novel biomass production,” *Carbohydr. Polym.*, vol. 76, no. 1, pp. 94–99, 2009.

Effect of Different Crosslinkers On the Mechanical Properties of Nanocrystalline Cellulose/Chitosan Film Composite

Sam Sung Ting^{1*}, Gan Pei Gie¹ and Muhammad Faiq bin Abdullah¹

¹School of Bioprocess Engineering, Universiti Malaysia Perlis (UniMAP), Kompleks Pusat Pengajian Jejawi 3, 02600 Arau, Perlis, Malaysia.

*E-Mail: stsam@unimap.edu.my

Abstract

Nanocrystalline cellulose (NCC) reinforced chitosan-based biodegradable film composites were prepared by solution casting. Two different crosslinkers were used in this study which were citric acid and glutaraldehyde, respectively. Both crosslinkers improved the tensile strength of the NCC/chitosan film composites significantly compared to the non-crosslinked film composites. However, the glutaraldehyde-crosslinked composites exhibited a better improvement in tensile strength compared to the citric acid-crosslinked composites. The glutaraldehyde-crosslinked composites showed the tensile strength of 40.1 MPa and 58.1 MPa for the neat chitosan film and the 4 wt% NCC/chitosan film, respectively. Fourier transform infrared spectroscopy (FTIR) analyses indicated the network formations of NCC and chitosan with the citric acid and glutaraldehyde crosslinkers by the imine linkage.

Keywords: Nanocrystalline Cellulose, Chitosan and Crosslink

1. Introduction

More than half a century ago, synthetic polymers were the main alternative for natural products in every aspect and it has become parts and parcel of our lives due to their easy processing, excellent barrier properties, and low cost [1]. However, the increased concern for environmental sustainability stimulates the use of renewable resources for producing biodegradable and environmental-friendly composites that could replace the synthetic polymers [2].

Chitosan [cationic (1-4)-2-amino-2-deoxy- β -D-glucan] is a natural biopolymer obtained from the deacetylation of chitin [3]. The development of chitosan-based film had been studied by many researchers. Its excellent properties such as film-forming capability, non-toxic, biodegradability, anti-microbial activity and good barrier property make it an ideal alternative for the reduction of environmental problems caused by synthetic polymers [4]. However, the poor mechanical property of chitosan has limited their usage when compared to synthetic polymer, especially in packaging field [5].

The addition of cellulose as reinforcing agent to

biopolymer is of particular interest due to their abundant source, low cost and biodegradability [6]. Furthermore, filler with smaller size could provide a higher surface area for better filler-matrix interfacial adhesion [7]. Therefore, cellulose materials with diameters in the nanometre range known as nanocrystalline cellulose (NCC) is developed. NCC is a rod-like crystalline cellulose prepared from acid hydrolysis with a diameter between 5 – 70 nm [8]. The production of NCC has garnered significant interest of researchers due to its remarkable properties such as excellent mechanical properties, high aspect ratio and high thermal resistance [9]. Both chitosan and NCC exhibit similar chemical structures and are expected to possess excellent biodegradability and biocompatibility when compounded into composites.

The crosslinking process is an important procedure in the production of NCC/chitosan film as the properties such as mechanical strength of the film are dependent on the crosslinking degree [10]. Falamarzpour et al. used adipic acid as a crosslinker for nanocellulose/chitosan composites and they observed that

the mechanical properties were improved significantly [10]. Similarly, Sionkowska et al. also observed a great improvement on tensile properties of tannic acid crosslinked chitosan film [11]. Therefore, in order to improve the mechanical properties of chitosan film composites for particular application, additives such as crosslinker and fillers are necessary. In this study, citric acid and glutaraldehyde were used as crosslinking agent for the NCC/chitosan film. The tensile properties of both non-crosslinked and crosslinked chitosan with and without the addition of NCC were compared. The interaction between crosslinkers (citric acid and glutaraldehyde) and chitosan was also investigated by using Fourier transform infrared (FTIR) spectroscopy.

2. Experimental Methods

2.1 Materials

Empty fruit bunch (EFB) was provided by Taclico Company Sdn. Bhd. EFB fibres were ground and sieved to obtain powder with a diameter less than 125 μm . Chitosan (degree of deacetylation 90.5%) was purchased from Cleo Shanghai Pharmaceutical, China. Sodium chlorite, sodium hydroxide and acetic acid were purchased from Sigma–Aldrich while sulphuric acid was purchased from Merck. Potassium carbonate was obtained from HmbG.

2.2 Preparation of NCC from EFB fibres

2.2.1 Pre-Treatments of EFB fibres

20g EFB fibres were treated with deep eutectic solvent (DES) at 80 °C for 2 hours. DES was made up of potassium carbonate and glycerol at a molar ratio of 1:7. Bleaching was then carried out at 80 °C for 2 hours. Both treatments were repeated for three times to purify cellulose by removing other non-cellulosic constituents.

2.2.2 Acid Hydrolysis of EFB Cellulose

Acid hydrolysis was performed by mixing the EFB cellulose with 64 wt% sulphuric acids at 45 °C for 45 minutes. The suspension obtained after acid hydrolysis was washed with distilled water and centrifuged repeatedly at 8000 rpm till the supernatant become turbid. The suspension was then sonicated for

10 minutes and stored in refrigerator at 4 °C for further use.

2.3 Preparation of NCC/Chitosan Composites

Chitosan solution (80 mL) was prepared by adding 1.5 wt% (1.2 g) of chitosan powder into 2 v/v% (1.6 mL) of acetic acid solution and heated at 60 °C for 4 hours. 10 wt% (95 μL) of glycerol and NCC were added into the solution and stirred for another hour. The solution was sonicated for 10 minutes for the removal of bubbles. The solution was then casted onto a plastic petri dish (12 x 10 cm) and dried in an oven at 50 °C for 48 hours. For crosslinked composites, 5wt% of citric acid and glutaraldehyde were added into the solution respectively. The solution was stirred vigorously until it was homogenized.

3. Characterization

3.1 Tensile Properties

The tensile properties were measured using Instron universal tensile testing machine (UTM) according to ASTM D882-A at a crosshead speed of 10mm/min. The specimens were cut into rectangular shape with a length of 10 cm and width of 1 cm. The film thickness was measured randomly using a micrometer at three locations and the average thickness was calculated. A total of 10 measurements of tensile strength and elongation at break were carried out for each formulation and the average values were obtained.

3.2 Fourier transform infrared spectroscopy (FTIR)

Infrared spectra of non-crosslinked and crosslinked NCC/chitosan film were determined by using a FTIR spectrophotometer of model PerkinElmer Spectrum 10 with an attenuated total reflectance (ATR) device. The spectra were recorded in a range of 4000 to 450 cm^{-1} with 16 scans and a resolution of 4 cm^{-1} .

4. Results and Discussion

4.1 Tensile Properties

Tensile properties of non-crosslinked, citric acid crosslinked and glutaraldehyde crosslinked neat chitosan and NCC reinforced chitosan film composites are shown in Figure 1. The tensile strength of chitosan composites

exhibited a significant increase with the addition of NCC. The increment could be caused by the increase of hydrogen bonding by the addition of high crystallinity index NCC [12]. Besides, the enhancement in stress transfer between NCC and chitosan and strong filler-matrix interaction had led to a remarkable improvement in the tensile strength [13]. Glutaraldehyde crosslinked chitosan composites displayed the highest tensile strength of 40.1 MPa and 58.1 MPa for 0% and 4% NCC loading, respectively. The crosslinking process has further increased the tensile strength by forming a more stable network between crosslinkers and matrix [13]. The good performance of crosslinked composites indicated the favorable interactions among crosslinkers, filler and matrix [10].

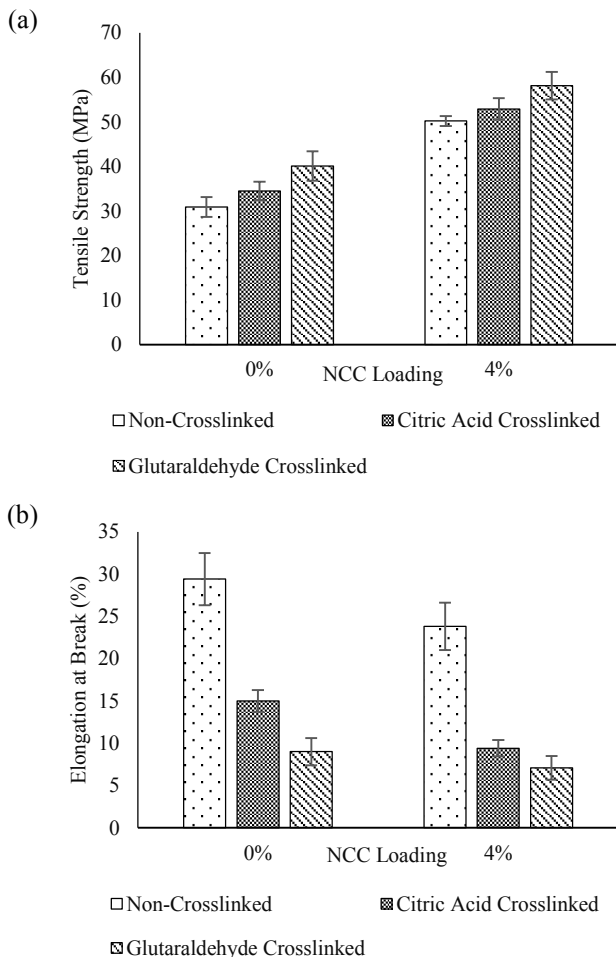


Figure 1: The (a) tensile strength and (b) elongation at break of non-crosslinked, citric acid crosslinked and glutaraldehyde crosslinked neat chitosan and NCC reinforced chitosan film composites

However, the addition of NCC and crosslinkers had a negative effect on the elongation at break of the

composites significantly. According to Ching, Rahman, Ching, Sukiman, & Chuah [14], the addition of highly crystalline NCC formed a strong intramolecular or intermolecular hydrogen bonding with chitosan and resulted in the decline of elongation at break. Furthermore, the addition of crosslinkers has limited the polymer chain mobility and flexibility of composites and decreased the elongation at break. The citric acid crosslinked chitosan composites displayed a higher elongation at break compared to glutaraldehyde crosslinked composites. This could be due to the plasticization effect of citric acid on the chitosan composites [15].

4.2 Fourier transform infrared spectroscopy (FTIR)

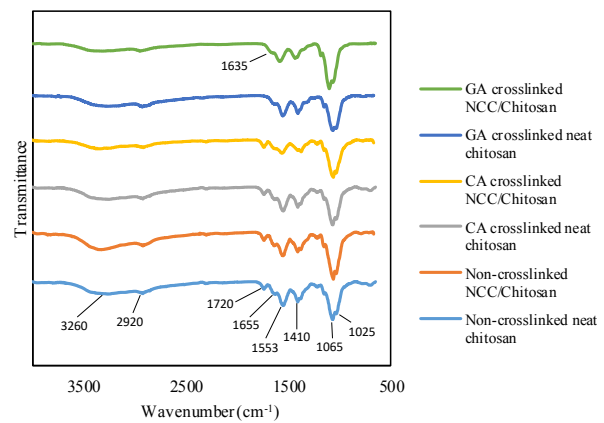


Figure 2: FTIR Spectra of non-crosslinked, citric acid crosslinked and glutaraldehyde crosslinked neat chitosan and NCC reinforced chitosan film composites

Figure 2 shows the comparative IR spectra of pristine non-crosslinked, citric acid crosslinked and glutaraldehyde crosslinked neat chitosan and NCC reinforced chitosan film composites. The non-crosslinked chitosan composites displayed a wide spectrum between 3600-3000 cm⁻¹ with a maximum transmittance at 3260 cm⁻¹ which attributed to the O-H and N-H stretching vibrations. The addition of NCC increased the intensity of the peak at 3260 cm⁻¹. This indicated that there was an increase in the number of hydrogen bonding between NCC and chitosan [16]. Peak at 2920 cm⁻¹ was assigned to symmetric and anti-symmetric C-H vibrations. Whereas, the peak at 1720 cm⁻¹ was the strong C=O stretching band which was the indication of carboxylic acid was due to the addition of acetic acid for the

dissolution of chitosan [17]. The similar peak could also be observed in citric acid crosslinked chitosan composites. The peaks at 1655 cm⁻¹, 1553 cm⁻¹ and 1410 cm⁻¹ were the characteristics of chitosan, which were amide I, II and III, respectively. The sharp peaks at 1065 cm⁻¹ and 1025 cm⁻¹ were related to the C-O-C stretching vibration. The incorporation of NCC has increased the peaks at 1065 cm⁻¹ and 1025 cm⁻¹ significantly.

The chemical crosslinking of chitosan composites with citric acid and glutaraldehyde has led to the formation of imine bonds C=N which could be noticed at 1635 cm⁻¹ [18]. The imine group or Schiff base was caused by the nucleophilic attack of the amine from chitosan with the crosslinking agents. Besides, it could also be noticed that the band at 3260 cm⁻¹ appeared to be lower for crosslinked film composites. It could be due to that the hydrogen bonding between NCC and chitosan is being interrupted by the crosslinkers [13].

5. Conclusion

NCC/chitosan film composites were successfully synthesized and chemical crosslinked using citric acid and glutaraldehyde respectively. Mechanical properties of chitosan film composites were enhanced by the incorporation of NCC. The tensile strength was improved remarkably by the addition of citric acid and glutaraldehyde as crosslinkers. NCC/chitosan film composites were chemically crosslinked which could be confirmed by the formation of imine group using FTIR.

References

- [1] S. Belbekhouche *et al.*, "Water sorption behavior and gas barrier properties of cellulose whiskers and microfibrils films," *Carbohydr. Polym.*, vol. 83, no. 4, pp. 1740–1748, 2011.
- [2] O. Adekomaya, T. Jamiru, R. Sadiku, and Z. Huan, "A review on the sustainability of natural fiber in matrix reinforcement - A practical perspective," *J. Reinf. Plast. Compos.*, vol. 35, no. 1, pp. 3–7, 2016.
- [3] M. Kouchak, A. Ameri, B. Naseri, and S. Kargar Boldaji, "Chitosan and polyvinyl alcohol composite films containing nitrofurazone: Preparation and evaluation," *Iran. J. Basic Med. Sci.*, vol. 17, no. 1, pp. 14–20, 2014.
- [4] D. Dehnad, Z. Emam-Djomeh, H. Mirzaei, S. M. Jafari, and S. Dadashi, "Optimization of physical and mechanical properties for chitosan-nanocellulose biocomposites," *Carbohydr. Polym.*, vol. 105, no. 1, pp. 222–228, 2014.
- [5] K. K. Gadghey and G. S. Sharma, "Investigation of Mechanical Properties of Chitosan Based Films: A Review," *Int. J. Adv. Res. Eng. Technol.*, vol. 8, no. 6, pp. 93–102, 2017.
- [6] M. B. K. Niazi, Z. Jahan, S. S. Berg, and Ø. W. Gregersen, "Mechanical, thermal and swelling properties of phosphorylated nanocellulose fibrils/PVA nanocomposite membranes," *Carbohydr. Polym.*, vol. 177, no. March, pp. 258–268, 2017.
- [7] H. M. C. de Azeredo *et al.*, "Nanocellulose Reinforced Chitosan Composite Films as Affected by Nanofiller Loading and Plasticizer Content," *J. Food Sci.*, vol. 75, no. 1, pp. 1–7, 2010.
- [8] Mohammad, T. Islam, M. M. Alam, A. Patrucco, A. Montarsolo, and M. Zoccola, "Preparation of Nanocellulose: A Review," *AATCC J. Res.*, vol. 1, no. 5, pp. 17–23, 2014.
- [9] H.-M. Ng *et al.*, "Extraction of cellulose nanocrystals from plant sources for application as reinforcing agent in polymers," *Compos. Part B Eng.*, vol. 75, pp. 176–200, 2015.
- [10] P. Falamarzpour, T. Behzad, and A. Zamani, "Preparation of Nanocellulose Reinforced Chitosan Films, Cross-Linked by Adipic Acid," *Int. J. Mol. Sci.*, vol. 18, no. 396, pp. 1–12, 2017.
- [11] A. Sionkowska, B. Kaczmarek, and K. Lewandowska, "Characterisation of chitosan after cross-linking by tannic acid," *Prog. Chem. Appl. Chitin its Deriv.*, vol. 19, pp. 135–138, 2014.
- [12] M. K. Mohamad Haafiz *et al.*, "Bionanocomposite based on cellulose nanowhisker from oil palm biomass-filled

- poly(lactic acid),” *Polym. Test.*, vol. 48, pp. 133–139, 2015.
- [13] V. Rubentheren, T. A. Ward, C. Y. Chee, and P. Nair, “Physical and chemical reinforcement of chitosan film using nanocrystalline cellulose and tannic acid,” *Cellulose*, vol. 22, no. 4, pp. 2529–2541, 2015.
- [14] Y. C. Ching, A. Rahman, K. Y. Ching, N. L. Sukiman, and C. H. Chuah, “Preparation and Characterization of Polyvinyl Alcohol- Based Composite Reinforced with Nanocellulose and,” *BioResources*, vol. 10, no. 2, pp. 3364–3377, 2015.
- [15] C. M. Yeng, S. Husseinsyah, and S. S. Ting, “A comparative study of different crosslinking agent-modified chitosan/corn cob biocomposite films,” *Polym. Bull.*, vol. 72, no. 4, pp. 791–808, 2015.
- [16] R. A. Khan *et al.*, “Mechanical and barrier properties of nanocrystalline cellulose reinforced chitosan based nanocomposite films,” *Carbohydr. Polym.*, vol. 90, no. 4, pp. 1601–1608, 2012.
- [17] E. S. Costa-júnior, E. F. Barbosa-stancioli, A. A. P. Mansur, W. L. Vasconcelos, and H. S. Mansur, “Preparation and characterization of chitosan / poly (vinyl alcohol) chemically crosslinked blends for biomedical applications,” *Carbohydr. Polym.*, vol. 76, no. 3, pp. 472–481, 2009.
- [18] M. M. Beppu, R. S. Vieira, C. G. Aimoli, and C. C. Santana, “Crosslinking of chitosan membranes using glutaraldehyde: Effect on ion permeability and water absorption,” *J. Memb. Sci.*, vol. 301, no. 1–2, pp. 126–130, 2007.

Development of low-cost hydrophobic sachet for storage of ethylene scavenger for use in extending fruit shelf life

Nisanart Naksin^{1,3}, Korakot Sombatmankhong², Pakorn Opaprakasit³, Wanida Chooaksorn⁴,
Nichakorn Pathumrangsarn⁵, Paiboon Sreearunothai^{3*}

¹Thailand Advanced Institute of Science and Technology (TAIST-Tokyo Tech), National Science and Technology Development Agency (NSTDA), Pathum-Thani, Thailand 12120

²National Metal and Materials Technology Center (MTEC), 114 Thailand Science Park, Pathum Thani, Thailand 12120

³School of Bio-Chemical Engineering and Technology, Sirindhorn International Institute of Technology, Thammasat University, Pathum Thani, Thailand 12120

⁴Environmental Science Department, Faculty of Science and Technology, Thammasat University, Pathum Thani, 12120

⁵Faculty of Science and Technology, Muban Chombueng Rajabhat University, Rachaburi, Thailand 70150

*Email: paiboon_sree@siit.tu.ac.th

Abstract

Postharvest loss is a great problem for fruit storage and exportation in Thailand. Ethylene scavenger based on KMnO_4 can help to extend fruit storage life by removing the ethylene gas which is involved in stimulating fruit ripening. However, the containing sachets of these scavengers are often made from special plastics in order to allow for both efficient gas permeability as well as resistance to water, causing them to still be expensive with potential environmental problems. Here, low-cost hydrophobic and gas-permeable cellulose sachet was developed. The hydrophobic and gas-permeable sachet was achieved by a simple wax emulsion based on natural fatty acids coating onto a cellulose teabag. The water contact angles of the sachet changed from 40° before coating to about 146° after coating. Scanning Electron Microscope (SEM) images showed a network of cellulose fiber with a lot of microporosities still remained after wax coat allowing for gas permeability. Fourier Transform Infrared Spectroscopy indicated efficient wax coating on the sachet rendering it into almost a superhydrophobic surface. The use of modified sachet containing ethylene scavenger (KMnO_4 impregnated on silica gel) in high humidity environment of banana fruit package was found to be effective for delaying ripening and maintenance qualities of fruit in term of skin color, weight loss, fruit firmness, and total soluble solids during storage.

Keywords: banana ripening, ethylene scavenger, hydrophobic cellulose sachet, wax coating

1. Introduction

The production and consumption of fruit and vegetables are increasingly important due to improve in quality of life and changes in dietary patterns of people. The fruit and vegetable sectors play a significant role to increase farm income, food security, and sustainable agriculture in developing countries. The production of fruits and vegetables in Thailand has increased by 31% and 69% respectively since 1987 [1]. However, this

sector suffers greatly from postharvest losses. In the Asia-Pacific Region, Thailand was estimated levels of postharvest loss of 17-35% [2]. For climacteric fruits, the postharvest management can be more complicated than that of non-climacteric fruit, due to the fact that climacteric fruits can continue to ripen, either naturally or artificially, after harvest due to the production of ethylene gas from the fruit's respiration themselves [3]. Ethylene gas produced can stimulate ripening [4], and shortens the

self-life of fruits and vegetables during storage [5] . Therefore, ethylene removal is vital in quality management and postharvest life of fruits and vegetables.

Potassium permanganate (KMnO_4) has been well known as a very effective ethylene scavenger and widely used to extend fruit storage life. KMnO_4 works by reacting with the ethylene gas [6],[7],[8] turning it into CO_2 , MnO_2 and KOH which do not stimulate fruit ripening. The produced CO_2 has further benefit of lowering fruit respiration suppressing ripening process. To increase the reactive area, KMnO_4 is usually dispersed on solid support such as clay, zeolites, alumina and silica gel [9] . These ethylene scavenger powders/beads are normally contained in the various types of packaging sachets such as plastic and papers which must have sufficient gas permeability to allow for ethylene gas to pass.

Commercial ethylene scavenger for extending shelf life of fruits exist under various trade names such as Ethysorb (StayFresh Ltd.), Freshkeep (Kurarey), and Acepack (Nippon Greener). They were made from potassium permanganate impregnated onto aluminum oxide, activated carbon, clay, zeolite, or silicon dioxide [9] . However, these commercial scavengers are still expensive, and have to be imported. The packaging sachets of these scavengers are often made from special plastics which can allow ethylene gas to pass as well as being able to withstand high humidity environment in fruit and vegetable storage. Some of materials used in these sachets are such as Tyvex® [10], [11] and porous polyethylene film [1 2] , leading to high cost. If hydrophobic sachets can be made quite simply, it will help the local fruit growers or exporters greatly. In addition, the use of plastic sachet generates more plastic wastes and environmental concern. Sachet made from cellulose provides an alternative since it is biodegradable and environmental friendly. However, cellulose sachets such as those used in tea bag tend to suffer from high water wettability which can cause the KMnO_4 to be leached out. The leached KMnO_4 can react with fruit skin causing brown stain or damage on fruit appearance.

In this work, the low-cost hydrophobic cellulose sachet for containing ethylene scavengers was developed based on using a simple wax coating. The wetting property of the modified cellulose sachet was determined by measuring water contact angles. The surface morphology and functional groups of the modified cellulose sachet were also studied using Scanning Electron Microscope (SEM) and Fourier Transform Infrared Spectroscopy (FTIR) . Finally, the sachet containing KMnO_4 -loaded silica gel was also tested for storage life extension of banana fruit as a representative climacteric fruit with high respiration rate and export importance [13]. The physicochemical changes of these bananas were also evaluated in terms of skin color, weight loss, fruit firmness, and total soluble solids.

2. Experimental Methods

2.1 Preparation of the ethylene scavenger and wax-coated hydrophobic sachet

The ethylene scavenger was prepared by using silica gel impregnated with KMnO_4 solution. Silica gel was purchased from Hi Dri Co.Ltd. in the form of spherical beads colorless type. The silica gel is added into KMnO_4 solution (2.5 g of KMnO_4 mixed with 100 ml of DI water) and stirred, before filtered out. The KMnO_4 impregnated silica gel is allowed to air dry, and then packed into a sachet made from cellulose. The concentration of potassium permanganate on the silica gel was determined followed that of Wills and Warton (2004) [14]. The concentration of potassium permanganate (KMnO_4) on the silica gel beads was determined to be 6.7 ± 1.4 mg/g.

The sachet used in this study was made from cellulose (21 gram/²) used typically as tea bag. The sachet can be wetted by water very well. The surface of the sachet was then modified by coating with a wax emulsion (FennoSize KD 364 MP) from Kemira Co. Ltd. The wax emulsion is an agent that can impart hydrophobicity and water resistance to paper and board. The wax emulsion was applied on both sides of sachet by a simple brushing.

2.2 Characterizations

The wetting property of sachet surface was investigated by measuring the water contact angles (WCA) of water droplets (5 μ L) on the surface using a sessile drops method [15]. The contact angle was measured using Dino-lite microscope after 30s of dropping the water onto the surface. Surface structure of the coated and uncoated sachet was also studied using Scanning Electron Microscope (SEM) images taken at various magnifications (Hitachi, S-3400N) and Fourier Transform Infrared Spectroscopy (FTIR) in the ATR mode (Nicolet iS5, diamond ATR) to study the structure and functional groups of the coated sachet compared to the original uncoated surface.

2.3 Testing of the developed sachet for banana ripening retardation

The fruit used in this study is a Namwa banana. The bananas were bought from a local market at a green mature stage, and were cleaned in water, blown dry and packed in a 40 μ m-thick polyethylene (PE) bag with the sachet containing 5g ethylene scavenger/kg banana. The bananas were divided into three groups, using the coated sachet, the un-coated sachet, and the control group. The conditions for storing these bananas were similar to the conditions used in banana exportation, which were the vacuum packaging (at 0.1 atm) in combination with low-temperature storage at 13°C using temperature-controlled refrigerator. Each experimental condition is conducted in triplicates based on complete randomized design [16]. The physicochemical quality changes of banana during storage were also evaluated which were total soluble solids (TSS), pulp firmness (PF), peel color, and percent weight lost (%WL). During ripening, there are many physiological changes. The pulp firmness of banana tends to decrease since the starch in tissues and pectin in cell wall were metabolized [17]. For TSS content, the enzyme activities convert starch to sugar during ripening increasing TSS [18]. The fresh weight loss also increased due to the loss of water from transpiration.

PF was evaluated by measuring a force in penetrating the pulp using a fruit penetrometer (GY-3, Sundoo™). The TSS content of the juice was measured

by using a refractometer (Hanna, HI96800). Peel color evolution was determined by taking a photo at the beginning of the storage (day 0) and after 14 days under the same lighting conditions. Weight loss (WL) was determined as the difference between the initial fresh weight and the final weight [19]. The percentages of change (% change) in all quality parameters during the storage time of 14 days were calculated.

2.4 Statistics Analysis

The Statistics Package for the Social Sciences (SPSS, version 17) was used for analysis of variance of the result data from experiment. The least significance difference (LSD) test at $p < 0.05$ was used for separation of means.

3. Results and Discussion

3.1 Surface morphology of sachet

The morphology of surface of the uncoated and coated sachet was characterized by SEM. Their images were shown in Fig. 1. The surface of sachet exhibited the network of cellulose fibers and microporosities that can allow gases to pass through. After coating, the surface of the sachet appeared as a smooth waxy-coating on all of the fiber structure indicate efficient coating of the emulsion wax. The holes on the coated surface are still visible indicating that ethylene gases can still pass through the sachet.

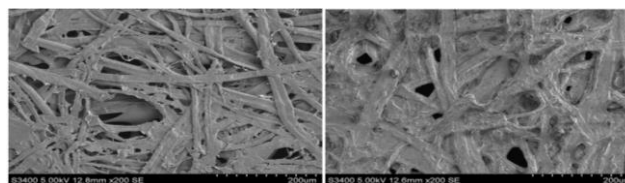


Fig. 1 SEM images of un-coated sachet (left) and wax-coated sachet (right) at 200X.

3.2 Water contact angle and wetting property of sachet

The wetting property of sachets was assessed by measuring the water contact angles (WCA) of water droplets on the uncoated sachet, coated sachet before use and after 14 days of used in fruit bags. The surface of uncoated sachet exhibited hydrophilicity with the WCA of only $37.2 \pm 2.6^\circ$ as shown in Fig. 2. The cellulose fiber which is a raw material of this sachet has a high affinity to water. As a result, the uncoated sachet can rapidly

absorb the water droplets onto surface. The coated sachet was also investigated for its water contact angles at the beginning and also after uses inside the banana bag. The result showed that the coated sachet surface has a hydrophobic surface with WCA of $146.8 \pm 9.7^\circ$. The sachet remained hydrophobic throughout the usage period with WCA still remained high of $145.6 \pm 3.5^\circ$ after 2 weeks of storing inside the banana bag. This indicates that the wax emulsion coating has also good durability even in prolong period of use under high humidity.

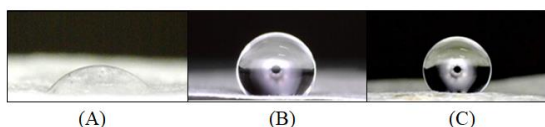


Fig. 2 Images of the water droplets on: (A) un-coated sachet surface; (B) wax-coated sachet surface before use; (C) wax-coated sachet surface after 14 days of use in the banana bag

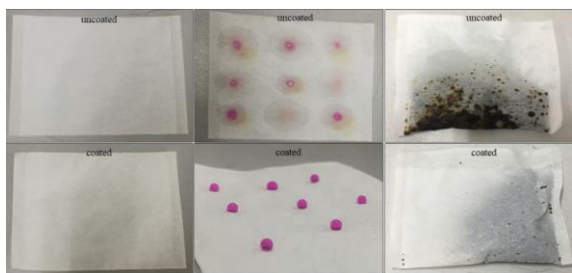


Fig. 3 Digital photographs of uncoated (top row) and wax-coated sachet (bottom row) showing their wetting properties (middle images), and the appearance after 14 days of use in the banana bag (rightmost)

Fig. 3 compares the wetting of the uncoated (top row), and coated sachets (bottom row) by the potassium permanganate solution. It can be seen that for the pristine uncoated sachet, the potassium permanganate solution can readily wet the sachet causing the brown stain, while the potassium permanganate solution droplet remains as a droplet and does not wet the sachet surface.



Fig. 4 Photos of the sachets inside the banana packaging during the storage for 7 days; (A) uncoated sachet inside banana packaging; (B) wax-coated hydrophobic sachet inside the banana packaging

Fig. 4 shows comparison of sachets containing potassium-permanganate loaded silica gel used inside the banana bag. It can be seen that for the uncoated sachet, potassium permanganate can be leached out from the uncoated sachet (Fig. 4A) and while the wax-coated sachet does not show any noticeable leaching of the KMnO_4 (Fig. 4B).

3.3 FTIR spectra of coated sachet

The FTIR spectra of uncoated sachet, and coated sachet were measured by FTIR spectrometer (Fig.5A). The band around $3100\text{-}3500\text{ cm}^{-1}$ corresponds to the -OH absorption band of the cellulose which can be clearly observed in the uncoated sachet. The uncoated sachet exhibited higher intensity of O-H absorption band, due to the hydroxyl group of cellulose which made the sachet hydrophilic [20]. The intensity of this band is reduced upon coating by the wax indicating that cellulose is effectively covered by the wax surface. In the coated sachet spectra (blue) exhibited the high sharp peak of -CH stretching at 2917 and 2847 cm^{-1} representing methyl groups of the alkyl chain of the wax. In addition, the characteristic absorption peak of alkyl chains as the fingerprint region which is hydrophobic tail of wax emulsion at 836 , 821 and 721 cm^{-1} were also observed indicating the wax emulsion coated the sachet very well rendering the hydrophobic property to the sachet surface.

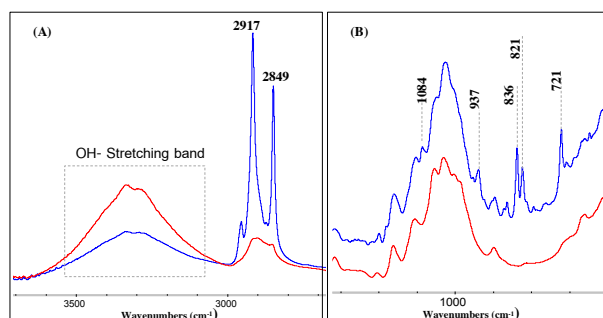


Fig. 5 FTIR spectra of the uncoated pristine sachet (red) and that of the wax-coated sachet (blue)

3.4 Application of ethylene scavenger and their sachet for fruit ripening retardation

To evaluate the performance of the developed ethylene scavengers and their sachets in real use, the developed sachets were tested in delay ripening of banana

Table 1 The quality evaluation of banana during storage of 14 days under various conditions

Conditions	Pulp Firmness (N)			TSS (°Brix)			%Weight loss
	Initial	Final	%Change	Initial	Final	%Change	
Control (no ethylene scavenger)	44.4 ^a	10.8 ^a	75.4 % ^a	1.4 ^a	5.4 ^a	298 % ^a	1.9% ^a
Uncoated sachet	36.7 ^a	30.4 ^b	19.5 % ^b	1.3 ^a	3.8 ^b	186 % ^b	1.3% ^{ab}
Coated sachet	43.5 ^a	34.8 ^b	17.3 % ^b	1.3 ^a	3.6 ^b	186 % ^b	1.1% ^b

Means within the same column followed by different superscript letters are significantly different ($p < 0.05$)

-under conditions that were used for export i.e. to store in vacuumed polyethylene bag at 13°C for 14 days, and changes in peel color, PF, TSS, and %WL evaluated.

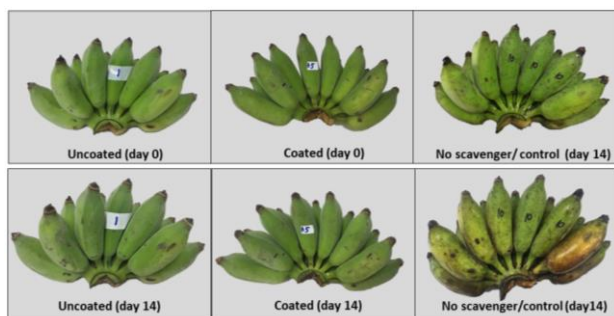


Fig. 6 Peel color evaluation of banana after 14 days of storage using ethylene scavengers in the uncoated sachets, coated sachets, and control (no scavenger used).

When considering the peel color of banana in each condition (Fig 6.), the result showed that after 14 days of storage, the banana in the control condition without the use of any ethylene scavenger changes to be more yellow indicating some partial ripening has taken place [17]. The peel color of banana using ethylene scavengers in both the coated and uncoated sachets still remain green similar to the initial appearance.

For PF, TSS and %WL, bananas in the control set without the use of ethylene scavengers showed again the largest loss of the pulp firmness, greatest increase in TSS, and largest %WL indicating the fruit had high physiological changes during the storage in the same trend as that of the peel color which indicated substantial ripening. The PF, TSS and %weight loss in the case of ethylene scavengers filled in the un-coated sachets or coated sachets showed similar performance. However, as observed earlier that no leaching of KMnO_4 to stain the banana skin was observed in the case when using coated sachets. These result of quality change and peel color of

banana during storage indicated that the using of coated sachets can extend and maintain the quality of banana (Table1).

4. Conclusion

This work demonstrates a simple route to prepare low-cost, hydrophobic, and gas permeable sachet for containing ethylene scavenger that can effectively be used in extending the storage of fruit under high humidity conditions or fruits that have high transpiration. The uncoated sachet has the WCA of about 40° and showed leaching of KMnO_4 due to wetting of the sachet. The wax-coated sachet showed very high water contact angle of 146° and hydrophobic surface. The coated sachet can be effectively used inside the banana bag preventing water wetting and the ethylene scavenger remained effectively dry without KMnO_4 leaching out causing stain on the banana skin. The application of ethylene scavenger contained in the coated sachet in combination with the use of low-temperature storage and partial vacuum packaging was found to be effective for extending storage life of banana. This treatment can maintain the physical and chemical quality of banana including peel color, firmness and total soluble solids during storage. The banana can also be ripened and tasted normally.

Acknowledgement

Authors gratefully acknowledge support from the Research Network for Higher Education in the Upper Central Region of Thailand, Office of the Higher Education Commission, and also from Center of Excellence in Materials and Plasma Technology (CoE M@PTech), Thammasat University. Authors would like to thank Mrs. Pranee Hemchuea who is head of 'Pathumrat' Banana Grower/Exporter Community

Enterprise for permission to study on the real banana export process and supplying, testing of the Namwa banana.

References

- [1] Food and Fertilizer Technology Center. (n.d., 23 April, 2018). *Postharvest Losses of Fruit and Vegetables in Asia*. Available: <http://www.ffc.agnet.org/library.php?func=view&id=20110630151214>.
- [2] D. R. S. Rolle, *Postharvest Management of Fruits and Vegetables in the Asia-Pacific Region*. 2006.
- [3] N. A. A. Hassan R. El-Ramady , Éva Domokos-Szabolcsy and M. F. Hussein S. Taha, *Postharvest Management of Fruits and Vegetables Storage*, vol. 15, no. JANUARY. 2015.
- [4] K. ABE and A. E. WATADA, "Ethylene Absorbent to Maintain Quality of Lightly Processed Fruits and Vegetables," *J. Food Sci.*, vol. 56, no. 6, pp. 1589–1592, 1991.
- [5] A. Coloma, F. J. Rodríguez, J. E. Bruna, A. Guarda, and M. J. Galotto, "Development of an active film with natural zeolite as ethylene scavenger," *J. Chil. Chem. Soc.*, vol. 59, no. 2, pp. 2409–2414, 2014.
- [6] E. Santosa, W. D. Widodo, and Kholidi, "The use of clay as potassium permanganate carrier to delay the ripening of raja bulu banana," *J. Hortik. Indones.*, vol. 1, no. 2, pp. 89–96, 2010.
- [7] D. F. P. Silva, L. C. C. Salomão, D. L. Siqueira, P. R. Cecon, and A. Rocha, "Potassium permanganate effects in postharvest conservation of the papaya cultivar Sunrise Golden," *Pesqui. Agropecuária Bras.*, vol. 44, no. 7, pp. 669–675, 2009.
- [8] D. Zagory, *Active Food Packaging*. Boston, MA: Springer US, 1995.
- [9] A. U. Malik, F. Siddiq, and M. Siddiq, "Packaging of Fresh Mangoes and Processed Mango Products," in *Handbook of Mango Fruit*, John Wiley & Sons, Ltd, 2017, pp. 131–149.
- [10] J. D. Petty, J. N. Huckins, and A. David, "(12) Patent Application Publication (10) Pub . No .: US 2002/0187020 A1," vol. 1, no. 19, 2002.
- [11] I. G. E. Gore, N. Branch, T. Roman, E. Orange, K. Wayne, and R. A. Gore, "United States Patent (19)," no. 19, 1998.
- [12] I. Ozdemir, F. Monnet, and B. Gouble, "Simple determination of the O₂ and CO₂ permeances of microperforated pouches for modified atmosphere packaging of respiring foods," *Postharvest Biol. Technol.*, vol. 36, no. 2, pp. 209–213, 2005.
- [13] R. Suthatham, "The Study of Effect Factor for Demand of Thai's Banana Export to Japan," Thammasat University, 2005.
- [14] R. B. H. Wills and M. A. Warton, "Efficacy of Potassium Permanganate Impregnated into Alumina Beads to Reduce Atmospheric Ethylene," *J. Amer. Soc. Hort. Sci.*, vol. 129, no. 3, pp. 433–438, 2004.
- [15] A. Liukkonen, "Contact Angle of Water on Paper Components: Sessile Drops versus Environmental Scanning Electron Microscope Measurements," *Scanning*, vol. 19, pp. 411–415, 1997.
- [16] G. Casella, "Completely Randomized Designs," *Stat. Des.*, pp. 43–90, 2006.
- [17] N. Siriboon and P. Banlusilp, "A Study on the Ripening Process of ' Namwa ' Banana," *AU J. Technol.*, vol. 7, no. 4, pp. 159–164, 2004.
- [18] A. Zewter, K. Woldetsadik, and T. S. Workneh, "Effect of 1-methylcyclopropene, potassium permanganate and packaging on quality of banana," *African J. Agric. Res.*, vol. 7, no. 16, pp. 2425–2437, 2012.
- [19] B. K. Dadzie and J. E. Orchard, *Routine post-harvest screening of banana/plantain hybrids: criteria and methods*. 1997.
- [20] J. Du *et al.*, "Effect of hydroxyl groups on hydrophilic and photocatalytic activities of rare earth doped titanium dioxide thin films," *J. Rare Earths*, vol. 33, no. 2, pp. 148–153, 2015.

Effects of Hydrophobic Starch/Nanosilica Hybrid Filler on Properties of Poly(lactic acid) Composites

Jindamas Supphasupiri¹ and Kawee Srikulkit^{2,3*}

¹Program in Petrochemistry and Polymer Science, Faculty of Science, Chulalongkorn University, Bangkok 10330

²Department of Materials Science, Faculty of Science, Chulalongkorn University, Bangkok 10330

³Center of Excellence in Petrochemicals and Material Technology, Chulalongkorn University, Bangkok 10330

Phone +66 9921 1178, *E-mail: kawee.s@chula.ac.th

Abstract

Starch/ SiO₂ composites were prepared and followed by surface hydrophobicity modification using hexadecyltrimethoxysilane (HDTMS) through surface silanization reaction. Resultant hydrophobic starch/ SiO₂ composite was melt mixed with PLA using a twin-screw extruder to obtain 10 wt% masterbatch. Again, 10 wt% masterbatch which was employed at high percent wt content was melt mixed with virgin PLA, resulting in PLA containing starch/ SiO₂ at various contents (1.0 wt, 3.0 wt, 5.0 wt%) using a twin-screw extruder (barrel zone temperature : 150/160/170/180/190 °C (die zone)). Injection molded samples were prepared for mechanical properties evaluation. Note that, 10 wt% masterbatch was subjected to injection molding straight away in one-step process. Results showed that 10 wt% masterbatch exhibited a significant improvement in the impact resistance by 17.35% and 12.62 % in all cases of 1.0 starch : 0.25 HDTMS and 1.0 starch : 1.0 HDTMS, respectively. In a similar manner, the 10 wt% composites exhibited an increase in tensile strength by 25.28 % and 18.77 % for 1.0 starch : 0.25 HDTMS and 1.0 starch : 1.0 HDTMS, respectively. Poor mechanical properties found at low percent loadings were associated to a significant depolymerization of those diluted composites due to twice thermal treatments of 10 wt% masterbatch. In case of 10 wt% starch/SiO₂/PLA composites, it could be concluded that hydrophobic starch/SiO₂ composites were able to reinforce PLA matrix as well as absorb impact energy. Finally, the addition of starch/ SiO₂ could favor landfill degradation of PLA via water absorption ability of starch which increased significantly. It is expected that enzymatic hydrolysis of starch will result in the formation of lactic acid and silicic acid which consequently catalyze the hydrolytic degradation (acid hydrolysis) of PLA. The hydrolytic degradation produces carboxylic acid end group which further accelerates the degradation rate.

Keywords: Poly(lactic acid), hydrophobic starch/SiO₂ composites, mechanical properties, water absorption.

1. Introduction

Nowadays, plastics are common commodity found in various products due to their good mechanical properties and versatility. However, plastics are extremely slow in degradation process. So that, biodegradable plastics have been intensively developed in order to search for non-biodegradable substitutes. At present, commercial bioplastics are available including poly(lactic acid)(PLA) and polybutylene succinate (PBS).

Poly(lactic acid) (PLA) [4] is an aliphatic thermoplastic polymer and has attracted more attention

recently because of its biodegradability. PLA has several advantage such as transparency, biocompatibility and melt processing. However, PLA has disadvantages such as processing difficulty due to poor thermal stability [1]. Even though PLA is a biodegradable polymer but the fast degradation is limited to only composting conditions due to its poor water absorption ability which is a key of hydrolysis process. In order to enhance hydrolytic degradation of PLA under landfill condition, the addition of hydrophilic fillers such as starch [2], silica (SiO₂) [3], and montmorillonite [8] provides synergistic effect due

to their capacity of generating acid donor which results in accelerating acid hydrolysis of PLA under landfill biodegradation. However, the main drawback of PLA/hydrophilic filler biocomposites is the problem of poor filler distribution, leading to agglomeration deriving from poor PLA-filler interaction [5-7] . A resulting problem of filler agglomeration could be solved by surface modification approach to alter the matrix-filler interaction [4]. In this study, water absorptivity of PLA was enhanced by the addition of starch/SiO₂ composites. Prior to filler loading, the composite requires proper surface modification in order to prevent agglomeration problem during melt-mixing process. In this research, starch/ SiO₂ composites was prepared and followed by surfaced hydrophobicity modification using Hexadecyl trimethoxysilane (HDTMS) through surface silanization reaction. PLA composites containing hydrophobic starch/SiO₂ were prepared using twin screw extruder. Then, injection molded samples were prepared for properties evaluation.

2.Experimental methods

2.1 Materials

Poly(lactic acid) ; PLA Ingeo 4043D grade was purchased from NatureWorks LLC. Company, USA. Tapioca starch flour was purchased from ETC International Trading Co., Ltd. Sodium silicate (50 wt%) for preparation of nanosilica particles is of commercial grade. Hexadecyltrimethoxysilane (HDTMS) was kindly supplied by Evonik. Nonylphenoethoxylate EO15 (EO15) under the trade name of TERGITOLTM (DOW Chemical Co., Ltd.) was kindly provided by Star Tech Chemical Co., Ltd. Commercial grade methanol was bought from local supplier.

2.2 Preparation of SiO₂ nanoparticles

1000 ml solution containing 55 g of 50 wt% sodium silicate was prepared. The pH value was adjusted to pH 2 with conc. H₂SO₄. The solution was left standing for 2 days to allow the formation of SiO₂ nanoparticles which was detected by laser light scattering. The colloidal solution was employed straight away in

preparing starch/SiO₂ composite to prevent the formation of SiO₂ gel.

2.3 Preparation and surface silanization of starch/ SiO₂ nanocomposites

500 g starch and 1000 ml SiO₂ colloidal solution from section 2.2 (5 wt% of starch) were stirred together to allow the precipitation of SiO₂ nanoparticles onto starch surface. As a result, starch/SiO₂ nanocomposites was obtained. Then, Hexadecyltrimethoxysilane emulsion (HDTMS/EO15/CH₃OH/H₂O) was added with vigorous homogenization. The pH value was adjusted to 1-2 by addition of H₂SO₄. To study the effect of degree of surface modification, two ratios of starch to HDTMS of 1.0:0.25 and 1.0:1.0 wt ratio were prepared, respectively. Resultant mixture paste was left standing freely for 2-3 days to achieve complete silanization reaction. Modified starch/SiO₂ was washed repeatedly until pH value became neutral and then dried in an oven at 65°C for at least 24 h to remove the moisture. Surface hydrophobicity was confirmed by FTIR analysis.

2.4 Preparation of poly(lactic acid) filled with hydrophobic starch/SiO₂ nanocomposite

PLA and hydrophobic starch/SiO₂ nanocomposite were oven dried at 65°C for at least 24 h. Then, PLA masterbatch containing 10% hydrophobic starch/ SiO₂ nanocomposite was prepared using a twin-screw extruder (LTE-26-44, Labtech Scientific, Labtech Engineering, Thailand). The temperature profile was set as follows : 190 (die zone) / 180/ 170/ 160/ 150 °C. Then, PLA composites with various hydrophobic starch/ SiO₂ nanocomposite contents of 1%, 3%, and 5% were prepared using the same twin-screw extruder. Composite compositions were summarized in Table 1.

Injection molded samples were prepared using an injection machine (NEX80, Nissei Injection Molding Machine). The temperature profile was set at 195 (die zone)/190/180/180/165/30 °C.

2.5 Morphology

A JSM-6480LV (JEOL Co. , Japan) Scanning electron microscope (SEM) was employed to study the morphology of starch/ SiO₂/PLA composites. Fractured

surface of samples were coated with gold layer prior to SEM observation.

2.6 Mechanical properties

The tensile test was carried out using with Universal Testing Machine (Instron 5566, U.S.A.) according to ASTM D638. The speed of crosshead and load cell were set at 5 mm/min and 10 KN, respectively.

Notched izod impact tests of the composites were performed on GT-T045-MD (Gotech testing machines, Taiwan) according to ASTM D256. The angle of the notch and impact energy were 45° and 1J. The dimension of the test sample was 12.7x63.5x(3.21-3.24) mm³. An average value of 5 samples per formulation was calculated.

Table 1. Composite compositions

Composite	PLA (g)	Masterbatch (g)
neat PLA	1000	-
PLA/1.0:0.25 ST:HDTMS 1%	1350	150
PLA/1.0:0.25 ST:HDTMS 3%	1050	450
PLA/1.0:0.25 ST:HDTMS 5%	750	750
PLA/1.0:0.25 ST:HDTMS 10%	-	1500
PLA/1.0:1.0 ST:HDTMS 1%	1350	150
PLA/1.0:1.0 ST:HDTMS 3%	1050	450
PLA/1.0:1.0 ST:HDTMS 5%	750	750
PLA/1.0:1.0 ST:HDTMS 10%	-	1500

ST = Starch

2.7 Water absorption properties

Samples were dried at 65°C in an oven for at least 24 h according to ASTM D570. The specimens were weighed (W_c) before submerging in distilled water for 2 h, 4 h, 6 h, 8 h, 24 h, 5 days, 15 days and 30 days, respectively. The samples were taken out and softly blotted with tissue paper or fabric to remove surface

water. The samples were then instantly weighed (W_w) and the percentage of water uptake (W_f) was calculated as follows:

$$\% W_f = \frac{W_w - W_c}{W_c} \times 100\% \quad (1)$$

2.8 Biodegradation test

The biodegradation test was carried out by soil burial test in the outdoor condition according to ASTM D5338. The samples were accurately weighed and then buried in separate holes with about 15 cm deep for 8 weeks (2 months). The pH value of soil was adjusted to 5-6 by watering with diluted citric acid solution. The percentage of weight loss was calculated for 4 and 8 weeks, respectively. The morphology was observed by SEM.

3. Results and Discussion

3.1 TEM analysis of SiO₂ nanoparticles

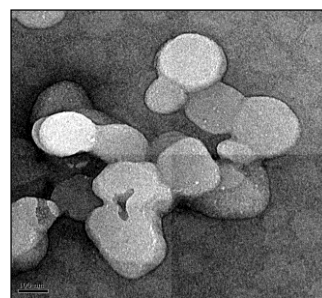


Figure 1. TEM images of SiO₂ nanoparticles.

Figure.1 shows a representative TEM image of SiO₂ nanoparticles prepared by precipitation technique. The image reveals both primary particle and agglomerate. A primary particle diameter and an agglomerate diameter are found 150 - 250 nm and 400 - 600 nm, respectively. The optimum conditions to achieve nanosized ranges with minimum agglomeration are as follows: sodium silicate concentration of 55 g/L, pH values between 1-2, room temperature and reaction time of 2 days. Longer reaction time than 2 days led to the formation of silica gel. The colloidal solution was employed straight away for preparing starch/SiO₂ composite.

3.2 Morphology of fracture surface of hydrophobic starch/SiO₂/PLA composites

Fig. 2(a-b) show SEM images of neat PLA and 10 wt% ST/SiO₂/PLA composite after impact testing. As seen, most of ST/SiO₂ particles (from 1.0 ST : 0.25

HDTMS) firmly adhered to PLA matrix, indicating that the good adhesion at the interphase between PLA and ST/SiO₂ composites.

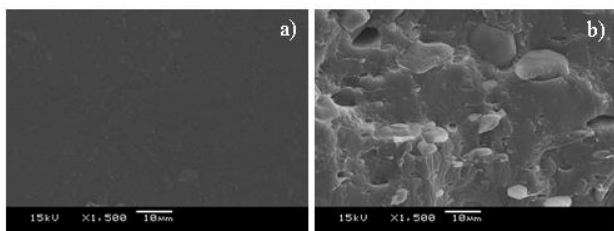


Figure 2. SEM images obtained from impact testing of (a) neat PLA (b) 10 wt% ST/SiO₂/PLA composite.

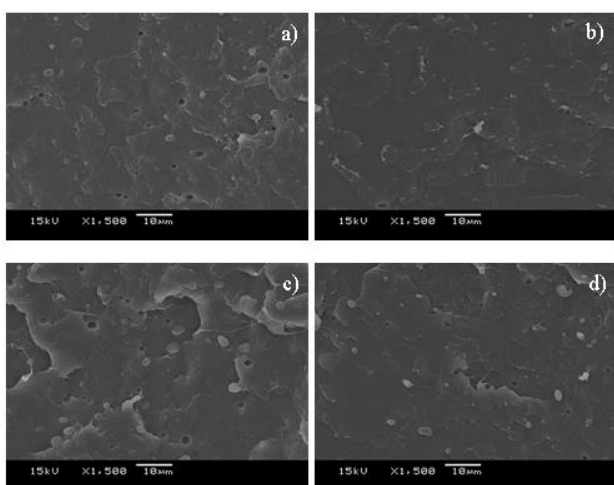


Figure 3. SEM images of (a) PLA/1.0 ST : 0.25 HDTMS 1% (b) PLA/1.0 ST : 1.0 HDTMS 1% (c) PLA/1.0 ST : 0.25 HDTMS 3% (d) PLA/1.0 ST : 1.0 HDTMS 3%

SEM images of ST/SiO₂/PLA composites with low percent loadings of composites after impact testing are shown in Fig. 3. Good dispersion was observed in all cases. However, poor adhesion indicated by the presence of holes is found in case of 1.0 ST : 0.25 HDTMS (Fig. 3a & c) due to incomplete surface modification when compared to 1.0 ST : 1.0 HDTMS. Partial surface modification led to difference in surface energy at the interphase, resulting in poor adhesion.

3.3 Mechanical properties

Fig.4a shows the impact strength of neat PLA and hydrophobic ST/SiO₂/ PLA composites. The notched impact strength of neat PLA is 2.84 kJ/ m². For hydrophobic ST/SiO₂/PLA composites, the impact strength increases with an increase in percent loading. 10 wt% ST/SiO₂/PLA composites exhibits the highest values of impact strength (3.28 kJ/ m² and 3.23 kJ/ m² for

PLA/1.0 ST : 1.0 HDTMS and PLA/1.0 ST : 0.25 HDTMS, respectively) . It can be claimed that hydrophobic ST/SiO₂ composites acted effectively as an energy absorber. The tensile strength values of all samples are shown in Fig.4b. Tensile strength values of composites at low percent loadings (1% , 3% , and 5%) decrease slightly. Slightly poor tensile strength found at low percent loadings was associated to a significant decrease in melt strength of those diluted composites due to twice thermal treatments of 10 wt% masterbatch. For 10 wt% ST/SiO₂/PLA composites, their tensile strength values increase notably, indicating that hydrophobic ST/SiO₂ composite as a reinforcing agent performed well for PLA.

3.4 Water uptake

Table 2. shows percent water absorption values for all samples taken after 600 h or 25 days. It can be seen that after 0.5 h, PLA containing 10 wt% 1.0 ST : 0.25 HDTMS 10% and PLA containing 1.0 ST : 1.0 HDTMS absorbed less water than neat PLA due to hydrophobicity of ST/SiO₂ composites. By time, starch slowly absorbed water, resulting in two fold increase in water uptake.

3.5 Biodegradation test

Soil burial test was conducted to study the biodegradation. After 2 months, all samples are unchanged in weight. However, composites become translucent as shown in Fig. 5. Composites surface is rougher when compared to neat PLA. SEM images were illustrated in the insert. It is obvious that cracks and holes are found in the images of composites particularly in cases of high ST/SiO₂ contents. In contrast, neat PLA remains intact after 2 months of burial test.

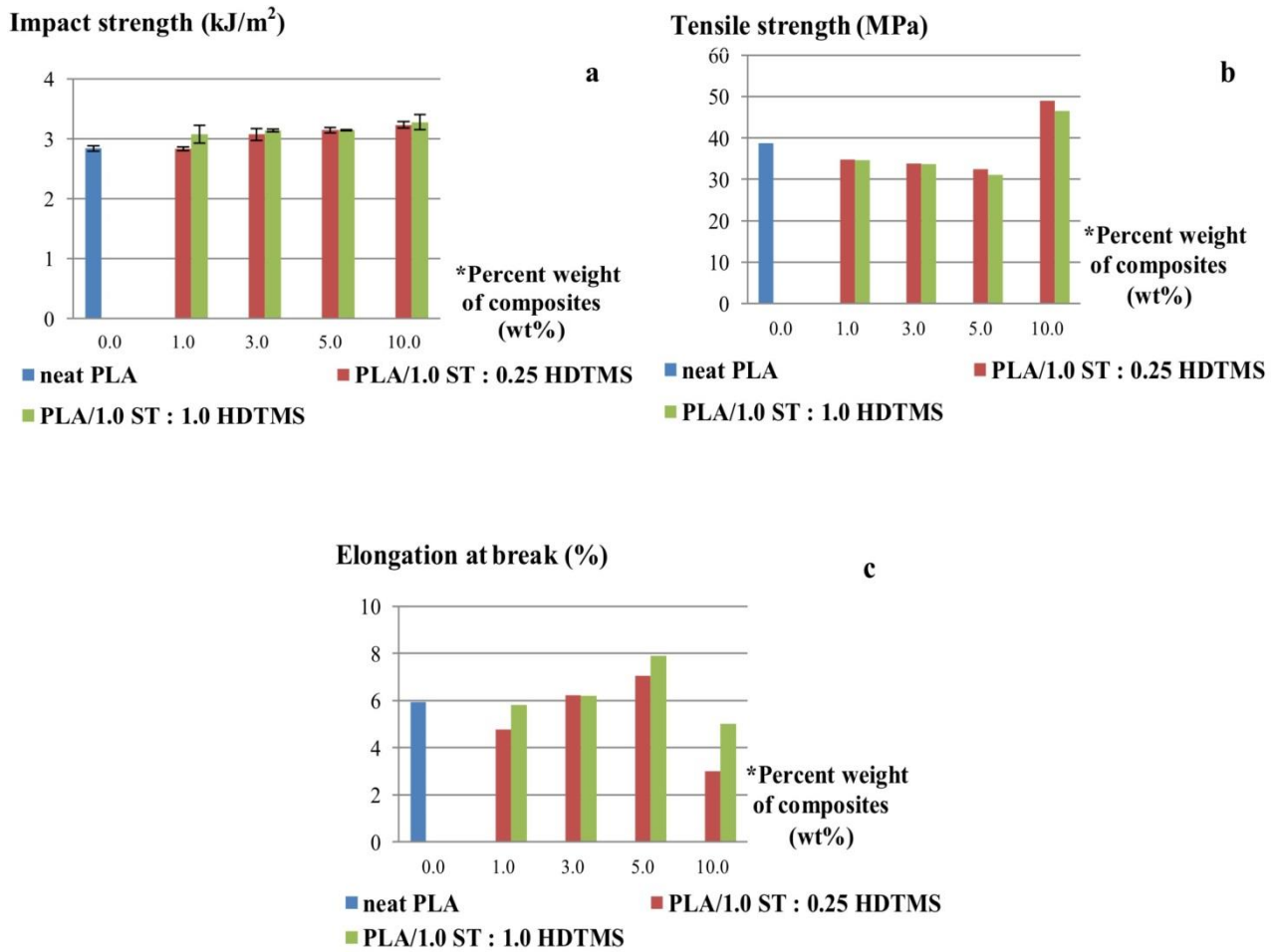


Figure 4. Mechanical properties of neat PLA and ST/ SiO₂/PLA composites. (a) impact strength; (b) tensile strength; (c) elongation at break.

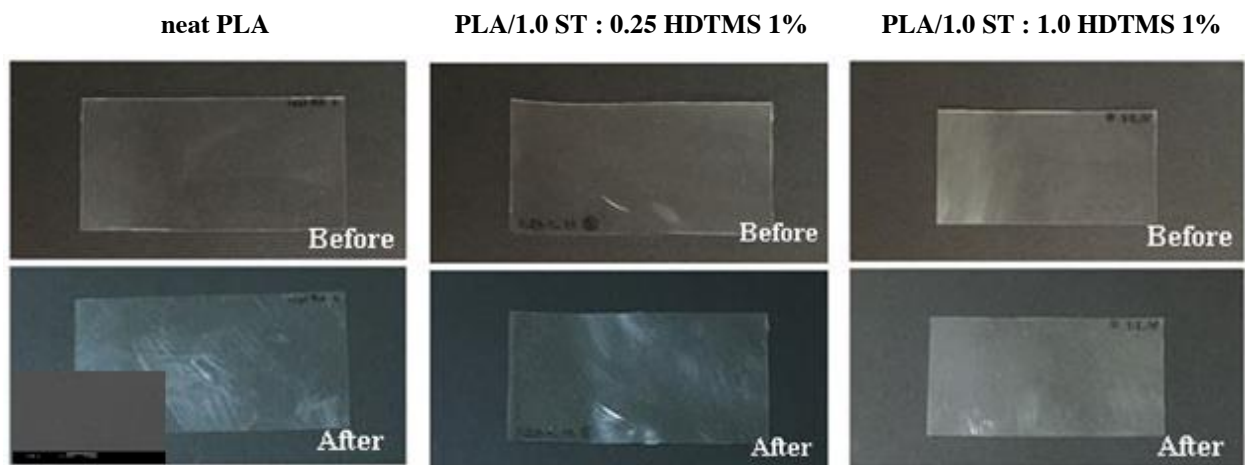


Fig 5. Images of neat PLA and ST/SiO₂/PLA composites before and after soil burial test for 2 months.

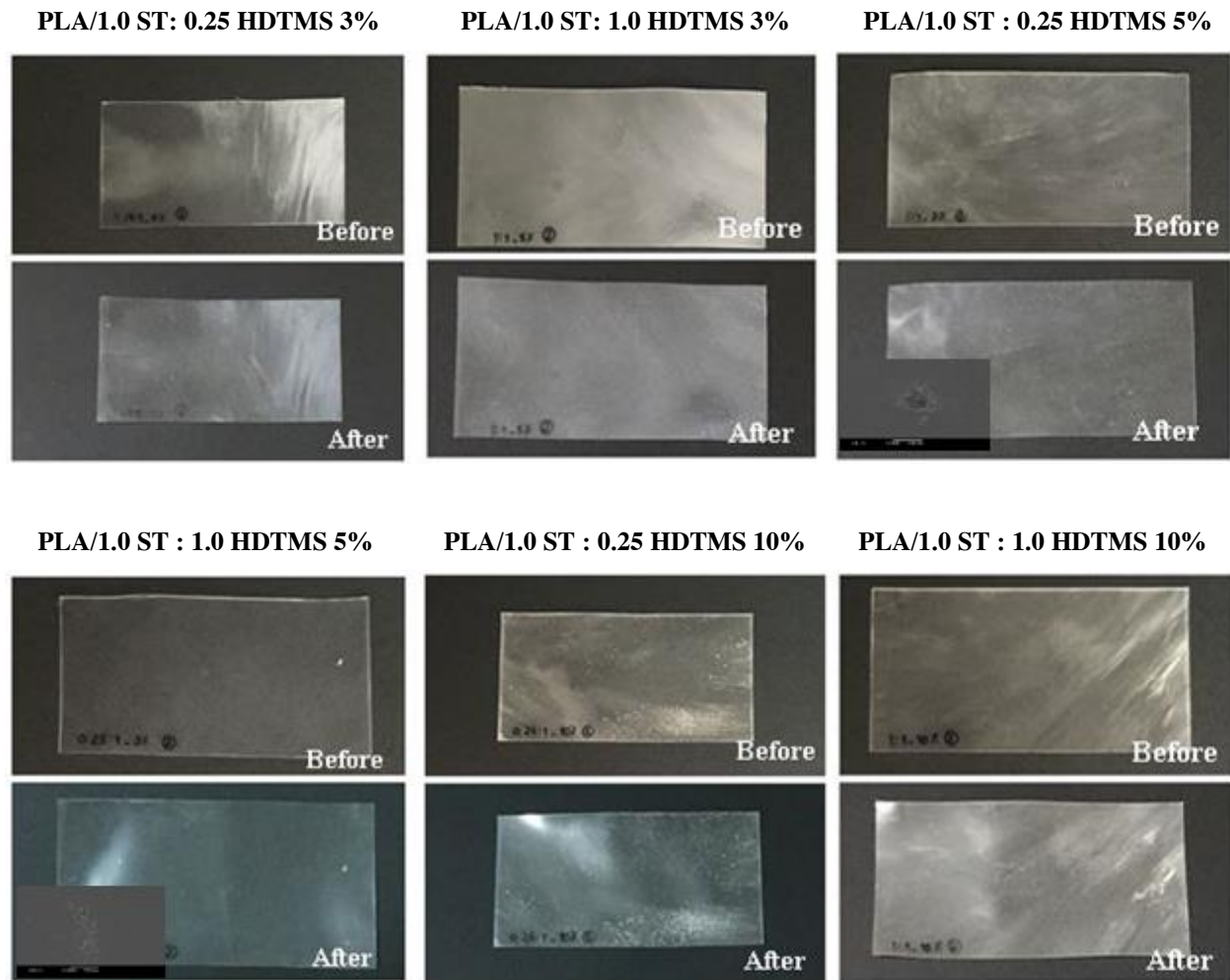


Fig 5. Images of neat PLA and ST/SiO₂/PLA composites before and after soil burial test for 2 months.

Table 2. Percentage of water absorption for all samples.

Time (h)	Water absorption (%)								
	Neat PLA	PLA/1.0 ST : 0.25 HDTMS				PLA/1.0 ST : 1.0 HDTMS			
		1.00%	3.00%	5.00%	10.00%	1.00%	3.00%	5.00%	10.00%
0.5	0.3801	0.3436	0.2615	0.2654	0.2222	0.5246	0.5211	0.5929	0.2474
2	0.2279	0.2846	0.6256	0.5567	0.3235	0.3843	0.3775	0.3617	0.5083
4	0.4579	0.5578	0.4599	0.3838	0.3859	0.6782	0.6555	0.4055	0.5482
6	0.6910	0.5951	0.7453	0.5908	0.6359	0.5466	0.6237	0.6991	0.6341
8	0.5187	0.4959	0.5226	0.6279	0.4620	0.3296	0.4977	0.3777	0.4897
24	0.6313	0.7634	0.7313	0.7878	0.6777	0.8508	0.7325	0.5911	0.9935
120 (5 days)	0.6862	0.7361	0.8776	1.0504	1.2299	0.7800	0.9851	0.6168	1.1674
360 (15 days)	0.9882	1.0905	0.9995	1.2342	1.4558	1.0636	1.1114	0.9766	1.7884
480 (20 days)	0.9882	1.0087	1.0483	1.2605	1.5813	1.1345	1.1872	1.0023	1.9374
600 (25 days)	0.9882	1.1723	1.0970	1.4443	1.5813	1.1345	1.2377	1.0280	2.0368

4. Conclusion

SiO₂ nanoparticle was synthesized by precipitation method. The synthesized SiO₂ nanoparticles were precipitated onto starch granules to obtain starch/SiO₂ composites. Further hydrophobicity surface modification of the composite was carried out using 0.25 : 1.0 and 1.0 : 1.0 wt ratios of HDTMS: starch/SiO₂. Then, PLA/hydrophobic starch/SiO₂ composites at hydrophobic ST/SiO₂ contents of 1 wt%, 3 wt%, 5 wt% and 10 wt% were prepared and evaluated for mechanical properties, water uptake and biodegradation. Results showed that in the presence of 10 wt% hydrophobic starch/SiO₂ composite, PLA composites exhibited significant increase in mechanical properties including impact strength and tensile strength, deriving from energy absorption and reinforcement performance of hydrophobic starch/SiO₂ composites. Two fold increase in water uptake was obtained. Notable change in physical appearance after soil burial test for 2 months was observed, implying the faster biodegradability when compared to neat PLA.

Acknowledgement

Authors are grateful for BEDO for financial support and thank IRPC public company limited for supporting sample preparation and QC testing.

References

- [1] Lim, L. T., Auras, R. and Rubino, M., “ Processing technologies for poly(lactic acid)”, *Progress in Polymer Science* : 820-852 (2008).
- [2] Jirawat, L., Supakij, S., Poonsub, T. and Manus, S., “ Compatibilized polylactic acid/ thermoplastic starch by reactive blend” , *Journal of Metals, Materials and Minerals* : 87-90 (2010).
- [3] Hafiz, A.A., Arshad, C. and Abdul, S., “Synthesis of quality silica gel ; optimization of parameters”, *Journal of Faculty of Engineering and Technology* : 1-14 (2009).
- [4] Lv, H., Song, S., Sun, S., Ren, L. and Zhang, H., “ Enhanced properties of poly(lactic acid) with silica nanoparticles” , *Polymers for Advanced Technologies* : 1156-1163 (2016).
- [5] Lai, S. M. and Hsieh, Y. T. , “ Preparation and properties of polylactic acid (PLA) / silica nano-composites”, *Journal of Macromolecular Science, Part B* : 211-228 (2016).
- [6] Marra, A., Silvestre, C., Duraccio, D. and Cimmino, S., “ Poly(lactic acid)/ zinc oxide biocomposite films for food packaging application” , *International Journal of Biological Macromolecules* : 254-262 (2016).
- [7] Jalalvandi, E., Majid, RA., Ghanbari, T. and Ilbeygi, H. , “ Effects of montmorillonite (MMT) on morphological, tensile, physical barrier properties and biodegradability of polylactic acid/ starch/ MMT nanocomposites” , *Journal of Thermoplastic Composite Materials* : 496-509 (2015).
- [8] Huang, M.F., Yu, J.G. and Ma, X.F., “Studies on the properties of montmorillonite - reinforced thermoplastic starch composites” , *Polymer* : 7017-7023 (2004) .

Preparation of Cellulose Hydrogel-coated Fertilizers for Agricultural Applications

Nuntaporn Sutayo¹, Somrudee Nilthong¹, Nattakan Soykeabkaew^{1,2} and Orawan Suwanton^{1,2,3*}

¹Science, School of Science, Mae Fah Luang University, Chiang Rai 57100

²Materials for Energy and Environment (MEE) Research Group, Mae Fah Luang University, Chiang Rai 57100

³Center of Chemical Innovation for sustainability (CIS), Mae Fah Luang University, Chiang Rai 57100

Phone +66 5391 6787, Fax +66 5391 6776, *E-Mail: o.suwanton@gmail.com

Abstract

In this study, the cellulose extracted from the pineapple leaves was used to coat the fertilizer. The different concentrations (i.e., 1.0, 1.5, and 2.0% w/v) of cellulose were used to prepare the cellulose hydrogel-coated fertilizers. The cellulose hydrogel-coated fertilizers were prepared by dissolving of pineapple leave cellulose in ionic liquid (IL). The cellulose hydrogel-coated fertilizers were characterized for their morphology, water swelling and weight loss, and release characteristics of potassium (K) from the cellulose hydrogel-coated fertilizers. The results showed that the fertilizer was successfully coated with the cellulose hydrogel as shown in the scanning electron microscopy (SEM) and Fourier Transform Infrared (FTIR) results. Both the water swelling and weight loss of the cellulose hydrogel-coated fertilizers in distilled water increased with increasing of immersion time. The released amounts of K from the samples increased and reached the plateau value at the longer immersion time. For release study in soil column, the lowest released amount of K was obtained at cellulose concentration of 2.0% w/v. Thus, the cellulose hydrogels prepared from different concentrations of cellulose had the different characters and release characteristics.

Keywords: Cellulose; Hydrogel, Pineapple leave, Fertilizer, Agriculture

1. Introduction

Thailand is one of an agricultural country in Asia. Therefore, the increase of agricultural products leads to the increase of agricultural wastes. These wastes must be eliminated by burning or embedding, so they become the pollution in daily life. Furthermore, the increase of crop products causes the high amount of fertilizer for growth. However, fertilizer is generally unable to control the release, thus plants are fed over the rate of nutrients from fertilizers affecting the soil. This problem can affect the agricultural products in the future. Therefore, the controlled release of fertilizer should be desired to match the plant requirement and decrease the negative environmental effects of over-fertilization [1].

Fertilizers are normally applied to the soils for improving the crop yields [2]. In general, fertilizers promote plant growth and they have many nutrients such as nitrogen (N), potassium (K), phosphorus (P), calcium

(Ca) and magnesium (Mg) for supporting of growth the crop [3,4]. However, the fertilizers cannot control the release rate when they are applied to the soil since they are immediately soluble in water and directly absorb into the soil. Therefore, the controlled release of fertilizers is important. Many researchers have been used polymers for coating fertilizers such as kraft pine lignin, polyacrylamide/methylcellulose/calcium montmorillonite composites, polyethylene, etc [5-7]. Hydrogel is one of the materials for coating fertilizers because the hydrogel-coated fertilizers can substantially delay the release of soluble nutrients compared with only soluble fertilizer [8,9]. Hydrogel is a three-dimensional network of polymer chains. It exhibits the ability to swell and retain a significant fraction of water within its structure, but will not dissolve in water [10]. It can be classified to natural and synthetic hydrogels. Since natural hydrogels are the eco-friendly environment, pH-neutrality after swelling, low price and biodegradability [10]. Therefore, the

natural hydrogels were used in many fields such as biomedical, food and agricultural applications [11-14]. Moreover, they can be used for coating fertilizers to control the release rate.

Cellulose is a polysaccharide polymer that connected with glycosidic bond at β -1,4 linkage. The chain length of the cellulose is more than 2,000 molecules [15]. In addition, the sources of cellulose are the agricultural products such as rice straw, banana rachis, a sugar cane and bagasse. Since pineapple leaves are one of the agricultural wastes in Chiang Rai, Thailand. Thus, the cellulose extracted from pineapple leaves is used in this study since it is non-toxic, eco-friendly, biodegradable, and low cost [16]. Moreover, it contains a high amount of hydroxyl group. So, it can be easily fabricated to the hydrogel [14].

In this study, the cellulose obtained from pineapple leaves was used for coating NPK fertilizers. The cellulose solution was prepared by dissolving cellulose in ionic liquid (AMIMCl). The NPK fertilizers were then coated with the cellulose hydrogels. After that, the cellulose hydrogel-coated fertilizers were characterized for their morphology, water swelling, and weight loss, and release characteristics of K from the cellulose hydrogel-coated fertilizers.

2. Experimental Methods

2.1 Materials

Cellulose sample derived from pineapple leaves was obtained from Materials for Energy and Environment (MEE) Research Group. 1-methylimidazole and allyl chloride were bought from Aldrich (USA). NPK fertilizer was purchased from MC agrochemicals Co., Ltd. (Thailand).

2.2 Preparation of ionic liquid

To prepare an ionic liquid (AMIMCl), 1-methylimidazole (400 mL) and allyl chloride (800 mL) at a molar ratio of 1.25:1.25 were added to a round-bottomed flask fitted with a reflux condenser for 8 h at 65 °C with stirring. The unreacted chemical reagents and other impurities were removed by vacuum distillation. The obtained AMIMCl was slightly amber.

2.3 Preparation of cellulose hydrogel-coated fertilizers

Cellulose was cut into small pieces and dried at 50 °C for 30 min in an oven before use. A known weight of cellulose was dissolved in 10 mL of AMIMCl. The mixture was heated and stirred until cellulose was completely dissolved to obtain cellulose solutions at different concentrations of 1.0%, 1.5%, and 2.0% w/v. The cellulose solution was poured into the polystyrene (PS) mold with a diameter of 6 mm and then a fertilizer pellet was added to each hole of PS mold that contained the cellulose solution. After that, the PS mold was immersed in distilled water 4 times and then allowed to dry at 50 °C for 2 h. Finally, the cellulose hydrogel-coated fertilizers were obtained.

2.4 Fourier transform infrared (FTIR) spectroscopy

The FTIR spectra of cellulose sample, fertilizer, and cellulose hydrogel-coated fertilizers were obtained by FTIR spectroscopy. The samples were ground into a powder and mixed with KBr powder. The powder mixture was compressed into a transparent disk and scanned from 4000 to 650 cm^{-1} using the average of 32 scans.

2.5 Morphology study

The morphological appearance of the cellulose hydrogel-coated fertilizers was investigated by scanning electron microscope (SEM). Each sample was coated with a thin layer of gold using sputtering device prior to observation by SEM.

2.6 Water swelling and weight loss evaluation

The water swelling and weight loss of the cellulose hydrogel-coated fertilizers were carried out in distilled water at 30 °C for 1, 3, 5, and 7 days and calculated according to the following equations:

$$\text{Water swelling (\%)} = \frac{M - M_d}{M_i} \times 100 \quad (1)$$

$$\text{Weight loss (\%)} = \frac{M_i - M_d}{M_i} \times 100 \quad (2)$$

where M is the weight of each sample after immersion in distilled water for 1, 3, 5, and 7 days, M_i is the initial weight of each sample in its dry state and M_d is the weight of each sample after immersion in distilled water for 1, 3, 5, and 7 days in its dry state.

2.7 Release of K from cellulose hydrogel-coated fertilizers

2.7.1 Actual K content

Each sample (~60 mg) was immersed in 10 ml of distilled water to dissolve fertilizer out of the sample. After that, 3 ml of the sample solution was measured by atomic absorption spectroscopy (AAS). The actual amount of K in the cellulose hydrogel-coated fertilizers was back-calculated from the obtained data against a predetermined calibration curve for K.

2.7.2 K release study

The release characteristics of K from the cellulose hydrogel-coated fertilizers were investigated in distilled water and soil.

The cellulose hydrogel-coated fertilizers (~20 mg) were immersed in 20 ml of distilled water at 30 °C. At time interval ranging from 30 min up to 7 days, 3 ml of the sample solution was removed and an equal amount of fresh distilled water was added. The amount of K was determined by AAS. Finally, the amount of K released from the cellulose hydrogel-coated fertilizers was back-calculated from the obtained data against a predetermined calibration curve for K.

The soil column was prepared by packing the soil in 5 cm long polyvinyl chloride (PVC) pipes with 1.6 cm internal diameter. The bottom end of each column was plugged with a plastic lid and the 2.5 g of soil was then added to the column. After that, the cellulose hydrogel-coated fertilizers were applied to each column and 2.5 g of soil was then added to the top of each column. 2 mL of distilled water was added into each column which was then covered with a plastic lid. The soil column of each sample and each time interval was analyzed for released K after 30 min up to 7 days. After each time, the soil from each column was taken out from the column and was dissolved in 10 mL of distilled water for 10 min to analyze of released K. The obtained solution was filtered and the amount of released K was measured by AAS.

3. Results and Discussion

3.1 Morphology of cellulose hydrogel-coated fertilizers

The morphology of the cellulose hydrogel-coated fertilizers was characterized by SEM. The overall and cross-section SEM images of the cellulose hydrogel-coated fertilizers at cellulose concentration of 2.0% w/v are shown in Figure 1. The cellulose hydrogel-coated fertilizers showed a spherical shape with rough surface of coated cellulose. The fertilizer was successfully coated with cellulose as shown in cross-section image (Figure 1b). In addition, the thickness of the coated cellulose layer at cellulose concentration of 1.0, 1.5, and 2.0% w/v was 182±22, 120±12, and 223±16 μm, respectively.

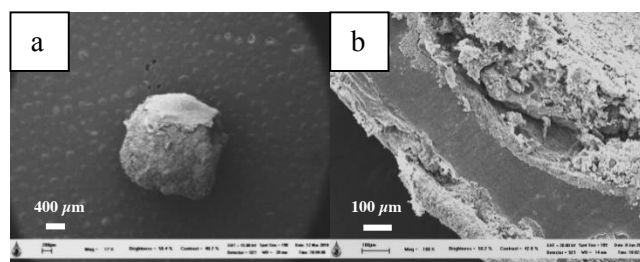


Figure 1. Selected SEM images of the cellulose hydrogel-coated fertilizers at 2% w/v of cellulose in (a) overall and (b) cross-section.

3.2 FTIR results

For FTIR spectrum of pure cellulose (Figure.2 a), the absorption peaks showed at the following wavenumbers (in cm^{-1}): 3314 (O-H stretching), 1385 (C-H stretching), and 1066 (C-O stretching) [17]. For FTIR spectrum of fertilizer (Figure 2 b), the absorption peaks showed at the following wavenumbers (in cm^{-1}): 3177 (O-H stretching), and 1420 (C-H bending of CH_2), 1112 (C-O stretching). In case of the cellulose hydrogel-coated fertilizers (Figure 2 c), the absorption peak at 1426 cm^{-1} was assigned to the C-H bending of CH_2 . This peak was shifted to a lower wavenumber indicating the destruction of the intramolecular hydrogen bond involving O at C6. The absorption peak at 1059 cm^{-1} was belonged to the C-O stretching in the amorphous region. The O-H stretching of cellulose showed a broad vibration band located in the range of 3000-3500 cm^{-1} . From these results, the spectrum of the cellulose hydrogel-coated fertilizers was similar to that of the fertilizer. Thus, it can be concluded that the fertilizer was successfully coated with the hydrogels.

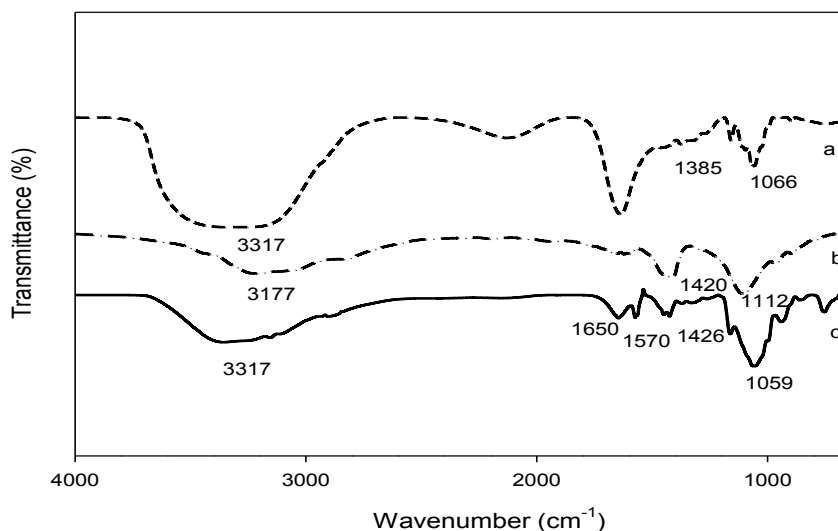


Figure 2. FTIR spectra of pure cellulose (a), fertilizer (b) and cellulose hydrogel-coated fertilizers (c).

3.3 Water swelling and weight loss of cellulose hydrogel-coated fertilizers

The water swelling of the cellulose hydrogel-coated fertilizers was investigated with varying concentrations of cellulose (i.e., 1.0%, 1.5%, and 2.0% w/v) after immersion in distilled water at 30 °C for 1, 3, 5, and 7 days and the results are shown in Figure 3. From Figure 3a, the water swelling of the cellulose hydrogel-coated fertilizers prepared from 1.0%, 1.5%, and 2.0% w/v of cellulose in distilled water after immersion for 1 day was 122.2%, 272.9%, and 189.1%, respectively. At 3 days, the value was 170.2%, 142.1%, and 132.4%, respectively. At 5 days, the value increased to 208.4%, 331.11%, and 221.8%, respectively. At 7 days, the value was 461.2%, 309.2%, and 183.5%, respectively.

For the weight loss (Figure 3b), the results showed that the weight loss of the cellulose hydrogel-coated fertilizers prepared from 1.0%, 1.5%, and 2.0% w/v of cellulose in distilled water for 1 day was 18.8%, 48.6%, and 26.4%, respectively. At 3 days, the value increased to 20.8%, 73.1%, and 49.4%, respectively. At 5 days, the value increased to 38.3%, 75.1%, and 48.4%, respectively. At 7 days, the value increased to 74.0%, 78.9%, and 60.9%, respectively.

From these results, the weight loss of the cellulose hydrogel-coated fertilizers was increased with increasing

of immersion time. These results might be the longer immersion time caused the coated cellulose hydrogels to have enough time to swell and let the fertilizer to diffusion out of the coated cellulose hydrogel.

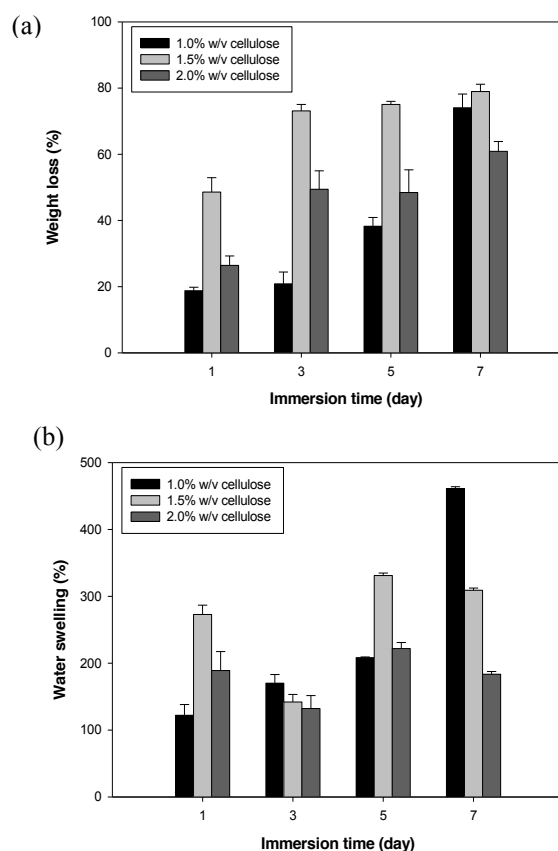


Figure 3. The water swelling (a) and weight loss (b) of the cellulose hydrogel-coated fertilizers in distilled water.

3.4 Release of potassium from cellulose hydrogel-coated fertilizers

The actual amount of K in the cellulose hydrogel-coated fertilizers was determined prior to investigating the release characteristics of K from these samples. The results showed that the actual amount of K (based on the sample weight) in the cellulose hydrogel-coated fertilizers prepared from 1.0%, 1.5% and 2.0% w/v of cellulose was 4.24%, 6.26%, and 3.39%, respectively. These values were later used to calculate the release characteristics of K from these hydrogels.

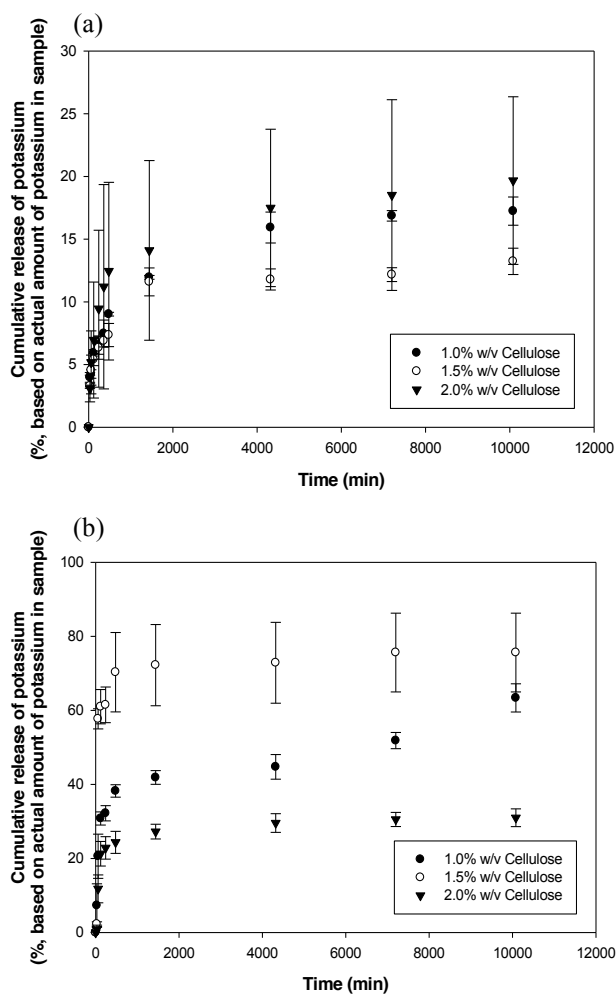


Figure 4. The release profiles of potassium from the cellulose hydrogel-coated fertilizers in distilled water (a) and soil column (b).

The release characteristics of K from the cellulose hydrogel-coated fertilizers prepared from 1.0%, 1.5% and 2.0% w/v of celluloses were investigated in distilled water and soil and the results are shown in Figure 4. For Figure 4a, a gradual increase in the released amount of K from these samples was observed. The released amount

of K from these samples reached the plateau value at the longer immersion time. From these results, the released amount of K from the samples was not significantly different in all conditions.

In the case of the soil column study, the release characteristics of K from the cellulose hydrogel-coated fertilizers were also investigated every 30 min up to 7 days (Figure 4b). The released amount of K from the hydrogels was rapidly increased within the first period, increased gradually afterward, and reached the plateau at the longer immersion time. In addition, the lowest released amount of K was obtained at cellulose concentration of 2.0% w/v. This might be due to the high amount of coated cellulose on the fertilizers. In comparison with the release study in distilled water, the much higher amount of K released from these samples was obtained in the soil column. This result might be due to the long submersion time in soil condition without dilution.

4. Conclusion

The cellulose hydrogel-coated fertilizers were successfully prepared to control the release rate of fertilizer for use in agricultural applications. From SEM image, the cellulose hydrogel-coated fertilizers showed a spherical shape with rough surface of coated cellulose. For the FTIR spectra, the results confirmed that the fertilizer was completely coated with the cellulose hydrogel. The weight loss of the cellulose hydrogel-coated fertilizers in distilled water increased with increasing immersion time. For release study in soil column, the lowest released amount of K was obtained at cellulose concentration of 2.0% w/v.

Acknowledgement

The authors would like to acknowledge the financial support from Mae Fah Luang University (MFU).

References

- [1] Cao H, Wang Z, He G, Dai J, Huan M, Wang S, Malhi SS. (2017), Tailoring NPK fertilizer application to

- precipitation for dryland winter wheat in the Loess Plateau. *Field Crops Research*, 209: 88-95.
- [2] Haynes RJ, Naidu R. (1998), Influence of lime, fertilizer and manure applications on soil organic matter content and soil physical conditions: a review. *Nutrient Cycling in Agroecosystems*, 51: 123-137.
- [3] Cole JC, Smith MW, Penn CJ, Cheary BS, Conaghan KJ. (2016), Nitrogen, phosphorus, calcium, and magnesium applied individually or as a slow release or controlled release fertilizer increase growth and yield and affect macronutrient and micronutrient concentration and content of field-grown tomato plants. *Scientia Horticulturae*, 211: 420-430.
- [4] Lombardo S, Pandino G, Mauromicale G. (2017), Minerals profile of two globe artichoke cultivars as affected by NPK fertilizer regimes. *Food Research International*, 100: 95-99.
- [5] García MC, Diez A, Vallejo A, Garcia L, Cartagena MC. (1996), Use of kraft pine lignin in controlled-release fertilizer formulations. *Industrial & Engineering Chemistry Research*, 35: 245-249.
- [6] Bortolin A, Aouada FA, Mattoso LH, Ribeiro C. (2013), Nanocomposite PAAm/methyl cellulose/montmorillonite hydrogel: evidence of synergistic effects for the slow release of fertilizers. *Journal of Agricultural and Food Chemistry*, 61: 7431-7439.
- [7] Yang X, Jiang R, Lin Y, Li Y, Li J, Zhao B. (2018), Nitrogen release characteristics of polyethylene-coated controlled-release fertilizers and their dependence on membrane pore structure. *Particuology*, 36: 158-164.
- [8] Mikkelsen RL. (1994), Using hydrophilic polymers to control nutrient release. *Nutrient Cycling in Agroecosystems*, 38: 53-59.
- [9] Rashidzadeh A, Olad A, Reyhanitabar A. (2015), Hydrogel/clinoptilolite nanocomposite-coated fertilizer: swelling, water-retention and slow-release fertilizer properties. *Polymer Bulletin*, 72: 2667-2684.
- [10] Ahmed EM. (2015), Hydrogel: Preparation, characterization, and applications: A review. *Journal of Advanced Research*, 6: 105-121.
- [11] Kakkar P, Madhan B. (2016), Fabrication of keratin-silica hydrogel for biomedical applications. *Materials Science and Engineering: C*, 66: 178-184.
- [12] Yasui G, Yamamoto Y, Shichinohe R, Funayama E, Oyama A, Hayashi T, Furukawa H. (2016). Neuregulin-1 released by biodegradable gelatin hydrogels can accelerate facial nerve regeneration and functional recovery of traumatic facial nerve palsy. *Journal of Plastic, Reconstructive & Aesthetic Surgery*, 69: 328-334.
- [13] Gregorová A, Saha N, Kitano T, Saha P. (2015), Hydrothermal effect and mechanical stress properties of carboxymethylcellulose based hydrogel food packaging. *Carbohydrate Polymers*, 117: 559-568.
- [14] Chang, C, Zhang L. (2011), Cellulose-based hydrogels: present status and application prospects. *Carbohydrate Polymers*, 84: 40-53.
- [15] Gupta VK, Carrott PJM, Singh R, Chaudhary M, Kushwaha S. (2016), Cellulose: a review as natural, modified and activated carbon adsorbent. *Bioresource Technology*, 216: 1066-1076.
- [16] Sannino A, Demitri C, Madaghiele M. (2009), Biodegradable cellulose-based hydrogels: design and applications. *Materials*, 2: 353-373.
- [17] Abderrahim B, Abderrahman E, Mohamed A, Fatima T, Absesselam T, Krim O. (2005), Kinetic thermal degradation of cellulose, polybutylene succinate and a green composite: Comparative study. *World Journal of Environmental Engineering*, 3: 95-110.

Rheological and Viscoelastic Properties of Poly(Butylene Succinate)/ Poly(Ethylene Terephthalate) Blends

Nattakarn Hongsriphan^{*}, Kiattisak Chutivasanaskun, Paphada Kantipongpipat, Jirawat Thanokiang,
and Pajaera Patanathabutr

Department of Materials Science and Engineering, Faculty of Engineering and Industrial technology,
Silpakorn University, Sanam Chan Palace Campus, Nakhon Pathom, 73000
Phone +66 3424 1708, Fax +66 3424 1708, *E-Mail: Hongsriphan_N@su.ac.th

Abstract

This work attempted to increase rigidity of poly(butylene succinate) or PBS by blending with poly(ethylene terephthalate) or PET. Since the melting temperatures of these polymers were vastly different, rheological properties were investigated using a parallel plate rheometer and analyzed by the power law model. Viscoelasticity and thermal properties of the obtained blends were evaluated by dynamic mechanical analysis and differential scanning calorimetry, respectively. PBS and PET were blended with weight ratios of 100/0, 90/10, 80/20, and 70/30 wt% in a typical melt blending or a reactive blending (adding glycidyl methacrylate of 3 phr and dicumyl peroxide of 0.5 phr). It was found that blending PET of 10-30 wt% into PBS increased complex viscosities at the processing temperature of PBS, and these viscosities were further increased by the reactive blending. Complex viscosity data showed pseudo-plastic behaviour that the power-law indices decreased with the increase of PET content. Viscosities were higher and pseudo-plastic behaviour was more pronounced in the reactive blending. Increasing PET content increased storage moduli of the blends, but the reactive blending reduced moduli due to decreasing of crystallinity of PET phases. Shifting of glass transition temperatures toward each other confirmed the transesterification between PBS and PET and polymer branching generated by GMA.

Keywords: Poly(butylene succinate); Poly(ethylene terephthalate); GMA; Power-law index; Storage modulus.

1. Introduction

Poly(butylene succinate) or PBS is a biodegradable aliphatic polyester which can be produced from renewable resources. PBS is obtained by polycondensation of 1,4-butanediol and succinic acid [1], so it is one of aliphatic polyesters that has melting temperature of 112-118°C and glass transition temperature of about -40 to -30°C [2]. PBS has elongation at break and tensile strength comparable with those of polypropylene (PP) and low-density polyethylene (LDPE), while its crystallization behavior is similar to that of polyethylene. Although it offers excellent impact strength, melt processability and chemical resistance, PBS's rigidity might not be satisfied for load-bearing application. In order to improve rigidity

for this kind of application, blending PBS with higher mechanical strength polymer is one solution to be considered. This work attempted to increase rigidity of PBS by melt blending with poly(ethylene terephthalate) or PET that is well known for its applications in engineering applications. Kint *et al.* [3] reported the reactive blending of commercial PET pellets and laboratory synthesized PBS at 290°C led to the formation of block PET/PBS copolyesters. The PET/PBS copolymers exhibited a pronounced hydrolytic degradability, which increased with the content in 1,4-butylene succinic unit. They demonstrated to point that hydrolysis mainly occurred on the aliphatic ester groups. In this research, PBS and PET were blended with weight ratios of 100/0, 90/10, 80/20, and 70/30 wt% in a typical

melt blending or a reactive blending (adding glycidyl methacrylate of 3 phr and dicumyl peroxide of 0.5 phr). Since the melting temperatures of commercially available PBS and commercial PET polymers were vastly different, their rheological properties were investigated via a parallel plate rheometer and analyzed using the power law model. Viscoelasticity and thermal properties of the obtained blends was evaluated by dynamic mechanical analysis and differential scanning calorimeter, respectively. The understanding of rheological and viscoelastic properties would be useful for melt processing of this kind of blend.

2. Experimental Methods

2.1 Materials

Poly(butylene succinate) (PBS) pellets (BioPBS[®], Grade FZ91PM) with MFI of 5.0 g/10 min (190°C, 2.16 kg) and a density of 1.26 g/cm³ was purchased from PTT MCC Biochem Company Ltd., Thailand. Poly(ethylene terephthalate) (PET) pellets (RAMAPET[®] Grade N1) with a density of 1.40 g/cm³ and an intrinsic viscosity of 0.80 dl/g was kindly supported by Indorama Polymer Public Company Limited, Thailand. Glycidyl methacrylate (GMA, ≥97% purity, boiling point of 189°C) and dicumyl peroxide (DCP, 98% purity, melting point of 39-41°C) were purchased from Sigma-Aldrich, Thailand. These chemicals were used as received.

2.2 Specimen preparation

Prior to melt compounding, PBS was dried at 60°C for 12 hours, while PET was dried at 120°C for 6 hours. The abbreviations and compositions of all blends are presented in Table 1.

The melt blending was carried out in a twin-screw extruder (SHJ-25, S/D 40, Yongteng, China) using a screw speed of 60 rpm. The temperature profile of extruder was set-up to allow melt blending with suitable melt strength for processing. For sample#1, the temperature profile was in the range of 100-130°C. For sample#2-7, the temperature profile was in a range of 130-260°C. And, for sample#8, the temperature profile was in a range of 210-260°C. Finally, processed resins were fabricated into sheets (15 x 15 x 1 mm³) by a

compression molding (LP-S-50, Labtech Engineering, Thailand) using hydraulic pressure of 1,000 MPa.

Table 1. Abbreviations and composition of the blends.

Sample	Abbreviations	PBS (wt%)	PET (wt%)	GMA (phr)	DCP (phr)
1	PBS100_G0	100	-	-	-
2	PBS90_G0	90	10	-	-
3	PBS80_G0	80	20	-	-
4	PBS70_G0	70	30	-	-
5	PBS90_G3	90	10	3	0.5
6	PBS80_G3	80	20	3	0.5
7	PBS70_G3	70	30	3	0.5
8	PET100_G0	-	100	-	-

2.3 Thermal property by DSC

Sample sheets were cut into small pieces (5-10 mg) for thermal property analysis by a differential scanning calorimeter (DSC Pyris 1, Perkin Elmer, USA). The tests were performed in a heat-cool-reheat mode from 50 to 270°C with a heating/cooling rate of 10°C/min. Melting temperature, crystallization temperature, and the degree of crystallinity were determined.

2.4 Complex viscosity by Parallel Plate Rheometer

Specimens (0.5 x 3.0 x 1 cm³) were used to study complex viscosity by a parallel plate rheometer (Physica MCR500, Anton Paar, Germany). The tests were run in a frequency sweep mode from 0.1 to 100 rad/s. The diameter of parallel plates was 25.0 mm. All samples were run testing at 150°C, except extruder PET (PET100_G0) was tested at 260°C. The preheat time was 3.0 min. This condition referred to processing temperature of neat PBS.

2.5 Viscoelasticity by Dynamic Mechanical Analyzer

Specimens (0.5 x 3.0 x 1 cm³) were used to study dynamic mechanical properties by a dynamic mechanical analyzer (EPLEXOR[®]25N, Gabo, Germany). The tests were run in a temperature sweep mode from 50 to 100°C with a heating rate of 2°C/min. The frequency was set at 10 Hz. Static strain was 1.0% and dynamic strain was 0.0-1.0%.

2.6 FTIR analysis

Samples were grinded into powder and mixed with KBr powder (dried at 90°C for 6 hours) and then pressed into a circular disc by a hydraulic pressing. The KBR discs were then analyzed by a Fourier transform infrared spectrometer (VERTEX 70, Bruker, Germany).

3. Results and Discussion

Figure 1 presents the 1st heating DSC thermograms showing the melting temperatures of extruded PBS, extruded PET, and PBS/PET blends. Extruded PBS melted at 116°C and extruded PET melted at 258°C. It is clearly seen that the melting temperatures of PBS and PET differed about 142°C. Melting temperatures, crystallization temperatures and the degree of crystallinity are presented in Table 2. Blending PBS with PET adding GMA/DCP or no adding reduced the melting temperature (T_m) of PBS implying that the melt blending had impact on crystal structures of PBS. When blending PET of 10-20 wt% into PBS, the crystallization temperatures (T_c) slightly shifted to higher temperatures. This indicated that the crystallized PET acted as nucleating agents for PBS molecules during PBS's crystallization. As a result, the degree of crystallinity (χ) increased with the presence of PET of 10-20 wt%.

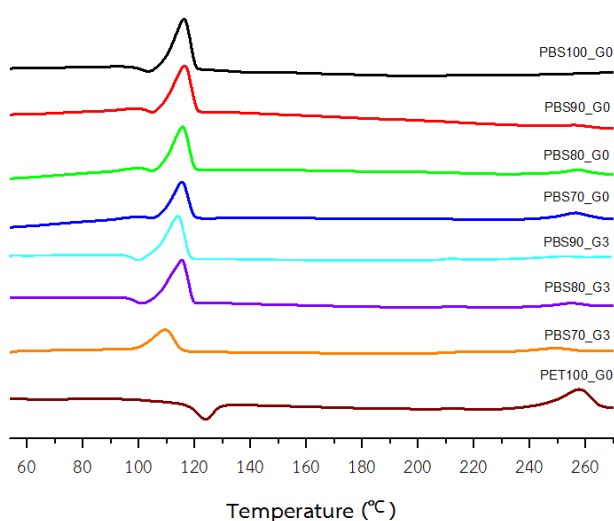


Figure 1. The 1st heating DSC thermograms of extruded neat PBS, extruded neat PET, and PBS/PET blends.

When PET of 30 wt% was blended into PBS, the T_c was shifted to occur at 100°C and the degree of

crystallinity was about the same of neat PBS. This suggested that too high content of PET could inhibit crystallization of PBS molecules. For PET, the degree of crystallinity was almost unchanged for blending PBS without adding GMA/DCP, however, the degree of crystallinity was reduced significantly when adding GMA/DCP. This was attributed to the forming of polymer branching or network that interrupted rigid PET molecules during the crystallization.

Table 2. Melting temperatures (T_m), crystallization temperatures (T_c) and the degree of crystallinity (χ).

Abbreviations	T_m (°C)		T_c (°C)		Degree of crystallinity (%)	
	PBS	PET	PBS	PET	PBS	PET
PBS100_G0	116.28	-	103.38	-	26.45	-
PBS90_G0	116.47	256.69	104.60	-	30.37	20.96
PBS80_G0	115.80	257.20	104.73	-	30.64	21.08
PBS70_G0	115.43	256.51	100.05	-	26.03	20.90
PBS90_G3	115.10	252.99	101.05	-	29.63	9.67
PBS80_G3	115.45	254.83	-	-	29.00	12.78
PBS70_G3	109.41	249.15	-	-	22.08	16.17
PET100_G0	-	257.83	-	129.98	-	20.74

Figure 2 shows complex viscosities of extruded PBS, extruded PET, and PBS/PET blends plotted against shear rates. Since data were plotted in a log-log scale, these curves were straight lines with negative slopes. This indicated pseudo-plastic behaviour of the polymers that the faster shear rate was the lower viscosity would be. Blending PET into PBS increased the complex viscosities of the blends. At 150°C, PET dispersed phases in the PBS matrix did not melt and was in the rubbery state, and thus they interrupted mobility of PBS molecules. The reactive blending with adding GMA/DCP further increased the complex viscosities of the blends. This confirmed the forming of polymer branching or networks due to a chemical reaction introduced by GMA and DCP [4].

From the complex viscosity data, the power-law model was applied in order to correlate with the pseudo-plastic behaviour. The power-law model could be written as the following equation.

$$\eta = K\dot{\gamma}^{n-1} \quad (1)$$

where η is shear viscosity, K is consistency index, $\dot{\gamma}$ is shear rate, and n is the power-law index. Data from figure 2 were fitted very well with this model, at which Table 3 summaries power-law indices, consistency indices, and correlation coefficient (R^2) after treated complex viscosities with the power-law model.

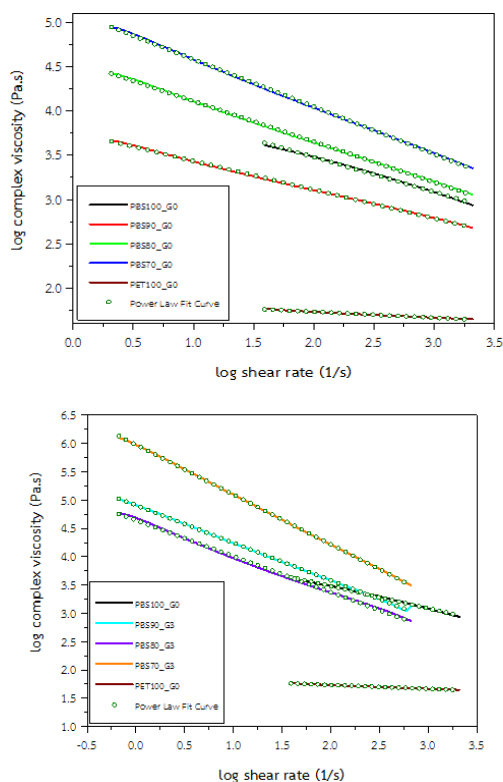


Figure 2. Complex viscosity of extruded PBS, extruded PET, and PBS/PET blends. All samples were tested at 150°C, except extruded PET was tested at 260°C.

From the calculated constants, it is found that adding PET into PBS reduced the power-law indices to be lower than that of neat PBS. Although PET dispersed phases inhibited mobility of PBS molecules, these rubbery dispersed phases would be easily stretched or oriented along with the applied shear stress. Similarly, adding GMA/DCP further reduced the power-law indices to be lower. Although occurrence of polymer branching or network increased melt viscosity, these polymer networks would be oriented by the applied shear stress as well.

Figure 3 shows storage moduli of extruded PBS, extruded PET, and PBS/PET blends from -50°C to 100°C. At about room temperature, PET is at its glassy state with much higher modulus, while PBS is at its rubbery state.

Therefore, blending PET into PBS increased storage moduli at room temperature with respect to the PET content. Compared with the same blend composition, adding GMA/DCP reduced storage moduli of the reactive blends slightly. Despite of compatibility improvement by adding GMA/DCP, reduction of crystallinity reduced the modulus of the PET dispersed phases as evident in DSC results.

Table 3. Power-law indices, consistency indices, and correlation coefficient after treated complex viscosities with the power-law model.

Abbreviations	Slope	n	K	R ²
PBS100_G0	-0.3929	0.6071	4.2651	0.9962
PBS90_G0	-0.3239	0.6761	3.7596	0.9992
PBS80_G0	-0.4578	0.5422	4.5683	0.9994
PBS70_G0	-0.5343	0.4657	5.1166	0.9994
PBS90_G3	-0.6634	0.3366	4.9076	0.9995
PBS80_G3	-0.6357	0.3643	4.6431	0.9977
PBS70_G3	-0.8805	0.1195	5.9774	0.9999
PET100_G0	-0.0669	0.9331	1.8683	0.9925

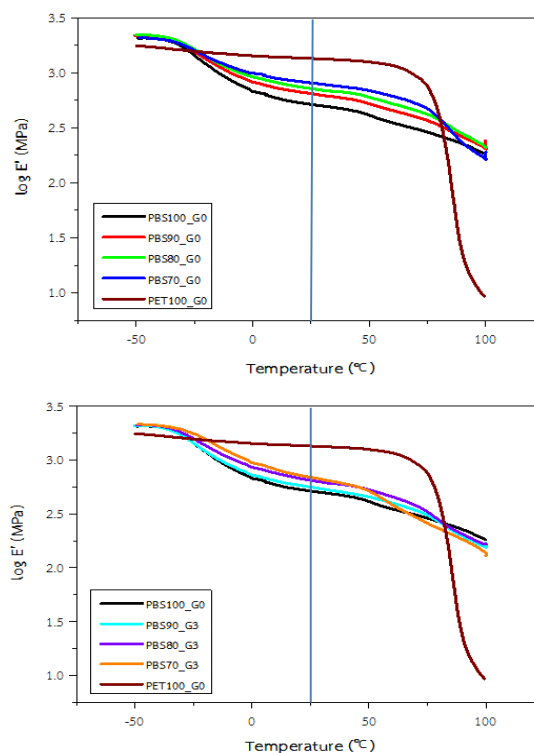


Figure 3. Storage modulus of extruded PBS, extruded PET, and the PBS/PET blends with no GMA and with GMA of 3 phr.

Figure 4 presents tan delta of extruded PBS, extruded PET, and PBS/PET blends. Peaks of tan delta indicated glass transition temperatures (T_g) of polymers. Table 4 summaries T_g of both PBS and PET phases. It is found that T_g of PBS and PET phases in all blends shifted toward each other. With the absence of GMA/DCP, the shifting of T_g implied that the transesterification between PBS and PET [5] took place. When melt blending with GMA/DCP, the chemical reaction between PBS and PET via GMA produced better compatibility [3] between phases resulting in clearly noticeable shifting of T_g .

Table 4. Glass transition temperatures (T_g) of PBS and PET phases obtained from peaks of tan delta.

Abbreviations	T_g (PBS), °C	T_g (PET), °C
PBS100_G0	-20.8	-
PBS90_G0	-19.9	85.5
PBS80_G0	-20.9	84.2
PBS70_G0	-21.2	85.4
PBS90_G3	-19.8	83.0
PBS80_G3	-16.6	79.9
PBS70_G3	-10.1	71.6
PET100_G0	-	87.7

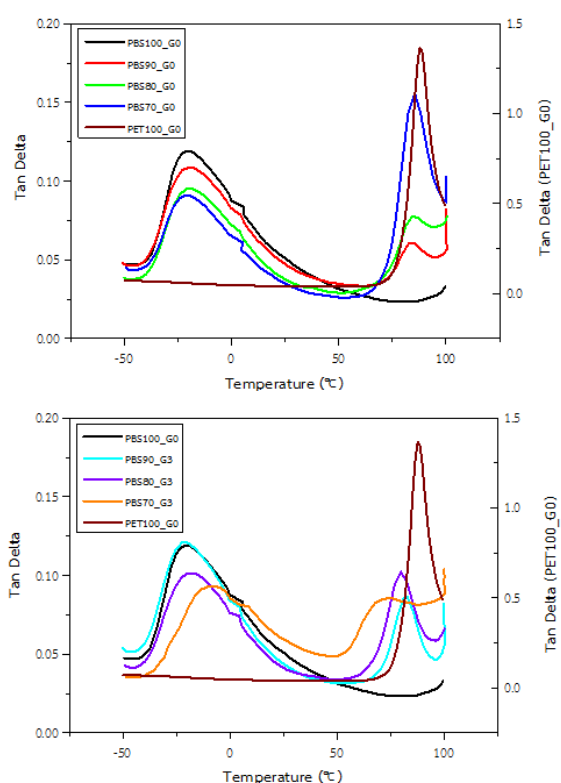


Figure 4. Tan delta of extruded PBS, extruded PET, and the PBS/PET blends with no GMA and with GMA of 3 phr.

Figure 5 shows FTIR spectra of extruded PBS, extruded PET, and PBS/PET blends with no GMA and with GMA/DCP of 3/0.5 phr. Table 5 and 6 present details of FTIR spectra wavenumbers and their assignments for functional groups of extruded polymers or polymer blends.

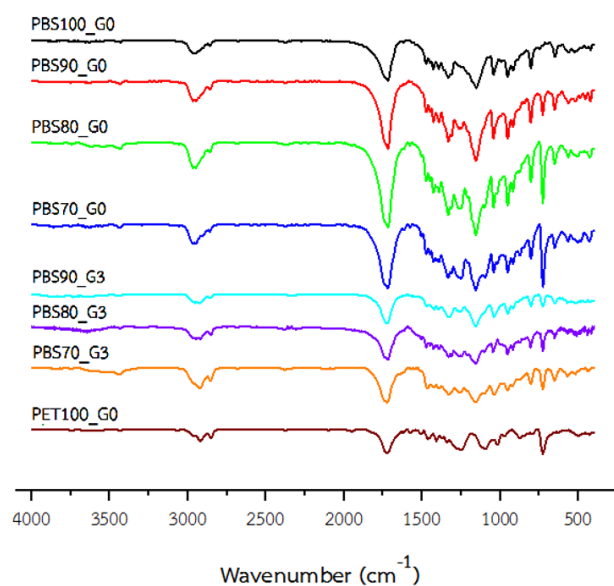


Figure 5. FTIR spectra of extruded PBS, extruded PET, and the PBS/PET blends with no GMA and with GMA of 3 phr.

Compared between extruded polymers and the blends without GMA, the shifting of carbonyl groups (esters) was attributed to the transesterification between PBS and PET molecules or the chain reaction by GMA that correlated very well to the shifting of T_g in DMA results. The hydroxyl end groups for the PBS/PET blends was still closed to that of PBS matrix. When adding GMA/DCP, the hydroxyl end groups of the blends were significantly shifted from 3663 cm⁻¹ to 3734 cm⁻¹. This supported the chain extension between the hydroxyl groups of PBS and PET molecules by GMA with the presence of initiator.

Table 5. FTIR spectra of extruded PBS and extruded PET.

Sample	Wavenumber (cm ⁻¹)	Assignments
Extruded PBS [6]	3663	hydroxyl end group
	3445	carbonyl overtone
	2972	C-H stretching
	1722	C=O stretching (aliphatic ester)
	1475	C-H bending
	1155	C-O-C asymmetric stretching
Extruded PET	3659	hydroxyl end group
	3450	carbonyl overtone
	2924	C-H stretching
	1730	C=O stretching (aromatic ester)
	1512	aromatic C-C stretching
	1468	C-H bending
	1269	asymmetric C-C-O stretching (carbon in aromatic ring)
	1105	C-O-C asymmetric stretching (ester)
	879	out of plane bending (aromatic C-H)
729	aromatic C-H wagging	

Table 6. FTIR spectra of the blends.

Sample	Wavenumber (cm ⁻¹)	Assignments
PET/PBS	3663	hydroxyl end group
	2972	C-H stretching
	1724	C=O stretching (aliphatic ester)
	1271	asymmetric C-C-O stretching (carbon in aromatic ring)
	1160	C-O-C asymmetric stretching (ester)
	810	out of plane bending (aromatic C-H)
	729	aromatic C-H wagging
PET/PBS/GMA/DCP	3734	hydroxyl end group
	2938	C-H stretching
	1723	C=O stretching (aliphatic ester)
	1554	aromatic C-C stretching
	1251	asymmetric C-C-O stretching (carbon in aromatic ring)
	1162	C-O-C asymmetric stretching (ester)
	804	out of plane bending (aromatic C-H)
725	aromatic C-H wagging	

4. Conclusion

Blending PET of 10-30 wt% into PBS increased the complex viscosities at PBS's processing temperature, and these viscosities further increased by the reactive blending using GMA of 3 phr and DCP of 0.5 phr. Complex viscosity data showed pseudo-plastic behaviour that the power-law indices decreased with the increase of PET content. The Pseudo-plastic behaviour was more pronounced in the reactive blending. Increasing PET content increased the storage moduli of the blends, but the reactive blending reduced these properties correlated to the decreasing of crystallinity of PET phases. Shifting of glass transition temperatures toward each other confirmed the transesterification reaction between PBS and PET and the chain reaction generated by GMA.

Acknowledgement

Department of Materials Science and Engineering, Faculty of Engineering and Industrial Technology, Silpakorn University is appreciated for the instrument and the financial support throughout this senior project.

References

- [1] Bordes, P., Pollet, E., and Avérous, L., "Nano-biocomposites: biodegradable polyester/nanoclay systems", *Progress in Polymer Science*, 34: 125-155 (2009).
- [2] Jamaluddin, N., Razaina, M. T., and Mohd Ishak, Z. A., "Mechanical and morphology behaviours of polybutylene (succinate)/thermoplastic polyurethane blend", *Procedia Chemistry*, 19: 426-432 (2016).
- [3] Kint, D. P. R., Alla, A., Deloret, E., Campos, J. L., and Munoz-Guerra, S., "Synthesis, characterization, and properties of poly(ethylene terephthalate)/poly(1,4-butylene succinate) block copolymers", *Polymer*, 44: 1321-1330 (2003).
- [4] Al-Itry, R., Lamnawar, K., and Maazouz, A., "Improvement of thermal stability, rheological and mechanical properties of PLA, PBAT and their blends by reactive extrusion with functionalized epoxy", *Polymer Degradation and Stability*, 97: 1898-1914 (2012).

[5] Sadik, T., Becquart, F., Majesté, J.-C., and Taha, M., "In-melt transesterification of poly(lactic acid) and poly(ethylene-co-vinylalcohol)", *Materials Chemistry and Physics*, 140: 559-569 (2013).

[6] Cai, Y., Lv, J., and Feng, J., "Spectral characterization of four kinds of biodegradable plastics: poly (lactic acid), poly (butylenes adipate-co-terephthalate), poly (hydroxy butyrate-co-hydroxyvalerate) and poly (butylenes succinate) with FTIR and Raman spectroscopy", *Journal of the Polymers and the Environment*, 21: 108-114 (2013).

Preparation and Properties of Biodegradable Citric Acid Modified Thermoplastic Rice Starch Films

Kittichai Sornsumdaeng¹, Panpailin Seeharaj^{1,2} and Jutarat Prachayawarakorn^{1,2*}

¹Department of Chemistry, Faculty of Science, King Mongkut's Institute of Technology Ladkrabang, Bangkok 10520

²Advanced Materials Research Unit, Faculty of Science, King Mongkut's Institute of Technology Ladkrabang, Bangkok 10520

Tel +66 2329 8400 ext 6235, Fax +66 2329 8428, *E-Mail : jutarat.si@kmitl.ac.th

Abstract

In order to increase mechanical strength and decrease high water absorption of thermoplastic starch (TPS); rice starch (RS), the smallest particle size, was chosen and modified by crosslink with tricarboxylic citric acid (CA). In this study, thermoplastic rice starch (TPRS) films prepared by casting technique and modified by different contents of CA, i.e. 0, 5, 10, 15, and 20 wt% (starch wt% basis) and properties were, then, analyzed. The results from FT-IR spectra showed that the additional peak position at 1734 cm⁻¹, assigned the C=O stretching was observed, indicating of ester carbonyl band. In addition, swelling behavior clearly decreased with increasing CA contents. SEM micrographs presented smoother morphology of TPRS films after cross-linked by CA. Moreover, strain at maximum load of TPRS films was found to increase with increasing content of CA.

Keywords: biodegradable; citric acid; cross-linked starch; modified starch

1. Introduction

Food packaging materials are always required with good mechanical strength, excellent barrier properties against water, high thermal stability and biodegradability [1]. Currently, materials that have been used in packaging industries are mainly prepared by using petroleum based plastic materials, since they are relatively cheap and convenient to use with excellent processing ability and durability [2-3].

From the past few years, researches have been focused on the development of biodegradable packaging by using bio-based polymers such as polysaccharides, proteins and derivative of lipids to replace petroleum-based plastic materials [2]. Among these bio-based polymers, starch is an ideal polysaccharide because it is inexpensive, renewable, non-toxic and biodegrade [3, 4]. Rice starch (RS) is the most suitable due to its smallest particle size and high surface area [5]. It was reported that packaging film made from RS showed high tensile strength and modulus than those of cassava starch. However, compared to common petroleum-based

thermoplastics, biodegradable RS products still reveal many disadvantages, such as low mechanical properties and high polarity [5, 8].

Cross-linking is a common approach to improve performance of starch for various applications. Starch and starch products have been cross-linked with various cross-linking agents e.g. citric acid (CA), epichlorohydrin and glutaraldehyde [6]. CA, a tricarboxylic acid, is an interesting choice since it is inexpensive and non-toxic [1]. It was mentioned that cross-linking caused the increase of gelatinization temperature and decrease of pasting temperature of starch [1-2, 4-5]. Furthermore, the addition of CA, lactic and malic acid into the gelatinized cassava starch led to the improvement of water resistance, thermal stabilities, mechanical properties and also rate of water transmission [4]. CA was found to form stable hydrogen bond interactions with corn starch and to prevent starch retrogradation [6]. The addition of CA to carboxymethylcellulose improved swelling behavior and

thermal properties [7]. Moreover, the addition of CA to potato starch-casted film could reduce both moisture solubility and retrogradation [9].

The objective of this research was to study properties of CA modified thermoplastic rice starch (TPRS) casted film in order to improve mechanical properties and water resistance. The effect of CA contents on properties of CA modified TPRS film was also investigated.

2. Experimental Methods

2.1 Materials

All raw materials used in this study are available as commercial products. RS was obtained from Cho Heng Rice Vermicelli Factory Co., Ltd. (Nakhon pathom, Thailand). CA was purchased from Union Chemical 1986 Co., Ltd. (Bangkok, Thailand) and glycerol (plasticizer) was supplied by Lab System Co., Ltd. (Bangkok, Thailand)

2.2 Sample preparation

Modified starch was prepared by mixing 7 g rice starch (10 wt%), 70 ml distilled water and 2.1 g (30 wt%) glycerol at the temperature of 78 ± 2 °C under stirring condition for 40 min until the solution mixture was pre-gelatinized [3-4], then, various CA contents, i.e. 0, 5, 10, 15, and 20 wt% (based on the initial dry weight of starch) were added and stirred for 3 min to ensure the completed compatibility. The films were dried for 6-8 h. at the temperature of 70 °C in a hot air oven (ULM 600/1, MEMMERT, USA). Then, the films were cured at the temperature of 150 °C for 10 min. The films were kept at 23 ± 1 °C (60% RH) in desiccator containing silica gel for 72 h before characterizing film properties.

2.3 FT-IR spectroscopic study

A sample was characterized by FT-IR analysis on a spectrum 2000 GX spectrometer (PerkinElmer, USA) using KBr disk technique with a resolution of 6 cm^{-1} using 20 scans per sample. Completed analysis was done at ambient temperature.

2.4 Swelling measurement

A sample with 1×1 inch (width x length) was placed in 250 mesh wire bag and immersed in distilled water at room temperature. The wire bag was hung up for 5 min to remove the excess solution, then, it was weighed until its weight was stabilized. The weight of the sample was measured for 1 - 72 h (i.e. 1, 2, 3, 4, 5, 6, and 72 h.) and recorded. The swelling was calculated as follows (Eq.1).

$$\% \text{ Swelling} = (W_e - W_o) / W_o \times 100 \quad (1)$$

where W_o and W_e were the dry and wet weight of the film, respectively. It should be noted that cross-linked film was thoroughly washed with excess water in order to remove unbound CA.

2.5 Morphology

A sample film was dried in a hot air oven and stored in a desiccator before examining by Scanning Electron Microscope (SEM), (FEI, quanta 250, USA). The sample was gold-sputter coated by an electro deposition technique to impart electrical conduction. Morphology of the film was operated at an accelerating voltage of 15 kV.

2.6 Mechanical properties

Tensile test was performed according to ASTM D-882 standard. A specimen was cut into rectangular shape with the dimension of $100 \times 15 \text{ mm}^2$ with a thickness of approximately 0.1 mm. Tensile properties i.e. stress at maximum load, Young's modulus and strain at maximum load were determined using Universal Testing Machine (LLOYD Instrument, LR 5K, UK) with 100 N load cell a crosshead speed of 50 mm/min. In each case, 10 specimens were tested and the average values were reported.

3. Results and Discussion

3.1 FT-IR spectroscopic study

FT-IR spectra of native TPRS film and various cross-linked TPRS films using CA contents of 0, 5, 10, 15, and 20 wt%. are shown in Figure 1. The absorption peak

observed at 3450 cm^{-1} was related to stretching vibration of O-H in RS and CA structures [5, 8]. In addition, all of the films showed similar peaks, except for the additional peak position in the cross-linked starch films at 1734 cm^{-1} . The band at 1734 cm^{-1} was ascribed to the ester carbonyl bands [6]. The presence of the carbonyl peak confirms the chemical cross-linked linkages between CA and RS components.

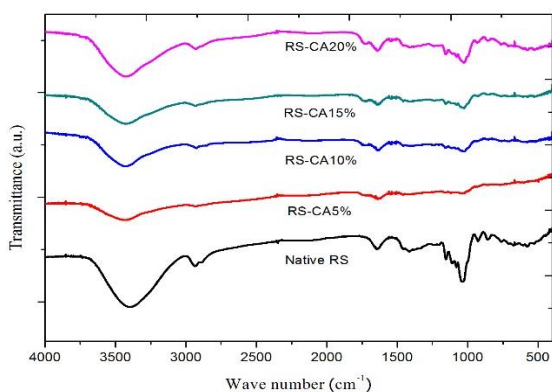


Figure 1. FT-IR spectra of native TPRS and different TPRS films modified by different contents of CA

3.2 Swelling behavior

The result of swelling behavior is shown in Figure 2. It was found that different TPRS films showed an increase of percentage of swelling with increasing immersion time. Besides, native TPRS films showed the highest swelling values. This is because native TPRS films contained abundant hydroxyl groups, preferred to form hydrogen bonds with water [7]. However, the swelling values of different cross-linked TPRS films were significantly decreased with increasing CA concentrations. The results confirm the cross-linking reaction, i.e., esterification reaction between CA and RS molecules (Figure. 1) which can reinforce the starch network both chemically and physically, thus resulting in lower percentage of swelling [7-8].

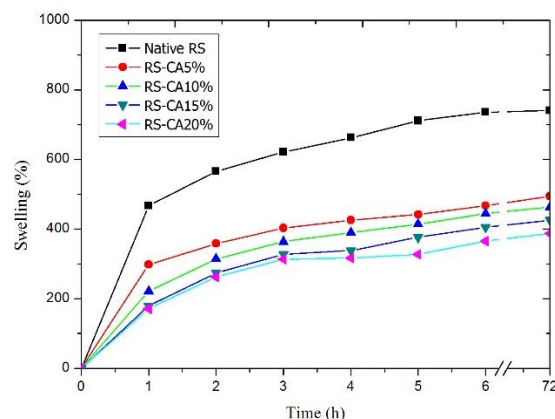


Figure 2. Swelling behavior of native TPRS and cross-linked TPRS films modified by different contents of CA

3.3 Morphology

Morphology of various TPRS films observed by SEM is presented in Figure 3. It can be seen that native TPRS film (Figure 3(a)) showed rough fractured surface morphology with some unmolten starch. The addition of CA into TPRS films (Figure 3(b)-3(e)) caused more smooth and homogeneous films, especially at high content of CA. This is caused by both cross-linking and hydrolysis of CA into starch chains.

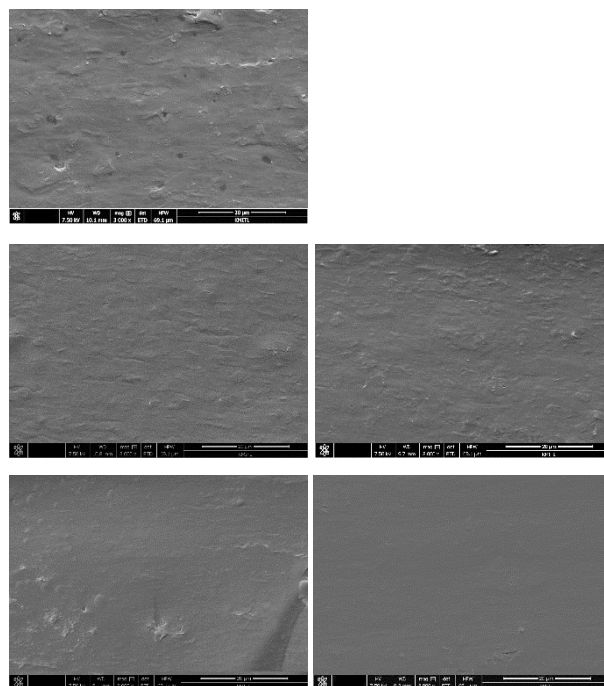


Figure 3. SEM micrographs of native and cross-linked TPRS films modified by different content of CA (a) 0 % (b) 5 % (c) 10 % (d) 15 % and (e) 20 %

3.4 Mechanical properties

The influence of different CA contents on mechanical properties of different TPRS films is shown in Figure 4. It was found that stress at maximum load obviously and Young's modulus tended to decrease considerably as CA content increased. As a result, strain at maximum load increased with increasing CA contents. This should be due to the result of cross-linking reaction between RS and CA as confirmed by FT-IR and SEM results [4]. It should be noted that TPRS film modified by CA showed significantly higher Young's modulus, stress and strain at maximum load than cassava starch film modified by CA [4]. Furthermore, stress at maximum load and Young's modulus for TPRS film modified by 20 wt% CA was comparable to LDPE commercial film [10].

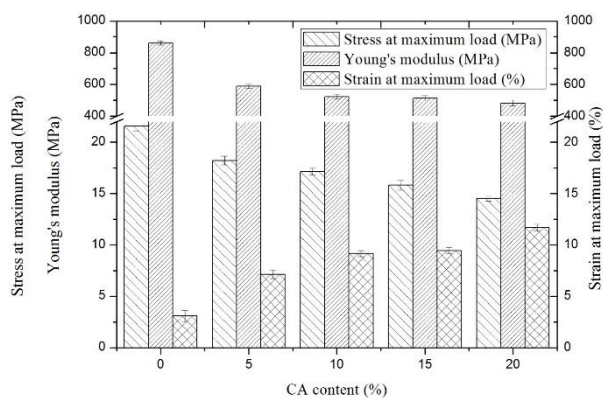


Figure 4. Mechanical properties of native TPRS and various cross-linked TPRS films modified by different contents of CA

4. Conclusion

TPRS films cross-linked by different contents of CA was successfully prepared. From FT-IR spectra, the wave number of 1734 cm^{-1} was observed, confirming of cross-linking reaction between CA and RS. In addition, the increase of CA concentration caused the decrease of the swelling behavior. SEM micrographs of different cross-linked TPRS films showed smoother cross-sectioned surface, especially at high CA content. Furthermore, the introduction of CA into TPRS films improve the mechanical properties, especially strain at maximum load. The CA-modified TPRS films can be used in food industries and packaging applications.

Acknowledgement

This research was financially supported by KMITL Research Fund. King Mongkut's Institute of Technology Ladkrabang.

References

- [1] Menzel, C., Olsson, E., Plivelic, T.S., Andersson, R., Johansson, C., Kuktaited, R., Jarnstrom, L. and Kocha, K., "Molecular structure of citric acid cross-linked starch films", *Carbohydrate Polymers* : 270–276 (2013).
- [2] Reddy, N. and Yang, Y., "Citric acid cross-linking of starch films", *Food Chemistry* : 702–711 (2010).
- [3] Kotharangannagari, K.V. and Krishnan, K., "Biodegradable hybrid nanocomposites of starch/lysine and ZnO nanoparticles with shape memory properties", *Materials and Design* : 590–595 (2016).
- [4] Prachayawarakorn, J. and Tamseekram, J., "Chemical modification of biodegradable cassava starch films by natural mono-, di- and tri-carboxylic acids", *Songklanakarin Journal of Science and Technology*, online articles.
- [5] Laohakunjit, N. and Noomhorm, A., "Effect of plasticizers on mechanical and barrier properties of rice starch film", *Starch* : 348-356 (2004).
- [6] Jiugao, Yu., Ning, W. and Xiaofei, M., "The effects of citric acid on the properties of thermoplastic starch plasticized by glycerol", *Starch* : 494-504 (2005).
- [7] Demitri, C., Sole, R. S., Scalera, F., Sannino, A., Vasapollo, G., Maffezzoli, A., Ambrosio, L. and Nicolais, L., "Novel super absorbent cellulose-based hydrogels crosslinked with citric acid", *Journal of Applied Polymer Science* : 2453–2460 (2008).
- [8] Wittaya, T., "Rice starch-based biodegradable films: properties enhancement", *Structure and Function of Food Engineering* : 103-134 (2012).
- [9] Olsson, E., Menzel, C., Johansson, C., Andersson, R., Koch, K. and Jarnstrom, L., "The effect of pH on hydrolysis, cross-linking and barrier properties of starch barriers containing citric acid", *Carbohydrate Polymers* : 1-30 (2013).

[10] Matweb material property data, 2018, Overview of materials for Low Density Polyethylene (LDPE), Film Grade, [online] Available :

<http://www.matweb.com/search/DataSheet.aspx?MatGUID=9ff98d958a714b2a8a00990a929d6f14>.

Influence of waste paper fiber on the physical properties of natural rubber graft cassava starch

Rangsima Jarusuwanwong, Lalisa Bunmechimma and Sa-Ad Riyajan*

Department of Chemistry, Faculty of Science and Technology, Thammasat University, Phahonyothin Road
Pathumthani, 12120, Thailand, *E-Mail: saadriyajan@hotmail.com

Abstract

The objective of this work was to study the preparation and properties of a novel biopolymer composite produced from waste paper (PF) and natural rubber-*graft*-cassava starch (NS) made by using water based route. The water resistance and toluene resistance of the polymer composite were enhanced after the addition of the PF compared to the pristine NS. The moisture content of the composite was mostly constant. But the moisture absorption increased as function of storage time and the PF content. The contact angle of the sample increased with increasing of the PF content. The swelling ratio, moisture content and moisture absorption of the specimen was improved after the incorporation of urea.

Keywords: Rubber, Composite, Blend, Latex, Waste

1. Introduction

Paper is a significant component of our daily life and likewise one of the most prominent cellulosic biomass wastes produced in an ample amount in several subjects. In recent years, solid wastes from waste paper which comes from office plays an important role in damaging the ecology of the earth and have raised serious environment issues. In previous work, recycling of one ton of waste paper can save 17 trees and 7000 gallons of water [1] which has great environmental and economic benefits. Therefore, how to make this paper from waste to wealth and use it in new approaches, i.e. recycling of office waste paper, have become a meaningful and challenging work. In the previous work, waste paper was used to raw material for building materials due to their advantageous properties, low environmental impact and low cost [2]. The waste paper use improved the workability of fresh cement [2], raw material for biogas [3-4] and filler for NR [5].

In case of NR, it was grafted with poly(dimethylaminoethyl methacrylate) [6], poly(lactic acid) [7], poly(methyl methacrylate) [8], poly(2-hydroxyethyl acrylate) [9] and starch [10]. For example, the natural rubber grafted cassava starch (NS) was produced as

polymer membrane for encapsulation of urea [11]. Results showed that the hydrophilicity of natural rubber (NR) was enhanced after the incorporation of the CS. The swelling ratio of the modified NR increased as function of the CS in water. The NS provided a good controlled-release for urea. The NS foam was produced by the addition of super cell (SC) as a blowing agent [12]. The optimum curing time decreases with increasing SC loading as observed using a moving die rheometer. A more open cell structure is produced by higher loadings of SC. Finally, the foam produced was used as an absorbent for oil. The NS foam provided a maximum percentage oil absorption of around 7 g g⁻¹.

Here, the PF was used a filler for the NS to improve the mechanical properties. The properties including moisture content, moisture absorption, swelling ratio and contact angle of the composite were investigated.

2. Experimental Methods

2.1 Preparation of the PF and NS

In the preparation of PF, waste paper were immersed in 10% NaOH solution for 24 h and then washed

with water until reaching neutral pH. The wet cellulose was mixed with 50%w/w sulfuric acid at 90°C for 5 h. At the end of the reaction, the suspension was centrifuged and washed with excess distilled water. This reaction was performed seven times. The diameter of dried cellulose fiber was determined under an optical microscopy (OM; Primo Star Company, Carl Zeiss). NS was prepared following the method outlined in our previous work [13]. Before use, the CS sample obtained was dried in an oven at 50 °C for 48 h. A CS solution was prepared by dissolving CS in distilled water containing 2% (v/v) of K₂S₂O₈ at 85 ± 3 °C for 1 h. After cooling, the gelatinized CS was mixed with 10 g of 0.5% w/w K₂S₂O₈ solution, and stirred at 60 °C for 45 min to obtain a modified CS. Then 86 g of 60% dry rubber content NR latex was mixed with 500 g of the 10% modified CS in the presence of Triton-X 100.

2.2. Preparation of polymer composite

The PF suspension with various contents was blended with 10% (w/v) of NS latex at room temperature by using a homogenizer (PL Trading International Co. Ltd.; Bangkok, Thailand). The effect of urea as plasticizer (Ajax Finechem pty ltd, New Zealand) on the properties of the NS composite was studied. In order to form a sheet of 0.45mm in thickness, the mixture was poured into a glass plate (10cm×10cm×0.5 cm) at ambient temperature.

2.3. Characterization

The film's moisture content (1 cm×1 cm) was analyzed by measuring the weight loss before and after drying in oven at 110 °C for 2 h and then was calculated from the following as shown in equation (1).

$$\% \text{ Moisture content} = (W_i - W_f) / W_i \times 100\% \dots \dots (1)$$

Water absorption test was performed in accordance with the ASTM standard E104. All specimens for water absorption were cut from the 80/20 CS/NR blend films with dimensions of 1 × 1 cm² and dried at 70 °C for 24 h. The dried samples were placed in a desiccator containing calcium sulfate (RH = 0%) for three days and afterwards

the initial weight of the samples were measured. The samples were then transferred into a desiccator containing potassium sulfate (RH = 98%) and the time taken to reach a constant weight was marked. The water absorption (WA) of the specimens was calculated as follows as shown in (2):

$$\text{Water absorption (\%)} = (W_1 - W_0) / W_0 \times 100 \dots \dots \dots (2)$$

where, W₁ is the weight of the sample at the time in 98% RH and W₀ is the initial sample weight exposure to 98% RH. An average value of the three replicates for each sample was reported.

The swelling ratio in both distilled water and toluene was determined. A sample of the 80/20 CS/NR blend films was weighed before being immersed in 25 mL of distilled water at room temperature for 7 hours. After that, the sample was reweighed after removing excess water from the surface of the beads with tissue paper. The swelling ratio was calculated as follows as shown in (3):

$$\text{Swelling ratio} = (W_4 - W_3) / W_3 \dots \dots \dots (3)$$

where W₃ is the initial dry weight of the sample (g) and W₄ is the weight of the swollen sample (g).

The water contact angle (WCA) was carried out on an OCA 20 (Dataphysics, Germany) to evaluate the hydrophilic performance of NS composite sheets. During testing, water drops of 2 µl were controlled by the syringe system of the tester and dispensed drop by drop onto the surface of the samples. The contact angle values were calculated using the contact angle meter software on basis of the droplet shape in the image. For each sample, measurements were repeated at several different positions, and its contact angle was finally determined by averaging these contact angle values from various measurements.

3. Results and Discussion

The influence of PF on the % moisture content of NS is presented in Figure 1. It was found that the moisture content of the NS was 5%. After the addition of PF into the

NS, the % moisture content of all samples decreased. The lowest moisture content was found when using 2 g PF.

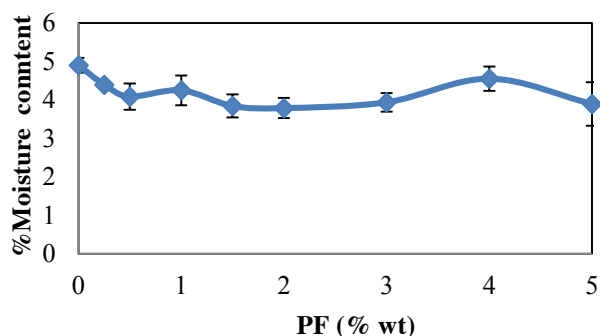


Figure 1 Influence of PF on the % moisture content of NS composite with different PF contents

However, when the amount of PF was over 2 %, the moisture content slightly increased owing to hydrophilic behavior of the PF [14]. Urea was applied to be a plasticizer for NS containing 5 % PF sample and results shown in Figure 2. At low amount urea, the moisture content of sample decreased. The minimum moisture content was found at 0.5 % urea. However, when the amount of urea increase from 0.5 to 1%wt, the moisture content of sample increased from 3 to 3.8% due to excess urea in the composite [15].

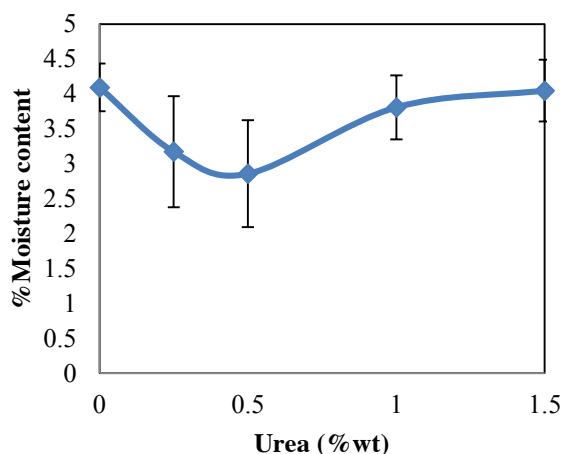


Figure 2 Influence of urea on the %moisture content of the NS composite with different PF contents

Moisture absorption of the NS composite was determined gravimetrically. The effect of the PF content and urea on the moisture absorption of the NS is presented

in Figure 3 and Figure 4, respectively. It was found that the moisture absorption of sample increased as a function of the PF. Thus, when NS samples were placed above the water vapor, the water vapor was absorbed on NS composite due to the larger intermolecular forces between water molecules and NS composite, and molecular diffusion happened from water molecule to NS composite. Subsequently, the water molecule was desorbed on the other side of NS composite and the water vapor permeability ended. The highest moisture absorption of the sample was found when using 5 % PF and its value was 20%. In case of urea, the moisture absorption of the sample increase dramatically after the incorporation of urea. For example, the moisture absorption of the NS composite the presence of 0.25% urea was 17%. When the amount of urea increased from 0.25% to 0.5%, the moisture absorption of sample increased from 17% to 20%. The maximum moisture absorption was observed when using 1.5%wt. These results are opposite with previous work [16]. They studied the effect of SiO₂ on the moisture absorption of poly(vinyl alcohol) (PVA)/chitosan blend. Results showed that the moisture absorption of this sample decreased after the silica. The PVA/chitosan blend with 0.6% silica is superior to the film without silica in preventing moisture transfer, which is required as a food package. High water vapor permeability of films significantly restricts their application as potential materials for food packaging.

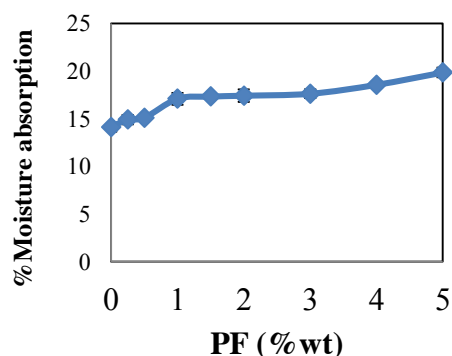


Figure 3 Influence of PF on the %moisture absorption of NS composite with different PF contents

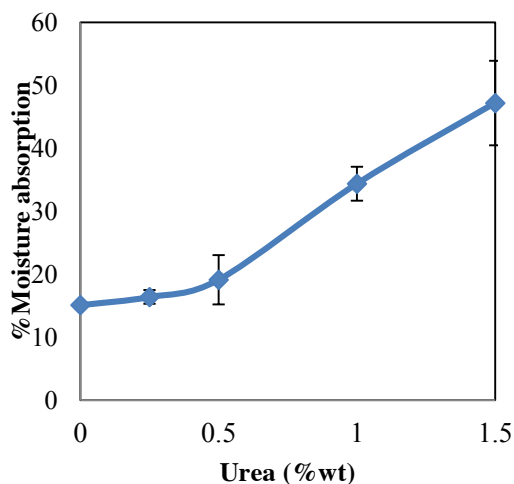


Figure 4 Influence of urea on the %moisture absorption of NS composite with different PF contents

The influence of PF on the swelling ratio of sample is presented in Figure 5. The swelling ratio of the NS was 130%. When the NS was blended with the PF at 0.25 %, the swelling ratio of sample was 140%. When the PF increased from 0.25 to 0.5 %, the swelling ratio of sample was 170%. However, when the amount of the PF was over 0.5 %, the swelling ratio of sample dramatically decreased as a function of the PF.

These results are similar to those of a previous study [17]. They studied the swelling ratio of bacterial cellulose / gelatin hydrogel in water. The swelling ratio of sample decreased as a function of the bacterial cellulose. This might be due to the formation of a more rigid hydrogel structure, which hindered the penetration of water molecules. Hence, the degree of water absorption and permeation decreased, which led to a reduction in the swelling ratio.

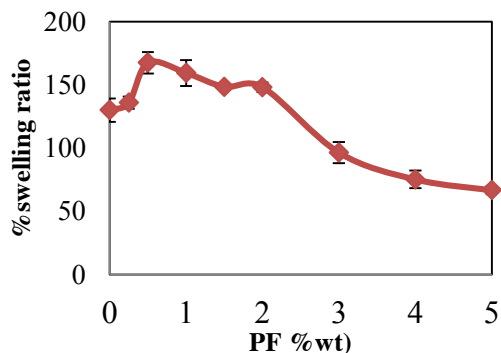


Figure 5 Influence of PF on the %swelling ratio of NS composite with different PF contents in toluene

In case of urea, the swelling ratio of sample decreased as a function of urea content owing to hydrophilic behavior of urea as shown in Figure 6.

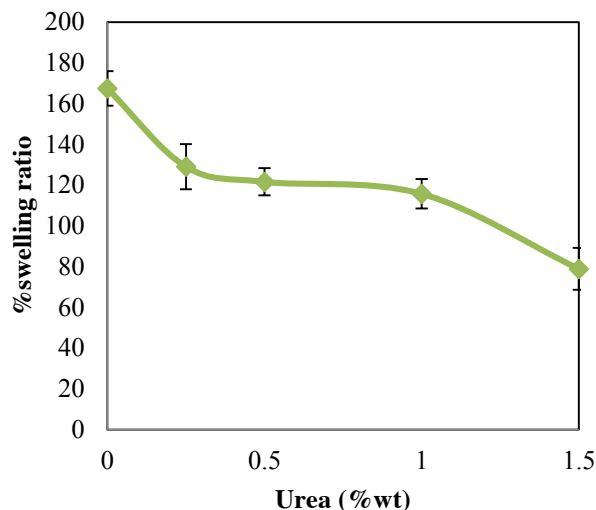


Figure 6 Influence of urea on the %swelling ratio of NS composite with different PF contents in water

Figure 7 represents the influence of PF on the swelling ratio of the NS in toluene. It is clear that the swelling ratio of sample decreased as function of PF content. For example, the swelling ratio of the NS in the presence of the PF at 3, 4 and 5 g was 210, 150 and 130%, respectively in toluene for 30 min. When the immersion time in toluene was 180 min, the swelling ratio of sample at 3, 4 and 5 g was 160, 116 and 109%, respectively.

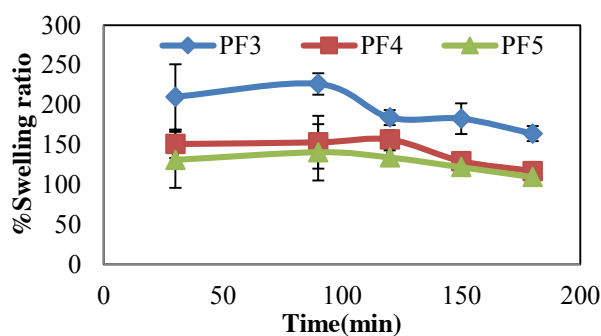


Figure 7 Influence of PF on the %swelling ratio of NS composite with different PF contents in toluene

In case of urea, the swelling ratio of sample decreased with increasing urea content as shown in Figure 8.

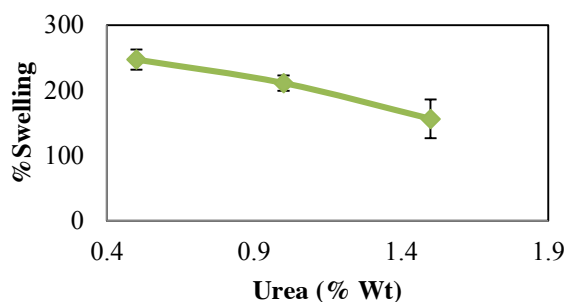
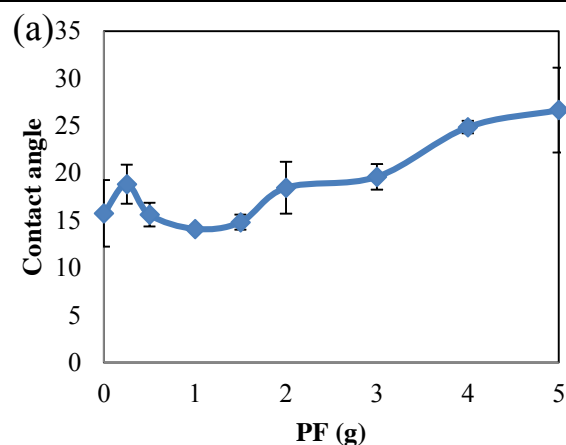


Figure 8 Influence of PF on the %swelling ratio of NS composite with different PF contents in toluene

To investigate the hydrophilic performance of NS composite prepared using different PF concentrations

The influence of PF on the contact angle is presented in Figure 9 (a). The contact angle of sample was 15° suggesting that NS films were hydrophilic. At low amount of the PF, the contact angle of sample was almost constant. However, the amount of the PF was more than 1 g, the contact angle of sample slightly increased as a function of PF. The maximum contact angle was found at 5 g PF.

The influence of the urea on the contact angle of sample is presented in Figure 9 (b). The contact angle of sample containing 0.3 g PF was 22°. When the amount of PF increased from 0.3 g to 0.5 g, the maximum contact angle was found. Then, the contact angle of sample decreased when the amount of urea was over 0.5 g. This was might be due to excess urea. This result might have arisen from the existence of hydrophilic hydroxyl groups in urea.



(b)

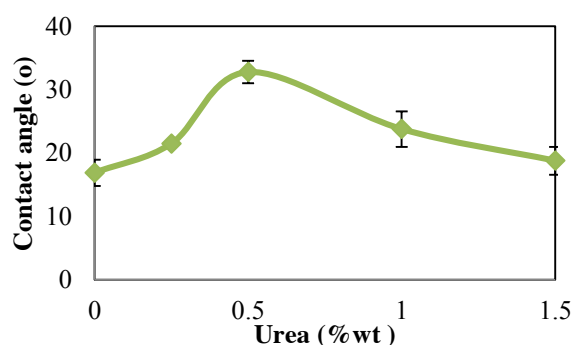


Figure 9 Influence of PF and urea on the contact angle of NS composite with different PF contents in toluene

4. Conclusion

The novel biopolymer composite was successfully made from the PF and NS by using water based route. The water resistance and toluene resistance of the polymer composite were enhanced after the addition of the PF compared to the pristine NS. The moisture content of the composite was mostly constant. But the moisture absorption of these samples increased as function of storage time and the PF content. The contact angle of the composite increased with increasing of the PF content. After the addition of urea, the swelling ratio, moisture content and moisture absorption of the specimen enhanced with the urea contents.

References

- [1] Joshi, G., Naithani, S., Varshney, V.K., Bisht, S.S., Rana, V. and Gupta P.K., Synthesis and characterization of carboxymethyl cellulose from office waste paper: a greener approach towards waste management, *Waste Management*, 38 (2015) 33-40.
- [2] Stevulova, N., Briancin, J. and Kostelanska, K., Investigation of waste paper cellulosic fibers utilization into cement based building materials, *Buildings*, 8 (2018) 43-49.
- [3] Rodriguez, C., Alaswad, A., El-Hassan, Z. and Olabi, A.G., Mechanical pretreatment of waste paper for biogas production, *Waste Management*, 68 (2017) 157-164.
- [4] Nishimura, H., Tan, L., Kira, N., Tomiyama, S., Yong Sun, K.Y., Tang Y.Q, Morimura, S. and Kid, K., Production of ethanol from a mixture of waste paper and kitchen waste via a process of successive liquefaction, presaccharification, and simultaneous saccharification and fermentation, *Waste Management* 67 (2017) 86-94.
- [5] Nashar, D.E.E., Abd-El-Messieh, S.L. and Basta A.H., Newsprint Paper Waste as a Fiber Reinforcement in Rubber Composites, *Journal of Applied Polymer Science*, 91 (2004) 469-478.
- [6] Jayadevan, J., Alex, R and Gopalakrishnanicker, U., Deproteinised natural rubber latex grafted poly(dimethylaminoethyl methacrylate) – poly(vinyl alcohol) blend membranes: Synthesis, properties and application, *International Journal of Biological Macromolecules*, 107 (2018) 1821-1834.
- [7] Wongngam, Y. and Pattamaprom, C., Synthesis and characterization of poly(lactic acid)-grafted natural rubber by reactive melt-blending technique, *Defect and Diffusion Forum*, 382 (2018) 7-11.
- [8] Moolsin, S., Saksayamkul, N. and Wichien, A.N., Natural rubber grafted poly(methyl methacrylate) as compatibilizer in 50/50 natural rubber/nitrile rubber blend, *Journal of Elastomers and Plastics*, 49(2017) 422-439.
- [9] Chueangchayaphan, W., Tanrattanakul, V., Chueangchayaphan, N., Muangsap, S. and Borapak, W. Synthesis and thermal properties of natural rubber grafted with poly(2-hydroxyethyl acrylate), *Journal of Polymer Research*, 24 (2017)107-114.
- [10] Riyajan, S.A. A Novel Hybrid 2,4-Dichlorophenoxy Acetate Bead from Modified Cassava Starch and Sodium Alginate with Modified Natural Rubber Coating, *Journal of Polymers and the Environment*, 26 (2018)1950-1961.
- [11] Riyajan, S.-A., Sasithornsonti, Y. and Phinyocheep, P., Green natural rubber-g-modified starch for controlling urea release, *Carbohydrate Polymers*, 89(2012)251-258.
- [12] Riyajan, S.A. and Keawittarit, P., A novel natural rubber-graft-cassava starch foam for oil/gasohol absorption, *Polymer International*, 65(2016) 491-502.
- [13] Riyajan, S. Robust and biodegradable polymer of cassava starch and modified natural rubber, *Carbohydrate Polymers*, 134 (2015) 267-277.
- [14] Lundgren, J.E. and Gudmundson, P. Moisture absorption in glass-fibre/epoxy laminates with transverse matrix cracks, *Composites Science and Technology*, 59 (1999) 1983-1991.
- [15] Wang, J.L., Cheng, F. and Zhu, P.X. Structure and properties of urea-plasticized starch films with different urea contents, *Carbohydrate Polymers*, 101 (2014) 1109-1115.
- [16] Yu Z., Li B., Chu J. and Zhang P. Silica in situ enhanced PVA/chitosan biodegradable films for food packages, *Carbohydrate Polymers*, 184 (2018) 214-220.
- [17] Treesuppharat W, Rojanapanthu P., Siangsanoh C., Manuspiya H. and Ummartyotin S. Synthesis and characterization of bacterial cellulose and gelatin-based hydrogel composites for drug-delivery systems. *Biotechnology Reports* 15 (2017) 84-91.

Effect of Glycerol Contents on Properties of Hydrogel Sponge from Basil Seed Mucilage

Siriporn Tantiwatcharothai¹ and Jutarat Prachayawarakorn^{1,2*}

¹ Department of Chemistry, Faculty of Science, King Mongkut's Institute of Technology Ladkrabang, Bangkok 10520

² Advanced Materials Research Unit, Faculty of Science, King Mongkut's Institute of Technology Ladkrabang, Bangkok 10520

Phone +66 2329 8400, Fax +66 2329 8428, *E-Mail: jutarat.si@kmitl.ac.th

Abstract

Due to a large capacity for hydration of basil seed mucilage (BSM), the objectives of this research were to prepare hydrogel sponge from BSM and investigate the effect of glycerol contents on properties of BSM hydrogel sponge. Different BSM hydrogel sponges were prepared by freeze-drying technique using various contents of glycerol i.e. 0 wt%, 15 wt% and 30 wt%, as a plasticizer. It was found that FTIR spectra showed a shift to lower wavenumber of O-H stretching peak by the addition of glycerol, indicating of new hydrogen bond formation between glycerol and BSM phases. SEM image also revealed interconnecting open-cell structure of pores in unplasticized BSM hydrogel sponge. BSM hydrogel sponges plasticized with glycerol presented tight network structure and narrow transport pores with the increase of glycerol content. Furthermore, the increase in glycerol contents clearly resulted in the increase of hardness but the decrease of thickness of BSM hydrogel sponges. In addition, the increase in glycerol content also resulted in a considerable increase in degree of swelling of BSM hydrogel sponges. Moreover, thermal decomposition temperature of BSM hydrogel sponge improved by the use of glycerol plasticizer.

Keywords: basil seed mucilage, freeze-drying, glycerol, hydrogel sponge

1. Introduction

Worldwide consumption of bioplastics has increased more than 600% in the past decades. This remarkable growth is resulted from the global trend of environmental awareness [1]. Hydrogels are physical or chemical cross-linked macromolecules forming a three dimensional network capable of retaining water without disintegrating. The use of natural polymers in hydrogels is advantageous due to their biodegradability and non-toxicity. Basil (*Ocimum americanum L.*) seed is one of an interesting product of Thailand. Basil seed mucilage (BSM) is high molecular weight heteropolysaccharide. It composes of D-glucose, D-galactose, D-mannose, L-arabinose, D-xylose, and L-rhamnose in the approximate proportions of 25:25:10:15:15:5, along with uronic acid [2, 3]. Basil seed offers a great potential for use as an emulsifying, foaming, thickening and gelling stabilizing agents in food and pharmaceutical industries. There was a few reports for the use of BSM. It was mentioned that BSM showed a

good potential to be used for edible films in various food applications and coatings. BSM film was transparent and presented good tensile strength and excellent barrier properties [4]. Additionally, thermostable ultra-thin BSM/PVA nanofibers was reported to be used for different applications in food sector such as bioactive encapsulation [5]. As a result of BSM water holding capacity, BSM is a novel natural source of polysaccharides and could potentially generate interesting polymer for water holding application such as hydrogel sponge. However, there is no report for the use of BSM as a material for hydrogel sponge.

The aim of this study was to prepare a new natural hydrogel sponge based on BSM and to examine physical, mechanical, thermal and microstructural properties of the hydrogel sponge as a function of varying concentration of glycerol as plasticizer (0, 15 and 30 wt% of BSM).

2. Experimental Methods

2.1 Hydrogel sponge preparation

BSM was obtained with hydration process. The basil seeds were soaked in distilled water at the ratio of seed: water at 1:30 for 1 h at room temperature. Then, the swollen seed was stirred with a blender for 1 min to scrape the mucilage layer off the seed surface. Separation of the mucilage from the swollen seeds was achieved by filtration with muslin cloth. The resulting mucilage was frozen at -40°C for 24 h in a deep freezer (DW-40L92, Haier, China), followed by lyophilization at -100°C for 24 h using a freeze dryer (Coolsafe 110-4, Scan Vac, Denmark) to obtain the dried BSM. For the preparation of hydrogel sponge from BSM with various concentration of glycerol, BSM was dissolved in distilled water (1%w/w) using glycerol as a plasticizer (0, 15, 30 wt% of BSM). The solutions were mechanically stirred using a magnetic stirrer at 40°C for 45 min. After that, the solution was refrigerated and lyophilization at the same condition as mentioned.

2.2 Hydrogel sponge characterization

2.2.1 Fourier Transform Infrared Spectroscopy (FT-IR)

Functional groups of different hydrogel sponges were analyzed by using Fourier-Transform Infrared (FTIR) Spectroscopy, (Perkin Elmer Model Spectrum GX, USA). The sample was tested by the transmission method in the range of 4000-600 cm⁻¹.

2.2.2 Hardness testing

Hardness testing was carried out according to technical standard method ASTM, D 2240 using type OO durometer, (Teclock, Japan). All the measurements were carried out at 50% relative humidity. The thickness of specimens was approximately 6 mm. 5 specimens were tested to obtain the average values.

2.2.3 Morphology

The morphology of BSM hydrogel sponge was observed using a scanning electron microscope (SEM), (LEO 1455VP, ZEISS, Germany). BSM hydrogel sponge was fractured in liquid nitrogen before the

examination. Prior the tests, the sample was covered with a thin layer of gold for thermal and electrical conduction.

2.2.4 Degree of swelling

BSM hydrogel sponge (20×20 mm²) was weighted and immersed in deionized water at room temperature for 48 h. The degree of swelling of hydrogel sponges were measured after immersing the sample for different periods of time, i.e. 0.5, 1, 2, 3, 4, 5, 6, 24 and 48 h. After swelling, the hydrogel sponge were taken out of water and removed water that adhered on the surface by gently blotting with tissue paper and immediately weighted. The degree of swelling (DS) was calculated by Eq.1

$$DS = \frac{m_w - m_0}{m_0} \times 100 \quad (1)$$

where m_0 and m_w were the weight of the hydrogel sponge before and after immersion.

2.2.5 Thermal properties

Derivative thermal gravimetric (DTG) analyses of a specimen was scanned within a temperature range of 30 to 600°C at the heating rate of 10°C/min under nitrogen atmosphere using thermogravimetric analyzer (Pyris I TGA HT, Perkin Elmer, USA).

3. Results and Discussion

3.1 Functional group analysis

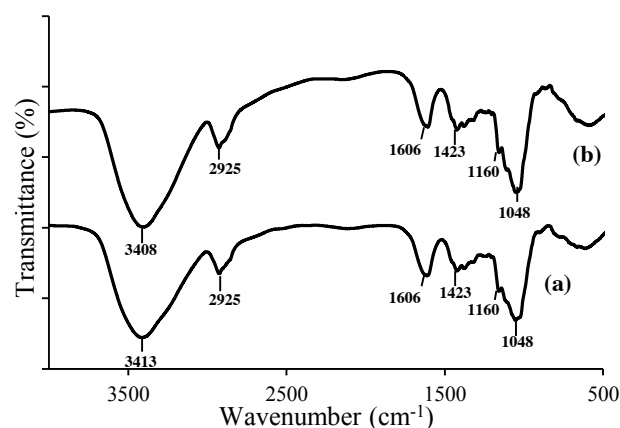


Figure 1 FT-IR spectra of different BSM hydrogel sponges (a) unplasticized (b) plasticized with 15%w/w of glycerol

Figure 1 shows FT-IR spectra of unplasticized and plasticized BSM hydrogel sponges. Two spectra presented similar characteristic peaks. The broad peak around 3400-3000 cm^{-1} was attributed to the complex vibrational stretching associated with free, inter- and intra-molecular hydroxyl groups. The peak position at 2925 cm^{-1} were arisen from the characteristic of C-H stretching. The wave numbers at 1606 cm^{-1} and 1423 cm^{-1} were caused by C=O asymmetric and symmetric stretching of free carboxylate, respectively. The presence of both peak positions confirmed the existence of uronic acid in BSM. In addition, the peaks at 1160 cm^{-1} and 1048 cm^{-1} were attributed to C-O and C-O-C stretching, respectively [3]. It should be noted that, a shift of the broad absorption band due to O-H stretching from 3413 to 3308 cm^{-1} was observed, indicating that hydrogen bonding occurred between BSM and glycerol molecules.

3.2 Scanning electron microscopy

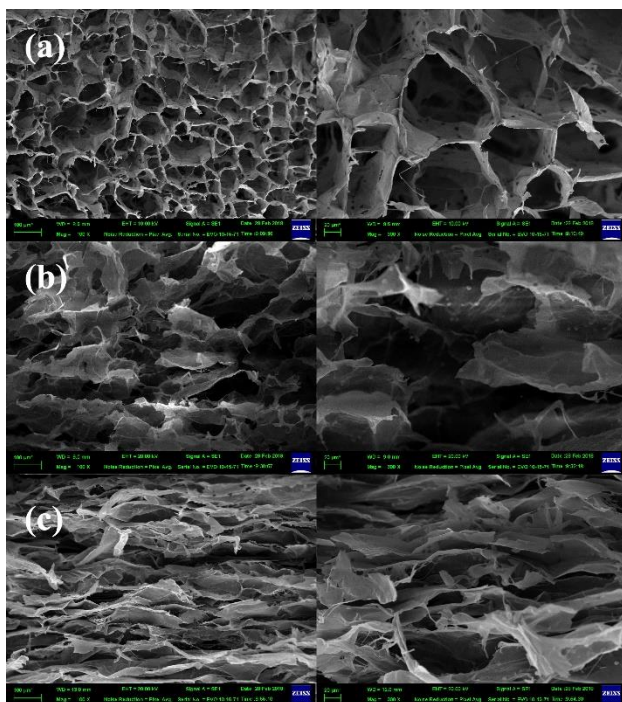


Figure 2 SEM images of different BSM hydrogel sponges (a) unplasticized (b) plasticized with 15%w/w of glycerol (c) plasticized with 30 wt% of glycerol; magnification of 100X (left) and 300X (right)

Figure 2 presents the microstructure of cross-section BSM hydrogel sponges at various contents of

glycerol. After prefreezing and freeze-drying, water in BSM solution became ice and, then, sublimed to be pores. It can be seen that, BSM hydrogel sponges represented interconnecting open-cell structures of pores. Unplasticized BSM hydrogel sponge (Figure 2(a)) showed many large round pores; on the other hand, BSM hydrogel sponges plasticized with glycerol (Figures 2(b) and 2(c)) presented different morphology. The round pores turned to be transported pores and tight network structure with increasing glycerol content. This could be caused by a plasticizing effect brought about better distribution of water in BSM during the mixing method. As a result, the pores were connected with each other after freeze-drying and turned to be transported pores.

3.3 Hardness properties

Thickness and hardness (shore OO) of different BSM hydrogel sponges are shown in Table 1. It can be observed that the thickness of BSM hydrogel sponges decreased with increasing glycerol contents. This is may be due to the plasticizing effect of glycerol which corresponded to SEM image (Figure 2). The pores were narrower and the network structure was tighter when glycerol content increased. For hardness (shore OO) testing, it was found that hardness increased with increasing of glycerol contents. The increase of hardness could be due to the decrease of distance between BSM layers and tighter network as seen in SEM images (Figure 2).

Table 1 Thickness and Hardness of different BSM hydrogel sponges

Sample	Thickness (mm)	Hardness (shore OO)
BSM/0%Gly	3.09 ± 0.43	13.20 ± 1.52
BSM/15%Gly	1.53 ± 0.26	33.17 ± 3.04
BSM/30%Gly	0.80 ± 0.14	49.33 ± 5.71

3.4 Swelling property

The degree of swelling of unplasticized and plasticized BSM hydrogel sponges is shown in Figure 3.

It can be seen that BSM hydrogel sponges show very high degree of swelling. Hydrogel sponges rapidly adsorbed water within 1 h; after that, lower amount of water was adsorbed and reached a plateau indicating that they became equilibrated. This result was higher than several reports [6-7]. Aloe vera and acacia gum hydrogel sponge were achieved a degree of swelling about 3,000% and 4,700%, respectively [6-7]. High degree of swelling of BSM hydrogel sponge could be due to hydrophilicity of $-\text{COOH}$ group of uronic acid in BSM molecules. In addition, there was significant difference between the degree of swelling of hydrogel sponges made from different glycerol contents. The degree of swelling increased significantly with an increase in glycerol content. This could be due to the plasticizing effect of glycerol. The glycerol diminished interactions between BSM molecules and a consequent increase of free volume and segmental motions, allowing water molecules to diffuse more easily and giving higher degree of swelling which suitable for hydrogel applications.

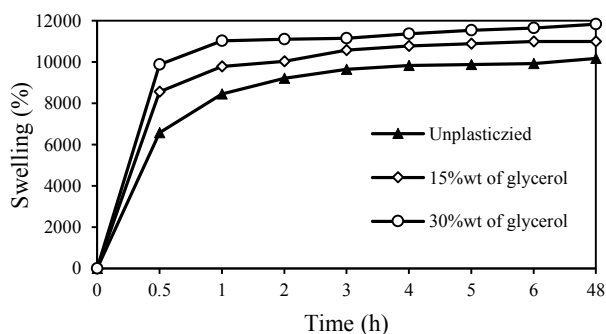


Figure 3 Degree of swelling of unplastized and plasticized BSM hydrogel sponges.

3.5 Thermogravimetric analysis

DTG thermograms of unplastized and plasticized BSM hydrogel sponges are shown in Figure 4. DTG analysis showed three thermal degradation steps for unplastized BSM hydrogel sponge. The first step was related to an initial weight loss due to moisture vaporization between 35- 100°C. The main degradation step at 255-340°C was due to thermal degradation of BSM. The third step at 410-460°C was due to continuous

decomposition of BSM. These results corresponded to the results reported by Khazaei N. *et al.* who reported thermal degradation temperature of BSM casted film [4]. For BSM hydrogel sponges plasticized with 15%w/w of glycerol, the additional degradation step at 120-210°C was observed. This step was caused by the thermal decomposition of glycerol in BSM hydrogel sponge.

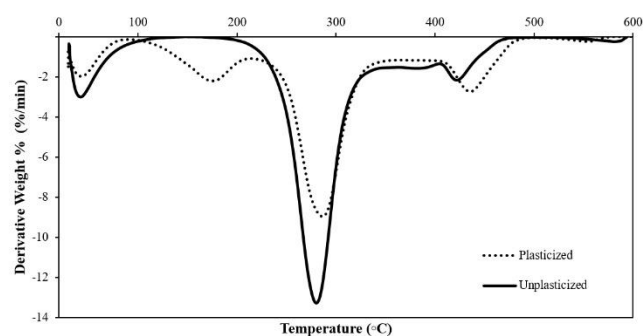


Figure 4. DTG thermograms of unplastized and plasticized BSM hydrogel sponges

It should be mentioned that BSM hydrogel sponges plasticized with glycerol showed higher degradation temperature than unplastized BSM hydrogel sponge. This should be due to the presence of hydrogen bonding between glycerol and BSM as confirmed by the shift of IR wavenumber (Figure 1).

4. Conclusion

BSM hydrogel sponges were successfully prepared by freeze-drying technique. For the results, FTIR spectra showed new hydrogen bond formation between BSM and glycerol, as a result from IR shift. SEM image presented interconnecting open-cell structure of pores in unplastized BSM hydrogel sponge. BSM hydrogel sponges plasticized with glycerol revealed tight network structure and narrow transport pores with the increase of glycerol content. Moreover, the increment of glycerol content resulted in the decrease of thickness and the increase of hardness, caused by the plasticizing effect of glycerol. Furthermore, degree of swelling substantially increased with increasing in glycerol content. For thermal

analysis, BSM hydrogel sponges plasticized with glycerol represented the improved decomposition temperatures, compared with unplasticized BSM hydrogel sponge.

Acknowledgment

This work was financially supported by KMITL Research Fund, King Mongkut's Institute of Technology Ladkrabang.

References

- [1] Ceresana Consulting; Worldwide consumption of biodegradable plastics from 2000-2008
- [2] Dick, M., Costa, T. M. and Gooma, A., "Edible film production from chia seed mucilage: Effect of glycerol concentration on its physicochemical and mechanical properties", *Carbohydrate Polymers* : 198-205 (2015).
- [3] Tabashi, A. J. and Razavi, S. M., "Functional properties and applications of basil seed gum: An overview", *Food Hydrocolloids* : 313-325 (2017)
- [4] Khazaei, N., Jouki, M. and Esmaili, M., "Characterization of new biodegradable edible film made from basil seed (*Ocimum basilicum* L.) gum", *Carbohydrate Polymers* : 199-206 (2014).
- [5] Kurd, F., Fathi, M. and Shekarchizadeh, H., "Basil seed mucilage as a new source for electrospinning: Production and physicochemical characterization", *International Journal of Biological Macromolecules* : 689-695 (2017)
- [6] Silva, S., Oliveira, M. and Mano, J., "Bio-inspired Aloe vera sponges for biomedical applications", *Carbohydrate Polymers* : 264-270 (2014)
- [7] Singh, B., Sharma, S. and Dhiman, A., "Acacia gum polysaccharide based hydrogel wound dressings: Synthesis, characterization, drug delivery and biomedical properties", *Carbohydrate Polymers*: 294-303 (2017)

Preparation and Properties of Thermoplastic Dialdehyde Cassava Starch Film by Sodium Metaperiodate

Sasikorn Poomkaew¹ and Jutarat Prachayawarakorn^{1,2*}

¹ Department of Chemistry, Faculty of Science, King Mongkut's Institute of Technology Ladkrabang, Bangkok 10520

² Advanced Materials Research Unit, Faculty of Science, King Mongkut's Institute of Technology Ladkrabang,
Bangkok 10520

Tel +668-3298400 ext.6235, Fax+66 2329 8428, *E-mail: jutarat.si@kmitl.ac.th

Abstract

Because of poor mechanical properties and hydrophilic characteristics of starch; in this study, dialdehyde starch (DAS) and thermoplastic dialdehyde starch (TPDAS) were prepared and characterized for biopolymer film application. DAS was prepared by periodate oxidation of starch with different mole ratios of starch/NaIO₄, i.e. 1:0, 1:0.25, 1:0.5, 1:0.75 and 1:1. The result indicated that aldehyde content increased with increasing mole ratio of NaIO₄ and the highest oxidation percentage of 80.61% was obtained. Then, different DAS with different aldehyde contents were fabricated by thermal process using glycerol as plasticizer to obtain TPDAS films. It was found from FT-IR spectra that the extra position peak at 1730 cm⁻¹, attributed to C=O stretching, was observed, indicating of peroxide oxidation in starch molecules. In addition, SEM micrographs of high mole ratio of NaIO₄ showed smooth morphology. Furthermore, stress at maximum load and Young's modulus of TPDAS films were obviously increased, with increasing mole ratio of starch/NaIO₄. Additionally, swelling power of different TPDAS films was significantly dropped, especially for 1:1 DAS.

Keywords: dialdehyde starch, modified starch, periodate oxidation, thermoplastic starch

1. Introduction

Nowadays, biopolymer film packaging has been interested due to their environmentally friendly nature. Many investigations have been emphasized on biodegradable materials to substitute for petroleum based materials such as plastics because of their slow decomposition. Starch is regarded as one of the most alternative materials due to its low cost, abundance and good film forming properties [1].

Cassava starch can be considered of great potential owing to its odorless, colorless, non-toxic and biodegradable characteristics. Unfortunately, some properties of thermoplastic native starch film need to be improved, for example, poor mechanical properties, high water absorption and low thermal properties. Accordingly, it is still required to be modified and oxidation is the one way to modify native starch (NS). For dialdehyde starch

(DAS), hydroxyl groups of starch can be replaced with the aldehyde groups which can be produced by controlled periodate oxidative cleavage of C₂ and C₃ bond of the anhydroglucose unit of native starch, leading to the decrease of hydrophilicity and crystallinity with increasing aldehyde content and the recrystallization of starch can be inhibited. It was reported that tensile strength and water vapor permeability were improved for thermoplastic dialdehyde starch (TPDAS) films with the increasing of aldehyde contents of DAS [2-3]. It was also mentioned that blended film of TPDAS – thermoplastic native starch (TPNS) was prepared from low dialdehyde content of DAS. The blended film showed non-homogeneous morphology and low mechanical properties due to the different non-compatible phases [4]. Therefore, in this study, various TPDAS films, obtained from DAS with

different dialdehyde contents, were prepared and tested for IR functional group, morphology, mechanical properties and swelling behavior, in comparison with TPNS.

2. Experimental Methods

2.1 Materials

Cassava starch was purchased from Chaopraya Phuchrai 2999 Co.,Ltd. (Kamphaengphet, Thailand). Sodium metaperiodate (NaIO₄) analytical grade was purchased from Italmar Co., Ltd. (Bangkok, Thailand). Glycerol was obtained from Lab System Co., Ltd. (Bangkok, Thailand), respectively.

2.2 Preparation of DAS

Firstly, the solution from starch and sodium periodate was prepared. Different mole ratios between cassava starch and NaIO₄ were 1:0, 1:0.25, 1:0.5, 1:0.75 and 1:1. The mixture was adjusted to pH 4.0 with hydrochloric acid under vigorous mechanical stirring. The reaction was maintained at 37 ± 2 °C for 4 h. Then, the slurry was filtered and washed by distilled water. After that, anhydrous ethanol was used to remove excess water. The obtained powder was dried in a hot air-oven (UF 110, Memmert GmbH Co. KG, Germany) at the temperature of 50 °C for 24 h and cooled down to room temperature. The dried powder was ground by a blender (EM-44A, Sharp Thai Co., Ltd., Thailand) and kept in a desiccator for further testing.

2.3 Preparation of DAS film

DAS powder, glycerol and distilled water were mixed together. Then, mixture was heated at the temperature 65 ± 5 °C as the gelatinization temperature of NS for 2 h for completed dissolving DAS powder. After that, the processed mixture were casted in a polypropylene tray and dried in the hot air-oven at the temperature of 55 °C for 24 h. TPNS film was also prepared by the same condition but the mixture was heated for 1 h.

2.4 Sample characterization

2.4.1 Determination of dialdehyde content

1 g. of dry sample was stirred in 300 ml. of distilled water. The sample was heated on a hot plate equipped by a magnetic stirrer. Next, the cooled solution was adjusted to pH 3.2 by 0.118 M hydrochloric acid and then 60 ml. of hydroxylamine hydrochloride solution was added. After that, the solution was heated at 40 °C for 4 h on the hot plate and titrated by 0.118 M. hydrochloric acid using methyl orange as an indicator. Aldehyde content was calculated by the following equation (1)

$$\text{CHO} = 0.118 \times 0.028 \times (V_{\text{control}} - V_{\text{sample}}) \times 100 \quad (1)$$

where V_{control} and V_{sample} were the volume of HCl used for titrating water and the sample, respectively.

2.4.2 FT-IR spectroscopic study

A sample was characterized by FT-IR on a spectrum GX spectrometer (Perkin Elmer, USA) using KBr disc technique in a wavenumber range from 4000 to 400 cm⁻¹ at a resolution of 4 cm⁻¹ with 6 scans per sample at ambient temperature.

2.4.3 Scanning electron microscope

A cross section sample was prepared by using liquid nitrogen and sputter-coated with thin layer of gold to prevent electrical charging during the observation. A sample was examined with scanning electron microscope (SEM: FEI, quanta 250, USA) and examined with a secondary electron detector using 5 kV of accelerating voltage.

2.4.4 Mechanical properties

A film with the dimension of 15 × 100 mm² was cut. Tensile properties were detected by Universal testing machine (QC-536 M1, Cometech Co., Ltd.) with 500 N load cell and crosshead speed of 50 mm/min in accordance with ASTM D 882-02. The film was conditioned at the temperature of 23 ± 1 °C and relative humidity of 60±5% before testing.

2.4.5 Swelling power

A dry film with the dimension of 10×10 mm² was cut and kept into the sieve sheet. Then, the film was immersed in distilled water at room temperature. The film was taken out at the end of soaking period, moisture on the surface of film was removed and the weight of film was

measured. Swelling power of the film was calculated as equation (2)

$$\text{Swelling power (\%)} = [(W_e - W_0) / W_0] \times 100 \quad (2)$$

where W_0 and W_e were the dry and wet weight of the film, respectively.

3. Results and Discussion

3.1 Aldehyde content

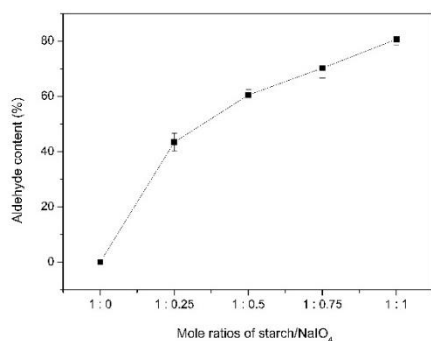


Figure 1 Aldehyde content of various DAS with different mole ratios of starch/NaIO₄.

The aldehyde contents (Figure 1) for different DAS, examined by titration method, were found to be 0%, 43.39%, 60.46%, 70.21% and 80.61%, when moles ratio starch/NaIO₄ of 1:0, 1:0.25, 1:0.5, 1:0.75 and 1:1 were used, respectively. The result could be explained that NaIO₄ cleavage at the C₂ and C₃ bond of the glucose unit [2], resulting in changing from carboxyl group (COOH) to aldehyde group (CHO). In addition, high content of NaIO₄ led to the increase of periodate oxidation in starch molecules.

3.2 FT-IR spectroscopy

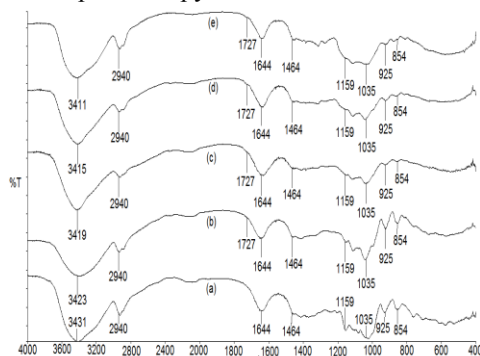


Figure 2 IR spectra from various TPDAS films with different mole ratios of starch/ NaIO₄ (a) 1:0 (b) 1:0.25 (c) 1:0.5 (d) 1:0.75 and (e) 1:1.

TPNS (1:0) film showed characteristic IR bond in Figure 2(a). It was found that, the broad absorption at 3000 to 3600 cm⁻¹ was from O-H stretching. Besides, the peak at 2800 to 3000 cm⁻¹ was attributed to C-H stretching and the small peak positions at 1190 to 950 cm⁻¹ were presented for C-O stretching [5]. The wavenumber at 1640 to 1650 cm⁻¹ was assigned for bending mode of retaining water in starch structure.

It should be mentioned that TPDAS films with different moles of NaIO₄ in Figure 2 (b, c, d, e and f) presented the increase intensity of the peak position at 1727 cm⁻¹, characteristic peak for C=O stretching of the aldehyde group at the C₂ and C₃ bond of the glucose unit. On the other hand, the intensity of wavenumber at 1159 cm⁻¹, ascribed to C-O stretching, was slightly lowered with the increasing content of NaIO₄ due to C₂ and C₃ positions as C-O bonds of the glucose unit were transformed into aldehyde bonds (C=O) by NaIO₄ oxidation [6]. The change in both peak intensities verified that NS was successfully reacted with NaIO₄.

3.3 Morphology

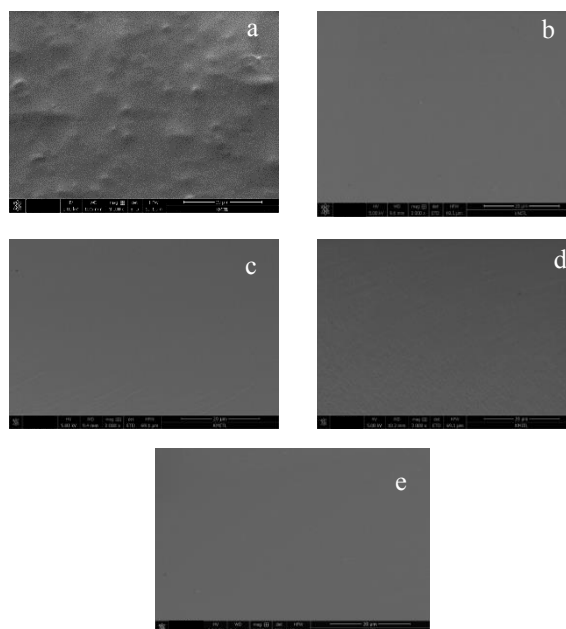


Figure 3 SEM micrographs of various TPDAS films with different mole ratios of starch/NaIO₄ (a) 1:0 (b) 1:0.25 (c) 1:0.5 (d) 1:0.75 and (e) 1:1.

SEM micrographs of the cross-section for TPNS film and different TPDAS films are shown in Figure 3. It

was found that cross section of TPDAS films showed smoother surface cross section than TPNS film. It could be explained that crystallinity of native granule starch were destroyed by increasing of NaIO₄ oxidation [2]. As a result, water and glycerol can enter easily into starch granular interior, disrupted inter- and intra-molecular hydrogen bonds and made granular starch plastication. From this result, TPDAS film showed more homogeneous morphology than TPNS film [4].

3.4 Mechanical properties

Mechanical properties of various TPDAS films are as shown in Figure 4. It was found that stress at maximum load (Figure 4 (a)) significantly increased from 1.00 MPa to 8.93 MPa when NaIO₄ content increased from 0 to 1. Similarly, Young's modulus (Figure 4 (b)) also increased from 0.42 MPa to 158 MPa. As a result, strain at maximum load (Figure 4 (c)) obviously declined from 174% to 16% when NS was modified with 1:1 mole ratio of starch/NaIO₄. The result demonstrated that for TPDAS films, C₂ and C₃ aldehyde group of the anhydroglucose unit could form inter- and intra-molecular hemiacetal and acetal cross-linking [2] and led to film stiffness. It should be noted that stress at maximum load of TPDAS films, especially for 1:1 starch/NaIO₄ mole ratio, was comparable to low-density polyethylene (LDPE) commercial film [7].

3.5 Swelling power

It was found from Figure 5 that TPNS film showed the highest swelling power. Because TPNS film consists of numerous of hydroxyl groups those prefers to form hydrogen bonds with water; therefore, TPNS film shows high hydrophilic properties. However, the swelling power of TPDAS films which immersed in water for 1 h significantly decreased from 142.97% to 50.56% when NS was modified with mole ratio of starch/NaIO₄ was 1:0.25. As expected, the lowest swelling power was obtained from TPDAS film with 1:1 starch/NaIO₄. The result demonstrated that TPDAS films formed inter- and intra-molecular hemiacetal and acetal cross-linking, brought

about the decrease of hydrophilic properties. The result was agreed with previous report from TPDAS-TPNS blended films [4].

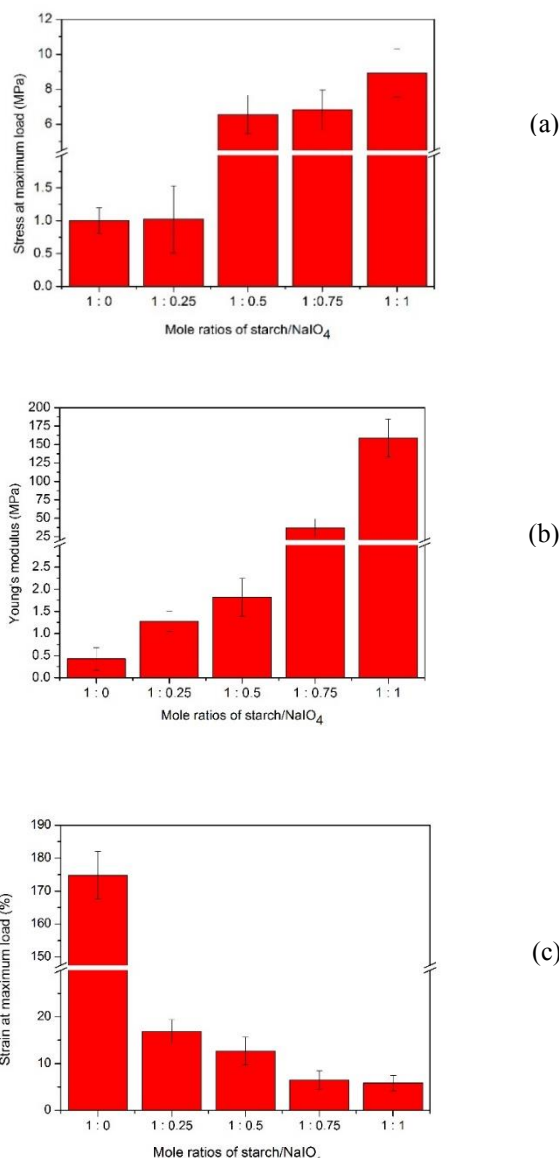


Figure 4 Mechanical properties: (a) stress at maximum load (b) Young's modulus and (c) strain at maximum load of various TPDAS films with different mole ratios of starch/ NaIO₄.

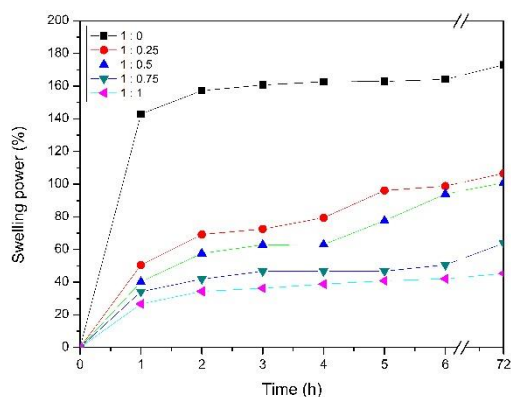


Figure 5 Swelling power of TPNS and TPDAS films with different mole ratios of starch/ NaIO₄.

4. Conclusion

Various dialdehyde contents of DAS and TPDAS films were successfully prepared. Aldehyde contents were found to increase with increasing periodate contents. From FT-IR spectra, the wavenumber at 1727 cm⁻¹, which indicated the C=O stretching of the aldehyde group at the C₂ and C₃ bond of the glucose unit, was observed. SEM micrographs of different TPDAS films also showed smooth morphology. In addition, both stress at maximum load and Young's modulus of several TPDAS films were substantially increased. Finally, the increase of mole ratios of starch/NaIO₄ also caused the considerable decrease of the swelling power due to inter- and intra-molecular hemiacetal and acetal cross-linking as the evidence of periodate oxidation of TPDAS films.

Acknowledgement

The authors express their sincere appreciation to KMITL Research Fund for supporting the study financially.

References

- [1] Luchese, L.C., Garrido, T., Spada, C.J., Tessaro, I.C. and De la Caba, K., "Development and characterization of cassava starch films incorporated with blueberry pomace", *International Journal of Biological Macromolecules* : 834-839 (2018).
- [2] Yu, J., Chang, P.R. and Ma, X., "The preparation and properties of dialdehyde starch and thermoplastic

dialdehyde starch", *Carbohydrate polymers* : 296-300 (2010).

[3] Zhang, S.D., Wang, X.L., Zhang, Y.R., Yang, K.K. and Wang, Y.Z., "Preparation of a new dialdehyde starch derivative and investigation of its thermoplastic properties", *Journal of Polymer Research* : 439-446 (2010).

[4] Komsai, P., "Dialdehyde cassava starch and cassava starch blended films", M.Sc. Thesis, Department of Chemistry, Faculty of science, King Mongkut's of Technology Ladkrabang, (2016).

[5] Kaewtatip, K. and Tanrattanakul, V., "Preparation of cassava starch grafted with polystyrene by suspension polymerization", *Carbohydrate Polymers* : 647-655 (2008).

[6] Dou, Y., Huang, X., Zhang, B., He, Ming., Yin, G. And Cui, Y., "Preparation and characterization of a dialdehyde starch crosslinked feather keratin film for food packaging application", *RSC Advances* : 27168-27174 (2015).

[7] Matweb material property data. 2018. Overview of materials for Low Density Polyethylene (LDPE), Film Grade. [online] Available: <http://www.matweb.com/search/DataSheet.aspx?MatGUID=9ff98d958a714b2a8a00990a929d6f14>

Encapsulation of Agrochemical *via* Chitosan-functionalized W₁/O/W₂ Double Emulsions

Chomphunut Thammapichai¹, Nuttaporn Pimpha², and Panya Sunintaboon^{1,3*}

¹Department of Chemistry, Faculty of Science, Mahidol University, Bangkok 10400, Thailand

²National Nanotechnology Center, National Science and Technology Development Agency, Pathum Thani 12120, Thailand

³Center for Sustainable Energy and Green Materials, Mahidol University, Nakorn Pathom 73170, Thailand

*E-Mail: panya.sun@mahidol.ac.th

Abstract

Encapsulation of Methomyl, a model of hydrophilic pesticide, was carried out as a W₁ phase in chitosan (CS)-functionalized W₁/O/W₂ double emulsions using a two-step emulsification. The W₁/O primary emulsion was firstly prepared by dispersing water soluble methomyl, vegetable oil, and 4%v/v polyglycerol polyricinoleate (PGPR) as a hydrophobic stabilizer. Among 3 types of vegetable oil: coconut oil, palm oil and soybean oils, when soybean oil was used, its respective W₁/O emulsion exhibited the lowest percentage of sedimentation index, indicating a better colloidal stability. Methomyl can be loaded up to 30% in the resulting W₁/O emulsions. Then, W₁/O/W₂ double emulsions can be prepared by using biopolymer complexes between CS and sodium carboxymethylcellulose (CMC) (or sodium lignosulfonate (LS)). It was shown that the CS/CMC and CS/LS complexes provided W₁/O/W₂ double emulsions with higher colloidal stability and the percentage of encapsulation efficiency (%EE) than when using only CS, CMC or LS. The complexes at 700ppmCS/500ppmCMC and 700ppmCS/200ppmLS provided 90% and 70% of the percentage of encapsulation efficiency (%EE) of O phase, respectively. Therefore, CS/LS complex resulted in better performance for the formation of colloidally stable double emulsions. The optical micrograph from optical microscope (OM) can confirm the successful preparation of W₁/O/W₂ double emulsions, which had positive zeta potentials (> +20 mV), and the sizes ranging from 2 to 15 μm

Keywords: Agrochemical, Double emulsion, Biopolymer complex, Agriculture

1. Introduction

Agriculture has been utilizing agrochemicals, which are referred as pesticides for protection of crops or plants against pests to support growth, and improve both quality and quantity of agricultural products. The parameters in the environment, including natural sunlight, water, and microorganisms could destroy or breakdown agrochemicals, leading to losses in their efficiency and activity. So, farmers have to use excessive agrochemicals directly into the fields to ensure the growth of plants. The excessive concentration of agrochemicals could possibly leave residues into the environment that would affect soil health, water, and air qualities. So, solutions to such problem is interesting and challenging.

Encapsulation technology is well known and has a high potential to solve this problem. As a result, agrochemicals can be used in the lower amount, be protected from deterioration by environmental factors, and have a controlled releasing behavior [1]. Many researchers have been attempting to develop methods for encapsulation both hydrophobic and hydrophilic agrochemicals. For example, layer-by-layer (LbL) method [2], emulsion cross-linking [3], membrane emulsification [1], and radiation-induced graft polymerization [4]. These methods require complicated conditions and processes. Thus, this work also attempted to develop a simple encapsulation method for agrochemicals.

Double emulsion is a complex emulsion system with two types of morphology: water-in-oil-in-water ($W_1/O/W_2$) and oil-in-water-in-oil ($O_1/W/O_2$) [5]. This system has been growing in interests for several industries, including food [6], cosmetics and pharmaceuticals [7] because it provides high percentage loading of both hydrophobic and hydrophilic active ingredients in the same micron-sized emulsion droplets with great distribution of the two components. Moreover, such encapsulation can protect active ingredients from detrimental effects from external phase or the environment. In general, there are two main pathways for the preparation of double emulsion, which are 1) one-step emulsification and 2) two-step emulsification [8]. Nowadays, the two-step emulsification method is more attractive than the one-step emulsification, because it does not use high temperature and complicate emulsifiers.

Herein, this work introduced CS-functionalized $W_1/O/W_2$ double emulsion system to encapsulate agrochemicals, potentially useful in agriculture application *via* the two-step emulsification method. In addition, the purposes of establishing this alternative method are to utilize bio-friendly materials, have a low cost method, and mild condition. Moreover, the utilization of complexes between cationic and anionic biopolyelectrolyte as the outer stabilizer were investigated. The cationic biopolymer used was Chitosan (CS), which possesses non-toxicity, biocompatibility, biodegradability, stimulation of seed germination and easily absorption into plant surfaces [9]. The anionic biopolymers selected were sodium carboxymethylcellulose (CMC), and sodium lignosulfonate (LS). The comparison in terms of colloidal stability of the resulting double emulsions from both complexes was also conducted. Moreover, after the resulting double emulsions were characterized by using techniques, including particle size, zeta potential, emulsion stability and encapsulation efficiency of oil and agrochemicals.

2. Experimental Methods

2.1 Materials

Methomyl was purchased from Sigma-Aldrich (USA). Coconut oil, palm oil and soybean oil were bought from a local supermarket. Polyglycerol polyricinoleate (PGPR) was supplied from Foodchem International Corporation (China). Chitosan (CS) was purchased from Seafresh Chitosan Lab (Thailand). The degree of deacetylation was ca. more than 95%, and the weight-average molecular weight was ca. 80-120 kDa. Carboxymethylcellulose sodium salt (CMC) was purchased from Sigma-Aldrich (USA). Sodium lignosulfonate (LS) was purchased from Tokyo chemical industry Co.,Ltd. (Japan).

2.2 Preparation of W_1/O primary emulsion

Methomyl as an inner aqueous phase (W_1) was mixed with a hydrophobic emulsifier, which is PGPR (4%v/v). Next, different types of vegetable oils, including coconut oil, palm oil and soybean oil, were added into the mixture, until total volume of mixture was equal to 30 mL. Then, the mixture was blended by using Ultrasonication with 30% of amplitude about 3 min to obtain W_1/O primary emulsion.

2.3 Aggregation behavior measurement

In order to find the optimum concentrations of positively charged CS and negatively charged CMC or LS. The concentration of CS was fixed at 700 ppm and that of anionic biopolymer was varied from 0 to 1500 ppm. The CS and anionic biopolymer were added into a glass bottle and mixed by using magnetic stirrer about 5 min to form a complex solution. Next, the turbidity of complex solution was determined by using UV-Vis spectrophotometer at a wavelength about 300 nm in transmittance mode. The percentage of transmittance was converted into turbidity by using the following equation:

$$\text{Turbidity} = 100 - \% \text{Transmittance} \quad (1)$$

2.4 Preparation of $W_1/O/W_2$ double emulsion

The double emulsion system was prepared by using homogenization at 9000 rpm of speed about 3 min. The concentration of outer aqueous phase (W_2) which is a complex solution of CS and anionic biopolymers was

selected at the concentrations below the critical aggregation concentration (CAC) point in order to have an excess CS to stabilize the double emulsion droplets. In the process, the resulting of W_1/O primary emulsions were added drop-wise to the outer aqueous phase (W_2) to form $W_1/O/W_2$ double emulsions. Then, the size and zeta potential of the resulting $W_1/O/W_2$ double emulsion were measured by using Mastersizer and Zetasizer instrument, respectively.

2.5 Sedimentation stability measurement of W_1/O primary emulsion

The resulting of W_1/O primary emulsion was transferred into a test tube that has 1.5 cm of internal diameter and 13 cm of height. It was kept at room temperature about 30 days to determine the percentage of sedimentation index. The percentage of sedimentation index was determined every 5 days by measuring the height of serum or unstable phase (H_S) and total emulsion phase (H_E) in the test tube, which is calculated by the following equation:

$$\text{Sedimentation index (\%)} = \frac{H_S}{H_E} \times 100 \quad (2)$$

Table 1 Main chemical compositions found in selected vegetable oils

Types of oil	Sat. fat (%)	Monounsat. fat (%)	Polyunsat. fat (%)
Coconut	92	6	2
Palm	50	40	10
Soybean	18	45	37

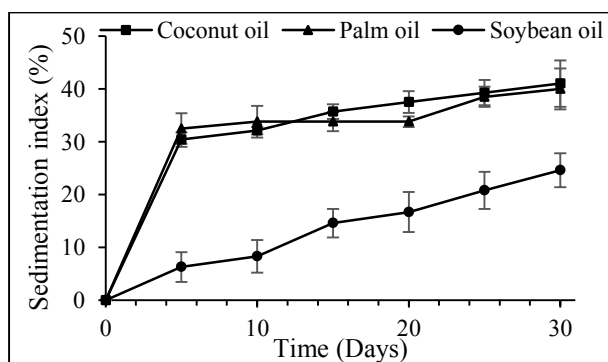


Fig.1. Percentage of sedimentation index of coconut oil, palm oil and soybean oil.

Table 2 Characteristics of W_1/O primary emulsion

Types of oil	Size (nm)
Coconut	286.8 ± 2.8
Palm	388.1 ± 1.7
Soybean	765.1 ± 2.1

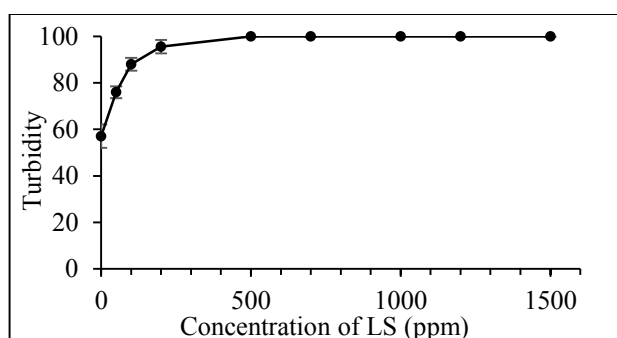
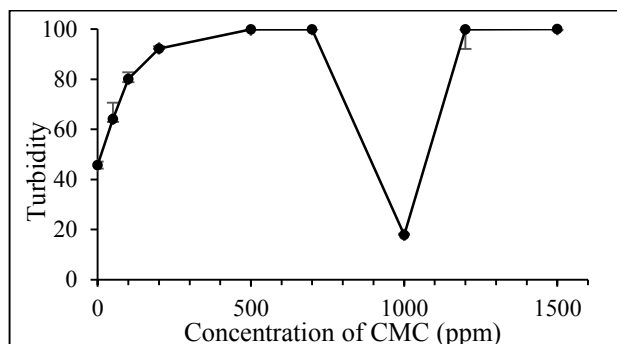


Fig.2. Turbidity measurement of CS/CMC and CS/LS complex stabilizers by using UV-Vis spectrophotometer

2.5 Determination of encapsulation efficiency (%EE)

The encapsulation efficiency was determined by using extraction method. The untrapped oil were separated from the double emulsion by partitioning with hexane. The hexane fraction was collected and evaporated by using a rotational evaporator. %EE was calculated using the following equation:

$$\text{EE (\%)} = \frac{W_{\text{Sample}} - W_{\text{Separated oil}}}{W_{\text{Sample}}} \times 100 \quad (3)$$

3. Results and Discussion

3.1 Preparation of W_1/O primary emulsion

Different types of vegetable oil as an oil phase (O) consist of different chemical compositions that could provide W_1/O with different properties. Thus, the study on the formation of W_1/O primary emulsion from various types of vegetable oils was our first concern. There are 3 types of vegetable oil selected for the investigation, which

were coconut oil, palm oil, or soybean oil. Their chemical compositions based on different types of fatty acids are shown in Table 1. The 30% of methomyl (W_1), 66% of O and 4% PGPR ratio by volume was fixed. The results from percentages of sedimentation index measured from the resulting W_1/O emulsion with soybean oil as an oil phase. The lower percentage of sedimentation index, the lower rate of phase separation, and the higher the colloidal stability. Furthermore, the sizes of W_1/O primary emulsions, as presented in Table 2, were increased when the composition of unsaturated fats increased. This result refers to the compatibility between PGPR and vegetable oils. PGPR has a hydrophilic-lipophilic balance (HLB) value is equal to 4.3 that refers to it has more hydrophobic parts in itself. Therefore, when PGPR stabilized in soybean oil, the sizes would show larger than palm oil and coconut oil, respectively.

Table 3

Characteristics of the resulting $W_1/O/W_2$ double emulsions

Complexes (ppm)	Size (μm)	Zeta potential (mV)
700CS	-	-
500CMC	-	-
700CMC	-	-
100LS	-	-
200LS	-	-
700CS/500CMC	8.512 ± 2.6	32.9 ± 2.5
700CS/700CMC	14.336 ± 1.6	0.10 ± 2.2
700CS/100LS	7.378 ± 1.5	23.8 ± 1.1
700CS/200LS	2.544 ± 1.7	28.8 ± 2.6



Fig.3 The resulting $W_1/O/W_2$ double emulsions with 700ppmCS/500ppmCMC, 700ppmCS/700ppmCMC, 700ppmCS/100ppmLS and 700ppmCS/200ppmLS complex stabilizer, respectively

3.2 Preparation of $W_1/O/W_2$ double emulsion

The volume ratio between W_1/O primary emulsion and W_2 was kept at 5:95. The CS, CMC, LS, CS/CMC

complex and CS/LS complex were used as stabilizers in W_2 phase to prepare $W_1/O/W_2$ double emulsions. The concentrations of these biopolymers were presented in Table 3. The concentrations of CS/CMC and CS/LS were below their respective CAC points, which can be observed by slope breaking of turbidity plots as shown in Fig.2. At these concentrations, the excessive amount of CS is expected that will result in a positive zeta potential value as measured from the stable $W_1/O/W_2$ double emulsion obtained. After preparation, the resulting $W_1/O/W_2$ double emulsions with CS, CMC, and LS showed high creaming layers, indicating unstable double emulsions. When the stabilizers were changed to CS/CMC and CS/LS complexes, the resulting $W_1/O/W_2$ double emulsions showed the milky-white emulsions and less creaming layer. It can be seen that the complex stabilizers provided the $W_1/O/W_2$ double emulsions with higher colloidal stability than their single biopolymer counterparts.

The concentration of each complex stabilizer was concerned to find the suitable concentration that could give more stability of the resulting $W_1/O/W_2$ double emulsions. From table 3, decreasing CS/CMC complex concentration from 700CS/700CMC to 700CS/500CMC ppm gave more electrostatic repulsion force to reduce droplet size of double emulsions. If the CS/CMC complex concentration was changed to above CAC point, such as 700CS/1000CMC ppm, the surface charge of resulting double emulsion would be negative, due to the excess of negatively charged CMC. Thus, such condition is not suitable for preparing positively charged CS-functionalized double emulsions.

When the type of complex stabilizer was changed to CS/LS complex, the results of size contrasted the CS/CMC. The sizes were increased when CS/LS complex concentration decreased from 700CS/200ppm to 700CS/100 ppm that come from the reason about less of hydrophobic part from LS to bind the oil portions. Thus, the coalescence mechanism was occurred. Furthermore, the zeta potentials of all biopolymer complex were in positive values, emphasizing the excess amount of CS in the complexes.

The morphology of the obtained $W_1/O/W_2$ double emulsions with CS/CMC and CS/LS complex stabilizers were shown in Fig. 4. It can be observed that the larger droplets have the smaller droplets, which is W_1/O primary emulsions, inside. These OMs could confirm that the $W_1/O/W_2$ double emulsions were successfully prepared

Table 4 Encapsulation efficiency of O phase in the resulting $W_1/O/W_2$ double emulsions

Complexes (ppm)	EE (%)
700CS/500CMC	79.5 ± 2.4
700CS/700CMC	76.3 ± 1.9
700CS/100LS	90.9 ± 1.7
700CS/200LS	98.3 ± 3.0

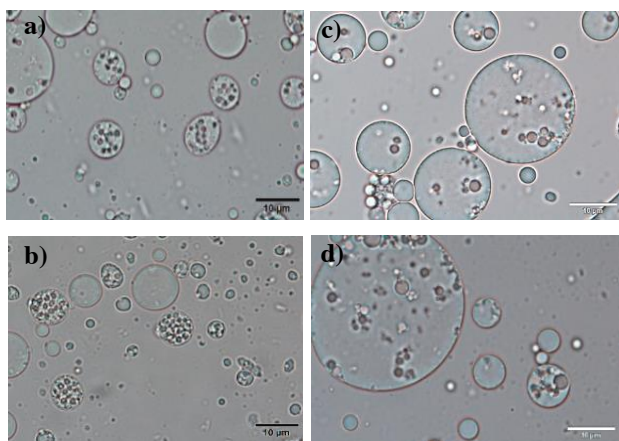


Fig.4. Optical micrographs (OMs) of the resulting $W_1/O/W_2$ double emulsions at different concentrations of complex stabilizers (a.) 700ppmCS/500ppmCMC, (b.) 700ppmCS/700ppmCMC, (c.) 700ppmCS/100ppmLS and (d.) 700ppmCS/200ppmLS

3.3 Determination of encapsulation efficiency (%EE) of O phase

From Table 4, the resulting $W_1/O/W_2$ double emulsions with CS/CMC and CS/LS gave the %EE of O phase about 70% and 90%, respectively. So, CS/LS complex had higher efficiency in the stabilization of $W_1/O/W_2$ double emulsion than CS/CMC complex did.

4. Conclusion

The $W_1/O/W_2$ double emulsion system could be applied in the encapsulation of hydrophilic pesticide with

the use of CS/CMC and CS/LS complex stabilizers. The biopolymer complex stabilizers can potentially stabilize the $W_1/O/W_2$ double emulsions than their single biopolymer counterparts (CS, CMC and LS). Both biopolymer complex stabilizers could affect size, surface charge, and encapsulation efficiency. CS/LS complex stabilizer gave the higher %EE of O phase in the $W_1/O/W_2$ double emulsions than CS/CMC complex stabilizer did. Therefore, CS/LS complex had more efficiency to provide $W_1/O/W_2$ double emulsions than CS/CMC. It can be postulated that these $W_1/O/W_2$ double emulsions have biocompatibility, low toxicity, enhanced activity, efficiency, stability of pesticide, and environmental safety. The preparation process for CS-functionalized $W_1/O/W_2$ double emulsions is also simple. Thus, this formulation can be performed and developed for being used in agricultural application.

Acknowledgement

This work was supported by Mahidol University and National Science and Technology Development Agency.

References

- [1] Liu, B., et al., "Construction of a controlled-release delivery system for pesticides using biodegradable PLA-based microcapsules". *Colloids Surf. B: Biointerfaces*, 144, 38-45 (2016).
- [2] Wang, X. and Zhao, J., "Encapsulation of the herbicide Picloram by using polyelectrolyte biopolymers as layer-by-layer materials". *J. Agric.Food Chem.*, 61(16), 3789-3796 (2013).
- [3] Kumar, S., et al., "Synthesis, characterization and on field evaluation of pesticide loaded sodium alginate nanoparticles". *Carbohydr. Polym.*, 101,1061-1067 (2014).
- [4] Yi, Z., et al., "Functionalized mesoporous silica nanoparticles with redox-responsive short-chain gatekeepers for agrochemical delive". *ACS Appl. Mater. Interfaces*, 7(18), 9937-9946 (2015).

- [5] Garti, N. and Bisperink C., Double emulsions: Progress and applications. *Curr. Opin. Colloid Interface Sci.*, 3(6), 657-667 (1998).
- [6] Li, B., et al., Synergistic effects of whey protein-polysaccharide complexes on the controlled release of lipid-soluble and water-soluble vitamins in W₁/O/W₂ double emulsion systems. *Int. J. Food Sci. Technol.*, 47(2), 248-254 (2012).
- [7] Bozkir, A. and Hayta G., Preparation and Evaluation of Multiple Emulsions Water-in-oil-in-water (w/o/w) as Delivery System for Influenza Virus Antigens. *J. Drug Target.*, 12(3), 157-164 (2004).
- [8] Lamba, H., Sathish K., and Sabikhi. L., Double Emulsions: Emerging Delivery System for Plant Bioactives. *Food Bioprocess Tech.*, 8(4), 709-728 (2015).
- [9] Kashyap, P.L., Xiang X., and Heiden P., Chitosan nanoparticle based delivery systems for sustainable agriculture. *Int. J. Biol. Macromol.*, 77, 36-51 (2015).

Starch Foams Based on Rice Starch/Rice Straw Fiber

Nisa Promsen, Suparada Tagan and Linda Thiraphattaraphun*

Division of Packaging Technology, Faculty of Agro-Industry, Chiang Mai University, Chiangmai 50100, Thailand

Phone +66 5394 8225, *E-Mail: linda.t@cmu.ac.th

Abstract

Environmentally friendly foam trays for packaging applications were prepared using the rice starch and the rice straw fiber. The starch foam trays were obtained by a baking process of the rice starch incorporating with the rice straw fiber content ranging from 2 to 10%. Both the rice starch foam and the rice starch foams with different rice straw fiber contents exhibited small and dense foam cells at the surface and large foam cells at the interior. The rice starch foam densities ranged from 0.151 to 0.188 g/cm³ by adding the rice straw fiber content of 2 to 10%. Moreover, the water absorption of the rice starch foams decreased with incorporating the rice straw fiber content of 2 to 10%. However, the flexural strength of the rice starch foam can be improved by adding the rice straw fiber content of 4 to 10%.

Keywords: starch foam, rice starch, rice straw

1. Introduction

Starch based foams have received attention as alternative materials to replace non-biodegradable petroleum-based foams. Starch is abundant biopolymer, inexpensive, environmentally friendly material and biodegradable material. The starch foams can be formed as loose-fill foam [1] and foam tray [2] for packaging applications. However, the starch foams are poor mechanical properties and sensitive to water. Therefore, adding the natural fibers to the starch foams is an alternative method to improve the mechanical properties and water sensitivity of the starch foams [3, 4]. In this work, the rice starch foam tray was prepared by a baking process. In addition, to overcome the starch foam problems, the rice straw fiber was selected to incorporate into the rice starch foam tray. Moreover, the rice straw fiber is an agricultural residue, non-toxic, large available amount and low-cost. Meanwhile, the appearance, color parameters, morphology, density, flexural strength, water absorption and water solubility index (WSI) of the rice starch foam and the rice starch foams with different rice straw fiber contents were investigated.

2. Experimental Methods

2.1 Materials

The rice starch was purchased from Thai Flour Industry Co., Ltd., Thailand. Rice straw (RD10) fiber was from Sanpatong, Chiangmai, Thailand. The rice straw fiber were prepared without chemical treatment and ground into an average size of 180 μm .

2.2 Foam preparation

The rice starch and distilled water with a ratio of 2:3 (weight:volume) were mixed with the rice straw fiber (0, 2, 4, 6, 8 and 10% by weight of the rice starch). A homogeneous batter was poured into a mold to form a foam tray (bottom size of 120 mm x 120 mm and thickness of 5 mm). Mold was placed in a compression molding machine (Model 4122, Carver Inc., U.S.A.) and heated at 165 °C for 25 min under a clamping force of 5000 lbs.

2.3 Characterization

The samples were stored at 23 \pm 2 °C, 50 \pm 2% relative humidity for 24 h prior to test 2.3.3 – 2.3.6.

2.3.1 Appearance and color parameters

The foam tray appearance was taken by a digital camera (Olympus OM-D E-M6, Japan). The color parameters were measured by a colorimeter (CR-410, Minolta Co, Ltd., Japan) with a CIE-Lab color scale. The color parameters were reported in L^* , a^* and b^* values; $L^* = 0$ (black) to $L^* = 100$ (white), $-a^*$ = (greenness) to $+a^*$ (redness) and $-b^*$ (blueness) to $+b^*$ (yellowness). The three different points of each sample were determined and reported from the averages of five samples.

2.3.2 Morphology

The sample surfaces and cross-sections were investigated by a stereo microscope (Leica S8 APO, Germany). The images were taken at 20× magnification with Leica application suite V3.3 software.

2.3.3 Density

The density was calculated as weight of sample divided by volume of sample. The samples were cut into the size of 25 mm x 100 mm. The sample thicknesses were measured using a thickness gauge (GT-313-A, Gotech Testing Machines Inc, Taiwan). The averages of five samples were reported.

2.3.4 Flexural test

The flexural beams were cut into the size of 25 mm x 100 mm. The flexural beam thicknesses were determined with a thickness gauge. The three-point bending mode was performed using a universal testing machine (Model HIKS, United Kingdom) with a load cell of 1000 N, cross-head speed of 2.5 mm/min and support span of 50 mm. The flexural strength was calculated as:

$$\text{Flexural strength (MPa)} = \frac{3FL}{2Wh^2} \quad (1)$$

where: F = applied load (N), L = support span (mm), W = width of beam (mm) and h = thickness of beam (mm). The reported values are the average of five measurements.

2.3.5 Water absorption

The samples were cut into the size of 25 mm x 50 mm and immersed in 100 ml of distilled water at 25 °C for 1 min. The water absorption was calculated using the equation given below:

$$\text{Water absorption (\%)} = \frac{(W_f - W_i)}{W_i} \times 100 \quad (2)$$

where: W_i = initial weight of sample (g) and W_f = final weight of sample after immersed in distilled water (g). The average values of five samples were reported.

2.3.6 Water solubility index (WSI)

The sample weight of 1 g was dispersed in 30 ml of distilled water in a centrifuge tube. The suspension was centrifuged at 6000 × g for 30 min by using a centrifugal (Sorvall super T21, USA). The supernatant was separated from sediment and poured into a filter paper. The solid in supernatant was dried in a hot air oven at 105 °C for 24 h.

The WSI was calculated as follow:

$$\text{WSI (\%)} = \frac{W_{ds}}{W_s} \times 100 \quad (3)$$

where: W_{ds} = weight of dry solid in supernatant (g) and W_s = weight of sample (g). The reported values are the averages of five measurements.

3. Results and Discussion

3.1 Appearance and color parameters

The rice starch foam tray and the rice starch foam trays with the rice straw fiber are shown in Fig. 1. Small holes and cracks were found at some surfaces and edges of all foam trays. As a result, it may be due to the water evaporates during the foam expansion. In addition, Salgado et al. [5] stated that several cavities or holes at the foam tray surface were probably due to the escape of steam bubble from the foam surface. Shogren et al. [2] also explained that steam, air voids or shrinkage and breaks during the foam drying may induce many holes on the foam surface. The rice starch foam tray was opaque and slight yellowish. Whereas, the rice starch foam trays with the rice straw fiber (2 to 10%) were darker and more

yellowish. The appearance colors also correlated to the color parameters as shown in Table 1.

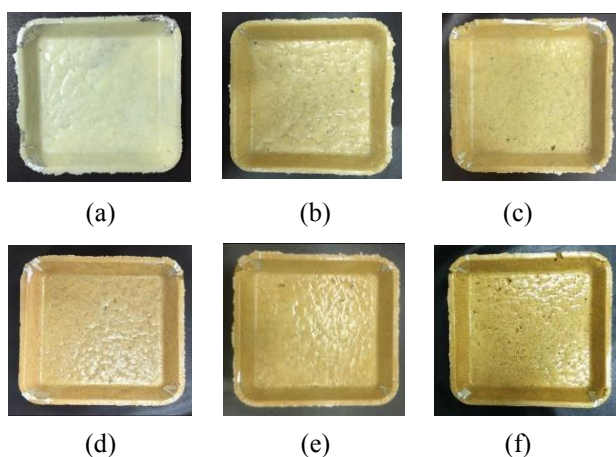


Fig. 1. The appearance of the rice starch foams with different rice straw fiber contents; (a) 0% rice straw fiber, (b) 2% rice straw fiber, (c) 4% rice straw fiber, (d) 6% rice straw fiber, (e) 8% rice straw fiber and (f) 10% rice straw fiber.

Table 1. Color parameters of the rice starch foams with different rice straw fiber contents.

Rice straw fiber (%)	L*	a*	b*
0	71.05 ± 2.42	-0.67 ± 0.14	5.13 ± 1.14
2	63.42 ± 3.28	1.62 ± 0.99	13.74 ± 2.76
4	63.32 ± 2.66	3.21 ± 0.57	17.64 ± 3.09
6	62.09 ± 2.15	4.15 ± 1.50	21.88 ± 1.91
8	59.69 ± 3.67	4.74 ± 0.63	17.99 ± 2.67
10	59.82 ± 2.26	5.49 ± 0.94	18.69 ± 3.31

It can be seen that the L* values decreased by adding the rice straw fiber (2 to 10%) to the rice starch foam. Also, the darker colors were seen on the rice starch foams with the rice straw fiber. Furthermore, the b* values increased by adding the rice straw fiber (2 to 10%) to the rice starch foam. Due to the yellowness characteristic of the natural fiber [4], more yellowish was seen on the starch foam trays containing the rice straw fiber as compared to

the rice starch foam tray without the rice straw fiber. The a* values also increased by adding the rice straw fiber (2 to 10%) to the rice starch foam. This represented more redness due to the effect of lignin in the natural fibers [4]. Furthermore, all L*, a* and b* values do not change with increasing the rice straw fiber contents from 4 % to 10%.

3.2 Morphology

Fig. 2 shows optical micrographs of the foam cross-sections.

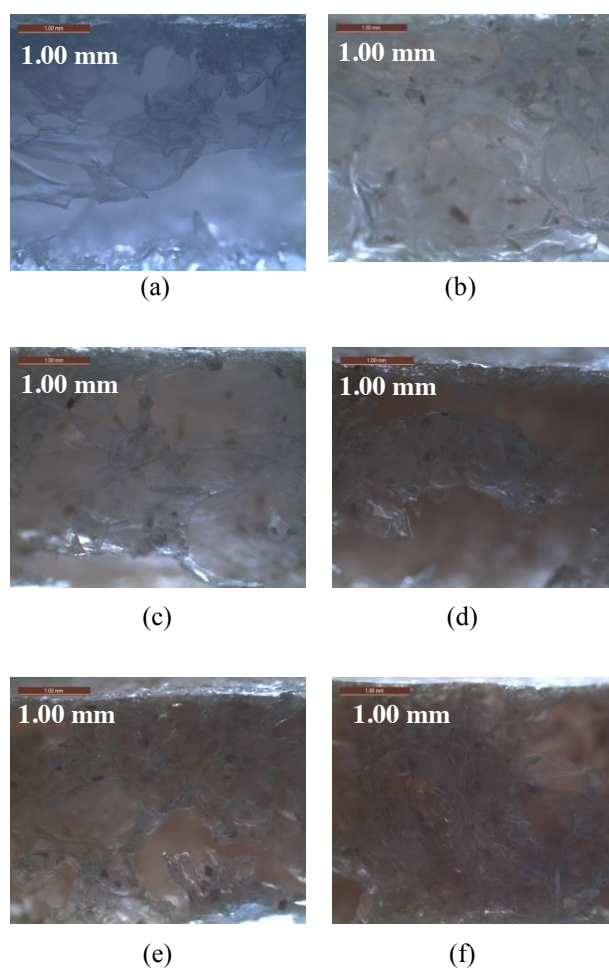


Fig. 2. Optical micrographs of the foam cross-sections; (a) 0% rice straw fiber, (b) 2% rice straw fiber, (c) 4% rice straw fiber, (d) 6% rice straw fiber, (e) 8% rice straw fiber and (f) 10% rice straw fiber.

Both the rice starch foam and the rice starch foams with the rice straw fiber (2 to 10%) exhibited two different foam cell structures. There are small and dense foam cells at the surface and large expanded foam cells at the interior

in both the rice starch foam and the rice starch foams with the rice straw fiber (2 to 10%). This different foam cells between surface and interior were obtained using a baking process and called as a sandwich-type structure [6]. Due to the foam expansion occurred by evaporating of the water in the starch paste. Thus, water can act as a blowing agent for the foam cell formation. In addition, Shogren et al. [2] pointed out that the rapidly drying of starch paste at the mold surface leads to interrupt the foam expansion. Therefore, the starch paste may not vastly expand. As the reduction of the foam expansion ability, therefore, it tends to induce small and dense foam cells at the foam surface. Shogren et al. [2] also stated that the large amounts of water evaporation at the mold interior lead to foam cell rapture. Thus, at the foam interior tends to induce the large foam cells. Similar foam cell structures were also obtained by Salgado et al. [5] and Yang et al. [6]. Moreover, from Fig. 2, as adding the rice straw fiber (2 to 10%) to the rice starch foam, no alignment of the rice straw fiber was observed. This is agreement with Lawton et al. [3] who mentioned the fiber cannot align in a baking process due to no flow direction in the machine. The optical micrographs of the foam surfaces are illustrated in Fig. 3. The foam cells in both the rice starch foam and the rice starch foams with the rice straw fiber (2 to 10%) are irregular shapes and sizes. Additionally, no alignment of the rice straw fiber (2 to 10%) was observed at the foam surfaces.

3.3 Density and flexural strength

From Table 2, it was observed that the rice starch foam density increased by incorporating the rice straw fiber content of 8 and 10%. In addition, the flexural strength of the rice starch foam can be improved by adding the rice straw fiber content of 4 to 10%. However, the flexural strength of the rice starch foam with the rice straw fiber content of 10% is lower than the rice starch foams with the rice straw fiber content of 6 and 8%. The decrease in flexural strength may be due to the non-uniform fiber distribution as mentioned by Lawton et al. [3] or the lack of the rice straw fiber in some areas of the rice starch foams. Therefore, the decrease in flexural strength of the rice

starch foams may have occurred by adding the high fiber content (10%).

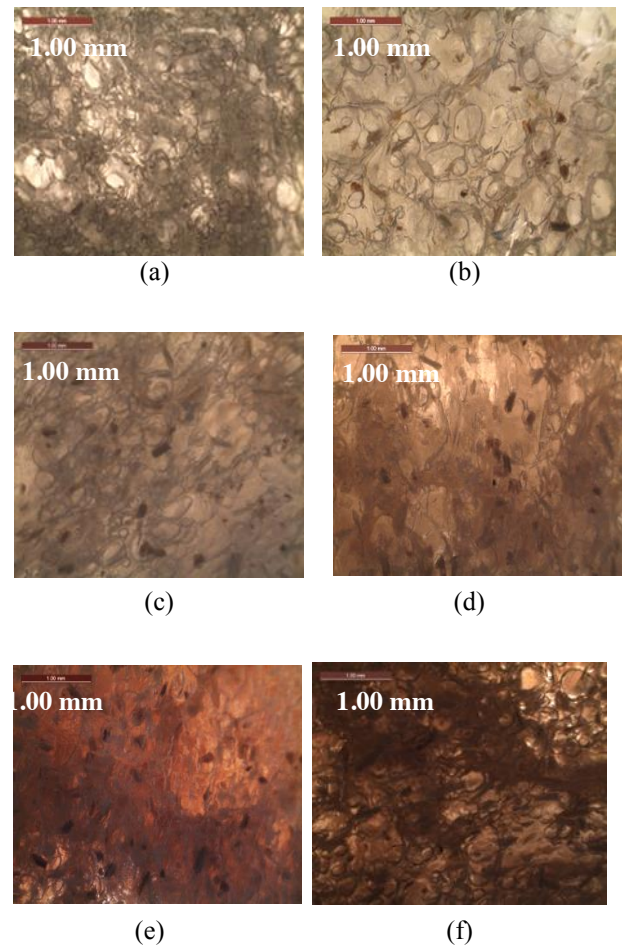


Fig. 3. Optical micrographs of the foam surfaces; (a) 0% rice straw fiber, (b) 2% rice straw fiber, (c) 4% rice straw fiber, (d) 6% rice straw fiber, (e) 8% rice straw fiber and (f) 10% rice straw fiber.

Table 2. Density and flexural strength of the rice starch foams with different rice straw fiber contents.

Rice straw fiber (%)	Density (g/cm ³)	Flexural strength (MPa)
0	0.161 ± 0.008	0.076 ± 0.012
2	0.151 ± 0.012	0.070 ± 0.017
4	0.165 ± 0.013	0.091 ± 0.013
6	0.170 ± 0.006	0.144 ± 0.019
8	0.193 ± 0.009	0.155 ± 0.010
10	0.188 ± 0.009	0.102 ± 0.018

3.4 Water absorption and water solubility index (WSI)

Water absorption and WSI of the rice starch foams with different rice straw fiber contents are given in Table 3.

Table 3. Water absorption and WSI of the rice starch foams with different rice straw fiber contents.

Rice straw fiber (%)	Water absorption (%)	WSI
0	70.41 ± 3.30	12.38 ± 0.44
2	58.15 ± 6.37	11.76 ± 0.75
4	60.76 ± 5.58	11.06 ± 0.34
6	60.86 ± 2.22	10.98 ± 0.45
8	53.02 ± 5.59	11.12 ± 0.39
10	47.42 ± 4.51	10.36 ± 0.90

The decreases in water absorption by incorporating the rice straw fiber (2 to 10%) to the rice starch foam were observed. In addition, the water absorption decreased with increasing the rice straw fiber content. Due to the cellulose in the natural fiber is less hydrophilic than the starch [7], therefore, the rice straw fiber may be decreased the hydrophilicity of the rice starch foam matrix. Moreover, the rice straw fiber may be blocked water to penetrate into the foam. Thus, these lead to the decrease in water absorption of the rice starch foam containing the rice straw fiber. However, WSI values do not change with adding the rice straw fiber (2 to 10%) to the rice starch foam.

4. Conclusion

The rice starch blended with the rice straw fiber can be prepared as environmentally friendly foam trays. The limit rice straw fiber content can be added to improve the flexural strength and water sensitivity of the rice starch foam. The rice starch foams with the rice straw fiber content of 4 to 10% exhibited higher flexural strength and lower water absorption than the only rice starch foam. In addition, randomly aligned rice straw fibers were dispersed throughout the rice starch foams. The further

environmentally friendly packaging applications may be developed using these rice starch composite foams.

Acknowledgement

The authors thank Faculty of Agro-Industry, Chiang Mai University for equipment support.

References

- [1] Mitrus, M. and Moscicki, L., "Extrusion-Cooking of Starch Protective Loose-Fill Foams", *Chemical Engineering Research and Design*, 92, 778-783 (2014).
- [2] Shogren, R. L., Lawton, J. W., Doane, W. M. and Tiefenbacher, K. F., "Structure and Morphology of Baked Starch Foams", *Polymer*, 39, 6649-6655 (1998).
- [3] Lawton, J. W., Shogrena, R. L. and Tiefenbacher, K. F., "Aspen Fiber Addition Improves the Mechanical Properties of Baked Corn Starch Foams", *Industrial Crops and Products*, 19, 41-48 (2004).
- [4] Mello, L. R. P. F. and Mali, S., "Use of Malt Bagasse to Produce Biodegradable Baked Foams Made from Cassava Starch", *Industrial Crops and Products*, 55, 187-193 (2014).
- [5] Salgado, P.R., Schmidt, V.C., Molina Ortiz, S. E., Mauri, A. N. and Laurindo, J. B., "Biodegradable Foams Based on Cassava Starch, Sunflower Proteins and Cellulose Fibers Obtained by a Baking Process", *Journal of Food Engineering*, 85, 435-443 (2008).
- [6] Yang, W., Shimizu, I., Ono, T. and Kimura, Y. "Preparation of Biodegradable Foam from Walnut Shells Treated by Subcritical Water", *Journal of Chemical Technology and Biotechnology*, 90, 44-49 (2015).
- [7] Dufresne, A. and Vignon, M. R. "Improvement of Starch Film Performances Using Cellulose Microfibrils", *Macromolecules*, 31, 2693-2696 (1998).

PVA/CaHPO₄ film from cockle shell for biodegradable film

Nattapong Pinpru¹ and Somsak Woramongkolchai^{1,2*}

¹Applied Chemistry, Faculty of Science, King Mongkut's Institute of Technology Ladkrabang, Bangkok, 10520

²Department of Chemistry, Faculty of Science, King Mongkut's Institute of Technology Ladkrabang, Bangkok, 10520

Phone +66 806191629, Fax +66 2329 8428, *E-Mail: kwosomsa@gmail.com

Abstract

Phosphate compounds was synthesized by a simple precipitation of initial compounds, CaCO₃ in calcite phase from cockle shell powders reacted with H₃PO₄, CaHPO₄ was obtained. The compounds were further characterized by FT-IR revealed the fundamental vibrations of PO₄³⁻ anion in structural compound, XRD indicated the phosphate compounds, SEM showed that there were clearly different in shapes and particle size. The PVA was mixed with obtained CaHPO₄ in the ratio of 100:0, 98:2, 96:4 and 94:6. Then it was cast into film for further characterization by SEM micrographs. It was edible portion shown that bio-plastic was dominated much more roughness and porosity. In addition, the mechanical properties of the bio-plastic were lower when compared to pure PVA before and after soil burial test. The percentage of weight loss for biodegradation was between 43.75 to 82.44%.

Keywords: Calcium hydrogen phosphate (CaHPO₄), Fertilizer, Poly vinyl alcohol (PVA), Bio-plastic

1. Introduction

Researchers have previously attempted to use cockle shell as raw materials for various industrial materials [1] according to the edible portion of shellfish is small, leaving a large amount of waste after processing the animal. Cockle shell is also easy to gather, a favorable trait of any raw material. At present, relatively light-toned seashells with little pigmentation (such as cockle shell and green mussel shell) are used as a calcium source [2].

Calcium hydrogen phosphate, (CaHPO₄) occurs in nature as a mineral [3]. It is an important substance used for many applications, such as in pharmaceutical industry biocompatibility and adsorbent [3]. Furthermore, It is also considerable for applying in agriculture technology as inorganic compound fertilizer [4]. They were first reported on aqueous solution precipitation preparation of CaHPO₄ by Vassett and Bedwell [5] then, Visser et al. [6, 7] determined the chemical structures and crystal structures of the series of these phosphates such as CaHPO₄, CaHPO₄H₂O, KMgHPO₄ and by FT-IR and XRD [5].

Development of biodegradable film using bio-filler such as phosphate compound as fertilizer has been applied in the field of degradable plastic and blend films for packaging and agriculture applications [8]. The blending of biodegradable bio-filler such as phosphate compounds with PVA or bio-polymer, has also received considerable attention. Beside, upon disposal, they are completely degraded by micro-organisms (bacteria and fungi), photo-degradation as energy sources and hydrolytic was in various environment such as soil, UV light, sea, sewage, environment and including global warming [8]. The selection of compatibility between bio-filler and polymer matrix must be concerned to improve degradation and release fertilizer of the bio-plastic in soil [8].

In this research, CaHPO₄ was prepared with cockle shell with H₃PO₄ by precipitation method. The bio-plastic with released fertilizers of phosphate compound, CaHPO₄ on the base of PVA/CaHPO₄ was further studied. The casting process was used to prepare specimens for investigation by fourier-transform infrared (FT-IR),

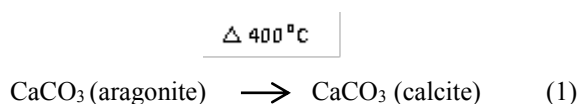
scanning electron microscope (SEM), weight loss and mechanical properties.

2. Experimental Methods

2.1 Preparation and Characterization of CaCO₃ in calcite phase from cockle shell powders.

CaCO₃ was prepared by cockle shell taken from various restaurants in Thailand. Approximately 500 g of shells as original without purification were washed by distilled water to scrub and remove dirt and then dried in an oven at 80 °C for 10 hr. The cockle shell was finely ground using grinder. The powders was sieved using a stainless steel sieve laboratory test with an aperture size 400 mesh to obtain micron-sized (37 μm in diameter) powders. The powders were finally packed into a polyethylene bag for further use in calcination processing.

CaCO₃ in calcite phase derived from CaCO₃ in aragonite phase as indicated in Eq. (1) were prepared with a chamber calciner [9]. A 50 g shells powder of CaCO₃ was placed in corundum crucible and put into the chamber of the calciner. The calciner was heated to 400 °C at a rate of 5 °C/min in a N₂ flow (0.8 L/min). The N₂ flow was maintained to prevent moisture in the atmosphere. The temperature was constant for 120 min and then cooled to room temperature.



The chemical composition of cockle shell powders was characterized by X-ray fluorescence spectrometry (XRF Bruker SRS3400 Germany). The decomposition patterns of shells powders were studied using a thermogravimetric analyzer (TGA Mettler Toledo 851e). TGA measurements were carried out from 25 to 900 °C at a heating rate 5 °C/min under nitrogen flow (10 ml/min) to prevent oxidation. Chemical analyses were performed using Fourier transform infrared spectrophotometer (FTIR Perkin Elmer) in the range of 400-4000 cm⁻¹ with 6 scans and the resolution of 4 cm⁻¹. The crystal powder was characterized by X-ray powder diffraction (XRD, Bruker D8 Advanced Germany) using CuKα

(λ = 0.15406 nm). The morphology and particle size of the synthesized nano-CaCO₃ were studied using a scanning electron microscope (SEM JEOL JSM 5800 LV) after coating the powders with gold.

2.2 Synthesis and characterization of CaHPO₄ fertilizer by precipitation method.

CaHPO₄ was prepared by precipitation technique by 50 ml of phosphoric acid (1 M of H₃PO₄) and 5 g of CaCO₃ in calcite phase from cockle shell. And then it was taken in to a 200 ml beaker with magnetic stirring at 250 rpm and room temperature for 10 min using a systematic multi-hotplate. A solution was formed by adding and mixing 100 ml of ethanol for precipitation CaHPO₄. The prepared sample was separated from the solution using a filter paper of size 18.0 cm (Filters Fioroni, China). The final products were dried for 24 hr. in an oven at 60 °C and packed into a polyethylene bag for further uses. Precipitates were firstly characterized by X-ray diffraction (XRD, Rigaku) to determine the material phases. The chemical bands were analyzed using Fourier-transformed infrared spectroscopy (FTIR, Di-gilab). The surface morphologies were studied using a scanning electron microscope (SEM, Zeiss).

2.3 Preparation and characterization of bio-composites film.

The composites of PVA and CaHPO₄ blends were processed into films by a casting method through varied PVA/CaHPO₄ with different ratio. Pure PVA film was prepared for control parameter. Pure PVA film forming solution (3%, w/w) was prepared by dissolving 3 g PVA in 97 ml distilled water for 60 min and then heated at 80 °C under 300 rpm magnetic stirring. The compositions of PVA, CaHPO₄ and deionized water (DI) were carefully mixed in various ratios (100:0, 98:2, 96:4 and 94:6 (PVA : CaHPO₄)). All mixtures were warmed and stirred at 80 °C under 300 rpm magnetic stirring for 60 for good blending. Finally, the solutions of 40.70 ml (30.70 g) of film forming solution were poured in polypropylene plastic rectangle plate (19x28 cm) and the mixture was evaporated in room temperature for 48 h to obtain the casting films. Films were

set conditioned at 30 °C and a relative humidity (RH) of 47 ± 3% RH for 48 h for further analysis.

3. Results and Discussion

3.1 Characterization of CaCO₃ in calcite phase of cockle shell.

3.1.1 The chemical composition of cockle shell powders.

Table 1. Composition of cockle shell powders obtained by X-ray fluorescence spectroscopy (XRF)

Oxide %	Cockle shell
CaO	96.20
Na ₂ O	1.950
MgO	0.377
SiO ₂	0.274
Cl	0.191
Fe ₂ O ₃	0.325
CuO	0.262
SrO	0.288

The chemical composition of the cockle shell powders by X-ray fluorescence spectrometry (XRF) was shown in Table 1. The chemical analysis of shell powders has been conducted to estimate the mineral composition and established the potential of shells wastes as bio-source of calcium carbonate (CaCO₃). The results were indicated that the shells were mainly composed of calcium in the form of calcium oxide (CaO) which could be represented more than 96.20 wt% of cockle shell. This is revealed that seashell is an attractive bio-source of high purified calcium carbonate which is in agreement with other studies [10].

3.1.2 TGA curves of cockle shell powders.

Thermal degradation of cockle shell powders was studied by thermogravimetric analysis (TGA). The evolution of the weight loss from 25 °C to 900 °C of shell powders is shown in Figure. 1. The degradation process takes place in two different stages. For Cockle shell powders, the first step occurs at relative low temperatures with a very small weight loss around 260-360 °C which is due to the degradation of the organic content of the cockle shells. The organic component was close to 1.26 wt% as calculated by a step analysis in the TG curve.

The second degradation step was occurred at higher temperatures and corresponded to the thermal decomposition of calcium carbonate which started at about 688.5 °C with a maximum decomposition of 753 °C. The total weight loss in this second degradation step was close to 42.99 wt% which was in total agreement with the theoretical decomposition of calcium carbonate as indicated in Eq. (2) [9]. The degradation of cockle shell powders led to approximately 98.74 wt% of CaCO₃ and a 1.26 wt% of organic component.

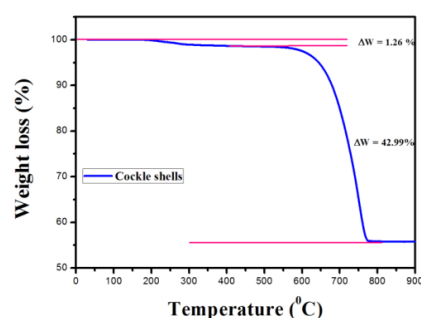


Figure 1. Thermal degradation of CaCO₃ in Cockle shell powders.

3.1.3 FT-IR patterns of CaCO₃ in calcite phase of cockle shell powders.

The FT-IR spectra of CaCO₃ from cockle shell powders before and after the calcination was shown in Figure 2. After calcination shell powder, the most prominent absorption peak of calcium carbonate was appeared at 1434 cm⁻¹ [10]. Another weak peak was observed at 1797 cm⁻¹ due to carboxylic stretching vibration [6]. The characteristic peaks which represent CO₃²⁻ that described the signature of calcite phase were observed at 876 and 712 cm⁻¹ [10]. These peaks were presented in CaCO₃ particles reflecting to the calcite phase in cockle shell.

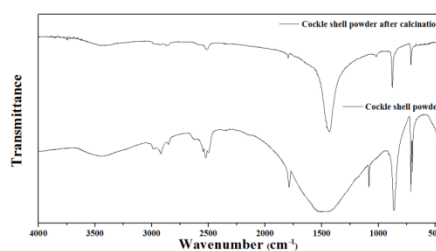


Figure 2. FT-IR spectra of cockle shell powders (a) before and (b) after calcination method.

3.1.4 XRD patterns of CaCO_3 in calcite phase of cockle shell powders.

To investigate the crystal structure in the cockle shell, the XRD analysis was conducted to calcination method. Fig 3 (c) and (d) are the XRD patterns of cockle shells powder before and after calcination, respectively. The XRD pattern peaks of (d) cockle shell powder after calcination match very well with the peaks of calcite CaCO_3 (JCPDS card No. 72-1937) reference (b) corresponding to Figure. 3 (a) [11]. This is confirmed completely synthesis CaCO_3 in calcite phase by calcination method at temperature of 450°C for 2 hr. with a rate of $5^\circ\text{C}/\text{min}$

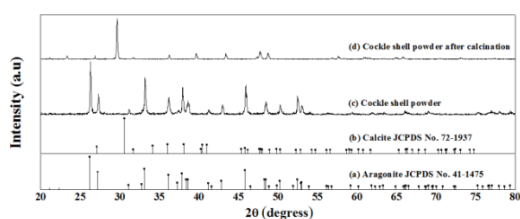


Figure 3. XRD patterns of (a) Aragonite JCPDS No. 41-1475 (b) Calcite JCPDS No.72-1937 (c) Cockle shell powder and (d) Cockle shell powder after calcination. The calcite phase was observed in XRD patterns that completely matched with the JCPDS card No. 72-1937 (b).

3.1.5 The morphology of CaCO_3 in calcite phase of shell.

The SEM micrographs of shell powders were shown in Figure 4. They were characterized cockle shells before calcination (a) after calcination (b). The surface of CaCO_3 (a) indicated dense and roughness. However, for all CaCO_3 (a), an inorganic fillers phase were agglomerate on the surface and lower dispersed in this area. The surface of CaCO_3 (b) was smoother than of CaCO_3 (a). Furthermore, the surface of all CaCO_3 (b) were shown highly dispersed. A morphology of CaCO_3 (b) was laminated form indicating calcite phase of CaCO_3 with corresponding to XRD results.

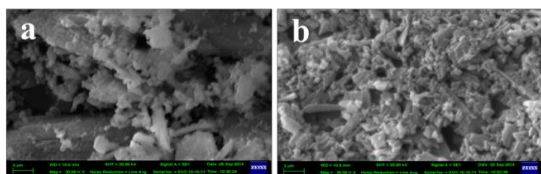


Figure 4. SEM micrographs of cockle shells powders (a) before (b) after calcination method.

3.2 Characterization of CaHPO_4 fertilizer

3.2.1 The FT-IR patterns of CaHPO_4 fertilizer.

The FT-IR spectrum of CaHPO_4 was shown a typical CaHPO_4 in Fig.5 The hydrogen phosphate anions dominated at least two broad bands around 2855 and 2385 cm^{-1} [12]. The possibility of interaction of second order modes with the fundamental O–H stretching vibrations was investigated. The band at 1216 cm^{-1} is due to the in-plane P–O–H bending. The band around at 913 cm^{-1} is out-of-plane P–O–H bending vibration [12]. There are all peaks to confirmed CaHPO_4 structure.

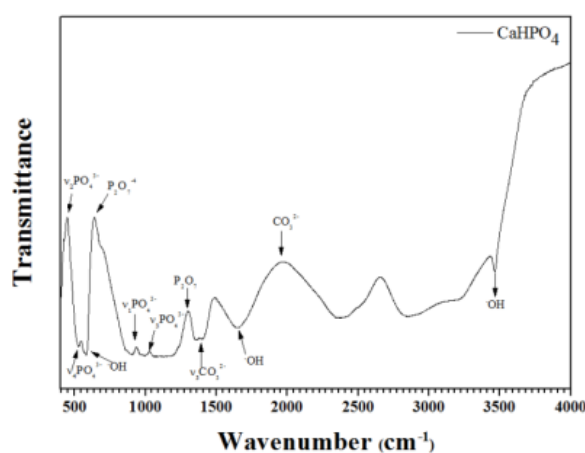


Figure 5. FT-IR patterns of CaHPO_4 fertilizer after reaction CaCO_3 in calcite phase of cockle shell powders with H_3PO_4 .

3.2.2 The XRD patterns of CaHPO_4 fertilizer.

The X-ray patterns of the CaHPO_4 powder obtained by precipitation technique were shown in Fig. 6. The X-ray patterns of CaHPO_4 was in good agreement with the corresponding JCPDS file (70-0359).

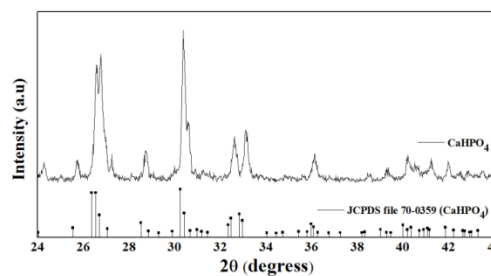


Figure 6. The XRD patterns of CaHPO_4 fertilizer.

3.2.3 The morphology of CaHPO₄ fertilizer.

There are different magnitude on the surface morphologies of the CaHPO₄. Fig.7. (a) and (b) were indicated typical SEM images of particles after synthesis CaCO₃ from cockle shell with H₃PO₄ by precipitation technique. In Fig. 7 (a), particles are well dispersed and higher distribution and greater surface area Fig.7 (b) was shown a high resolution SEM images of CaHPO₄ particles similar to laminated. These results were clearly evidenced that the particles are highly crystalline and dispersion

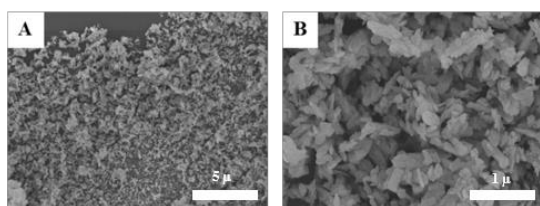


Figure 7. SEM micrographs of CaHPO₄ with difference magnitude (a) 1000x (b) 3,000x

3.3 Characterization of PVA/CaHPO₄ composite film

3.3.1 Morphology of composite film

The cross-sectional surface morphologies of composites film with different ratio of CaHPO₄ fertilizer was shown in Fig. 8. (a, c, e and f) before soil burial test and Fig.8. (b, d, f and h) after soil burial test for 4 weeks. This was revealed the CaHPO₄ could be dispersed into the PVA polymer matrix. The PVA/CaHPO₄ composites film indicated the roughness surface for each formula because CaHPO₄ had ability to pulled out from surface.

3.3.2 Mechanical properties testing.

The tensile strength, elongation at break and Young's modulus of PVA/CaHPO₄ composite films were shown in Table 2. Tensile strength and elongation at break of PVA/CaHPO₄ blends were decreased as increasing CaHPO₄ content. The decreasing mechanical properties were due to weaker interfacial adhesion between CaHPO₄ and PVA matrix leading to lower elongation at break. The tensile strength of 2%, 4%, and 6% of CaHPO₄ was also decreased when compare to pure PVA. The filler CaHPO₄ content indicated a non-reinforcing filler. For Young's modulus values were also decreased when CaHPO₄ increased because Young's modulus was closely related to

the rigid domains of the material. The lower to mechanical properties was also supported by the SEM images Fig. 8 (c, e and g)

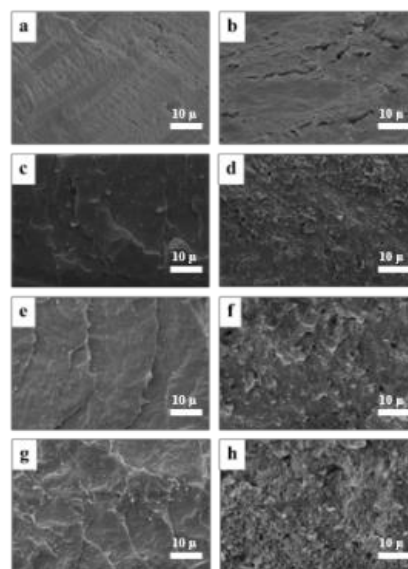


Figure 8. The cross-sectional surfaces SEM images of PVA (a) and PVA/CaHPO₄ composite film with different ratios of CaHPO₄ fertilizer (c, e and g) before soil burial test and Fig.8. (b, d, f and h) after soil burial test for 4 weeks.

Table 2 Mechanical properties of composite films before soil burial test.

Blend	Tensile strength (MPa)	Elongation at break (%)	Young's Modulus (MPa)
PVA	7.12±0.13	89.45±11.23	12.33±0.21
PVA/2%CaHPO ₄	5.62±0.25	60.82±6.71	24.88±4.58
PVA/4%CaHPO ₄	4.22±0.67	55.65±6.78	32.11±2.23
PVA/6%CaHPO ₄	3.07±0.28	41.86±3.67	57.24±7.88

3.3.3 Biodegradation by soil burial test.

Biodegradation test was conducted using soil burial test. Different PVA/CaHPO₄ composites were buried under soil surface for 4 weeks, then the tensile test was carried out and characterized surface morphologies of composite film by SEM. The biodegradation was indicated to decrease of the tensile strength, elongation at break and Young's modulus (Table 3) because the PVA and CaHPO₄ component was degraded by microorganism existed such as water fungi and bacteria in soil. This was also because

the composite could be absorbed water from the soil. The occurrence of these factor in various part of the composite was enhanced to decreasing to mechanical properties. The results were suggested that the addition of the CaHPO₄ into the PVA polymer matrix could accelerate the biodegradation of composite film. As supported by the SEM analysis in Fig. 8. (b, d, f and h), cavities and crack were initiated appearance during the 4 weeks of microorganism activities.

Table 3 Mechanical properties of composite films after soil burial test.

Blend	Tensile strength (MPa)	Elongation at break (%)	Young's Modulus (MPa)
PVA	5.12±1.26	60.45±9.38	8.33±1.42
PVA/2%CaHPO ₄	3.62±0.68	51.71±3.35	18.49±3.64
PVA/4%CaHPO ₄	2.22±0.29	40.65±2.14	23.25±3.17
PVA/6%CaHPO ₄	0.67±0.14	31.93±2.46	41.36±4.41

For the SEM images of composite film after soil burial test exposure were shown in Fig. 8. (b, d, f and h), The surface of these films which contain high CaHPO₄ were more degraded than composite film containing low CaHPO₄. These composites film was dominated some cavities from degradation of CaHPO₄ and further large interconnected holes. These results proved that degradation efficiency of high content of CaHPO₄ was much better than low content of CaHPO₄. This result was corresponding to weight loss as shown in Table 4.

3.3.4 Weight loss of composite film.

The average weight loss measurement of composite film was carried out to study their biodegradation by soil burial test. The weight loss of different samples compared to before and after soil burial test was shown in Table 4.

After soil burial test, the noticeable degradation rate of CaHPO₄ was revealed a maximum degradation of 82.44% w/w with a composite film containing 6% of CaHPO₄ for 4 weeks. The higher CaHPO₄ content, the more biodegradation of CaHPO₄ in PVA were shown.

Table 4 The average weight loss of different samples compare to before and after soil burial test.

Blend	Before (g)	After (g)	Weight loss (%)
	Avg.	Avg.	
PVA	0.80	0.35	43.75
PVA/2%CaHPO ₄	0.96	0.57	59.38
PVA/4%CaHPO ₄	1.24	0.95	76.61
PVA/6%CaHPO ₄	1.31	1.08	82.44

4. Conclusion

The CaCO₃ was prepared in calcite phase from cockle shell by aqueous solution precipitation technique. The techniques of FTIR, XRD and SEM were selected use to characterize the composition of cockles shell powder. The results were all confirmed that the CaCO₃ were completely synthesis. It was then to synthesized with H₃PO₄ to get CaHPO₄ fertilizer. This was successfully revealed by all the same previous techniques. Bio-composite was further prepared by blending PVA with CaHPO₄ fertilizer in various ratios, these was shown that the higher the addition of CaHPO₄ into PVA, the more degradation film was obvious. However, the lower the mechanical properties were appeared to both before and after soil burial test.

References

- [1] M. Mohamed, S. Yusup, and S.Maitra., "Decomposition study of calcium carbonate in cockle shells", *Journal of Engineering Science and Technology*, vol. 7, no. 1, pp. 1–10 (2012).
- [2] A. J. Awang-Hazmi, A. B. Z. Zuki, M. M. Nordin, A. Jalila, and Y. Norimah., "Mineral composition of the cockle (*Anadara Granosa*) shells of west coast of peninsular Malaysia and its potential as biomaterial for use in bone repair", *Journal of Animal and Veterinary Advances*, vol. 6, no. 5, pp. 591–594 (2007).
- [3] Guo-Chung Dong, Jui-Sheng Sun, Chun-Hsu Yao, George J. Jiang, Chin-Wang Huang and Feng-Huei Lin., "A study on grafting and characterization of HMDI-modified calcium hydrogenphosphate", *J. Biomaterials*. 22, 3179-3189 (2001).

- [4] Zhang, S., Huang, S.-W. and Zhang., “Dehydration characteristics of struvite-K pertaining to magnesium potassium phosphate cement system in non-isothermal condition” *J. Thermal Analysis and Calorimetry*, p. 111, 35-40 (2013).
- [5] Mathew, M. and Schroeder, LW., “Crystal structure of a struvite analogue, $MgKPO_4 \cdot 6H_2O$ ”, *J. Acta Crystallogr*, 11–13 (1979).
- [6] Graeser, S., Postl, W., Bojar, H-P., Berlepsch, P. and Armbruster., “Growth and characterization of Struvite-K crystals”, *J Mineral*, P., 20, 629–33 (2018)
- [7] Luff, BB. and Reed, RB., “Thermodynamic properties of magnesium potassium orthophosphate hexahydrate”, *J. Chem Eng Data*, 25, 310–312 (1980).
- [8] Alcantara, M.T.S., Brant, A.J.C., Giannini, D.R., Pessoa, J.O.C.P., Andrade, A.B., Riella, H.G. and Lugao A.B., “Influence of dissolution processing of PVA blends on the characteristics of their hydrogels synthesized by radiation—Part I: Gel fraction, swelling, and mechanical properties”, *J. Radiation Physics and Chemistry*, 81, 1465-1470 (2012).
- [9] N.A. Rashidi, M. Mohamed, S. Yusup., “Calcination condition on decomposition of calcium carbonate in waste cockle shell to calcium oxide using thermal gravimetric analysis”, *J. Engineering and Technology*, 60, 818-823 (2011).
- [10] V. Fombuena, L. Bernardi, O. Fenollar, T. Boronat, R. Balart., “Characterization of green composites from biobased epoxy matrices and bio-fillers derived from seashell wastes”, *J. Materials and Design*, 57, 168-174 (2014).
- [11] A. Devarajan, M. Abdul Khadar, K. Chattopadhyay., “Effect of ball milling on chemically synthesized nanoparticles of $CaCO_3$ ”, *J. Materials Science and Engineering*, 452-453, 395-400 (2007).
- [12] Guo-Chung Donga, Jui-Sheng Sunb, Chun-Hsu Yaoc, George J. Jianga, Chin-Wang Huanga, Feng-Huei Lind., “A study on grafting and characterization of HMDI-modified calcium hydrogen phosphate” *J. Biomaterials*, 3179–3189, (2001).

Preparation and Property Improvement of Stereocomplexed PLL/PDL-PEG-PDL Blends

Aphinan Saengsrichan¹, Puttinan Meepowpan¹, Patnarin Worajittiphon¹, Robert Molloy^{1,2} and Winita Punyodom^{1,2*}

¹Department of Chemistry, Faculty of Science, Chiang Mai University, Chiang Mai, Thailand 50200

²Materials Science Research Center, Faculty of Science, Chiang Mai University, Chiang Mai, Thailand 50200

Phone: +66-5394-3341-5, Fax: +66-5389-2277, *E-mail: winitacmu@gmail.com

Abstract

Poly(L-lactide) (PLL) is biodegradable, compostable and producible from renewable resources. However, its inherent brittleness and low heat distortion temperature (HDT) prohibit its widespread industrial application. Therefore, great effects have been made to improve its thermal resistance, processability and toughness by controlling its structure and morphology. In this research, stereocomplexed polylactide (Sc-PL) was prepared by the solution blending of PLL with poly(D-lactide) (PDL) and poly(D-lactide)-*b*-poly(ethylene glycol)-*b*-poly(D-lactide) (PDL_n-PEG_m-PDL_n) triblock copolymers. The results showed that the Sc-PL had a melting temperature at 218 °C which is approximately 43 °C higher than that of PLL or PDL. The addition of 40 wt % PDL₈₇-PEG₁₈₂-PDL₈₇ to PLL could significantly increase the elongation at break of the PLL/PDL-PEG-PDL blended films as a result of the combined effects of stereocomplexation between the PLL and PDL and plasticization by the PEG. In addition, the PLL/PDL-PEG-PDL blended films showed a higher thermal stability than PLL alone at temperatures above 375 °C. The biodegradation of Sc-PL films on exposure to a controlled composting environment at 58±2 °C under aerobic conditions was studied alongside PLL and PDL. These results showed that the Sc-PL films were compostable with 100% biodegradability similar to PLL and PDL.

Keywords: Property improvement; stereocomplexed PLL/PDL-PEG-PDL; biodegradation; composting

1. Introduction

Poly(L-lactide) (PLL) is known as one of the biodegradable polymers which can be decomposed in a moist aerobic environment [1-2]. Since PLL is compostable, it has been viewed as a promising material to reduce the plastics waste problem. The low toxicity of PLL along with its environmentally benign characteristics has made PLL an ideal candidate for food packaging, tableware and for other consumer products [3].

However, PLL is limited by its brittleness and low heat distortion temperature which affect its mechanical and thermal properties. Ways to improve the mechanical and thermal properties of PLL include block copolymerization, plasticization, and polymer blending. More recently, stereocomplexation has also shown great promise whereby the two enantiomeric forms of PLL and poly(D-lactide) (PDL) are mixed to form stereocomplexed crystallites. Block copolymerization of PDL with flexible

polymer such as poly(ethylene glycol) (PEG) helps to achieve a good balance between toughness and crystallization [4-5]. PEG is also an attractive polymer for biomedical applications. It can be used as a plasticizing agent for PLL to give increased elongation without too much decrease in tensile strength [6]. Many researchers have studied the crystallization behavior of enantiomeric blends of PLL by blending with low molecular weight PDL-PEG-PDL copolymers. The crystallization rate, thermal resistance, and toughness of PLL were all improved due to the plasticization effect of the flexible PEG segments and the increased interfacial affinity between PEG and the PLL matrix induced by stereocomplexation [7-8].

In a previous study, the *in vitro* hydrolytic degradation behavior of PLL/PDL blends compared with pure PLL and PDL was carried out at 37 °C. The

hydrolytic degradation rate of PLL/PDL blends was found to lower than pure PLL and PDL in terms of the number-average molecular weight (\bar{M}_n) and weight loss [9-10].

This could be explained by the enantiomeric blends of PLL and PDL having higher crystallinity and crystal stability from the stronger hydrogen bonds and dipole-dipole interactions between the enantiomeric PLL chains [11].

In this work, we have prepared the PLL/PDL-PEG-PDL blends by the solution casting method using chloroform as the solvent. The mechanical, thermal and morphological properties of the Sc-PL were characterized and the biodegradation of PLL/PDL-PEG-PDL blends, PLL and PDL under controlled composting condition at 58 ± 2 °C were compared.

2. Experimental Methods

2.1 Materials

L-lactic acid was purchased from Archer Daniels Midland. D-lactic acid was purchased from Musashino Chemical Laboratory. PEG ($\bar{M}_n = 8000$) and stannous octoate, Sn(Oct)₂, was purchased from Sigma-Aldrich. All other reagents were analytical grade and used as received.

2.2 Synthesis of PLL, PDL and PDL-PEG-PDL triblock copolymers

PLL and PDL were synthesized by ring-opening polymerization (ROP) of L-lactide and D-lactide using stannous octoate as initiator. PDL-PEG-PDL triblock copolymers were also synthesized by the ROP of D-lactide and PEG. Polymerizations were carried out at 120 °C for 24 h. After the reaction was complete, the products were dissolved in chloroform and precipitated in excess cold methanol. The PLL, PDL and copolymers were dried in a vacuum oven at 50 °C to constant weight.

2.3 Sc-PL film preparation

PLL/PDL_n-PEG_m-PDL_n were prepared by the solution blending of PLL with synthesized poly(D-lactide)-*b*-poly(ethylene glycol)-*b*-poly(D-lactide) (PDL_n-PEG_m-PDL_n) triblock copolymers. After solvent

evaporation at room temperature, films were cut into rectangular-shaped 1x7 cm test pieces. The thickness of the polymer films was approximately 50 μm.

2.4 Characterization of polymer films

Thermal and morphological properties of the polymer films were studied using a PerkinElmer differential scanning calorimeter (DSC7). Each sample (3-5 mg) was placed into an aluminum pans and heated from 0-250 °C at a rate of 10 °C /min under a nitrogen gas atmosphere. The mechanical properties of the polymer films were investigated using an LRX⁺ (Lloyd Instrument) universal tensile testing machine at a crosshead speed of 5 mm/min.

2.5 Biodegradation of polymer films

The biodegradation of the PLL, PDL and Sc-PL polymer films was studied at the Thailand Institute of Scientific and Technological Research (TISTR). Briefly, the carbon dioxide accumulation was determined from the microbial degradation in compost under controlled conditions. Mixtures of compost with 1% test material (polymer films were ground into a powder of particle size less than 1 mm.), or positive reference, or negative reference were incubated within closed containers at 58 ± 2 °C (total bacteria about 10⁸ colonies forming unit per gram compost). The carbon dioxide (CO₂) of microbial degradation activity in the system was determined during incubation periods of 39 days. Each treatment was carried out in triplicate.

3. Results and Discussion

3.1 Structural characterization of PDL-PEG-PDL

The ¹H-NMR spectrum of the PDL_n-PEG_m-PDL_n copolymer is shown in Fig 1. The methine proton (–CH, *d*) and methyl proton (–CH₃, *a*) signals were evident at $\delta = 5.2$ ppm and at 1.6 ppm respectively. The ethylene oxide protons signal (–OCH₂CH₂, *b*) appeared at $\delta = 3.7$ ppm. The PDL content as determined from the ¹H-NMR peaks, was found to be 87 mole%. The multiplicity of the methine proton (*c*) peak at the chain ends of the copolymer and the

last methylene proton (*f*) unit on PEG confirmed the reaction between PEG and DL [12-13]. Molecular weights of PLL and PDL were 43,000 and 61,000 g/mol as determined by dilute-solution viscosity. The molecular weights of the synthesized copolymers were also calculated by ¹H-NMR using CDCl₃ as a solvent by comparing the intensities of the PLL methine proton and PEG methylene proton. The molecular weights of the PDL_n-PEG_m-PDL_n copolymer after calculated was calculated as 20,500 g/mol [14].

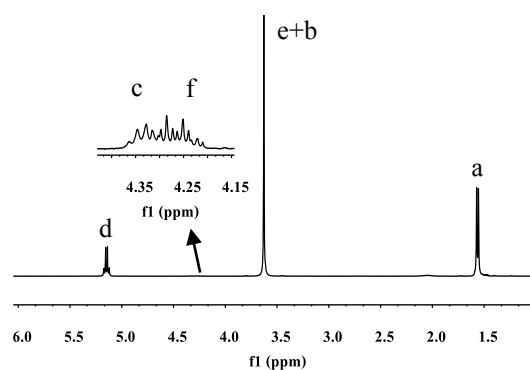


Fig. 1 ¹H NMR spectrum of PDL_n-PEG_m-PDL_n copolymer

3.2 Stereocomplexation of PLL/PDL₈₇-PEG₁₈₂-PDL₈₇

Figure 2 shows the DSC curves of the PLL/PDL₈₇-PEG₁₈₂-PDL₈₇ blends in different weight ratios. While PLL showed a melting peak around 175.3 °C, there was also a new peak around 215-220 °C due to stereocomplexation of PLL and PDL₈₇-PEG₁₈₂-PDL₈₇. When the L/D weight ratio reached 60/40, the blend had only a single melting peak around 220 °C. This indicated that complete stereocomplexation of PLL could be achieved at L/D ratios of 60/40-50/50 without the presence of homocrystals. The second DSC heating runs in Figure 2 of the PLL/PDL₈₇-PEG₁₈₂-PDL₈₇ blends do not show any significant melting point differences from the first heating runs which, shows good stereocomplex reformability in the PLL/PDL-PEG-PDL blends [2, 7, 12, 14].

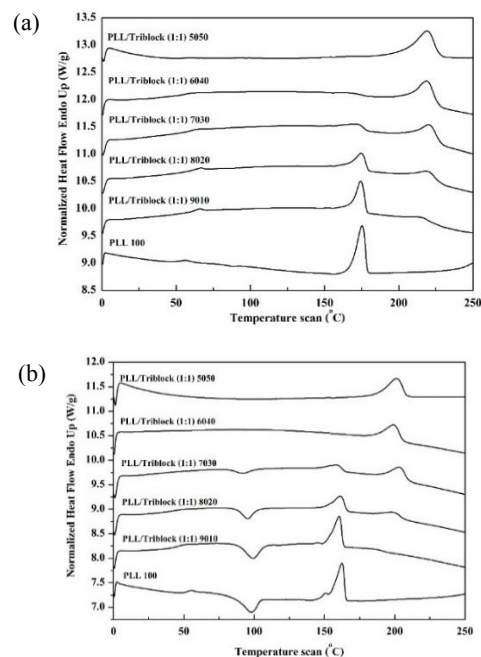


Fig. 2 DSC thermogram of PLL/PDL₈₇-PEG₁₈₂-PDL₈₇ in various composition (a) first heating run and (b) second heating run.

3.3 Mechanical properties of PLL/PDL₈₇-PEG₁₈₂-PDL₈₇

Figure 3 shows the mechanical properties of the PLL/PDL₈₇-PEG₁₈₂-PDL₈₇ blend films. Tensile strength and percentage elongation at break are plotted as a function of PDL₈₇-PEG₁₈₂-PDL₈₇ copolymer addition. A slight decrease in tensile strength can be observed with increasing PDL₈₇-PEG₁₈₂-PDL₈₇ content in the polymer blend. The tensile behavior reflects the synergistic effect of stereocomplexation and PEG plasticization in the copolymer. For the percentage elongation at break, there is no obvious increase when 10 wt% PDL₈₇-PEG₁₈₂-PDL₈₇ was added but there was a dramatic increase with 40 wt% PDL₈₇-PEG₁₈₂-PDL₈₇ loading. This increase in elongation at break can be attributed to the fact that a critical PEG content for plasticization is reached at 40 wt% PDL₈₇-PEG₁₈₂-PDL₈₇ is added. However, the elongation at break decreases slightly when 50 wt% of the copolymers is added which might be caused by a physical crosslinking effect in the stereocomplex that limits extensibility [2, 4, 7, 12-13].

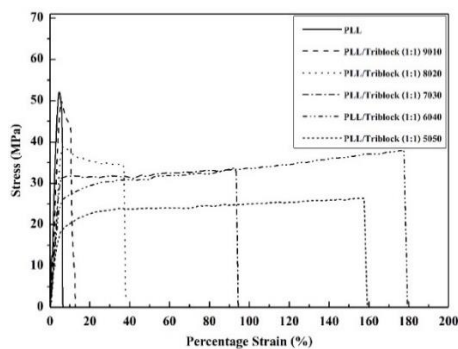


Fig. 3 Mechanical properties of PLL/PDL₈₇-PEG₁₈₂-PDL₈₇ blends at different compositions.

3.4 Biodegradation testing

The biodegradabilities of PLL, PDL and PLL/PDL₈₇-PEG₁₈₂-PDL₈₇ were evaluated compared with microcrystalline cellulose and polyethylene as positive and negative controls under controlled composting conditions in the laboratory. The compost testing conditions were as follows: temperature (58±2 °C); aerobic conditions; 50% relative humidity. The test method used was based on the determination of the CO₂ evolved [15]. In accordance with biodegradability testing, Table 1 compares the biodegradabilities of PLL, PDL and PLL/PDL₈₇-PEG₁₈₂-PDL₈₇ in term of % biodegradability as 97.5±9.2, 100.0±9.5 and 100.0±9.9 respectively. The first stage degradation of PLL is hydrolysis of the main chain ester bonds to water-soluble compounds and lactic acid. This is followed by metabolization via bulk erosion of these products into CO₂, water and biomass by a variety of microorganisms [16-17]. Furthermore, the size and shape of the test material also plays an important role in biodegradation. Since the PLL, PDL and PLL/PDL₈₇-PEG₁₈₂-PDL₈₇ were all ground into powders of particle size less than 1 mm, they all had high surface areas so that a large fraction of the test material could be in contact with moisture and microorganisms for hydrolysis and enzymatic degradation to occur rapidly [18-19].

Table 1 The percentage of biodegradability of PLL, PDL and PLL/PDL₈₇-PEG₁₈₂-PDL₈₇ blend.

Code	Biodegradability (%)	
	Mean	SD (%)
Control ^{1/}	-	-
R ⁺ ^{2/}	97.9	9.6
R ⁻ ^{3/}	0.0	5.4
PLL ^{4/}	97.5	9.2
PDL ^{4/}	100.0	9.5
PLL/PDL ₈₇ -PEG ₁₈₂ -PDL ₈₇ (60/40) ^{4/}	100.0	9.9

^{1/} The cumulative CO₂ has occurred by microbial degradation activity in compost. (not include CO₂ in containers)

^{2/} The cumulative CO₂ has occurred by cellulose microcrystalline biodegradation. (cellulose microcrystalline is easy to decompose in the natural; refer to ASTM D5338)

^{3/} The cumulative CO₂ has occurred by polyethylene sheet biodegradation. (polyethylene sheet are difficult to decompose in the natural; refer to ASTM D5338)

^{4/} The cumulative CO₂ has occurred by test material biodegradation.

4. Conclusion

PLL/PDL-PEG-PDL (60:40 wt %) films achieved full stereocomplexation with a T_m of around 200-220 °C, which is approximately 40-50 °C higher than virgin PLL or PDL, while the addition of 40 wt % PDL-PEG-PDL to PLL could significantly increase the elongation at break of the PLL/PDL-PEG-PDL blended films. The PLL/PDL₈₇-PEG₁₈₂-PDL₈₇ films could degrade under composting conditions with a percentage biodegradability closed to those of PLL and PDL alone.

Acknowledgment

The authors gratefully acknowledge the financial support from the National Research Universities (NRU) Scholarship program. Furthermore, we also thank the Thailand Institute of Scientific and Technological Research (TISTR) for carrying out the preliminary biodegradability testing.

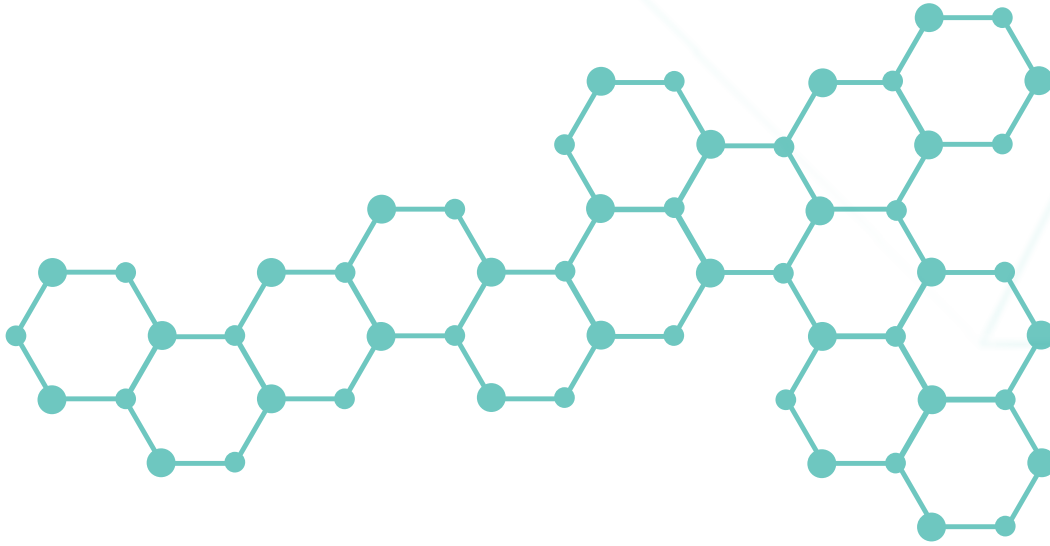
References

- [1] Jiang, L., Wolcott, M.P., Zhang, J. "Study of biodegradable polylactide/poly(butylene adipate-co-terephthalate) blends", *Biomacromolecules*, 199-207 (2006).

- [2] Liu, Y., Shao, J., Sun, J., Bian, X., Feng, L., Xiang, S., Sun, B., Chen, Z., Li, G., Chen, X., "Improved mechanical and thermal properties of PLLA by solvent blending with PDLA-*b*-PEG-*b*-PDLA", *Polymer Degradation and Stability*, 10-17 (2014).
- [3] Lima, L.T., Auras, R., Rubinob, M., "Processing technologies for poly(lactic acid)", *Progress in Polymer Science*, 820-852 (2008).
- [4] Han, L., Yu, C., Zhou, J., Shan, G., Bao, Y., Yun, X., Dong, T., Pan, P., "Enantiomeric blends of high-molecular-weight poly(lactic acid)/poly(ethylene glycol) triblock copolymers: Enhanced stereocomplexation and thermomechanical properties", *Polymer*, 376-386 (2016).
- [5] Tsuji, H., "Poly(lactic acid) stereocomplexes: A decade of progress", *Advanced Drug Delivery Reviews*, 97-135 (2016).
- [6] Rathi, S., Chen, X., Coughlin, E.B., Hsu, S.L., Golub, C.S., Tzivani, M.J., "Toughening semicrystalline poly(lactic acid) by morphology alteration", *Polymer*, 4184-4188 (2011).
- [7] Song, Y., Wang, D., Jiang, N., Gan, Z., "Role of PEG segment in stereocomplex crystallization for PLLA/PDLA-*b*-PEG-*b*-PDLA blends", *ACS Sustainable Chemistry & Engineering*, 1492-1500 (2015).
- [8] Fukushima, K., Kimura, Y., "Stereocomplexed polylactides (Neo-PLA) as high-performance bio-based polymers: their formation, properties, and application", *Polymer International*, 626-642 (2006).
- [9] Tsuji, H., "In vitro hydrolysis of blends from enantiomeric poly(lactide)s. 1. Well-stereocomplexed blend and non-blended films", *Polymer*, 3621-3630 (2000).
- [10] Tsuji, H., Tsuruno, T., "Accelerated hydrolytic degradation of Poly(L-lactide)/Poly(D-lactide) stereocomplex up to late stage", *Polymer Degradation and Stability*, 477-484 (2010).
- [11] Andersson, S.R., Hakkarainen, M., Inkinen, S., Sodergard, A., Albertsson, A.C., "Polylactide stereocomplexation leads to higher hydrolytic stability but more acidic hydrolysis product pattern", *Biomacromolecules*, 1067-1073 (2010).
- [12] Tacha, S., Saelee, T., Khotasen, W., Punyodom, W., Molloy, R., Worajittiphon, P., Meepowpan, P., Manokruang, K., "Stereocomplexation of PLL/PDL-PEG-PDL blends: Effects of blend morphology on film toughness", *European Polymer Journal*, 308-318 (2015).
- [13] Han, L., Yu, C., Zhou, J., Shan, G., Bao, Y., Yun, X., Dong, T., Pan, P., "Enantiomeric blends of high-molecular-weight poly(lactic acid)/poly(ethylene glycol) triblock copolymers: Enhanced stereocomplexation and thermomechanical properties", *Polymer*, 376-386 (2016).
- [14] Jing, Z., Shi, X., Zhang, G., Lei, R., "Investigation of poly(lactide) stereocomplexation between linear poly(L-lactide) and PDLA-PEG-PDLA tri-block copolymer", *Polymer International*, 1399-1407 (2015).
- [15] American Standard Test Method (ASTM), Standard Test for Determining Aerobic Biodegradation of Plastic Materials Under Controlled Composting Conditions, ASTM D 5338-98 (2003).
- [16] Lucas, N., Bienaime, C., Belloy, C., Queneudec, M., Silvestre, F., Nava-Saucedo, J.-E., "Polymer biodegradation: Mechanisms and estimation techniques", *Chemosphere*, 429-442 (2008).
- [17] Shah, A.A., Hasan, F., Hameed, A., Ahmed, S., "Biological degradation of plastics: A comprehensive review", *Biotechnology Advances*, 246-265 (2008).
- [18] Kijchavengkul, T., Auras, R., "Perspective compostability of polymers", *Polymer International*, 793-804 (2008).
- [19] Kale, G., Kijchavengkul, T., Auras, R., Rubino, M., Selke, S.E., Singh, S.P., "Compostability of bioplastic packaging materials: An overview", *Macromolecular Bioscience*, 255-277 (2007).

BMED

BIOMEDICAL POLYMERS



Synthetic Strategies for Molecularly Imprinted Polymer of Very-Low-Density Lipoprotein

Suticha Chunta¹ and Peter A. Lieberzeit^{2*}

¹Department of Clinical Chemistry, Faculty of Medical Technology, Prince of Songkla University, Thailand 90110

²Department of Physical Chemistry, Faculty for Chemistry, University of Vienna, Austria 1090

Phone +43-1-4277-52341, Fax +43-1-4277-852341, *E-Mail: peter.lieberzeit@univie.ac.at

Abstract

Designing biomimetic receptors, namely molecularly imprinted polymers (MIPs), have become of substantial interest for clinically relevant analytes. Herein, we report the strategies for synthesis the selective polymer of very-low-density lipoprotein (VLDL), which is exploited as a cardiovascular biomarker, as well as low-density lipoprotein and high-density lipoprotein. VLDL-MIP, comprising co-polymers of methacrylic acid and N-Vinyl pyrrolidone at the ratio of 1:1 crosslinked with ethylene glycol dimethacrylate, were screened on 10 MHz dual-electrode quartz crystal microbalances (QCM) for binding ability investigation. Such MIP yields much higher sensor response towards VLDL (2967 Hz) than other lipoprotein species (112 Hz of LDL, 302 Hz of HDL), indicating that MIP favors VLDL very strongly. Successful imprinting of VLDL-MIP inherently opens up a novel field in the area of molecular imprinting that is potentially useful in clinical analysis.

Keywords: Molecularly imprinted polymer, very-low-density lipoprotein, quartz crystal microbalance

1. Introduction

Synthetic polymers, namely molecularly imprinted polymers (MIPs), have increasingly become of interest as artificial, biomimetic receptor materials. MIPs efforts have been reported in a broad range of potential areas such as separation sciences [1], bio/chemical sensors [2], catalysis [3] and drug delivery [4]. MIPs can be synthesized via molecular imprinting approach as presented in Figure 1.

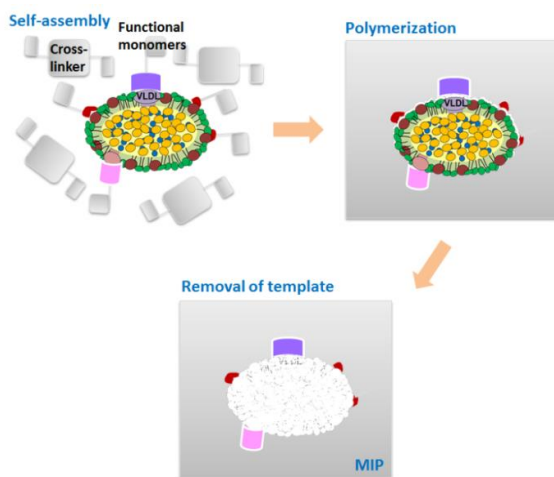


Figure 1 Principle of MIPs synthesis

In principle, the desired template is firstly assembled to functional monomer(s) in the presence of crosslinker through covalent or non-covalent interactions, forming the polymer matrix. After template removal, this polymer network reveals selective binding cavities that are complementary to the template in dimensions, shape, and positioning of functional groups [5].

As previously mentioned for polymer synthesis, MIPs need to be optimized by varying a range of parameters including: type of template, types of monomer, solvents, polymerization time, pressure, and temperature [2]. To date, MIPs have been synthesized successfully for wide a range of analytes from small organic molecules (e.g. pesticides, pharmaceutical [6], nucleic acids [7], etc.) [2], to large bio(macro)molecules (e.g. proteins [8], cholesterol [9], phospholipids [10], sugars [11], etc.). In addition, MIP-based sensors of clinically relevant species deserve special attention to apply in clinical diagnosis and therapeutic monitoring, for instance to investigate species of virus [12] or bacteria [13] and also to determine the amount of human serum albumin (HSA) in serum [14],

creatinine in urine [15], and cancer biomarkers [16]. To date, imprinting approach of such large biochemical compounds is still a challenge because they are flexible and also expose a large number of functional groups on their surfaces. In recent years, MIPs of lipoprotein aggregates, namely low-density lipoprotein (LDL) [17] and high-density lipoprotein (HDL) [18], have been successfully synthesized as sensing biomimetic selective elements to detect LDL and HDL, respectively. Both lipoproteins are critical biomarkers in clinical analysis for assessing coronary heart disease (CHD). The lipoproteins used are more challenging templates than “simple” proteins, because lipoproteins surfaces reveal large numbers of functional groups of three constituents comprising amphipathic phospholipids (PL), free cholesterols (FC), and apolipoproteins (AP), which are all available to interact with functional monomers.

Herein, we present MIP strategies for very-low-density lipoprotein (VLDL) which is also an important biomarker for CHD diagnosis as well as LDL and HDL. Polymer optimization turned out to be one of the main challenges. The reason is that VLDL, LDL and HDL comprise of similar types of surface constituents but differ by the ratios of these constituents and hence also slightly in diameter as shown in Table 1.

Table 1. Characteristics of lipoprotein classes

Class	Size (nm)	Surface potential (mV)	% Composition				
			Core		Surface		
			T	C	F	P	A
		G	E	C	L	P	
LDL	18-25	-4.5 to -7.0	6	42	8	22	22
HDL	9-12	-10.5 to -12.5	4	13	6	27	50
VLDL	30-80	-7.0 to -10.5	55	12	7	18	18

TG: Triglycerides, CE: cholesteryl ester

2. Experimental Methods

Quartz crystal microbalance (QCM)-based sensor was chosen for these studies because it provides straightforward measuring, generating mass signals from binding between selective MIPs and VLDL particles. Ten MHz AT-cut quartz crystals with dual gold-electrode were used as the transducer. All chemicals/reagents used were

purchased as analytical grade or the highest available synthetic grade.

2.1 Preparation of Standard Lipoprotein Solutions

All standard lipoprotein solutions, i.e., VLDL, LDL, and HDL, were isolated from human sera via density gradient ultracentrifugation as described in our previous work [17]. Purity/identity and cholesterol concentration of each lipoprotein fraction (namely VLDL-C, LDL-C, HDL-C) were evaluated using agarose gel electrophoresis and homogeneous enzymatic colorimetry, respectively.

2.2 Synthesis and Screening of VLDL-MIP

VLDL-MIP was firstly synthesized followed the LDL-MIP recipes [17], comprising co-polymers of methacrylic acid and N-Vinyl pyrrolidone (ratio at 3:2) crosslinked with ethylene glycol dimethacrylate (EGDMA). This solution was prepolymerized under UV light approaching the gel state, which is suitable for coating the respective electrodes of QCM. Then, the VLDL template stamp was pressed into the prepolymer film on the first electrode of QCM to yield the MIP. The polymer on the untreated side of the electrode leads to so-called non-imprinted polymer (NIP) and used as a reference.

2.3 Testing Binding Ability of MIP via QCM

For QCM sensor operation, the baseline signals were obtained via 10 mM phosphate buffer saline (PBS) until reaching the equilibrium state. Binding ability of VLDL to recognition cavities on VLDL-MIP was determined by exposing the sensor system to standard VLDL solutions at the concentration of 80 mg/dL.

2.4 Testing of Selectivity for MIP

The sensor was exposed to each standard lipoprotein solution comprising of VLDL-C, LDL-C, and HDL-C standard solutions at the same concentration of 80 mg/dL, respectively.

3. Results and Discussion

3.1 Optimization of VLDL-MIP Synthesis

Figure 2 shows the first QCM responses of both MIP and NIP-coated electrodes (MAA/VP at the ratio 3:2 as LDL-MIP) when exposing them to 80 mg/dL standard VLDL-C solution. This leads to a decreased frequency by -1020 Hz on the MIP side and -875 Hz on the NIP side, corresponding to -145 Hz mass effect. This response confirms successful imprinting. Additionally, all bound VLDL can be removed again by washing sequences with 10% aqueous solution of acetic acid, followed by 0.1% SDS solution, and deionized water to regenerate MIP. However, the MIP response is rather small, namely, less than a factor of 2 between MIP and NIP. One reason for this is that VLDL and LDL contain different ratios of surface constituents as aforementioned.

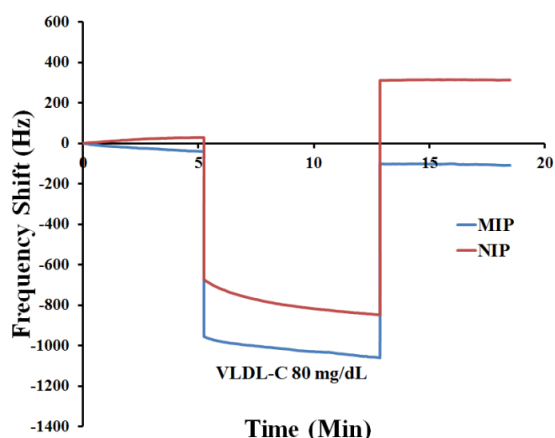


Figure 2 Frequency response of VLDL-MIP (MAA:VP 3:2) exposed to 80 mg/dL VLDL-C solution

Then, the exact mixing ratio of MAA and VP was investigated to enhance sensitivity. Figure 3 presents all sensor outcomes of five various ratios of mixing functional monomers. Sensor response of MAA and VP at the ratio of 1:1 provides the highest frequency shift by -2805 Hz on the MIP side and +278 Hz on the NIP side. Hence, this functional monomer ratio was chosen as VLDL-MIP for all further experiments. Non-Sauerbrey behavior of NIP side have been observed in biomolecules due to being weakly bound and the retention of some mobility on flat surfaces, leading to increased frequency signals [19].

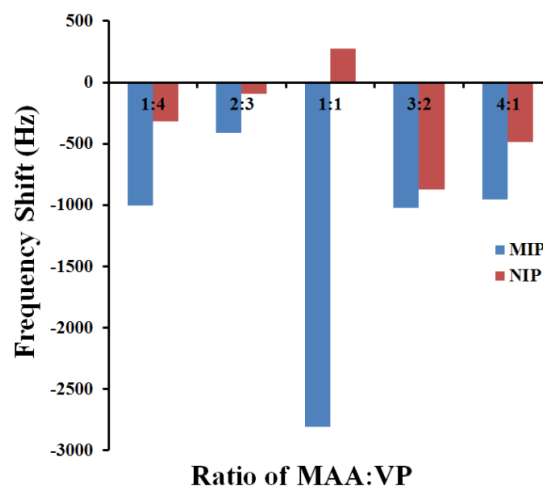


Figure 3 Sensor responses of MIP and NIP obtained for different monomer ratios toward 80 mg/dL VLDL-C

3.2 Selectivity of VLDL-MIP

Figure 4 reveals the sensor response for QCM-coated VLDL-MIP and NIP toward a standard VLDL-C, LDL-C, and HDL-C standard solutions, respectively. After loading VLDL-C, MIP coated electrode led to a substantial frequency signal of -2967 Hz. While LDL-C and HDL-C addition yielded small negative frequency signals on the MIP side of -112, and -302 Hz, respectively. NIP again obtains positive frequency shifts of 21 and 81 Hz, respectively. Based on all results presented it can be said that VLDL-MIP favors VLDL strongly.

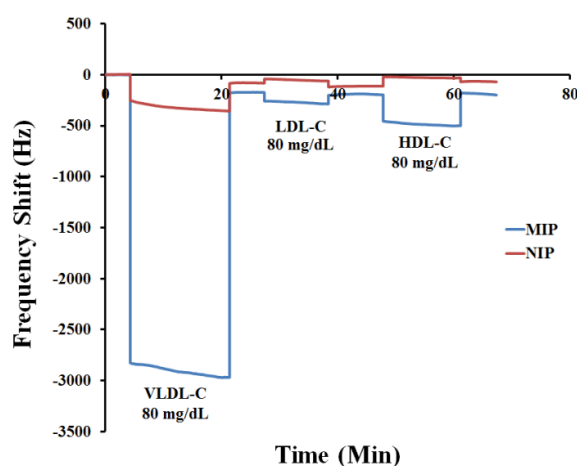


Figure 4 Sensor responses toward vary lipoprotein standards at the concentration of 80 mg/dL

4. Conclusion

All results indicate successful imprinting of VLDL-MIP, which is indeed fit both morphological and functional variances between the lipoprotein species very well. Next step will comprise of the full evaluation of the sensor for direct VLDL assessment in serum. This approach can be introduced instead of indirect (via Friedewald equation) VLDL calculation method.

Acknowledgment

This project was supported by the ASEAN-European Academic University Network (ASEA-UNINET) for preparation of standard lipoprotein solutions.

References

- [1] Yang S, Wang Y, Jiang Y, Li S, Liu W. Molecularly Imprinted Polymers for the Identification and Separation of Chiral Drugs and Biomolecules. *Polymers*. 2016;8(6):216.
- [2] Whitcombe MJ, Chianella I, Larcombe L, Piletsky SA, Noble J, Porter R et al. The rational development of molecularly imprinted polymer-based sensors for protein detection. *Chemical Society Reviews*. 2011;40(3):1547-71.
- [3] Liu J-q, Wulff G. Functional Mimicry of the Active Site of Carboxypeptidase A by a Molecular Imprinting Strategy: Cooperativity of an Amidinium and a Copper Ion in a Transition-State Imprinted Cavity Giving Rise to High Catalytic Activity. *Journal of the American Chemical Society*. 2004;126(24):7452-3.
- [4] Alvarez-Lorenzo C, Concheiro A. Molecularly imprinted polymers for drug delivery. *Journal of Chromatography B*. 2004;804(1):231-45.
- [5] Hussain M, Wackerlig J, Lieberzeit P. Biomimetic Strategies for Sensing Biological Species. *Biosensors*. 2013;3(1):89.
- [6] Suedee R, Srichana T, Rattananont T. Enantioselective Release of Controlled Delivery Granules Based on Molecularly Imprinted Polymers. *Drug Delivery*. 2002;9(1):19-30.
- [7] Sreenivasan K. Synthesis and evaluation of molecularly imprinted polymers for nucleic acid bases using aniline as a monomer. *Reactive and Functional Polymers*. 2007;67(10):859-64.
- [8] Phan N, Sussitz H, Lieberzeit P. Polymerization Parameters Influencing the QCM Response Characteristics of BSA MIP. *Biosensors*. 2014;4(2):161.
- [9] Spizzirri UG, Peppas NA. Structural Analysis and Diffusional Behavior of Molecularly Imprinted Polymer Networks for Cholesterol Recognition. *Chemistry of Materials*. 2005;17(26):6719-27.
- [10] Jang R, Kim KH, Zaidi SA, Cheong WJ, Moon MH. Analysis of phospholipids using an open-tubular capillary column with a monolithic layer of molecularly imprinted polymer in capillary electrochromatography-electrospray ionization-tandem mass spectrometry. *Electrophoresis*. 2011;32(16):2167-73.
- [11] Parmpi P, Kofinas P. Biomimetic glucose recognition using molecularly imprinted polymer hydrogels. *Biomaterials*. 2004;25(10):1969-73.
- [12] Wangchareansak T, Thitithanyanont A, Chuakheaw D, Gleeson MP, Lieberzeit PA, Sangma C. Influenza A virus molecularly imprinted polymers and their application in virus sub-type classification. *Journal of Materials Chemistry B*. 2013;1(16):2190-7.
- [13] Dickert FL, Hayden O. Bioimprinting of Polymers and Sol-Gel Phases. Selective Detection of Yeasts with Imprinted Polymers. *Analytical Chemistry*. 2002;74(6):1302-6.
- [14] Cieplak M, Szwabinska K, Sosnowska M, Chandra BKC, Borowicz P, Noworyta K et al. Selective electrochemical sensing of human serum albumin by semi-covalent molecular imprinting. *Biosensors and Bioelectronics*. 2015;74:960-6.
- [15] Lee M-H, Tsai T-C, Thomas JL, Lin H-Y. Recognition of creatinine by poly(ethylene-co-vinylalcohol) molecular imprinting membrane. *Desalination*. 2008;234(1):126-33.
- [16] Selvolini G, Marrazza G. MIP-Based Sensors: Promising New Tools for Cancer Biomarker

- Determination. *Sensors* (Basel, Switzerland). 2017;17(4):718. Chunta S, Suedee R, Lieberzeit PA. Low-Density Lipoprotein Sensor Based on Molecularly Imprinted Polymer. *Analytical Chemistry*. 2016;88(2):1419-25.
- [17] Chunta S, Suedee R, Lieberzeit PA. High-density lipoprotein sensor based on molecularly imprinted polymer. *Analytical and Bioanalytical Chemistry*. 2018;410(3):875-83.
- [18] Pomorska A, Shchukin D, Hammond R, Cooper MA, Grundmeier G, Johannsmann D. Positive Frequency Shifts Observed Upon Adsorbing Micron-Sized Solid Objects to a Quartz Crystal Microbalance from the Liquid Phase. *Analytical Chemistry*. 2010;82(6):2237-42.

Cordyceps militaris* extract-loaded chitosan nanoparticles and their release characteristics*Jittap Pranjan**¹ and Orawan Suwanton^{1,2*}¹School of Science, Mae Fah Luang University, Chiang Rai 57100²Center of Chemical Innovation for Sustainability (CIS), Mae Fah Luang University, Chiang Rai 57100

Phone +66 5391 6787, Fax +66 5391 6776, *E-Mail: o.suwanton@gmail.com

Abstract

Cordyceps militaris (CM) is commonly used as a tonic and therapeutic herb in Asia. It has the antitumor, antiaging, antibacterial, and antioxidant activities. To extend shelf life, improve stability, control and sustain release of CM extract, the encapsulation of CM extract was employed in the form of nanoparticles. In this study, the chitosan nanoparticles (CS-NPs) were prepared by ionic gelation method. The CM-loaded CS-NPs were fabricated by mixing chitosan (CS) solution (i.e. 0.5%, 1%, and 2% w/v) with CM extract and then crosslinked with sodium tripolyphosphate (STPP) solution (0.5% w/v). The morphology of the CM-loaded CS-NPs was characterized by Field Emission Scanning Electron Microscopy (FE-SEM). In addition, the size and polydispersity index (PDI) of the CM-loaded CS-NPs were characterized by Zetasizer. From the results, the samples showed the agglomeration of particles in shape with a rough surface. The CM-loaded CS-NPs had the particle size ranging from 471 to 953 nm and PDI ranging from 0.43 to 0.66. The release profiles of CM from the CM-loaded CS-NPs showed a burst release in the first period time and reached the plateau at the longer immersion time.

Keywords: Chitosan, Nanoparticles, Ionic gelation, *Cordyceps militaris***1. Introduction**

Cordyceps militaris (CM) is a rare fungus of medicinal mushroom, which is commonly used as a tonic and therapeutic herbs of the Chinese for many years. CM consists of 2 parts which are stroma (fruit body) and caterpillar body (dead body of host larva). CM has shown a broad range of health effect on the antitumor, antiaging, antibacterial and antioxidant activities [1-5]. Because it contains many active ingredients, including polysaccharides, nucleosides, and sterols such as mannoglucan, galactose, exopolysaccharides, cordycepin, adenosine, guanosine, and ergosterol [2, 6-8].

Nowadays, nanotechnology is gaining more attention in the industry because of its small particle size. The nanometer level allows nanoparticles to penetrate into the stratum corneum and penetrate deep into the skin through the channel of the hair follicle. Moreover, it enhances the effectiveness of essential substances to the skin. Polymeric nanoparticles can be prepared in several

ways such as solvent evaporation, polymerization, desolvation, and ionic gelation [9-10]. Nanoencapsulation is an effective way to increase the stability of important substances and prevent the reaction with other substances. The small size of particles has the potential to increase the efficiency of the substance [11-12]. Chitosan (CS) is one of the most common biopolymers. It is a polysaccharide and obtained from the shells, shellfish, crabs, or the wall of fungi. It is used in pharmaceutical and biomedical applications due to its availability, good biocompatibility, and other desirable characteristics [13-14]. Moreover, it is inexpensive and digestible, making it is a promising vehicle for the development of drug delivery system.

The present work, the CM-loaded CS-NPs were prepared by ionic gelation. This process is unique because it not only provides very tiny particles or nanoparticles but also avoids the use of high temperature. The objective of this work was to prepare the CM-loaded CS-NPs. The CM-

loaded CS-NPs were characterized for their morphology, particle size, PDI, encapsulation efficiency (EE), and loading capacity (LC). Finally, the release profiles of CM extract from the CM-loaded CS-NPs were investigated.

2. Experimental Methods

2.1. Materials

CS (weight-average molecular weight = 22 kDa) was purchased from Bio21 (Thailand). Sodium tripolyphosphate (STPP) was purchased from Sigma-Aldrich (USA). Ethanol was purchased from Ajax Finechem (Australia). Acetic acid was purchased from EMSURE (Germany). Hydrochloric acid was purchased from QR&C (New Zealand). *Cordyceps militaris* was obtained from MG Cordy Gold Company Ltd. (Thailand).

2.2. Extraction of *Cordyceps militaris* extract

5 g of dried CM was soaked in 30 ml of ethanol and distilled water (i.e., 100:0, 80:20, 60:40, 40:60, 20:80 and 0:100). After three days, the extracted solution was centrifuged to separate supernatant and precipitate. Then, the precipitate was extracted again in the mixture of ethanol and distilled water for two times. The supernatant of the extract solution was evaporated using a rotary evaporator at 45 °C. The crude CM extract was lyophilized to get a brown paste of the crude CM extract.

2.3. HPLC analysis

HPLC conditions were as follows: Column, C18-reverse phase; mobile phase, methanol:distilled water (20%:80% v/v); flow rate, 1.0 ml/min; UV detection, 260 nm; and injection quantity, 30 µl. The CM extract was dissolved in ethanol:distilled water (20:80) and then filtered through a 0.22 µm membrane filter prior to injection. Quantitative analysis of cordycepin was conducted by evaluating the peak area on the basis of a standard curve. Peaks of cordycepin were identified by their retention time of the standard compounds.

2.4. Antioxidant activity of *Cordyceps militaris* extract

The CM extract was dissolved in an ethanol and distilled water (60:40). Then, the various concentrations (0.012, 0.023, 0.047, 0.094, 0.188, 0.375 and 0.750 mg/ml) of CM extract solutions were mixed with 1 ml of 100 µM 2,2-diphenyl-1-picrylhydrazyl (DPPH). After that, the solutions were kept in a dark room for 30 min at room temperature. The free radical scavenging activity of the CM extract was determined by UV-Vis spectrophotometer at the wavelength of 517 nm. Then, the antioxidant activity (%) was calculated from the following equation;

$$\%AA = \frac{A_{\text{control}} - A_{\text{sample}}}{A_{\text{control}}} \times 100 \quad (1)$$

Where A_{control} and A_{sample} are the absorbance values of the testing solution without and with CM extract.

2.5. Preparation of *Cordyceps militaris* extract-loaded chitosan nanoparticles

CS solutions (i.e., 0.5%, 1%, and 2% w/v) were prepared by dissolving the different amounts of chitosan in 1% v/v acetic acid. After that, the CM extract (0.75 mg/ml) was added solution to the CS solution under continuous stirring. Next, STPP solution (0.5% w/v) was added to the CS solution under stirring for 30 min at room temperature. After that, the suspended nanoparticles were centrifuged at a speed 6,000 rpm at 25 °C for 20 min and washed with distilled water for several times. Finally, the nanoparticles were dispersed in distilled water by sonication. The nanoparticle suspension was then immediately dried by freeze-drying process.

2.6. Morphology and particle size study

The morphological appearances of the CM-loaded CS-NPs were examined by FE-SEM. One drop of the dilute sample solution was dropped on a carbon film and let air-dried before viewing.

The particle size and PDI were determined by dynamic light scattering (DLS) and the results were reported as the mean value.

2.7. Encapsulation efficiency and loading capacity

The CM-loaded CS-NPs was dissolved in 1 M HCl at 45 °C for 30 min. After that, the ethanol was added to the solution to extract CM extract and the solution was then centrifuged at 9,000 rpm for 1 min at room temperature. The solution was measured by UV- vis spectrophotometer at the wavelength of 260 nm. Finally, the values of EE and LC were calculated according to the following equations;

$$\%EE = \frac{\text{Weight of loaded CM extract}}{\text{Weight of initial CM extract}} \times 100 \quad (2)$$

$$\%LC = \frac{\text{Weight of loaded CM extract}}{\text{Weight of sample}} \times 100 \quad (3)$$

2.8. Release study

The release characteristics of CM extract from the CM-loaded CS-NPs were investigated by the dialysis bag diffusion technique. Each sample was placed in the dialysis bag containing PBS solution (molecular weight cut-off of 12,000-14,000). After that, the dialysis bag was immersed the flask containing PBS solution (pH 7.4) at 37 °C for different time points. After a specified time, 1 ml of sample was withdrawn and fresh medium was refilled. The sample solution was characterized by UV- Vis spectrophotometer at the wavelength of 260 nm to determine the released amount of CM extract.

3. Results and Discussion

3.1 The content of cordycepin

The content of cordycepin from CM extract can be determined by the peak area of HPLC graphs. The content of cordycepin in each extraction was 0.33%, 0.52%, 1.24%, 1.40%, 1.63% and 0.90% for 0:100, 20:80, 40:60, 60:40, 80:20 and 100:0 of ethanol:distilled water, respectively. The maximum of cordycepin content was 1.63% for ethanol:distilled water (80:20). This extraction was used in further study to determine the antioxidant activity.

3.2 Antioxidant activity of *Cordyceps militaris* extract

The antioxidant activity of CM extract was investigated by the DPPH assay. The results are shown in

Figure 1. The antioxidant activity of CM extract was increased with increasing concentration of CM extract and the maximum antioxidant activity was 81% at CM extract concentration of 0.75 mg/ml. The DPPH scavenging results demonstrated that the CM extract probably contained the substances that were proton. The polysaccharide was the key component exhibiting the antioxidant activity [15].

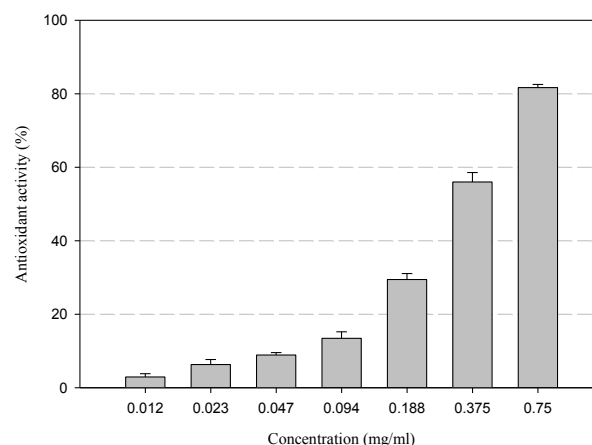


Figure 1. Antioxidant activity of *Cordyceps militaris* extract

3.3 Morphology and particle size study

The CM-loaded CS-NPs were prepared by an ionic gelation. The nanoparticles occur from the interaction between positively charged CS and negatively charged STPP at room temperature. From FE-SEM image, the spherical shape with aggregation of particles was obtained (Figure 2). From Table 1, the particle size of CM-loaded CS-NPs prepared from CS concentration of 0.5%, 1.0%, and 2.0% w/v was 517.0±25.5, 471.2±7.1, and 953.4±44.6 nm, respectively. The large sizes of these particles might be due to the agglomeration of nanoparticles during the preparation process for DLS test. PDI is a parameter used to define the particle size distribution, which is expressed as dimensionless number extrapolated from autocorrelation function in photon correlation spectroscopy. The value of PDI may vary from 0.01 (mono dispersed particles) to 0.5-0.7, whereas, PDI > 0.7 indicates a broad particle size distribution of the formulation. From the results, the PDI of CM-loaded CS-

NPs prepared from CS concentration of 0.5%, 1.0%, and 2.0% w/v was 0.46 ± 0.02 , 0.43 ± 0.02 , and 0.66 ± 0.02 , respectively. Normally, the particles sizes of CS-NPs depend largely on the concentration of CS and STPP solutions. For the success of CS with nanosized, the concentration of CS and STPP should be controlled at a suitable range [16].

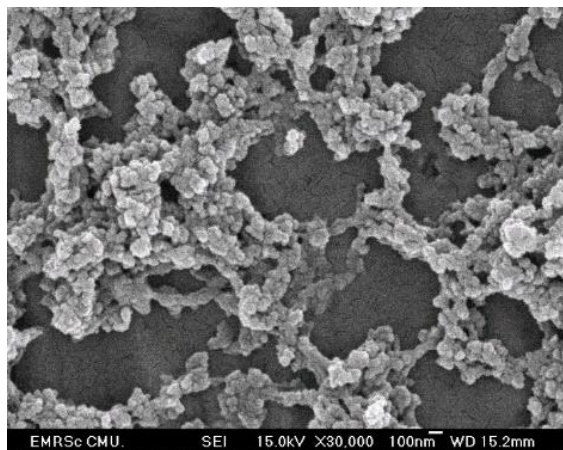


Figure 2. The FE-SEM image of CM-loaded CS-NPs (1% w/v CS)

3.5 Release study

The release profiles of CM extracts from CM-loaded CS-NPs are shown in Figure 3. The release profile showed an initial burst release about 40% in the first 1 h and then gradually increased and reached the plateau at the longer diffusion time in all samples. Generally, the nanoparticles occur the burst release on the first period due to the three different mechanisms of drug release from nanoparticles system: (a) release from the surface of particles, (b) diffusion through the swollen rubbery matrix and (c) release due to polymer erosion [18]. So, the burst release at the first period was attributed to the some of the CM extract which was weakly bound to the surface area of the nanoparticles, than to the CM extract incorporated in nanoparticles. The maximum released amount of CM was 96.0%, 95.3%, and 86.8% from 0.5%, 1.0%, and 2.0% w/v CS, respectively. So, the released amount of CM from the CM-loaded CS-NPs decreased with increasing concentration of CS.

Table 1. The particles size, PDI, EE, and LC of the CM-loaded CS-NPs

Concentration of CS (%w/v)	Particle size (nm)	PDI	EE (%)	LC (%)
0.5	517.0 ± 25.5	0.46 ± 0.02	16.34 ± 0.77	2.33 ± 0.17
1.0	471.2 ± 7.1	0.43 ± 0.02	28.23 ± 1.08	2.24 ± 0.14
2.0	953.4 ± 44.6	0.66 ± 0.02	15.26 ± 4.40	2.13 ± 0.07

3.4 Encapsulation efficiency and loading capacity

EE is the percentage of CM extract loading content that can be entrapped into CS-NPs. From Table 1, the percentage of EE and LC were calculated from equation (2) and (3). The %EE of CM-loaded CS-NPs was 16.34%, 28.23%, and 15.26% for 0.5%, 1.0% and 2.0% w/v of CS, respectively. The maximum EE (28.23%) was found at 1.0% w/v of CS. However, the %LC of CS-NPs was not different (2.13%-2.33%). The samples prepared using a high initial weight ratio of CS to drug showed the decreased value of EE. This might be due to the saturation of drug loading into CS-NPs. However, the EE and LC values obtained from this study were not different from the previous report [17].

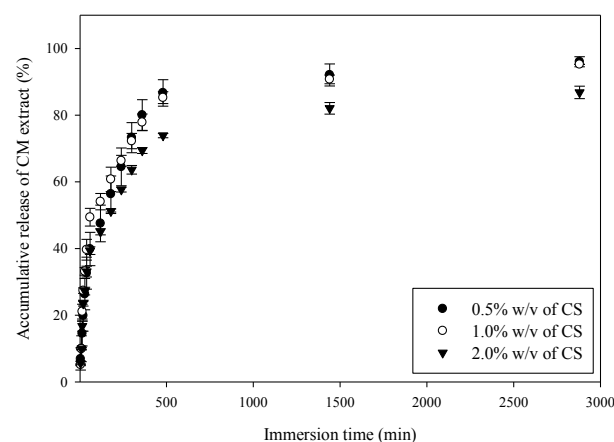


Figure 3. Cumulative release of CM-loaded CS-NPs at CS concentrations of 0.5, 1.0, and 2.0% w/v

4. Conclusion

The CM-loaded CS-NPs were successfully prepared by ionic gelation. The CM extract at extraction of ethanol:distilled water (80:20) showed the maximum cordycepin (1.63%). The CM-loaded CS-NPs nanoparticle showed the spherical shape with some agglomerations. The particle size was ranging between 417 and 953 nm and PDI ranged between 0.43 and 0.66. The %EE of CM-loaded CS-NPs nanoparticles was not related to the concentration of CS while %LC was not significantly different in all conditions. The released amount of CM decreased with increasing concentration of CS. The maximum released amount of CM was 96.0% at CS concentration of 0.5% w/v.

Acknowledgment

The authors would like to acknowledge the Research and Researchers for Industries-RRI M.Sc. scholarship (MSD60I0006) and MG Cordy Gold Co., Ltd. for financial support and the authors also grateful to Center of Chemical Innovation for Sustainability (CIS) and Scientific and Technological Instruments Center (STIC), Mae Fah Luang University.

References

[1] Buenz, E.J., Bauer, B.A., Osmundson, T.W., Motley, T.J., "The traditional Chinese medicine Cordyceps sinensis and its effects on apoptotic homeostasis", *J. Ethnopharmacol.*, 96, 19-29 (2005).

[2] Ji, D.B., Ye, J., Li, C.L., Wang, Y.H., Zhao, J., Cai, S.Q., "Antiaging Effect of Cordyceps sinensis Extract", *Phytother. Res.*, 23, 116-122 (2009).

[3] Wang, J., Kan, L., Nie, S., Chen, H., Cui, S.W., Phillips, A.O., Phillips, G.O., Li, Y., Xie, M., "A comparison of chemical composition, bioactive components and antioxidant activity of natural and cultured Cordyceps sinensis", *LWT - Food Sci. Technol.*, 63, 2-7 (2015).

[4] Shashidhar, M.G., Giridhar, P., Sankar, K.U., Manohar, B., "Bioactive principles from Cordyceps sinensis: A potent food supplement – A review", *J. Funct. Foods*, 5, 1013-1030 (2013).

[5] Yan, J.K., Li, L., Wang, Z.M., Leung, P.H., Wang, W.Q., Wu, J.Y., "Acidic degradation and enhanced antioxidant activities of exopolysaccharides from Cordyceps sinensis mycelial culture", *Food Chem.*, 117, 641-646 (2009).

[6] Kim, S.D., "Isolation, Structure and Cholesterol Esterase Inhibitory Activity of a Polysaccharide, PS-A, from Cordyceps sinensis", *J. Korean Soc. Appl. Biol. Chem.*, 53(6), 784-789 (2010).

[7] Wu, Y., Hu, N., Pan, Y., Zhou, L., Zhou, X., "Isolation and characterization of a mannoglucan from edible Cordyceps sinensis mycelium", *Carbohydr. Res.*, 342, 870-875 (2007).

[8] Leung, P.H., Zhao, S., Ho, K.P., Wu, J.Y., "Chemical properties and antioxidant activity of exopolysaccharides from mycelial culture of Cordyceps sinensis fungus Cs-HK1", *Food Chem.*, 114, 1251-1256 (2009).

[9] Nagavarma B.V.N., Yadav H., Ayaz A., Vasudha L. S., Shivakumar H.G., "Different Techniques for Preparation of Polymeric Nanoparticles- a Review", *Asian J. Pharm. Clin. Res.*, 5(3), 16-23 (2012)

[10] Reis, C.P., Neufeld, R.J., Ribeiro, A.J., Veiga, F., "Nanoencapsulation I. Methods for preparation of drug-loaded polymeric nanoparticles", *Nanomedicine*, 2, 8-21 (2006).

[11] Neethirajan, S., Jayas, D.S., "Nanotechnology for the food and bioprocessing industries", *Food and Bioprocess Technology*, 4, 39-47 (2011).

[12] Huang, Q., Yu, H., Ru, Q., "Bioavailability and delivery of nutraceuticals using nanotechnology", *J. Food Sci.*, 75, R50-R57 (2010).

[13] Ji J., Hao S., Wu D., Huang R., Xu Y., "Preparation, characterization and in vitro release of chitosan nanoparticles loaded with gentamicin and salicylic acid" *Carbohydr. Polym.*, 85, 803–808 (2011).

[14] No H.K., Kim S.H., Lee S.H., Park N.Y., Prinyawiwatkul W., "Stability and antibacterial activity of chitosan solutions affected by storage temperature and time", *Carbohydr. Polym.*, 65, 174-178 (2006).

[15] Lin R., Liu H., Wu S., Pang L., Jia M., Fan K., Jia S., Jia L., "Production and in vitro antioxidant activity of

exopolysaccharide by a mutant, *Cordyceps militaris* SU5-

08", *Int. J. Biol. Macromol.*, 51, 153-157 (2012)

[16] Zhao J., Wu J., "Preparation and characterization of the fluorescent chitosan nanoparticle probe," *Chin. J. Ana. Chem.*, 34(11), 1555-1559 (2006).

[17] Hosseini S.F., Zandi M., Rezaei M, Farahmandghavi F., "Two-step method for encapsulation of oregano essential oil in chitosan nanoparticles: Preparation, characterization and in vitro release study" *Carbohydr. Polym.*, 95, 50-56 (2013).

[18] Agnihotri, S.A., Mallikarjuna N.N., Aminabhavi T.M., "Recent advances on chitosan-based micro- and nanoparticles in drug delivery", *J. Control. Release*, 100, 5-28 (2004).

Preparation of Poly(Lactic Acid)/Alumina Composites For Dentistry Application

Nathawat Kanchanawaleekun^{1*}, Nattakarn Hongsriphan¹, and Pajaera Patanathabutr¹

¹Department of Materials Science and Engineering, Faculty of Engineering and Industrial Technology, Silpakorn University, Sanam Chan Place Campus, Nakhon Pathom 73000, Thailand
Phone +66 3424 1708, Fax +66 3424 1708, *E-mail: kanchanawalee_n@silpakorn.edu

Abstract

Currently, the polymeric material used to fabricate temporary crowns in dentistry application is poly(methyl methacrylate) (PMMA), which is non-biobased polymer and fabricated by milling. This research objective is aimed to find polymeric materials to replace PMMA and be able to fabricate by 3D printing technique, which could provide faster making of temporary crowns. Poly(lactic acid) (PLA), the most applicable biodegradable polymer, was processed by alumina powder in the ratio of 5, 10, 15 and 20% by weight. Alumina surface was modified with (3-Aminopropyl) triethoxysilane (APTES) at 10% by weight compared to alumina powder. The obtained composites were characterized rheological and mechanical properties in order to determine the optimized formulation for fabrication using 3D printing technique. It was found that higher alumina content in the PLA composites increased flexural modulus but decreased elongation at break. Rheological property results showed that the PLA composite adding silane-treated alumina of 10 wt% had the highest storage and loss modulus. In addition, the optimum condition for 3D printing of the PLA/alumina composite filament will be further studied.

Keywords: Poly(lactic acid); Composite; Temporary crowns; and 3D Printing

1. Introduction

Temporary crown is the curing method that works well in dental patients. Temporary crown is a restoration of damaged or broken teeth from many causes, for example by occlusion or by time and teeth with very large perforation to work efficiently as before. The curing method is composed of many processes and steps. The duration of the curing might take twice since it requires molding temporary crown in the dental laboratory to create the perfect size that fits the patient and dismantling the temporary crown and attaching the permanent crown with the teeth, then checking and adjusting as appropriate. [1]

Currently, temporary crown is made from acrylic polymer, such as poly(methyl methacrylate) or PMMA [2] which is not either bio-based material and biodegradable. In this work, we propose to find the polymeric material that is suitable and can be used to make a temporary crown using 3D-printing technology [3] to reduce the duration of making the temporary crown. Poly(lactic acid) or PLA, a bio-based and biodegradable polymeric material, was compounded with alumina powder, in order to make them

look more like a real tooth and have better mechanical performance. Since PLA and alumina have different hydrophilicity, alumina surface was treated with 3-aminopropyltriethoxysilane (APTES) in order to improve compatibility and dispersion of the fillers during the compounding. In this report, thermal and rheological properties of composite compounds were evaluated and compared with extruded neat PLA. Also, composite compounds were injection molded into specimens to determine improvement of mechanical properties by means of flexural testing.

2. Experimental Methods

PLA pellets, Ingeo 4032D extrusion grade, was purchased from NatureWorks (USA). The polymer has a density of 1.24 g/cm³ and MFI of 3.9 g/10 min (190°C, 2.16 kg). Alumina powder was purchased from Sigma-Aldrich (USA) with the average particle size of 100 μm. 3-aminopropyltrieth-oxysilane (APTES) was purchased from Sigma-Aldrich (USA) and used as received.

Table 1. Thermal properties of neat PLA and PLA/alumina composites.

Sample	First heating						Second heating					
	T _g	T _{cc}	T _m	H _{cc}	H _m	%X _c	T _g	T _{cc}	T _m	H _{cc}	H _m	%X _c
	(°C)	(°C)	(°C)	J/g	J/g	(%)	(°C)	(°C)	(°C)	J/g	J/g	(%)
Neat PLA	58.82	100.11	169.72	24.23	32.84	9.26	60.24	109.26	168.23	26.87	32.91	6.49
5% Alumina	58.77	99.11	169.31	24.09	33.40	10.54	60.31	101.76	167.97	21.76	34.23	14.11
10% Alumina	59.32	98.63	169.78	23.54	33.33	11.70	60.33	100.79	168.37	22.59	34.58	14.32
15% Alumina	58.58	96.36	169.63	19.80	27.89	10.23	58.44	98.83	167.97	13.52	28.48	18.92
20% Alumina	57.70	95.41	169.39	17.59	29.22	15.63	60.24	99.33	167.97	14.50	28.38	18.66

APTES of 10 wt% was dissolved in water/ethanol mixture (30/70 w/w). Then, alumina powder was suspended in the solution at 80°C with mechanical stirring continuously for 3 hours, and then was filtered and dried at 120°C for 18 hours. [4, 5].

Prior to compounding, PLA and APTES silane treated alumina particles were dried in a vacuum oven at 60°C for 24 hours. The composites were melt compounded using a twin-screw extruder (SHJ-25, S/D 40, Yongteng, China) using the barrel temperature profile of 150-180°C and a screw speed of 20 rpm. The extrudate was cooled down in water bath and the pull-off speed was set to obtain the extrudate diameter of 1.7 mm for 3D-printing. Neat PLA extrudate/filament was also prepared under the same condition. Some of them were pelletized and injection molded (Plus 350/75, Battenfeld, Austria) into rectangular specimens for flexural testing.

Differential scanning calorimetry (DSC) was performed under nitrogen atmosphere using a differential scanning calorimeter (TGA/DSC1, Mettler Toledo, USA). Extrudates were cut into 7-10 mg samples and tested in a heat-cool-reheat mode with a heating rate of 5°C/min from 30 to 180°C. Flexural modulus and Flexural strength were evaluated in accordance to ASTM D792 using an universal testing machine (Model 5969, Instron Engineering Corporation, USA). The testing was carried out with a crosshead speed of 5 mm/min. Rheological properties was determined using a rotational rheometer (ARES-G2, TA Instruments, USA). The testing condition was performed in a frequency sweep mode (0.01-100 rad/s) at 180°C with a strain of 80%.

3. Results and Discussion

3.1 Differential scanning calorimetry (DSC)

Thermal properties from DSC studies are presented in Table 1. Typically, shifting of glass transition temperature (T_g) is used to determine compatibility between polymer matrix and additive or fillers. In this study, shifting of T_g was slightly changed to indicate interaction between PLA molecules and silane treated alumina particles. In cooling step, crystallization temperatures (T_c) were not observed in all samples. However, the cold crystalline temperatures (T_{cc}) decreased when the content of APTES treated alumina particles increased. This was attributed to silane-treated alumina acted as nucleating agents [6] during applying thermal energy above the T_g for PLA molecules to crystallize. For crystal melting temperatures (T_m), it was found that adding silane treated alumina did not alter T_m in both the first and second heating scans. This indicated that silane treated alumina did not affect the crystal structures of PLA although these alumina reduced the T_{cc}. The degree of crystallinity (X_c) increased with the presence of silane treated alumina. Comparing between the first and second heatings, the X_c of the second heating scan was somewhat higher. This supported the annealing effect of the PLA/alumina composites that the slower heating/cooling rate, was the higher degree of crystallinity could be obtained. Therefore, the printing condition that favors annealing of the composite material would provide higher rigidity due to higher degree of crystallinity.

3.2 Rheological properties by rotational rheometer

Figure 1 shows the complex viscosity of neat PLA and PLA/alumina composites tested at 180°C. It was found that all samples showed Newtonian behaviour at the frequency lower than 10 rad/s, then the shear-thinning behaviour (non-Newtonian) was present for all materials. At high frequency, filler content did not affect on complex viscosities which they were in the closed values. At low frequency, adding silane-treated alumina impacted on complex viscosities significantly. Hassanabadi *et al.* [7] suggested that from a morphological point of view, percolation was the concentration that due to an increase of filler concentration, particles started to interconnect and form a network structure.

Only PLA composite adding silane-treated alumina of 10 wt% had significantly higher complex viscosity than neat PLA, while the others had lower complex viscosities. Moreover, the onset of non-Newtonian behaviour in the PLA/alumina 10 wt% occurred at lower frequency than the rest of them. This could be attributed that APTES treated alumina of 10 wt% was the percolation concentration that alumina particles (particle size of 100 μm) could form effective particle-particle interaction which required high shear stress for mobility of PLA molecules. However, such networks were broken down when increasing alumina content higher than 10 wt%.

The Fused Deposition Modeling (FDM) is the machine that will be used to fabricate these composite filaments into products by 3D-printing technique. The opening diameter and the length of the printing head is 4 mm and 8 mm, respectively. The printing speed could be varied in the range of 30-50 mm/s, which gives the volumetric flow rate (\dot{Q}) (cross-sectional area times speed) to be 377-628 mm³/s.

From the relationship between volumetric flow rate (\dot{Q}) and shear rate ($\dot{\gamma}$) in pipe, $\dot{\gamma} = 4\dot{Q}/(\pi R^3)$, the calculated shear rate would be about 60-100 s⁻¹. Therefore, the fabrication of PLA/alumina filament using this machine will be in the shear thinning region. The higher printing speed is the lower complex viscosity of the composite. However, the alumina content would rarely affect on complex viscosity.

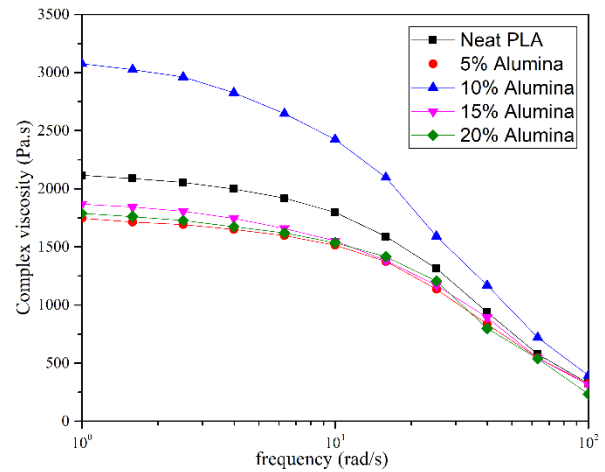


Figure 1. Complex viscosities of neat PLA and PLA/alumina composites with different alumina content (at 180°C).

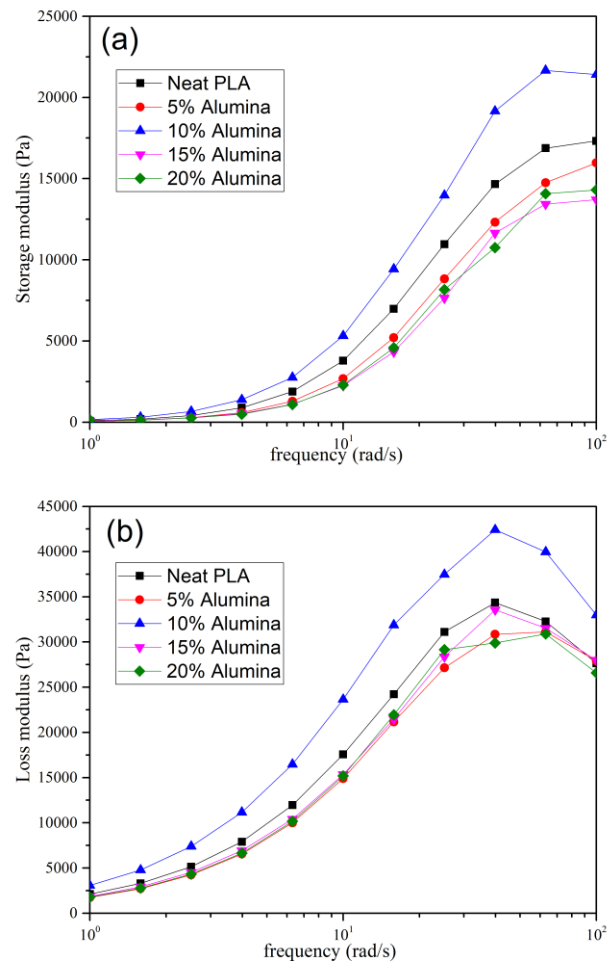


Figure 2. Storage and loss modulus of neat PLA and PLA/alumina composites with different alumina content: (a) Storage modulus (b) Loss modulus (at 180°C).

Storage and loss modulus of neat PLA and PLA/alumina composites plotted in logarithm scale were shown in Figure 2(a) and 2(b), respectively. Storage modulus represents elastic response of the materials when subjected to dynamic loading. It is seen that the composites were solid-like at high frequency, which the PLA/alumina 10 wt% had the highest storage modulus. Typically, peaks of loss modulus could be used to indicate compatibility between polymer matrix and fillers. Similarly to shifting of T_g in the DSC results, the peaks of loss modulus did not differ significantly.

3.3 Flexural properties of injection molded specimens

In order to study effect of alumina content on mechanical properties of the PLA/alumina composites, composite compounds were injection molded into specimens and tested in accordance to ASTM-D790. Flexural modulus and flexural strength for neat PLA and PLA/alumina composites with different alumina content are shown in Figure 3(a) and 3(b), respectively.

It was found that flexural modulus increased when silane-treated alumina content higher than 10 wt%. This was in agreement with the study by Kasuga *et al.* [8] that the modulus of elasticity of PLA composite did not increase when adding calcium carbonate of 10 wt% compared to neat PLA and increased when adding calcium carbonate more than 20 wt%. They used ^{13}NMR spectra to suggest bonding between carboxyl groups and calcium ions. Since alumina particles in this study was APTES treated, the interfacial adhesion between PLA matrix and silane treated alumina particles was expected to improve although there was slightly shifting in T_g observed in DSC results. Moreover, increasing the degree of crystallinity of PLA when adding silane treated alumina would improve rigidity of the PLA matrix.

In contrast, flexural strength was reduced with the presence of fillers [9] indicating the interfacial adhesion between PLA matrix and silane-treated alumina particles was not sufficient enough to dissipate loading energy between phases. Also, this might be attributed to dispersed alumina particles inhibited disentanglement of PLA

molecules during the extension, so that the higher filler loading reduced the flexural strength of the composites.

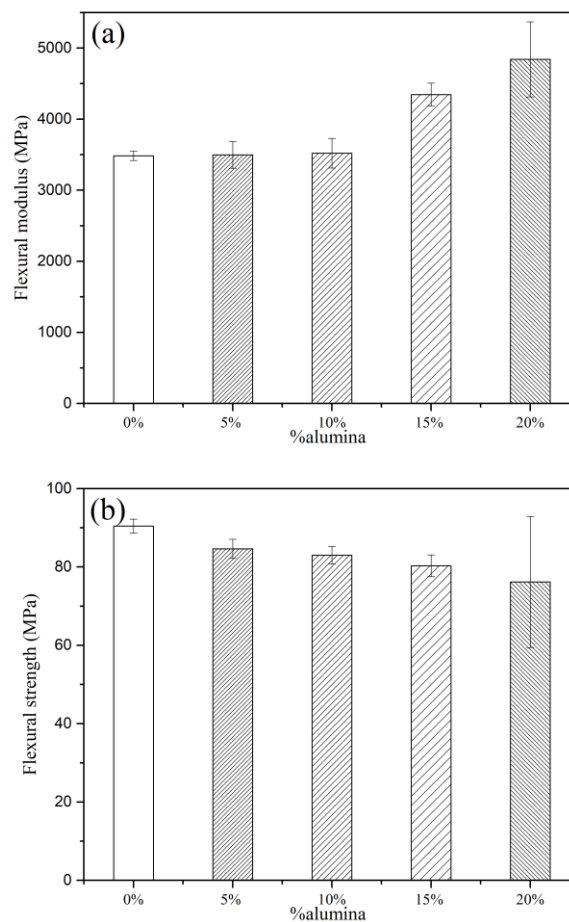


Figure 3. Flexural properties of neat PLA and PLA/alumina composites with different alumina content: (a) Flexural modulus (b) Flexural strength.

4. Conclusion

In this report, the composites between PLA and APTES treated alumina were successfully prepared with the loading between 5-20 wt%. These composites could be extruded into filaments ready for 3D-printing fabrication. From DSC results, it showed that adding silane-treated alumina did not change the T_m of PLA, and increased the degree of crystallinity due to silane treated alumina acting as nucleating agents. Rheological results indicated that the silane treated alumina of 10 wt% could be the percolation content that gave the highest complex viscosity and storage modulus. However, flexural modulus of the injection molded specimen was increased when the silane treated alumina content was more than 10 wt%. The

optimum condition for 3D-printing of these PLA/alumina composite filaments will be further studied.

References

- [1] Raghavan, R. N., *Ceramics in Dentistry* 2012.
- [2] Totu, E. E., Nechifor, A. C., Nechifor, G., Aboul-Enein, H. Y., and Cristache, C. M., "Poly(methyl methacrylate) with TiO₂ nanoparticles inclusion for stereolithographic complete denture manufacturing – the future in dental care for elderly edentulous patients?", *Journal of Dentistry*, 59: 68-77 (2017).
- [3] Tahayeri, A., Morgan, M., Fugolin, A. P., Bompolaki, D., Athirasala, A., Pfeifer, C. S., Ferracane, J. L., and Bertassoni, L. E., "3D printed versus conventionally cured provisional crown and bridge dental materials", *Dental Materials*, 34: 192-200 (2018).
- [4] Tran, T. P. T., Bénézet, J.-C., and Bergeret, A., "Rice and Einkorn wheat husks reinforced poly(lactic acid) (PLA) biocomposites: Effects of alkaline and silane surface treatments of husks", *Industrial Crops and Products*, 58: 111-124 (2014).
- [5] Xie, Y., Hill, C. A. S., Xiao, Z., Militz, H., and Mai, C., "Silane coupling agents used for natural fiber/polymer composites: A review", *Composites Part A: Applied Science and Manufacturing*, 41: 806-819 (2010).
- [6] Scaffaro, R., Lopresti, F., and Botta, L., "PLA based biocomposites reinforced with *Posidonia oceanica* leaves", *Composites Part B: Engineering*, 139: 1-11 (2018).
- [7] Hassanabadi, H. M., Wilhelm, M., and Rodrigue, D., "A rheological criterion to determine the percolation threshold in polymer nano-composites", *Rheologica Acta*, 53: 869-882 (2014).
- [8] Kasuga, T., Maeda, H., Kato, K., Nogami, M., Hata, K., and Ueda, M., "Preparation of poly(lactic acid) composites containing calcium carbonate (vaterite)", *Biomaterials*, 24: 3247-3253 (2003).
- [9] Hakimelahi, H. R., Hu, L., Rupp, B. B., and Coleman, M. R., "Synthesis and characterization of transparent alumina reinforced polycarbonate nanocomposite", *Polymer*, 51: 2494-2502 (2010).

The applicability of PMAMPC-functionalized Fe₃O₄NPs for biosensor application

Supannika Boonjammian, Thanida Trakulsujaritchok and **Piyaporn Na Nongkhai***

Department of Chemistry and Center of Excellence for Innovation in Chemistry, Faculty of Science,
Burapha University, Chonburi, 20131, Thailand

Phone +66 3810 3067, Fax +66 3839 3494, *E-Mail: piyapornn@buu.ac.th

Abstract

In this work, poly[(methacrylic acid)-*co*-(2-methacryloyloxyethyl phosphorylcholine)] (PMAMPC) was used to modify the surface of magnetite nanoparticles (Fe₃O₄NPs) with a suitable dual functionality for biosensor application. PMAMPC was easily coated on Fe₃O₄NPs surface via coordination between carboxyl group of MA unit in copolymer and Fe atom on the Fe₃O₄NPs surface. The present of PMAMPC on the surface of Fe₃O₄NPs prevented the nonspecific adsorption of protein and made them more suitable for Fe₃O₄NPs-based biosensor. The free carboxyl groups on the surface of PMAMPC-Fe₃O₄NPs were available for biotin immobilization that acted as sensing probes. The applicability of biotin immobilized PMAMPC-Fe₃O₄NPs for biospecific detection of streptavidin molecules was investigated. The biotin immobilized PMAMPC-Fe₃O₄NPs showed the specific binding with streptavidin molecules which was monitored by a simple flocculation assay. These result showed the possibility of PMAMPC-Fe₃O₄NPs for an instrument-free biosensor.

Keywords: Biosensor, Magnetite nanoparticles, Protein adsorption

1. Introduction

At present, magnetite nanoparticles (Fe₃O₄NPs), have been subjected to biosensor application [1-6]. To enhance the performance in these applications, the functionalization of the Fe₃O₄NPs' surface is particularly importance. Ideally, the functionalization should provide active functional groups for attaching active biomolecules that acted as sensing probes for biospecific detection of targeted molecules [1-4]. In addition, the resistant of nonspecific biomolecules adsorption on the Fe₃O₄NPs' surface also require for high selective and sensitive Fe₃O₄NPs-based biosensor [2-3, 7-8].

In our previous work, the novel PMPC-based copolymer, namely poly[(methacrylic acid)-*co*-(2-methacryloyloxyethyl phosphorylcholine)] (PMAMPC), was used to coat the gold sensor chip for surface plasmon resonance (SPR) technique. The carboxyl groups from the methacrylic acid units in copolymer were useful for attaching active biomolecules. On the other hand, the MPC

units were also advantageous to suppress unwanted nonspecific adsorption [7]. From these, PMAMPC-based SPR sensor provided a high detection efficiency of the targeted molecules in diluted blood plasma samples. However, this PMAMPC-based SPR sensor needs specialized equipment, an SPR instrument, for detection which is an expensive instrument.

Therefore, this research aimed to explore the applicability of Fe₃O₄NPs coated with PMAMPC (PMAMPC-Fe₃O₄NPs) for an instrument-free biosensor application. We expect that the free carboxyl groups on the surface of PMAMPC-Fe₃O₄NPs can be used for immobilization of biomolecules. From the ability to suppress the nonspecific adsorption of phosphorylcholine groups (PC) in MPC units, our biosensor should provide a high selectivity and sensitivity. We also introduced a simple and instrument-free detection assay, flocculation, for detection of target analyte which can be easily seen by naked-eye.

2. Experimental Methods

2.1 Preparation of PMAMPC-functionalized Fe₃O₄NPs

PMAMPC was used to modify the surface of Fe₃O₄NPs using the same synthetic methodology as published by our previous work [9]. Firstly, Fe₃O₄NPs were synthesized by chemical co-precipitation method. FeCl₃·6H₂O (298 mg, 1.10 mmol) and FeCl₂·4H₂O (114 mg, 0.57 mmol) were dissolved in DI water 20 mL at room temperature and added to a three-neck flask under nitrogen atmospheric condition at 60 °C. The solution was stirred at 750 rpm for 30 min before six milliliter of NH₄OH (28%w/v) was added. The black colloid solution was observed and continuously mechanical stirred for 1 h. Secondly, 0.5 mL of PMAMPC solution (80 mg/mL) was subsequently added to the continue stirred black colloid solution. The reaction was continuously stirred for 1 h and cooled down to room temperature. The black colloidal were separated by a magnet, washed with DI water several times to remove unreacted chemical and stored by suspension in water.

2.2 Protein Adsorption study

Lysozyme (Lyz) and bovine serum albumin (BSA) were used as a model protein for proteins adsorption study. Lyz or BSA was dissolved in phosphate buffered solution (PBS, 10 mM, pH 7.4). A 500 μL of proteins solution (1 mg/mL) was added to 500 μL of Fe₃O₄NPs and PMAMPC-Fe₃O₄NPs colloidal (2 mg/mL) and incubated under shaking condition at room temperature for 30 min. Then, the particles were magnetically separated. Supernatant was collected and the remaining proteins were analyzed by Bio-Rad protein assay. The amount of proteins adsorption on the Fe₃O₄NPs and PMAMPC-Fe₃O₄NPs was calculated by equation 1

$$q_e = (C_0 - C_e)V/m \quad (1)$$

Where q_e was the amount of protein adsorption (mg/g), C_0 and C_e were the protein concentrations before and after adsorption (mg/mL) respectively, V was the volume of the aqueous phase (mL), m was the weight of the nanoparticles (g).

2.3 Immobilization of biotin probe

The carboxyl groups of PMAMPC were firstly activated by mixed solution of EDC (50 mg/mL) and NHS (50 mg/mL) coupling agent. Suspended PMAMPC-Fe₃O₄NPs were added to an aqueous solution of EDC/NHS and incubated at room temperature for 30 min. The activated PMAMPC-Fe₃O₄NPs were separated from the solution by a magnet and washed with DI water three times. Then, the activated PMAMPC-Fe₃O₄NPs were resuspended in the solution of O-(2,9- aminoethyl)-O'-[2-biotinylaminoethyl]octaethylene glycol (NH₂-biotin) in DI water for overnight at room temperature. After incubation step, the nanoparticles were separated and re-suspended in DI water. The amount of biotin probe immobilization on the PMAMPC-Fe₃O₄NPs was calculated by equation 1 where q_e was the amount of biotin probe immobilization (mg/g), C_0 and C_e were the NH₂-biotin concentrations before and after immobilization (mg/mL), respectively, V was the volume of the aqueous phase (mL), and m was the weight of the nanoparticles (g).

2.4 Streptavidin detection

Flocculation assay for streptavidin (SA) detection in sample was carried out as follows: 10 μL of biotin immobilized PMAMPC-Fe₃O₄NPs dispersion (1 mg/mL) in DI water and 50 μL of aqueous solution streptavidin (0.1 mg/mL) were added into Eppendorf tube and adjusted the total volume to 100 μL. The mixture was incubated at room temperature. BSA was used instead of SA for selectivity study by using the same protocol of SA detection.

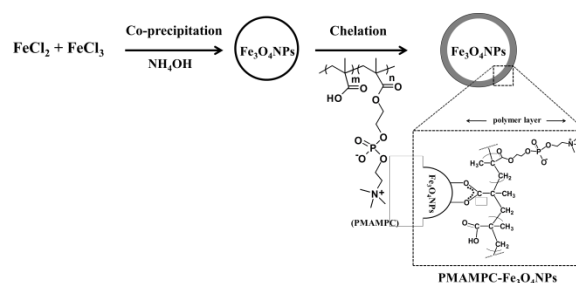


Figure 1. Scheme for the preparation of PMAMPC-Fe₃O₄NPs

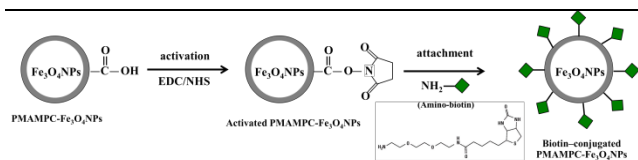


Figure 2. Scheme for the immobilization of biotin probe onto PMAMPC-Fe₃O₄NPs

3. Results and Discussion

The PMAMPC-functionalized magnetic nanoparticles (PMAMPC-Fe₃O₄NPs) were synthesized by “one-pot” reaction with two-step addition. The Fe₃O₄NPs were firstly formed by chemical co-precipitation of ferrous/ferric ions in alkaline medium and then polymer solution was directly added to Fe₃O₄NPs suspension providing a coating of polymer on Fe₃O₄NPs (Figure 1). The FT-IR spectra confirmed the success of PMAMPC anchored on the surface of Fe₃O₄NPs by chemical bonding base on chelating (Figure 3). The characteristic FT-IR peak of both Fe₃O₄NPs and PMAMPC was observed. In addition, the presence of chelating bond between carboxyl group of MA unit in copolymer and Fe atom was appeared at 1589 cm⁻¹ and 1412 cm⁻¹ which may be assigned to the symmetric and asymmetric C-O stretching of carboxylate groups, agreeing with previous report [4, 10].

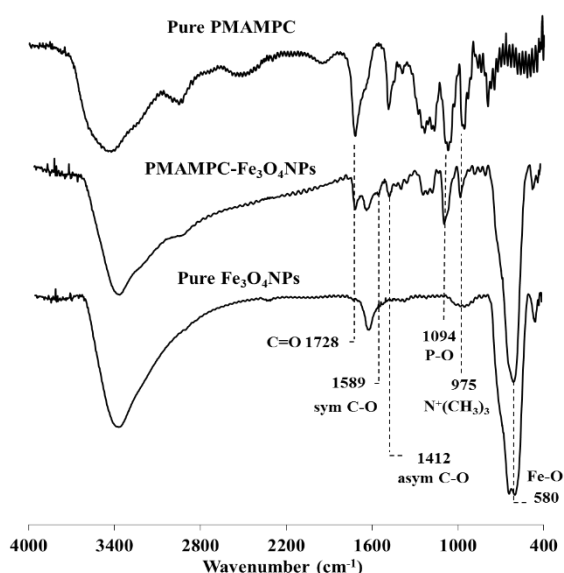


Figure 3. FT-IR spectra of pure Fe₃O₄NPs, PMAMPC-Fe₃O₄NPs, and pure PMAMPC

The morphology and particles size of pure Fe₃O₄NPs and PMAMPC-Fe₃O₄NPs were characterized by transmission electron microscopy (TEM). The TEM images of both samples showed a spherical shape and nanometer size in range of 9-15 nm (Figure 4). The optical images of colloidal NPs after dispersion in DI water for 1 h are displayed in Figure 4 (insert picture). PMAMPC-Fe₃O₄NPs provided more colloidal stability than pure Fe₃O₄NPs without any precipitation while pure Fe₃O₄NPs started to aggregate and precipitate to the bottom of vial (red arrows in Figure 4A). This result showed that the coating of hydrophilic PMAMPC improves the stability of nanoparticles.

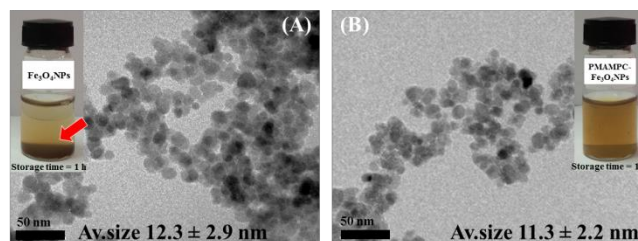


Figure 4. TEM and optical images of pure Fe₃O₄NPs (A) and PMAMPC-Fe₃O₄NPs (B)

The magnetic properties of pure Fe₃O₄NPs and PMAMPC-Fe₃O₄NPs were measured at room temperature using vibrating sample magnetometer (VSM). It could be seen in Figure 5 that the saturation magnetization of the Fe₃O₄NPs slightly decreased after PMAMPC coating.

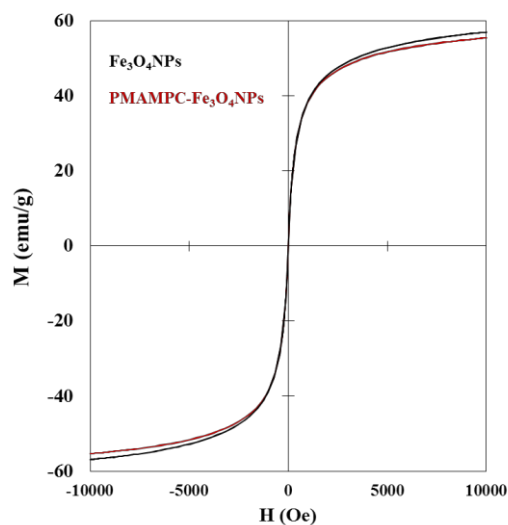


Figure 5. Magnetization curves of pure Fe₃O₄NPs and PMAMPC-Fe₃O₄NPs

In order to future apply for biosensor application, non-specific protein adsorption of PMAMPC-Fe₃O₄NPs was investigated. As expected, PMAMPC-Fe₃O₄NPs had a low proteins adsorption of both positive and negative charge protein compared with pure Fe₃O₄NPs (Figure 6). This result showed that the present of PMAMPC on the surface of Fe₃O₄NPs prevented the nonspecific adsorption of protein.

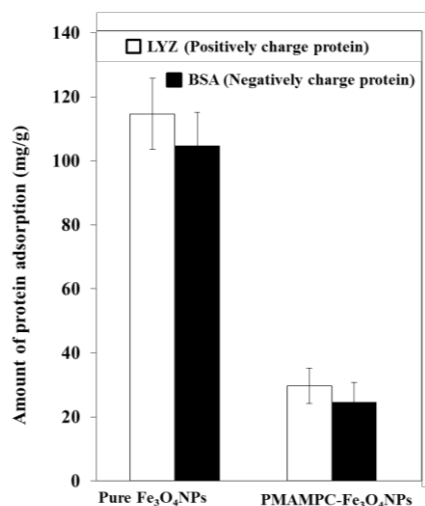


Figure 6. Protein adsorption study of pure Fe₃O₄NPs and PMAMPC-Fe₃O₄NPs

In the final part, the applicability of PMAMPC-Fe₃O₄NPs for biosensor was examined. The sensing probe was immobilized on PMAMPC-Fe₃O₄NPs via an amide bond formation between the amino group of NH₂-biotin and the carboxyl group of the MA unit in the PMAMPC (Figure 2). The UV-vis spectrum of initial NH₂-biotin solution before and after immobilization step showed in Figure 7 having the characteristic absorption peak at 290 nm. After immobilization step, the decrease of absorption peak was observed. This result demonstrated the success of biotin immobilization on PMAMPC-Fe₃O₄NPs. The amounts of immobilized biotin were calculated in term of biotin mass per nanoparticles mass, Q (mg/g) and found to be 970.22 mg/g. The immobilized biotin probe on PMAMPC-Fe₃O₄NPs was used for detecting the target molecule which is streptavidin (SA) in sample solution. The concept of flocculation assay based on the aggregation of magnetic nanoparticles induced by the interaction of immobilized biotin probe on magnetic nanoparticles and streptavidin molecules was proposed. The flocculation

phenomenon was clearly observed in case of biotin immobilized PMAMPC-Fe₃O₄NPs when SA was added (Figure 8B). The lowest detectable concentration of streptavidin was found at 50 ng/μL or 830 pM. In case of PMAMPC-Fe₃O₄NPs without biotin probe immobilization, the flocculation of nanoparticles was not observed where SA was added (Figure 8A). This result indicated that the interaction between SA and PMAMPC-Fe₃O₄NPs without sensing probe was not occurred. Moreover, the selectivity of biotin probe was also investigated by detecting BSA instead of SA in which the flocculation was not observed (Figure 8C).

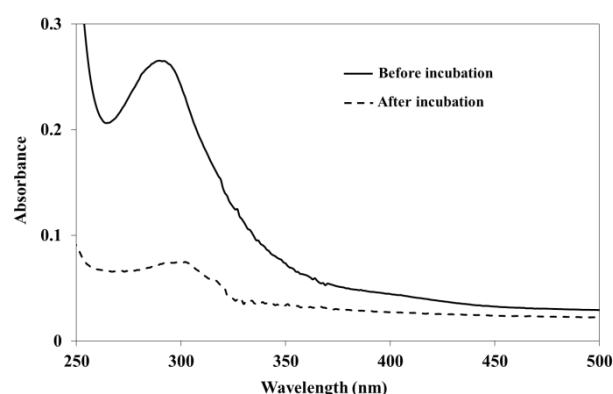
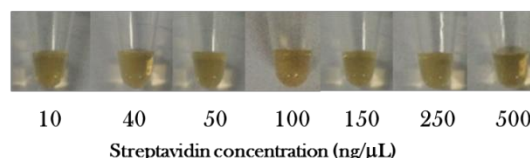
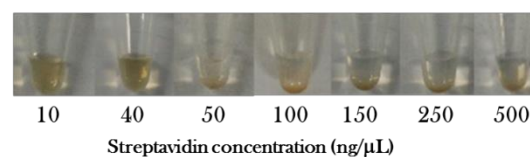


Figure 7. The UV-vis spectra of NH₂-biotin solution before and after incubation with activated PMAMPC-Fe₃O₄NPs

(A) PMAMPC-Fe₃O₄NPs + streptavidin



(B) Biotin-conjugated PMAMPC-Fe₃O₄NPs + streptavidin



(C) Biotin-conjugated PMAMPC-Fe₃O₄NPs + BSA

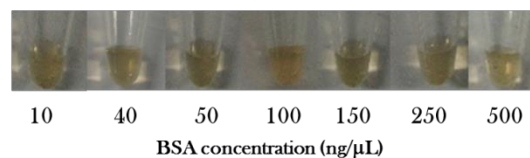


Figure 8. The photograph of (A) PMAMPC-Fe₃O₄NPs after adding SA, (B) biotin-conjugated PMAMPC-Fe₃O₄NPs after adding SA and (C) biotin-conjugated PMAMPC-Fe₃O₄NPs after adding BSA

4. Conclusion

The functionalization of Fe₃O₄NPs surface by PMAMPC coating showed an excellent colloidal stability in water media and also showed a low protein adsorption in compared with uncoated Fe₃O₄NPs. The carboxyl groups of PMAMPC-Fe₃O₄NPs are readily available for the covalent attachment of sensing probe for target molecules detection. The applicability of PMAMPC-Fe₃O₄NPs for biosensor was examined by flocculation assay in which the interaction of immobilized sensing probes on magnetic nanoparticles and target molecules induced the aggregation and flocculate out of solution. The results have demonstrated that PMAMPC-Fe₃O₄NPs are potential to use for biosensor application.

Acknowledgment

This work was financially supported by the Research Grant of Burapha University through National Research Council of Thailand (Grant no. 72/2559). Financial support from the Center of Excellence for Innovation in Chemistry (PERCH-CIC) was gratefully acknowledged.

References

[1] Yang, M., Guan, Y., Yang, Y., Xia, T., Xiong, W., Wang, N., & Guo, C., "Peroxidase-like activity of amino-functionalized magnetic nanoparticles and their applications in immunoassay". *Journal of Colloid and Interface Science*, 405, 291–295 (2013).

[2] Yan, X., Gao, L., Zhuang, J., Nie, L., Zhang, J., Zhang, Y., Gu, N., Wang, T., Feng, J., Yang, D., & Perett, S., "Intrinsic peroxidase-like activity of ferromagnetic nanoparticles". *Nature Nanotechnology*, 2, 577–583 (2007).

[3] Zhang, Z., Wang, Z., Wang, X., & Yang, X., "Magnetic nanoparticle-linked colorimetric aptasensor for the detection of thrombin". *Sensors and Actuators B*, 147, 428–433 (2010).

[4] Woo, M. -A., Kim, M., Jung, J. H., Park, H. S., Seo, T. S., & Park, H. G., "A Novel Colorimetric Immunoassay Utilizing the Peroxidase Mimicking Activity of Magnetic

Nanoparticles". *International Journal of Molecular Sciences*, 14, 9999–10014 (2012).

[5] Park, K. S., Kim, M. I., & Park, H. G., "Label-Free colorimetric detection of nucleic acids based on target-induced shielding against the peroxidase-mimicking activity of magnetic nanoparticles". *Small*, 7(11), 1521–1525 (2011).

[6] Li, X., Wen, F., Creran, B., Jeong, Y., Zhang, X., & Rotello, V. M., "Colorimetric protein sensing using catalytically amplified sensor arrays". *Small*, 8, 3589–3592 (2012).

[7] Akkhat, P., Kiatkamjornwong, S., Yusa, S. I., Hoven, V. P., & Iwasaki, Y., "Development of a novel antifouling platform for biosensing probe immobilization from methacryloyloxyethyl phosphorylcholine-containing copolymer brushes" *Langmuir*, 28(13), 5872–5881 (2012).

[8] Wiarachai, O., Vilaivan, T., Iwasaki, Y., & Hoven, V. P., "Clickable and Antifouling Platform of Poly [(propargyl methacrylate)-ran-(2-methacryloyloxyethyl phosphorylcholine)] for Biosensing Applications" *Langmuir*, 32(4), 1184–1194 (2016).

[9] Boonjammian, S., Trakulsujaritchok, T., & Na Nongkhai, P., "Preparation and characterization of PMAMPC-functionalized MNPs by one-pot reaction" *International Polymer Conference of Thailand*. 6, 425–429 (2016).

[10] Wang, G., Zhang, X., Skallberg, A., Liu, Y., Hu, Z., Mei, X., & Uvdal, K., "One-step synthesis of water-dispersible ultra-small Fe₃O₄ nanoparticles as contrast agents for T1 and T2 magnetic resonance imaging" *Nanoscale*, 6, 2953–2963 (2014).

Improvement in Mechanical Property of Hydroxyapatite Reinforced Chitosan/Collagen Scaffolds for Bone Tissue Engineering

Nareerat Thongtham¹, Suwimon Boonrungsiman², Orawan Suwanton^{1,3*}

¹School of Science, Mae Fah Luang University, Chiang Rai, 57100

²National Nanotechnology Center, National Science and Technology Development Agency, PathumThani, 12120

³Center of Chemical Innovation for Sustainability (CIS), Mae Fah Luang University, Chiang Rai 57100

Phone +6653916787, Fax +66 53916776, *E-Mail: o.suwanton@gmail.com

Abstract

The aim of this work was to improve properties of the scaffolds fabricated from biopolymer chitosan (CS) and collagen (Col). The blended CS/Col scaffold was reinforced with hydroxyapatite (HA) at different concentrations (i.e., 0, 2.5, 5 and 10%w/v). The HA/CS/Col composite scaffolds were fabricated by freeze-drying method. These composite scaffolds were characterized for their morphology, chemical structure, compressive modulus, water swelling, and weight loss behaviors. The morphology of all the composite scaffolds was three-dimensional porous structure. The HA/CS/Col composite scaffolds at 10%w/v HA showed the small porous structure and high compressive modulus when compared to the others. In addition, the addition of HA into the composite scaffolds caused the water swelling and weight loss behaviors to decrease. Thus, the addition of HA into the scaffolds could improve the physical and mechanical properties of the composite scaffolds for use in bone tissue engineering applications.

Keywords: Hydroxyapatite, Chitosan, Collagen, Composite scaffolds, Freeze-drying

1. Introduction

Bone is an important organ since bone has a number functions including protection, movement, leverage, mineral storage and a source of hematopoietic cell. The bone fracture is caused to handicapped and dies. There are many sources of bone fracture such as car accident, sports injuries and osteoporosis disease. Bone healing is the natural process. The treatment revolves around giving the bone optimum conditions to heal itself but the limitation gap must be less than 800 μm to 1 mm [1]. Therefore, it is necessary to make the implanting scaffolds that can degrade or resorb *in vivo*.

The scaffolds represent as a temporary material to promote cell growth and differentiate into the new tissue [2]. The ideal scaffold should be biodegradable, biocompatible, promote bone regeneration and mimic the characteristic properties of natural bone. Since bone is a hard tissue that is a composite between organic and inorganic matrixes [3].

Therefore, the strength of the scaffold is considered as one of a requirement of bone.

Since hydroxyapatite (HA) is a mineral that possesses an organized structure inducing the unique properties of bone such as toughness and stiffness. Thus, HA is also widely used to improve mechanical properties and bioactivities of bone scaffolds because it has biocompatibility, osteoconductivity, non-toxicity and composition significantly similar to nature bone [4]. Honssen et al. studied the mechanical properties of HA-gelatin scaffolds via solvent casting process and they found that the composite scaffolds had the maximum tensile strength of 37.13 MPa. Thus, these materials were potential candidates for tailoring bone tissue engineering [5].

Chitosan (CS) and collagen (Col) are natural polymers that have been widely used in tissue engineering. Particularly, Col is a natural extracellular matrix, which has been extensively applied to fabricate bone scaffolds owing to its biocompatibility, biodegradability, ability to

support cell attachment, proliferation, and differentiation [6]. However, the disadvantage of Col scaffolds is poor mechanical properties for load-bearing applications [7]. Therefore, the combination of Col and an inorganic component to improve mechanical properties has been considered. Kane et al. developed HA-Col scaffolds by freeze-dry technique. The results showed that the compressive modulus of these scaffolds was up to ~1 MPa and the scaffolds had high porosity of 85-90% with interconnected pore of ~300-400 μm [8]. CS is another natural polymer which is derived from N-acetyl-D-Glucosamine (acetylated unit) of chitin, expressing potential for biomedical application due to the glucosamine unit in the polymer molecules [9]. Despite, the poor stability of CS [10], CS has also been used in bone scaffolds due to its biocompatibility, suitability for cell adhesion, proliferation and antibacterial activities [11]. In order to improve stability of CS for long term system, blending with other polymers or combining with HA is proposed. Wang et al. reported that artificial bone was fabricated from Col/CS/HA using phase separation technique. As a result, the matrix was observed to be three-dimensional porous structure with pore-size of 100-200 μm [12]. Moreover, this range of pore size was appropriate for scaffold in osteoblast growth [13].

In this work, the HA/CS/Col composite scaffolds were fabricated by freeze-dry method. Various concentrations of HA (i.e., 0, 2.5, 5, and 10% w/v) were added into the scaffolds to study the physical and mechanical properties of the scaffolds. These composite scaffolds were characterized for their morphology, chemical structure, compressive modulus, water swelling, and weight loss to define the optimum formula of these scaffolds for use in bone tissue engineering.

2. Experimental Methods

2.1 Materials

All the raw materials used in this work were purchased from Sigma-Aldrich as follows: (1) Medium-molecular weight CS (75-85% deacetylated). (2) Type I Col from bovine Achilles tendon. (3) HA reagent grade.

2.2 Scaffold fabrication

1% w/v Col solution was prepared by dissolving Col in 2.5% v/v aqueous acetic solution. While, 1% w/v CS was prepared by dissolving CS in 2.5% v/v aqueous acetic solution. After that, the CS and Col solutions were mixed. The HA was added into the mixture solution with different concentrations (i.e., 0, 2.5, 5, and 10% w/v). Then, the mixture solution was crosslinked with 0.25% v/v glutaraldehyde. The solution was then homogenized by vortex mixer until the homogeneous solution was obtained. After that, the solution was transferred to mold and finally freeze-dried to fabricate the HA/CS/Col composite scaffolds.

2.3 Field- Emission scanning electron microscopy (FE-SEM)

The morphological appearance of the HA/CS/Col composite scaffolds was investigated by FE-SEM (JEOL, JSM-6301F) with operating voltage at 5 kV.

2.4 Fourier transform infrared (FTIR) spectroscopy

Pure and cross linked of Col and CS scaffolds and the HA/CS/Col composite scaffolds were analyzed using FTIR spectroscopy (Nicolet 6700, Thermo Scientific). The samples were scanned at wave number in the range from 500-4000 cm^{-1} .

2.5 The compressive modulus

The compressive modulus of the HA/CS/Col composite scaffolds was investigated by an universal testing machine (Instron Machine Model 5566) using a 1 kN. The scaffolds were compressed at the crosshead speed of 1 mm/min until the loaded cell attained 100 N. The compressive modulus was calculated in the 2-6% strain, from smaller extent in the first region of deformation that considered as an elastic region [14].

2.6 Water swelling

The water swelling behavior of the HA/CS/Col composite scaffolds were measured in phosphate buffer solution (PBS, pH 7.4) at 37 °C for 30 min, 1 h, 3 h, 3, and 5 days. The wet scaffolds after immersion in PBS (M_t)

were weighed. Later, the scaffolds were dried in an oven and weighed (M_2). The water swelling (%) was calculated according to the following equation,

$$\text{Water swelling} = \frac{M_1 - M_2}{M_1} \times 100 \% \quad (1)$$

2.7 Weight loss

The weight loss of the HA/CS/Col composite scaffolds was carried out in PBS (pH 7.4) at 37 °C for 6 h, 1 and 5 days. The weight loss was calculated according to the following equation;

$$\text{Weight loss} = \frac{M_d - M_i}{M_i} \times 100 \% \quad (2)$$

Where M_d is the weight of each sample after submersion in the buffer solution for specified time in its dry state. M_i is the initial weight of each sample.

3. Results and Discussion

3.1 Morphology

The HA/CS/Col composite scaffolds were fabricated by the freeze-drying technique. The freeze-drying technique is widely used for fabricating three-dimensional porous structures based on ice crystal formation. From Figure 1, the CS/Col (without HA) scaffolds exhibited less organized porous structure with pore size of $71.56 \pm 22.38 \mu\text{m}$ while the HA/CS/Col composite scaffolds at HA concentrations of 2.5 and 5% w/v showed more organization with larger pore size of 78.23 ± 17.30 and $78.28 \pm 33.17 \mu\text{m}$, respectively. However, the composite reinforced with 10% w/v HA exhibited smaller pore size ($50.72 \pm 26.82 \mu\text{m}$) and less organized structure when compared to the HA/CS/Col composite scaffolds reinforced with 2.5% and 5% HA. Thus, the amount of HA added into the CS/Col solution affected the porous structure of the composites. The porous scaffolds reinforced with hydroxyapatite and β -tricalcium phosphate (TCP) showed pore sizes above $80 \mu\text{m}$ that improved the bone ingrowth [15].

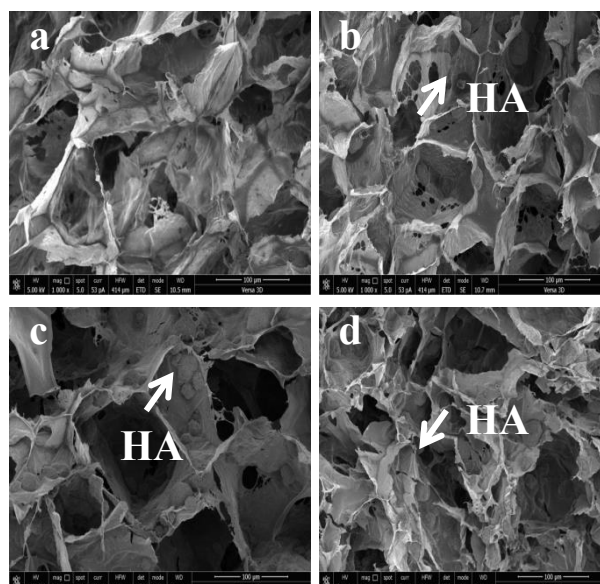


Figure 1. Morphology of the HA/CS/Col composite scaffolds at HA concentration of a) 0%, b) 2.5%, c) 5%, and d) 10% w/v

3.2 FTIR analysis

The HA/CS/Col composite scaffolds were characterized to analyze the chemical structure of CS, Col, and HA and the results are shown in Figure 2. The functional group of Col was observed at wave number of 1653 , 1558.48 and 1418.32 cm^{-1} indicating amide 1, amide 2, and amide 3, respectively. The peaks at $3600-3700 \text{ cm}^{-1}$ and $2800-2950 \text{ cm}^{-1}$ were identified as OH^- group of CS. The broad peak of PO_4^{3-} group was observed at 569 , 603.72 , 962.48 , and 1039.63 cm^{-1} suggesting the presence of HA. When compared between the pure and crosslinked of Col and CS scaffolds, the board peak of crosslinked scaffolds was shipped to lower wave number. It was identified that the structure of scaffolds was changed after crosslinking.

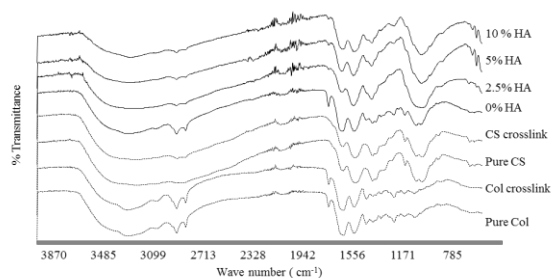


Figure 2. FTIR spectra of pure and crosslinked of Col and CS scaffolds and the HA/CS/Col composite scaffolds at different HA concentrations of 0, 2.5, 5, and 10% w/v

3.3 Compressive modulus

The compressive modulus of the HA/CS/Col composite scaffolds was tested by using a universal testing machine and the results are shown in Figure 3. The compressive modulus of the HA/CS/Col composite scaffolds at different HA concentrations of 0, 2.5, 5, and 10% w/v was 0.022 ± 0.010 , 0.029 ± 0.010 , 0.040 ± 0.010 , and 0.072 ± 0.010 MPa, respectively. From the results, the compressive modulus of the composite scaffolds increased with increasing HA content corresponding to the previous report of Calabrese et al. [16]. Thus, the addition of HA into the scaffolds improved the compressive modulus of the scaffolds.

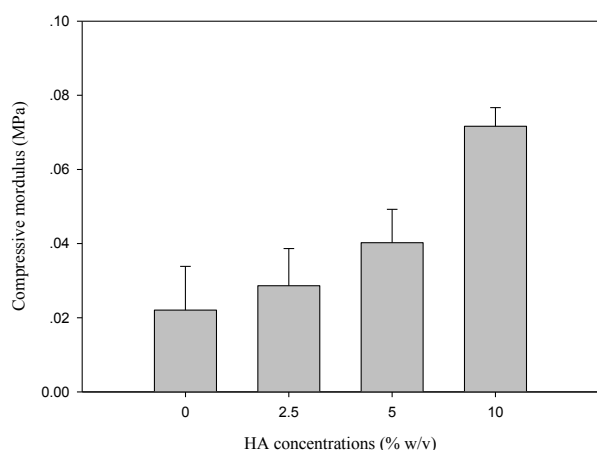


Figure 3. The compressive modulus of the HA/CS/Col composite scaffolds at different HA concentrations of 0, 2.5, 5, and 10% w/v

3.4 Water swelling

The water swelling of the HA/CS/Col composite scaffolds was determined by immersion of the scaffolds in PBS at pH of 7.4 at 37 °C and the results are shown in Figure 4. When the composite scaffolds with- and without HA were compared, the scaffolds without HA exhibited higher water swelling than the scaffolds with HA. Increasing concentration of HA resulted in a reduction of the water swelling since the higher content of HA decreased the pore size in the HA/CS/Col composite scaffolds. However, the water swelling increased with increasing submersion time, which can be observed after 30 min immersion. The water swelling of the HA/CS/Col composite scaffolds at different HA concentrations of 0, 2.5, 5, and 10% w/v was $\sim 2005\%$, $\sim 686\%$, $\sim 277\%$ and $\sim 195\%$, respectively. For longer submersion time (i.e. 5 days), the water swelling of these scaffolds increased up to $\sim 3246\%$, $\sim 1109\%$, $\sim 416\%$ and $\sim 291\%$, respectively.

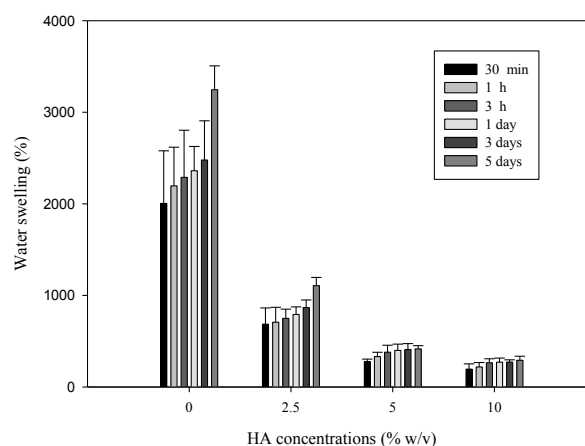


Figure 4. The water swelling of the HA/CS/Col composite scaffolds at different HA concentrations of 0, 2.5, 5, and 10% w/v

3.5 Weight loss

To examine the weight loss of the HA/CS/Col composite scaffolds, the samples were immersed in PBS at pH of 7.4 at 37 °C for 6 h, 1 day, and 5 days. From Figure 5, the weight loss of the HA/CS/Col composite scaffolds decreased with increasing HA content. However, the weight loss of these scaffolds increased with increasing submersion time. The weight loss of the HA/CS/Col

composite scaffolds at different HA concentrations of 0, 2.5, 5, and 10% w/v was ~6.79%, ~3.44%, ~2.98%, and ~2.18%, respectively. After immersion for 5 days, the value increased to ~10.71%, ~5.07%, ~2.98%, and ~2.35%, respectively. Therefore, it can be concluded that the addition of HA into the scaffolds increased the stability of the HA/CS/Col composite scaffolds.

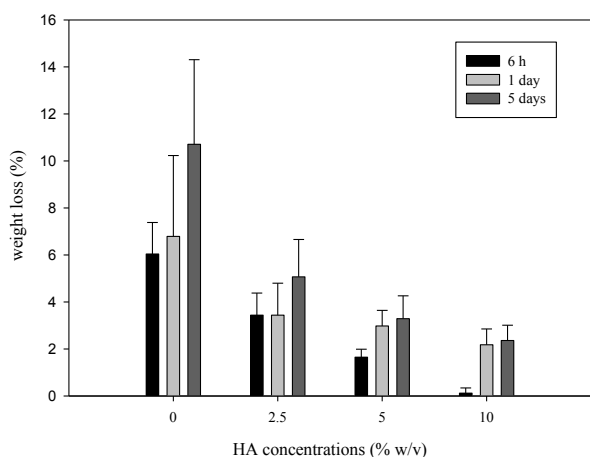


Figure 5. Weight loss of the HA/CS/Col composite scaffolds at different HA concentrations of 0, 2.5, 5, and 10% w/v

4. Conclusion

The HA/CS/Col composite scaffolds at different concentrations of HA (i.e., 0, 2.5, 5, and 10% w/v) were fabricated by freeze-drying method. The morphology of those composite scaffolds showed three dimensional porous structures but the pore size decreased with increasing HA concentration. The compressive modulus of the composite scaffolds increased with increasing HA concentration. For the water swelling and weight loss behaviors of the composite scaffolds decreased with increasing HA concentration but increased with increasing submersion time. Therefore, it can be concluded that the HA content affected the properties of the scaffolds by improving the stability and mechanical properties of the composite scaffolds to be used in long term system of bone cell culture.

Acknowledgement

The authors would like to acknowledge the Thailand Graduate Institute of Science and Technology (TGIST) under the National Science and Technology Development Agency (NSTDA), Grant No.TG-55-99-59-042M for financial support and the authors also grateful to the Nano Characterization Laboratory, National Nanotechnology Center and Scientific and Technological Instruments Center (STIC), Mae Fah Luang University.

References

- [1] Kaderly, R.E., "Primary bone healing", *Seminars in Veterinary Medicine & Surgery (Small Animal)*, 6:5-21. (1991).
- [2] Sachlos, E., Czernuszka, J. T., "Making tissue engineering scaffolds work. Review: the application of solid freeform fabrication technology to the production of tissue engineering scaffolds", *European Cells & Materials*, 5:39-40 (2003).
- [3] Boskey, A.L., Roy, R., "Cell culture systems for studies of bone and tooth mineralization", *Chemical Review*, 108:4716-4733 (2008).
- [4] Bose, S., Tarafder, S., "Calcium phosphate ceramic systems in growth factor and drug delivery for bone tissue engineering a review", *Acta Biomaterialia*, 8:1401-1421 (2012).
- [5] Hossan, M.J., Gafur, M.A., Karim, M.M., Rana, A.A., "Mechanical properties of Gelatin-Hydroxyapatite composite for bone tissue engineering", *Bangladesh Journal of Scientific and Industrial Research*, 50:15-20. (2015).
- [6] Hiraoka, Y., Kimura, Y., Ueda, H., Tabata, Y., "Fabrication and biocompatibility of collagen sponge reinforced with poly (glycolic acid) fiber", *Tissue Engineering*, 9:1101-1112 (2003).
- [7] Harley, B.A., Leung, J.H., Silva, E. C., Gibson, L.J., "Mechanical characterization of collagen-glycosaminoglycan scaffolds", *Acta Biomaterialia*, 3:463-474 (2007).

- [8] Kane, R.J., Weiss-Bilka, H.E., Meagher, M.J., Liu, Y., Gargac, J.A., Niebur, G.L., Roeder, R.K., “Hydroxyapatite reinforced collagen scaffolds with improved architecture and mechanical properties”, *Acta Biomaterialia*, 3:16-25 (2015).
- [9] Hsu, S.H., Whu, S.W., Tsai, C.L., Wu, Y.H., Chen, H.W., Hsieh, K.H., “Chitosan as scaffold materials: effects of molecular weight and degree of deacetylation”, *Journal of Polymer Research*, 11:141-147 (2004).
- [10] Szymańska, E., Winnicka, K., “Stability of chitosan—a challenge for pharmaceutical and biomedical applications”, *Marine Drugs*, 13:1819-1846 (2015).
- [11] Di Martino, A., Sittering, M., Risbud, M.V., “Chitosan: a versatile biopolymer for orthopaedic tissue-engineering”, *Biomaterials*, 26:5983-5990 (2005).
- [12] Wang, Y., Zhang, L., Hu, M., Liu, H., Wen, W., Xiao, H., Niu, Y., “Synthesis and characterization of collagen-chitosan-hydroxyapatite artificial bone matrix”, *Journal of Biomedical Materials Research Part A*, 13:244-252 (2008).
- [13] Agrawal, C., Ray, R.B., “Biodegradable polymeric scaffolds for musculoskeletal tissue engineering”, *Journal of Biomedical Materials Research Part A*, 55:141-150 (2001).
- [14] Diba, M., Kharaziha, M., Fathi, M. H., Gholipourmalekabadi, M., Samadikuchaksaraei, A., “Preparation and characterization of polycaprolactone/forsterite nanocomposite porous scaffolds designed for bone tissue regeneration”, *Composites Science and Technology*, 72:716-723 (2012).
- [15] Galois, L., Mainard, D., “Bone ingrowth into two porous ceramics with different pore sizes: an experimental study”, *Acta Orthopaedica Belgica*, 70:598-603 (2004).
- [16] Calabrese, G., Giuffrida, R., Fabbi, C., Figallo, E., Furno, D.L., Gulino, R., Memeo, L., “Collagen-hydroxyapatite scaffolds induce human adipose derived stem cells osteogenic differentiation in vitro”, *PLoS One*, 11:e0151181 (2016).

Synthesis and Characterization of Hydrogels Composed of crosslinked poly(vinyl alcohol) and *Mesona chinensis* Extract for Biomedical Use as Wound dressings.

Chadaporn Srimai^{1,2}, Runglawan Somsunan^{2*}

¹Master's Degree Program in Chemistry, Department of Chemistry, Faculty of Science, Chiang Mai University, Chiang Mai, 50200, Thailand

²Department of Chemistry, Faculty of Science, Chiang Mai University, Chiang Mai, Thailand 50200

Phone +66 5394 3341 ext. 121, Fax: +66 5389 2277, *E-mail: r.somsunan@gmail.com

Abstract

In this research, the hydrogels composed of crosslinked poly(vinyl alcohol) and *Mesona chinensis* extract were studied. The hydrogel wound dressings were prepared by dissolving the poly(vinyl alcohol) in the *Mesona chinensis* extract solution and polymerized at 70°C using glutaraldehyde as a cross-linking agent. It was found that the gel fraction of hydrogel with the *Mesona chinensis* had lower than that of the crosslinked poly(vinyl alcohol). From the mechanical properties test, it showed that adding the *Mesona chinensis* decreased the stress and increased the percentage strain of the hydrogels. The hydrogel-water interaction was also investigated by mean of the water vapour transmission rate (WVTR). The results show that WVTR of hydrogels composed of *Mesona chinensis* extract had higher WVTR than that of pure PVA hydrogel. In addition, the internal structure of the hydrogel was examined to confirm the porosity of the hydrogel by scanning electron microscopy. In conclusions, all results showed that the prepared hydrogels have a potential for wound dressing application.

Keywords: poly(vinyl alcohol); *Mesona chinensis* extract ; wound dressing ; hydrogel

1. Introduction

An ideal wound dressing should be flexible, provide a moist environment to the wound bed, absorb the excess of exudate, protect the wound from infection and exhibit good adhesion and adequate mechanical properties [1]. It also should be antimicrobial, nontoxic and biocompatible [2]. Nowadays, there are many kinds of materials for use as wound dressings currently available in world markets. Among these, hydrogels are one of the best choices to be applied for wound dressing because they are excellent materials and have all the properties required for wound dressings. These are capable of absorbing contaminated exudates and safely retaining them within the gel structure, which provides microclimate that stimulates and regulates all cellular activities and nutritional processes during the individual phases of wound healing [3]. Hydrogels can be removed from the wound without pain, risk of wound irritation, impermeable

to bacteria, thermally insulating and soft to the touch. In addition, they also allow the proper gaseous and water vapor exchange between environment and wound [4]. Poly(vinyl alcohol) (PVA) is one of the interesting candidates to prepare hydrogel for biomedical applications due to its low toxicity and good biocompatibility [5]. However, PVA hydrogel possesses insufficient elasticity, is a stiff membrane, and very limited hydrophilicity characteristics, which restricts its use alone as a wound dressing polymeric material. In the last few decades, the use of polysaccharides has increased intensively, particularly in biomedical applications. *Mesona chinensis* polysaccharide (MCP) is an anionic plant polysaccharide found in the extract of the herb *Mesona chinensis* and is widely used in Asian countries to prepare a gel dessert known as grass jelly. The main constituents isolated from *Mesona chinensis* are polysaccharides, flavonoids, terpenoids polyphenols, etc [6].

In this research, a novel hydrogel based on poly(vinyl alcohol) as a synthetic polymer and *Mesona chinensis* polysaccharide as a natural component were synthesized by thermal-initiation polymerization. The hydrogel sheets were characterized and evaluated physical properties, mechanical properties and water vapour transmission rate (WVTR).

2. Experimental Methods

2.1 Materials

PVA and potassium persulfate were supplied by BDH chemicals Ltd poole, England. The dried *Mesona chinensis* leaves and stems were received from Chonburi Province, Thailand. Glutaraldehyde was supplied by Loba Chemie Pvt. Ltd., India.

2.2 Preparation of *Mesona chinensis* extract

Dried *Mesona chinensis* leaves and stems 30 g was boiled in 400 mL of water by reflux condensation at 100°C for 4 hr. The extract solution was filtered through filter cloth. The extract was then powdered by freeze drying process. The extraction yield from *Mesona chinensis* leaves and stems was 8.52% (w/w).

2.3 Hydrogel preparation

2.3.1 Synthesis of poly(vinyl alcohol) hydrogels

PVA powder was first dissolved in distilled water and continuously stirred to form homogeneous mixture with heating at 60-70°C made up 5, 10, 15 and 20%w/v. Potassium persulfate (0.5%w/v) and glutaraldehyde (0.5%w/v) were added to PVA solution as an initiator and cross-linking agent, respectively. The polymerization began at 70°C for 6 hrs. The prepared hydrogel sheets were then removed from the mold and kept in a plastic bag.

2.3.2 Synthesis of hydrogels composed of poly(vinyl alcohol) and *Mesona chinensis* extract.

The hydrogel wound dressings were prepared by dissolving the poly(vinyl alcohol) in the *Mesona chinensis* extract solution and continuously stirred to form homogeneous mixture with heating at 60-70 °C. PVA in the final solution made up 5, 10, 15 and 20%w/v.

Potassium persulfate and glutaraldehyde 0.5%w/v were added into this solution under gentle stirring. Then, the mixed solution was poured into mold and polymerized in an oven at 70°C for 8 hrs. The hydrogel sheet was removed from mold and kept in a plastic bag.

2.4 Gel fraction

After polymerization, the hydrogel samples were freed from the mold and cut into samples of 1×1cm². The three samples of each condition were dried under vacuum at 45 °C. The weight of each sample (W_a) was recorded and then soaking it in an excess of water which replaced every day for 3 days to remove residual monomer. After purification, the swollen hydrogel samples were then dried again at 45 °C under vacuum to constant weight (W_b). The percentage gel fraction (GF) was calculated from the following equation:

$$\%GF = (W_b/W_a) \times 100 \quad (1)$$

2.5 Mechanical properties

In order to estimate the mechanical properties of hydrogel, the synthesized hydrogel sheets were cut into rectangular shapes of 1 × 7 cm². Then stress and percentage strain were measured by using a Universal Testing machine (Lloyds LRX) at a cross-head speed of 10 mm/min with a pre-load of 0.01 N, load cell of 100 N, and gauge length of 5 cm. The stress and percentage strain of each composition were investigated. At least five measurements for each sample were recorded and a mean value was calculated.

2.6 Morphology

The morphological structures of the hydrogels were studied by using LV-Scanning Electron Microscope (SEM,JSM 5910 LV) at an accelerating voltage of 15 kV. The hydrogels after swelling in water (to an equilibrium state) were freeze-dried using a freeze drier and fixed to a stub before coating with gold in a vacuum chamber, then observed and photographed.

2.7 Water vapour transmission rate

The water vapour transmission rate (WVTR) through the hydrogel were measured using the standard ASTM E96-93 water cup method. To measure WVTR, circular-shaped test specimens were cut from the hydrogel sheets with an overall diameter 7 cm. The circular-shaped hydrogel was mounted at the top of the aluminum cup contain distilled water to a level 1.9 ± 0.6 cm. from the top of specimen. The edges of the sample were sealed with paraffin wax. After that, the water cups were placed in an incubator at 35 ± 1 °C and a relative humidity of 55-60% and weighed every 1 hr for 8 hr. The WVTR was calculated from equation 2.

$$WVTR = G/tA = G/t/A \quad (2)$$

Where G represents the weight change in g, t represents time in hr., A represents the test area in m² and WVTR represents the rate of water vapour transmission in g m⁻² hr⁻¹.

3. Results and Discussion

3.1 Gel fraction

The changes of the gel fraction of PVA/ *Mesona chinensis* extract hydrogels versus the PVA content in the system are shown in Fig. 1. The gel fraction of the hydrogel with only PVA and no *Mesona chinensis* extract was about 94-96% and relatively high, suggesting that PVA was almost completely cross-linked. The results showed that adding the *Mesona chinensis* extract the gel fraction decreased to 80-84%. During thermal-initiation polymerization, the cross-linking strength of *Mesona chinensis* extract was weaker than that of PVA. Generally, as the gel fraction decreased, the strength of the gel was weakened but the flexibility was increased. Therefore, *Mesona chinensis* extract could be used to control both the strength and flexibility of hydrogel. Because it reduced the cross-linking reaction and, consequently, the gelation process [7].

3.2 Mechanical properties

To investigate the influence of *Mesona chinensis* extract on the mechanical properties of the hydrogels, their percentage strain and stress at break were evaluated as shown in Fig. 2. It showed that *Mesona chinensis* extract hardly affected the percentage strain, as seen in Fig. 2(A). However, it decreased the stress (Fig. 2(B)). This is due to, after blending *Mesona chinensis* extract with PVA, the cross-linking density of the hydrogel was decreased [8] and also polysaccharide in *Mesona chinensis* produced less stiff and more elastic hydrogels.

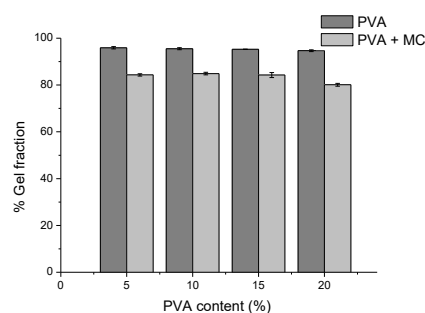
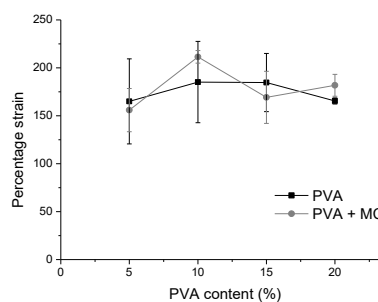
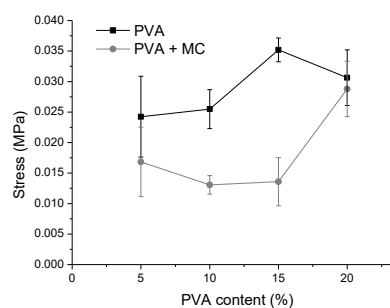


Figure 1: The gel fraction of PVA hydrogels and hydrogels composed of PVA and *Mesona chinensis* extract.



(A)



(B)

Figure 2: Percentage strain (A) and stress (B) at break of PVA hydrogels and hydrogels composed of PVA and *Mesona chinensis* extract.

3.3 Scanning Electron Microscopy

Wound dressing structures should normally be porous, which are permeable for water vapor and wound exudates. The permeability of wound exudate can prevent bullae formation. In this study, as seen in Fig. 3, the PVA hydrogel showed a network structure with holes and pores in the one with lower PVA content. For the hydrogel with higher PVA content, holes and pores on the surface were lost. Adding the *Mesona chinensis* extract, the hydrogel exhibited a more porous structure with a greater distribution of holes and pores [9]. Moreover, the average size of pores in the hydrogels composed of PVA and *Mesona chinensis* extract became increasingly large, and relatively loose network with increasing of PVA content.

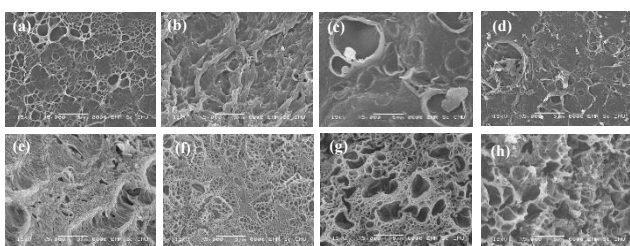


Figure 3: SEM micrographs of the surface of (a) PVA 5% (b) PVA 10% (c) PVA 15% (d) PVA 20% hydrogels and hydrogel composed of PVA and *Mesona chinensis* extract (e) PVA 5% (f) PVA 10% (g) PVA 15% and (h) PVA 20%

3.4 Water Vapour Transmission Rate (WVTR)

The WVTR of hydrogels at different interval times after crosslinked hydrogels were put into a moisture-rich environment is shown in Fig. 4. It was found that the *Mesona chinensis* extract had a significant effect on the WVTR for hydrogel composed of PVA and *Mesona chinensis* extract. This showed in a higher WVTR than pure PVA hydrogel at all compositions. From the gel fraction, when *Mesona chinensis* extract is added into hydrogel, a lower gel fraction than pure PVA hydrogel is seen. Therefore, contributing to an increase the WVTR. Moreover, the SEM micrographs showed the average size of pores in the PVA hydrogel became increasingly large, and relatively loose network when adding *Mesona chinensis* extract into hydrogel. So, the *Mesona chinensis* extract had a significant effect on the WVTR for hydrogel.

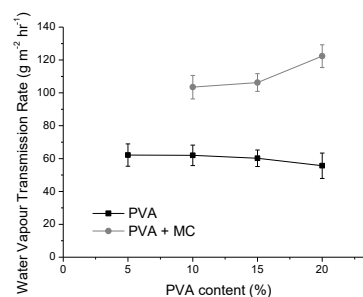


Figure 4: The water vapour transmission rate of PVA hydrogel and hydrogel composed of PVA and *Mesona chinensis* extract.

4. Conclusion

The influence of the *Mesona chinensis* extract on the properties of a PVA hydrogel was studied. All results demonstrated good correlation between the structure and the properties of hydrogel. In this study, the hydrogels composed of PVA and *Mesona chinensis* extract showed higher water vapour transmission rate than that of PVA hydrogel. Moreover, the added *Mesona chinensis* extract improved the mechanical properties of the prepared hydrogel, especially for the hydrogels with PVA 10% and 20%. The morphology of hydrogels containing *Mesona chinensis* extract showed more porosity than that of PVA hydrogels. It can be concluded that all obtain results indicate that the prepared hydrogels have a potential for wound dressing application.

Acknowledgement

The research reported in this paper was supported by the Graduate School, Chiang Mai, Thailand and Chiang Mai University. Department of Chemistry, Chiang Mai University, Chiang Mai, Thailand. The authors also wish to thank the Science Achievement Scholarship of Thailand (SAST) for financial support.

References

- [1] Pereira, R., Mendes, A. and Bártolo, P.J., Evaluating the properties of an alginate wound dressing for skin repair. *Advanced Materials Research*, 2013. 683: p. 141-144.

- [2] Wang, T., Zhu, X.K., Xue, X.T. and Wu D.Y., Hydrogel sheets of chitosan, honey and gelatin as burn wound dressings. *Carbohydrate Polymers*, 2012. 88(1): p. 75-83.
- [3] Singh, B. and Pal, L., Radiation crosslinking polymerization of sterculia polysaccharide-PVA-PVP for making hydrogel wound dressings. *International Journal of Biological Macromolecules*, 2011. 48(3): p. 501-510.
- [4] Dhivya, S., Padma, V.V., and Santhini, E., Wound dressings - a review. *Biomedicine*, 2015. 5(4): p. 24-28.
- [5] Kamoun, E.A., Chen, X., Mohy Eldin, M.S. and Kenawy, E.S., Crosslinked poly(vinyl alcohol) hydrogels for wound dressing applications: A review of remarkably blended polymers. *Arabian Journal of Chemistry*, 2015. 8(1): p. 1-14.
- [6] Coviello, T., Matricardi, P., Marianecchi, C. and Alhaique, F., Polysaccharide hydrogels for modified release formulations. *Journal of Controlled Release*, 2007. 119(1): p. 5-24.
- [7] Kim, J.O., Park, J.K., Kim, J.H., Jin, H.J., Yong, C.S., Li, D.X., et al., Development of polyvinyl alcohol-sodium alginate gel-matrix-based wound dressing system containing nitrofurazone. *International Journal of Pharmaceutics*, 2008. 359(1-2): p. 79-86.
- [8] Hwang, M.R., Kim, J.O., Lee, J.H., Kim, Y.I., Kim, J.H., Chang, S.W., et al., Gentamicin-loaded wound dressing with polyvinyl alcohol/dextran hydrogel: gel characterization and in vivo healing evaluation. *American Association of Pharmaceutical Scientists*, 2010. 11(3): p. 1092-103.
- [9] Zhang, D., Zhou, W., Wei, B., Wang, X., Tang, R., Nie, J. and Wang, J., Carboxyl-modified poly(vinyl alcohol)-crosslinked chitosan hydrogel films for potential wound dressing. *Carbohydrate Polymers*, 2015. 125: p. 189-99.

Fabrication of High Magnification Microscope Lens using Confined Sessile Drop Technique

Wisansaya Jaikandee^{1,2,3}, Sanong Ekgasit^{2,*}, Supeera Nootchanat³, Parintorn Jangtawee², Porapak Suriya¹,
Chutiparn Lertvachirapaiboon³, Kazunari Shinbo³, Keizo Kato³, Akira Baba³

¹Program in Petrochemical and Polymer Science, Faculty of Science, Chulalongkorn University, Thailand

²Sensor Research Unit, Department of Chemistry, Faculty of Science, Chulalongkorn University, Thailand

³Graduate School of Science and Technology, Niigata University, Japan

Phone +66 2218 7591, Fax +66 2218 7585 * E-mail: sanong.e@chula.ac.th*

Abstract

Polymeric lens could be an alternative with lower cost of production in order to decrease the expensive expenditure for fabrication of exceptional quality lenses, which is usually unavoidable. In this work, we present an uncomplicated method to fabricate polymeric plano-convex lens (PCL), bi-convex lens (BCL) and ball lens (BL) using high reflective optical polymer (Polydimethylsiloxane, PDMS by Dow Corning and Norland Optical adhesive 61, NOA61 by Norland Products). Confined sessile drop is a modified technique that is used for the fabrication lenses.

Keywords: Plano-convex lens, Gibb inequality condition, elastomeric optics, confined sessile drop,

1. Introduction

Nowadays, plano-convex lens (PCL) fabrication has been developed by several methods, such as replica molding [1], thermal reflow process [2], inkjet printing [3], hanging droplet[4], needle moving [5], and confined sessile drop [6] and etc. They have been widely used with the smartphones as smartphone microscopes since the smartphones play an important role in people's daily life. Smartphones also have variety features and are also the key of today's communication. Meanwhile, the fabrication methods of biconvex lens (BCL) and ball lens (BL) are not popular and very difficult to perform. Both BCL and BL were fabricated with many methods such as novel optofluidic flexible meniscus-biconvex lens system[7], photoresist[8], liquid mold[9], thermal reflow process [10] and etc. They are usually used in specific works.

In this research, we developed the fabrication method of PCL, BCL and BL for high magnification by Confined sessile drop technique. The size of liquid volume control on the lens substrate can be varied as 2.5, 3.0, 4.0, 5.0 and 6.0 mm, to adjust magnification of lenses. The polymers used to form lenses are Polydimethylsiloxane (PDMS) and Norland optical adhesive 61 (NOA61). Both polymers have good optical properties, for instance, clear

and colorless when it hardens, light can transmission more than 95%, high flexibility, high reflective index of 1.42 for PDMS and 1.56 for NOA61, suitable to fabricate polymer lenses. Fabricated NOA61 with higher magnification than PDMS lenses under the confined sessile drop technique and the use of optical polymers allows researchers to develop high quality lenses that will be used in complex applications.

2. Experimental Methods

2.1 Chemicals

Polydimethylsiloxane (PDMS, Sylgard 184) was purchased from Dow corning and Norland optical adhesive 61 (NOA61) was purchased from Norland products incorporated. All chemicals have structure and unique optical properties.

2.2 Fabrication of lens substrates

Lens substrate was prepared by transparent elastomeric PDMS (ePDMS) films with less than 0.6 mm thickness and was drill to use as a circle disk by 2.5 to 6.0 mm-diameter sizes of hollow puncher (Fig. 1A).

Fabrication starts from preparing homogeneous liquid PDMS (IPDMS) precursor by mixing PDMS base and curing agent in ratio 10:1 w/w, respectively. After mixing, the homogeneous IPDMS precursor was degassed in a vacuum desiccator removing residue of all air bubbles and solvent around 1 hr. The homogeneous IPDMS precursor was filled in the prepared acrylic molds with of 50x50 cm² and was left overnight at room temperature (~30°C) in order to cure the IPDMS into bubble-free films. The ePDMS films drilled by 2.5 to 6.0 mm-diameter sizes of hollow puncher to the circular ePDMS films (lens substrates) and kept in a dust-free desiccator until usage.

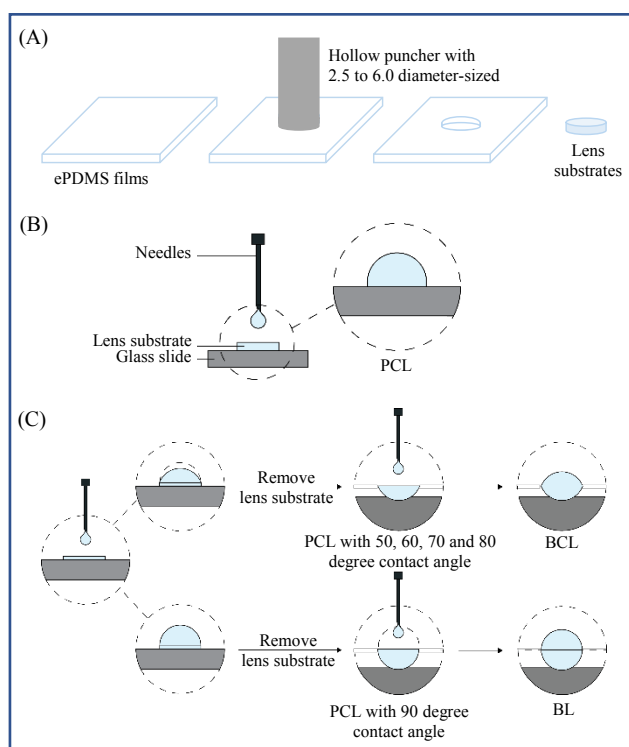


Figure 1. Fabrication process of (A) Lens substrates that using ePDMS film with the thickness of 0.6 mm and the diameter of circular lens substrates was tuned by changing the size of hollow punchers, (B) Plano-convex lenses and (C) Bi-convex lens and Ball lens.

2.3 Fabrication of Plano-convex lenses

Plano-convex lenses (PCL) fabricated using confined sessile drop technique with PDMS and NOA61. Both aliquot of polymers were dropped on 2.5 to 6.0 mm-diameter sizes lens substrates on the top cleanliness glass slide, as shown in fig 1B. The aliquot of polymers spread out to edge of lens substrates and surface tension force

assist to axisymmetrically spread into a spherical cap. The aliquot of polymers was left for 5 mins to reach equilibrium and spread into a stable spherical cap before curing by thermal curing at 60°C for 30 mins for PDMS and an 1 hour of UV curing by ultraviolet light with maximum absorption within the range of 320-380 for NOA61. The PDMS Plano-convex lenses (PDMS-PCL) and NOA61 Plano-convex lenses (NOA61-PCL) with reproducible curvature, focal length, resolution and magnification were fabricated.

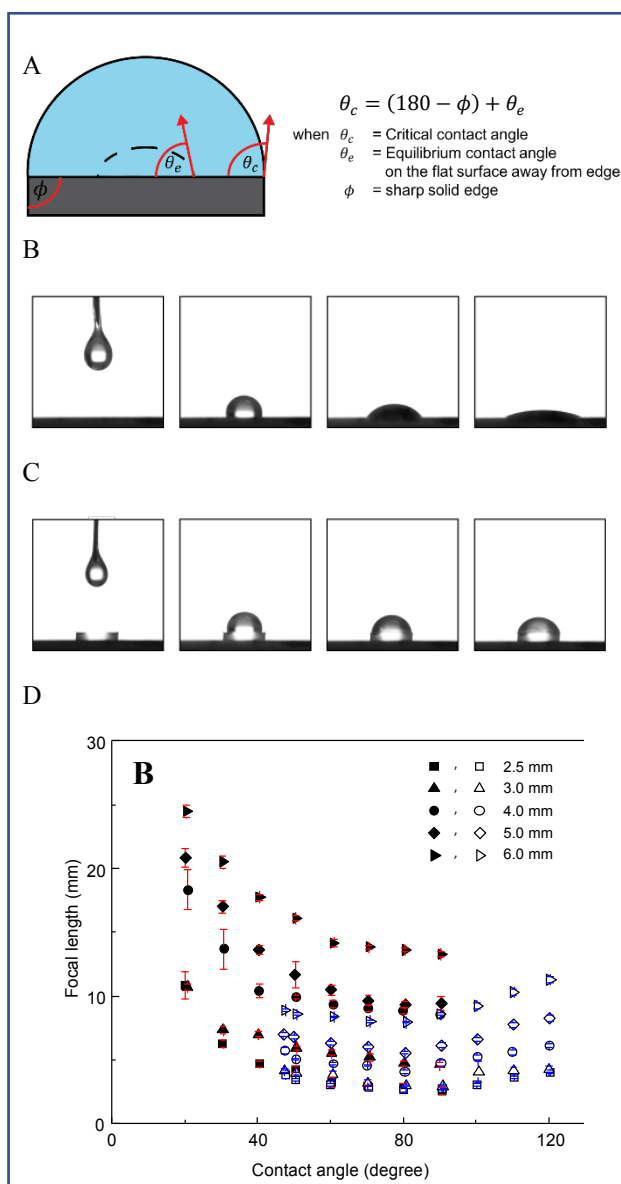


Figure 2. Schematic of (A) Gibbs's inequality condition, (B) the liquid polymers drop on flat surface without edge, (C) the liquid polymers drop on lens substrate with sharp edge and (D) a relationship between focal length and contact angle of plano-convex lenses obtained from PDMS and NOA61.

2.4 Fabrication of Bi-convex lenses and Ball lenses

Bi-convex lenses (BCL) and Ball lenses (BL) fabricated from PCL, as shown on fig 1C. The PCL with 2.5, 3.0 and 4.0 diameter sizes lens substrates that have contact angle 50, 60, 70, 80 and 90 degrees. After that PCL was turned upside down and then drop the aliquot of polymers on base of PCL.

3. Results and Discussion

3.1 Fabrication and Testing of PCL

Plano-convex lens formation with confine sessile drop technique can be formed by dropping IPDMS or INOA61 onto lens substrates. According to Gibb's inequality equation (Fig 2A.), when liquid polymers are dropping onto a flat surface without the edges (fig 2B.), it is found that polymers can disperse until the liquid polymer flatten along the surface. At the same time, the liquid polymer was dropped on the lens substrates which has angle of the edge (ϕ) 90 degrees, as shown on fig 2C. The liquid polymer dispersed to the edge and formed PCL. The critical contact angle (θ_c) of PCL will be varied according to its volume. The equilibrium contact angle (θ_e) depends on polymers. IPDMS and INOA61 have an equilibrium contact angle about 0 degrees and 47 degrees, respectively. Critical contact angle calculated from Gibb's inequality equation, will represent the possible maximum volume of the liquid polymers on lens substrate. In contrast, if the liquid polymer was added until the contact angle is more than the critical contact angle, the liquid polymer cannot control its shape on the lens substrates and spread out of the edge and cannot form PCL.

Curvature of lens is related to contact angle that is controlled by the volume of the liquid polymer dropping on the lens substrate. Therefore, the formation of PCL (PDMS-PCL and NOA61-PCL) on the same diameter-sized of lens substrate but different curvature, has different focal length.

On fig 2D shows between PDMS PCL and NOA61 have differential the relative curvature of lens on the same diameter-sized of lens substrate. In the same polymer and same diameters-size, when the curvature of the lens is low,

the focal length is low too. Any other way, when the curvature of the lens is high, the focal length is high too. However, higher curvature of NOA61-PCL show difference focal length from the PDMS PCL. The focal length of the NOA61-PCL is reduced until an equilibrium contact angle more than 90 degrees. In addition, the lens substrate with a diameter ranging from 2.5-6.0 mm (2.5, 3.0, 4.0 and 6.0) affected the focal length as well. In the same contact angle PCL formation on different diameters-size of lens substrates, both PDMS-PCL and NOA61-PCL are effected. The focal length of the PCL is less, when PCL were formed on small diameters-size lens substrates.

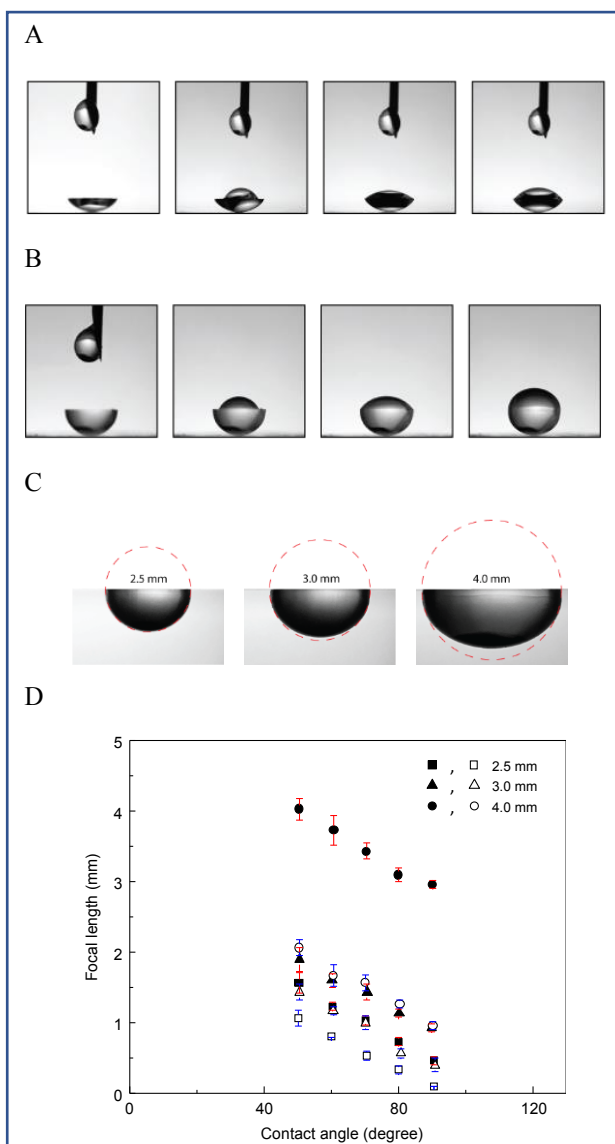


Figure 3. Optical image show the formation of (A) biconvex lens, (B) ball lens, (C) selection of hemispherical lens for ball lens fabrication and (D) a relationship between focal length and contact angle of plano-convex lenses obtained from PDMS and NOA61.

Lens maker's equation that the focal length is invert variation with reflective index of lens materials means the PDMS-PCL and NOA61-PCL have different focal length, even if they are the same condition of formation. The magnification power is calculated according to the expression: Magnification $X = 250/FL$, where FL is the focal length in mm.[6] On fig 3D, considering PDMS-PCL and NOA61-PCL that were formed on the same diameters-size of lens substrates, the PDMS-PCL have a greater focal length than the NOA61-PCL, that means the NOA61-PCL have higher magnification the PDMS PCL. The focal length of the NOA61-PCL is lower than PDMS-PCL, because NOA61 ($n = 1.56$) is a polymer with a higher refractive index than PDMS ($n = 1.42$).

3.2 Fabrication and Testing of BCL and BL

Biconvex lenses (BCL) can be formed on any base-size of the PCL. The curvature of the lens can be adjust by controlling the volume of the liquid polymer droplet. Moreover, the PCL used as the base for forming the biconvex lens that have the curvature half of the circle will be able to form the ball lens (BL) with the equilibrium contact angle at 90 degrees. Fig 4C shows that only PCL with diameter of 2.5 mm and equilibrium contact angle 90 degrees can formed BCL and BL while 3.0 and 4.0 mm diameter substrate PCL cannot, even with equilibrium contact angle 90 degrees. The relationship between the equilibrium contact angle and the focal length of BCL (PDMS-BCL and NOA61-BCL) that have the equilibrium contact angle are 50, 60, 70, 80 and 90 degrees are shown in fig 4D. The result shows that the equilibrium contact angle and the focal length is direct variation. The PDMS BCL and NOA61 BCL which forming on different the equilibrium contact angle on the same base-size of both PCL have a different focal length and can be explained from Lens's maker equation as same as PCL. The PDMS-BCL has a focal length greater than the NOA61-BCL because the refractive index of the PDMS is lower than the NOA61. In the same way, the focal length of both BCL is decreased when the equilibrium contact angle is decreased too. In addition, the 2.5-4.0 diameters-sizes of lens substrates affect the focal length as well. When both BCL

were forming the with the same equilibrium contact angle on the different diameters-size of lens substrates, both BCL that formed on a small diameter-size of lens substrate have less focal length than large diameter-size of lens substrate.

3.3 Target

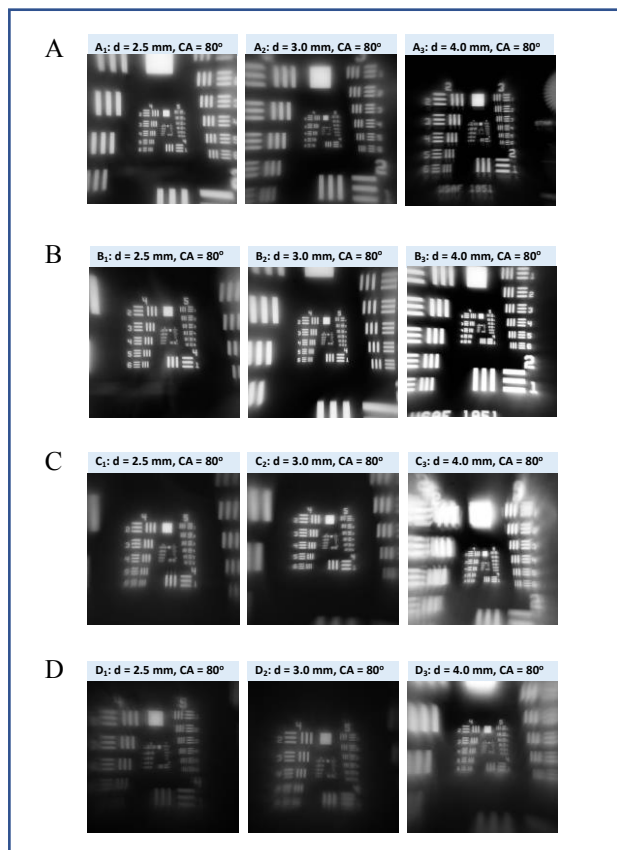


Figure 4. An image of 1951 USAF resolution test target was captured by PDMS Plano-convex lens (A_1 - A_3), NOA61 Plano-convex lens (B_1 - B_3), PDMS Bi-convex lens (C_1 - C_3), and NOA61 Bi-convex lens (D_1 - D_3) comparing the lenses by 2 polymers (PDMS, NOA61) that was forming

The optical resolution of fabricated lenses such as PDMS-PCL (fig 4A), PDMS-BCL (fig 4B), NOA61-PCL (fig 4C), NOA61-BCL (fig 4D) and NOA61-BL (fig 4F), was tested by attach fabrication lenses on smartphone camera (iPhone7, Apple Inc.) and took a photograph of 1951 USAF Resolution Target (Combined Resolution and Distortion Test Targets, 18 mm x 18 mm, Thorlabs, Inc.). The flash light of iPod (iPod touch , Apple Inc.) was used as light source with wax paper to diffuse light under 1951

USAF Resolution Target state and use NOIR mode effect in iPhone to take photograph as transmission mode of optical microscopy. After that, the resolution of the fabricated was measured lenses with plot profile mode of ImageJ program. In the group 4 element 2, PDMS-PCL have lower resolution than the NOA61-PCL. In addition, PDMS-PCL and NOA61-PCL that formed on the small diameter-size of lens substrate have higher resolution.

4. Conclusion

The uncomplicated, rapid, low cost, size and shape controllable lens fabricating method was presented. PCL, BCL and BL can be fabricated by confined sessile drop technique. In addition, the BLC and can be fabricated on base of PCL which provide the magnification as high as 250x.

Acknowledgement

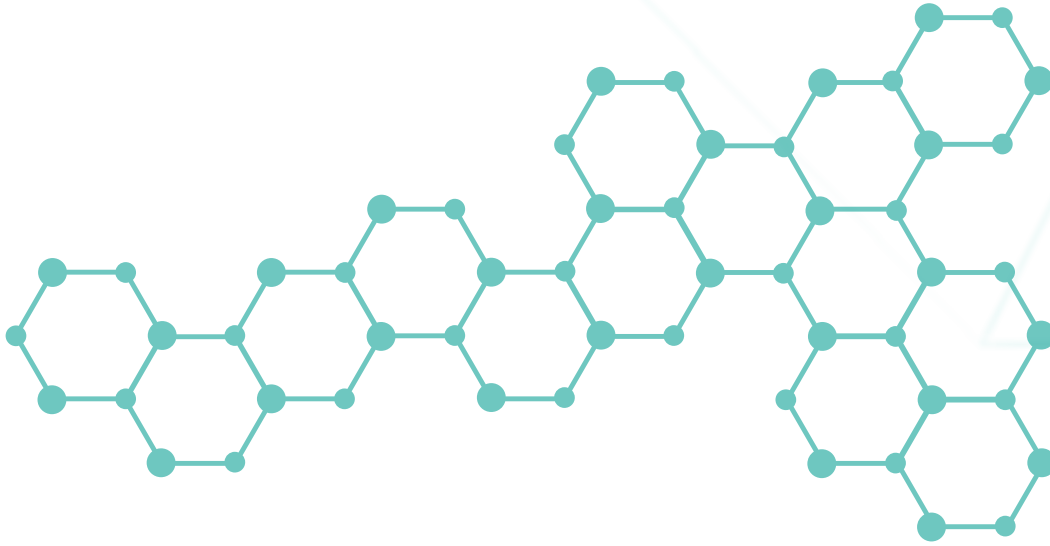
This research was supported by the Development and Promotion of Science and Technology Talents (DPST) Project Thailand, Sensor research unit (SRU) Chulalongkorn University, Thailand and Graduate school of Science and Technology, Niigata University, Japan.

References

- [1] Shih, T.-K.; Chen, C.-F.; Ho, J.-R.; Chuang, F.-T., Fabrication of PDMS (polydimethylsiloxane) microlens and diffuser using replica molding. *Microelectron. Eng.* 2006, 83 (11-12), 2499-2503.
- [2] Hsieh, H. T.; Lin, V.; Hsieh, J. L.; Su, G. D. J., Design and fabrication of long focal length microlens arrays. *Opt. Commun.* 2011, 284 (21), 5225-5230.
- [3] Sung, Y. L.; Jeang, J.; Lee, C. H.; Shih, W. C., Fabricating optical lenses by inkjet printing and heat-assisted in situ curing of polydimethylsiloxane for smartphone microscopy. *J. Biomed. Opt.* 2015, 20 (4), 047005.
- [4] Fuh, Y.-K.; Lai, Z.-H., A fast processing route of aspheric polydimethylsiloxane lenses array (APLA) and optical characterization for smartphone microscopy. *Opt. Commun.* 2017, 385, 160-166.
- [5] Amarit, R.; Kopwittaya, A.; Pongsoon, P.; Jarujareet, U.; Chaitavon, K.; Porntheeraphat, S.; Sumriddetchkajorn, S.; Koanantakool, T., High-quality large-magnification polymer lens from needle moving T technique and thermal assisted moldless fabrication process. *PLoS One* 2016, 11(1), e0146414. doi:10.1371/journal.pone.0146414
- [6] Ekgasit, S.; Kaewmanee, N.; Jangtaewee, P.; Thammacharoen, C.; Donphoongpri, M., Elastomeric PDMS planoconvex lenses fabricated by a confined sessile drop technique. *ACS Appl. Mater. Interfaces.* 2016, 8 (31), 20474-20482.
- [7] Feng, G.-H. and Y.-C. Chou (2009). "Fabrication and characterization of optofluidic flexible meniscus-biconvex lens system." *Sensors and Actuators A: Physical* **156**(2): 342-349.
- [8] Shyu, R. F., et al. (2007). "Micro-ball lens array fabrication in photoresist using PTFE hydrophobic effect." *Microsystem Technologies* **13**(11): 1601-1606.
- [9] Zhu, X., et al. (2016). "Micro-ball lens structure fabrication based on drop on demand printing the liquid mold." *Applied Surface Science* **361**: 80-89.
- [10] Ren, H., et al. (2013). "A plano-convex/biconvex microlens array based on self-assembled photocurable polymer droplets." *Journal of Materials Chemistry C* **1**(44).
- [11] Chan, H. N., et al. (2017). "Point-of-care testing: applications of 3D printing." *Lab Chip* **17**(16): 2713-2739.

RUBB

RUBBERS/ELASTOMERS



Development of Styrene Butadiene Rubber (SBR) Nanocomposites Reinforced with Polyethylene Glycol (PEG) Treated nano Titanium Dioxide (TiO₂)

Kumarjyoti Roy^{1*} and Pranut Potiyaraj¹

¹ Department of Materials Science, Faculty of Science, Chulalongkorn University, Bangkok 10330

Phone +66647456004, *E-Mail: kukumarjyotiroy@gmail.com

Abstract

The present paper mainly deals with the suitable utilization of sol-gel derived nano titanium dioxide (TiO₂) to enhance the properties of styrene butadiene rubber (SBR). Surface of nano TiO₂ was modified by two surfactants namely polyethylene glycol (PEG) and polypropylene glycol (PPG). The cure, mechanical and thermal properties of SBR nanocomposites were investigated in presence of both unmodified and surface modified nano TiO₂. The result revealed that PEG treated nano TiO₂ was much more efficient to improve the resulting properties of SBR nanocomposites in comparison to unmodified nano TiO₂. Thus, the present study successfully reports the development of SBR nanocomposites reinforced with PEG treated nanoTiO₂.

Keywords: Rubber, reinforcement, mechanical properties, thermal properties.

1. Introduction

Simply, rubber nanocomposites are important in academic and industrial field of research due to its wide application range. Several research papers have been published previously associated to the application of some common nanostructure particles like carbon nano tube [1-3], nano clay [4-6], nano calcium carbonate [7-9] etc. in rubber chemistry. In most cases, the nanoparticles have been utilized as filler to improve several properties of rubber compounds [1-9]. Now, degree of dispersion of nano filler within the rubber matrix is the key parameter that determines level of improvement of rubber compounds in presence of nano filler [10]. Thus, homogeneous dispersion of nano filler is mandatory to achieve maximum level of enhancement of rubber compounds in presence of nano filler [10]. However, due to its hydrophilic nature, the nano fillers are not able to disperse uniformly within the hydrophobic rubber matrix [10-12]. As a result, surface treatment of nano fillers is necessary in order to increase its hydrophobicity.

Several studies have been reported by different researchers [12-15] based on the utilization of various surfactants like polyethylene glycol (PEG), polypropylene glycol (PPG), cetyltrimethylammonium

bromide (CTAB) etc. for modifying the surface of nanoparticles. Undoubtedly, the utilization of surfactant provides interesting route to modify the surface of nanoparticles.

Presently, styrene butadiene rubber (SBR) is the most important synthetic rubber in rubber related industry. Major part of SBR is utilized in the tire production industry. The main aim of the present article was to study the efficiency of surface treated nano TiO₂ as filler to improve desired properties of SBR nanocomposites. Thus, the present work undoubtedly delivers a new chapter on the development of rubber technology by the appropriate use of nanotechnology.

2. Experimental Methods

2.1 Materials

Styrene butadiene rubber (SBR 1502: Synthetic and Chemicals Ltd. India), zinc oxide (Merck, Germany), stearic acid (Loba Chemie, India), sulfur (Loba Chemie, India), tetrabenzylthiuramdisulfide (TBzTD) (Apollo tyre Ltd., India) were used as received. Polyethylene glycol (PEG, M_w = 400) and polypropylene glycol (PPG, M_w = 2000) were also supplied by Merck (Germany) company. Nano TiO₂ was synthesized by sol-gel method using the procedure given by Behnajady et al. [16]. Surface of

Nano TiO₂ was modified following the procedure given by Roy et al. [17].

2.2 Preparation of SBR composites

Both unmodified and surface modified nano TiO₂ filled SBR nanocomposites were prepared in a two-roll mixing mill at room temperature. The total mixing procedure was completed in 15 minutes for all nano TiO₂ filled SBR samples. During mixing the speed of the one roll was fixed at 20 rpm and that of the other at 24 rpm to obtain the friction ratio 1:1.2. Mixing composition of different SBR nanocomposites was presented in Table 1.

Table 1. The formulation of studied vulcanizates in parts per hundred parts of rubber (phr)

Formulation	Compound designation						
	M1	M2	M3	M4	M5	M6	M7
SBR	100	100	100	100	100	100	100
ZnO	5	5	5	5	5	5	5
Stearic acid	2	2	2	2	2	2	2
TBzTD	4.9	4.9	4.9	4.9	4.9	4.9	4.9
Sulfur	0.5	0.5	0.5	0.5	0.5	0.5	0.5
Untreated nano TiO ₂	-	0.5	1	1.5	2	-	-
PEG treated nano TiO ₂	-	-	-	-	-	1.5	-
PPG treated nano TiO ₂	-	-	-	-	-	-	1.5

2.3 physical measurements

The cure properties of different vulcanizates were calculated using the Monsanto Rheometer R-100 at 3 degree arc for 160 °C. The mechanical properties like modulus at 100% (M₁₀₀) elongation, tensile strength (T.S.) and elongation at break (E.B. in %) were measured according to ASTM D 412-51 T using dumbbell shaped test pieces in an Amsler (Sweden) tensile tester. Thermogravimetric analysis (TGA) of SBR vulcanizates were performed using a TA instrument (Q 5000) under nitrogen flow from 20 °C to 800 °C with a heating rate of 10 °C/min. Fourier transform infrared (FTIR) spectra of unmodified and PEG modified nano TiO₂ were measured on a Perkin-Elmer L 120-000A spectrometer.

3. Results and Discussion

3.1 Cure characteristics of SBR nanocomposites

The cure characteristics of SBR nanocomposites are elucidated in view of torque difference (R_{∞}), optimum cure time (t_{90}), scorch time (t_2) and cure rate index (CRI). The effects of both unmodified and surface modified nano TiO₂ on the cure characteristics of SBR vulcanizates are illustrated in Table 2. R_{∞} is the measure of difference between highest torque (M_H) and lowest torque (M_L). Cure study showed that there was a very small improvement in the value of R_{∞} for SBR nanocomposites containing unmodified nano TiO₂ in comparison to unfilled SBR vulcanizate. However, there was a considerable enhancement in the value of R_{∞} in presence of 1.5 phr surface modified nano TiO₂. Thus, surface modified nano TiO₂ interacts more effectively with SBR matrix than unmodified one. Again, it was observed that PEG treated nano TiO₂ interacts much better with SBR matrix as compared to PPG treated nano TiO₂. The value of R_{∞} was about 40% greater for M6 containing 1.5 phr PEG treated nano TiO₂ than M1 i.e. unfilled SBR.

Table 2. Cure and mechanical properties of SBR nanocomposites in presence of unmodified and surface modified nano TiO₂

Sample code	R_{∞} dNm	t_{90} min	CRI = $100/(t_{90}-t_2)$ min ⁻¹	M ₁₀₀ MPa	T.S. MPa	E.B. (%)
M1	30	8	16.66	0.98	1.66	350
M2	32	7.75	17.39	1.08	1.79	345
M3	34	7.5	18.18	1.10	1.86	340
M4	35.5	7.5	18.18	1.13	2.07	340
M5	34.5	7.5	18.18	1.11	2.04	340
M6	42	7	22.22	1.38	2.52	300
M7	41	7	21.05	1.22	2.24	315

There was a reduction in the value of optimum cure time (t_{90}) for SBR nanocomposites in presence of

both unmodified and surface modified nano TiO₂. Thus, both unmodified and surface modified nano TiO₂ were capable to activate the vulcanization reaction of SBR. Actually, there was a chance of generating more heat during milling of nano TiO₂ filled SBR compounds due to additional friction as compared to unfilled system. This might be responsible for the acceleration of cure process and reduction of cure time in nano TiO₂ filled SBR compounds. It was observed that unmodified nano TiO₂ was able to increase the value of CRI up to 1.5 phr loading level. Above 1.5 phr loading level, there was a reduction in the CRI value of SBR nanocomposites due to the agglomeration of nano TiO₂ [7]. Both PEG and PPG modified nano TiO₂ were much more efficient to activate cure reaction of SBR nanocomposites as compared to unmodified nano TiO₂. The CRI value was observed to improve by 22.22% and 15.79% for M6 and M7 respectively in comparison to M1 i.e. unfilled SBR.

3.2 Mechanical properties of SBR nanocomposites

Table 2 represents the effect of both unmodified and surface modified nano TiO₂ on the improvement of mechanical properties of SBR nanocomposites. As shown in Table 2, the value of M₁₀₀ increased regularly due to addition of unmodified nano TiO₂ into SBR matrix up to 1.5 phr loading level. The value of M₁₀₀ was observed to improve by 13.77% for M4 in comparison to that value of M1 i.e. unfilled SBR. Above 1.5 phr loading level, the value of M₁₀₀ decreased due to the agglomeration of TiO₂ nanoparticles within the rubber matrix [7]. Now, there was an excellent improvement in the value of M₁₀₀ for SBR nanocomposites in presence of surface modified nano TiO₂. This might be due to the enhancement of interfacial interaction between rubber matrix and nano TiO₂ after surface treatment of nano TiO₂ by PEG and PPG. But, surface capping of nano TiO₂ was much more superior in presence of PEG as compared to PPG. This might be due to the smaller size of PEG molecule in comparison to PPG molecule [12]. Thus, PEG treated nano TiO₂ was able to cause greater enhancement in the modulus value as compared to either untreated or PPG treated nano TiO₂ and the value of M₁₀₀ showed a

remarkable increase by 39.88% for M6 in comparison to M1 i.e. unfilled SBR.

At same loading level, both PEG and PPG modified nano TiO₂ were much more capable to enhance the tensile strength of SBR nanocomposites as compared to unmodified nano TiO₂. In fact, surface treated nano TiO₂ had greater hydrophobicity than unmodified one. This was the important factor in developing excellent compatibility between surface modified nano TiO₂ and hydrophobic SBR matrix. Consequently, surface modified TiO₂ nanoparticles were much more homogeneously dispersed within the SBR matrix as compared to unmodified nano TiO₂. More importantly, the tensile strength value showed a remarkable increment by 51.81% for M6 and by 34.94% for M7 in comparison to M1 i.e. unfilled SBR. However, the value of tensile strength gives general indication that PEG treated nano TiO₂ has better hydrophobic character in contrast to PPG treated nano TiO₂. The value of elongation at break remains almost unaffected for different SBR nanocomposites due to addition of unmodified nano TiO₂. But, the value of elongation at break decreased due to addition of surface modified nano TiO₂ into the SBR matrix.

3.3 Thermal properties of SBR nanocomposites

Thermogravimetric analysis (TGA) curves of various SBR vulcanizates are shown in Figure 1. TGA study indicated that rapid degradation region of SBR vulcanizates shifted higher temperature in presence of PEG treated nano TiO₂ in comparison to both untreated and PPG treated nano TiO₂. Thus, PEG treated nano TiO₂ offers greater thermal stability for SBR vulcanizates as compared to either untreated or PPG treated nano TiO₂. Differential thermogravimetric analysis (DTG) curves of various SBR vulcanizates are shown in Figure 2. DTG study was utilized to calculate the onset decomposition temperature (T_i) and the temperature at which the rate of decomposition is maximum (T_{max}). The T_i values of SBR nanocomposites were recorded at 310, 345, 319 °C for 1.5 phr loading of untreated, PEG treated and PPG treated nano TiO₂ respectively, while T_i value of unfilled SBR was 295 °C. The T_i value clearly confirmed that PEG modified nano TiO₂ was able to produce considerably

greater thermal stability for SBR nanocomposites than unmodified or PPG modified nano TiO₂. Actually, the uniform dispersion of PEG modified nano TiO₂ within the SBR matrix restricted the thermal motion of rubber chain within the network structure. This fact was responsible for the noticeably greater thermal stability of SBR nanocomposites due to addition of PEG modified nano TiO₂ into the SBR matrix.

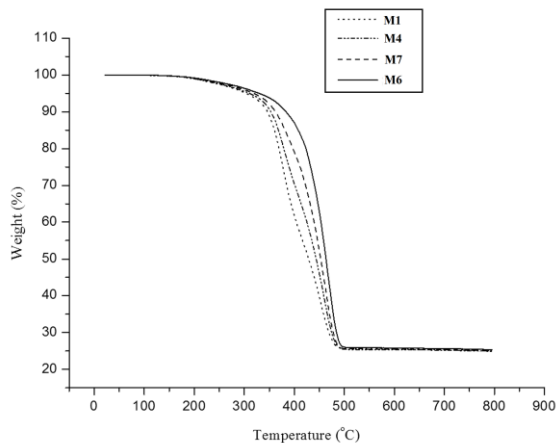


Figure 1. TGA curves of SBR vulcanizates

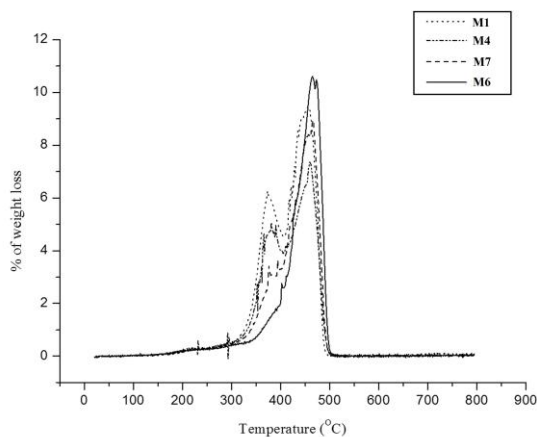


Figure 2. DTG curves of SBR vulcanizates

3.4 FTIR study

FTIR study was utilized to provide a probable mechanism of interaction between PEG and nano TiO₂. Figure 3a represents the FTIR spectra of unmodified TiO₂ nanoparticles. The peak around 2800 to 3000 cm⁻¹ indicates the stretching vibration of the C-H bond [12]. Thus, in the FTIR spectra of PEG modified nano TiO₂ (Figure 3b), the significant peak at about 2913 cm⁻¹ indicated the C-H stretching vibration in the PEG which

is present on the surface of nano TiO₂. Now, presence of surface hydroxyl group was characterized by the broad peak between 3200 cm⁻¹ to 3600 cm⁻¹ [12]. The strong peak of surface hydroxyl group was transferred towards the lower wave number region in the FTIR spectra of nano TiO₂ after surface modification with PEG. The probable mechanism of interaction between PEG and nano TiO₂ is shown in Figure 4. In a very simple way, during surface modification of TiO₂ nanoparticles by PEG, the hydrogen bonds were formed between surface hydroxyl groups of nano TiO₂ and PEG. As a result, the characteristic band of surface hydroxyl group for PEG modified nano TiO₂ was transferred towards lower wave number region [15].

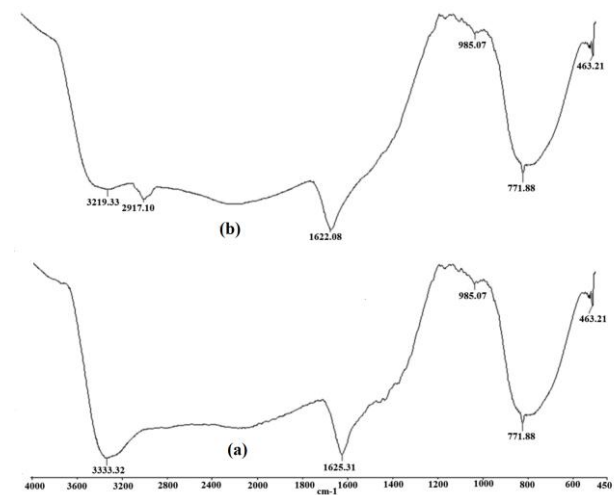


Figure 3. FTIR spectra of (a) untreated and (b) PEG treated nano TiO₂

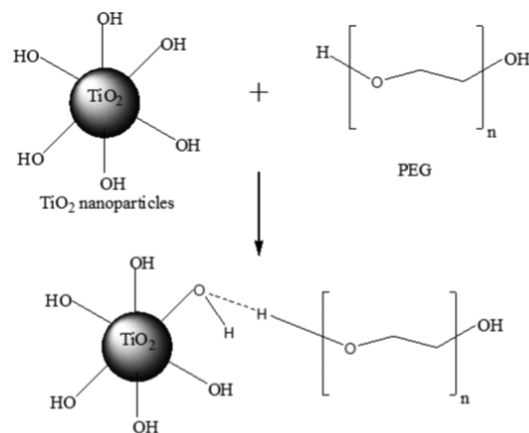


Figure 4. Probable mechanism of interaction between PEG and nano TiO₂

The characteristic band of surface hydroxyl group appeared at 3333 and 3319 cm^{-1} for untreated and PEG treated nano TiO_2 respectively.

4. Conclusion

The main goal of this work was to compare the resulting properties of SBR nanocomposites based on both unmodified and surface modified nano TiO_2 . The surface of nano TiO_2 was modified by PEG and PPG. The surface modification causes excellent improvement in the interfacial interaction between nano TiO_2 and SBR matrix. As a result, surface modified nano TiO_2 was much more effective to enhance mechanical and thermal properties of SBR nanocomposites as compared to unmodified nano TiO_2 . Out of two surface modifiers, PEG was more efficient surface modifier than PPG for TiO_2 nanoparticles. Therefore, PEG modified nano TiO_2 will be applicable in rubber industry to improve mechanical and thermal properties of SBR nanocomposites.

Acknowledgment

One of the authors, Kumarjyoti Roy would like to thank postdoctoral fellowship supported by Ratchadaphiseksomphot Endowment Fund, Chulalongkorn University for fellowship assistance.

References

- [1] Kueseng, P., Sae-oui, P., Sirisinha, C., Jacob, K. I. and Rattanasom, N., "Anisotropic studies of multi-wall carbon nanotube (MWCNT) filled natural rubber (NR) and nitrile rubber (NBR) blends", *Polymer Testing*, 32, 1229–1236 (2013).
- [2] Kueseng, P., Sae-oui, P. and Rattanasom, N., "Mechanical and electrical properties of natural rubber and nitrile rubber blends filled with multi-wall carbon nanotube: Effect of preparation methods", *Polymer Testing*, 32, 731–738 (2013).
- [3] Cadambi, R. M. and Ghassemieh, E., "Optimized Process for the Inclusion of Carbon Nanotubes in Elastomers with Improved Thermal and Mechanical Properties", *Journal of Applied Polymer Science*, 124, 4993–5001 (2012).
- [4] Sookyung, U., Nakason, C., Thaijaroen, W. and Vennemann, N., "Influence of modifying agents of organoclay on properties of nanocomposites based on natural rubber", *Polymer Testing*, 33, 48–56 (2014).
- [5] Chakraborty, S., Kar, S., Dasgupta, S., Mukhopadhyay, R., Bandyopadhyay, S., Joshi, M. and Ameta, S. C., "Study of the properties of in-situ sodium activated and organomodified bentonite clay – SBR rubber nanocomposites – Part I: Characterization and rheometric properties", *Polymer Testing*, 29, 181–187 (2010).
- [6] Diez, J., Bellas, R., Ramírez, C. and Rodríguez, A., "Effect of Organoclay Reinforcement on the Curing Characteristics and Technological Properties of SBR Sulphur Vulcanizates", *Journal of Applied Polymer Science*, 118, 566–573 (2010).
- [7] Balachandran, M. and Bhagawan, S. S., "Mechanical, Thermal, and Transport Properties of Nitrile Rubber–Nanocalcium Carbonate Composites", *Journal of Applied Polymer Science*, 126, 1983–1992 (2012).
- [8] Roy, K., Alam, M. N., Mandal, S. K. and Debnath, S. C., "Silica-coated nano calcium carbonate reinforced polychloroprene rubber nanocomposites: influence of silica coating on cure, mechanical and thermal properties", *Journal of Nanostructure in Chemistry*, 6, 15-24 (2016).
- [9] Roy, K., Alam, M. N., Mandal, S. K. and Debnath, S. C., "Effect of sol–gel modified nano calcium carbonate (CaCO_3) on the cure, mechanical and thermal properties of acrylonitrile butadiene rubber (NBR) nanocomposites", *Journal of Sol-Gel Science and Technology*, 73, 306-313 (2015).
- [10] Kim, J., Oh, T. and Lee, D., "Morphology and rheological properties of nanocomposites based on nitrile rubber and organophilic layered silicates", *Polymer International*, 52, 1203-1208 (2003).
- [11] Mishra, S., Shimpi, N. G. and Mali, A. D., "Investigation of photo-oxidative effect on morphology and degradation of mechanical and physical properties of nano CaCO_3 silicone rubber composites", *Polymers for Advanced Technologies*, 23, 236-246 (2012).

- [12] Taghvaei-Ganjali, S., Malekzadeh, M., Farahani, M., Abbasian, A. and Khosravi, M., "Effect of Surface-Modified Zinc Oxide as Cure Activator on the Properties of a Rubber Compound Based on NR/SBR", *Journal of Applied Polymer Science*, 122, 249-256 (2011).
- [13] Ma, X. K., Lee, N. H., Oh, H. J., Kim, J. W., Rhee, C. K., Park, K. S. and Kim, S. J., "Surface modification and characterization of highly dispersed silica nanoparticles by a cationic surfactant", *Colloids and Surfaces A: Physicochemical and Engineering Aspects*, 358, 172-176 (2010).
- [14] Qu, Y., Wang, W., Jing, L., Song, S., Shi, X., Xue, L. and Fu, H., "Surface modification of nanocrystalline anatase with CTAB in the acidic condition and its effects on photocatalytic activity and preferential growth of TiO₂", *Applied Surface Science*, 257, 151-156 (2010).
- [15] Sudha, M., Senthilkumar, S., Hariharan, R., Suganthi, A. and Rajarajan, M., "Synthesis, characterization and study of photocatalytic activity of surface modified ZnO nanoparticles by PEG capping", *Journal of Sol-Gel Science and Technology*, 65, 301-310 (2013).
- [16] Behnajady, M. A., Eskandarloo, H., Modirshahla, N. and Shokri, M., "Sol-Gel Low-temperature Synthesis of Stable Anatase-type TiO₂ Nanoparticles Under Different Conditions and its Photocatalytic Activity", *Photochemistry and Photobiology*, 87, 1002-1008 (2011).
- [17] Kumarjyoti Roy, Swapan Kumar Mandal, Md Najib Alam, Subhas Chandra Debnath, A comparison between polyethylene glycol (PEG) and polypropylene glycol (PPG) treatment on the properties of nano-titanium dioxide (TiO₂) based natural rubber (NR) nanocomposites, *Polymer Bulletin*, 73, 3065-3079.

Influence of Free Fatty Acid in Eco-Friendly Oil on Physical Properties of Carbon Black-Filled Styrene Butadiene Rubber and Natural Rubber Blend

Siwarote Boonrasri^{1*}, Naruemon Thongkong¹ and Pongdhorn Sae-Oui²

¹Faculty of Engineering and Agro-industry, Maejo University, Chiang Mai 50290

²MTEC, National Science and Technology Development Agency (NSTDA), Pathumthani 12120

Phone +66 5387 8123, Fax +66 5349 8902, *E-Mail: siwarote.b@maejo.mju.ac.th

Abstract

The rubber industry has used palm oil as a plasticizer. Different palm oil processes produce a variety of free fatty acid (FFA) content ranging from 2% to 30%. This research investigated the effect of FFA in palm oil on properties of rubber blend. The palm oil was mixed with 75/25 styrene-butadiene rubber and natural rubber (SBR/NR) blend, 30 phr of carbon black and the vulcanizing agents. The amount of palm oil was fixed at 20 phr while its FFA (lauric acid, oleic acid and stearic acid) content was varied from 10-30%. The physical properties of the rubber blend were then examined. The results show that increasing FFA content in palm oil decreased minimum torque and Mooney viscosity while scorch time, cure time and torque difference were increased. Due to the increase of crosslink density, hardness and tensile strength of the rubber blend were increased with increasing FFA content. The vulcanizate properties were slightly affected by the FFA type, i.e., lauric acid gave slightly better mechanical properties than the other fatty acids.

Keywords: free fatty acid; palm oil; carbon black; rubber; properties

1. Introduction

Plasticizers are widely used in rubber to facilitate mixing of rubber and filler and also shaping of filled-rubber compounds. The commonly used plasticizers are petroleum oils of which distillate aromatic extract (DAE) oils have been widely used particularly in the tire industry [1]. However, it has been reported that DAE oils contain relatively high content of polycyclic aromatics (PCA) which have been identified or suspected as carcinogens having toxic effects on human organisms [2]. Consequently, there have been extensive interests in the uses of eco-friendly oils as possible alternative processing oils to the petroleum-based oils including soybean oil [3], rice bran oil [4, 5], linseed oil [6, 7], rubber seed oil [8, 9], castor oil [10], citrus oil [11] and palm oil [12, 13]. Additionally, Jayewardhana and co-workers [12] reported that palm oil is a better alternative plasticizer in place of petroleum based aromatic oils which have been reported as carcinogenic. In addition, palm oil has the best heat resistance ability. Ismail and co-workers [14] found that

reversion decreased with increasing palm oil fatty acid concentration, whereas fatigue life showed an increasing trend.

The present work studied the use of palm oil as a possible plasticizer to replace the toxic petroleum-based oils. However, different palm oil processes yield different levels of free fatty acid (FFA), ranging from 2% to 30%. This research investigated the effect of FFA content in palm oil on properties of carbon black filled 75:25 styrene-butadiene rubber and natural rubber (SBR/NR) blend. The viscosity, cure characteristics and mechanical properties of the rubber blend were examined.

2. Experimental Methods

2.1 Materials

NR (STR 5) used in this study was purchased from Thai Rubber Latex Corporation (Thailand) Public Co., Ltd. Stearic acid and zinc oxide were obtained from Chemmin Co., Ltd. Sulfur was supplied by Siam Chemical Public Co., Ltd. and accelerators namely 2-mercaptobenzothiazole (MBT) and tetramethylthiuram

disulfide (TMTD) was purchased from Reliance Technochem Co., Ltd. Palm oil was obtained from Morakot Industries PCL. SBR 1502, lauric acid, oleic acid and carbon black (N330) were all purchased from Lucky Four Co., Ltd.

2.2 Compound Preparation

The rubber compounds used in this study were prepared according to the formulation shown in Table 1 using a laboratory two-roll mill (Model YFTR-8, YFM) in accordance with the method described by the American Society for Testing and Materials (ASTM D 3184).

Table 1. The compound formulation used in the present study

Ingredients	Content, phr ^a
SBR 1502	75.0
STR 5	25.0
ZnO	5.0
Stearic acid	0.5
N330	30.0
MBT	1.0
TMTD	0.5
Sulphur	2.0
Palm oil ^b	20.0

^a Parts per hundred rubber (phr)

^bThe amount of palm oil was fixed at 20 phr while its FFA (lauric acid, oleic acid and stearic acid) content was varied from 10-30%.

2.3 Rubber Viscosity Testing

After mixing, Mooney viscosity was measured by using a Mooney viscometer (Mooney 2000, Gibitre) at the test temperature of 100°C.

2.4 Cure Characteristics Testing and Sample Preparation

Cure characteristics of the rubber blend compounds were determined using a moving die rheometer (MDR, UR-2010, U-can dynatex Inc.) at 150°C as per ISO 6502. The rubber compounds were vulcanized by compression molding at 150°C in an electrically-heated hydraulic press (HPC-100(D), Oomn sem-automatic moulding press) according to their optimum cure time (tc90) obtained from the MDR. The vulcanized samples were stored at room temperature for at least 24 h before testing.

2.5 Mechanical property measurements

Hardness of the 6-mm-thick specimen was measured at room temperature according to ISO 7619-1 with a Shore A durometer. At least 6 readings at different

areas were taken and the average value was reported.

Tensile properties were measured using a universal testing machine (Model 5566, Instron), in accordance with ISO 37. The dumbbell (die Type 1) for tensile tests was cut from the rubber vulcanized sheets having thickness of approximately 2 mm. The values of tensile properties were the average of 3 measurements. For swelling test, the vulcanized specimens (3 cm x 1 cm x 2 mm) were prepared, weighed using an analytical balance and, then immersed in toluene. The specimens were kept at room temperature for a few days and weighed regularly until a constant weight was observed.

3. Results and Discussion

3.1 Effect of FFA on Rubber Viscosity

Mooney viscosities of the carbon black-filled compounds containing different FFA types and contents are shown in Fig. 1. It can be seen that Mooney viscosity of the compounds is not significantly affected by the FFA type. However, the Mooney viscosity shows decrease with increasing FFA content. This may be attributed to the increasing plasticization effect of the FFA used in this study. Mooney viscosity is commonly considered as a representative of the uncured stock's elastic modulus and also provides valuable information about a compound's processability [15]. This result indicates that all types of FFA in palm oil improve the processability of the rubber compounds.

3.2 Effect of FFA on Cure Characteristics

Fig. 2 and 3 show results of scorch time (ts2) and cure time (tc90) of the carbon black-filled compounds containing different FFA types and contents. Again, cure characteristics of the carbon black-filled compounds do not appear to be significantly affected by the FFA type. However, both ts2 and tc90 tend to slightly increase with increasing FFA content. This may be due to the acidity effect of FFA which delays the build-up of torque to the levels which decide ts2 and tc90 values. This shows that FFA is similar to other well-known retarders like benzoic acid, which retard the onset of vulcanization when excessive amount is present [16].

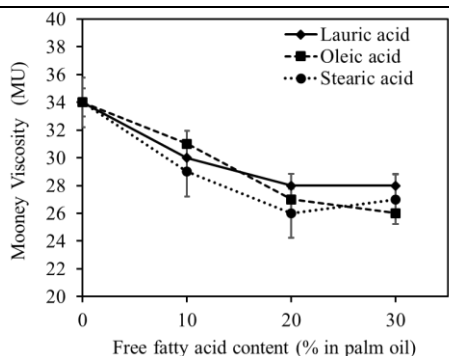


Fig. 1 Mooney viscosity of the carbon black–filled rubber compounds containing different FFA types and contents

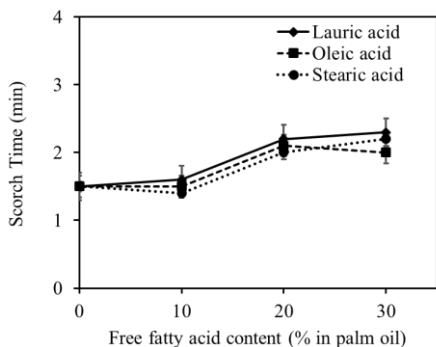


Fig. 2 Scorch time of the carbon black–filled compounds containing different FFA types and contents

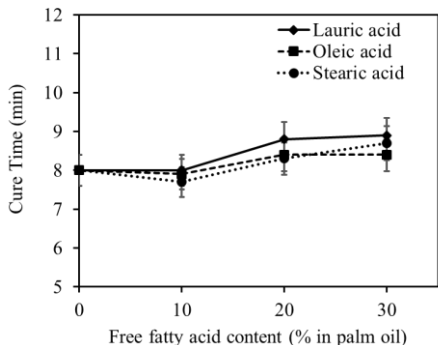


Fig. 3 Cure time of the carbon black–filled compounds containing different FFA types and contents

Minimum torque (ML) of the carbon black–filled rubber compounds containing different FFA types and contents is shown in Fig. 4. Clearly, FFA type does not significantly affect ML of the carbon black–filled compounds. However, the ML decreases with increasing FFA content. This can be attributed to the plasticization effect. The results correspond well with those obtained from Mooney viscosity as previously mentioned.

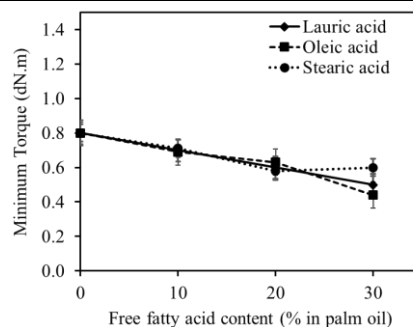


Fig. 4 Minimum torque of the carbon black–filled compounds containing different FFA types and contents

Fig. 5 shows the torque difference (Max. torque - Min. torque) of the carbon black–filled compounds containing different FFA types and contents. The results show that the torque difference of the carbon black–filled compounds depend on FFA type, i.e., lauric acid tends to provide slightly higher torque difference than other fatty acid, probably due to its saturated and small molecule. Furthermore, The number of the FFA molecules decreases with increasing the fatty acid size since the FFA content was fixed. The increment in the torque difference values indicates that an increase of FFA content causes more efficient use of sulphur leading to a higher degree of crosslinking. Barton and Hart [17, 18] reported in their previous works on MBT accelerated system that there was an increment in crosslinking with increasing fatty acid content in the rubber compounds. Higher concentration of soluble zinc stearate complex in hydrocarbon causes faster desulphuration of crosslinking and most of the crosslinking formed was mono and disulphidic. Similar observation has also been made in the carbon black–filled rubbers in which palm oil fatty acid improves torque difference [14].

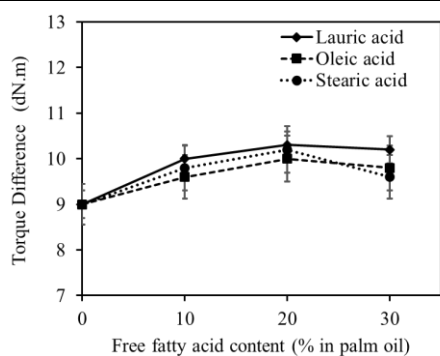


Fig. 5 Torque difference of the carbon black-filled compounds containing different FFA types and contents

3.3 Effect of FFA on Physical Properties of the Vulcanizates

Generally, swelling is inversely proportional to the crosslink density [5]. Therefore, one would expect a relationship between the torque difference value and the swelling index. Such a relationship can be observed from the results given in Fig. 5 and Fig. 6. Fig. 6 shows swelling of the carbon black-filled vulcanizates. As can be seen, the swelling results agree well with the torque difference results, i.e., lauric acid gives slightly higher crosslink density than stearic acid and oleic acid, respectively. The swelling shows decrease with increasing FFA content. The improved crosslink density can be used to explain the results.

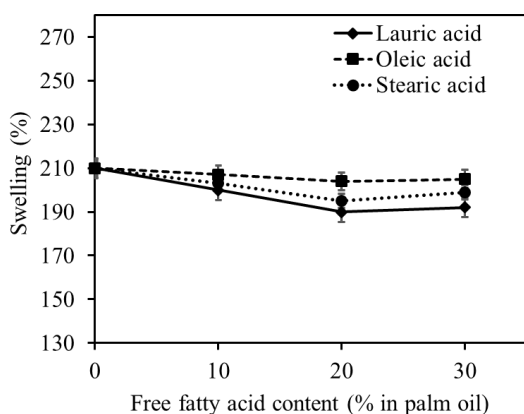


Fig. 6 Swelling of the carbon black-filled vulcanizates containing different FFA types and contents

Fig. 7 illustrates the hardness values of carbon black-filled vulcanizates containing different FFA types and contents. At any given FFA content, variations of the hardness value among the vulcanizates containing different oil types were observed. As expected, lauric acid

gives slightly higher crosslink density and, thus, hardness than other fatty acids. Due to the increase of crosslink density as previously mentioned from torque difference and swelling results, hardness tends to increase slowly with increasing FFA content.

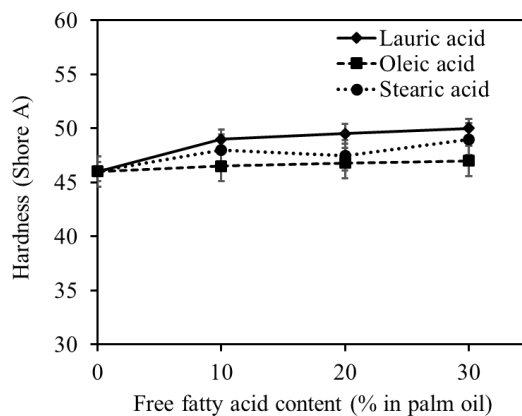


Fig. 7 Hardness of the carbon black-filled vulcanizates containing different FFA types and contents

Tensile strength of the carbon black-filled vulcanizates containing different FFA types and contents is displayed in Fig. 8. It can be observed that FFA type shows noticeable effects on tensile strength of the lauric acid system are slightly higher than those of the other fatty acid systems. In addition, the tensile strength of the rubber vulcanizate are found to increase with increasing FFA content. This can be explained by the improved crosslink density of FFA as previously mentioned.

It can be noted that the vulcanizate containing oleic acid gives the lowest tensile strength when compared at the same FFA content. This is because the oleic acid has a double bond in its molecular structure which could consume curatives in the system by reacting with sulphur as shown in Fig. 9 whereas the other FFAs do not have double bonds. It is also found that tensile strengths of the carbon black-filled vulcanizates are initially increased with increasing FFA content up to a certain point and thereafter tend to level off. Similar observation has also been reported by Barton and Hart [17,18].

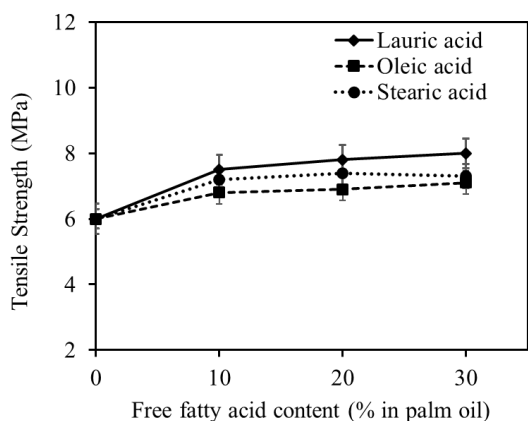


Fig. 8. Tensile strength of the carbon black-filled rubber vulcanizates containing different FFA types and contents

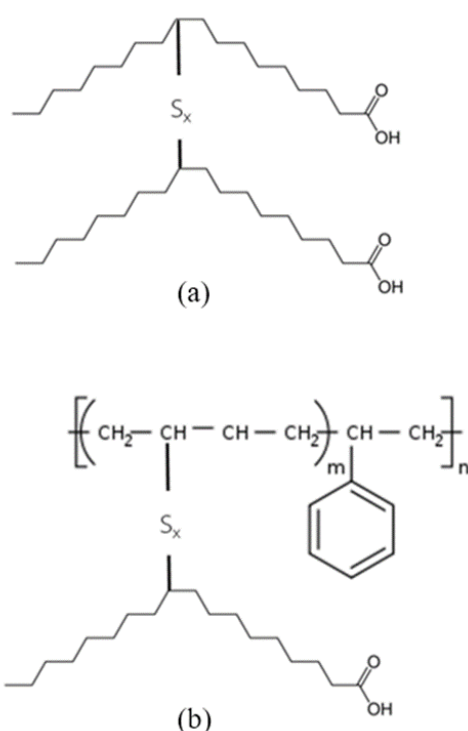


Fig. 9 Proposed crosslink reaction (a) oleic acid to oleic acid (b) oleic acid to rubber

4. Conclusion

The present study reveals that increasing FFA content in palm oil decreased minimum torque and Mooney viscosity while scorch time, cure time and torque difference were increased. Due to the increase of crosslink density, hardness and tensile strength of the rubber blend were increased with increasing FFA content. It was also found that the mechanical properties of the carbon black-filled vulcanizates depended slightly on FFA type, that is,

lauric acid gave slightly higher hardness, and tensile strength than the other fatty acids.

Acknowledgment

Financial support from Faculty of Engineering and Agro-industry Maejo University is acknowledged.

References

- [1] W. Hofmann, *Rubber technology handbook* New York, U.S.A. : Hanser Publishers, 1989.
- [2] A. Tarantini, A. Maître, E. Lefèbvre, M. Marques, A. Rajhi, and T. Douki, "Polycyclic aromatic hydrocarbons in binary mixtures modulate the efficiency of benzo[a]pyrene to form DNA adducts in human cells," *Toxicology*, vol. 279, pp. 36-44, 2011.
- [3] K. Sahakaro and A. Beraheng, "Epoxidized natural oils as the alternative safe process oils in rubber compounds," *Rubber Chemistry and Technology*, vol. 84, pp. 200-214, 2011.
- [4] A. P. Kuriakose and G. Rajendran, "Use of rice-bran oil in the compounding of styrene butadiene rubber," *Journal of Materials Science*, vol. 30, pp. 2257-2262, 1995.
- [5] A. P. Kuriakose and M. Varghese, "Use of rice bran oil and epoxidized rice bran oil in carbon black-filled natural rubber-polychloroprene blends," *Journal of Applied Polymer Science*, vol. 90, pp. 4084-4092, 2003.
- [6] S. Mishra and N. G. Shimpi, "Mechanical and flame-retarding properties of styrene-butadiene rubber filled with nano-CaCO₃ as a filler and linseed oil as an extender," *Journal of Applied Polymer Science*, vol. 98, pp. 2563-2571, 2005.
- [7] P. Raju, V. Nandan, and K. N. K. Sunil, "A study on the use of linseed oil as plasticiser in natural rubber compounds," *Journal of Rubber Research*, vol. 11, pp. 147-162, 2008.
- [8] R. Joseph, R. Alex, V. S. Vinod, C. K. Premalatha, and B. Kuriakose, "Studies on epoxidized rubber seed oil as plasticizer for acrylonitrile butadiene rubber,"

- Journal of Applied Polymer Science*, vol. 89, pp. 668-673, 2003.
- [9] V. Nandan, R. Joseph, and K. E. George, "Rubber seed oil: A multipurpose additive in NR and SBR compounds," *Journal of Applied Polymer Science*, vol. 72, pp. 487-492, 1999.
- [10] T. R. Kukreja, R. C. Chauhan, S. Choe, and P. P. Kundu, "Effect of the doses and nature of vegetable oil on carbon black/rubber interactions: Studies on castor oil and other vegetable oils," *Journal of Applied Polymer Science*, vol. 87, pp. 1574-1578, 2003.
- [11] L. Hockensmith, "Yokohama begins making eco-friendly E-Spec tire," *Rubber & Plastics News*, vol. 37, pp. 20-20, 2007.
- [12] W. G. D. Jayewardhana, G. M. Perera, D. G. Edirisinghe, and L. Karunanayake, "Study on natural oils as alternative processing aids and activators in carbon black filled natural rubber," *Journal of the National Science Foundation of Sri Lanka*, vol. 37, pp. 187-193, 2009.
- [13] G. Chandrasekara, M. K. Mahanama, D. G. Edirisinghe, and L. Karunanayake, "Epoxidized vegetable oils as processing aids and activators in carbon-black filled natural rubber compounds," *Journal of the National Science Foundation of Sri Lanka*, vol. 39, pp. 243-250, 2011.
- [14] H. Ismail and H. Anuar, "Palm oil fatty acid as an activator in carbon black filled natural rubber compounds: dynamic properties, curing characteristics, reversion and fatigue studies," *Polymer Testing*, vol. 19, pp. 349-359, 2000.
- [15] J. S. Dick, C. Harmon, and A. Vare, "Quality assurance of natural rubber using the rubber process analyzer! Presented at a meeting of the Rubber Division, American Chemical Society, Anaheim, California, 6-9 May 1997.
- [16] R. P. Dinsmore, "Stearic and Oleic Acids as Rubber-Compounding Ingredients," *Rubber Chemistry and Technology*, vol. 2, pp. 619-622, 1929.
- [17] B. C. Barton and E. J. Hart, "Variables Controlling the Cross-Linking Reactions in Rubber," *Rubber Chemistry and Technology*, vol. 26, pp. 510-521, 1953.
- [18] B. C. Barton and E. J. Hart, "Variables Controlling the Cross-Linking Reactions in Rubber," *Industrial & Engineering Chemistry*, vol. 44, pp. 2444-2448, 1952.

Study the Effects of NCO Index on Mechanical Properties of Natural Rubber -based Cationic Waterborne Polyurethane – New Approach to Water-based Adhesive Applications

Nathapong SUKHAWIPAT¹, Nitinart SAETUNG^{1*}, Anuwat SAETUNG², Jean-Francois PILARD³

and Sophie BISTAC⁴

¹Department of Materials Science and Technology, Faculty of Science,
Prince of Songkla University, Songkhla, Thailand. 90110

²Department of Rubber Technology and Polymer, Faculty of Science and Technology,
Prince of Songkla University, Pattani, Thailand. 94000

³IMMM, UMR CNRS 6283, Le Mans Université, Faculté des Sciences,
72085 Le Mans Cedex 9, France.

⁴Université de Haute Alsace, LPIM, 3 rue Alfred Werner 68093 Mulhouse, France.
Phone +66 805475881, *E-Mail: Nitinart.s@psu.ac.th

Abstract

The main purpose of this work was to investigate the isocyanate (NCO) index on mechanical properties of cationic waterborne polyurethane (cWPU) from hydroxyl telechelic natural rubber (HTNR) fixing molecular weight of HTNR about 2800 g. mol⁻¹ in case of with and without chain extender. The obtained cWPUs were stable in water with milky-blue appearance. In addition, NCO index is directly affected on dispersion stability of cWPU latex. The particle sizes of cWPUs were increased by increasing NCO index in both cases. It was increased from 59 nm to 94 nm in case of without chain extender and 76 to 193 nm in case of adding chain extender. cWPUs were well-dispersed with NCO index from 100 to 150 in case of without chain extender while with chain extender NCO index of 100 to 125 systems were well-dispersed. The shelf life was at least 6 months. NCO index is strongly affected on mechanical properties of cWPU in both cases by showing higher mechanical properties with increasing NCO index. The inversion of soft elastic to hard plastic behavior were observed. However, the addition of chain extender gives higher mechanical properties than those without. Moreover, a possibility and extension of this research work is used for adhesive application.

Keywords: hydroxyl telechelic natural rubber, waterborne polyurethane, renewable material, isocyanate index, Adhesive

1. Introduction

Cationic waterborne polyurethane (cWPU) is interesting for our group because of their intense applications. This type of WPU is now playing in a vital role of new access adhesive because many previous works had been reported that cWPU showed very high adhesion with various anionic and other ionic materials, especially glass, paper, and leather [1-3]. The other intense applications are widely used in many sectors of industrials such as automotive applications [2], fabric coating [4], novel electrolyte [5] and in a special field of gene carrier [6, 7] and also DNA transfection [8]. In this work, cWPU

is an interesting choice for advanced materials in case of water-based adhesive applications.

Ordinary, cWPUs are based on petroleum source polyols, chemicals in the class of polyether and polyester [4-6, 9-11]. These petroleum based polyols are very stress against environmentally friendly. To reduce its use, some classes of modified plant oil from natural based cWPU such as soybean oil were studied [3, 12], but there are too limited in physical and mechanical properties resulting from the low molecular weight of starting materials. Therefore, our group interested in natural rubber, renewable and green material, which can be modified *via*

reactive double bond along the molecular chain of *cis*-1,4-polyisoprene [13]. This material possesses excellent physical properties, especially high tensile and tear strength, remarkable elastic behavior, which have not yet been competed by synthetic elastomers [13, 14]. There are many works reported by our group about PU from natural rubber [15-18]. In our previous work [15], mechanical properties of synthesized cWPU were too weak while cWPUs with the good mechanical properties and strength suited to the adhesive application need.

In the recent years, many works improved the cWPU strength for applying in industrial work by providing methods such as extended polymer chain [19], grafted with melamine [20] and grafted with acrylate group [21, 22]. For the literature reviews on anionic WPU, the studies had been reported that NCO index is one of the main effects on WPU properties and its strength [18, 23]. Anionic WPU base on natural rubber had been studied and reported, but cWPU have no report yet.

Therefore, the objectives of this work were to improve cWPU mechanical strength by studying the effects of NCO index on mechanical properties of cWPU from hydroxyl telechelic natural rubber with various NCO index by studying in case of with and without chain extender condition to be used a new approach to water-based adhesive applications. Accordingly, pH values of the system, emulsion stability, emulsion particle size were investigated. The mechanical properties and surface wettability were also studied.

2. Experimental Methods

2.1 Materials

The hydroxyl telechelic natural rubber with molecular weight about $2800 \text{ g}\cdot\text{mol}^{-1}$ (HTNR2800) was synthesized through a selective degradation of natural rubber according to the procedure previously reported by our group [13]. HTNR2800 was used as a polyol in the synthesis of cWPU.

99% *N*-methyl diethanol amine (NMDEA), 98% 2,4-Toluene diisocyanates (TDI), and dibutyltindilaurate (DBTL) were purchased from Sigma-Aldrich (Germany).

95% acetic acid (CH_3COOH) and 99.5% ethylene glycol (EG) were purchased from Carlo Erba (Italy).

2.2 Preparation of cWPUs and Characterizations

cWPUs were synthesized by applying the process of our previous works [15, 16, 18]. HTNR and NMDEA were fixed at 1 mole and 2.25 mole, respectively, while TDI and EG were varied as shown in recipes **Table 1**. With controlled, about 20% TSC, HTNR2800, NMDEA and MEK were mixed in the reactor equipped with stirrer set, nitrogen inlet, condenser and thermal controller. Under the temperature of 70°C , TDI was slowly dropped into the reaction of mixture with a various amount of NCO index from 100 to 150. After the stable condition for 4 hours, EG was slowly dropped into the system for 30 minutes. For non-EG content of cWPU, the step of EG dropping was skipped. Then, the system was cooled and neutralized by acetic acid for 1 hour followed by slowly dropping deionized water with the reaction time of 30 minutes with high speed, respectively. Finally, MEK solvent was removed by rotary evaporator to obtain only well-dispersed cWPU in water medium. The structure of synthesized cWPUs were confirmed by ^1H NMR and FTIR as shown in our previous works [13, 15, 17].

cWPU dispersions were investigated. Particle size and size distribution of synthesized cWPU were characterized by Nano-ZS particle sizer (Malvern Instruments Company, UK). The stability of cWPU was studied by keeping the cWPU in the storage vial at room temperature. The appearance of dispersion was observed. Also, Total solid content (TSC) of cWPUs were collected by differential weight before and after drying. cWPU about 1 g was placed in an aluminium tray and drying in air oven under the temperature of 70°C overnight.

cWPU films were formed by casting into Teflon molds with the cavity depth of 0.3 mm. After mold casting, emulsion solution was left at room temperature for 7 days. Then emulsion solution was dried in an oven at 70°C for 24 hours. Mechanical properties of cWPU film were tested following ISO37 with die type 2. The films were characterized by using Instron machine (Model 3365). The apparatus was equipped with 100 N load cell and extensor grip included laser sensor for measuring their elongation

with crosshead speed of 100 mm.min⁻¹. Hydrophobicity and hydrophilicity were analyzed by Contact angle using Data physics apparatus (Model: OCA 15EC, input: 55W, Line voltage: 12 V DC, Fuses: 6.3 AT) with sessile drop method. Average water contact angle with individual droplet volume of 7 µl was determined in 3 separate measurements with a different position for each sample. Average oil contact angle for hydrophilicity measurement using 4- stoke motorcycle engine oil with individual droplet volume of 6 µl was determined in 3 separate measurements with a different position for each sample.

3. Results and Discussion

Table 1. cWPU recipe and the physical properties of cWPU

Code	NCO index	TSC (%)	Stability	Particle size (nm)	
				size	PDI
cWPU6	100 ^a	21.02	Stable ^c	59.8	0.14
cWPU7	100 ^b	16.67	Stable ^c	76.5	0.438
cWPU19	125 ^a	18.72	Stable ^c	83.8	0.224
cWPU20	150 ^a	19.23	Stable ^c	94.2	0.253
cWPU22	125 ^b	N/A	Stable ^c	192.7 and 36.1	0.428
cWPU23	150 ^b	17.73	Unstable	N/A	N/A

cWPU recipe (by mole): HTNR 1, NMDEA 2.25, and TDI

(various Index)

^awithout EG,

^bwith EG 1 mole

^cstable more than 6 months

This work was divided into two parts – with adding 1 mole EG and without EG formula. These cWPU showed well-dispersed with milky-blue appearance latex as shown in **Fig. 1** and shelf life is more than 6 months with the total solid content (TSC) about in range of 17 – 21%. pH values of these cWPU were approximately 4 which indicated that overdose of acetic was neutralized into the amine functional group of NMDEA for making sure that all positions were cationic.

Stabled cWPU was found in NCO index of 100 – 150 for without EG content system while with EG at 1 mole was stable in NCO index of 100 – 125. Coagulated cWPU was found in the unstable system with the increase of isocyanate index. These accessed isocyanates reacted with water in cWPU latex to form the urea hard segments and

carbon dioxide gas [18, 23, 24]. The appearance of urea would be gathered and coagulated due to insufficient emulsifier to stabilize in water. Dimensional particle sizes were increased by increasing level of NCO index. In case of non- EG, the particles size of cWPU was slightly increased from 59.8 to 83.8 and 94.2 nm by NCO index levels of 100, 125 and 150, respectively. Similarly, the particles size of cWPU with EG was increased from 76.5 to 192.7 nm by NCO index levels of 100 and 125, respectively. The particle size distribution depends on prepolymer viscosity, ionic group position, chain rigidity and soft segment structure [18]. In this work, it is because of two reasons. For large particle size, it observed in side of folded main chain of cWPU with normal reaction in synthesis process while the smaller size range might be the reaction of excess isocyanate and short chain cWPU randomly or urea form in the system [18, 23, 24]. It was related with trend of anionic WPU based on NR result that the particle size increase with increasing NCO index level [18]. Also, the reaction was run randomly to get long chain with active functional group to rise the particle size with higher NCO levels.

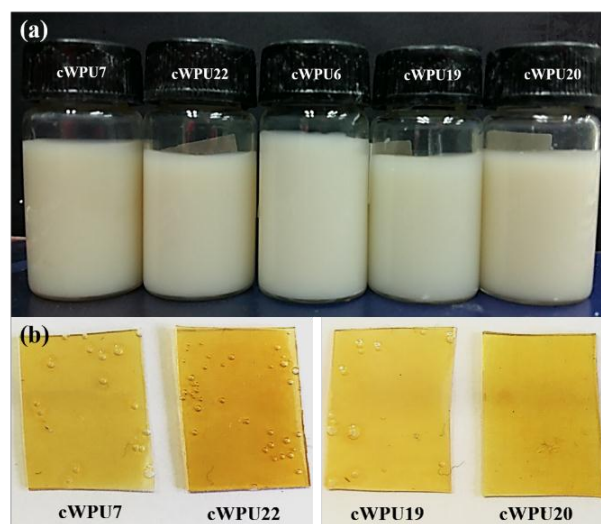


Fig. 1. Appearance of cWPU base on natural rubber with different NCO index (a) cWPU latex and (b) cWPU films

Fig. 1 compares the physical appearances of film of cWPU with a different NCO index. The samples showed that the increasing level of NCO index or adding EG effected to the strength of films. In this study, cWPU film in case of the NCO index of 100 without EG could not

formed as strength film. Also, the increasing level of NCO index change the color of films from yellow to yellowish brown due to the optical properties [25].

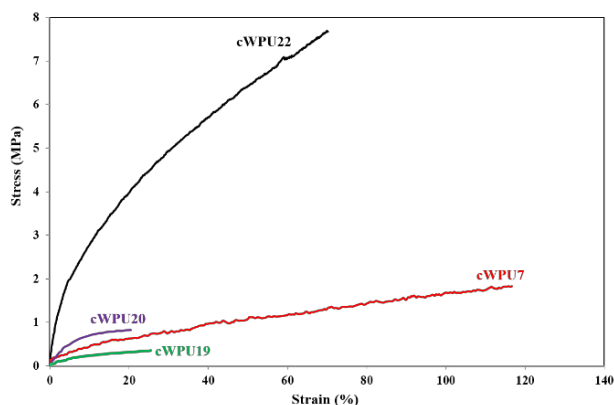


Fig. 2. Stress vs strain curves of cWPU films

Mechanical properties of cWPU films were indicated by stress-strain curves as shown in **Fig. 2** and listed in **Table 3**. In case of non-EG, the properties of films were up by increasing NCO levels from 125 to 150. Tensile strength of films were 0.32 and 0.82 MPa, Young's modulus values were 0.95 and 1.21 MPa, and Elongation at break values were 26.05 and 20.65 % for cWPU19 and cWPU20, respectively. In addition, adding EG series, it could be increased the mechanical properties. The tensile strength were 1.83 and 7.76 MPa, Young's modulus values were 1.14 and 20.52 MPa, and Elongation at break values were 116.64 and 72.32 % for cWPU7 and cWPU22, respectively. It was observed that they showed the same trend of mechanical properties when composed with higher NCO index. Moreover, the comparison of strength in series of NCO index 125, non-EG content (cWPU19) and EG content (cWPU22), jumped into 7 fold times by adding EG as chain extender because of long chain and chain entanglement that was explained in our previous work [15].

Table 2. Contact angle of cWPU films images.



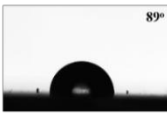

Codes	Water Contact Angle	Oil Contact Angle
cWPU7	 91°	 35°
cWPU22	 89°	 32°

Table 3. Contact angle values and mechanical properties of cWPU films.

Code	Contact angle (°)		Young's modulus (MPa)	Tensile Strength (MPa)	Elongation at break (%)
	W	O			
cWPU6	90	39	N/A	N/A	N/A
cWPU7	91	35	1.14 ± 0.23	1.83 ± 0.19	116.64 ± 1.38
cWPU19	88	37	0.95 ± 0.17	0.32 ± 0.03	26.05 ± 0.11
cWPU20	76	36	1.21 ± 0.22	0.82 ± 0.13	20.65 ± 0.31
cWPU22	89	32	20.52 ± 0.25	7.76 ± 0.33	72.32 ± 1.27

Note: W = water, O = Oil

Table 2 showed figures of water contact angle and oil contact angle for hydrophobicity and hydrophilicity of cWPU films and they were summarized in **Table 3**. Hydrophilicity was increased by increasing NCO levels in both cases. In case of non-EG, water contact angle values were 90, 88, and 76 degree while oil contact angle values were 39, 37, and 36 degree for NCO index of 100, 125, and 150, respectively. In condition of adding EG, water contact angle values were 91 and 89 degree while oil contact angle values were 35 and 32 degree for NCO index of 100 and 125, respectively. The contact angle result were not different because most of the ingredients were natural rubber part which is non polar structure [15]. On the other hand, water contact angle value which was dramatically dropped in system of NCO index of 150 because of high polarity of the presence of urea. These contact angle values were relatively hydrophilic and easier to wet many material surfaces [26]. That was a good parameter to pave the way for adhesive application.

4. Conclusion

The results show that cWPU based on natural rubber with increasing NCO index was successfully synthesized. All cWPU were well-dispersed, and the particle sizes of dispersions were in range of 58 to 193 nm. cWPU system was prepared in aqueous with TSC of approximately 20 and with pH value of 4. In addition, the increasing NCO index and EG led to increased mechanical properties.

Moreover, the contact angle results were relatively hydrophilic and easier to wet many material surfaces. An implication of this is the possibility that could be used as good adhesive applications. Further research should assess the impact of environmentally friendly by using renewable resource and solvent-free, and its mechanical strength is properly used for many applications.

Acknowledgement

This work was supported by Science Achievement Scholarship of Thailand; Natural Rubber Innovation Research Institute (Grant No. SCI581152S-0); Rubber products Development Group, Faculty of Science (Grant No. ACDS5910-01) and the Graduate school of Prince of Songkla University, Thailand.

References

- [1] Zain N M, Roslin E N, Ahmad S, "Preliminary study on bio-based polyurethane adhesive/aluminum laminated composites for automotive applications", *Int. J. Adhes. Adhes.*, 71, 1-9 (2016).
- [2] Sundar S, Vijayalakshmi N, Gupta S, Rajaram R, Radhakrishnan G, "Aqueous dispersions of polyurethane-polyvinyl pyridine cationomers and their application as binder in base coat for leather finishing", *Prog. Org. Coat.*, 56, 178-184 (2006).
- [3] Lu Y, Larock R C, "Soybean oil-based, aqueous cationic polyurethane dispersions: Synthesis and properties", *Prog. Org. Coat.*, 69, 31-37 (2010).
- [4] El-Sayed A A, Kantouch F A, Kantouch A, "Preparation of cationic polyurethane and its application to acrylic fabrics", *J. Appl. Polym. Sci.*, 121, 777-783 (2011).
- [5] Liu L, Wu X, Li T, "Novel polymer electrolytes based on cationic polyurethane with different alkyl chain length", *J. Power Sources*, 249, 397-404 (2014).
- [6] Yang T-f, Chin W-k, Cherng J-y, Shau M-d, "Synthesis of Novel Biodegradable Cationic Polymer: N,N-Diethylethylenediamine Polyurethane as a Gene Carrier", *Biomacromolecules*, 5, 1926-1932 (2004).
- [7] Cheng J, Tang X, Zhao J, Shi T, Zhao P, Lin C, "Multifunctional cationic polyurethanes designed for non-viral cancer gene therapy", *Acta Biomater.*, 30, 155-167 (2016).
- [8] Hung W C, Shau M D, Kao H C, Shih M F, Cherng J Y, "The synthesis of cationic polyurethanes to study the effect of amines and structures on their DNA transfection potential", *J. Controlled Release*, 133, 68-76 (2009).
- [9] Li P, Shen Y, Yang X, Li G, "Preparation and properties of waterborne cationic fluorinated polyurethane", *Journal of Polymer Research*, 19, 1-10 (2011).
- [10] Li J, Zhang X, Gooch J, Sun W, Wang H, Wang K, "Photo- and pH-sensitive azo-containing cationic waterborne polyurethane", *Polym. Bull.*, 72, 881-895 (2015).
- [11] Xin H, Shen Y, Li X, "Novel cationic polyurethane-fluorinated acrylic hybrid latexes: Synthesis, characterization and properties", *Colloids. Surf. A. Physicochem. Eng. Asp.*, 384, 205-211 (2011).
- [12] Lu Y, Larock R C, "Synthesis and properties of grafted latices from a soybean oil-based waterborne polyurethane and acrylics", *J. Appl. Polym. Sci.*, 119, 3305-3314 (2011).
- [13] Saetung A, Rungvichaniwat A, Campistron I, Klinpituksa P, Laguerre A, Phinyocheep P, Pilard J F, "Controlled degradation of natural rubber and modification of the obtained telechelic oligoisoprenes: Preliminary study of their potentiality as polyurethane foam precursors", *J. Appl. Polym. Sci.*, 117, 1279-1289 (2010).
- [14] Klinklai W, Kawahara S, Mizumo T, Yoshizawa M, Sakdapipanich J T, Isono Y, Ohno H, "Depolymerization and ionic conductivity of enzymatically deproteinized natural rubber having epoxy group", *Eur. Polym. J.*, 39, 1707-1712 (2003).
- [15] Sukhawipat N, Saetung N, Pilard J-F, Bistac S, Saetung A, "Synthesis and characterization of novel natural rubber based cationic waterborne polyurethane—Effect of emulsifier and diol class chain extender", *J. Appl. Polym. Sci.*, 135, 45715 (1 - 12) (2017).
- [16] Saetung A, Kaenhin L, Klinpituksa P, Rungvichaniwat A, Tulyapitak T, Munleh S, Campistron I, Pilard J F, "Synthesis, characteristic, and properties of

- waterborne polyurethane based on natural rubber", *J. Appl. Polym. Sci.*, 124, 2741-2752 (2012).
- [17] Sukhawipat N, Saetung N, Saetung A In *Synthesis of Novel Cationic Waterborne Polyurethane from Natural Rubber and its Properties Testing*, 2016 6th International Conference on Key Engineering Materials (ICKEM 2016), Hongkong, Alexander M. Korsunsky, Chobin Makabe, Haider F. Abdul Amir, Nindhia, T G T, Eds. Trans Tech Publications: Hongkong, 19-23, (2016).
- [18] Saetung A, Tsupphayakorn-ake P, Tulyapituk T, Saetung N, Phinyocheep P, Pilard J-F, "The chain extender content and NCO/OH ratio flexibly tune the properties of natural rubber-based waterborne polyurethanes", *J. Appl. Polym. Sci.*, 132, 42505 (1 of 12) (2015).
- [19] Choi J, Moon D S, Jang J U, Yin W B, Lee B, Lee K J, "Synthesis of highly functionalized thermoplastic polyurethanes and their potential applications", *Polymer*, 116, 287-294 (2017).
- [20] Cakić S M, Ristić I S, Cincović M M, Stojiljković D T, János C J, Miroslav C J, Stamenković J V, "Glycolyzed poly(ethylene terephthalate) waste and castor oil-based polyols for waterborne polyurethane adhesives containing hexamethoxymethyl melamine", *Prog. Org. Coat.*,
- [21] Hinrichsen G, *Polyurethane handbook* 2nd ed.; Akademie Verlag GmbH: **1994**; Vol. 45, pp.
- [22] Li P, Shen Y, Yang X, Li G, "Preparation and properties of waterborne cationic fluorinated polyurethane", *J Polym Res*, 19, 9786 (2011).
- [23] Lin W-T, Lee W-J, "Effects of the NCO/OH molar ratio and the silica contained on the properties of waterborne polyurethane resins", *Colloids. Surf. A. Physicochem. Eng. Asp.*, 522, 453-460 (2017).
- [24] Fuensanta M, Jofre-Reche J A, Rodríguez-Llansola F, Costa V, Iglesias J I, Martín-Martínez J M, "Structural characterization of polyurethane ureas and waterborne polyurethane urea dispersions made with mixtures of polyester polyol and polycarbonate diol", *Prog. Org. Coat.*, 112, 141-152 (2017).
- [25] Rai R N, Kant S, Reddi R S B, Ganesamoorthy S, Gupta P K, "Solid state synthesis, crystal growth and optical properties of urea and p-chloronitrobenzene solid solution", *J. Solid State Chem.*, 233, 244-251 (2016).
- [26] Liu H, Li C, Sun X S, "Soy-oil-based waterborne polyurethane improved wet strength of soy protein adhesives on wood", *Int. J. Adhes. Adhes.*, 73, 66-74 (2017).

Microphase Separation on Thermal/Dynamic Mechanical Properties of Olefin Block Copolymer-Thermoplastic Elastomers

Orrathai Chamnan, Nanwarinparch Pucknansawhet and Chantima Deeprasertkul¹

¹School of Polymer Engineering, Institute of Engineering, Suranaree University of Technology, Nakhon Ratchasima 30000

Phone +66 4422 4434, Fax +66 4422 4605, E-Mail: chantima@sut.ac.th

Abstract

Thermal and dynamic mechanical properties of olefin multiblock copolymers (OBC) were investigated. Two preparation conditions were applied as to prepare OBCs with and without the phase separated structure. Annealing at 220°C over a period of time of 60 min was chosen for the phase separation. Results obtained from differential scanning calorimetry showed that the melting temperatures are relatively the same either with or without the phase separation. Dynamic mechanical behavior of OBC solid samples was generally the same for both conditions. Except that in the phase-separated samples, the additional loss peak was observed at 0-10°C which is higher than its glass transition temperature. Some restricted large scale structure must be formed.

Keywords: thermoplastic elastomer, olefin block copolymer, microphase separation, storage modulus

1. Introduction

Thermoplastic elastomers (TPEs) are materials exhibiting elastomeric behavior and possessing thermoplastic processability. Block copolymer with microphase separation characteristic is a typical class of TPEs. Olefin multiblock copolymers (OBCs) recently synthesized via chain shuttling process have shown these microphase separation. The OBCs are alternating multiblock ethylene-comonomer copolymers, comprised of the crystallizable blocks (low comonomer content) alternating with the amorphous blocks (high comonomer content) [1]. The multiblock copolymers exhibit the behavior ranging from thermoplastic to elastomeric depending on the amount of crystallizable (hard) and amorphous (soft) blocks [2]. Under stress-strain curve, the multiblock copolymer with more soft blocks show

elastomeric behavior and that with more hard blocks behave like semicrystalline thermoplastics with yielding.

Phase separation of block copolymers has drawn much attention in research as it can provide the ordered structures with wide range of applications. Studies showed that microphase separation (or mesophase separation as larger domain size than normally obtained from typical block copolymers) was observed in OBCs with high comonomer content [3-6]. Our previous work on viscoelastic behavior of OBC melts has shown that in the low frequency region, the observed liquid behavior changed to the elastic behavior when annealed for a period of 60 min at 220°C. The constant storage modulus $|G'|$ of 10^4 Pa was obtained which is lower than typical rubbery plateau modulus (about 10^6 Pa) of linear homopolymer [7]. It suggested that some elastic structure with larger interlocking length between hard-soft phase separated structure than entanglement length was formed in the melt

during annealing. In this work, we aimed to compare the thermal and dynamic mechanical thermal properties of solid OBC samples as prepared under the condition with and without phase separation.

2. Experimental Methods

2.1 Materials

Three olefin multiblock copolymers (OBCs) with the same density of 0.866 g/cm^3 and different melt flow indices were used. Melt flow index was measured according to ASTM D1238 (2.16 kg, 190°C). The samples were designated as OBC_x_A or OBC_x_B, where x is its MFI. A, and B is the preparation condition with and without phase separation, respectively. These Dow Chemicals polyolefins were purchased from Chemical Innovation (Thailand).

2.2 Differential Scanning Calorimetric Analysis

DSC measurements were conducted on PerkinElmer PYRIS (Diamond) calorimeter under N_2 atmosphere. Thin circular disk (1 mm thickness) samples were compression molded (Gotech model GT-7014-A30) either condition A at 160°C for 15 min or B at 220°C for 60 min before quenching. Each specimen under condition A was heated from 50 to 160°C (first heat), isothermally at 160°C for 15 min, then cooled to 50°C (cooling) and heated up to 160°C (second heat) at the heating rate of $10^\circ\text{C}/\text{min}$. For the samples under preparation condition B, the scanning temperature was changed from 160°C to 220°C .

2.3 Dynamic mechanical thermal analysis

Dynamic mechanical properties of the solid samples were measured in torsion mode under N_2 atmosphere using the AR-G2 rheometer. Multiple frequency (1-10 Hz) with temperature ramp from -100 to 30°C at a rate of $10^\circ\text{C}/\text{min}$ was varied. Strain of 0.2% was applied. Rectangular-shape samples (with dimension of

$1.3 \times 5.0 \times 0.25 \text{ cm}^3$) were compression molded (Gotech model GT-7014-A30) either condition A at 190°C for 20 min or B at 220°C for 60 min before quenching.

3. Results and Discussion

3.1 Thermal Properties

DSC thermograms of OBC5_A and OBC5_B are presented in Figure 1 and 2. On the first heating curve, the endothermic peak was observed. The melting temperature is about 122°C for both conditions. The first heating is considered to present the effect of preparation condition. The results indicate that the presence of phase separation does not affect the thermal properties of OBC5. Isothermally heating inevitably erases thermal history. Upon cooling, the exothermic crystallization temperatures are 97°C for A and B, much lower than the T_m . Undercooling is typical for polymer. Double melting peaks were clearly observed on the second heating. Similar results were obtained on OBC1 and OBC15. Thermal properties of all samples are summarized in Table 1.

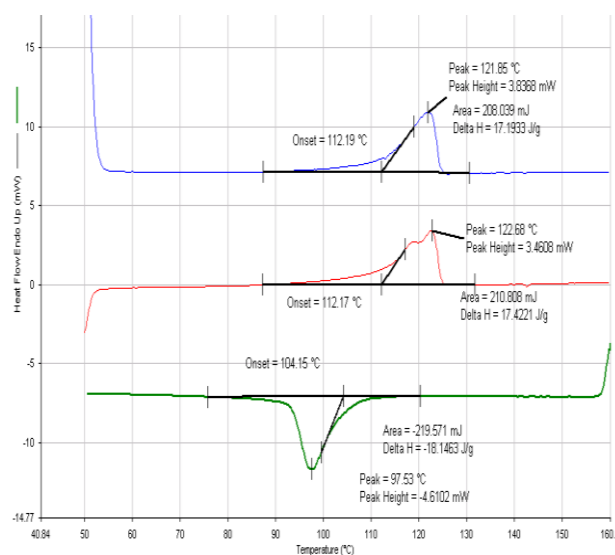


Figure 1 DSC curves (top: 1st heating, middle: 2nd heating, bottom: cooling) of OBC5_A

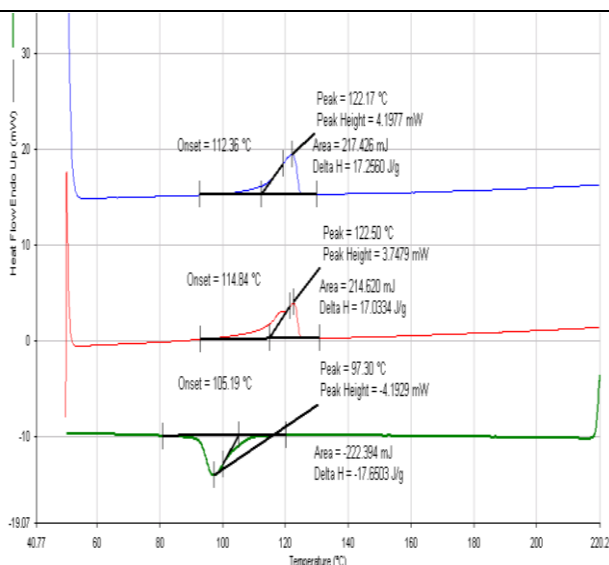


Figure 2 DSC curves (top: 1st heating, middle: 2nd heating, bottom: cooling) of OBC5_B samples

Table 1 Thermal properties of OBCx samples

OBCs	1 st heating		Cooling	
	T _m (°C)	ΔH _m (J/g)	T _c (°C)	ΔH _c (J/g)
OBC1_A	120.0	17.4	86.3	19.9
OBC1_B	120.3	18.1	87.4	19.7
OBC5_A	121.8	17.2	97.5	18.1
OBC5_B	122.1	17.2	97.3	17.7
OBC15_A	120.5	17.1	99.0	15.5
OBC15_B	119.5	20.1	96.6	19.2

3.2 Dynamic mechanical behavior of solid OBC

Figure 3 shows the dynamic properties of all OBCs obtained at frequency of 1 Hz. For a series prepared at 190°C (OBCx_A), the storage modulus (G') is relatively high (~7x10⁸ Pa) at low temperature and drops at -60 to -50°C then levels off to ~5x10⁶ Pa. This transition is considered as the glass transition temperature (T_g) belonging to the amorphous region. Only one transition was noticed. For a series prepared at 220°C with 60 min annealing time (OBCx_B), the glass transition was observed at the same temperature range. The additional transitions at -90, and 0 to 10°C was clearly seen. These

additional relaxations appeared at far below both their melting and crystallization temperatures, suggesting neither melting nor crystallization transition.

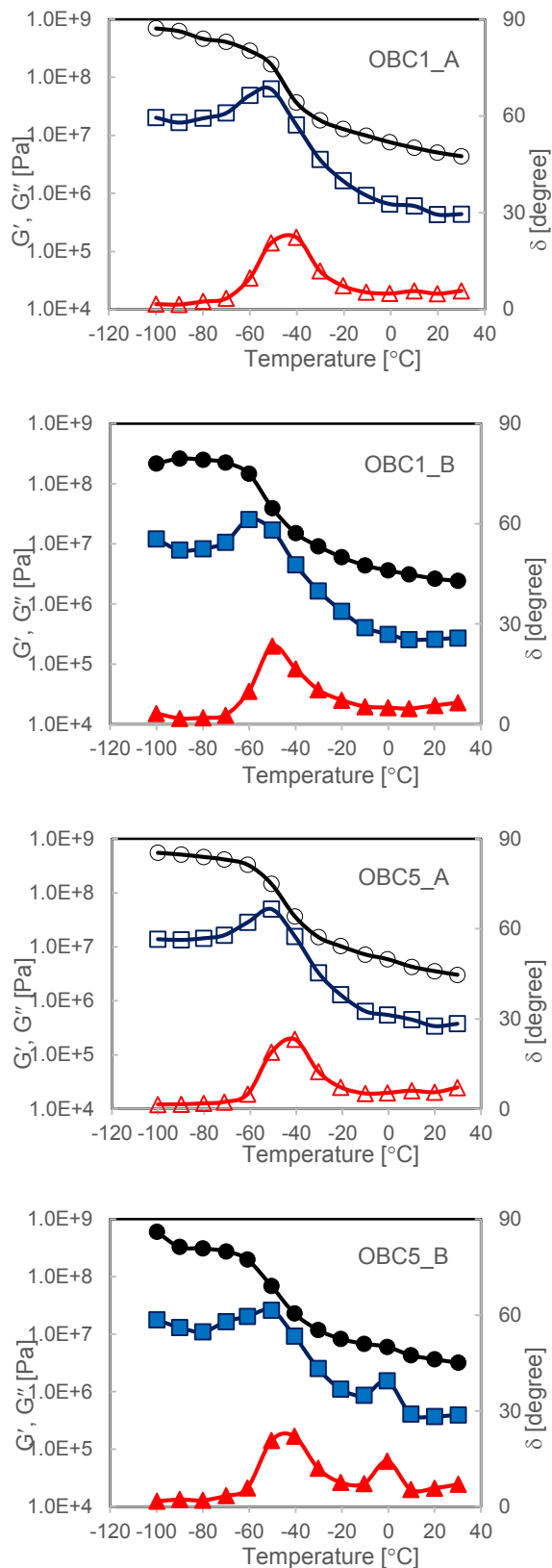


Figure 3 Dynamic mechanical properties of OBCx_A and OBCx_B at frequency of 1 Hz (circle: G', square: G'', triangle: phase shift δ)

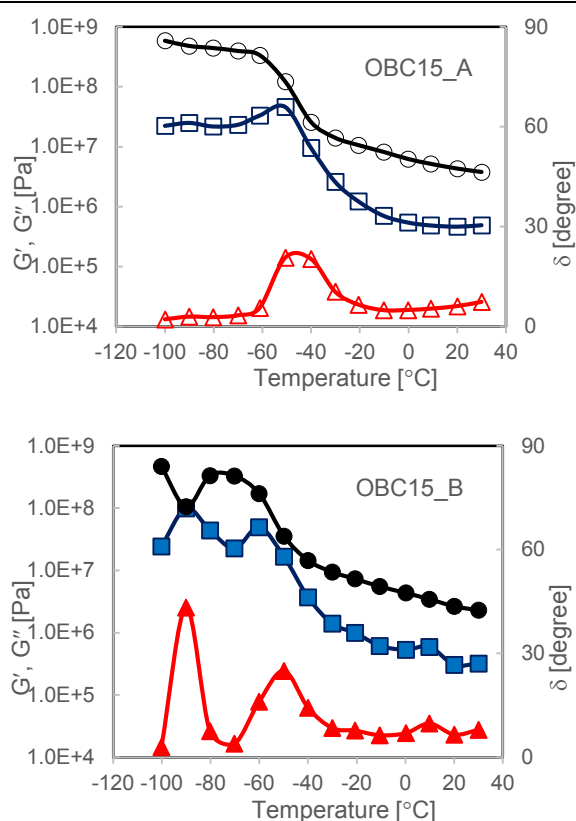


Figure 3 (cont'd) Dynamic mechanical properties of OBCx_A and OBCx_B at frequency of 1 Hz (circle: G' , square: G'' , triangle: phase shift δ)

The loss peak at -90°C is attributed to the motion of side groups of comonomer [8]. With low molecular weight of OBC15, this motion can be easily observed. Well above the T_g but far below the melting temperature, the loss peaks at 0 to 10°C must belong to the relaxation of chains in some restricted region such as chains in between the interlocking hard-soft phase separated structure or restricted amorphous phase in the hard crystallizable phase region. However, this relaxation was not observed in OBC1 at frequency of 1 Hz. By varying frequency from 1 to 10 Hz, OBC1_B showed the additional loss peak at low temperature of -20°C with the highest loss at 7.9 Hz (not shown here). It suggests that there be the natural frequency corresponding to the relaxation process of chains in these restricted regions. Beyond 30°C , the samples were soft and lost their shape for the dynamic measurements. In general, the dynamic mechanical properties (the magnitude of G'

and G'') of solid OBCs were not affected by the microphase separation.

4. Conclusion

Thermal and dynamic mechanical properties of solid olefin block copolymers were investigated. The presence of microphase structure was noticed in the dynamic mechanical properties of solid OBC as the additional relaxation occurs at the temperature in between the T_g and T_m transitions. This attributes to some more restricted region than T_g but less restricted than T_m which likely supports the occurrence of microphase separation in the melt at 220°C . Nevertheless, the phase separation hardly affect the magnitude of storage modulus and the thermal transition temperature.

References

- [1] Arriola D.J., Carnahan E.M., Hustad P.D., Kuhlman R.L., Wenzel T.T., *Science*, **312**, 714-719 (2006).
- [2] Wang H.P., Khariwala D.U., Cheung W., Chum S.P., Hiltner A., Baer E., *Macromolecules*, **40**, 2852-2862 (2007).
- [3] Park H.E., Dealy J.M., Marchand G.R., Wang J., Li S., Register R.A., *Macromolecules*, **43**, 6789-6799 (2010).
- [4] Liu G., Guan Y., Wen T., Wang X., Zhang X., Wang D., Lib X., Loos J., Chen H., Walton K., Marchand G., *Polymer*, **52**, 5221-5230 (2011).
- [5] He P., Shen W., Yu W., Zhou C., *Macromolecules*, **47**, 807-820 (2014).
- [6] Guoming Liu, Yu Guan, Tao Wen, Xiwei Wang, Xiuqin Zhang, Dujin Wang, Xiuhong Li, Joachim Loos, Hongyu Chen, Kim Walton, Gary Marchand., *Polymer*, **52**, 5221-5230 (2011).
- [7] Phatthanuwat P., Deeprasertkul C., *Proceeding of International Polymer Conference of Thailand [PCT-6]*, Bangkok, Thailand, 181-184 (2016).
- [8] Haynes, W.M. (ed.). *CRC Handbook of chemistry and physics*. 96th ed (2015-2016). CRC Press, Boca Raton (2014).

Study of Porous Pipes made from GRT/NR/Reclaimed Rubber Reinforced with Waste Tire Fibers for Agricultural Applications

Pattawee Pinitkul¹, Boonharn Ou-udomying², and Ittipol Jangchud^{1*}

¹ Department of Chemistry, Faculty of Science, King Mongkut's Institute of Technology Ladkrabang, Bangkok 10520

² Saeng Thai Rubber Co., Ltd., Samrong-Tai, Prapadaeng, Samut Prakarn 10130

Phone +66 1349 3585, Fax +66 2564 6445, *E-Mail: ittipol.ja@kmitl.ac.th

Abstract

In this research, reinforced porous pipes as water irrigation for agriculture applications were studied. The pipes were made from natural rubber (NR), reclaimed rubber (RR) and ground rubber tire (GRT). A blowing agent and kicker were used to create open-cell structures. Short fibers from ground ply waste were used to reinforce the porous pipes. Mixtures were compounded by a kneader and shaped into porous pipe by a single-screw extruder. Pipe samples were vulcanized by a hot air oven. Ratio of the GRT to based rubbers (NR and RR) was fixed at 60:40. Factors affecting of porous pipe properties were studied, e.g., carbon black (CB) loading (30, 50 and 70 phr) and waste tire fibers (WTF) loading (0-6 phr). Porous pipe properties were investigated, such as, cure characteristics, mechanical properties, morphology, burst pressure, %diameter swell and water permeability rate. It was found that open-cell porous pipe could be produced. CB loading was found at 50 phr as shown by the maximum tensile strength. Reinforcing effects of WTF on pipe properties were studied at a fixed CB loading (50 phr). By increasing WTF loading, optimum point was found at 4 phr. By adding the WTF, %diameter swell and burst pressure were clearly improved. It can be proven that the reinforced porous pipes have a high potential for commercial use as water irrigation system.

Keywords: Porous pipes, Natural rubber, Reclaimed rubber, Ground rubber tire (GRT), Waste tire fibers (WTF)

1. Introduction

Worn-out tires have always been concerned environmentally and economically. Efficient Recycling methods of used tires have been studied and drawn more attentions.[1] Products using wastes from worn tires would represent great environmental benefits and economic savings for communities.[2] In this research, ground rubber tire (GRT), waste tire fibers (WTF) and reclaim rubber (RR) derived from worn tires were used to produce reinforced porous pipes as agricultural irrigation equipment. Porous pipes have been proved to be an effective water irrigation method due to low water consumption, less water evaporation, and direct-to-root system. Both on-ground and under-ground porous pipe systems can be carried out. Commercial porous pipes are usually made from plastics such as polyolefins.[3]

Attempts to produce porous pipes from rubbers were unsuccessfully done due to low pressure resistance, high % diameter swell, and non-linear water rate at high pressures.[4] Short fibers can be used to reinforce rubbers yielding high modulus, high strength and low creep [5-6]. Short nylon fibers reinforced natural rubber-reclaimed rubber blends were studied for cure characteristics and mechanical properties [7]. Effects of fiber-matrix adhesion, aspect ratio of filler, fiber dispersion and orientation, nature of matrix and type of fiber on the extent of reinforcement were also studied [8-10]. In this study, porous pipes were made from natural rubber (NR), reclaimed rubber (RR), ground rubber tire (GRT) and waste tire fibers (WTF). Factors affecting porous pipes properties were studied, such as, NR/RR ratios, carbon black loading, WTF loading, and blowing agent loading. Porous pipe properties were investigated, such as,

RUBB-P2

mechanical properties, physical properties, morphology, and water permeability.

2. Experimental Methods

2.1 Materials

STR20 natural rubber (NR) was purchased from MBJ Enterprise Co., Ltd. (Bangkok, Thailand). Reclaim rubber (RR), 30 mesh ground rubber tire (GRT) and waste tire fibers (WTF) were obtained from Saeng Thai Rubber Co., Ltd.. UCD-105 grade reclaim rubber (RR) has 50% rubber content, 29% carbon black content, and Mooney Viscosity (ML1+4 (100°C)) of 52. WTF with diameter of 0.027 mm and 3-4 mm in length were used in this work. N-330 Carbon black (Thai Carbon Product Co., Ltd.) was used as a main reinforcing filler. N-cyclohexyl-2-benzothiazyl sulfenamide (CBS), sulfur (S), zinc oxide (ZnO) and stearic acid were used for the curing system. A blowing agent and kicker (proprietary) were used to create open-cell structures.

2.2 Preparation of waste fiber masterbatches

40% masterbatch of WTF in NR was prepared by using a kneader. NR was first masticated in kneader mixer for 1 min with a rotor speed of 40 rpm and 70 °C. Then, WTF was gradually added during 3 min loading time. Fiber masterbatch was then rolled into sheet on a two-roll mill. Sheeted rubber compound was conditioned at room temperature (25°C) for 24 hr.

2.3 Mixing and extrusion

Rubbers, WTF, GRT, carbon black and all chemical ingredients were mixed by using a kneader with a rotor speed of 40 rpm and 70 °C. Compound formulas were shown in **Table 1**. Ratio of the GRT to based rubbers (NR and RR) was fixed at 60:40. Total mixing time was kept constant at 17 min. Compound samples were shaped into porous pipes by a single-screw extruder with a screw speed of 30 rpm at 60 °C. Diameters of the die were 14 mm (inside) and 18 mm (outside). Pipe samples were vulcanized by a hot air oven.

Table 1 Formulas of porous pipes in this work

Materials	C ₃₀ F ₀	C ₅₀ F ₀	C ₇₀ F ₀	C ₅₀ F ₂	C ₅₀ F ₄	C ₅₀ F ₆
NR	50	50	50	50	50	50
RR	100	100	100	100	100	100
GRT	150	150	150	150	150	150
WTF	-	-	-	2	4	6
CB	30	50	70	50	50	50

2.4 Characterization and testing

Mooney viscosity (ML1+4 @ 100°C) of compound samples was determined by using a Mooney viscometer (ViscTech®, TechPro). Tensile properties were determined by using a universal testing machine (UTM), HIWA-200 at a crosshead speed of 500 mm/min. Mechanical properties were determined according to ASTM D412. Cryogenic fractured surfaces of porous samples were observed with a scanning electron microscope (SEM) (FEI, Quanta 400). Water permeability and %diameter swell of porous pipes with changing water pressure were determined according to ASTM D3767-03. Burst test of porous pipes was determined according to ASTM D622.

3. Results and Discussion

Porous pipe made from GRT mixed NR/RR in this work can be shown in **Figure 1**. Effects of CB loading on mechanical properties of porous pipes were shown in **Figure 2**. As CB was increased to 50 phr, tensile strength of the pipe was increased. However, tensile strength at 70 phr CB loading was declined. It might derive from poor filler dispersion at high CB loadings. SEM micrographs of porous samples were shown in **Figure 3**.



Figure 1 Porous pipe made from GRT mixed NR/RR

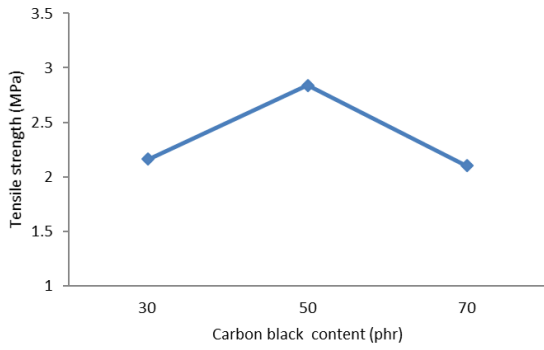


Figure 2 Effects of CB loading on tensile strength of porous pipe samples

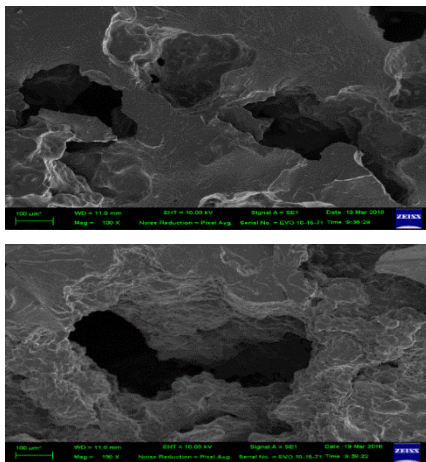


Figure 3 SEM micrographs of fractured samples (50 and 70 phr CB loading).

By fixing CB loading at 50 phr, effects of waste tire fiber (WTF) loading were studied and shown in **Figure 4**. It was found that mechanical properties of rubber vulcanizates had a trend to increase to an optimum loading (4 phr) as WTF loading was increased. As expected, properties in machine direction (MD) were slightly higher than those in transverse direction (TD). As shown in **Figure 5**, Mooney viscosity of rubber compounds was increased as WTF content was increased. High viscosity of compounds with WTF was found since WTF with high degree of fibrillation was capable of interacting via mechanical interlocking, leading to strong filler network formation.

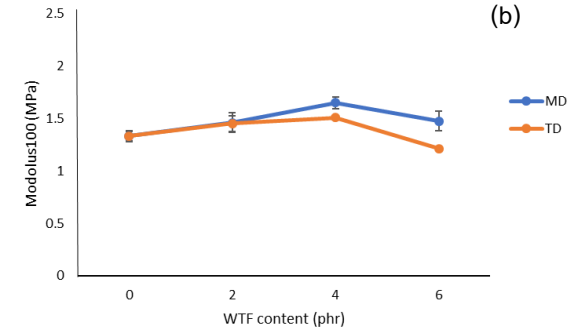
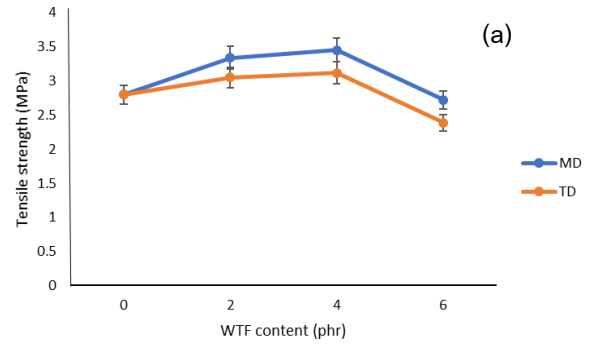


Figure 4 Effects of WTF loading on (a) tensile strength and (b) modulus100 of porous pipe samples

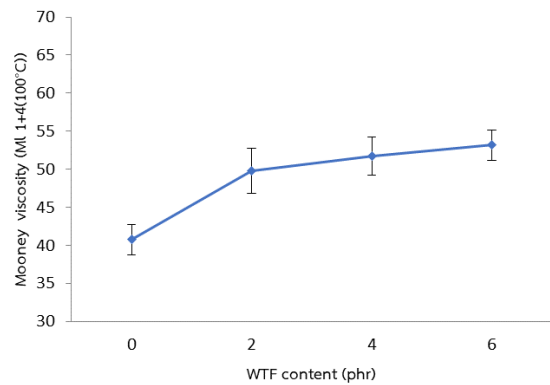


Figure 5 Effects of WTF loading on Mooney viscosity ML 1+4 (100 °C)

Figure 6 displays SEM micrographs of fractured samples with 4 phr WTF. It was revealed that WTF dispersion in rubber matrix was good. However, interfacial adhesion of WTF and rubber was not so good since fiber pulled-out and adhesion failure were observed.

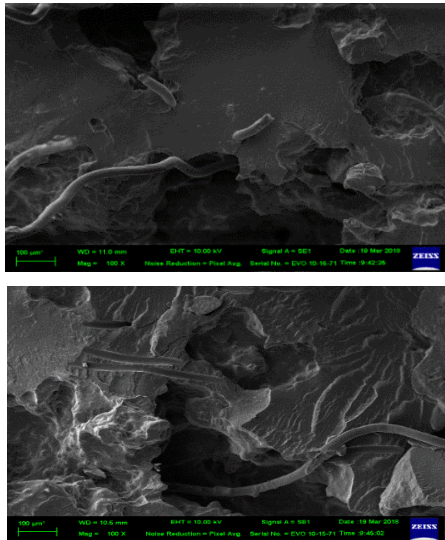


Figure 6 SEM micrographs of fractured samples with WTF (4 phr)

%Diameter swells of porous pipes as affected by water pressure were shown in **Figure 7**. Effects of CB and WTF reinforcement were observed clearly as %swell was significantly decreased when CB and WTF were added in the compounds. %Diameter swell of porous pipe can be related to water permeability as shown in **Figure 8**. As expected, %swell and water permeability rate were increased as water pressure was increased. CB alone (C50F0) could reinforce pipe samples. However, CB together with WTF (C50F4) showed better reinforcement. More linear water permeation was observed when water pressure was increased. **Figure 9** shows burst pressure of pipe samples. It was found that burst pressure was improved dramatically when both CB and WTF were used to reinforce porous pipes.

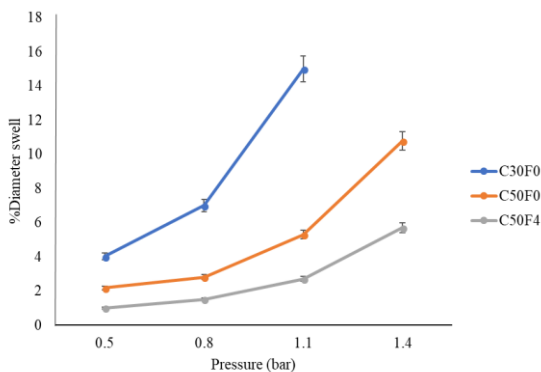


Figure 7 %Diameter swell of porous pipes affected by water pressure and fillers

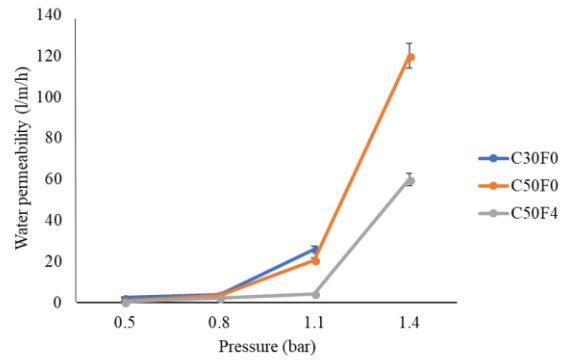


Figure 8 Water permeability of porous pipes affected by water pressure and fillers

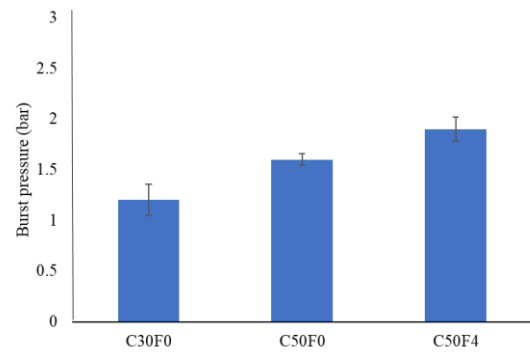


Figure 9 Burst pressure of porous pipes showing effects of fillers

4. Conclusion

In this work, study of porous pipes made from natural rubber (NR), reclaimed rubber (RR) and ground rubber tire (GRT) was carried out as water irrigation for agriculture. Effects of carbon black (CB) and waste tire fibers (WTF) reinforcement were studied. Mechanical properties of vulcanizates had a trend to increase to an optimum fiber loading (4 phr) as WTF loading was increased. Hybrid composites of CB and WTF showed advantageous mechanical properties. By adding the WTF, %diameter swell and burst pressure were clearly improved. It can be proven that the reinforced porous pipes have high potentials for commercial use as water irrigation system.

Acknowledgement

The authors would like to express their sincere appreciation to KMITL Research Fund and Saeng Thai Rubber Co., Ltd. for supporting this study.

References

- [1] Kenzo F., Mitsumasa M., Hirotaka O. Recycling Technology of Tire Rubber. J. JSAE. A Toyota Central Research and Development Laboratories, Inc., Nagakute., 259–264 (2001).
- [2] Xin G-Zhan G, X., Hui Lu , C. and Lian G, M. Preparation of Rubber Composites from Ground Tyre Rubber Reinforced with Waste-tyre Fibre through Mechanical Milling. J. appl. Polym. Sci., 103, 4087–4094. (2007).
- [3] James E. Turner, Southlake, Tex. Underground Irrigation Porous Pipe. Patent 4,003,408., United States Patent (1997).
- [4] Sumana J. Production of Porous Pipe made from Natural Rubber and Ground Rubber tire., Thesis of KMITL, Thailand. (2004).
- [5] Bhowmick, A.K. and Stephens, H.I. Handbook of Elastomers, New York: Marcel Dekker, 241–264. (1994)
- [6] Foldif, A.P. Reinforcement of Rubber through Short Individual Filaments. Rubber. Chem. Technol., 49, 379–389. (1976)
- [7] Sreeja T.D. and Kutty S.K.N. Cure Characteristics and Mechanical Properties of Short Nylon Fiber Reinforced Natural Rubber–Reclaimed Rubber Blends, Polymer-Plastics Technology and Engineering, 42:2, 239-252, (2003)
- [8] Seemas, A. and Kuttyk, S.K.N. Effect of an Epoxy-Based Bonding Agent on the Cure Characteristics and Mechanical Properties of Short Nylon Fiber Reinforced Acrylonitrile-Butadiene Rubber Composites. J. appl. Polymer. Sci., 99, 532–539. (2006)
- [9] Geethamma, Kala Prasad V.G., Groenin G. and Thomas S. Dynamic Mechanical Behaviour of Short Coir Fibre Reinforced Natural Rubber Composites. Composites: Part A, 36, 1499–1506. (2005)
- [10] Soltani S., Nader G. and Ghoreishy M.H.R. Mechanical and Rheological Properties of Short Nylon Fiber NR/SBR Composites. J. Rubb. Res., 13(2), 110–124. (2010)

Influence of Sulphur Crosslink Type on the Strain-induced Crystallization of Sulphur-Vulcanized Natural Rubbers by *In-situ* Synchrotron WAXD

Watcharin Sainumsai^{1,2*}, Shigeyuki Toki^{2,3,4} and Krisda Suchiva^{2,3}

¹Program in Rubber and Polymer Technology, Faculty of Science and Technology, Songkhla Rajabhat University, Songkhla, 90000, Thailand

²Department of Chemistry, Faculty of Science, Mahidol University, Nakorn Pathom, 73170 Thailand

³National Metal and Materials Technology Center, National Science and Technology Department Agency, Pathum Thani 12120, Thailand

⁴Department of Chemistry, State University of New York at Stony Brook, NY, 11794-3400, USA

Phone +66 7433 6949, Fax +66 7426 0261, *E-Mail: watcharin.sa@skru.ac.th

Abstract

Strain-induced crystallization (SIC) of varied crosslink structures of vulcanized natural rubber (NR) were compared by using synchrotron X-ray. The sulphur crosslink type (mono-, di- and poly-sulphidic) was controlled by changing the sulphur to accelerator ratio (2.67, 0.50 and 0.10) using CBS as an accelerator. The onsets of SIC occurred at the strain (defined as $\lambda = (l-l_0)/l_0$ with l_0 is the initial sample length) of 2.24 for NR vulcanizates which contain mainly monosulphidic and disulphidic crosslinks (the EV-cured and the SEV-cured system). For the CV-cured NR vulcanizate, the crosslinks of which are dominated by polysulphidic type, SIC began to appear at the higher strain of 2.63. Thus, it appears that short sulphidic crosslinks favour the initiation of SIC. The rate of SIC was found to be slightly higher for the NR vulcanizate which contains a large amount of polysulphidic crosslinks (the CV-cured system) than for the samples which contain mainly monosulphidic and disulphidic crosslinks (the SEV-cured and the EV-cured systems). However, the CV-cured system showed the smaller development of crystallinity during deformation than did the SEV- and EV-cured samples but the final crystalline fraction at the rupture point was higher.

Keywords: Strain-induced crystallization, Natural rubber, Crosslink type

1. Introduction

Sulphur vulcanized natural rubber (V-NR) performs great mechanical properties such as tensile strength (20-30 MPa), strain at break (800-1000 %), tough fatigue resistance and large hysteresis loss without any fillers. On the contrary, synthetic polyisoprene (IR) has not been manufactured as a competitor of NR because of its inferior mechanical properties, although IR has been used as a processing agent [1].

After vulcanization, three-dimensional network of chemical crosslink is a vital element of vulcanized rubber to be stretched to large strain and to recover back to the original shape due to an entropy response. Sulphur

vulcanization system creates three kinds of structures of crosslink such as one sulphur bridge (-C-S-C-), two sulphurs bridge (-C-S-S-C-) and several sulphurs bridge (-C-S-S_x-S-C-, x = 1-6), called as mono-, di- and poly-sulphidic crosslinks, respectively [2-4]. It has been considered that monosulphidic rich compound is good for heat resistance and the polysulphidic rich compound is good for flexibility.

The value of crosslink density is calculated through macroscopic measurements of swell or of modulus, although microscopic studies revealed that crosslink is distributed heterogeneously by small angle neutron scattering (SANS) [5,6]. Sulphur vulcanization is

accompanied with zinc oxide, stearic acid and accelerators, therefore, zinc oxide (which is crystal and makes cluster) attracts sulphur and accelerator, then creates higher crosslink density area around zinc oxide. The molecular weight of polymer chains between crosslink points may have a broad distribution due to the heterogeneous distribution of crosslink points, although we calculate one value of crosslink density in a macroscopic sample. According to the theory of rubber elasticity of non-Gaussian chain, the extensibility of vulcanized rubber is limited by the molecular weight of polymer chains between crosslink [7-8]. In the case of polysulphidic, a crosslink bridge itself can be deformed like a chain since sulphur atoms make long chains and networks which are called as amorphous sulphur or plastic sulphur or rubber sulphur at certain conditions. Although the binding energy of polysulphidic is lower than monosulphidic and disulphidic, polysulphidic rich IR show the smaller amount of radicals than monosulphidic rich IR. Therefore, polysulphidic crosslink structure seems to be not broken down easier than other sulphides, but be deformed as a kind of elastic chains [9-12].

SIC of sulphur vulcanized NR has been studied extensively by X-ray [13-16]. It is reported that crosslink density does not change the onset strain of SIC although the higher crosslink density samples create the larger amount of SIC at larger strain [17-18]. The size of crystallites does not grow during deformation and the increase of crystalline fraction is caused by the increase of the number of crystallites [17-19]. The onset strain of SIC of vulcanized natural rubber (V-NR) is smaller than the one of vulcanized synthetic polyisoprene rubber (V-IR), although the maximum crystalline fraction of V-NR and V-IR are almost the same [20-21]. The onset strain of SIC of V-NR is larger than the one of un-vulcanized NR [22-25]. Inhomogeneous distribution of crosslink density may create the size distribution of the local crystallites [26]. Recent instantaneous deformation experiments disclosed the mechanism of SIC and classified SIC into fast (50-100 ms) and slow (2.5-4.0 sec) crystallization processes [21,26]. The slow SIC accompany with stress relaxation. This research deals with slow SIC. Polysulphidic rich

carbon black filled V-NR compound shows the larger amount of SIC than monosulphidic rich compound and accomplished the highest tensile strength of 42.5 MPa at an official competition in 2004 [27-28]. This suggests that filler does not hinder SIC.

The purpose of this paper is to study the sulphur vulcanization of NR accelerated with N-cyclohexyl-2-benzothiazyl sulphenamide (CBS). Three compounds of Sulphur/CBS were prepared at the same level of crosslink density. The ratio of sulphur and accelerator is varied as 2.67, 0.50 and 0.10. The compounds are called as conventional vulcanization (CV), semi-effective vulcanization (SEV) and effective vulcanization (EV). In the present paper the attention is mainly directed to study the influences of vulcanization system on the tensile properties.

2. Experimental Methods

2.1 Materials

Commercial grade of Standard Thai Natural Rubber, 5L grade (STR-5L) was used. The compositions and cure time of compounds are shown in Table 1. Rubber compounds were prepared by using a laboratory-sized two-roll mill (model LRM150, Lab Tech Engineering) at the set temperature of 40°C. Rubber was masticated for 2 minutes, stearic acid, zinc oxide, an accelerator (CBS) were mixed for 2 minutes. Then, sulphur was added and mixed for 2 minutes. Finally, passing the rolled batch endwise through the mill six times and passing the batch four times through the mill, folded it back on itself each time. The total mixing time is 8 minutes.

Table 1. Composition and sample preparation conditions of the samples

Ingredients	Quantity (phr)		
	CV	SEV	EV
NR ^a	100	100	100
Zinc Oxide	5	5	5
Stearic acid	1	1	1
CBS ^b	0.75	1.82	4.60
Sulphur	2.00	0.91	0.46
Sulphur/CBS ratio	2.67	0.50	0.10
Cure time (min) ^c	13	19	28

^aNR: STR 5L, ^bAccelerator: CBS (N-cyclohexyl-2-benzothiazyl sulphenamide), ^cCuring temperature 150°C

The rubber compounds were left at room temperature for 24 hours before testing. Vulcanization was carried out in an electrically heated hydraulic press at 150°C using the optimum cure time (T_{c90}) previously determined with a moving die rheometer (TechPro MD+) at 150°C. The ratio of sulphur and accelerator CBS is varied as 2.67, 0.50 and 0.10. The compounds are called as conventional vulcanization (CV), semi-effective vulcanization (SEV) and effective vulcanization (EV).

2.2 Determination of crosslink density

The total crosslink densities of the vulcanized rubber were calculated from the equilibrium swelling in toluene by the Flory-Rehner equation [29-30]. The values of the constant used in the calculation were the molar volume of the swelling solvent $V_s = 107 \text{ cm}^3/\text{mole}$ and the rubber-solvent interaction parameter $\chi = 0.393$ [31].

2.3 Determination of sulphur crosslink structures

The contents of mono-, di- and poly-sulphidic crosslink structures were determined using the method described by Cunneen and Russell [2,32-33]. The concentration of the polysulphidic crosslink was evaluated from the equilibrium swelling in piperidine and propane-2-thiol, the concentration of the monosulphidic crosslink was evaluated from of the equilibrium swelling in piperidine and n-hexanethiol. Finally, the concentration of disulphidic crosslink was calculated from the total

crosslink density, polysulphidic and monosulphidic crosslink densities previously determined.

2.4 Strain-induced crystallization (SIC) measurement

In-situ wide-angle X-ray diffraction (WAXD) measurements were carried out at the X27C beamline in the National Synchrotron Light Source (NSLS), Brookhaven National Laboratory (BNL). The wavelength of X-ray was 0.1371 nm. A CCD X-ray detector (MAR, USA) was used to record the two-dimensional wide-angle X-ray diffraction (WAXD) patterns for quantitative image analyses. The typical image acquisition time for each scan was 30 sec. The data analysis software package (POLAR) used was developed by Stony brook Technology and Applied Research at Stony Brook, New York. The tensile machines allowed the symmetric stretching of the sample, permitting the focused X-ray to illuminate the same sample position during deformation. The chosen deformation rate was 10 mm/min. The stress-strain curves during extension were collected at 25°C in the uniaxial deformation mode.

3. Results and Discussion

3.1 Network characteristics of NR vulcanizates

It is well known that the ratio of sulphur to accelerator in accelerated-sulphur vulcanization system has a significant influence on the network structure and properties of the rubber vulcanizates [34-37]. Depending on the ratio, the sulphur vulcanization can be classified into three types: conventional (CV), semi-efficient (SEV) and efficient (EV) vulcanizing systems [38-39]. Each system can result in a network structure with different combinations of polysulphidic, disulphidic and monosulphidic crosslink. The network characteristics of the NR vulcanizates used for the present study, including the crosslink density and the type of sulphidic crosslinks, are summarized in Table 2. It can be seen that the total crosslink densities of the 3 types of NR vulcanizates are comparable and are in the range of $7.66 \pm 0.12 \times 10^{-5} \text{ mole/cm}^3$.

Table 2. Total crosslink density (ν_T), and the concentration of mono-, di- and polysulphidic crosslink of NR vulcanizates with different curing systems

Crosslink Concentration and Type	CV	SEV	EV
Total crosslink density ($\times 10^{-5}$ mole/cm ³)	7.78	7.55	7.65
Monosulphidic crosslink	0.00	0.08	3.99
Disulphidic crosslink	0.75	3.38	2.05
Polysulphidic crosslink	7.03	4.09	1.61
Percentage			
Monosulphidic crosslink, (%)	0	0.98	52.17
Disulphidic crosslink, (%)	9.68	44.77	26.81
Polysulphidic crosslink, (%)	90.32	54.25	21.02

The distributions of sulphur crosslink types in different NR vulcanizates are graphically shown in Fig. 1. Regarding the sulphur crosslink type, the NR vulcanizate cured with the EV system, contains mostly monosulphides (an average of 52.17%), while only an average of 21.02% crosslinks are polysulphides, and 26.81% crosslinks are disulphides. On the other hand, for the NR vulcanizate cured with the CV system, only an average of 9.68% crosslinks are disulphides, while most of the crosslinks are polysulphides (an average of 90.32%). The SEV-cured vulcanizate contains a more balanced structure with 0.98% of monosulphides, 44.77% disulphides and 54.25% polysulphides.

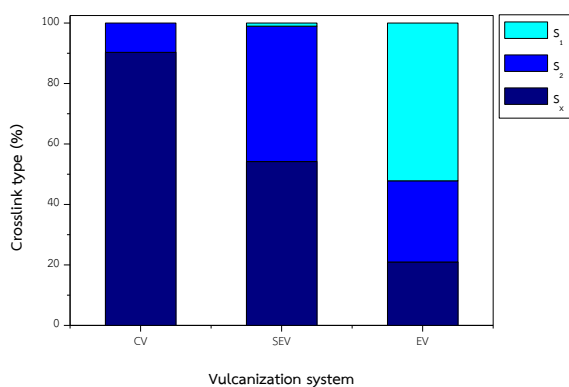


Fig. 1. The percentage of mono-, di- and poly-sulphidic crosslink of accelerated-sulphur vulcanized NR vulcanizates with different vulcanizing systems

3.2 WAXD patterns and scattering profiles

Ordinary 2D WAXD pictures can be changed to 3D WAXD by z-axis as the relative intensity of X-ray and the maximum intensity is colored as orange in each picture. In order to show the changes clearly during deformation, 3D images are tilted to 45 degree to the vertical line of the figure (In 2D expression, the stretching direction is vertical and SIC crystals align to the stretching direction completely). The stress-strain curves (up to the mechanical rupture point) and selected 3D WAXD patterns during deformation (at 10 mm/min rate) of NR vulcanizates with CV vulcanizing systems are shown in Fig. 2. Each WAXD image was taken at the strain indicated by the arrow. It is seen that stress generally increased with elongation for all samples.

3D WAXD patterns exhibited an amorphous halo at strain below 3.0. At strain 4.0, the several weak but distinct crystalline reflections were seen. These reflections appeared in smaller numbers than in the fully crystallized patterns (e.g. at strain 5.0). These reflections are caused by the first-formed strain-induced crystallites. By contrast, at strains above 5.0 (e.g. strain 6.0 and 7.0), the WAXD patterns exhibited clear oriented crystalline reflections from a monoclinic unit cell with crystal dimension, $a=1.25$ nm, $b=0.89$ nm, $c=0.81$ nm, and $\gamma=92^\circ$, as previously reported by Bunn [40-41]. It is interesting to see that, even at high elongation or at the breaking point, the non-oriented amorphous halo still persists, which is consistent with the previous finding that a substantial amount of amorphous chains remain unstretched even at high extension [34,42-43]. This result means that molecules in the amorphous part did not orient much and most of the rubber chains remained random in direction. Moreover, the fraction of unoriented crystallites is negligible because no circle patterns can be observed except for the amorphous halo for every vulcanizing system.

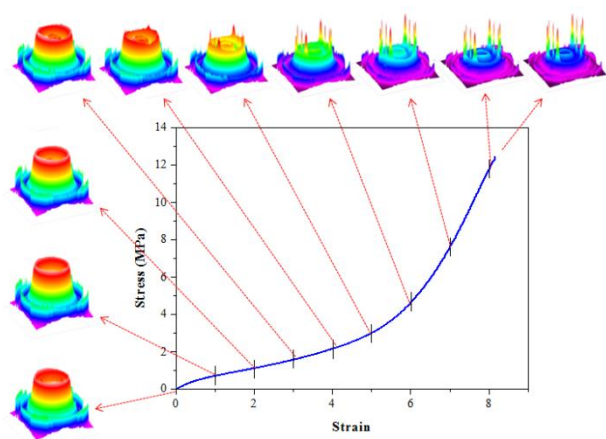


Fig. 2. Stress-strain curve and selected WAXD patterns in 3D expression of CV-NR. Each image was taken at the strain indicated by the arrows

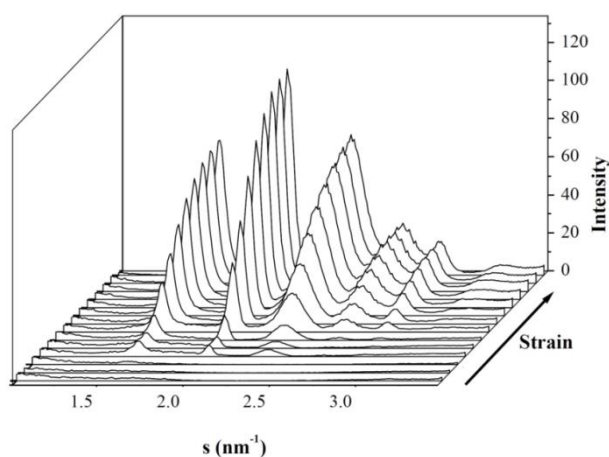


Fig. 3. Integrated WAXD intensity profiles as a function of scattering vector “s” of NR vulcanizates with CV vulcanizing system

The integral intensities as a function of scattering vector “s” at each strain are shown in Fig. 3. It is clear that the reflection intensities increase with strain smoothly up to the mechanical rupture point. All vulcanizing systems exhibited the similar tendency. However, the reflection intensities were slightly different. These indicate that the anisotropic fraction of NR vulcanizates with three vulcanizing systems may be different. Mass fractions will be discussed later.

3.3 The amount of strain-induced crystalline fraction

Crystalline and oriented amorphous fractions were determined from the one-dimensional integrated profiles

of the WAXD. The detail of the calculation is explained earlier. Crystalline fraction increases with strain during deformation and the oriented amorphous fraction does not increase significantly as shown in Fig. 4. The oriented amorphous seems to be a precursor of strain-induced crystals. The remaining un-oriented amorphous is around 80%. This value coincides with previous literatures [15,17-18,43]. Oriented amorphous fraction is much smaller than crystalline fraction and all the samples show the same tendency, therefore we focus on crystalline fraction hereafter.

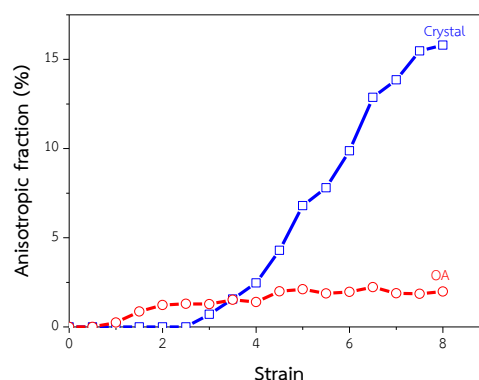


Fig. 4. Anisotropic fraction: crystal (Crystal: □) and oriented amorphous (OA: ○) at varying strains of CV-cured NR vulcanizate

The crystalline fractions of NR vulcanizates cured with CV, SEV and EV vulcanizing systems during deformation are shown in Fig. 5. The crystal fractions of them start to increase at strain around 2.5. The progress of SIC formed are not linear but are S-shaped curves, which are consistent with the results reported by Tosaka and coworkers [18,21]. Different crosslink structures with almost the same total crosslink density show similar behavior of crystal fraction during deformation. Polysulphide rich shows lower crystal fraction at small strain and reach the highest crystal fraction at the strain at break, compared to EV and SEV. The three crystal fractions seem to reach saturated level at large strain. Polysulphidic crosslink may decrease the stress (or strain) concentration to the local area by their flexibility to delay SIC at small strain and create more SIC at the strain at break.

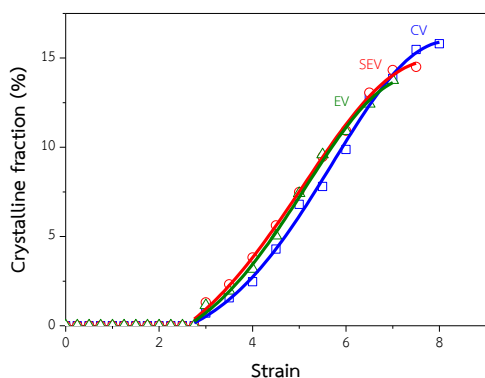


Fig. 5. Crystalline fraction at varying strains of CBS-accelerated NR cured with different vulcanizing systems

3.4 On-set and rate of strain-induced crystallization

The onset of strain-induced crystallization is the strain at which the crystalline reflections in the integrated profile begins to appear. The values of the onset strain at which SIC begins to form as a function of vulcanizing systems are plotted in Fig. 6. It can be seen that the onsets of SIC exhibited by NR vulcanizates cured with SEV and EV systems occurred at the same strain of 2.24. For the CV-cured NR vulcanizate, SIC occurred at a higher strain of 2.63. The delay in SIC exhibited by the CV-cured vulcanizate is probably due to the presence of high percentage of polysulphidic crosslinks in this rubber sample, making alignment of the NR molecules taken at higher strains.

The crystallization rate reflects a relative SIC rate as described earlier. Similarly to the effect of crosslink type on the onset of SIC, the crosslink type was found to have an influence on the rate of SIC as shown in Fig. 6. The rate of SIC was found to be slightly higher for the CV-cured sample than for the SEV-cured or the EV-cured counterparts. In general, the rate of SIC showed the decrease with increasing monosulphidic crosslinks. Perhaps, the short monosulphidic crosslinks, or disulphidic crosslinks for the same reason, restrict movement of the rubber chains, therefore, has a retarding effect on crystallization process.

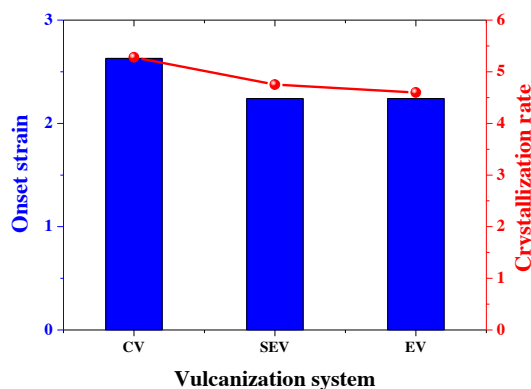


Fig. 6. Onset strain at which SIC occurred and crystallization rate for CBS-cured NR vulcanizates cured with different vulcanizing systems

For the effects of sulphur crosslink types, mono-, di- and poly-sulphidic crosslinks, which are different in length on SIC, the results revealed that SIC takes place easier with short sulphur crosslinks (mono- and di-sulphidic crosslinks) as were seen from the strains at which SIC begin and also the crystallization rate. However, long crosslinks (polysulphidic) allow the greater formation of the crystalline fraction (15.8% for polysulphidic crosslink V.S. 13.8 and 14.5% for mono- and di-sulphidic crosslinks) and hence higher tensile strength exhibited by the CV-cured samples. The well-known higher tensile strength of the CV-cured rubber vulcanizates compared with the EV-cured and the SEV-cured vulcanizates may, thus, be attributed to the ability to form the larger crystalline fraction of the former which also gives rise to the possibility of developing the greater level of orientation in the sample, leading finally to high strength.

4. Conclusion

The onsets of SIC occurred at the strain of 2.24 for NR vulcanizates which contain mainly monosulphidic and disulphidic crosslinks. For the vulcanizate of which is dominated by polysulphidic type, SIC began to appear at the higher strain of 2.63. The rate of SIC was found to be slightly higher for the NR vulcanizate which contains a large amount of polysulphidic crosslinks than for the samples which contain mainly monosulphidic and disulphidic crosslinks. The vulcanizate that was

crosslinked mainly by polysulphidic crosslinks exhibited the smaller development of crystallinity during deformation than those that contain the majority of disulphidic and monosulphidic crosslinks but the final crystalline fraction at the rupture point was higher.

Acknowledgement

The author would like to express his gratitude to SKRU and MU for financial support throughout this work and the National Synchrotron Light Source (NSLS), Brookhaven National Laboratory (BNL), New York, USA for synchrotron WAXD measurement facility.

References

- [1] Gent AN. *Engineering with rubber*, Oxford University Press, Oxford, U.K., 1992.
- [2] Cunneen JI, Russell RM. *Rubber Chem. Technol.* 1970, 43, 1215.
- [3] Saville B, Watson AA. *Rubber Chem. Technol.* 1967, 40, 100.
- [4] Nakauchi H, Utsunomiya T, Masuda K, Inoue S, Naito K. *Nippon Gomu Kyoukaishi*, 1987,60, 267.
- [5] Ikeda Y, Higashitani N, Hijikata K, Kokubo Y, Morita Y, Shibayama M, Osaka N, Suzuki T, Endo H, Kohjiya S. *Macromolecules*, 2009, 42, 2741.
- [6] Ikeda Y, Yasuda Y, Hijikata K, Tosaka M, Kohjiya S. *Macromolecules*, 2008, 41, 5876.
- [7] Treloar LRG. *The physics of rubber elasticity*. Re-published Oxford University Press: Oxford, U.K., 2005.
- [8] Boyce MC, Arruda EM. *Rubber Chem Technol.* 2000, 73, 504.
- [9] Ito M, Takizawa A. *Kautsch Gummi Kunst KGK*, 2012, 65, 24.
- [10] Toki S, Takagi R, Ito M, Hsiao BS. *Polymer*, 2011, 52, 2453.
- [11] Posadas P, Malmierca MA, González-Jiménez A, Ibarra L, Rodríguez A, Valentin JL, Nagaoka T, Yajima H, Toki S, Che J, Rong L, Hsiao BS. *eXPRESS Polymer Letters*, 2016, 10, 2.
- [12] Suzuki N, Ito M, Yatsuyanagi F. *Polymer*, 2005, 46, 193.
- [13] Katz JR. *Naturwissenschaften*, 1925, 13, 410.
- [14] Clark GL, Wolthuis E, Smith WH. *J. National Bureau. Standard*, 1937, 19, 479.
- [15] Toki S, Sics I, Ran S, Liu L, Hsiao BS, Murakami S, Senoo K, Kohjiya S. *Macromolecules*, 2002, 35, 6578.
- [16] Karino T, Ikeda Y, Yasuda Y, Kohjiya S, Shibayama M. *Bio-macromolecules*, 2007, 8, 693.
- [17] Trabelsi S, Albouy PA, Rault, J. *Macromolecules*, 2003, 36, 7624.
- [18] Tosaka M, Murakami S, Poompradub S, Kohjiya S, Ikeda Y, Toki S, Sics I, Hsiao BS. *Macromolecules*, 2004, 37, 3299.
- [19] Che J, Burger C, Toki S, Rong L, Hsiao BS, Amnuayporn Sri S, Nimpai boon A, Sakdapipanich, J. *Macromolecules*, 2012, 45, 6491.
- [20] Toki S, Sics I, Hsiao BS, Murakami S, Tosaka M, Poompradub S, Kohjiya S, Ikeda Y. *J. Polym. Sci., Polym. Physics ed.* 2004, 42, 956.
- [21] Tosaka M, Senoo K, Sato K, Noda M, Ohta N. *Polymer*, 2012, 53, 864.
- [22] Toki S, Hsiao BS, Amnuayporn Sri S, Sakdapipanich J. *Polymer*, 2009, 50, 2142.
- [23] Amnuayporn Sri S, Toki S, Hsiao BS, Sakdapipanich J. *Polymer*, 2012, 53, 3325.
- [24] Toki S, Che J, Rong L, Hsiao BS, Amnuayporn Sri S, Nimpai boon A, Sakdapipanich, J. *Macromolecules*, 2013, 46, 5238.
- [25] Sainumsai W, Toki S, Amnuayporn Sri S, Nimpai boon A, Sakdapipanich J, Rong L, Hsiao BS, Suchiva K. *Rubber Chem Technol.* 2017, 90, 728.
- [26] Candau N, Lagmach R, Chazau L, Chenal JM, Gauthier C, Biben T, Munch E. *Macromolecules*, 2014, 47, 5815.
- [27] Minouchi N. *Nippon Gomu Kyoukaishi*, 2004, 77, 235.
- [28] Toki S, Minouchi N, Sics I, Hsiao BS, Kohjiya S. *Kautsch Gummi Kunst KGK*, 2008, 61, 85.
- [29] Flory PJ, Rehner J. *J. Chem. Phys.* 1943, 11, 521.
- [30] Flory PJ. *J. Chem. Phys.* 1950, 18, 108.
- [31] Brydson JA. *Rubber Chemistry*, Applied Science Publishers Ltd., London, 1978.
- [32] Mitchell JC, Meier DJ. *J. Polym. Sci. A-2*, 1968, 6, 1689.

- [33] Studebaker MI, Nabors LG. *Rubber Chem. Technol.* 1959, 32, 941.
- [34] Bateman L, Cunneen JI, Moore CG, Mullins L, Thomas AG. In: L. Bateman (Ed.), *The chemistry and physics of Rubber-like substances*, Maclaren, London, 1963.
- [35] Lal J. *Rubber Chem. Technol.* 1970, 43, 664.
- [36] Baldwin FP, Ver Strate G. *Rubber Chem. Technol.* 1972, 45, 709.
- [37] Gonzalez L, Valentin JL, Fernandez-Torres A, Rodriguez A, Marcos-Fernandez A. *J. Appl. Polym. Sci.* 2005, 98, 1219.
- [38] Bruzzone M, Carbonaro A, Gargani L. *Rubber Chem. Technol.* 1978, 51, 907.
- [39] Valle LFR, Gargani L. *Rubber Chem. Technol.* 1978, 51, 863.
- [40] Bunn CW. *Proc. Roy. Soc. A*, 1941, 180, 40.
- [41] Boochathum P, Chiewnawin S. *Eur. Polym. J.* 2001, 37, 429.
- [42] Toki S, Sics I, Ran S, Liu L, Hsiao BS *Polymer*, 2003, 44, 6003.
- [43] Toki S, Sics I, Ran S, Liu L, Hsiao BS, Murakami S, Tosaka M, Kohjiya S, Poompradub S, Ikeda Y, Tsuo AH. *Rubber Chem. Technol.* 2004, 77, 317.

Effect of Maturation and Compounding Latex on Properties of Nitrile Latex Gloves

Siri Krirkmanee¹ Ittipol Jangchud¹, Suchet Khaenyook², and Suparat Rukchonlatee^{1,3*}

¹Department of Chemistry, Faculty of Science, King Mongkut's Institute of Technology Ladkrabang (KMITL), Bangkok, 10520, Thailand

²Department of Continuous Improvement, Ansell (Thailand) Co., Ltd., Bangkok, 10520, Thailand

³Polymer Synthesis and Functional Materials Research Unit, Faculty of Science, KMITL, Bangkok, 10520, Thailand
Phone +66 2329 8000 ext. 6251, Fax +66 2329 8428, *E-Mail: suparat.ru@kmitl.ac.th

Abstract

Compounding and maturation are ones of the most important steps in rubber latex manufacturing process. Those steps affect not only rubber properties but also processing time and %defective products. In this work, some effects of compounding and maturation of acrylonitrile butadiene rubber (NBR) latex on glove properties were studied. Properties of nitrile latex compound during maturation were monitored every 24 hours until 96 hours including pH, %coagulum and morphology of coagulum particles. Glove samples were prepared by coagulation of the nitrile latex compound using coagulant dipping process. Properties of nitrile gloves were studied including %swelling, pre-vulcanized relaxed-modulus (PRM), tensile strength and rubber modulus. It was found that pH slightly decreased while %coagulum slightly increased with maturation time. As maturation time was increased, %swelling of nitrile latex films reduced while PRM and tensile properties had trends to increase. These results corresponded to the increase of crosslinked rubber molecules. It was found that tensile properties of nitrile gloves were not significantly changed after 48 hours maturation time. This implied that over-matured nitrile latex compound could cause poor film formation. It was confirmed that maturation time of nitrile latex compound played a major role on the film formation and in-turn controlling rubber desirable properties.

Keywords: Nitrile latex compound, Maturation time, Nitrile gloves

1. Introduction

The present worldwide demand for the synthetic gloves continues to grow due to viral outbreaks and pandemics [1]. Switch from natural rubber to synthetic rubbers has been particularly evident in medical, examination, investigation and diagnosis gloves. The aim has been to avoid the risk of type-I hypersensitivity associated with natural rubber [2]. Synthetic nitrile gloves are an alternative ideal when latex allergies are of concern. Therefore, nitrile latex is a popular choice in the gloves industry. Manufacturing process of nitrile gloves is a multi-stage process including mainly latex compounding, maturation, dipping, testing and packing. Latex compound maturation is one of the most important aspects in manufacturing latex products [3]. There has been an issue of excessive amount of time used for target compound

maturation in the production of nitrile gloves. It results in over capability of tank stirrer and also lengthen the time used for production of nitrile gloves. In previous work [3], effect of maturation on properties of NR latex compounds was studied. It was found that viscosity of latex compounds slightly increased but pH and ammonia content slightly decreased with time. Swelling ratio of latex film was slightly decreased with time up to 96 hours. Maturation allows sulfur to gradually react with rubber. During maturation latex particles were swollen due to crosslinking with sulfur, inclusion of compounding ingredients and/or breakdown in colloidal stability of the latex. Changes in average particle diameters of latex would generally be detected [4]. Ruslimie et.al [5] studied effect of pre-vulcanization time on the latex particles, surface morphology and strength of epoxidized natural rubber latex films. It was found that structure of the

pre-vulcanized latex particles was suspected to be reminiscent of the influx of vulcanizing reagents in the rubber particles. The influx of these reagents into the interior of the latex particles was deemed as a prerequisite for crosslinking. It was reported that during pre-vulcanization, rubber molecules crosslinking activity had taken place inside discrete rubber particles dispersed in the aqueous phase. In this work, effects of maturation time of NBR latex in glove manufacturing process were carried out to monitor optimum processing properties and good properties of finished products.

2. Experimental Methods

2.1 Materials

Latex proprietary formula was shown in Table 1. Acrylonitrile butadiene latex (Nipol[®]), the total solid content (TSC) of the latex was 45% wt. Other compounding ingredients were commercial grade and used as received. Dispersions of 50% sulfur, 50% ZnO, accelerator and green pigment were provided by Ansell (Thailand) Co., Ltd.

2.2 Preparation of nitrile latex compound

Nitrile latex compound was prepared using a mixing tank with a batch size of 5,000 g. Nitrile latex was allowed to stir for 15 minutes with 5 rpm rotor speed. Other ingredients were slowly added as per amount required in formulation into latex under agitation and then allowed stirring for minimum 15 minutes. Compound was adjusted at a total solid content (TSC) of 35%wt with distilled water. After complete addition of each step, a homogeneous mixture was achieved by continuously stirring at least 30 minutes.

2.3 Glove sample preparation

After compounding, NBR latex compound was used for glove preparation via continuously dipping process. First, formers were cleaned by dipping in hot water and then preheated before dipping in a coagulant solution tank. After drying, formers were dipped in nitrile latex compound tank. Then formers with gelled latex film underwent pre-leaching, beading and curing in an oven before powdering. Finally, NBR latex gloves were stripped

off the formers. The dipping process was repeated in the same NBR latex compound tank every 24 hours until 96 hours.

Table 1 Formula of nitrile latex compound

Materials	phr (dry wt.)
Nitrile raw latex	100
Stabilizer A	0.4
ZnO dispersion	1.6
Sulfur	1.0
Accelerators	1.7
Antioxidant	0.5
Stabilizer B	0.4
Green pigment	1.0

2.4 Characterization and testing

pH values of nitrile latex compound was measured with pH meter (Orion Star[™] A111), at room temperature.

Coagulum content was measured with mixing 100 ml nitrile latex compound with 5% sodium lauryl sulfate. The compound was then filtered through a nylon filter (200 mesh). Residue on the nylon filter was dried and calculated in terms of percentage to TSC of the sample latex according to the following equation (1).

$$\text{Coagulum content (\%)} = \frac{W_2 - W_1}{W_0 \times \%TSC} \times 1,000 \quad (1)$$

when W_0 is weight of the latex sample, W_1 is weight of nylon sieve (200 mesh), W_2 is weight of nylon sieve and dry coagulum.

Morphology of coagulum was revealed using a Scanning Electron Microscope (SEM) (Quanta[®] 250; FEI) at accelerating voltage of 25 kV. All samples were coated with gold prior to examination.

Determination of swelling index involved the immersion of 25.4 diameter disks of rubber film in a mixed solvent. First, a ceramic plate was dipped into the coagulant solution and removed slowly. Then, it was allowed to dry at room temperature for 1 minute, before dipping into nitrile latex compound for 18 seconds. The films were dried at 100 °C for 10 minutes and then cut with a hole punch diameter of 25.4 mm. The sample was immersed in a Petri dish having solvent mixtures (40% wt

chloroform/ 60%wt toluene) and allowed to swell for 15 minutes. Then the latex dish was carefully withdrawn from solvent and put into clean petri dish which was placed on graph paper to record the swollen latex sample size. Calculation of the percentage of swell index can be shown as equation (2)

$$\% \text{Swelling ratio} = \frac{(D_1 - D_0)}{D_0} \times 100 \quad (2)$$

when D_0 is the diameter of hole punch (25.4 mm) and D_1 is the diameter of swollen latex films.

PRM test has been described the degree of nitrile latex prevulcanization by measurement of elastic tensile modulus at 100% extension of film dried down from nitrile latex [6]. Firstly, nitrile latex films were prepared using ceramic plate and allowed to dry at 70°C for 5 minutes. Nitrile film specimens were cut into size of 15×100 mm² and tested using a universal testing machine (UTM model 2519-104, Instron Co., Ltd.). Film specimens were stretched with a speed of 500 mm/min to 100% extension and held. After 1 minute the load in Newtons exerted by the film was recorded and then calculated for PRM.

Tensile properties of the gloves were also examined using UTM. The tensile properties including tensile strength, rubber modulus at 100%, 300% and 500% extensions were measured according to ASTM D412-15a with the gauge length of 25 mm.

3. Results and Discussion

3.1 pH of nitrile latex compound

Figure 1 presents pH of nitrile latex compound at ambient temperature with different maturation times. The pH of nitrile latex compound slightly decreased as the maturation time was increased from 0 to 96 hours. This might derive from ammonia evaporation during maturation. As the manufacturing process is controlled pH in the range of 9.50-10.80, thus the reduction of pH should not be significantly affected the process.

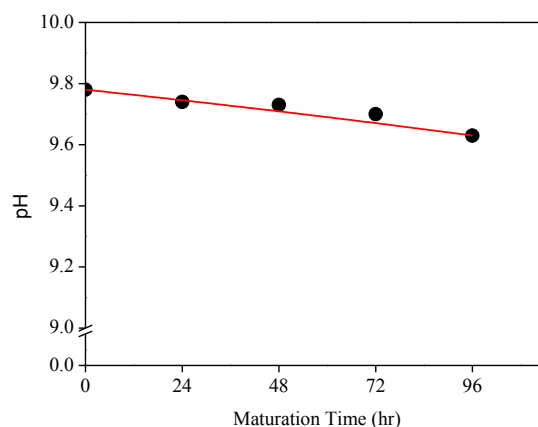


Figure 1 Effect of maturation time of nitrile latex compound on pH at ambient temperature

3.2 Coagulum of nitrile latex compound

As seen in Figure 2, %coagulum of nitrile latex compound increased from 0.0024 to 0.0066 % with increasing maturation time from 0 to 96 hours. This derived from prevulcanized nitrile latex particles with vulcanizing agents. The enhanced solubility of sulfur and accelerator in the latex aqueous phase during maturation would facilitate sulfur prevulcanization. The important step of the reaction was the formation of sulfur-accelerator species in the aqueous phase of the latex. These species or their derivatives then transferred into the rubber phase and crosslinked rubber molecules therein. Moreover, the high shear force during maturation causing ammonia evaporation and destabilization of latex particles leading to coagulation of nitrile latex compound.

Figure 3 illustrates morphology of coagulum particles of nitrile latex compound. The coagulum particles show spherical shape and randomly distributed on nylon filter (200 mesh). The particle diameters of coagulum were about 70 to 80 μm. During maturation the latex particles were swollen due to crosslinking with sulfur, inclusion of compounding ingredients and/ or breakdown in colloidal stability of the latex.

3.3 Solvent swelling of nitrile latex films

Solvent swelling is a measurement of the effect of the solvent mixtures, resulting change in volume of latex film which is exposed to solvents [7].

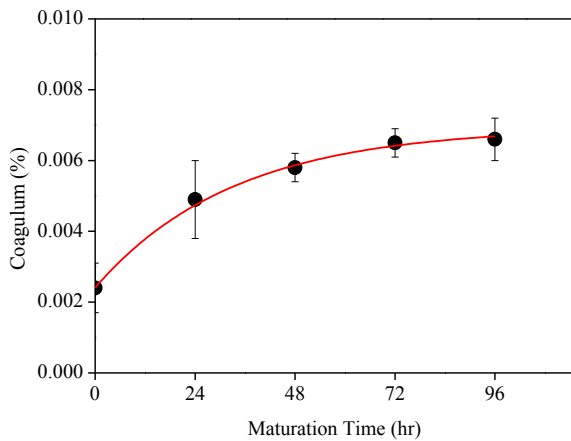


Figure 2 Effect of maturation time of nitrile latex compound on percentage of coagulum

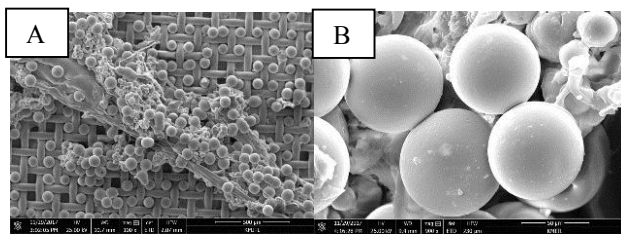


Figure 3 SEM images of coagulum particles of nitrile latex compound; (A) 100X, and (B) 900X. The scale bar represents 500 μm and 50 μm respectively

Figure 4 shows the %swelling at ambient temperature. The latex film without maturation at (0 hour) was discarded as it was, while the %swelling of latex film was slightly decreased with increasing maturation times (24 to 96 hours). By increasing maturation time, vulcanizing agents were allowed to gradually react with rubber molecules. Thus, the rubber chains were chemically crosslinked together and restricted the diffusion of solvent molecules. During solvent swelling in vulcanized rubber, diffusion of the solvent into rubber matrix expands the rubber network and thus weakens the molecular interaction between chains. Therefore, the results indicated an increase in crosslink formation after 24 hours while the crosslink formation after 48 hours maturation is slightly altered.

3.4 PRM of nitrile latex films

Figure 5 shows that the pre-vulcanized relaxed-modulus (PRM) of nitrile latex film slightly increased with

longer maturation time. The highest PRM value of 0.7734 MPa was at 96 hours maturation. The longer the maturation time, the greater the stage of pre-vulcanized rubber corresponding to % coagulum and swelling results.

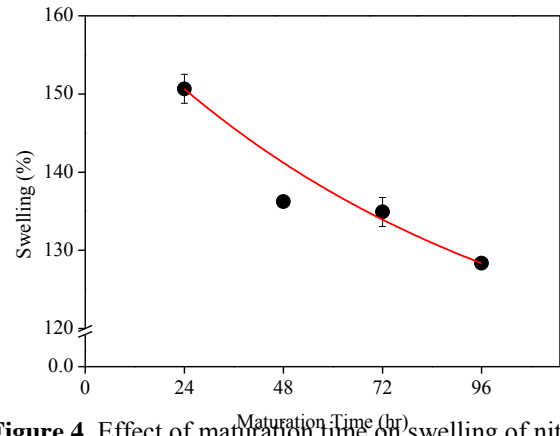


Figure 4 Effect of maturation time on swelling of nitrile latex films

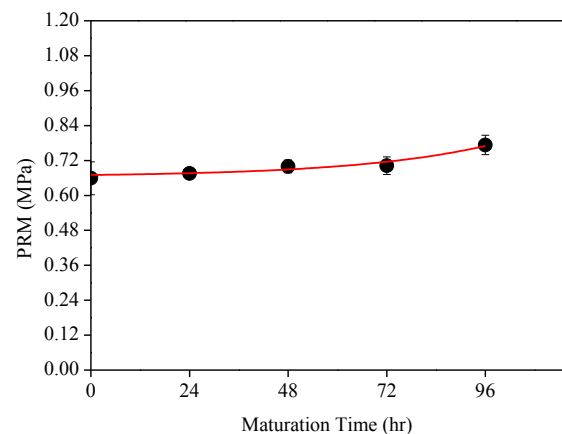


Figure 5 Effect of maturation time of nitrile latex films on pre-vulcanized relaxed-modulus (PRM)

3.5 Tensile properties of nitrile latex gloves

Tensile strength of nitrile latex gloves at different maturation times is illustrated in Figure 6. The tensile strength increased with increasing maturation times and then, after 48 hours maturation time, the tensile strength was insignificantly changed. It is probably a consequence of decreasing ability of latex particles to coalesce and fully integrate as the concentration of crosslinks in the latex particles increased. Moreover, the partially vulcanized particles might retard the diffusion of the rubber molecules and thus hindered further gradual coalescence of the latex particles in the films. Hence the nitrile latex film surface remained rough and uneven for the highly crosslinked

latex films. Similar trends were also observed for rubber modulus at 100% and 300% extensions (Figure 7).

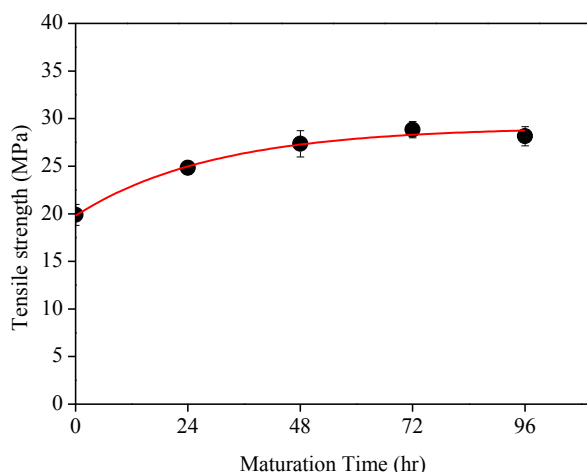


Figure 6 Tensile strength of nitrile latex films with different maturation times

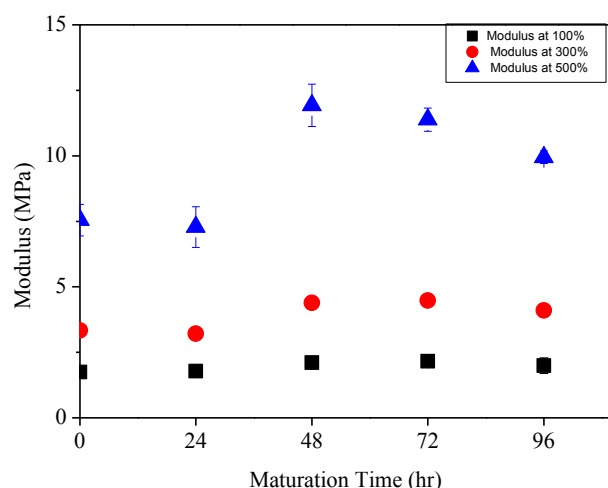


Figure 7 Modulus at 100%, 300% and 500% extensions of nitrile latex films with various maturation times

Effects of maturation time of the nitrile latex compound on rubber modulus can be clearly seen at 500% extension as the rubber modulus decreased after 48 hours maturation time (Figure 7). This implies that the over-matured nitrile latex compound could cause poor film formation. Thus, tensile properties were decreased after an optimum maturation time.

4. Conclusion

It can be seen that pH of nitrile latex compound slightly decreased with time. The percentage of coagulum of latex compound slightly increased with time. Nitrile latex particles were prevulcanized with vulcanizing agent leading to swelling of latex particles and coagulation of nitrile latex compound. Percentage of swelling of nitrile latex films reduced while PRM and tensile properties results showed increment as maturation time was increased. However, after 48 hours maturation time, the tensile strength was not significantly changed. Over matured nitrile latex compound could cause poor film formation. Thus, it could be suggested that 48 hours maturation time in this work was adequate to achieve the effective crosslinking in nitrile latex gloves.

Acknowledgement

Authors would like to thank Department of Chemistry, Faculty of Science, King Mongkut's Institute of Technology Ladkrabang (KMITL) and Ansell (Thailand) Co., Ltd. for their supports.

References

- [1] Cabanes, N., Lgea, J.M. and Hoz, B., "Latex Allergy", *Journal of Investigational Allergology and Clinical Immunology*, 22: 313-330 (2012)
- [2] Akabane, T. "Production method & market trend of rubber gloves", *Nippon Gomu Kyokaishi*, 9: 369-373 (2015).
- [3] Chaowanich, C. and Nitthi-uthai, N., "Effect on maturation time on properties of latex compound", *Thailand materials science and technology conference*, Bangkok, National Metal and Materials Technology Center, (2005).
- [4] Myers, M.E., Wims, A.M. and Lee, W.R. "Latex maturation studies by low angle light scattering photometry", *Rubber Chemistry and Technology*, 46: 464-469 (1973).
- [5] Ruslimie, C.A., Norhanifah, M.Y., Fatimah Rubaizah, M.R., and Asrul, M. "Effect of Pre-vulcanisation Time on the Latex Particles, Surface Morphology and Strength of

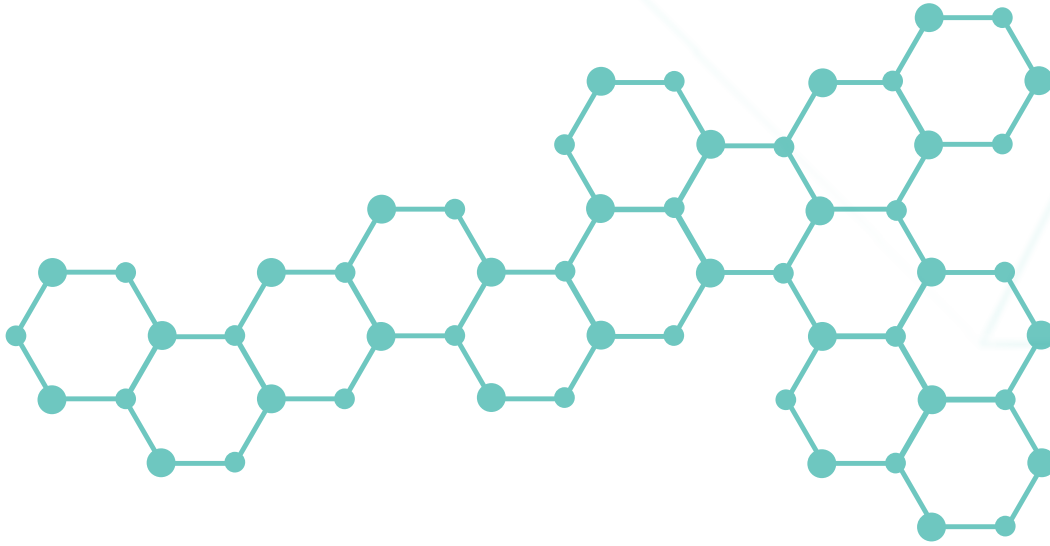
Epoxidised Natural Rubber Films”, *In International Conference on Chemical*, 3: 64-69 (2015).

[6] Blackley, D.C. “Method for assessing the degree of vulcanization of prevulcanized natural rubber latex”, *Polymer Latices Science and Technology*, London, Chapman and Hall : 450-453 (1997).

[7] Porter, M., Rawi, R. and Rahm, S.A., “Chemistry of the Latex Pre Vulcanisation Process”, *Journal of Natural Rubber Research*. 7: 85 – 101 (1992).

COMP

POLYMER BLENDS AND COMPOSITES



Effects of Fiber Surface Modifications on Mechanical Properties of Pineapple Leaf Fiber -**Acrylonitrile Butadiene Styrene (PALF-ABS) Composites**

Nanthaya Kengkhetkit¹, Taweechai Amornsakchai², Pornsawan Amornsakchai³ and Thanita Boonmee⁴

¹Faculty of Science and Agricultural Technology, Rajamangala University of Technology Lanna, Phitsanulok Campus, Muang, Phitsanulok 65000, Thailand

²Center of Sustainable Energy and Green Materials, Department of Chemistry and Center of Excellence for Innovation in Chemistry, Faculty of Science, Mahidol University, Phuttamonthon 4 Road, Salaya, Nakhon Pathom 73170, Thailand.

³Faculty of Liberal Arts, Rajamangala University of Technology Rattanakosin, Salaya Campus, Salaya, Nakhon Pathom 73170, Thailand.

⁴Science Lab Center, Faculty of Science, Naresuan University, Muang, Phitsanulok 65000, Thailand
Phone: +66 (0) 5529-8437, Fax: +66 (0) 5526-2789, E-Mail: nanthaya@rmutl.ac.th

Abstract

In this work the effects of surface modifications on the mechanical properties of pineapple leaf fiber (PALF) - acrylonitrile butadiene styrene (PALF-ABS) composites were investigated. The results show that fiber surface modifications is dramatically affected on the improvement in mechanical properties of ABS composites. Composite with UPALF display only increase in tensile modulus while that with TPALF show the improvement both in tensile and flexural properties, especially in its strengths, due to the presence of higher fraction of fine fiber and fibrillated bundles. However, significant improvement in tensile and flexural properties of PALF-ABS composite was found when using benzene diazonium salt treatment for PALF. Composite with TBZDA has greater mechanical properties than that of UPALF and TPALF systems. SEM of fracture surface, and heat distortion temperature of some systems will be presented.

Keywords: pineapple leaf fiber, acrylonitrile butadiene styrene, benzene diazonium salt treatment

1. Introduction

An awareness of the impacts of climate change and the consequent need to reduce CO₂ emissions requires a greater focus on environmentally-friendly products [1]. These demands have led to the current trend for composites to be focused on bio-based materials. Many natural fibers such as sisal, flax, jute, coir, oil palm, silk, banana fiber and pineapple leaf fiber (PALF) have been studied for use as reinforcements in composite materials [2-4].

Acrylonitrile butadiene styrene (ABS) is a thermoplastic terpolymer made by polymerizing styrene

and acrylonitrile in the presence of polybutadiene. The properties are created by rubber toughening, where fine particles of elastomeric are dispersed throughout the rigid matrix. Normally, ABS can be used between 20 and 80°C as its mechanical properties vary with temperature [5]. ABS is a widely used engineering thermoplastic due to its good mechanical properties, chemical resistance, toughness, dimensional stability, good surface appearance, and easy processing characteristics [6-9]. ABS also has some limitations like low thermal stability, poor flame resistance, and low mechanical properties compared to other engineering plastics. Many works showed the

improvement of ABS performance by addition of inorganic materials like glass fiber [8,10] or nano-fillers [7, 11–12]. Some works have also studied ABS composites with natural fiber such as kenaf [13], plam fiber [14], cotton fiber [15], broom fiber [16] and hemp fiber [16].

For Thailand, pineapple is one of the most important commercial crops. After harvesting, a large amount of pineapple leave waste are left largely unused in the field. Recently the work in our laboratory has shown that high quality short PALF can be separated from pineapple leaves by using a simple method [17]. The PALF from this method has higher fraction of elementary fiber and defibrillated bundle than that obtained from other conventional methods. The reinforcement effectiveness of this PALF has been demonstrated [17-24]. However, to achieve the great reinforcement effectiveness, the interfacial adhesion between hydrophobic matrix and hydrophilic PALF should be improved. In this work, short PALF reinforced ABS composites containing 20% w/w of PALF were studied. Three types of PALF were used, i.e. untreated as-prepared PALF (UPALF) and sodium hydroxide washed PALF (TPALF) and benzene diazonium salt (TBZDA). Effect of surface modification methods on mechanical properties of the composites was investigated. The tensile flexural and impact measurements were used to evaluate the mechanical properties of PALF-ABS composites. SEM of fracture surface and heat distortion temperature of some systems will be also investigated.

2. Experimental Methods

2.1 Materials

2.1.1 Polymer Matrix

Acrylonitrile Butadiene Styrene; ABS (POLYLAC@PA717C) was obtained from Chi Mei Corporation. The density and melt flow index of this polymer matrix are 1.04 g/cm³ and 1.3 g/10 min, respectively.

2.1.2 PALF Separation

Fresh pineapple leaves were collected from cultivation areas in the Kok Kwai District, Amphor Ban Rai, Uthai Thani Province, Thailand. PALF was separated from pineapple leaves using disc-milling method in our laboratory [17] resulting in a range of diameter and an average diameter of 3-68 μm and 18.70 μm, respectively [17].

2.2 PALF Surface Modification

NaOH pretreatment: Untreated PALF (UPALF) were soaked in 10 %wt sodium hydroxide solution at room temperature for 30 min, using a solution: fiber ratio of 30:1 (by weight). After treatment, fiber was washed with water until pH~7. The sodium hydroxide washed PALF (TPALF) was dried in hot air oven at 80 °C for 48 hrs.

Benzene diazonium salt treatment [25]: Benzene diazonium salt was synthesized by the standard diazotization method. The solution was kept in a freezer with maintaining temperature 0-5°C prior to the chemical treatment of PALF. TPALF was submerged in 5%NaOH solution and kept the mixtures in a freezer until the temperature of the mixture is about 0-5°C. A cooled solution of benzene diazonium salt was poured slowly into the mixture with constant stirring and kept for about 10 min. The treated fibers (TBZDA) were taken out, washed with soap solution followed by water and finally dried in hot air oven for 24hrs. The reaction scheme shows in Fig.1 as follow:

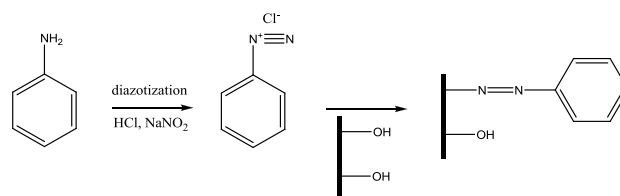


Fig. 1 Reaction scheme of benzene diazonium salt treatment [26]

2.3 Composite Preparation

ABS composites with 20% w/w of PALF were prepared in two steps. First, PP and fiber were melt mixed on a two roll mill for 30 min. The temperature of the front and back roll were 185°C and 175°C, respectively. The mixture was taken out with slight melt stretching while keeping the fiber orientation to form prepreg. The prepreg was then compression molded to form a uniaxial composite sheet of 1 and 3 mm thickness at a temperature of 185°C under a pressure of 500 psi for 5 min, followed by cooling under the pressure of 1,000 psi for 5 min.

2.4 Characterization Techniques

Tensile testing was carried out on a universal testing machine (Instron 4469, High Wycombe, UK) with a 1 kN load cell. The specimen was cut along the fiber direction to a strip of 10 mm wide with a scroll saw. The gauge length was 50 mm and the extension rate was 5 mm/min. Secant modulus at 1% stain and tensile strength were determined.

Flexural testing was carried out by using a universal testing machine (Instron 4469, High Wycombe, UK) at a strain rate of 1.28 mm/min with load cell at 1 kN. The specimens were 80 mm length, 10 mm width and 3 mm thickness. The span length was 48 mm. Flexural modulus and flexural strength were determined at 1% and 5% strain, respectively.

The impact strength, fracture initiation energy and fracture propagation energy were measured on a notched Izod impact testing machine (Radmana ITR-2000, McVan Instruments, Australia). The impact specimens were 60 mm length, 12 mm width and 3 mm thickness. The samples were notched with a Davenport notch cutting apparatus to a depth of about 1.3 mm.

The reported values of tensile properties, flexural properties and impact properties were averaged from five specimens

The heat deflection temperature (HDT) was measured by a DMA (Q800, TA Instruments, USA) with the three-point bending mode. The specimens used for this analysis were 50 mm length, 12 mm width and 3 mm thickness. The specimens were heated at the rate of 2° C /min from 35 to 160° C under a constant load of 0.455 MN/m² and the HDT was determined as the temperature at which the specimen deflection reached 0.25 mm.

The morphology of some treated PALF was observed with a scanning electron microscope (SEM) (S2500, Hitachi, Japan). Impact fracture morphology of some composites system was also investigated with SEM (Hitachi Tabletop Microscope; model TM 1000, Japan).

3. Results and Discussion

The morphology of some treated PALF is shown in Fig.2. After washed with NaOH, the cementing substances are removed. TPALF (high magnification, Fig.2b)) shows clearly cleaner and rougher surface than UPALF (Fig. 2a). Moreover, TPALF (low magnification) has a higher fraction of thin fiber and fibrillated bundles. After benzene diazonium salt treatment, the surface morphology of TBZDA shows similar to that of TPALF.

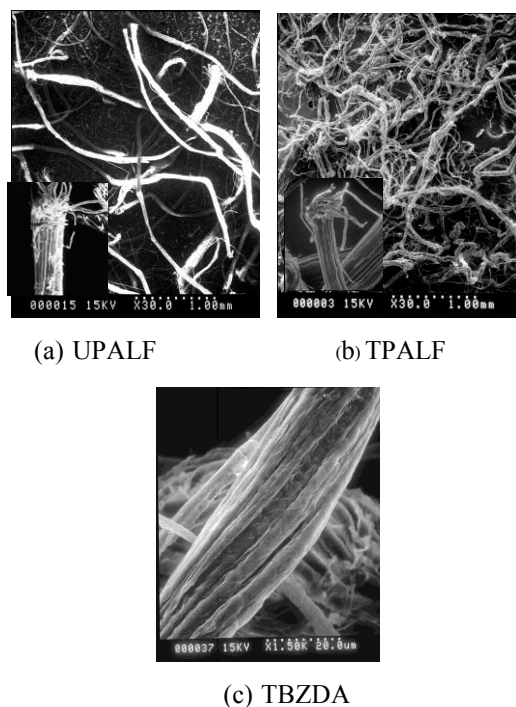


Fig. 2 SEM images of various PALF types

Fig.3 displays tensile properties of ABS composites.

The addition of UPALF in ABS composite strongly increases the tensile modulus but no improvement in tensile strength. However, due to the presence of fine fiber and fibrillated bundles, the use of TPALF as a reinforcing agent provides the superior strength performance than that of UPALF-ABS composite and neat ABS while no effect on tensile modulus. Interestingly, TBZDA-ABS composite provides the highest values of tensile modulus and strength.

The flexural properties of the ABS composites is shown in Fig.4. This result showed the little improvement in flexural modulus and strength when adding UPALF. The use of finer fiber like TPALF provides higher effectiveness. Moreover, using TBZDA in composite provides the greatest enhancement in flexural properties. This result showed that the great reinforcement effectiveness of TBZDA in ABS composites was found. This may be due to not only the presence of fine fiber and fibrillated bundles but also the increase of interfacial interaction between phenyl group of TBZDA and styrene group in ABS matrix.

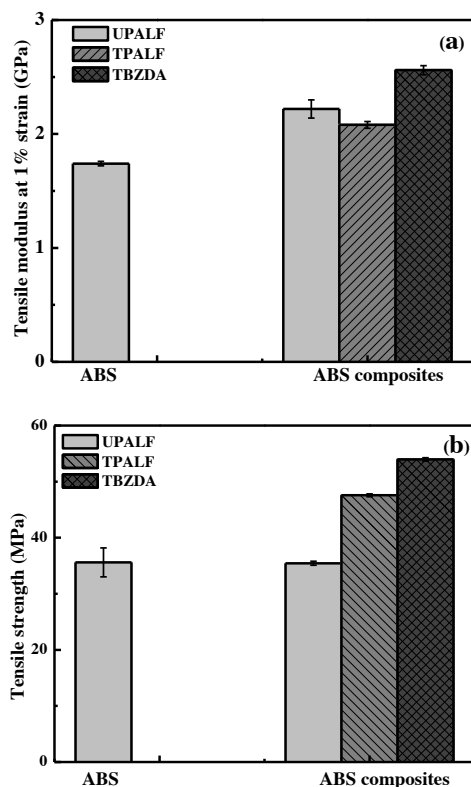


Fig. 3 Tensile properties of 20% PALF-ABS composites with various surface treatments

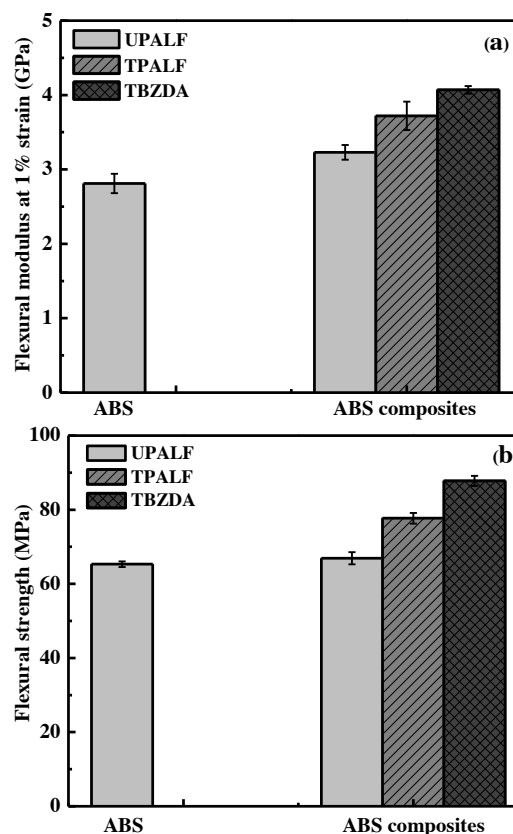


Fig. 4 Flexural properties of 20% PALF-ABS composites with various surface treatments

Fig. 5 shows the impact properties of PALF-ABS composite. Comparing with neat ABS, it is found that the impact strength of all types PALF-ABS composites decrease with the addition of PALF in the ABS. A dramatic drop has been observed in the both fracture initial energy and impact strength. It may be due to the addition of highly stiff fiber in the tough ABS matrix, the mechanism of energy absorption has changed. However, the reduction in impact strength normally observed on the addition of rigid fillers in to tough polymer matrix. The similar results have been observed by many works [11, 12].

From the SEM images in Fig.6 (a) and (b) show the impact fracture surfaces of TPALF-ABS composite and TBZDA-ABS composite, respectively. In the case of impact testing, the composites with too strong interfacial interaction makes the deformation and fracture mechanism change from fiber pull out Fig.6(a) to brittle fracture as clearly shown in Fig.6(b). The impact fractured surface of

TBZDA-ABS composite shown in Fig.6(b) reveals the smaller gap between fiber and matrix which indicates the more compatibility between TBZDA and ABS matrix when compared with TPALF-ABS composite (Fig.6(a)). It obviously displays the poor interfacial adhesion between TPALF and ABS matrix while clearly reveals ABS wetted on TBZDA surface. It indicates the strong interfacial adhesion formation which lead to good stress transfer between TBZDA and ABS matrix. It results in the great mechanical performances of TBZDA-ABS composite.

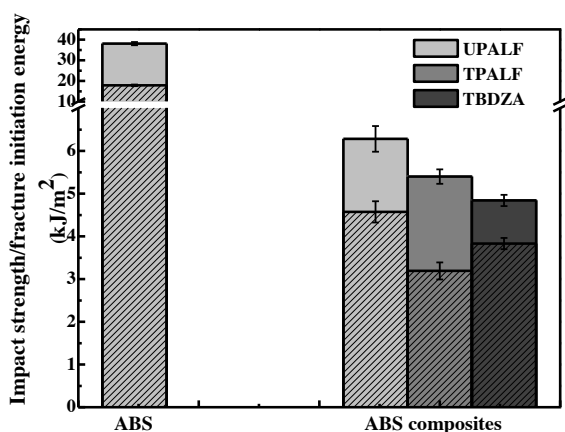


Fig. 5 Impact properties of 20% PALF-ABS composites with various surface treatments (The shaded and unshaded areas represent corresponding fracture initiation and fracture propagation energies of the composites, respectively.)

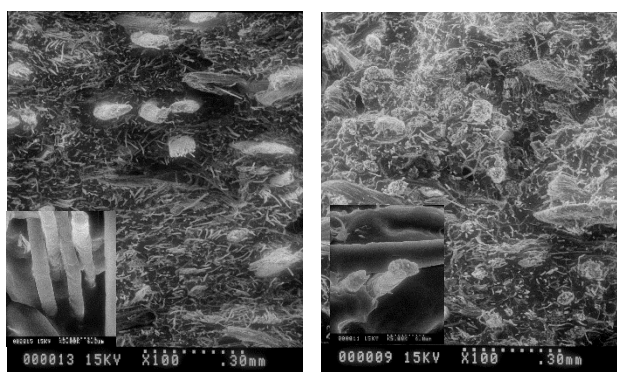


Fig. 6 SEM images of the impact fracture surface of PALF-ABS composites

Heat distortion temperature (HDT) of neat ABS and ABS composites is shown in Table 1. HDT refers to the polymer's ability to tolerate a standard load at elevated

temperatures. Normally, the HDT of neat ABS is approximately 87 °C. The addition of 20%w/w of PALFs, the HDT of all ABS composites is higher than that of neat ABS. This is due to the ability of fiber can retard the deformation of ABS chain at high temperature. Using finer fibers provide the little increase of HDT. However, the HDT of ABS composites is not affected by the types of treated PALF.

Table 1 Heat distortion temperature of ABS and ABS composites

PALF-ABS composites	HDT(°C)@ 0.455 MPa
Neat ABS	87.7±0.58
20UPALF	91.5±0.50
20TPALF	93.5±0.50
20TBZDA	93.3±0.87

4. Conclusion

From these results, it is shown that PALF can be used as a reinforcement for ABS matrix. Although, the use of UPALF studied show slight effect on composites properties. However, alkali treated PALF (TPALF) providing higher fraction of finer fiber, TPALF composite show higher properties than UPALF composite. Using benzene diazonium salt treatment provides the strong improvement in tensile and flexural properties. This can be attributed to higher fraction of fine fiber in the matrix and stronger TBZDA-ABS interfacial adhesion which is clearly seen in the SEM micrographs.

Acknowledgment

The authors gratefully acknowledge the financial supports of Rajamangala University of Technology Lanna (RMUTL) Phitsanulok, the Center of Excellence for Innovation in Chemistry (PERCH-CIC), Office of the Higher Education Commission and National Research Council of Thailand (NRCT).

References

- [1] Pervaiz, M. and Sain M.M., “Carbon storage potential in natural fiber composites”, *Resour. Conserv. Recycl.* 2003;39(4):325–340.
- [2] Mohanty, A.K., Misra, M., Drzal, L.T., Selke, S.E., Harte, B.R. and Hinrichsen, G., “Natural fibers, biopolymers, and biocomposites: an introduction”, In: Mohanty, A.K., Misra, M. and Drzal, L.T. (ed.s.) *Natural fibers, biopolymers, and biocomposites*. Boca Raton: CRC Press: 1–35 (2005).
- [3] Siqueira, G., Bras, J. and Dufresne, A., “Cellulosic bionanocomposites: a review of preparation, properties and applications”, *Polymers*. 2010;2:728–765.
- [4] Bledzki, A.K. and Gassan, J., “Composites reinforced with cellulose based fibres”, *Prog. Polym. Sci.* 1999; 24:221–274.
- [5] “Acrylonitrile Butadiene Styrene (ABS),” 2018. Available from: http://en.wikipedia.org/wiki/Acrylonitrile_butadiene_styrene [cited date: 27-4-2018]
- [6] Owen, R. S. and Harper, F. J., “Mechanical, microscopical and fire retardant studies of ABS Polymers”, *Polym. Degrad. Stab.* 1999;64:449–455.
- [7] Modesti, M., Besco, S., Lorenzetti, A., Causin, V., Marega, C., Gilman, W.J., Fox, M.D., Trulove, C.P., De Long, C. H. and Zammarano, M., “ABS/ clay nanocomposites obtained by a solution technique: influence of clay organic modifiers”, *Polym. Degrad. Stab.* 2007; 92:2206–2213.
- [8] Ozkoca, G., Bayramb, G. and Bayramlic, E., “Effects of polyamide 6 incorporation to the short glass fiber reinforced ABS composites: an interfacial approach”, *Polymer*. 2004;45:8957–8966.
- [9] Mantovani, L.G., Canto, B.L., Junior, H.E. and Pessan, A. L., “Toughening of PBT by ABS, SBS and HIPS systems and the effects of reactive functionalized copolymers”, *Macromol. Symp.* 2001;176:167–180.
- [10] Oriya, A. and Rajvaidya, R., “Characterization of ABS composites reinforced short glass fiber”, *IMPACT : IJRET*. 2015; 3(10): 35–42.
- [11] Pandey, A.K., Kumar, R., Kachhavah V.S. and Kar, K.K., “Mechanical and thermal behaviours of graphite flake reinforced acrylonitrile butadiene styrene composites and their correlation with entanglement density, adhesion, reinforcement and C factor”, *RSC Adv.* 2016, DOI: 10.1039/C6RA09236E.
- [12] Pour R.H., Hassan, A., Soheilmoghaddam M. and Bidsorkhi, H.C., “Mechanical, thermal, and morphological properties of graphene reinforced polycarbonate/acrylonitrile butadiene styrene nanocomposites”, *POLYM. COMPOS.* 2016;37:1633–1640.
- [13] Mohammad, N. N. B. and Arsad A., “Mechanical, thermal and morphological study of kenaf fiber reinforced rPET/ ABS composites”, *Malaysian Polymer Journal*. 2013;8(1):8–13.
- [14] Neher, B, Bhuiyan, M.M.R., Kabir, H., Qadir, M.R., Gafur, M. A. and Ahmed, F., “Study of mechanical and physical properties of palm fiber reinforced acrylonitrile butadiene styrene composite”, *Mater. Sci. Appl.* 2014;5: 39–45.
- [15] Martins. J.N., Klohn, T.G., Bianchi, O., Fiorio, R. and Freire, E., “Dynamic mechanical, thermal, and morphological study of ABS/textile fiber composites”, *Polym. Bull.* 2010; 64:497–510.
- [16] Durante, M., Leone, C., Ussorio, M. and Visconti, I.C., “Solution impregnation of natural fibres/ABS matrix composites”, In s Galiotis, C., (ed. s.) *Proceeding of European Conference on Composites Materials ECCM-11* Patras, Greece: 1–8 (2004).
- [17] Kengkhetkit, N. and Amornsakchai, T., “Utilisation of pineapple leaf waste for plastic reinforcement: 1. A novel extraction method for short pineapple leaf fiber”, *Ind. Crops Prod.* 2012;40:55–61.
- [18] Kengkhetkit, N. and Amornsakchai, T., “A new approach to “Greening” plastic composites using pineapple leaf waste for performance and cost effectiveness”, *Mater. Des.* 2014;55:292–299.
- [19] Kalapakdee, A. and Amornsakchai, T., “Mechanical properties of preferentially aligned short pineapple leaf fiber reinforced thermoplastic elastomer: effects of fiber content and matrix orientation”, *Polym. Test.* 2014;37:36–44.

[20] Prukkaewkanjana, K., Thanawan, S. and Amornsakchai, T., “High performance hybrid re-inforcement of nitrile rubber using short pineapple leaf fiber and carbon black”, *Polym. Test.* 2015;45:76–82.

[21] Wisittanawat, U., Thanawan, S. and Amornsakchai, T., “Mechanical properties of highly aligned short pineapple leaf fiber reinforced nitrile rubber composite: effect of fiber content and Bonding Agent”, *Polym. Test.* 2014;35:20–27.

[22] Wisittanawat, U., Thanawan, S. and Amornsakchai, T., “Remarkable improvement of failure strain of preferentially aligned short pineapple leaf fiber reinforced nitrile rubber composites with silica hybridization”, *Polym. Test.* 2014;38:91–99.

[23] Nopparut, A. and Amornsakchai, T., “Influence of pineapple leaf fiber and its surface treatment on molecular orientation in, and mechanical properties of, injection molded nylon composites” *Polym Test.* 2016;52:141–149.

[24] Panyasart, K., Chaiyut, N. and Amornsakchai, T. and Santawitee, O., “Effect of surface treatment on the properties of pineapple leaf fibers reinforced polyamide 6 composites” *Energy Procedia* 2014;56:406–413

[25] Kabir, M.A., Huque, M.M., Islam, M.R. and Bledzki, A.K., “Mechanical properties of jute fiber reinforced polypropylene composites: effect of chemical treatment by benzene diazonium salt in alkaline medium” *BioResources*, 2010;5:1618–1625.

[26] Ibrahim, M. “Preparation of cellulose and cellulose derivative azo compounds”, *Cellulose* 2002;9:337–349.

Effects of Type and Amount of Additives in Polypyrrole Composites on Metal Adsorption and Chemical Oxygen Demand Reduction

Aopeak Imvittaya¹, Neungrutai Saesaengseerung¹, Amornpon Changsuphan¹,

Panida Singra¹, Woraphong Janetanakit¹, Kamonrat Liabsiri^{1,2}, and Sirirat Sangkarak¹

¹Department of Science Service, Ministry of Science and Technology, Ratchathewi, Bangkok 10400, Thailand

²Department of Chemistry, Faculty of Science, Mahidol University, Bangkok 10400, Thailand

Phone +66 2201 7233, Fax +66 2201 7213, *E-Mail: aopeak@dss.go.th

Abstract

This work describes syntheses of polypyrrole (PPy) and its composites by chemical polymerizations of pyrrole monomers using iron (III) chloride as an initiator in aqueous solutions. Activated carbon (AC) and coconut fibers (CF) were used as additives in the composites. The PPy, the composites, and the raw materials including AC and CF were employed as adsorbents to remove heavy metal (copper ions) and chemicals in the synthetic wastewater. The effects of type and amount of additives in the composites on the efficiency of heavy metal and chemical oxygen demand (COD) reduction in the wastewater were investigated. Amounts of copper ions and COD values after treating the wastewater with the PPy and the raw materials were also determined and compared with the performance of the composites. The morphology and chemical structure of the PPy and the composites were characterized by using Scanning Electron Microscopy (SEM) and Fourier-Transform Infrared Spectroscopy (FTIR), respectively. Their thermal properties were also obtained by using Differential Scanning Calorimetry (DSC). The results indicate that the COD reduction efficiencies of the PPy, AC, and CF are approximately 60, 30, and 2% respectively. In addition, the AC and CF almost completely removed the copper ions from the wastewater, but the metal reduction efficiency of the PPy is less than 50%. The PPy-AC composites show the highest COD reduction efficiency up to about 75% and the highest metal reduction efficiency around 56%. Unlike the COD reduction efficiency, the higher the CF amount in the composite, the higher the copper removal efficiency.

Keywords: Polypyrrole, Conductive polymer, Composite, Metal adsorption, COD removal

1. Introduction

Wastewater is a main pollution found in many places all over the world, especially in the undeveloped and developing countries. Generally, wastewater treatment process can be classified into three main processes including physical, biological, and chemical treatment processes. These three processes have their limitations. The physical process cannot remove chemicals and heavy metals from the wastewater. The biological process takes

longer time than other processes, and some chemical compounds in the wastewater cannot degrade biologically.

For the chemical process, the chemicals used for the wastewater treatment are not only expensive, but also increase the chemical oxygen demand (COD) value in the wastewater.¹ Besides the three main wastewater treatment processes, there is also an effective one called physical-chemical process such as surface adsorption and ion exchange.²⁻⁴

Polypyrrole is one of well-known conducting polymers for a wide area of applications such as chemical sensors, polymeric batteries, surface coatings, electrochromic materials, electronic devices, and functional membranes, etc.²⁻⁵ Moreover, polypyrrole is also used for water treatment because of the ion exchange and adsorption properties.^{6,7} Many research studies focused on using conducting polymers and their composites for removing heavy metals and chemicals such as lead, nickel, cadmium, arsenic, chromium, iron, copper, hormones and dyes, from water.^{3,7}

An adsorbent mostly used for the water purification is activated carbon or activated charcoal. High porosity and surface area of the activated carbon facilitates the adsorption of molecules. Furthermore, biomass such as sawdust and rice husk ash is also used as an adsorbent to remove heavy metals and chemicals from water. This is caused by a variety of functional groups in their chemical structures (such as lignin and cellulose) which can form strong bonds with the molecules or ions in water.^{1,8}

This research project aims to develop the polymer composites from pyrrole monomers, activated carbon and coconut fibers for removing chemical compounds in order to decrease COD in the wastewater. Coconut fibers are used in the project because of its ready availability, abundance, and cost.

2. Experimental Methods

2.1 Materials

Pyrrole (Sigma-Aldrich, 98% purity), activated carbon (AC) (Merck, 99.96% purity), iron (III) chloride (Sigma-Aldrich, 97% purity), mercury (II) sulphate (Fisher Chemical, 99.3% purity), potassium dichromate (Merck, 99.96% purity), potassium hydrogen phthalate (KHP) (Merck, 99.97% purity), silver sulphate (Merck, 98.5% purity), sodium hydroxide (Merck, 99% purity), sulfuric acid (Lobachemie, AR grade, 98%), and nitric acid (Merck, Emsure ISO grade, 65%) were purchased. Milli-Q water was

used in all experiments. Coconut fibers (CF) were purchased from a local store, dried at 60 °C for 10 hours, ground prior to use.

2.2 Syntheses of polypyrrole and the composites

All syntheses were carried out at 20 °C for 3 hours by using iron (III) chloride as an initiator and Milli-Q water as a media. The mole ratio of pyrrole:iron (III) chloride used for all syntheses was 1:4.

For polypyrrole-AC composites, the weight ratio of pyrrole:AC was varied as follows 4:1, 1:1, 1:4, and 1:9. However, the weight ratio of pyrrole:AC for the polypyrrole-AC-NP composites was fixed as 1:1. The weight ratios of pyrrole:AC:NP were 10:10:80, 25:25:50, and 40:40:20.

After 3-hour polymerization, black powder products of polypyrrole and the composites were washed and filtered thoroughly with Milli-Q water. Then, the products were dried in the oven at 60 °C for 24 hours

2.3 Characterization

The morphology and chemical structure of polypyrrole and the composites were characterized by using Scanning Electron Microscopy (SEM, JEOL JSM-6610LV) and Fourier-Transform Infrared Spectroscopy (FTIR, BRUKER VERTEX70) with Attenuated Total Reflection (ATR) technique, respectively. Thermal properties of the composites were also obtained by using Differential Scanning Calorimetry (DSC, METTLER TOLEDO DSC1/400W). DSC data were obtained by using a heating rate of 10 °C/min from 30 to 500 °C.

2.4 Chemical oxygen demand (COD) reduction test

Activated carbon, coconut fibers, polypyrrole and the composites were used as adsorbents for reducing COD from the synthetic wastewater No. 1. The synthetic wastewater No. 1 prepared from KHP had initial COD value equal to 500 mg/L. The amount of adsorbent and the synthetic wastewater No. 1 used in each test batch were

0.08 g and 25 mL, respectively. The experiment was performed by stirring the adsorbent and synthetic wastewater No.1 at 25 °C for 8 hours. Then, the treated water was filtered and stored at 4 °C prior to COD measurement within 24 hours. The COD value of the treated water in each test batch was determined by using closed-reflux colorimetric technique according to standard method for the examination of water and wastewater, AWWA, APHA, WEF, 22nd edition (2012), part 5220D.⁹

2.5 Copper removal test

Removal of copper ions from the synthetic wastewater No.2 was performed in batch. The synthetic wastewater No. 2 was 1 mg/L copper solution. Other experimental parameters were similar to those of the COD reduction test. The amount of copper ions in the treated water was measured by using Fast Sequential Atomic Absorption Spectrometer (FSAAS).¹⁰

3. Results and Discussion

3.1 COD reduction

The data of the COD reduction test are shown in Figure 1. The COD reduction efficiency of polypyrrole (60.3%) was higher than those of activated carbon (30.15%) and coconut fibers (2.31%). When activated carbon was added to 10% w/w in the polypyrrole composite, the COD reduction efficiency was increased up to almost 75%. From the data of the PPy-AC-CF composites, the higher the CF amounts, the lower the COD reduction efficiency. It is possibly due to degradation of coconut fibers.

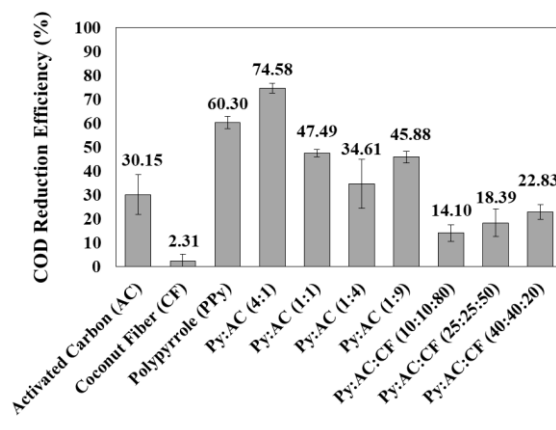


Figure 1. COD reduction efficiency (%) of activated carbon, coconut fibers, polypyrrole, and the composites.

3.2 Copper removal

The data of copper removal test are presented in Figure 2. Activated carbon and coconut fibers could adsorb copper ions up to almost 100%, while the copper adsorption efficiencies of polypyrrole was less than 35%. Unlike the COD reduction data of the PPy-AC-CF composites, the higher the amounts of coconut fibers, the higher the copper adsorption efficiency. It is presumably caused by the strong bonds between the functional groups in the coconut fiber structure with the copper ions in the synthetic wastewater.

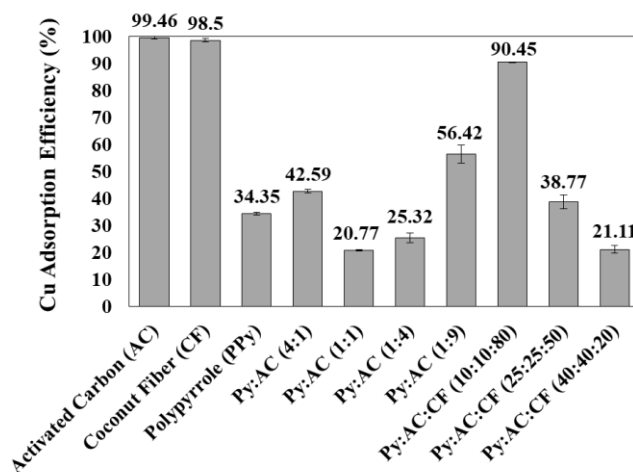


Figure 2. Copper adsorption efficiency (%) of activated carbon, coconut fibers, polypyrrole, and the composites.

3.3 Chemical structure, morphology, and thermal property

The FT-IR spectra of coconut fibers, activated carbon, polypyrrole, and the composite are presented in Figure 3. The region of FT-IR spectra from 1200-700 cm^{-1} represents the fingerprint region of each compound. C-H bending vibrations and benzene ring bands are present in this region. Also, C-C and C-N single bond stretches are expected at around 1100-1000 cm^{-1} . O-H and N-H bands are found in the range of 3500-2900 cm^{-1} .

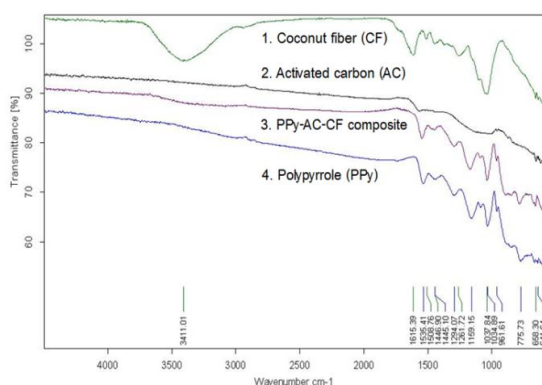


Figure 3. The FT-IR spectra of coconut fibers, activated carbon, polypyrrole, and the composite.

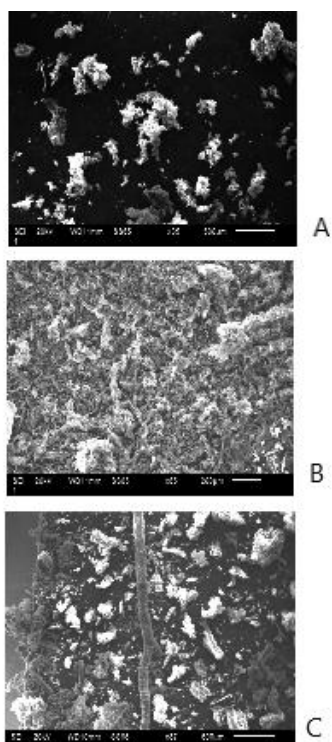


Figure 4. The SEM images of polypyrrole (A), PPy-AC composite and PPy-AC-CF composite

The distributions of polypyrrole and additives in the composites are illustrated in Figure 4. The SEM image (B) showed that activated carbon thoroughly dispersed in the polymer matrix. However, in the SEM image (C) coconut fibers were likely to agglomerate in the polymer matrix.

The DSC data of polypyrrole and the composites with different amounts of activated carbon and coconut fibers were displayed in Table 1. An example of the DSC thermograms of the composites was shown in Figure 5. Glass transition temperatures (T_g) of polypyrrole and the composites were present between 155-192 $^{\circ}\text{C}$. T_g of the composites depended on amounts of activated carbon and coconut fibers in the composites. It is probably because of bonding between the additives and polymer chain. When the amount of AC ranging from 50-90%wt were added into the composites, T_g of the composites increased. On the other hand, T_g of the composites were inversely proportional to the amount of CF.

Table 1. The DSC data of polypyrrole and the composites with different additive contents.

AC content (wt%)	CF content (wt%)	T_g ($^{\circ}\text{C}$) Onset
0	0	164.99
20	0	156.79
50	0	171.83
80	0	172.17
90	0	172.66
40	20	192.09
25	50	165.25
10	80	155.43

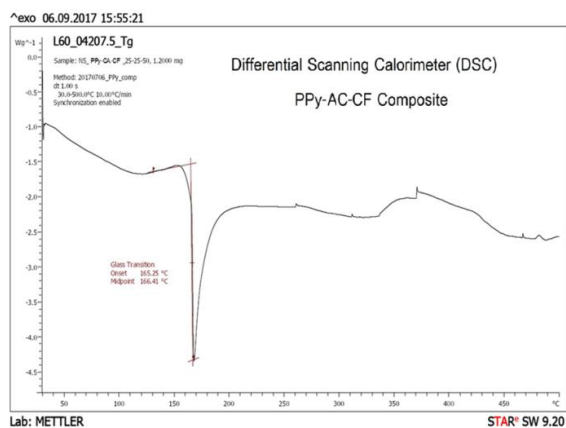


Figure 5. The DSC thermogram of the PPy-AC-CF composite.

4. Conclusion

The polypyrrole composite containing 20% w/w activated carbon significantly reduced both COD (74.58%) and amount of copper ions (42.59%). Moreover, the composite containing 80% w/w coconut fiber and 10% w/w activated carbon efficiently removed copper ions (approx. 90.45%). We found that polypyrrole was such a great COD remover, while activated carbon and coconut fibers were good adsorbents for copper removal. However, the agricultural by-products such as coconut fibers were not the appropriate additives in the polypyrrole composites for reducing COD, because they possibly degraded to increase COD in the wastewater.

Acknowledgement

The financial support of this research project has been granted by Department of Science Service, Ministry of Science and Technology, Thailand

References

- [1] MO, J., Hwang, J. E., Jegal, J., and Kim, J., "Pretreatment of a dyeing wastewater using chemical coagulants", *Dyes and Pigments*, 2007, 72(2), 240-245.
- [2] WEIDLICH, C., MARIGOLD, K. M., and Jüttner, K., "Technical application of conducting polymers for water treatment", *Synthetic metals*, 2001, 119(1-3), 263-264.

- [3] PHAL, S., Thammakhet, C., Thavarungkul, P., and Kanatharana, P., "Miniaturized tea bag filled with polypyrrole for micro-solid phase extraction of estrogens", *Pure and Applied Chemistry International Conference (PACCON) 2015 Proceedings (Analytical Chemistry)*, 2015, 8-11.

- [4] DIN, M. I., et. al., "Evaluation of conductive polymers as an adsorbent for eradication of As (III) from aqueous solution using inductively coupled plasma optical emission spectroscopy (ICP-OES)", *International Journal of Science and Engineering*, 2014, 6(2), 154-162.

- [5] ZOLEIKANI, L., Issazadeh, H., and ZareNezhad, B., "Preparation of new conductive polymer nanocomposites for cadmium removal from industrial wastewaters", *Journal of Chemical Technology and Metallurgy*, 2015, 50(1), 71-80.

- [6] EISAZADEH, H., "Removal of arsenic in water using polypyrrole and its composites", *World Applied Sciences Journal*, 2008, 3(1), 10-13.

- [7] KRISHNANI, K. K., et al., "Hexavalent chromium removal mechanism using conducting polymers", *Journal of hazardous materials*, 2013, 252, 99-106.

- [8] GHORBANI, M., and Eisazadeh, H., "Removal of COD, color, anions and heavy metals from cotton textile wastewater by using polyaniline and polypyrrole nanocomposites coated on rice husk ash", *Composites Part B: Engineering*, 2013, 45(1), 1-7.

- [9] International Standard, ISO 6060: 1989. "Water quality-Determination of chemical oxygen demand".

- [10] Hosseini, S., Ekramul Mahmud, N.H.M., Yahya, R. B., Ibrahim, F., Djordjevic, I., "Polypyrrole conducting polymer and its application in removal of copper ions from aqueous solution", *Materials Letters.*, 149 (2015). 77-80.

The Adsorption of Copper Ions onto Semi-interpenetrating Polymer Network Hydrogel Composed of HEMA and HEC

Amlika Rungrid¹, Runglawan Somsunan²

¹Master's Degree Program in Chemistry, Department of Chemistry, Faculty of Science,
Chiang Mai University, Chiang Mai, 50200, Thailand

²Department of Chemistry, Faculty of Science, Chiang Mai University, Chiang Mai, Thailand 50200
Phone +66 5394 3341 ext. 121, Fax: +66 53 89 2277, E-mail: r.somsunan@gmail.com

Abstract

In this study, the semi-interpenetrating polymer network (semi-IPN) hydrogel fabricated by UV polymerization of 2-hydroxyethyl methacrylate (HEMA) and different contents of hydroxyethyl cellulose (HEC) were investigated regarding their compositions for copper ion adsorption. The compositions of the prepared semi-IPN hydrogel were confirmed by Fourier transform infrared spectroscopy (FTIR). The gel contents of the hydrogel were in the range of 82-98 %. Equilibrium water content and swelling ratio were 44-64 % and 79-84 %, respectively. It was found that the equilibrium water content and swelling ratio of semi-IPN hydrogel decreased as increasing of the hydroxyethyl cellulose contents. From copper ion adsorption study, it shows that the adsorption capacity and the percentage adsorption were in the range of 0.98-1.36 mg/g and 10-13 %, respectively. It can be concluded that adding a relatively inexpensive natural product, in this case hydroxyethyl cellulose, can be utilized to good effect in the development of a high value-added product for metal ions adsorption.

Keywords: 2-hydroxyethyl methacrylate; hydroxyethyl cellulose; semi-interpenetrating polymer network; adsorption

1. Introduction

Water contamination has become a serious environmental problem. Many researches have been focused on the removal of heavy metal ion in waste water. At present, there are different water treatment methods such as chemical precipitation, membrane filtration, solvent extraction, electrolysis, reverse osmosis, ion exchange, adsorption, bioremediation, solvent extraction, etc. [1]. Among these techniques, adsorption has been recognized as one of the most popular methods due to its simplicity of operation, cost effectiveness, high efficiency, easy recovery, regeneration capacity and sludge-free operation [2]. The efficiency of the adsorption depends on the performance of adsorbents. An ideal adsorbent for

heavy metal ion removal includes large surface area and high adsorption capacity, suitable pore size and volume, mechanical stability, compatibility, easy accessibility, ease of regeneration, cost effectiveness, environmental friendliness, simple processing procedures and high selectivity [3]. The material that meets these criteria is hydrogel.

Hydrogels are 3D-structured networks which can be formed by physical or chemical crosslinking using any water-soluble polymer or various monomers with tailored functional groups. Depending on the nature of hydrogel networks, hydrogel can be divided into ‘‘physically’’ and ‘‘chemically’’ crosslinked hydrogels, which can be

distinguished by reversible and irreversible interactions. Multi-component hydrogels based on semi-interpenetrating polymer networks (semi-IPN) or Full-interpenetrating polymer networks (full-IPN) have shown large enhancement in the adsorption of metal ions from water. Interpenetrating polymer networks (IPN) consists of two (or more) networks, at least one of them being synthesized and/or cross-linked within the immediate presence of the other, without any covalent bonds between them, which cannot be separated unless chemical bonds are broken [4]. IPNs have been developed as a convenient method to prepare multi-component polymer materials, which provided a feasible route to modify the properties of natural polymer-based hydrogels [5]

Natural polymers like cellulose, starch and chitosan, have increased usage in synthesis of hydrogels for the removal of metal ions from water systems. These polymers separate metal ions by binding through adsorption and chelation. The hydrogels obtained from cellulose have been interested for heavy metal ions adsorption, because the structure has many hydroxyl groups which can enhance the adsorption of heavy metal ion by strong interaction between the hydroxyl group and heavy metal ion [6]. In addition, they also have internal porous structure, are eco-friendly, cost-effective, and have a high specific surface area.

The 2-hydroxy methyl methacrylate (HEMA) is another chosen as adsorbent hydrogel, due to as a two-dentate chelating co-monomer [7] It is a nontoxic, hydrophilic and biocompatible material [8] Addition, HEMA is a synthetic water-soluble vinyl monomer that could be crosslinked by free radical polymerization forming poly(hydroxyethyl methacrylate) (pHEMA) and the absorptivity of copper ion was 0.84 mg/g [9]. Also, HEMA can form interpenetration network structure with other polymers for heavy metal ions adsorption such as poly(acrylic acid-co-2-hydroxyethyl methacrylate) [10], poly(acrylamide-co-2-hydroxyethyl

methacrylate [11], poly(methyl methacrylate-co-2-hydroxyethyl methacrylate) [9] and poly(2-hydroxyethyl methacrylate-co-2-hydroxyethyl acrylate) [12]. So, the fabrication of synthetic pHEMA and natural HEC using UV radiation produces a new interesting useful properties.

In this study, the semi-interpenetrating polymer network (semi-IPN) hydrogels based on 2-hydroxy methyl methacrylate (HEMA) and hydroxyethyl cellulose (HEC) for Cu²⁺ adsorption were prepared. The chemical structure of the semi-IPN hydrogels were confirmed by Fourier transform infrared spectroscopy (FTIR). Some structural parameters, such as gel content, swelling ratio and water content were also examined. The obtained results will be provided for use as heavy metal adsorbent.

2. Experimental Methods

2.1 Chemicals

The following chemicals were purchased from Fisher Scientific, UK: copper (II) sulfate (CuSO₄) and ammonia solution (25%). 2-hydroxyethyl methacrylate (HEMA) was purchased from Sigma-Aldrich, USA. Hydroxyethyl cellulose (HEC) was obtained from Shinetsu, Japan. Ethylene glycol dimethacrylate (EGDMA) and potassium persulfate (KPS) were purchased from Fluka, Germany.

2.2 Semi-IPN hydrogel synthesis

For synthesis of semi-IPN hydrogel, HEC aqueous solution (0, 1, 2, 3, and 4 %w related to the total weight of HEMA, there used symbols are IPN0, IPN1, IPN2, IPN3, and IPN4) was prepared by dissolving HEC powder in deionized water at 40 °C with stirring for 30 min, and then the solution was kept at room temperature for 24 h to ensure complete dissolution and homogeneity. After adding HEMA (30 %w/v) containing EGDMA (2.0 %w related to the total of HEMA weight) and KPS (0.5 %w related to the total of HEMA weight) under continuous

stirring, the polymerization was carried out by UV lamps at 354 nm for 90 min.

2.3 Gel content and swelling behaviors

The hydrogels were cut into 1.0 cm x 1.0 cm, immersed in distilled water to remove any unreact component for 3 days and dried at 40 °C to a constant weight. The gel content was calculated as follows:

$$\text{Gel content} = \frac{m_d}{m_o} \times 100 \quad (1)$$

where, m_o and m_d are the weight of dry gel before and after purification, respectively.

To study the swelling behaviors of hydrogel, each hydrogel was immersed in water at room temperature. The hydrogels were allowed to swell to equilibrium and weighted m_e . The equilibrium water content (EWC) and percent swelling (SR) were calculated as following:

$$\text{EWC} = \frac{m_e - m_d}{m_e} \times 100 \quad (2)$$

$$\text{SR} = \frac{m_e - m_d}{m_d} \times 100 \quad (3)$$

2.4 Adsorption studies

For environmental conditions experiments, the hydrogel adsorbent was immersed in 200 mg/L of Cu^{2+} solution at pH 5.0. After being shaken for 60 min at 30 °C (Schutzart DIN 40050- IP20, Memmert). The residual concentration of Cu^{2+} was measured by UV- visible spectrophotometer (Lambda 25, PerkinElmer) at 605 nm, which adding the ammonium solution as a colored indicator. The removal efficiency (% removal) and adsorption capacity (q_e) at equilibrium were calculated in the following equation:

$$\% \text{ removal} = \frac{C_o - C_e}{C_o} \times 100 \quad (4)$$

$$q_e = \frac{C_o - C_e}{m} \times V \quad (5)$$

where C_o and C_e are the initial and equilibrium concentration of metal ion solution (mg/L). V is the volume

of metal ion solution (L) and m is the weight of the hydrogel adsorbent (g).

For a standard plot of concentration of Cu^{2+} , it was plotted the absorbance of 10 ppm, 50 ppm, 100 ppm, 200 ppm 300 ppm and 400 ppm Cu^{2+} solution observed in UV- visible spectrophotometer at 605 nm. The linearity of response was $r^2 = 0.9987$.

2.5 Statistical methods

The data was analyzed by one-way ANOVA of variance and Tukey's multiple comparisons test, by using Graph Pad Prism version 6.00 (Graph Pad Software, La Jolla, CA, USA). The result was reported with mean \pm SD and statistically significant of data differences were specified with $P < 0.05$.

3. Results and Discussion

3.1 Appearances of semi-IPN hydrogels before and after adsorption of Cu^{2+} .

Figure 1 illustrated the appearances of IPN2 before and after adsorption of Cu^{2+} . The dried IPN2 without Cu^{2+} (Fig. 1(a)) was completely transparent. Besides, Fig. 1(b) showed the swollen of IPN2 without Cu^{2+} , which appeared white and translucent. After adsorption of Cu^{2+} , the dried of samples appeared blue and transparent in Fig. 1(c), which referred that Cu^{2+} molecules might be absorbed into the matrix of IPN2.

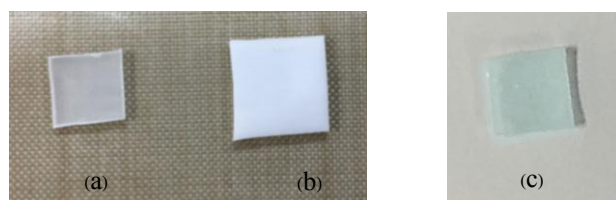


Figure 1: The appearances of IPN2 before and after adsorption in Cu^{2+} solution. (a) The dried hydrogel without Cu^{2+} . (b) The swollen of IPN2 without Cu^{2+} . (c) The dried IPN2 with Cu^{2+} .

3.2 Gel content

Gel contents of the prepared hydrogels were in the range of 82-98%. It was found that, IPN0 (without HEC) was less than all samples. When HEC contents increase, the gel content of all samples were not different significantly and reached the maximum value at 98% which was very high gel content. Addition, the average value of data of gel content with increasing HEC from 0 to 4% w/w_{HEMA} were analyzed by one-way ANOVA. For ANOVA analysis showed that P<0.0001, which indicate that means there is significant difference between the data.

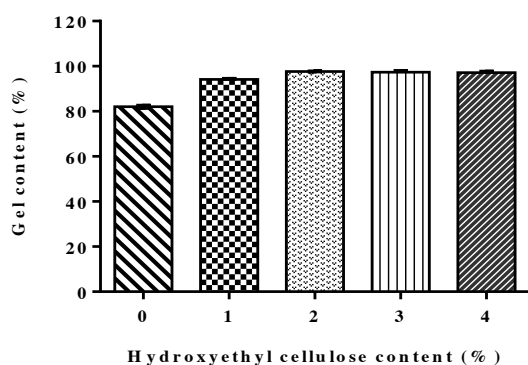


Figure 2: Gel contents of the semi-IPN hydrogels containing different amounts of HEC.

3.3 Water content and swelling ratio

A noticeable property of the hydrogel is its ability to swell in aqueous media without dissolving in it. The hydrogel swelling is a consequence of the balance between cohesive and dispersive forces on the hydrated polymer chains [13]. The swelling test results of different amounts of HEC hydrogels in water at room temperature. It can be seen from Fig. 3 that equilibrium swelling ratio (SR) of the hydrogel decreased from 184 to 79% as the amount of HEC increased from 0 to 4% w/w_{HEMA}. This result corresponded to the equilibrium water content (EWC), as can be seen in Fig. 4. These results were expected, because increasing HEC concentration allows for higher hydrophobic component. The structures of pHEMA and HEC are shown in Fig. 5. From ANOVA comparison between different HEC content, it was found

that P<0.0001 for SR and EWC, which indicate that there is significant difference between the data.

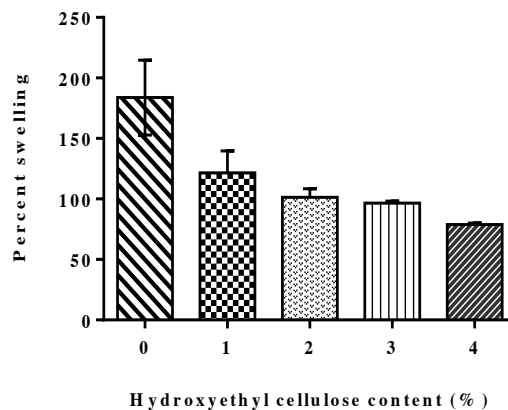


Figure 3: Equilibrium swelling ratio of the semi-IPN hydrogels containing different amounts of HEC.

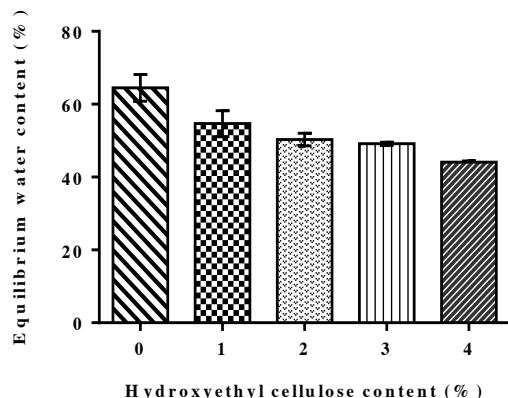


Figure 4: Equilibrium water content (EWC) of the prepared semi-IPN hydrogels containing different amounts of HEC.

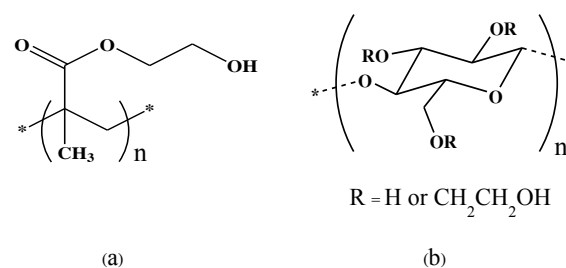


Figure 5: Structures of (a) pHEMA and (b) HEC.

3.4 FT-IR

The FTIR spectra of monomer and semi-IPN hydrogels were shown in Fig. 6. As can be observed, the HEC monomer showed a broad band at 3,200-3,600 cm^{-1} revealed the O-H stretching vibration and band at 2,800-3,000 cm^{-1} represents the C-H stretching vibration, while a band at 1,018 and 1,070 cm^{-1} were the characteristic bands for C-O-C stretching vibration [14]. In addition, glucose ring presents at 1,653 cm^{-1} [15]. For the HEMA monomer showed a band at 1,725 cm^{-1} , which was the characteristic stretching band for the ester carbonyl group (C=O), and bands at 1,160 and 1,070 cm^{-1} which were indicated with the stretching vibrations of C-O of the ester carbonyl group [16]. All synthesized hydrogels showed the characteristic peaks with similar to both HEMA and HEC which includes O-H stretching (3,200-3,600 cm^{-1}), C-H stretching (2,800- 3,000 cm^{-1}), C=O stretching (1730 cm^{-1}), C-O stretching (1000-1200 cm^{-1}) and glucose ring (1,653 cm^{-1}). Moreover, when comparing with the spectrum of prepared hydrogels and HEMA monomer, it found that the C=C stretching (1,635 cm^{-1}) disappeared. This can be confirmed the successful of the polymerization.

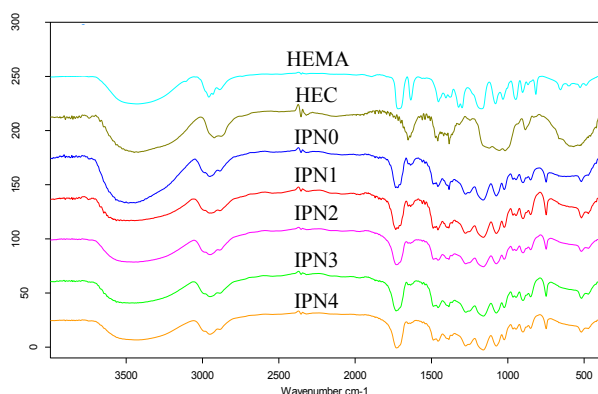


Figure 6: FTIR spectra of monomer and semi-IPN hydrogels.

3.5 Adsorption studies

Experiments were carried out in the solution pH 5 at 30 °C. In preliminary results showed that copper complex started to precipitate above pH 5, as similar

results obtained by other researchers [17]. At low pH, the hydrogen ions (H^+) compete with the metal ions for the sorption sites in the sorbent, the overall surface charge on the adsorbent becomes positive and hinders the binding of positively charged metal ions. In another hand, at high pH values higher ($\text{pH} > 5.0$), the precipitation of insoluble metal hydroxides takes place and might restricts the true adsorption studies [18]. In this study, the semi-IPN hydrogel 2.0 cm x 2.0 cm were immersed in 10 mL of 200 mg/L Cu^{2+} solution, at temperature 30 °C for 60 min. After adsorption, the Cu^{2+} concentrations remain in the solution were determined. The adsorption capacity and %removal of all semi-IPN hydrogel was shown in Table 1. It shows that the adsorption capacity and the percentage adsorption were not different significantly and in the range of 0.98-1.36 mg/g and 10-13 %, respectively. ANOVA analysis showed that $P > 0.05$ for different HEC concentrations, which indicate that there is no significant difference between the data.

Table 1: The adsorption capacity of semi-IPN hydrogels.

Adsorbents	Adsorption capacity (mg/g) *	%removal
IPN0	1.37 ± 0.17	13 ± 1.7
IPN1	0.98 ± 0.36	10 ± 3.4
IPN2	1.36 ± 0.02	12 ± 0.0
IPN3	1.32 ± 0.16	12 ± 1.5
IPN4	1.35 ± 0.14	12 ± 1.6

* $P = 0.3894$

4. Conclusion

In the present work, semi-IPN hydrogels based on HEMA and HEC have been prepared by UV-radiation and its adsorptions properties for removal of Cu^{2+} from aqueous solution were examined. The results confirmed that this method can be used suitably and successfully to fabricate the semi-IPN hydrogel. The semi-IPN hydrogel properties was feasible controlled by varying the hydroxyethyl

cellulose content. It was found that the equilibrium water content and swelling ratio of semi-IPN hydrogel decreased as increasing of the hydroxyethyl cellulose contents. The adsorption capacity was not different significantly. It can be concluded that adding a relatively inexpensive natural product, in this case hydroxyethyl cellulose, can be employed in the development of the adsorbent for metal ions adsorption.

Acknowledgement

The research reported in this paper was supported by the Graduate School, Chiang Mai, Thailand and Chiang Mai University. Department of Chemistry, Chiang Mai University, Chiang Mai, Thailand. The authors also wish to thank the Science Achievement Scholarship of Thailand (SAST) for financial support.

References

- [1] Bakhtiari, N. and Azizian, S. "Adsorption of copper ion from aqueous solution by nanoporous MOF- 5: A kinetic and equilibrium study." *Journal of Molecular Liquids*, 206, 114-118 (2015).
- [2] Zheng, Y. and Wang, A. "Removal of heavy metals using polyvinyl alcohol semi- IPN poly(acrylic acid) / tourmaline composite optimized with response surface methodology." *Chemical Engineering Journal*, 162(1), 186-193 (2010).
- [3] Yuan, S., Zhang, P., Yang, Z., Lv, L., Tang, S. and Liang, B. " Successive grafting of poly(hydroxyethyl methacrylate) brushes and melamine onto chitosan microspheres for effective Cu(II) uptake." *Int J Biol Macromol*, 109, 287-302 (2018).
- [4] Dragan, E. S., "Advances in Interpenetrating Polymer Network Hydrogels and Their Applications." *Pure Appl. Chem.* 86(11), 1707-1721 (2014).
- [5] Wang, X., Hou, H., Li, Y., Wang, Y., Hao, C. and Ge, "A novel semi-IPN hydrogel: Preparation, swelling properties and adsorption studies of Co (II)". *Journal of Industrial and Engineering Chemistry*, 41, 82-90 (2016).
- [6] Huang, Z., Wu, Q., Liu, S., Liu, T. and Zhang, B. A novel biodegradable beta-cyclodextrin-based hydrogel for the removal of heavy metal ions. *Carbohydr Polym*, 2013. 97(2): 496-501.
- [7] Soleyman, R., Pourjavadi, A., Monfared A. and Khorasani, Z. "Novel salep-based chelating hydrogel for heavy metal removal from aqueous solutions". *Polymers for Advanced Technologies*, 27(8), 999-1005 (2016).
- [8] Akgöl, S., Kaçar, Y., Özkara, S., Yavuz, H., Denizli, A. and Arica, M. Y. Immobilization of catalase via adsorption onto l- histidine grafted functional pHEMA based membrane. *Journal of Molecular Catalysis B: Enzymatic*, 15(4), 197-206 (2001).
- [9] Moradi, O., Aghaie, M., Zare, K., Monajjemi, M. and Aghaie, H. "The study of adsorption characteristics Cu²⁺ and Pb²⁺ ions onto PHEMA and P(MMA-HEMA) surfaces from aqueous single solution" . *Journal of Hazardous Materials*, 170(2), 673-679 (2009).
- [10] He, Y.-F., Zhang, L., Wang, R.-M., Li, H.-R. and Wang, Y. Loess clay based copolymer for removing Pb(II) ions. *Journal of Hazardous Materials*, 227-228, 334-340 (2012).
- [11] Chauhan, G. S., Chauhan, S., Sen, U. and Garg, D. " Synthesis and characterization of acrylamide and 2-hydroxyethyl methacrylate hydrogels for use in metal ion uptake studies". *Desalination*, 243(1), 95-108 (2009).
- [12] Meherchi, L., Chabane Sari, S.M., Senoudi, A.R., Zargou, S. and Benmouna, F. "Adsorption kinetics of gold nanoparticles on [P(HEMA-co-HEA)] swollen hydrogels" *J. Mater. Environ. Sci.* 6 (8), 2221-2228 (2015).
- [13] Souda, P. and Sreejith, L. "Magnetic hydrogel for better adsorption of heavy metals from aqueous solutions". *Journal of Environmental Chemical Engineering*, 3(3), 1882-1891 (2015).
- [14] Mabrouk, M., Chejara, D.R., Mulla, J.A.S., Badhe, R.V., Choonara, Y.E., Kumar, P., du Toit L.C. and Pillay, V. "Design of a novel crosslinked HEC- PAA porous hydrogel composite for dissolution rate and solubility enhancement of efavirenz" . *International Journal of Pharmaceutics*, 490(1), 429-437 (2015).
- [15] Kim, Y., Kim, Y.K., Kim, S., Harbottle, D. and Lee, J.W. "Nanostructured potassium copper hexacyanoferrate-cellulose hydrogel for selective and rapid cesium

adsorption". *Chemical Engineering Journal*, 313, 1042-1050 (2017).

[16] Hu, X., Wang, Y., Zhang, L., Xu, M., Dong, W. and Zhang, J. "Redox/pH dual stimuli-responsive degradable Salecan-g-SS-poly(IA-co-HEMA) hydrogel for release of doxorubicin". *Carbohydrate Polymers*, 155, 242-251 (2017).

[17] Demiral, H. and Güngör, C. " Adsorption of copper(II) from aqueous solutions on activated carbon prepared from grape bagasse" . *Journal of Cleaner Production*, 124, 103-113 (2016).

[18] Wang, L. , " Application of activated carbon derived from ‘waste’ bamboo culms for the adsorption of azo disperse dye: Kinetic, equilibrium and thermodynamic studies" . *Journal of Environmental Management*, 102, 79-87. (2012).

**Effect of Ethylene Ethyl Acrylate Copolymer on Mechanical Properties of Polymer Composite
from Polypropylene Mixed with Barium Sulfate**

Nattharanet Treeraritchalerm¹ and Suparat Rukchonlatee^{1,2*}

¹Department of Chemistry, Faculty of Science, King Mongkut's Institute of Technology Ladkrabang (KMITL),
Bangkok, 10520, Thailand

²Polymer Synthesis and Functional Materials Research Unit, Faculty of Science, KMITL, Bangkok, 10520, Thailand
Phone +66 2329 8000 ext. 6251, Fax +66 2329 8428, *E-mail : kjsupara@gmail.com

Abstract

This research studied the effect of ethylene ethyl acrylate copolymer (EEA) on mechanical properties of polymer composite from polypropylene (PP) mixed with barium sulfate (BaSO₄). The BaSO₄ content was constant at 30% by weight and the weight ratio of PP/EEA blends was varied at 95/5, 90/10, 85/15 and 80/20. The melt blends of PP/EEA/ BaSO₄ were carried out using an internal mixer at 190°C with a 100-rpm rotor speed for 15 min. All of specimens were prepared via an injection molding process at a die temperature of 210°C. It was found an addition of EEA in the composite did not affect on the crystalline region of PP even though EEA contents were increased. SEM micrographs showed that the compatibility between polymer and BaSO₄ was improved when EEA was presented. Tensile strength of PP/EEA/BaSO₄ was the highest when using PP/EEA blend ratio at 95/5; however, this property was declined when increasing EEA content and remain stable at 10-20%wt of EEA due to the softness and flexibility of EEA. In addition, Young's modulus and hardness of composite reduced with increasing EEA loading. On the other hand, impact resistance representing toughness of composites was enhanced significantly.

Keywords: polymer composite, polypropylene, ethylene ethyl acrylate copolymer, barium sulfate

1. Introduction

Polypropylene (PP) is a semi-crystalline polyolefin which is one of the most widely used thermoplastic materials as commodity plastics. It has a comparably light weight, low price and easy processability. One of the major benefits of PP is that it can be easily copolymerized with other polymers or combined into a composite plastic, allowing for more robust engineering applications.

Development of polymer such as polymer modification, polymer blends or polymer composite is aimed to achieve a system with more useful structures or functions. Polymer composites are very popular due to

their low cost and simple fabrication methods. Generally, polymers are organic compounds. Therefore, the polymer has moderate strength. Rigid particles fillers, such as, calcium carbonate (CaCO₃) [2] and barium sulfate (BaSO₄) [3] have been introduced into polymers to improve the necessary mechanical strength or stiffness to the composites.

The polymer-filler interfacial adhesion has been generally suggested to be one of the most important factors controlling the mechanical properties of composites, especially in the polymer composite with the difference of polarity between the polymer and the filler [4]. Therefore,

the improvement of interfacial adhesion should be developed to enhance composite properties.

In the previous work [5], effect of CaCO_3 on mechanical properties of high density polyethylene (HDPE) was studied. It was found that the yield stress and the percentage of elongation at break were decreased when CaCO_3 was presented. This is caused by the low compatibility and interfacial adhesion between CaCO_3 and HDPE; however, Young's modulus was improved. The addition of dispersing agent (stearic acid), coupling agent (silane coupling agent) or compatibilizer (PP-g-MA) improved the compatibility between the matrix and fillers. As a result, the mechanical properties of composites were increased [6-7]. Generally, on the impact resistance, the addition of inorganic fillers has an embrittling effect on polymers and results in a significant decrease of toughness although the compatibility was improved [6].

Current studies reinforce PP in order to have greater mechanical properties; reinforcing materials include rigid particles fillers. One of them is BaSO_4 , a kind of neutral filler having non-toxic, high whiteness and excellent chemical resistance. [8]

The aim of this work was to improve the compatibility of composite between non-polar polymer; PP and polar filler; BaSO_4 with the use of EEA because EEA is ethylene copolymer containing the polar part of ethyl acrylate and non-polar part of ethylene. Moreover, EEA also has high flexibility. This would help the composite to be tougher and/or reinforced simultaneously in the system containing rigid inorganic particles.

2. Experimental Methods

2.1 Materials

PP, 1100NK grade (density = 0.95 g/cm^3 , MFI ($230^\circ\text{C}/2.16 \text{ kg}$) = $11.0 \text{ g}/10\text{min}$) was a product of IRPC Pub Co., Ltd. EEA, AMPLIFY™ EA101 (density = 0.93 g/cm^3 , MFI ($190^\circ\text{C}/2.16 \text{ kg}$) = $6.0 \text{ g}/10\text{min}$, acrylate content = 18.5%

was a product of Dow Chemical (Thailand) Co., Ltd. BaSO_4 , SY1250 precipitated grade (density = 4.50 g/cm^3 , particle size = $3.0 \mu\text{m}$) was kindly supplied by TOA paint (Thailand) Co., Ltd. Xylene, a commercial grade was used as solvent for EEA extraction.

2.2 Preparation of PP/EEA/ BaSO_4 composite

In this study, BaSO_4 content was constant at 30% by weight. The PP/EEA/ BaSO_4 at various ratios of PP/EEA blends (95/5, 90/10, 85/15 and 80/20) were prepared. The sample formulas are presented in Table 1.

The melt blends of PP/EEA/ BaSO_4 were carried out using an internal mixer at 190°C with a 100-rpm rotor speed for 15 min. After grinding the compounds, all of specimens were prepared via an injection molding process at a die temperature of 210°C .

Table 1 Formula of PP/EEA/ BaSO_4 composites with BaSO_4 constant of 30%wt.

Formula	Polymer weight ratio (70% of polymer in the composites)	
	PP	EEA
P100B30	100	0
P95E5B30	95	5
P90E10B30	90	10
P85E15B30	85	15
P80E20B30	80	20

Remark: P is PP, E is EEA and B is BaSO_4

2.3 Characterization and testing

Melt flow index of the composites were carried out at 230°C with the weight of 2.16 kg, according to ASTM D1238. The capillary die was 2.095 mm in diameter. Five extrudates were cut and the average weight value was obtained.

Morphology of the composite was examined using a scanning electron microscope (SEM, model JSM 5410 LV, Jeol). Prior to the observation, the specimens were cryogenically cracked in liquid nitrogen. For observing

EEA dispersion, the fractured surface was sonicated in xylene at 60°C for 3 h to selectively extract the EEA phase.

Crystallinity behaviors of PP and EEA in the composites, including crystalline melting temperature (T_m), crystallization temperature (T_c) and percentage of crystallinity, were measured via a differential scanning calorimeter (DSC, model DSC7, PerkinElmer) under a nitrogen atmosphere. The samples were heated from room temperature to 220°C with a heating rate of 10°C/min. After that, the samples were cooled down at a cooling rate of 10°C/min. The percentages of crystallinity of PP and EEA were calculated using melting enthalpy of sample according to the following equation.

$$\%Crystallinity = \frac{\Delta H_f \times 100}{\Delta H_f^0} \times \frac{100}{\% \text{ of polymer in the sample}} \quad (1)$$

Where ΔH_f is the enthalpy of the melting, ΔH_f^0 is the enthalpy of 100% crystalline of PP (207 J/g) or EEA (293 J/g, taken from PE based sample) [9].

Tensile properties of samples were performed according to the ASTM D638 on dumbbell shaped specimen with a gauge length of 30 mm using a universal testing machine (UTM, model QC-536 M1, Comotech). The test conditions used were: cross head speed of 50 mm/min and load cell of 2 kN. Tensile strength at break, elongation at break and Young's modulus were reported.

Impact properties of composites were performed according to the ASTM D256 using a Izod impact tester (model QC-639 P, Astro Instrument) Before testing, specimens were notched with a root radius of 0.254 mm and a depth of 2.54 mm were cut on one side of the specimen. Impact strength was calculated by dividing the impact energy in kJ by the area of the specimen.

Hardness of composites were performed according to the ASTM D2240 using shore D Durometer hardness tester (Intro enterprise Co., Ltd.) with a dead load of 5 kg, reading after pressing the probe on the specimen for 5 sec.

3. Results and Discussion

3.1 Melt flow index

Melt flow index (MFI) analysis of composites is shown in Figure 1. The MFI values of composite slightly decrease by increasing EEA loading. This is caused by the fact that EEA has an acrylate group, which is a rough structure that could hinder the movement of the polymer chain. Therefore, the polymer becomes more difficult to move, implying higher viscosity.

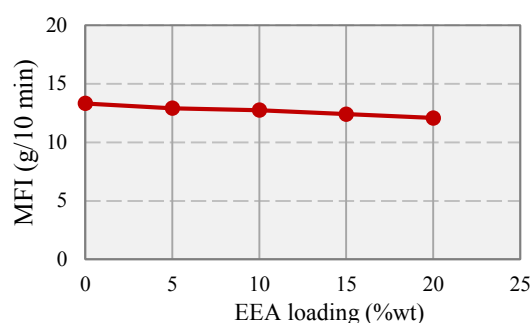


Figure 1 MFI of PP/EEA/BaSO₄ composite with various EEA loadings

3.2 Morphology of PP/EEA/BaSO₄ composite

SEM micrographs at the magnification of 6,000x of the fractured surface of the PP/BaSO₄ (P100B30) and the PP/EEA/BaSO₄ with PP/EEA blend ratio at 95/5 (P95E5B30) are demonstrated in Figures 1(a) and (b), respectively.

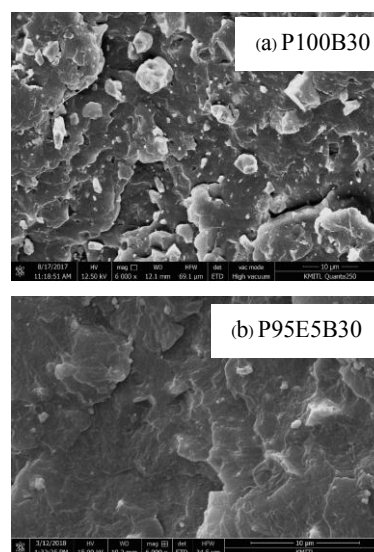


Figure 2 SEM micrographs (6000x) of cryogenically fractured surface of composites

In Figure 2(a), the white particles represent BaSO₄. There are a variety of sizes, both single and aggregate particles (about 2-8 μm), indicating that BaSO₄ particles are not well dispersed in the PP matrix. Additionally, some particles were pulled out from PP, showing weak interfacial adhesion between BaSO₄ particles and PP. This is because of low compatibility between BaSO₄ and PP, as the result of the different polarity. In addition, the compatibility between PP and BaSO₄ is improved when EEA is added. This is obviously seen in Figure 2(b), the BaSO₄ particles are firmly embedded in the polymer. This could be attributed to the presence of polar part (ethyl acrylate group) and non-polar part (ethylene chain) in EEA.

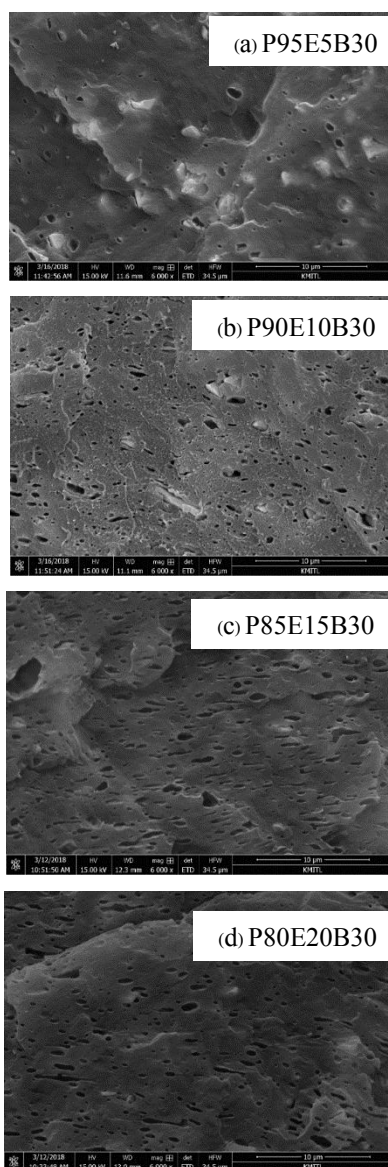


Figure 3 SEM micrographs (6000x) of cryogenically fractured surface of PP/EEA/BaSO₄ after EEA extraction

Figure 3 shows SEM micrographs of the fractured surface of the PP/EEA/BaSO₄ with the different PP/EEA ratios after EEA extraction. The pores and white particles represent extracted EEA and solid BaSO₄, respectively. The PP/EEA blends are immiscible. This is because of the solubility parameter (δ) of EEA and PP are 9.2 (cal/cm³)^{1/2} and 8.2 (cal/cm³)^{1/2}, respectively. It implies that EEA has relatively higher polarity than PP. However, EEA could be well dispersed and distributed in PP because EEA has a part of structure which is non-polar as PP. Most pores of EEA are spherical shape at lower EEA loadings (Figures 3(a) and (b)) and seen to be more cylindrical when the sincreasing EEA loading (Figures 3(c) and (d)). In addition, the amount of BaSO₄ particles in the Figures 3(a)-(d) are lesser than that observed in P100B30 (Figure 2(a)) and some of the particles left in the samples are located in the pores. It is indicated that some BaSO₄ was extracted with EEA. This is because of a good compatibility between BaSO₄ and EEA due to dipole-dipole interaction, leading to an improved interfacial adhesion of the polar BaSO₄ in the PP/EEA/BaSO₄ composites.

3.3 Thermal properties

The PP/EEA/BaSO₄ composites were examined for thermal properties using DSC and results are shown in Table 2. It was observed that T_m , T_c and percentage of crystallinity of PP in all of the samples were in the same range (170-173°C, 111-115°C and 41-46%, respectively), while EEA (100%EEA) has T_m , T_c and percentage of crystallinity at 104°C, 75°C and 9.8%, respectively. This is because PP/EEA blends are immiscible as obviously seen in Figure 3. Therefore, the addition of EEA could not interfere the crystallization of PP in the composite. However, the crystallinity of EEA (about 3-5%) in the composites can be found only when having high PP/EEA blend ratios in P85E15B30 and P80E20B30.

Table 2 T_m , T_c and crystallinity of PP and EEA in the PP/BaSO₄ composite

Formula	T_m (°C)	T_c (°C)	Crystallinity (%)	
			PP	EEA
PP	172	113	45.3	-
EEA	104	75	-	9.8
P100B30	173	115	42.5	-
P95E5B30	171	114	46.6	-
P90E10B30	170	111	45.0	-
P85E15B30	171	111	45.4	5.1
P80E20B30	170	111	41.0	3.6

3.4 Tensile properties

Figure 4 shows the tensile properties of PP/EEA/BaSO₄ with various EEA loadings

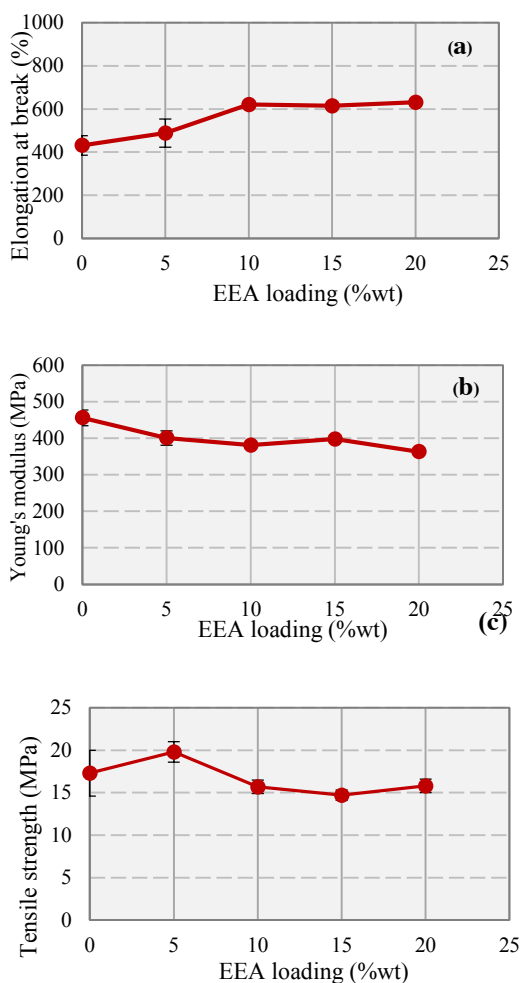


Figure 4 Tensile properties of PP/EEA/BaSO₄ composite with various EEA loadings

It shows that the elongation at break is steady increased when EEA is incorporated, as a result of two main reasons Firstly, the EEA could improve the compatibility between BaSO₄ and PP as confirmed from morphological result. Secondly, EEA has a superior flexibility compared to PP, so the composites are able to be more elongated before broken when increasing EEA.

As observed from SEM micrographs (Figure 2), it shows that the compatibility between PP and BaSO₄ was improved with EEA addition. Tensile strength of composite with 5 %wt of EEA (P95E5B30) was the highest; however, this value was decreased and remained stable at 10-20%wt of EEA. This result was corresponding to the softer and more flexible of EEA as compared with PP. In addition, Young's modulus of the composites was slightly decreased with increasing EEA loading.

3.5 Impact resistance and hardness properties

Figure 5 shows the impact strength and the hardness of PP/EEA/BaSO₄ composites with various EEA loadings. It was found that the impact resistance of PP/EEA/BaSO₄ composites is increased with increasing EEA.

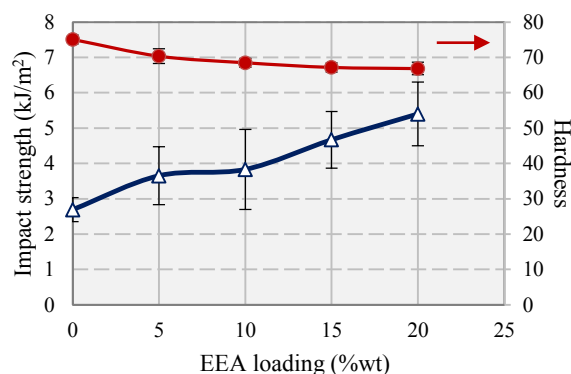


Figure 5 Impact strength and hardness of PP/EEA/BaSO₄ composite with various EEA loadings

The increased in impact resistance was due to the softness and flexibility of EEA leading to better impact force transfer and greater absorbed energy. Additionally, better compatibility between BaSO₄ and PP in the composite, as mentioned in SEM micrographs (Figures 1 and 2) would help to enhance this property. Conversely, the

hardness of PP/EEA/BaSO₄ composite was decreased when increasing EEA.

4. Conclusion

This study obviously demonstrated that the compatibility between PP and BaSO₄ was improved with EEA addition. It was confirmed from morphological results. The MFI of composite was reduced when EEA was added due to the difficult movement of EEA chain. PP/EEA is an immiscible blend, therefore an addition of EEA in the composite did not affect on the crystalline region. On the mechanical properties, the tensile strength of PP/EEA/BaSO₄ composite was the highest value with 5%wt of EEA loadings. Nevertheless, the Young's modulus and hardness of composites were decreased.

This study successfully improves the compatibility between PP and BaSO₄ using EEA leading to better toughness representing by higher impact resistance of the PP/EEA/BaSO₄ composites.

Acknowledgement

Authors would like to thanks TOA paint (Thailand) Co. Ltd. for providing BaSO₄ and SCG Chemicals Co., Ltd. for providing EEA. The financial support from Department of Chemistry, Faculty of Science, King Mongkut's Institute of Technology Ladkrabang (KMITL) has also been greatly appreciated.

References

- [1] Addeo, A. and Pasquini, N. 2005. **Polypropylene handbook**. Munich: Hanser Publishers.
- [2] Beg, M.D.H. and Zaman, H.U., "Effect of CaCO₃ Contents on the Properties of Polyethylene Nanocomposites Sheets". *Fibers and Polymers*, 15: 839-846 (2014).
- [3] Zuiderduin, W.C.J. Westzaan, C. Huetink, J. and Gaymans, R. J. , " Toughening of polypropylene with calcium carbonate particles". *Polymer*, 44:261-275 (2003)

- [4] Martínez de Arenaza, I. Sadaba, N. Larrañaga, A. Zuza, E. and Sarasua, J. R. , " High toughness biodegradable radiopaque composites based on polylactide and barium sulphate". *European Polymer Journal*, 73:88-93 (2015)
- [5] Bartzak, Z., Argon, A. S., Cohen, R. E. and Weinberg, M., "Toughness mechanism in semicrystalline polymer blend: II High-density polyethylene toughened with calcium carbonate filler particles". *Polymer*, 40: 2347-2365 (1999).
- [6] Wang, K. Jingshen, W. Ye, L. and Zeng, H. , "Mechanical Properties and Toughening Mechanisms of Polypropylene/Barium Sulfate Composites". *Composites : Part A*. 34 : 1199-1205 (2003).
- [7] Uttasuradee, M. and Rukchonlatee, S. 2015. "Property Improvement of Linear Low Density Polyethylene/Barium Sulfate Composites for Sea Fishery Application." 416-419. In Pure and Applied Chemistry International Conference 2015 (PACCON2015). Bangkok.
- [8] Zweifel, H. Maior, R. and Schiller, M. 2009. **Plastics additives handbook**. 6nd ed. Munich: Hanser Publishers.
- [9] B. Wunderlich, "Thermal Analysis". *Academic Press*, 417-431 (1990).

Modification of Natural Filler-filled PLA with Ethylene Ethyl Acrylate Copolymer

Nisakorn Watchara¹, Chonlada Ritvirulh^{1,2} and Suparat Rukchonlatee^{1,2}

¹Department of Chemistry, Faculty of Science, King Mongkut's Institute of Technology Ladkrabang (KMITL), Bangkok 10520, Thailand.

²Polymer Synthesis and Functional Materials Research Unit, Faculty of Science, KMITL, Bangkok, 10520, Thailand.
Phone +66 2329 8000 ext. 6251, Fax +66 2329 8428, *E-mail : kjsupara@gmail.com

Abstract

This research studied on the properties of natural filler filled-poly(lactic acid) (PLA) with ethylene ethyl acrylate copolymer (EEA). The filler loadings studied were 5, 10, 20 and 30 wt% and the EEA content was constant at the PLA/EEA weight ratio of 90/10. The sample compounds were prepared using an internal mixer and the samples were formed using an injection molding machine. The natural filler was characterized using several techniques. The XRD pattern confirmed that the natural filler had the characteristics of quartz showing the crystal structure with (100) and (011) planes and it composed of 86.10 wt% SiO₂. Its flake-like morphology with various sizes ranging from 200 nm to 3 μm was observed using SEM. The filler was surface modified with aminofunctional silane beforehand and the amount of the silane attached to the filler surface was detected using TGA and found about 0.48 wt%. From the effect of filler loading, it was found that an increase in filler contents resulted poor filler dispersion in all filled-PLA samples although good filler distribution was observed. This is due to the strong affinity between Si-OH groups of filler, leading to agglomerated filler particles. Therefore, deterioration of tensile and impact properties of filled-PLA were observed when increasing filler loading (0-30 wt%). EEA could enhance the impact strength and %elongation at break of the filled-PLA but reduce tensile strength and Young's modulus of the filled-PLA. This is because of the softness and flexibility of EEA structure.

Keywords: PLA, EEA, filled-PLA, Natural filler

1. Introduction

Plastics have been used for a long time for centuries, and are getting more and more, because of the development of technological advances. This makes possibility to increase the capacity of plastic production to meet the needs of human beings. Plastics are used to replace many kinds of materials such as metal, wood, etc. Because the plastic is strong, low density, light weight easily transportable, resistant to corrosion and good electrical insulation; however, plastics have limitations, such that most plastics are made from synthetic polymers and very few used plastics could be recycled. Most plastics

are not biodegradable and use a long degradation period. This leads to environmental problem. Therefore, biodegradable plastics are increasingly used to reduce the problem of environmental management.

Poly(lactic acid) (PLA) is an aliphatic polyester derived from lactic acid and is one of the promising biodegradable polymers. PLA is made of renewable resources, such as sugarcane, corn starch, cassava roots, chip or starch [1]. PLA has good mechanical properties and excellent transparency. Unfortunately, the usages of PLA

are limited due to poor thermal stability inherent brittleness and low melt strength.

A previous work [2] developed the toughness of PLA blend with ethylene vinyl acetate copolymer (EVA) at a PLA/EVA ratio of 80/20 and the amount of vinyl acetate (VA) was varied from 0-90 wt%. The compatibility of PLA/EVA was low when PLA was blended with EVA having low VA content due to difference in polarity. As the results, low adhesion between PLA and EVA phases was obtained and large dispersed phase sizes of EVA were observed. Therefore, improvement of PLA/EVA toughness was achieved when EVA having high VA content (up to 50%) was employed. In addition, the PLA/EVA blends (having 50% VA content) showed increasing in impact strength when increasing EVA loading. This is because of a good compatibility between PLA and EVA.

Moreover, in other works, PLA mixed with various nanofillers for example, ZnO [3], bamboo charcoal particles [4] and silica particles [5] were reported. It was found that silica nanoparticles were difficult to uniformly disperse in the PLA matrix [5]. So surface modification of silica particles was required. The most frequently used technique for modification is the use of coupling agent. 3-glycidoxypropyltri-methoxysilane (KH-560) was applied to modify silica particles. From SEM, it was found that PLA and KH-560 modified SiO₂ had good compatibility due to the chemical reaction between the epoxy groups of KH-560 and the carboxyl groups of PLA. Moreover, the mechanical properties were improved when little amount of SiO₂ particles were added into PLA.

In this work, the properties of PLA with natural filler contents varying from 0-30 wt% was studied. Also ethylene ethyl acrylate copolymer (EEA) was loaded in the filled-PLA to improve some properties of filled-PLA.

2. Experimental Methods

2.1 Materials

Polylactic acid (PLA) grade: Ingeo™ 3052D was purchased from Nature Works LLC. The specific gravity and melt flow index (MFI) of the PLA are 1.24 and 14 g/10 min (210°C/2.16 Kg), respectively. Ethylene ethyl acrylate copolymer (EEA) grade: AMPLIFY™ EA101 (ethyl acrylate, EA content 18.5 wt%) was a product of Dow Chemical (Thailand) Co., Ltd. The density and MFI of the EEA were 0.931 g/cm³ and 6 g/10 min (190°C/2.16 Kg), respectively. The AKITFIT AM (natural filler modified with aminofunctional silane) was supplied from Benh Meyer Chemical (Thailand) Co., Ltd.

2.2 Preparation of Samples

PLA, EEA and natural filler were dried at 50°C for 24 h before use. The filler contents were 5, 10, 20 and 30 wt% as shown in Table 1. PLA/filler compounds were melted by an internal mixer (MX500-D75L90; Chareon Tut Co., Ltd.) at 170°C with a 100 rpm rotor speed for 15 min. Then the samples were grounded by plastic grinder (Bosco A600; Bosco Engineering Co., Ltd.) and shaped via an injection molding machine.

Table 1 Sample composition

Samples	Composition (wt%)		
	PLA	EEA	A
PLA	100	-	-
P95A5	95	-	5
P90A10	90	-	10
P80A20	80	-	20
P70A30	70	-	30
P90E10A5	85.5	9.5	5

Note: P, E and A represent PLA, EEA and AKITFIT AM, respectively

2.3 Material Characterization

The morphology of natural filler was inspected using scanning electron microscope (SEM, JSM-5410LV; JEOL Co., Ltd.), operated at 20 kV. The filler surfaces were coated with gold prior investigation. For elemental analysis, the filler was determined using the x-ray fluorescence spectrometer (XRF, SRS 3400; Bruker Technology Co., Ltd.).

The crystal structure of natural filler was studied using X-ray diffractometer (D8 Advance; Bruker Technology Co., Ltd), operating with a scanning range from 10° to 80° at a rate of $0.04^\circ/\text{min}$.

The amount of aminofunctional silane attached to the filler surface was examined by PerkinElmer thermogravimetric analyzer (Pyris 1 TGA; PerkinElmer Co., Ltd.). The temperature range of the thermal analyzer was between 150 and 400°C in air zero atmosphere.

2.4 Sample testing

To observe the filler dispersion in the filled-PLA using SEM operated at 10 Kv, the samples were cryogenically cracked in liquid N_2 . Then, the cross-sectional surface area of sample was coated with gold prior investigation.

The tensile strength, % elongation at break and Young's modulus were measured using Universal testing machine (UTM, QC-536M1; Comotech Testing Machines Co., Ltd.) according to ASTM D638. The samples were performed with a load cell of 2 KN, a test speed of 10 mm/min and a gauge length of 30 mm.

The impact strength was examined according to ASTM D256 by Impact tester (QC-639P; Astro Instrument Co., Ltd.). The samples were notched using Ceast (7686; Yasuda Seiki Seisakusho Co., Ltd.).

3. Results and Discussion

3.1 Characterization of filler

SEM micrograph of natural filler is shown in Figure 1 and it can be noticed that the natural filler is mostly agglomerated with flake-like morphology and has various sizes ranging from 200 nm to 3 μm .

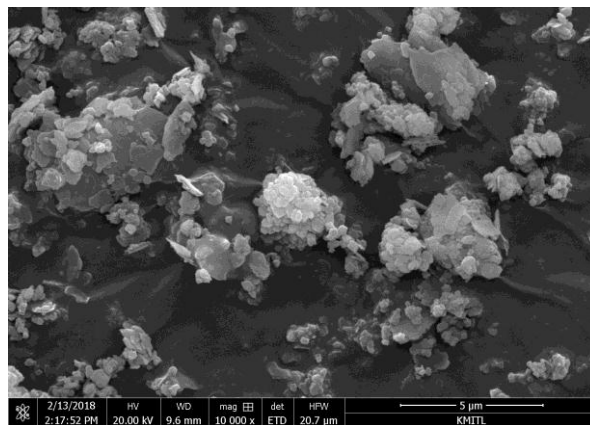


Figure 1 SEM micrograph of the natural filler at 10000x

The XRD pattern of natural filler is illustrated in Figure 2. The result reveals diffraction peaks at 2θ equal to 23° and 27° associated with (100) and (011) planes, respectively, which are the characteristics of quartz. This agrees with the XRF results which confirmed the natural filler mainly comprising 86.10 wt% SiO_2 .

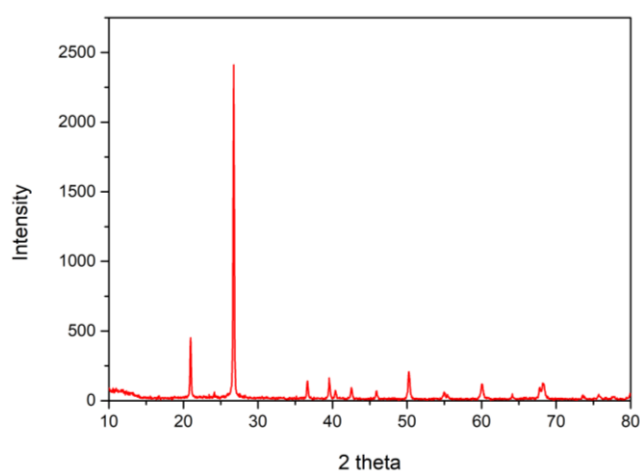


Figure 2 XRD pattern of the natural filler

The amount of aminofunctional silane attached to the filler surface was determined using TGA. The result

shows the onset and decomposition temperatures of the aminofunctional silane at 220°C and 230°C, respectively (Figure 3). In addition, the amount of aminofunctional silane is about 0.48 wt% detected on the filler surface.

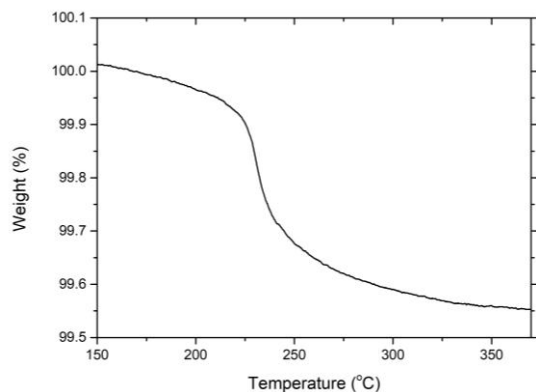


Figure 3 TGA diagram of the natural filler

3.2 Effect of filler loading

3.2.1 Morphology of filled-PLA

The cross-sectional area of the PLA and filled-PLA are demonstrated in Figure 4. The white particles in the filled-PLA specimens are the natural filler while only smooth surface is observed in PLA specimen. Good filler distribution seems to be in all filled-PLA specimens and this could be because both PLA and natural filler are polar. Most of filler particles embed in PLA. Nevertheless, poor filler dispersion can be seen in the specimens at high filler loadings. This is owing to the strong affinity between Si-OH groups of filler [6] and various small particle sizes of filler, leading to agglomerated filler particles as seen in Figure 1.

3.2.2 Tensile properties

Tensile strength, Young's modulus and %elongation at break of PLA and filled-PLA are exhibited in Figure 5. It can be seen that tensile strength, %elongation at break and Young's modulus of filled-PLA are decreased with filler loading. This could be because the filler particles were so small and mostly agglomerated, resulting in poor filler dispersion in PLA matrix, as noticed in Figure 4. It could be assumed that an interaction of hydrogen bonding

between amino-functional silane of filler and carboxyl group of PLA was weak.

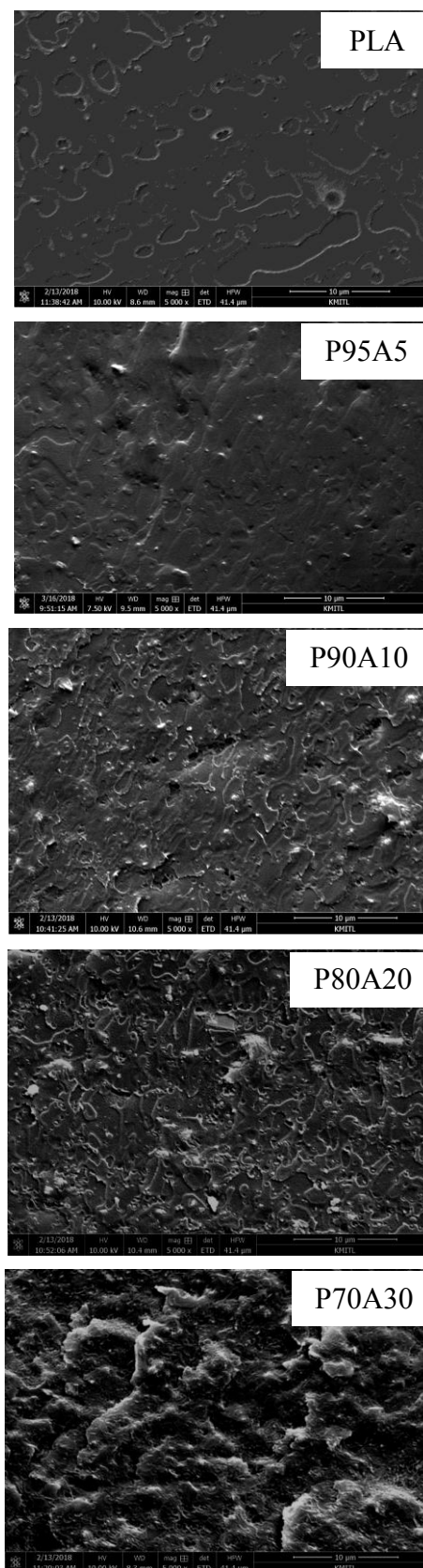


Figure 4 SEM micrographs of PLA with various filler loadings at 5000x

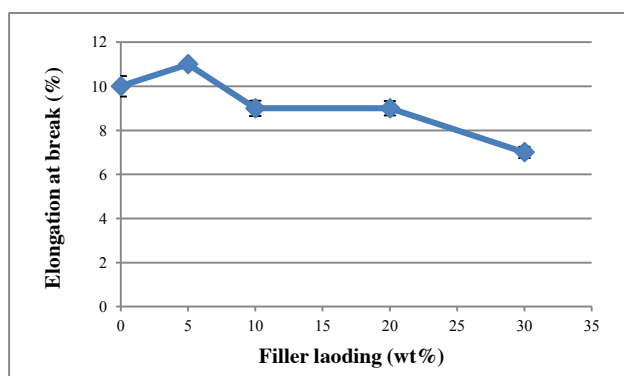
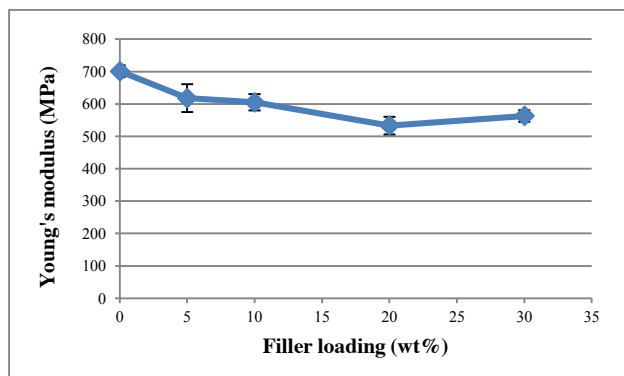
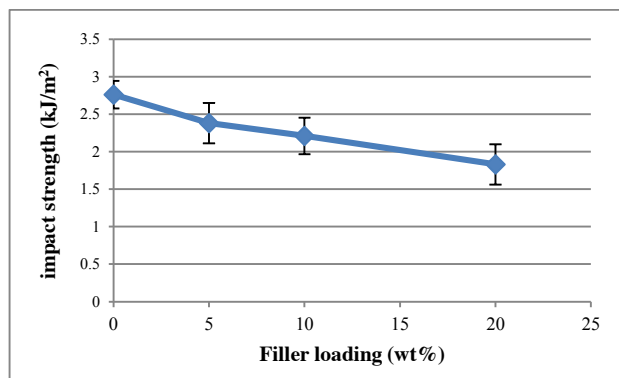
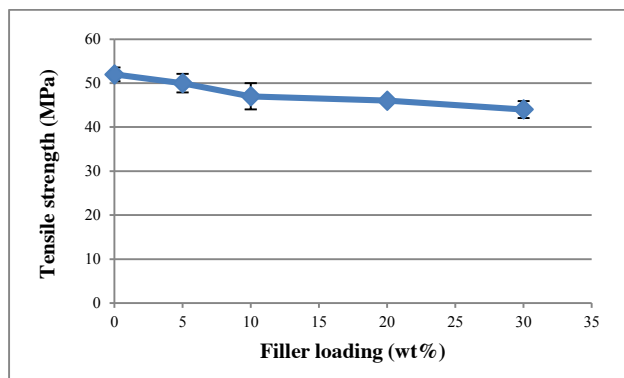


Figure 5 Tensile properties of filled-PLA with various filler loadings

3.2.3 Impact properties

Figure 6 shows the impact strength of PLA and filled-PLA. It is shown that the impact strength of filled-PLA is less than that of PLA and clearly displays a decreasing trend with filler loading. This is because the higher the filler content the poorer the filler dispersion in PLA matrix, as mentioned earlier. In addition, the rigidity of filler particles act as stress concentrator, and thus the samples could not easily absorb the impact energy.

Figure 6 Impact strength of filled-PLA with various filler loadings

3.3 Effect of EEA addition

From the effect of filler loading, it was found that the natural filler became poorer dispersion in the filled-PLA at higher filler loadings. Therefore, the property investigation of filled-PLA with EEA was carried out at 5 wt% natural filler content. The selected EEA loading was constant at the PLA/EEA weight ratio of 90/10.

3.3.1 Tensile properties

The tensile properties of PLA, filled-PLA and filled-PLA with EEA are shown in Figure 7. The presence of EEA in the P90E10A5 sample obviously reduces tensile strength and Young's modulus but slightly enhances %elongation at break of the filled-PLA. This is because EEA is an elastomeric copolymer having softness and flexibility.

3.3.2 Impact properties

As expected, the impact strength of the filled-PLA with EEA is the greatest among the tested samples (Figure 8). This is because EEA is an elastomeric copolymer having high flexibility as compared with PLA. The elastomeric characteristic of EEA enabled to absorb impact energy and retarded propagation during the impact deformation

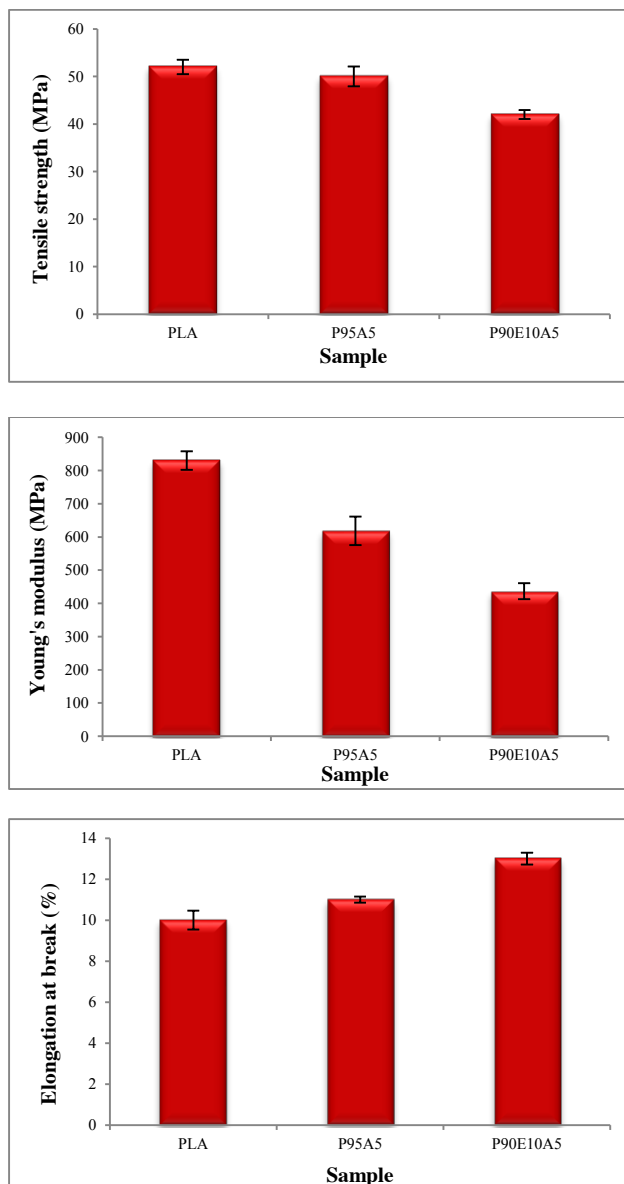


Figure 7 Tensile properties of PLA, filled-PLA and filled-PLA with EEA

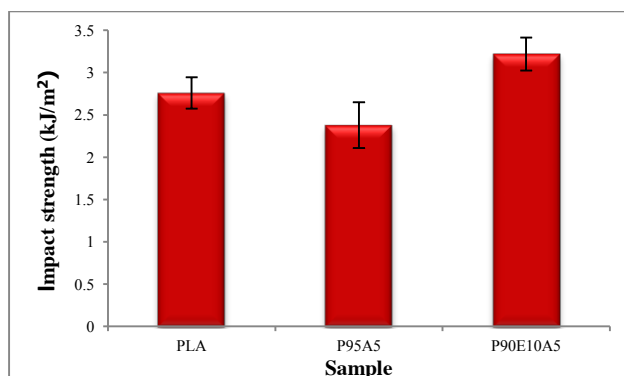


Figure 8 Impact strength of PLA, filled-PLA and filled-PLA with EEA

4. Conclusion

The natural filler used was classified to be quartz having 86.10 wt% SiO₂ and the surface was treated with 0.48 wt% of aminofunctional silane. Deterioration of tensile and impact properties of filled-PLA were observed when increasing filler loading (0-30 wt%). This could be due to the weak interaction of hydrogen bonding between aminofunctional silane of filler and carboxyl group of PLA. EEA could enhance the impact strength and % elongation at break of the filled-PLA but reduce tensile strength and Young's modulus of the filled-PLA. This is because of the softness and flexibility of EEA structure.

Acknowledgement

The authors would like to express their sincere thanks to Behn Meyer Chemical (Thailand) Co., Ltd. for supporting the natural filler. The financial support from Department of Chemistry, Faculty of Science, KMITL has also been appreciated.

References

- [1] Hamad, K., Kaseem, M., Deri, F. and Ko, Y. G., "Mechanical properties and compatibility of polylactic acid/polystyrene polymer blend", *Materials Letters*: 409-412 (2016).
- [2] Ma, P., Hristova-Bogaerds, D.G., Goossens, J.G.P., Spoelstra, A.B., Zhang, Y. and Lemstra, P.J., "Toughening of poly (lactic acid) ethylene - co - vinyl acetate copolymer with different vinyl acetate contents." , *European Polymer Journal*: 146-154 (2012).
- [3] Marra, A., Silvestre, C., Duraccio, D. and Cimmino, S., "Polylactic acid/zinc oxide biocomposite films for food packaging application." , *Journal of Biological Macromolecules International*: 254-262 (2016).
- [4] Ho, M., Lau, K., Wang, H. and Hui, D., "Improvement on the properties of polylactic acid (PLA) using bamboo charcoal particles." , *eXPRESS Polymer Letters*: 190-199 (2009).

-
- [5] Lv, H., Song, S., Sun, S., Ren, L. and Zhang, H., “Enhanced properties of poly(lactic acid) with silica nanoparticles”, *Polymers Advanced Technologies*: 1156-1163 (2015).
- [6] Lai, S. and Li, P., “Effect of Thermoplastic Polyurethane-Modified Silica on Melt-Blended Poly(Lactic Acid) (PLA) Nanocomposites.”, *Polymers & Polymer Composites*: 583-591 (2017).

Effect of Foaming Agent on Natural Rubber Foam for Oil Spill Cleanup

Siripak Songsaeng¹, Patchanita Thamyongkit² and Sirilux Poompradub^{3,4,5*}

¹Program in Hazardous Substance and Environmental Management, Chulalongkorn University, Bangkok 10330

²Department of Chemistry, Faculty of Science, Chulalongkorn University, Bangkok 10330

³Department of Chemical Technology, Faculty of Science, Chulalongkorn University, Bangkok 10330

⁴Center of Excellence on Petrochemical and Materials Technology, Chulalongkorn University, Bangkok 10330

⁵Green Materials for Industrial Application Research Unit, Faculty of Science, Chulalongkorn University, Bangkok 10330, Thailand

Phone +66 2218 7518, Fax +66 2218 7627, E-Mail : sirilux.p@chula.ac.th

Abstract

Oil spill is one of the most serious environmental problems in both short-term and long-term effects. Various techniques have been applied to remove spilled oil. In the present study, natural rubber (NR) is more interesting to design as an oil sorbent foam. The effect of foaming agent concentration of rubber foams with and without carbon black (CB) on the physical properties and oil sorption capacity was investigated. The physical properties, in terms of relative density and porosity of NR foam, were depending on the foaming agent and filler content. For oil sorption study, the increase of foaming agent content in NR foam did not enhance the oil sorption capacity due to the decrease in rubber content. CB may also prevent the bubble generation in NR foam. However, the presence of CB in NR foam composite could enhance the strength of rubber foams during the regeneration.

Keywords: rubber foam, hydrophobic property, porous material, oil sorption

1. Introduction

Over the year, oil spillage has been noted as a big environmental concern. Oil spill accidents mostly happen during extraction, industrial processes and also storage leakage. In 2010, the Deepwater Horizon oil spill is considered to be the largest oil spill in the petroleum industry's history. Approximately 200 million gallons of oil were released into the ocean.^(1,2) One of the conventional method for oil spill cleanup is using of sorbent material. Several materials have been used for oil sorbents which can be categorized into three main groups; inorganic minerals, synthetic materials and organic products.⁽³⁾ Inorganic minerals including perlite, vermiculites or sorbent clay, show poor buoyancy and low oil sorption

capacity. In terms of synthetic materials, polypropylene (PP) or polyurethane (PU) foam are the most widely used in oil spill cleanup because their potential oil removal.^(4,5) These synthetic materials cannot environmentally degrade as compared with natural products. Furthermore, large-scale production of sorbent materials cannot be compromised by a high cost of production and a great waste generation. Consequently, natural products, especially natural rubber (NR), becomes more interesting to replace the synthetic sorbents.⁽⁶⁾

NR or *cis*-1,4 polyisoprene is a renewable polymeric material which mostly obtained from *Hevea brasiliensis*. NR is generally known as a hydrophobic material that is very useful for oil sorbent material in the

state of rubber foam.⁽⁷⁾ Rubber composite is the simplest way to enhance the physical properties and oil sorption capacity. Carbon-based material is widely used as a reinforcing filler in rubber technology to improve the mechanical, thermal or electrical properties of rubber. Carbon black (CB) is the most popular filler added into the rubber compound due to its ability to enhance the strength, extensibility, fatigue resistance and abrasion resistance properties of rubber vulcanizate.⁽¹⁴⁾ Mostly, CB is mainly used in tires for UV stabilizer, and conductive or insulating agent in a variety of rubber, plastic, ink and coating applications. In this study, the rubber foams were prepared by latex mixing with foaming agent and followed by the vulcanization. The effect of foaming agent concentration on physical properties and oil sorption capacity of NR foam with and without CB was investigated. The morphology of rubber foams was examined by using scanning electron microscope (SEM). Finally, the reusability of NR foam was examined for 15 cycles.

2. Experimental Methods

2.1 Material

NR latex and all curing agents were supplied by Rubber Research Institute of Thailand (Bangkok, Thailand). All curing agents for rubber foam compounding were including 10% potassium oleate (K-oleate), 50% sulfur dispersion, 50% zinc diethyldithiocarbamate (ZDEC) dispersion, 50% zinc-2-mercaptobenzthiazole (ZMBT) dispersion, 50% wingstay-L, 33% dipropylene Glycol (DPG) dispersion, 50% zinc oxide (ZnO) dispersion, and 12.5% sodium silicofluoride (SSF) dispersion. Commercial carbon black powder (N339) was supplied from Eonik Company. Crude oil with viscosity 1.2 cP was received from PTT Public Company limited.

2.2 Preparation of NR foam and NR composite foam

167 g of high ammonia NR latex (60% dry rubber content) was added into a cake mixer. Various contents of

K-oleate (1.5, 2.0, 2.5 phr) were slowly added into NR latex to produce the foam and the mixture was agitated for 10 min. After that, 2.0 phr of sulfur dispersion, 1.0 phr of ZDEC dispersion, 1.0 phr of ZMBT dispersion, 1.0 phr of wingstay-L dispersion were poured in the mixture and continuously mixed for 1 min. 0.67 phr of DPG dispersion and 5.0 phr of ZnO dispersion were added into NR latex mixture and stirred for 1 min. Lastly, 1.0 phr of SSF dispersion were added to the latex mixture and stirred at room temperature for 30 sec. Un-gelled NR was will quickly pour into an aluminum mould and vulcanized at 100 °C for 2 h. The vulcanized NR foam was washed by water to remove unreacted elements and dried in oven at 60 °C for 24 h.⁽⁶⁾

To prepare composite NR foam, 1 phr of carbon black was dissolved in K-oleate and stirred until their homogeneity. Then carbon black suspension was poured into NR latex and mixed with curing agents by cake mixer. Finally, the rubber compounding was put into an aluminum mould and vulcanized at 100 °C for 2 h.

2.3 Characterization of rubber foam

Relative density and porosity of rubber foam can be calculated according to Eqs. (1) and (2)^(6,7)

$$\text{Relative density (RD)} = \frac{\text{Foam Density}}{\text{Solid density}} \quad (1)$$

$$\text{Porosity (\%)} = \left(1 - \frac{\text{Foam Density}}{\text{Solid density}}\right) \times 100 \quad (2)$$

Morphology of rubber foams was observed by scanning electron microscope (SRM) (JEOL, JSM-6480LV, Japan) under the accelerating voltage of 20 kV.

Oil sorption test was followed by ASTM F726-12. A cubic shape foam (1×1×1 cm³) was weighed before immersing into crude oil. A foam was floated freely for 15 min and let drain for 30 sec. The fully adsorbed foam was weighed and oil sorption capacity was calculated based on Eq. (3). The sorption capacity (Q) of the rubber foam was determined from the initial weight of absorbent

foam (W_f) and the equilibrium weight foam (W_e). The Q value of sample foam was replicated for 5 times to find the average value.

$$Q \text{ (g g}^{-1}\text{)} = \frac{(W_e - W_i)}{W_i} \quad (3)$$

Foam reusability was studied to investigate the capacity of foam for each sorption-desorption cycle. The absorbed oil can be desorbed by squeezing. Oil recovery efficiency were determined according to Eq. (4). Oil recovery efficiency (RE) is a percentage of mass ratio of the total amount of absorbed oil and the weight of absorbed foam for each cycle.

$$\text{RE (\%)} = \frac{(W_e - W_i)}{W_i} \quad (4)$$

3. Results and Discussion

3.1 Effect of foaming agent content on physical properties of rubber foam

In this study, the foaming agent used to generate bubble in NR latex is K-oleate. Figure 1 shows the effect of foaming agent content on the relative density and the porosity of NR and CB/NR foams. With increasing the foaming content (1.5, 2.0 and 2.5 phr), the relative density of rubber foams became decreased, while the porosity tended to be increased. However, it was found that the relative density of CB/NR foams was higher than that of the NR foam. By the inclusion of CB, the efficiency of foaming agent was dropped. During preparation, the volume of rubber compounding became decreased because the CB particles obstructed the bubble generation in foam compounding, resulting in the decrease in porosity of composite materials. Accordingly, the physical properties of rubber foams were depending on either foaming agent concentration or fill content.

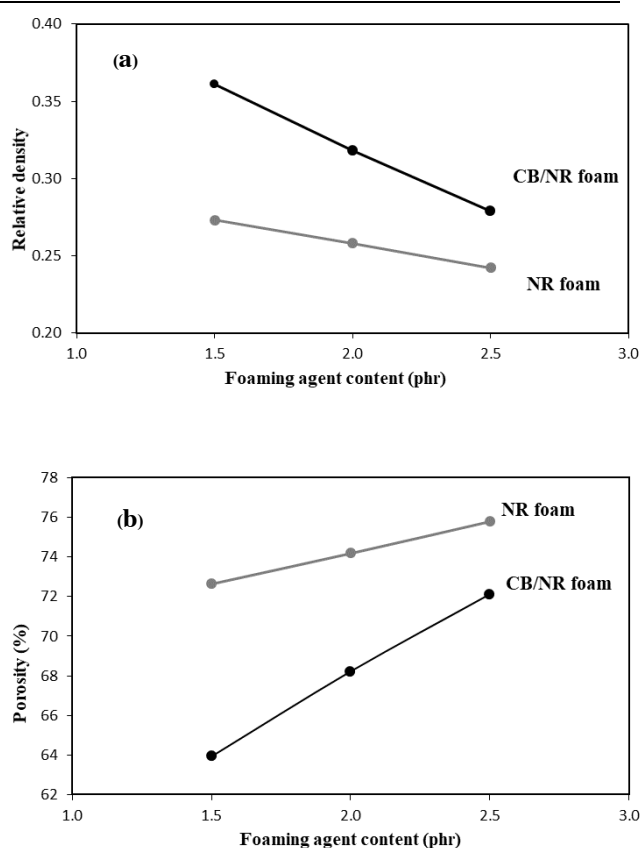


Figure 1 Effect of foaming agent content on (a) the relative density and (b) porosity of rubber foams.

3.2 Oil sorption capacity of rubber foam

The effect of foaming agent content on the oil sorption capacity of NR and CB/NR foams was shown in Fig 2. This result showed that the increase of foaming agent content of rubber foams without CB did not affect the oil sorption capacity. It may be due to the decrease of rubber content by fixing the constant volume (1 cm^3) during oil absorption test. Accordingly, the oil sorption capacity of rubber foams did not show the different capacity among three conditions. However, the ability of crude oil absorption in NR foams ($17\text{-}19 \text{ g g}^{-1}$) was close to synthetic foam of PU (20 g g^{-1}).⁽⁸⁾ The result confirmed that NR foams can be replaced to synthetic rubber foams.

In contrast, the oil sorption capacity of CB/NR foams was lower than that of NR foam. This result confirmed that the inclusion of CB may obstruct the generation of porosity in rubber foams as discussed in section 3.1.

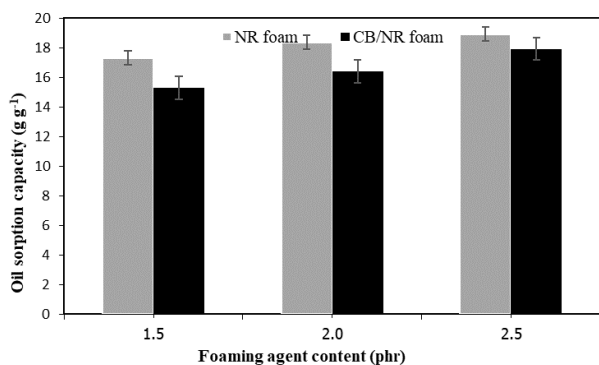


Figure 2 Effect of foaming agent content on the oil sorption capacity of NR and CB/NR foams.

As seen in Fig. 3, the morphology of rubber foam with and without CB of 2.5 phr K-oleate was different. The rubber foams showed the close-cell structure and one cell structure contained the large pore size with large cell structure. While in the case of CB/NR foam, the small cell size with small pore size per cell was obtained.

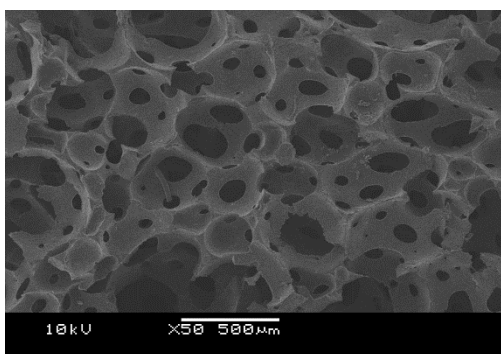
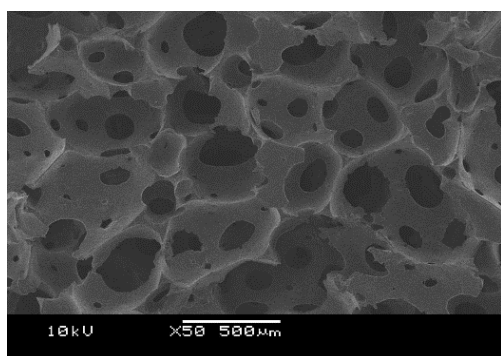


Figure 3 Morphology of (a) NR foam and (b) CB/NR foam with 2.5 phr K-oleate

Accordingly, the oil absorption capacity of CB/NR foam was lower than that of NR foam. The enhancement of oil sorption capacity was overcome by the increase of pore size to provide more space for oil absorption.^[8]

3.3 Recovery of oil and reusability of rubber foams

One of the most important properties of oil sorbent materials is reusability. The reusability refers to recovery of spilled oil and to reduce the production cost of sorbent materials. Figure 4 shows the oil recovery efficiency of rubber foams for 15 cycles. In the first cycle, 95% of absorbed oil could be recovered from both NR and CB/NR foams. After that, oil recovery efficiency of NR foams slightly decreased due to the trap of oil residual inside the rubber pores. However, the oil recovery efficiency of CB/NR was quite higher than that of NR foam in the other cycles. This result could be explained that for several times of reusability, the NR foam surface was destroyed by squeezing. The appearance of rubber foams before and after oil absorption was showed in Fig. 5. With the inclusion of CB, the good surface of rubber foam was clearly observed. Therefore, the advantage of adding CB is to improve the strength of rubber foams.

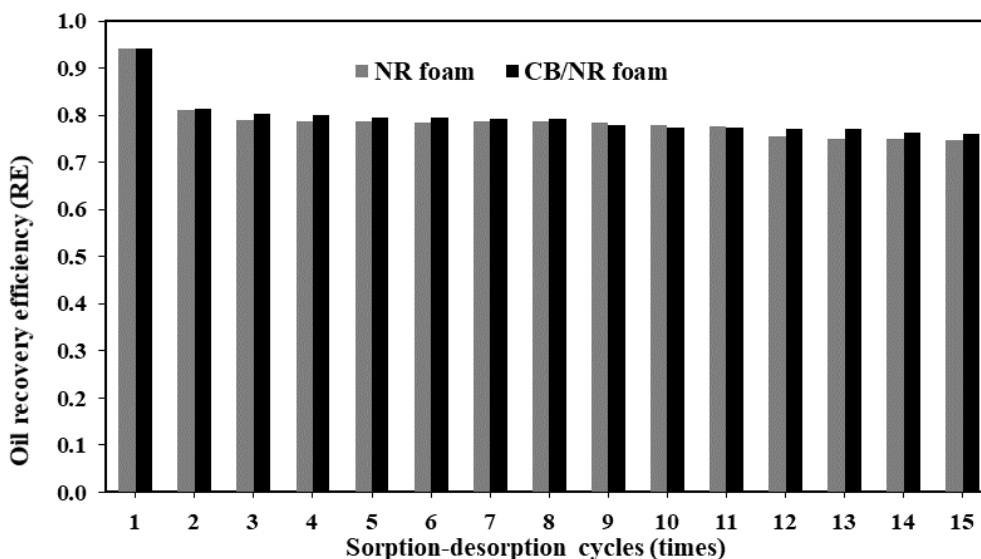


Figure 4 The percentage of oil recovery efficiency for 15 cycles.

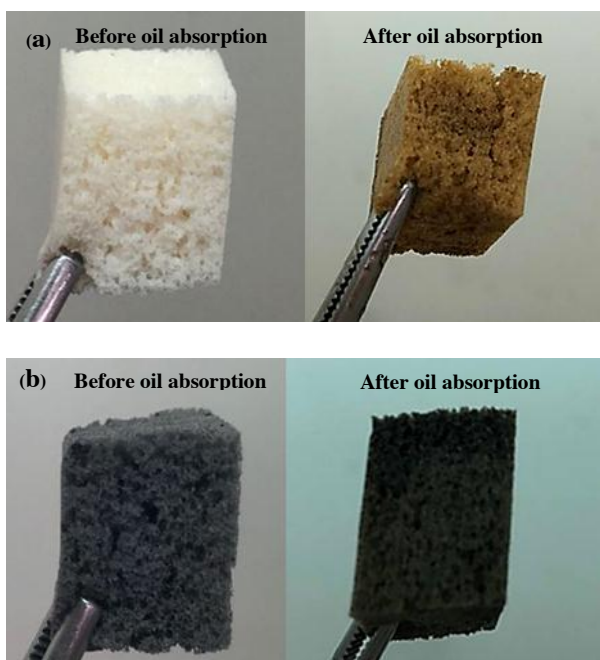


Figure 5 Appearance of rubber foams before and after oil absorption for 15 cycles of (a) NR foam and (b) CB/NR foam.

The oil sorption capacity and the strength for reusability of rubber foams were depending on reinforcing filler. To enhance oil sorption capacity of composite rubber foams, carbon-based materials with high surface area, i.e. activated carbon, carbon nanotube or graphene, are interesting to use in rubber technology

4. Conclusion

In this study, the oil sorption materials form NR with and without CB were prepared. The density of rubber foam decreased with increasing foaming agent content. The oil sorption capacity of NR foam was higher than that of NR foam with CB. This may be because CB prevented the foam generation. Morphological study also confirmed that the large pore size of NR foam was obtained when compared to NR foam with CB. However, the presence of CB could be improved the strength of material. This is the advantage to use rubber foam with CB for reusability in oil spill cleanup applications.

Acknowledgement

The financial support was provided by program in Hazardous Substance and Environmental Management and Green Materials for Industrial Application Research Unit, Chulalongkorn University.

References

[1] Adebajo, M. O. , Frost, R. L. , Klopogge, J. T. , Carmody, O., & Kokot, S. (2003). Porous materials for oil spill cleanup: a review of synthesis and absorbing properties. *Journal of Porous materials*, 10(3), 159-170.

- [2] Al-Majed, A. A., Adebayo, A. R., & Hossain, M. E. (2012). A sustainable approach to controlling oil spills. *Journal of environmental management*, 113, 213-227.
- [3] Behnood, R., Anvaripour, B., Jaafarzade Haghghi Fard, N., & Farasati, M. (2013). Application of natural sorbents in crude oil adsorption. *Iranian Journal of Oil & Gas Science and Technology*, 2(4), 1-11.
- [4] Asadpour, R., Sapari, N. B., Tuan, Z. Z., Jusoh, H., Riahi, A., & Uka, O. K. (2013). Application of Sorbent materials in Oil Spill management: A review. *Caspian Journal of Applied Sciences Research*, 2(2).
- [5] Choi, H. M., & Cloud, R. M. (1992). Natural sorbents in oil spill cleanup. *Environmental science & technology*, 26(4), 772-776.
- [6] Bayat, A., Aghamiri, S. F., Moheb, A., & Vakili-Nezhaad, G. R. (2005). Oil spill cleanup from sea water by sorbent materials. *Chemical engineering & technology*, 28(12), 1525-1528.
- [7] Ratcha, A., Samart, C., Yoosuk, B., Sawada, H., Reubroycharoen, P., & Kongparakul, S. (2015). Polyisoprene modified poly (alkyl acrylate) foam as oil sorbent material. *Journal of Applied Polymer Science*, 132(42).
- [8] Keshavarz, A., Zilouei, H., Abdolmaleki, A., Asadinezhad, A., & Nikkhah, A. A. (2016). Impregnation of polyurethane foam with activated carbon for enhancing oil removal from water. *International journal of environmental science and technology*, 13(2), 699-710.
- [9] Kausar, A. (2017). Contemporary applications of carbon black-filled polymer composites: An overview of essential aspects. *Journal of Plastic Film & Sheeting*, 8756087917725773.
- [10] Pinto, J., Athanassiou, A., & Fragouli, D. (2016). Effect of the porous structure of polymer foams on the remediation of oil spills. *Journal of Physics D: Applied Physics*, 49(14), 145601.
- [11] Roslim, R., Hashim, M. A., & Augurio, P. T. (2012). Natural latex foam. *J. Eng. Sci*, 8, 15-27.
- [12] Santos, O. S. H., da Silva, M. C., Silva, V. R., Mussel, W. N., & Yoshida, M. I. (2017). Polyurethane foam impregnated with lignin as a filler for the removal of crude oil from contaminated water. *Journal of hazardous materials*, 324, 406-413.
- [13] Gui, X., et.al (2013). Magnetic and highly recyclable macroporous carbon nanotubes for spilled oil sorption and separation. *ACS applied materials & interfaces*, 5(12), 5845-5850.
- [14] Bijarimi, M., Zulkafli, H., & Beg, M. D. H. (2010). Mechanical Properties of Industrial Tyre Rubber Compounds. *Journal of Applied Sciences(Faisalabad)*, 10(13), 1345-1348.

Process and Property Relationship of Pineapple Leaf Fiber/PHBV Composites

Pongsathorn Chaleerat¹, Rapeephun Dangtungee^{1,2}, Suchart Siengchin^{1,2,3,*}

¹Department of Materials and Production Engineering (MPE), The Sirindhorn International Thai - German Graduate School of Engineering (TGGS), King Mongkut's University of Technology North Bangkok, 1518 Pibulsongkram Road, Bangsue, Bangkok 10800, Thailand

²Center of Innovation in Design and Engineering for Manufacturing (CoI-DEM), King Mongkut's University of Technology North Bangkok, 1518 Pracharaj 1 Road, Wongsawang, Bang sue, Bangkok 10800, Thailand

³Natural Composite Research Group, King Mongkut's University of Technology North Bangkok, 1518 Pracharaj 1 Road, Wongsawang, Bang sue, Bangkok 10800, Thailand

*E-mail: suchart.s.pe@tggs-bangkok.org

Abstract

The great impacts of improve the mechanical, thermal, and selected other properties of bio-polymers using natural fibers such as sisal and flax [1,2]. The preparation technique recognized earlier that has a strong impact on the properties. The aim of this research is to study on comparing the effect of different preparing techniques, volume fraction of natural fiber reinforced on bio-polymer, and how they affect selected mechanical, thermomechanical and water absorption properties. Natural fiber bio-composites composed of poly(hydroxybutyrate-co-hydroxyvalerate) (PHBV) as a matrix and Pineapple leaf fibers (PALF) as a reinforcement. The solution casting and compression molding techniques used to production of composites. The PALF were prepared by immersing in NaOH (5%) solution for 1 hour at room temperature. The treated PALF were wash by tap water until pH 7 and air dried at 80°C for 24 hours then cut into the length of approximately 0.5 mm. In the solution casting techniques, PHBV/PALF mixed in chloroform that use as solvent. The mixture stirring constantly at 60°C, stirred for 30 minutes then cast on glass plate and dried in the oven at 70°C for 1 hour. In the compression molding technique, after melt mixing compound in the kneader (at 160°C for 15 minute and rotor speed of 60 rpm), the compounds were compression molded by a hot press. The mechanical properties of the PALF/PHBV composite films were evaluated by tensile and dynamic mechanical analysis (DMA). Moreover, the water uptake of the composites was calculated. The preliminary results are in line with the expectation of increasing tensile modulus. This was as the result of improvement of PALF dispersion in PHBV matrix for solution casting and compression molding technique.

Keywords: Poly(hydroxybutyrate-co-hydroxyvalerate)(PHBV), Pineapple leaf fibers(PALF), Solution casting, Compression molding

1. Introduction

A few years ago, Awareness of environmental issues causing demand to reduce environmental pollution increased. Led to the new direction of research and development to environment-friendly. Bio-composites are

optional that gain more attention nowadays due to their biodegradability behaviour. Bio-composites compose with two part, first is fiber and another is matrix biodegradable polymer. There are so many kinds of biodegradable polymer that available in the world such as PLA, PHBV that have the potential to be used in bio-composites. Poly(hydroxybutyrate-co-hydroxyvalerate) (PHBV) is one of a kind of biodegradable polymer in polyhydroxyalkanoate group (PHAs) [3], mostly used in food packaging and rubbish bag due to its biodegradability. But PHBV has been limited by processing window and mechanical properties. PHBV be often reinforced by natural fibers to improve the mechanical properties. Natural fibers are the most optional to use as a reinforced material due to their advantage, renewable and full biodegradable. Pineapple leaf fiber (PALF) is natural fiber that has better mechanical properties such as high specific strength, flexural and torsion rigidity[4]. Many researchers interested in PALF properties and used PALF as a reinforcement material in bio-composites. For example of PALF reinforced as reinforcement materials, George and coworker have been investigated on the effect of short pineapple leaf fiber reinforced on low-density polypropylene that was prepared by melt-mixing and solution-mixing methods and the result shows that the mechanical properties were found to be enhanced and elongation at break reduced with increasing fiber loading[5]. Mohammad and co-works have been investigating the processing ability of PALF and sugarcane bagasse as a raw material for a disposable plate at different heat compression temperatures. The result shows that the higher heat treatment indicates to be beneficial for PALF as a comparison to the bagasse and increase of heat shows of the specimen changing circumstances of composition characteristic[6]. However, the different preparing techniques effect on properties of bio-composites. By using the natural fiber for reinforcing biodegradable polymer, in this research focus on comparing the technique to prepare bio-composite films

and the effect of volume fractions of PALF reinforced PHBV composites.

2. Experimental Methods

2.1 Fiber treatment

The PALF were prepared by immersing in NaOH (5%) solution for 1 hour at room temperature. The treated PALFs were wash by tap water until pH 7 then air dried at 80°C for 24 hours and cut into the length of approximately 0.5 mm.

2.2 Fabrication of composites

In the solution casting techniques, PHBV/PALF were mixed in chloroform that was used as a solvent. The mixture was stirred constantly at 60°C, stirring for 30 minutes then cast on a glass plate and dried in the oven at 70°C for 1 hour as shown in Fig. 1a. In the compression molding technique, after melt mixing in the kneader (at 160°C for 15 minute and rotor speed of 60 rpm), the compounds were compression molded by a hot press as shown in Fig. 1b.

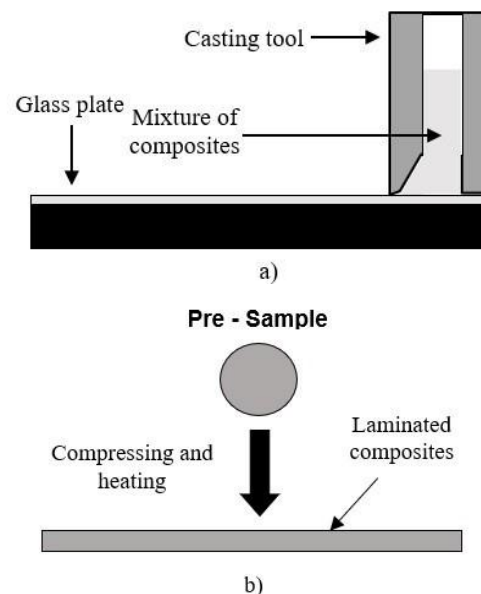


Figure. 1 Schematic of (a) solution casting And Compression molding (b)

2.3 Mechanical properties

Tensile properties were investigated by using Testometric M500-25AT, The Testometric Company Ltd., UK, with load cell of 100 N. The sample were cut to size 5 x 70 mm. Pull at 5 mm/min with intial distance between the grips of 25 mm.

Dynamic mechanical analysis (DMA) was used in tension mode on a DMA 1 METTLER TOLEDO, METTLER TOLEDO (Thailand) Ltd., at 1 Hz to investigated thermal dynamic properties of composite films.

2.4 Water absorption

Water absorption of PHBV composites was carried out according to ASTM D570-98 standard test method. PHBV composites were cut into specimens rectangular (25 × 60 × 0.1 mm³) and then immersed in a distill water bath over a period of 312 hours.

3. Results and Discussion

3.1 Tensile properties

The tensile modulus and tensile strength of PHBV composites as a function of PALF contents by different preparing technique are shown in Fig. 2 and 3. respectively. It was observed that the value of tensile modulus in solution casting technique higher than compression molding technique and the highest was found at PHBV with 3 wt.% PALF loading, the tensile modulus increased 13.88 % compared to the neat PHBV. Nevertheless, the tensile modulus in case of the 5,7 and 10 wt.%, PALF composites slightly decreased. Many factors be influential for tensile properties of natural fiber composites such as length, distribution, and orientation of fiber[7]. However, the tensile strength of PHBV composites decreased with addition fiber contents. This could be related to the high PALF loading and the adhesion between fibers and matrix were not perfectly bonded between fiber and matrix. From Fig. 3, It can be noticed that the results of tensile strength of PHBV composites from the solution casting technique

not much different than that the PHBV composites from the compressing molding technique.

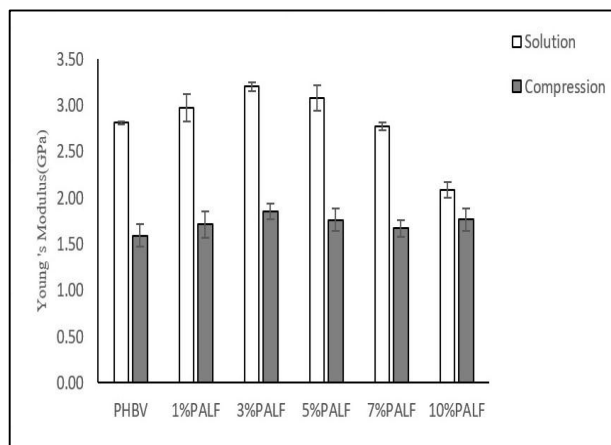


Figure. 2 Tensile modulus of PHBV/PALF of soluton casting and compression molding technique

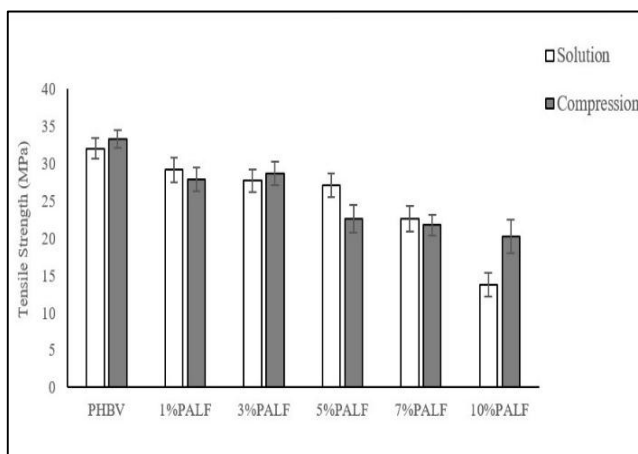


Figure. 3 Tensile strength of PHBV/PALF of solution casting and compression molding technique

3.2 Dynamic mechanical properties

Fig. 4 shows the storage modulus of PHBV composites of solution casting technique with temperature under dynamic conditions. The storage modulus of PHBV/PALF from solution casting technique displays a gradually decreased at 55 °C. The addition of 1, 3 and 5 wt.% of PALF loading has shown the higher value of storage modulus than that of the neat PHBV. whereas, the storage modulus of 7 and 10 wt.% PALF/PHBV composite decreased approximately 3.3% and 22.81 % compared to the neat PHBV. The storage modulus of PHBV composites from compression molding technique has shown in Fig. 5.

The storage modulus of composites from compression technique displays a gradually fall at a temperature around 60 °C. The addition of 1 and 3 wt.% of PALF loading has shown the higher value of storage modulus than that of the neat PHBV. However, the addition of 5, 7 and 10 wt.% loading PALF shown start decreased in storage modulus compare to 3 wt% loading PALF.

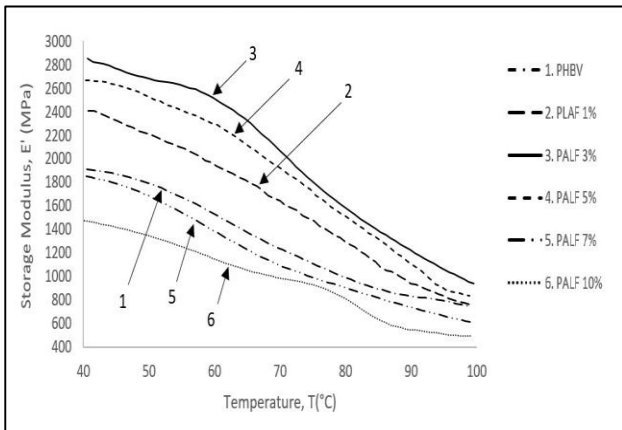


Figure. 4 Storage modulus of PHBV/PALF of solution casting technique

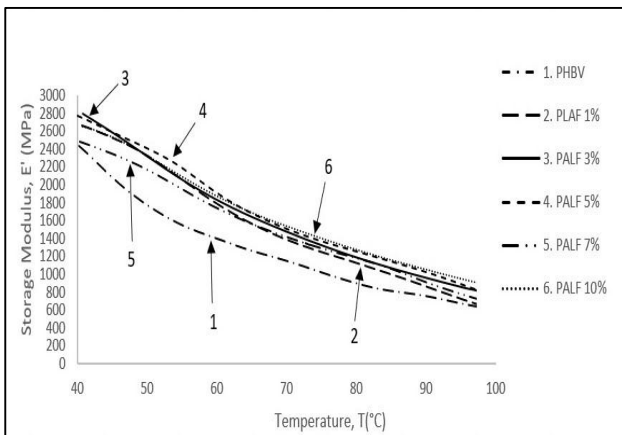
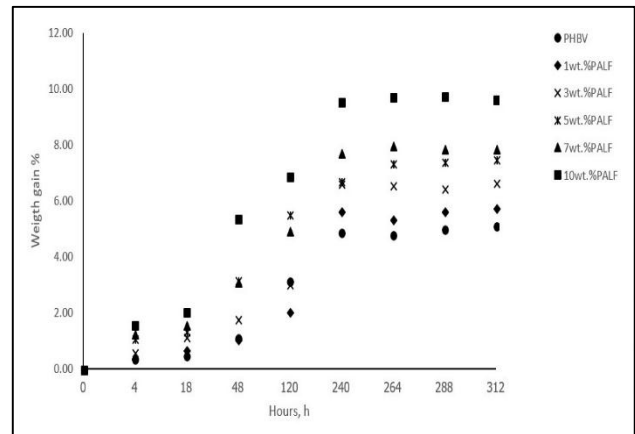


Figure. 5 Storage modulus of PHBV/PALF of compression molding technique

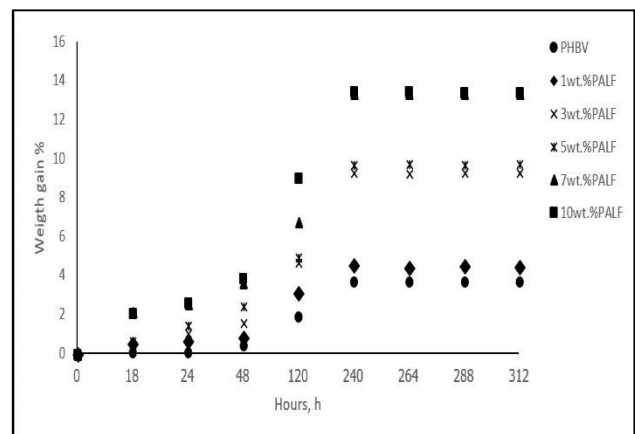
3.3 Water absorption

The water absorption of PHBV composites from solution casting technique as a function of time shown in fig. 6a. The neat PHBV recorded water uptake value at 5.13 % after subject to water absorption at 312 hr. The PALF/PHBV composites show a large amount of water

absorption. The water absorption of 10 wt.% PALF/PHBV composites for 120 hr and 312 hr increased by 6.89 % and 9.66 % respectively compared with the neat PHBV. The water absorption of PHBV/PALF composites increased with increasing fiber contents. For the water absorption of PHBV composites from compression molding technique as a function of time shown in fig. 6b. The neat PHBV recorded water uptake value at 3.72 % after subject to water absorption at 312 hr. The water absorption of 10 wt.% PALF/PHBV composites for 120 hr and 312 hr increased by 9.0% and 13.43 % respectively compare with the neat PHBV.



a)



b)

Figure. 6 Water absorption of PHBV/PALF of solution casting (a) and compression molding (b) technique

4. Conclusion

The objective of this work was to study the effect of comparing preparation techniques, volume fraction of natural fiber reinforced bio-polymer on mechanical, dynamic mechanical properties and water absorption. The preliminary results showed that, the tensile modulus of composites from solution casting technique are better than the tensile modulus of composites from compression molding technique as shown in fig. 2. The highest value of tensile modulus was found at PHBV with 3 wt.% PALF from solution casting technique with increased by 13.88% compared with the neat PHBV. The tensile strength of the two techniques are not different that much. The dynamic mechanical properties, the highest storage modulus of PHBV-reinforced PALF from solution casting technique was found at 3 wt.% PALF and the highest storage modulus from compression molding technique was found at 3 wt.% PALF. Both storage modulus results were compliance with result from tensile modulus. Incorporation of PALF increased the water uptake of the PHBV composites on both technique.

References

- [1] S. Siengchin, Reinforced Flax mat/modified Polylactide (PLA) Composites: Impact, Thermal and Mechanical Properties, *Mechanics of Composite Materials*. 50 (2014) 257-266.
- [2] R. Dantungee, J. Tengsuthiwat, P. Boonyasopon, S. Siengchin, Sisal natural fiber / clay reinforced poly(hydroxybutyrate-co-hydroxyvalerate) hybrid composites, *Journal of Thermoplastic Composite Materials* : 28 879-895 (2015).
- [3] E. Bugnicourt, P. Cinelli, A. Lazzeri, and V. Alvarez, Polyhydroxyalkanoate (PHA): Review of synthesis, characteristics, processing and potential applications in packaging, *Express Polymer Letter* : 791-808 (2014).
- [4] M. Asim, K. Abdan, M. Jawaid, M. Nasir, Z. Dashtizadeh, M. Ishak, and M. E. Hoque, "A Review on Pineapple Leaves Fibre and Its Composites", *International Journal of Polymer Science* : 2015.

[5] J. George, S. Bhagawan, N. Prabhakaran, and S. Thomas, "Short pineapple-leaf-fiber-reinforced low-density polyethylene composites," *Journal Applied Polymer Science* : 843–854 (1995).

[6] M. S. Mustapa, S. D. Sabdin, M. Tobi, A. Latif, M. S. Wahab, M. Yunus, M. Radzi, and Y. Yusof, *The effects of heat and compression on moisture content and water absorption of PALF/sugarcane bagasse composition in disposable plate production* : (2014).

[7] Singh, S., Mohanty, A. K., Sugie, T., Takai, Y., Hamada, H. "Renewable resource based biocomposites from natural fiber and polyhydroxybutyrate-covalerate (PHBV) bioplastic." *Composites Part A: Applied Science and Manufacturing*.39(5), pp. 875-886. 2008

Ag/PDMS Nanocomposite for Flexible Conductive Stripes

Porapak Suriya¹, Supeera Nootchanat³, Parintorn Jangtawee², Wisansaya Jaikeandee¹, Chutiparn Lertvachirapaiboon³, Akira Baba³, Sanong Ekgasit^{2*}

¹Program in Petrochemistry and Polymer Science, Faculty of Science, Chulalongkorn University, Bangkok 10330

²Sensor Research Unit, Department of Chemistry, Faculty of Science, Chulalongkorn University, 254 Phaya Thai Road, Patumwan, Bangkok 10330, Thailand

³Graduate School of Science and Technology, Niigata University, 8050, Ikarashi 2-nocho, Nishi-ku, Niigata 950-2181, Japan

Phone +66890828021, *E-Mail: sanong.e@chula.ac.th

Abstract

In this work, we present a facile, simple, and low-cost fabrication method for the fabrication of PDMS-silver nanocomposite which is an alternative flexible conductive substrate. Columnar silver acetate was synthesized and transformed to silver nanostructures with three-dimensional porous structures by thermal decomposition. Columnar silver acetate strongly adhered onto a surface of polydimethylsiloxane (PDMS) and exhibited excellent mechanical properties and high conductivity under a static mechanical strain including stretching, bending, and twisting. This could be due to the formation of columnar silver acetate network in PDMS matrix. We also compare the characteristics of columnar silver acetate between synthesis grade and commercial grade. Moreover, we demonstrate an application of columnar silver acetate as a flexible conductive stripe for electronics device as sensor for arduino robot arm.

Keywords: Flexible conductive, PDMS nanocomposite, silver acetate, silver nanostructure.

1. Introduction

Due to various potent applications, fabrication of flexible conductive materials has been in the field of interest of scientists for more decades. Nowadays, several researches have been demonstrated to be successful in flexible conductive polymer. For instance, using polydimethylsiloxane (PDMS) with silver for stretchable electrode¹, elastic electrical circuits², electronics bandage³, stretchable circuit⁴, transparent electrode⁵ with their excellent properties about electricity even there were under stress as stretching, bending, and twisting. Furthermore, flexible conductive materials can apply in many fields, electrical field⁶, medical field³.

In this research, we reported a facile, simple and low-cost approach to fabricate flexible conductive stripe which comprised of PDMS and silver nanostructure (PDMS/Ag). The silver nanostructure was prepared by columnar silver acetate microstructures (Csams) and was reduce sintering effect by adding 0.1 w% of PDMS base. The flexible conductive stripe can exhibit excellent mechanical properties and high conductivity under a static mechanical strain including stretching, bending, and twisting.

2. Experimental Methods

2.1 Synthesis of silver acetate

Silver acetate was prepared as follow: 200 mL ethyl acetate, 20 mL acetic acid, and 20 mL hydrogen peroxide were mixed together. After that, the mixture was poured

into beaker, which contains 8 g silver metal. Wrap the beaker with aluminium foil and stir the mixture at room temperature for 7 days, white powder could be obtained after filtration and purify by ethyl acetate for several times.

2.2 Thermal decomposition of silver acetate

PDMS/Ag stripe can be prepared following: 0.3 g of silver acetate powder (99%, Sigma Aldrich) dispersed in 3 ml ethyl acetate and adding 0.003 g PDMS base. After mixing, the mixture was casted on glass slide, which covered by 1.5x6.5 cm² polyimide tape (Kapton tape), and silver acetate film will be heated at 200°C for 10 minutes for thermal decomposition to transform to silver nanostructure film.

2.3 Fabrication of Ag/PDMS stripe

PDMS was prepared by mixing PDMS base and curing agent (SYLGARD® 184, Dow Corning) with a ratio of 10:1 and degassed by vacuum pump for 1 hour. After that the mixture was poured onto the silver nanostructure film which was casted on glass slide at 1 mm thickness, and cured at 60°C for 3 hours after curing, cutting and peeling off PDMS/Ag stripe.

2.4 Characterization of both silver acetate with and without PDMS base

2.4.1 Raman spectroscopy

In order to determine the different functional group of silver acetate with and without PDMS base mixture. It is necessary to confirm by Raman technique. We use DXR Raman microscope (Thermo Scientific) with a 532-nm excitation laser. Laser power at 10 mW was used with 50 μm slit aperture. The specimens were silver acetate with and without 0.1 w% of PDMS base including before and after thermal decomposition.

2.4.2 Scanning Electron Microscopy

To determine the structure of the silver nanoparticles on a silver acetate columnar. We use Scanning electron microscope (SEM), JEOL JSM-6510 to observe the structure of silver acetate with and without 0.1 w% of PDMS base including before and after thermal

decomposition. We also characterized the elements from Scanning electron microscopy with energy dispersive X-ray spectroscopy (SEM/EDX).

2.4.3 Optical microscopy

After Ag/PDMS stripe was fabricated, we observe the porous three-dimension structure of silver acetate while stretching, before and after stretching by using Optical microscope (OM), Carl Zeiss Axio Scope, A1 with a CCD camera (Carl Zeiss, AxioCam HRc).

2.4.4 Electrical resistance measurement

Three types of mechanical device, stretching, bending, and twisting were made using 3D printer. Electrical resistances were measured by using two-point probe with mechanical testing device. In order to measure the electrical resistance, there are two types of characteristics that have to be used. The first type is measurement of the change of electrical resistance by continuously force the mechanical stress onto the Ag/PDMS stripes. The next type is measurement of the change of electrical resistance with 10 cycles of deformation, under stretching, bending, and twisting.

3. Results and Discussion

3.1 Formation of silver acetate before and after decomposition

3.1.1 SEM micrographs

The prominent point of silver acetate is their structure, columnar shape, and porous three-dimension structure. Figure 1 shows the different silver acetate with and without PDMS base mixing between synthesis grades (A, B, C) and commercial grades from Sigma Aldrich (D, E, F). Synthesis grades (A, B, C) of silver acetate have a width of 1 μm each columnar while commercial grades (D, E, F) have 5 μm. The small silver acetate columnar is able to cover the area of substrate without the need for large quantities. Therefore, in this work we use synthesized

silver acetate. Furthermore, adding of PDMS base into the silver acetate solution before thermal decomposition can reduce sintering and cracking effect of silver porous three-dimension nanostructure network (C, F). The optimum amount of PDMS base is 0.1w%. If PDMS base was loaded more than 0.1w%, PDMS base induced silver nanoparticles to disperse into PDMS matrix and silver acetate cannot form to columnar shape and also cannot form to a film.

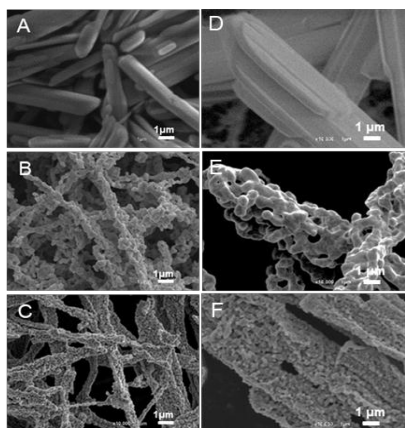


Figure 1 SEM micrographs of silver acetate synthesis grade, before (A), after (B) thermal decomposition, and 0.1w% of PDMS base mixture (C). And silver acetate commercial grade from Sigma Aldrich before (D), after (E) thermal decomposition, and 0.1w% of PDMS base mixture (F).

3.1.2 SEM/EDX

To determine the element of the silver acetate with and without PDMS base mixing, Scanning Electron Microscopy coupled with Energy Dispersive X-ray (SEM/EDX) was used.

Figure 2 shows element percentage changing before and after thermal decomposition. When bare silver acetate (A) transform to bare silver nanostructure (B) percentage of Ag increased while carbon decreased, because acetate group was decomposed after thermal decomposition. Furthermore, when silver acetate/PDMS base (C) transform to silver nanostructure/PDMS base (D), the percentage of Ag increased while Si remained the same

percentage because PDMS base was not completely decomposed.

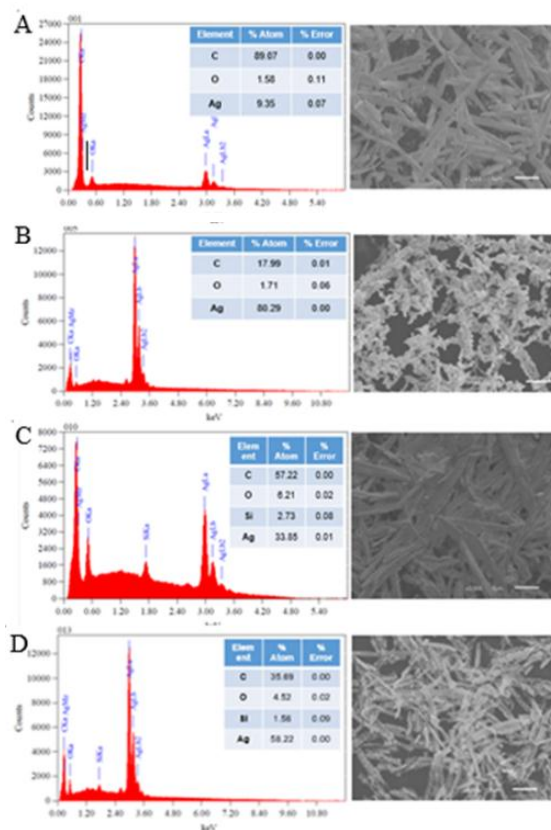


Figure 2 Scanning Electron Microscopy coupled with Energy Dispersive X-ray (SEM/EDX) spectra of (A) bare silver acetate, (B) bare silver nanostructure, (C) silver acetate/PDMS base, (D) silver nanostructure/PDMS base.

3.1.3 Raman spectroscopy

Figure 3 shows how silver acetate was decomposed to silver nanostructure and the digital images of thermal decomposition profile of silver acetate with and without PDMS base mixing. Raman signal shows that C-H stretching dispersed while D band and G band appeared after thermal decomposition (Figure 3A). However, C-H stretching signal of silver acetate/PDMS base was not completely decomposed.

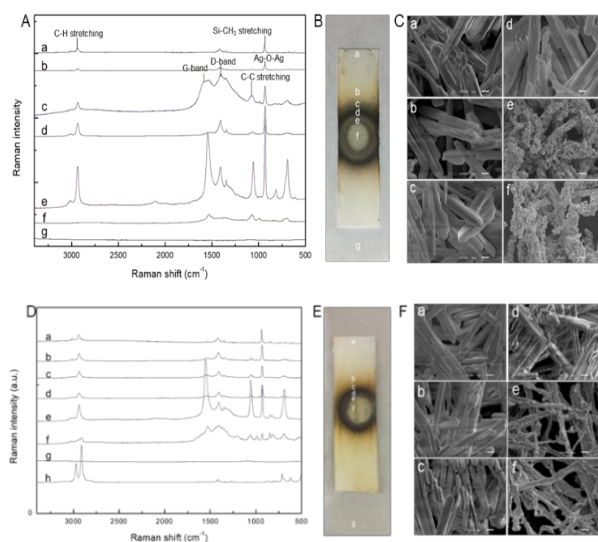


Figure 3 Comparison between (A) Thermal decomposition Raman spectra of bare silver acetate to silver nanostructure. (B) Digital images and (C) SEM micrographs of thermal decomposition profile of bare silver acetate. And (D) Thermal decomposition Raman spectra of silver acetate/PDMS base to silver nanostructure/PDMS base. (E) Digital images and (F) SEM micrographs of thermal decomposition profile of silver acetate/PDMS base.

3.1.4 Physical properties of Ag/PDMS stripe

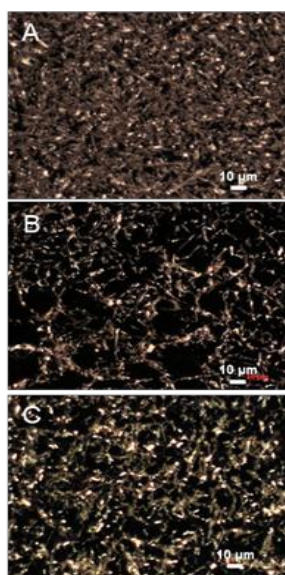


Figure 4 Optical microscope images of (A) Ag/PDMS conductive stripe before stretching ($R=5.0 \Omega$), (B) while stretching with 22% ($R=6.2 \Omega$), and (C) after release stretching ($R=5.2 \Omega$).

Figure 4 shows feature of silver nanostructure network which was mixed with 1w% of PDMS base in PDMS matrix when it was stretched. Before stretching (A), the porous structure was three-dimensional network covering all area of PDMS matrix. While 22% of stretching (B), the structure was stretched and empty space was occurred. After stretch releasing (C), the structure was recovered to porous three-dimension. It does not look like the previous structure because when it was stretched, some of the silver nanostructure was cracked. That is why resistivity increased after stretching.

3.1.5 Electrical resistance testing

Comparison of electrical resistance of three structures of the Ag/PDMS conductive stripes, 1) bare silver acetate, 2) silver acetate/PDMS base 0.1 w%, and 3) Evaporated silver metal.

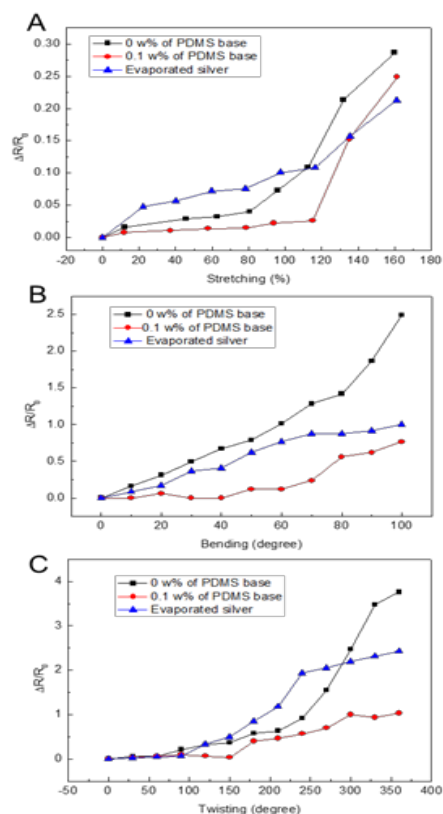


Figure 5 Relative change of electrical resistance ($R-R_0/R_0$) of Ag/PDMS stripe under various stretching percentages of three types of 1) bare silver acetate, 2) silver acetate/PDMS base 0.1 w%, and 3) evaporated silver metal.

Figure 5 shows three conditions of electrical resistance testing, stretching (A), bending (B), and twisting (C). In general, silver acetate which was mixed with PDMS base 0.1 w% (red line) has the lowest resistivity because PDMS base was as buffer and reduced sintering effect inside of porous three-dimension silver nanostructure network when it was under stress by stretching, bending, and twisting.

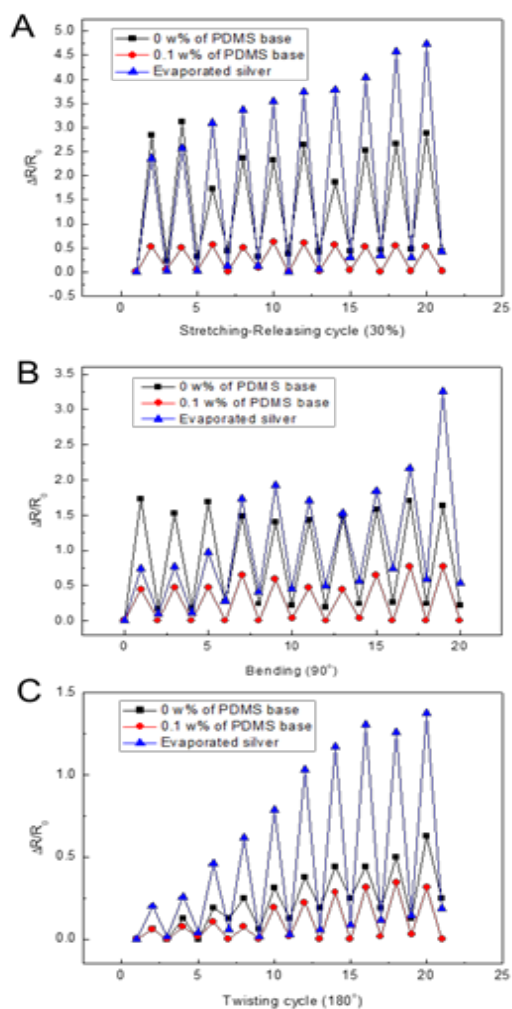


Figure 6 The change of electrical resistance ($R-R_0/R_0$) of Ag/PDMS stripe with 10 cycles of deformation under (A) stretching, (B) bending, and (C) twisting of three types of 1) bare silver acetate, 2) silver acetate/PDMS base 0.1 w%, and 3) evaporated silver metal.

The change of electrical resistance with 10 cycles of deformation under 30% stretching (A), 90° bending (B), and 180° twisting (C) of three types is shown in figure 6.

Generally, silver acetate which was mixed with PDMS base 0.1 w% (red line) has the lowest resistivity and reproducibility. While bare silver acetate and evaporated silver metal as black line and blue line respectively, show resistance increasing when stress is increased. Therefore, in this work we fabricated Ag/PDMS from condition of silver acetate which was mixed with PDMS base 0.1 w%.

4. Application

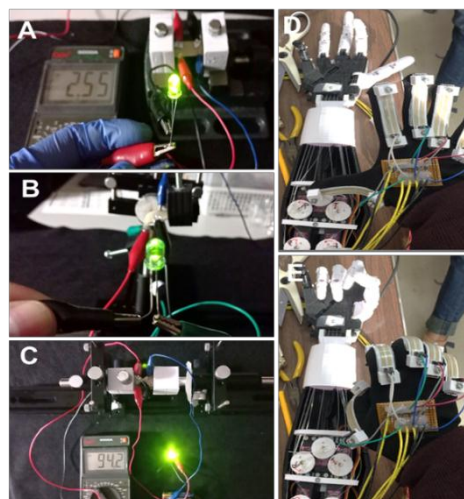


Figure 7 Pictures showing LEDs working while Ag/PDMS was under (A) stretching, (B) bending, and (C) twisting. And (D, E) Application of Ag/PDMS flexible conductive stripe for electronics device using for arduino sensor of robot arm.

Even Ag/PDMS stripes which was mixed with 0.1 w% of PDMS base, was under (A) stretching, (B) bending, and (C) twisting, LEDs still works, as shown in Figure 7.

Ag/PDMS stripe can apply to be flexible conductive polymer sensor for electronics device as sensor for arduino of robot arm as shown in D and E.

5. Conclusion

In this work, we present a facile, simple, and low-cost fabrication method for the fabrication of PDMS-silver nanocomposite which is an alternative flexible conductive substrate. Columnar silver acetate was synthesized and transformed to silver nanostructures with three-dimensional porous structures by thermal decomposition.

Adding of PDMS base into the silver acetate solution before thermal decomposition for reducing sintering effect of silver porous three-dimension nanostructure because silver nanostructure was inserted by PDMS base, when the structure was stretched, PDMS base could recover cracking of the porous structure. Moreover, Silver nanostructure porous three-dimension structure was also coated by PDMS base for reducing silver oxide.

Ag/ PDMS stripe can apply to be flexible conductive polymer sensor for electronics device as sensor for arduino robot arm.

Acknowledgement

This work was supported by Sensor Research Unit (SRU) at Department of Chemistry, and Program in Petrochemistry and Polymer Science, Chulalongkorn University. And Electric Engineering, Faculty of Engineer, Niigata University and the program on " Co- creative Dormitory-type Group-work for SciTech Students in Japan and Mekong Countries with Regional Collaboration (G-DORM) " , which Niigata University has been implementing under the Inter-University Exchange Project of MEXT.

References

- [1] Kim, J.; Park, J.; Jeong, U.; Park, J. W., Silver nanowire network embedded in polydimethylsiloxane as stretchable, transparent, and conductive substrates. *Journal of Applied Polymer Science* **2016**, *133* (33).
- [2] Hu, Y.; Zhao, T.; Zhu, P.; Zhu, Y.; Shuai, X.; Liang, X.; Sun, R.; Lu, D. D.; Wong, C.-P., Low cost and highly conductive elastic composites for flexible and printable electronics. *J. Mater. Chem. C* **2016**, *4* (24), 5839-5848.
- [3] Jeon, J.-Y.; Ha, T.-J., Waterproof Electronic-Bandage with Tunable Sensitivity for Wearable Strain Sensors. *ACS applied materials & interfaces* **2016**, *8* (4), 2866-2871.
- [4] Sun, J.; Jiang, J.; Bao, B.; Wang, S.; He, M.; Zhang, X.; Song, Y., Fabrication of Bendable Circuits on a

Polydimethylsiloxane (PDMS) Surface by Inkjet Printing Semi-Wrapped Structures. *Materials* **2016**, *9* (4), 253.

[5] Liu, H. S.; Pan, B. C.; Liou, G. S., Highly transparent AgNW/ PDMS stretchable electrodes for elastomeric electrochromic devices. *Nanoscale* **2017**, *9* (7), 2633-2639.

[6] Zhou, W.; Bai, S.; Ma, Y.; Ma, D.; Hou, T.; Shi, X.; Hu, A., Laser-Direct Writing of Silver Metal Electrodes on Transparent Flexible Substrates with High-Bonding Strength. *ACS applied materials & interfaces* **2016**, *8* (37), 24887-92.



List of Sponsors and Exhibitors

Sponsors

Platinum

- ❖ PTT Global Chemical Public Company Limited
- ❖ Aditya Birla Chemicals (Thailand) Co., Ltd.
- ❖ Bara Scientific Co., Ltd.

Gold

SCG Chemicals Co., Ltd.

Silver

Bruker BioSpin AG

Bronze

- ❖ IRPC Public Company Limited
- ❖ The Thailand Research Fund (TRF)

Support Students' Conference Registration Fee

M.B.J. Enterprise Co., Ltd.

Booth Exhibitors

- ❖ Becthai Bangkok Equipment & Chemical Co., Ltd.
- ❖ HORIBA (Thailand) Ltd.
- ❖ LMS Instruments Co., Ltd.
- ❖ Richtech Paint Co., Ltd.
- ❖ S.M. Chemicals Supplies Co., Ltd.
- ❖ Synchrotron Light Research Institute (Public Organization)
- ❖ Technovation International Co., Ltd.
- ❖ Vana Science Co., Ltd.

Abstract Book Co-Sponsor

Siam Synthetic Latex Co., Ltd.

Proceedings Publication

The proceedings for PCT-8 are published online, and can be downloaded from Polymer Society of Thailand website:

<http://www.thaipolymersociety.org/pst>



Polymer Society of Thailand

The Polymer Society of Thailand (PST) was founded on November 15, 1999, by a group of Polymer scientists who realized the increasing importance of the rapidly growing local petrochemical and polymer industries. Furthermore, with also the increasing number of polymer scientists and polymer degree courses to support the needs of human resources of the industries, it was thought that the Thai Polymer community would need a center for connecting different sectors in order to bring about effective development of the Thai petrochemical and polymer industries. Thus, the Polymer Club was established in 1991 and was later changed to the Polymer Society of Thailand in 1999.

Objectives:

1. To be a focal point for
 - coordinating collaborations among polymer scientists and persons or groups who are interested in polymer areas from both government and industrial sectors.
 - disseminating information and news related to polymer activities in Thailand.
 - representing the Thai polymer community in coordinating with relevant organizations domestically and internationally.
2. To promote the development of polymer science, technology and engineering in Thailand to international level.

Collaboration:

1. Memorandum of Collaboration Agreement with The Japan Society of Polymer Processing (JSPP)
2. Member of Pacific Polymer Federation (PPF)
3. Member of the Federation of Asian Polymer Societies (FAPS)
4. Member of The International Rubber Conference Organization (IRCO)
5. Memorandum of Agreement of the Society of Rubber Science and Technology, Japan (SRSJ)

Address:
73/1 room 412 NSTDA Building
Ministry of Science and Technology
Rama 6 Rd. Rajdathevi, Bangkok, THAILAND 10400
Email: tps@thaipolymersociety.org
June 14th 2018



**“ANNUAL MEETING IN POLYMER SCIENCE
AND TECHNOLOGY FOR ACADEMIC RESEARCH
AND INDUSTRIAL DEVELOPMENT”**

Organized by Polymer Society of Thailand